Contents

The Elements of Statistical Learning

Data Mining, Inference and Prediction

Chapter 1: Introduction

Jerome Friedman   Trevor Hastie   Robert Tibshirani

July 2, 2001

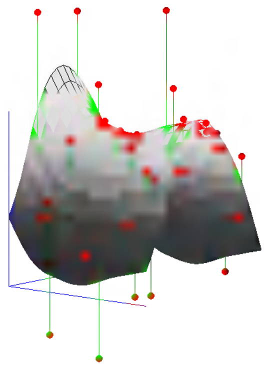

1
Introduction

Statistical learning plays a key role in many areas of science, finance and industry. Here are some examples of learning problems:

- Predict whether a patient, hospitalized due to a heart attack, will have a second heart attack. The prediction is to be based on demographic, diet and clinical measurements for that patient.
- Predict the price of a stock in 6 months from now, on the basis of company performance measures and economic data.
- Identify the numbers in a handwritten ZIP code, from a digitized image.
- Estimate the amount of glucose in the blood of a diabetic person, from the infrared absorption spectrum of that person's blood.
- Identify the risk factors for prostrate cancer, based on clinical and demographic variables.

The science of learning plays a key role in the fields of statistics, data mining and artificial intelligence, intersecting with areas of engineering and other disciplines.

This book is about learning from data. In a typical scenario, we have an outcome measurement, usually quantitative (like a stock price) or categorical (like heart attack/no heart attack), that we wish to predict based on a set of *features* (like diet and clinical measurements). We have a *training set* of data, in which we observe the outcome and feature measurements

TABLE 1.1. *Average percentage of words or characters in an email message equal to the indicated word or character. We have chosen the words and characters showing the largest difference between* `spam` *and* `email`.

	`george`	`you`	`your`	`hp`	`free`	`hpl`	`!`	`our`	`re`	`edu`	`remove`
`spam`	0.00	2.26	1.38	0.02	0.52	0.01	0.51	0.51	0.13	0.01	0.28
`email`	1.27	1.27	0.44	0.90	0.07	0.43	0.11	0.18	0.42	0.29	0.01

for a set of objects (such as people). Using this data we build a prediction model, or *learner*, which will enable us to predict the outcome for new unseen objects. A good learner is one that accurately predicts such an outcome.

The examples above describe what is called the *supervised learning* problem. It is called "supervised" because of the presence of the outcome variable to guide the learning process. In the *unsupervised learning problem*, we observe only the features and have no measurements of the outcome. Our task is rather to describe how the data are organized or clustered. We devote most of this book to supervised learning; the unsupervised problem is less developed in the literature, and is the focus of the last chapter.

Here are some examples of real learning problems that are discussed in this book.

Example 1: Email Spam

The data for this example consists of information from 4601 email messages, in a study to try to predict whether the email was junk email, or "spam." The objective was to design an automatic spam detector that could filter out spam before clogging the users' mailboxes. For 3601 email messages, the true outcome (email type) `email` or `spam` is available, along with the relative frequencies of 57 of the most commonly occurring words and punctuation marks in the email message. This is a supervised learning problem, with the outcome the class variable `email`/`spam`. It is also called a *classification* problem.

Table 1.1 lists the words and characters showing the largest average difference between `spam` and `email`.

Our learning method has to decide which features to use and how: for example, we might use a rule like

$$\text{if } (\texttt{\%george} < 0.6)\ \&\ (\texttt{\%you} > 1.5) \quad \begin{array}{l}\text{then } \texttt{spam} \\ \text{else } \texttt{email}.\end{array}$$

Another form of rule would be:

$$\text{if } (0.2 \cdot \texttt{\%you} \;-\; 0.3 \cdot \texttt{\%george}) > 0 \quad \begin{array}{l}\text{then } \texttt{spam} \\ \text{else } \texttt{email}.\end{array}$$

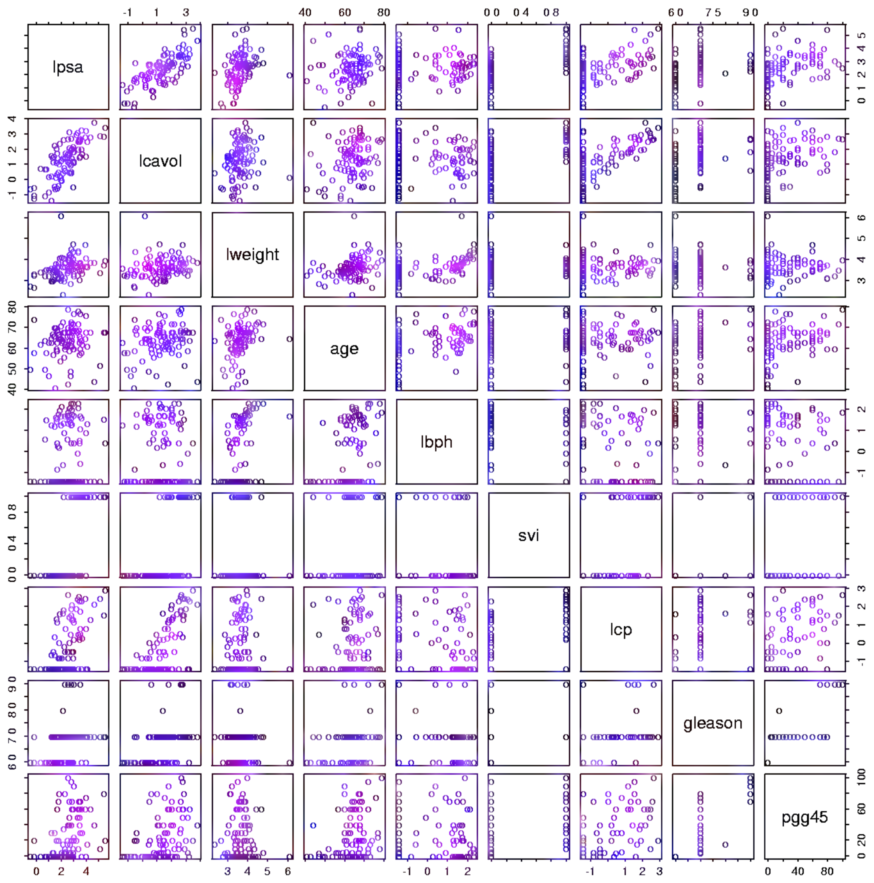

FIGURE 1.1. *Scatterplot matrix of the prostate cancer data. The first row shows the response against each of the predictors in turn. Two of the predictors,* `svi` *and* `gleason`*, are categorical.*

For this problem not all errors are equal; we want to avoid filtering out good email, while letting spam get through is not desirable but less serious in its consequences. We discuss a number of different methods for tackling this learning problem in the book.

Example 2: Prostrate Cancer

The data for this example, displayed in Figure 1.1, come from a study by **?** that examined the correlation between the level of prostate specific antigen and a number of clinical measures, in 97 men who were about to receive a radical prostatectomy.

The goal is to predict the log-cancer-volume (`lcavol`) from a number of measurements including log prostate weight `lweight`, age, log of benign

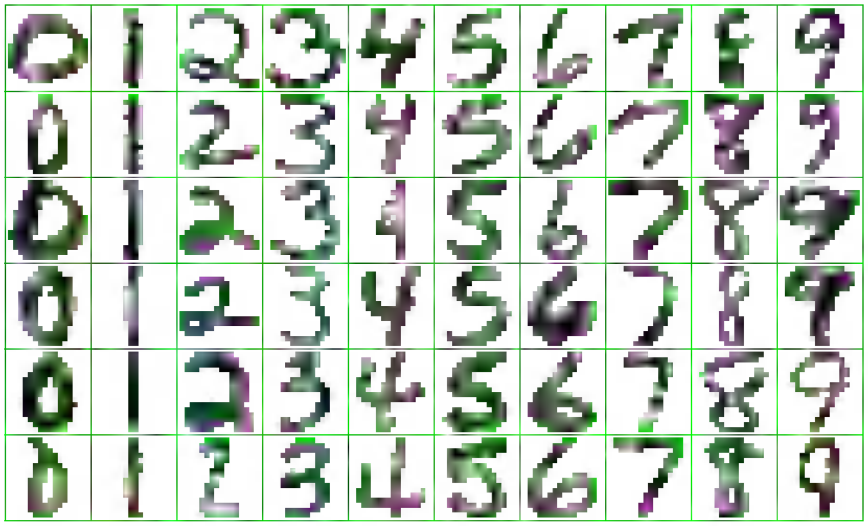

FIGURE 1.2. *Examples of handwritten digits from U.S. postal envelopes.*

prostatic hyperplasia amount `lbph`, seminal vesicle invasion `svi`, log of capsular penetration `lcp`, Gleason score `gleason`, and percent of Gleason scores 4 or 5 `pgg45`. Figure 1.1 is a scatterplot matrix of the variables. Some correlations with `lcavol` are evident, but a good predictive model is difficult to construct by eye.

This is a supervised learning problem, known as a *regression problem*, because the outcome measurement is quantitative.

Example 3: Handwritten Digit Recognition

The data from this example come from the handwritten ZIP codes on envelopes from U.S. postal mail. Each image is a segment from a five digit ZIP code, isolating a single digit. The images are 16×16 eight-bit grayscale maps, with each pixel ranging in intensity from 0 to 255. Some sample images are shown in Figure 1.2.

The images have been normalized to have approximately the same size and orientation. The task is to predict, from the 16×16 matrix of pixel intensities, the identity of each image $(0, 1, \dots, 9)$ quickly and accurately. If it is accurate enough, the resulting algorithm would be used as part of an automatic sorting procedure for envelopes. This is a classification problem for which the error rate needs to be kept very low to avoid misdirection of mail. In order to achieve this low error rate, some objects can be assigned to a "don't know" category, and sorted instead by hand.

Example 4: DNA Expression Microarrays

DNA stands for deoxyribonucleic acid, and is the basic material that makes up human chromosomes. DNA microarrays measure the expression of a gene in a cell by measuring the amount of mRNA (messenger ribonucleic acid) present for that gene. Microarrays are considered a breakthrough technology in biology, facilitating the quantitative study of thousands of genes simultaneously from a single sample of cells.

Here is how a DNA microarray works. The nucleotide sequences for a few thousand genes are printed on a glass slide. A target sample and a reference sample are labeled with red and green dyes, and each are hybridized with the DNA on the slide. Through fluoroscopy, the log (red/green) intensities of RNA hybridizing at each site is measured. The result is a few thousand numbers, typically ranging from say -6 to 6, measuring the expression level of each gene in the target relative to the reference sample. Positive values indicate higher expression in the target versus the reference, and vice versa for negative values.

A gene expression dataset collects together the expression values from a series of DNA microarray experiments, with each column representing an experiment. There are therefore several thousand rows representing individual genes, and tens of columns representing samples: in the particular example of Figure 1.3 there are 6830 genes (rows) and 64 samples (columns), although for clarity only a random sample of 100 rows are shown. The figure displays the data set as a heat map, ranging from green (negative) to red (positive). The samples are 64 cancer tumors from different patients.

The challenge here is to understand how the genes and samples are organized. Typical questions include the following:

(a) which samples are most similar to each other, in terms of their expression profiles across genes?

(b) which genes are most similar to each other, in terms of their expression profiles across samples?

(c) do certain genes show very high (or low) expression for certain cancer samples?

We could view this task as a regression problem, with two categorical predictor variables—genes and samples, with the response variable being the level of expression. However, it is probably more useful to view it as *unsupervised learning* problem. For example, for question (a) above, we think of the samples as points in 6830−dimensional space, which we want to *cluster* together in some way.

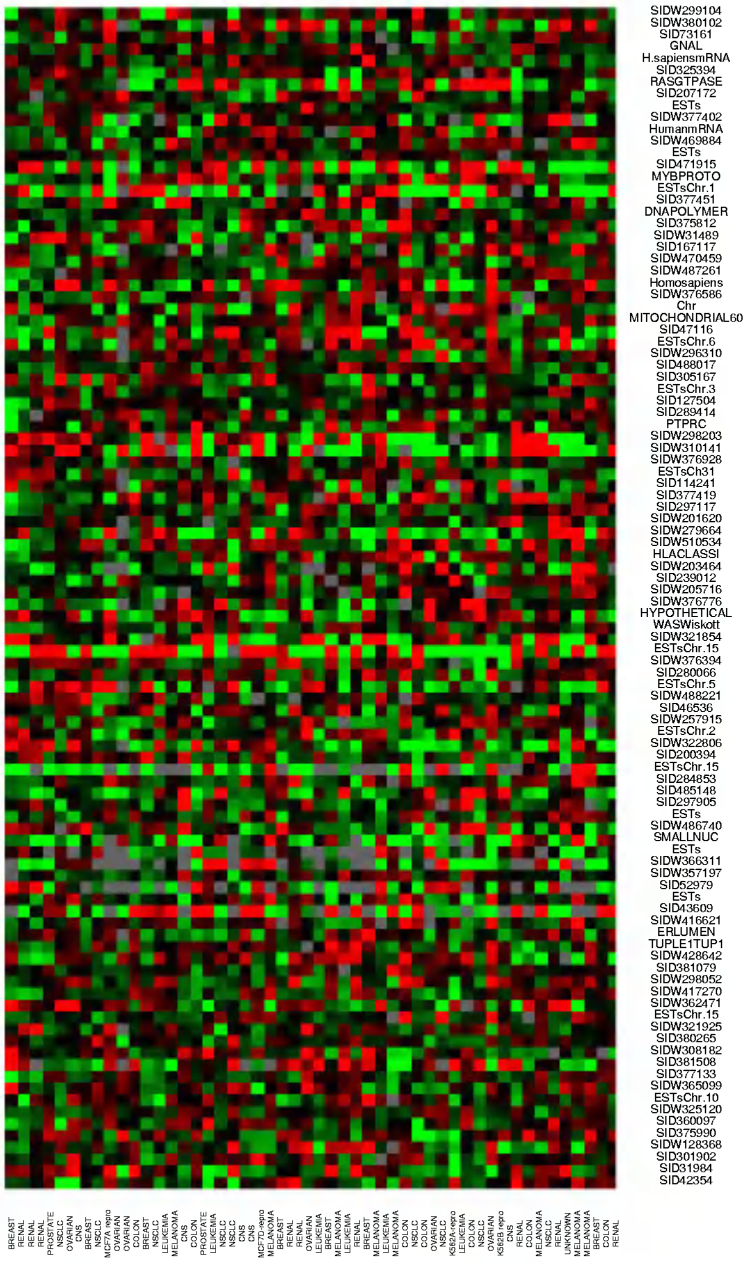

FIGURE 1.3. *DNA microarray data: expression matrix of 6830 genes (rows) and 64 samples (columns), for the human tumor data. Only a random sample of 100 rows are shown. The display is a heat map, ranging from bright green (negative, under expressed) to bright red (positive, over expressed). Missing values are gray. The rows and columns are displayed in a randomly chosen order.*

Who Should Read this Book

This book is designed for researchers and students in a broad variety of fields: statistics, artificial intelligence, engineering, finance and others. We expect that the reader will have had at least one elementary course in statistics, covering basic topics including linear regression.

We have not attempted to write a comprehensive catalog of learning methods, but rather to describe some of the most important techniques. Equally notable, we describe the underlying concepts and considerations by which a researcher can judge a learning method. We have tried to write this book in an intuitive fashion, emphasizing concepts rather than mathematical details.

As statisticians, our exposition will naturally reflect our backgrounds and areas of expertise. However in the past eight years we have been attending conferences in neural networks, data mining and machine learning, and our thinking has been heavily influenced by these exciting fields. This influence is evident in our current research, and in this book.

How this Book is Organized

Our view is that one must understand simple methods before trying to grasp more complex ones. Hence after giving an overview of the supervising learning problem in Chapter 2, we discuss linear methods for regression and classification in Chapters 2 and 4. In Chapter 5 we describe splines, wavelets and regularization/penalization methods for a single predictor, while Chapter 6 covers kernel methods and local regression. Both of these sets of methods are important building blocks for high-dimensional learning techniques. Model assessment and selection is the topic of Chapter 7, covering the concepts of bias and variance, overfitting and methods like cross-validation for choosing models. Chapter 8 discusses model inference and averaging, including an overview of maximum likelihood, Bayesian inference and the bootstrap, the EM algorithm, Gibbs sampling and bagging, A related procedure called boosting is the focus of Chapter 14.

In Chapters 9–12 we describe a series of structured methods for supervised learning, with Chapters 9 and 10 covering regression and Chapters 11 and 12 focussing on classification. Finally, in Chapter **??** we describe methods for unsupervised learning.

At the end of each chapter we discuss computational considerations important for data mining applications, including how the computations scale with the number of observations and predictors. Each chapter ends with Bibliographic Notes giving background references for the material.

We recommend that Chapters 1–4 be first read in sequence. Chapter 7 should also be considered mandatory, as it covers central concepts that pertain to all learning methods. With this in mind, the rest of the book can be read sequentially, or sampled, depending on the reader's interest.

The symbol indicates a technically difficult section, one that can be skipped without interrupting the flow of the discussion.

Book Website

The website for this book is located at

`http://www-stat.stanford.edu/ElemStatLearn`

It contains a number of resources, including many of the datasets used in this book.

Note for Instructors

We have successively used this book as the basis for a two-quarter course, and with additional materials, it could even be used for a three-quarter sequence. Exercises are provided at the end of each chapter. It is important for students to have access to good software tools for these topics. We used the S-PLUS programming language in our courses.

References

Stamey, T., Kabalin, J., McNeal, J., Johnstone, I., Freiha, F., Redwine, E. & Yang, N. (1989), 'Prostate specific antigen in the diagnosis and treatment of adenocarcinoma of the prostate ii. radical prostatectomy treated patients', *Journal of Urology* **16**, 1076–1083.

2
Overview of Supervised Learning

2.1 Introduction

The first three examples described in Chapter 1 have several components in common. For each there is a set of variables that might be denoted as *inputs*, which are measured or preset. These have some influence on one or more *outputs*. For each example the goal is to use the inputs to predict the values of the outputs. This exercise is called *supervised learning*.

We have used the more modern language of machine learning. In the statistical literature the inputs are often called the *predictors*, a term we will use interchangeably with inputs, and more classically the *independent variables*. The outputs are called the *responses*, or classically the *dependent variables*.

2.2 Variable Types and Terminology

The outputs vary in nature among the examples. In the glucose prediction example, the output is a *quantitative* measurement, where some measurements are bigger than others, and measurements close in value are close in nature. In the famous Iris discrimination example due to R. A. Fisher, the output is *qualitative* (species of Iris) and assumes values in a finite set $\mathcal{G} = \{$*Virginica*, *Setosa* and *Versicolor*$\}$. In the handwritten digit example the output is one of 10 different digit *classes*: $\mathcal{G} = \{0, 1, \ldots, 9\}$. In both of these there is no explicit ordering in the classes, and in fact often descriptive labels rather than numbers are used to denote the classes. Qualitative variables are also referred to as *categorical* or *discrete* variables as well as *factors.*

For both types of outputs it makes sense to think of using the inputs to predict the output. Given some specific atmospheric measurements today and yesterday, we want to predict the ozone level tomorrow. Given the grayscale values for the pixels of the digitized image of the handwritten digit, we want to predict its class label.

This distinction in output type has led to a naming convention for the prediction tasks: *regression* when we predict quantitative outputs, and *classification* when we predict qualitative outputs. We will see that these two tasks have a lot in common, and in particular both can be viewed as a task in function approximation.

Inputs also vary in measurement type; we can have some of each of qualitative and quantitative input variables. These have also led to distinctions in the types of methods that are used for prediction: some methods are defined most naturally for quantitative inputs, some most naturally for qualitative and some for both.

A third variable type is *ordered categorical*, such as *small, medium* and *large*, where there is an ordering between the values, but no metric notion is appropriate (the difference between medium and small need not be the same as that between large and medium). These are discussed further in Chapter 4.

Qualitative variables are typically represented numerically by codes. The easiest case is when there are only two classes or categories, such as "success" or "failure," "survived" or "died." These are often represented by a single binary digit or bit as 0 or 1, or else by -1 and 1. For reasons that will become apparent, such numeric codes are sometimes referred to as *targets.* When there are more than two categories, several alternatives are available. The most useful and commonly used coding is via *dummy variables.* Here a K-level qualitative variable is represented by a vector of K binary variables or bits, only one of which is "on" at a time. Although more compact coding schemes are possible, dummy variables are symmetric in the levels of the factor.

We will typically denote an input variable by the symbol X. If X is a vector, its components can be accessed by subscripts X_j. Quantitative outputs will be denoted by Y, and qualitative outputs by G (for group). We use uppercase letters such as X, Y or G when referring to the generic aspects of a variable. Observed values are written in lowercase; hence the ith observed value of X is written as x_i (where x_i is again a scalar or vector). Matrices are represented by bold uppercase letters; for example, a set of N input p-vectors $x_i,\ i = 1, \ldots, N$ would be represented by the $N \times p$ matrix $\mathbf{X}$. In general vectors will not be bold, except when they have N components; this convention distinguishes a p-vector of inputs x_i for the ith observation from the N-vector $\mathbf{x}_j$ consisting of all the observations on variable X_j. Since all vectors are assumed to be column vectors, the ith row of $\mathbf{X}$ is x_i^T, the vector transpose of x_i.

For the moment we can loosely state the learning task as follows: given the value of an input vector X, make a good prediction of the output Y, denoted by $\hat{Y}$ (pronounced "y-hat"). If Y takes values in $\mathbb{R}$ then so should $\hat{Y}$; likewise for categorical outputs, $\hat{G}$ should take values in the same set $\mathcal{G}$ associated with G.

For a two-class G, one approach is to denote the binary coded target as Y, and then treat it as a quantitative output. The predictions $\hat{Y}$ will typically lie in $[0, 1]$, and we can assign to $\hat{G}$ the class label according to whether $\hat{y} > 0.5$. This approach generalizes to K-level qualitative outputs as well.

We need data to construct prediction rules, often a lot of it. We thus suppose we have available a set of measurements (x_i, y_i) or (x_i, g_i), $i = 1, \dots, N$, known as the *training data*, with which to construct our prediction rule.

2.3 Two Simple Approaches to Prediction: Least Squares and Nearest Neighbors

In this section we develop two simple but powerful prediction methods: the linear model fit by least squares and the k-nearest-neighbor prediction rule. The linear model makes huge assumptions about structure and yields stable but possibly inaccurate predictions. The method of k-nearest neighbors makes very mild structural assumptions: its predictions are often accurate but can be unstable.

2.3.1 Linear Models and Least Squares

The linear model has been a mainstay of statistics for the past 30 years and remains one of our most important tools. Given a vector of inputs $X = (X_1, X_2, \dots, X_p)$, we predict the output Y via the model

$$\hat{Y} = \hat{\beta}_0 + \sum_{j=1}^{p} X_j \hat{\beta}_j. \tag{2.1}$$

The term $\hat{\beta}_0$ is the intercept, also known as the *bias* in machine learning. Often it is convenient to include the constant variable 1 in X, include $\hat{\beta}_0$ in the vector of coefficients $\hat{\beta}$, and then write the linear model in vector form as an inner product

$$\hat{Y} = X^T \hat{\beta}, \tag{2.2}$$

where X^T denotes vector or matrix transpose (X being a column vector). Here we are modeling a single output, so $\hat{Y}$ is a scalar; in general $\hat{Y}$ can be a K–vector, in which case β would be a $p \times K$ matrix of coefficients. In the $(p+1)$-dimensional input–output space, $(X, \hat{Y})$ represents a hyperplane. If the constant is included in X, then the hyperplane includes the origin and is a subspace; if not, it is an affine set cutting the Y-axis at the point $(0, \hat{\beta}_0)$. From now on we assume that the intercept is included in $\hat{\beta}$.

Viewed as a function over the p-dimensional input space, $f(X) = X^T\beta$ is linear, and the gradient $f'(X) = \beta$ is a vector in input space that points in the steepest uphill direction.

How do we fit the linear model to a set of training data? There are many different methods, but by far the most popular is the method of *least squares*. In this approach, we pick the coefficients β to minimize the residual sum of squares

$$\text{RSS}(\beta) = \sum_{i=1}^{N}(y_i - x_i^T\beta)^2. \tag{2.3}$$

$\text{RSS}(\beta)$ is a quadratic function of the parameters, and hence its minimum always exists, but may not be unique. The solution is easiest to characterize in matrix notation. We can write

$$\text{RSS}(\beta) = (\mathbf{y} - \mathbf{X}\beta)^T(\mathbf{y} - \mathbf{X}\beta), \tag{2.4}$$

where $\mathbf{X}$ is an $N \times p$ matrix with each row an input vector, and $\mathbf{y}$ is an N-vector of the outputs in the training set. Differentiating w.r.t. β we get the *normal equations*

$$\mathbf{X}^T(\mathbf{y} - \mathbf{X}\beta) = 0. \tag{2.5}$$

If $\mathbf{X}^T\mathbf{X}$ is nonsingular, then the unique solution is given by

$$\hat{\beta} = (\mathbf{X}^T\mathbf{X})^{-1}\mathbf{X}^T\mathbf{y}, \tag{2.6}$$

and the fitted value at the ith input x_i is $\hat{y}_i = \hat{y}(x_i) = x_i^T\hat{\beta}$. At an arbitrary input x_0 the prediction is $\hat{y}(x_0) = x_0^T\hat{\beta}$. The entire fitted surface is characterized by the p parameters $\hat{\beta}$. Intuitively, it seems that we do not need a very large data set to fit such a model.

Let's look at an example of the linear model in a classification context. Figure 2.1 shows a scatterplot of training data on a pair of inputs X_1 and X_2. The data are simulated, and for the present the simulation model is not important. The output class variable G has the values `GREEN` or `RED`, and is represented as such in the scatterplot. There are 100 points in each of the two classes. The linear regression model was fit to these data, with the response Y coded as 0 for `GREEN` and 1 for `RED`. The fitted values $\hat{Y}$ are

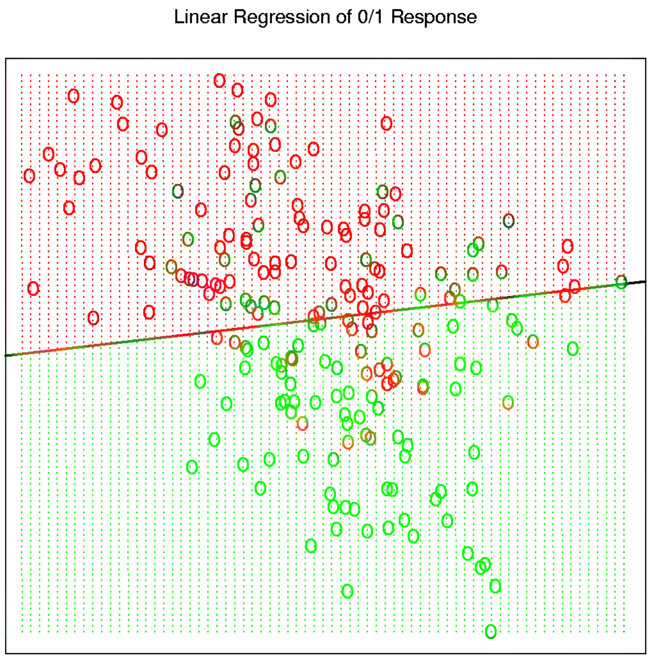

FIGURE 2.1. *A classification example in two dimensions. The classes are coded as a binary variable—*GREEN $= 0$, RED $= 1$*—and then fit by linear regression. The line is the decision boundary defined by $x^T\hat{\beta} = 0.5$. The red shaded region denotes that part of input space classified as* RED*, while the green region is classified as* GREEN.

converted to a fitted class variable $\hat{G}$ according to the rule

$$\hat{G} = \begin{cases} \texttt{RED} & \text{if } \hat{Y} > 0.5, \\ \texttt{GREEN} & \text{if } \hat{Y} \leq 0.5. \end{cases} \tag{2.7}$$

The set of points in $\mathbb{R}^2$ classified as RED corresponds to $\{x : x^T\hat{\beta} > 0.5\}$, indicated in Figure 2.1, and the two predicted classes are separated by the *decision boundary* $\{x : x^T\hat{\beta} = 0.5\}$, which is linear in this case. We see that for these data there are several misclassifications on both sides of the decision boundary. Perhaps our linear model is too rigid— or are such errors unavoidable? Remember that these are errors on the training data itself, and we have not said where the constructed data came from. Consider the two possible scenarios:

Scenario 1: The training data in each class were generated according to two bivariate Gaussian distributions with uncorrelated components and different means.

Scenario 2: The training data in each class came from a mixture of 10 low-variance Gaussian distributions, with individual means themselves distributed as Gaussian.

A mixture of Gaussians is best described in terms of the generative model. One first generates a discrete variable that determines which of the component Gaussians to use, and then generates an observation from the chosen density. In the case of one Gaussian per class, we will see in Chapter 4 that a linear decision boundary is the best one can do, and that our estimate is almost optimal. The region of overlap is inevitable, and future data to be predicted will be plagued by this overlap as well.

In the case of mixtures of tightly clustered Gaussians the story is different. A linear decision boundary is unlikely to be optimal, and in fact is not. The optimal decision boundary is nonlinear and disjoint, and as such will be much more difficult to obtain.

We now look at another classification and regression procedure that is in some sense at the opposite end of the spectrum to the linear model, and far better suited to the second scenario.

2.3.2 Nearest-Neighbor Methods

Nearest-neighbor methods use those observations in the training set $\mathcal{T}$ closest in input space to x to form $\hat{Y}$. Specifically, the k-nearest neighbor fit for $\hat{Y}$ is defined as follows:

$$\hat{Y}(x) = \frac{1}{k} \sum_{x_i \in N_k(x)} y_i, \tag{2.8}$$

where $N_k(x)$ is the neighborhood of x defined by the k closest points x_i in the training sample. Closeness implies a metric, which for the moment we assume is Euclidean distance. So, in words, we find the k observations with x_i closest to x in input space, and average their responses.

In Figure 2.2 we use the same training data as in Figure 2.1, and use 15-nearest-neighbor averaging of the binary coded response as the method of fitting. Thus $\hat{Y}$ is the proportion of GREEN's in the neighborhood, and so assigning class RED to $\hat{G}$ if $\hat{Y} > 0.5$ amounts to a majority vote in the neighborhood. The colored regions indicate all those points in input space classified as GREEN or RED by such a rule, in this case found by evaluating the procedure on a fine grid in input space. We see that the decision boundaries that separate the GREEN from the RED regions are far more irregular, and respond to local clusters where one class dominates.

Figure 2.3 shows the results for 1-nearest-neighbor classification: $\hat{Y}$ is assigned the value y_ℓ of the closest point x_ℓ to x in the training data. In this case the regions of classification can be computed relatively easily, and correspond to a *Voronoi tessellation* of the training data. Each point x_i

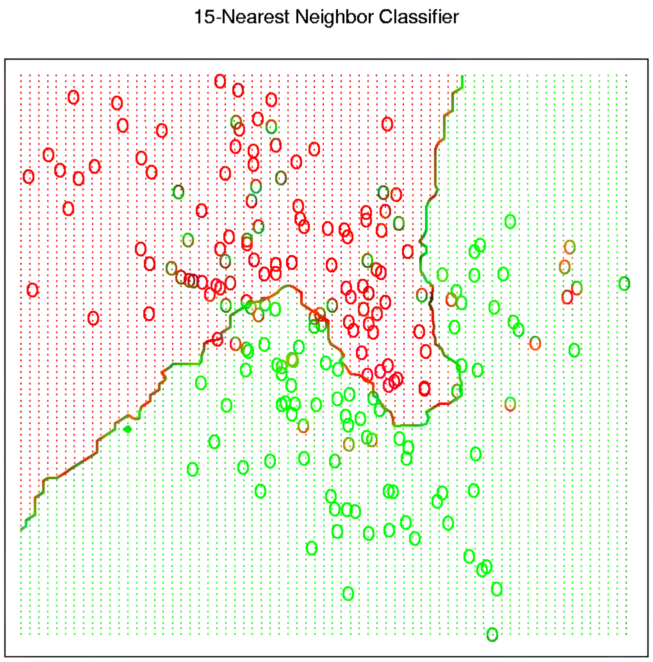

FIGURE 2.2. *The same classification example in two dimensions as in Figure 2.1. The classes are coded as a binary variable* (`GREEN` $= 0$, `RED` $= 1$) *and then fit by* 15*-nearest-neighbor averaging as in (2.8). The predicted class is hence chosen by majority vote amongst the* 15*-nearest neighbors.*

has an associated tile bounding the region for which it is the closest input point. For all points x in the tile, $\hat{G}(x) = g_i$. The decision boundary is even more irregular than before.

The method of k-nearest-neighbor averaging is defined in exactly the same way for regression of a quantitative output Y, although $k = 1$ would be an unlikely choice.

In Figure 2.2 we see that far fewer training observations are misclassified than in Figure 2.1. This should not give us too much comfort, though, since in Figure 2.3 *none* of the training data are misclassified. A little thought suggests that for k-nearest-neighbor fits, the error on the training data should be approximately an increasing function of k, and will always be 0 for $k = 1$. An independent test set would give us a more satisfactory means for comparing the different methods.

It appears that k-nearest-neighbor fits have a single parameter, the number of neighbors k, compared to the p parameters in least-squares fits. Although this is the case, we will see that the *effective* number of parameters of k-nearest neighbors is N/k and is generally bigger than p, and decreases with increasing k. To get an idea of why, note that if the neighborhoods

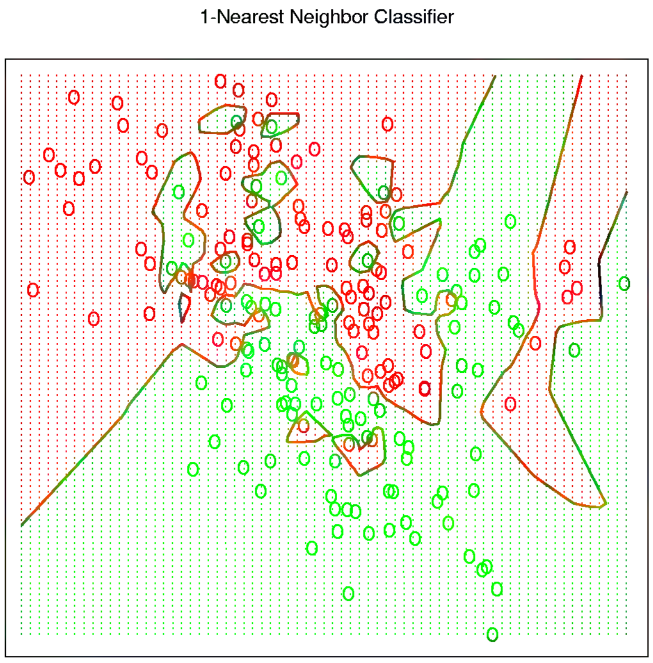

FIGURE 2.3. *The same classification example in two dimensions as in Figure 2.1. The classes are coded as a binary variable* (GREEN $= 0$, RED $= 1$), *and then predicted by* 1*-nearest-neighbor classification.*

were nonoverlapping, there would be N/k neighborhoods and we would fit one parameter (a mean) in each neighborhood.

It is also clear that we cannot use sum-of-squared errors on the training set as a criterion for picking k, since we would always pick $k = 1$! It would seem that k-nearest-neighbor methods would be more appropriate for the mixture Scenario 2 described above, while for Gaussian data the decision boundaries of k-nearest neighbors would be unnecessarily noisy.

2.3.3 From Least Squares to Nearest Neighbors

The linear decision boundary from least squares is very smooth, and apparently stable to fit. It does appear to rely heavily on the assumption that a linear decision boundary is appropriate. In language we will develop shortly, it has low variance and potentially high bias.

On the other hand, the k-nearest-neighbor procedures do not appear to rely on any stringent assumptions about the underlying data, and can adapt to any situation. However, any particular subregion of the decision boundary depends on a handful of input points and their particular positions, and is thus wiggly and unstable—high variance and low bias.

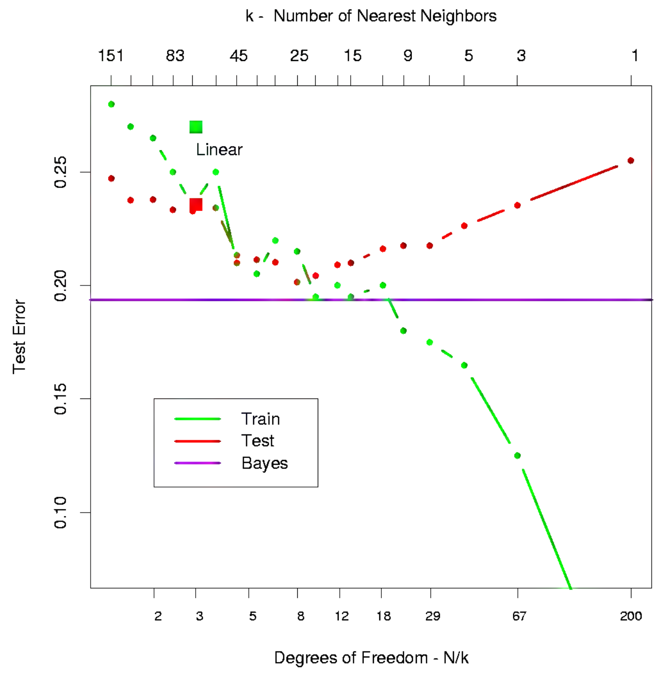

FIGURE 2.4. *Misclassification curves for the simulation example used in Figures 2.1, 2.2 and 2.3. A single training sample of size* 200 *was used, and a test sample of size* 10,000*. The red curves are test and the green are training error for k-nearest-neighbor classification. The results for linear regression are the bigger green and red dots at three degrees of freedom. The purple line is the optimal Bayes Error Rate.*

Each method has its own situations for which it works best; in particular linear regression is more appropriate for Scenario 1 above, while nearest neighbors are more suitable for Scenario 2. The time has come to expose the oracle! The data in fact were simulated from a model somewhere between the two, but closer to Scenario 2. First we generated 10 means m_k from a bivariate Gaussian distribution $N((1,0)^T, \mathbf{I})$ and labeled this class GREEN. Similarly, 10 more were drawn from $N((0,1)^T, \mathbf{I})$ and labeled class RED. Then for each class we generated 100 observations as follows: for each observation, we picked an m_k at random with probability 1/10, and then generated a $N(m_k, \mathbf{I}/5)$, thus leading to a mixture of Gaussian clusters for each class. Figure 2.4 shows the results of classifying 10,000 new observations generated from the model. We compare the results for least squares and those for k-nearest neighbors for a range of values of k.

A large subset of the most popular techniques in use today are variants of these two simple procedures. In fact 1-nearest-neighbor, the simplest of all, captures a large percentage of the market for low-dimensional problems.

The following list describes some ways in which these simple procedures have been enhanced:

- Kernel methods use weights that decrease smoothly to zero with distance from the target point, rather than the effective 0/1 weights used by k-nearest neighbors.
- In high-dimensional spaces the distance kernels are modified to emphasize some variable more than others.
- Local regression fits linear models by locally weighted least squares, rather than fitting constants locally.
- Linear models fit to a basis expansion of the original inputs allow arbitrarily complex models.
- Projection pursuit and neural network models consist of sums of non-linearly transformed linear models.

2.4 Statistical Decision Theory

In this section we develop a small amount of theory that provides a framework for developing models such as those discussed informally so far. We first consider the case of a quantitative output, and place ourselves in the world of random variables and probability spaces. Let $X \in \mathbb{R}^p$ denote a real valued random input vector, and $Y \in \mathbb{R}$ a real valued random output variable, with joint distribution $\Pr(X, Y)$. We seek a function $f(X)$ for predicting Y given values of the input X. This theory requires a *loss function* $L(Y, f(X))$ for penalizing errors in prediction, and by far the most common and convenient is *squared error loss*: $L(Y, f(X)) = (Y - f(X))^2$. This leads us to a criterion for choosing f,

$$\begin{aligned} \mathrm{EPE}(f) &= \mathrm{E}(Y - f(X))^2 && (2.9)\\ &= \int (y - f(x))^2 \Pr(dx, dy), && (2.10) \end{aligned}$$

the expected (squared) prediction error. By conditioning[*] on X, we can write EPE as

$$\mathrm{EPE}(f) = \mathrm{E}_X \mathrm{E}_{Y|X}\left([Y - f(X)]^2 | X\right) \qquad (2.11)$$

and we see that it suffices to minimize EPE pointwise:

$$f(x) = \mathrm{argmin}_c \mathrm{E}_{Y|X}\left([Y - c]^2 | X = x\right). \qquad (2.12)$$

[*]Conditioning here amounts to factoring the joint density $\Pr(X, Y) = \Pr(Y|X)\Pr(X)$ where $\Pr(Y|X) = \Pr(Y, X)/\Pr(X)$, and splitting up the bivariate integral accordingly

The solution is

$$f(x) = \mathrm{E}(Y|X = x), \tag{2.13}$$

the conditional expectation, also known as the *regression* function. Thus the best prediction of Y at any point $X = x$ is the conditional mean, when best is measured by average squared error.

The nearest-neighbor methods attempt to directly implement this recipe using the training data. At each point x, we might ask for the average of all those y_is with input $x_i = x$. Since there are typically at most one observation at any point x, we settle for

$$\hat{f}(x) = \mathrm{Ave}(y_i|x_i \in N_k(x)), \tag{2.14}$$

where "Ave" denotes average, and $N_k(x)$ is the neighborhood containing the k points in T closest to x. Two approximations are happening here:

- expectation is approximated by averaging over sample data;
- conditioning at a point is relaxed to conditioning on some region "close" to the target point.

For large training sample size N, the points in the neighborhood are likely to be close to x, and as k gets large the average will get more stable. In fact, under mild regularity conditions on the joint probability distribution $\Pr(X, Y)$, one can show that as $N, k \to \infty$ such that $k/N \to 0$, $\hat{f}(x) \to \mathrm{E}(Y|X = x)$. In light of this, why look further, since it seems we have a universal approximator? We often do not have very large samples. If the linear or some more structured model is appropriate, then we can usually get a more stable estimate than k-nearest neighbors, although such knowledge has to be learned from the data as well. There are other problems though, sometimes disastrous. In Section 2.5 we see that as the dimension p gets large, so does the metric size of the k-nearest neighborhood. So settling for nearest neighborhood as a surrogate for conditioning will fail us miserably. The convergence above still holds, but the *rate* of convergence decreases as the dimension increases.

How does linear regression fit into this framework? The simplest explanation is that one assumes that the regression function $f(x)$ is approximately linear in its arguments:

$$f(x) \approx x^T\beta. \tag{2.15}$$

This is a model-based approach—we specify a model for the regression function. Plugging this linear model for $f(x)$ into EPE (2.9) and differentiating we can solve for β theoretically:

$$\beta = [\mathrm{E}(XX^T)]^{-1}\mathrm{E}(XY). \tag{2.16}$$

Note we have *not* conditioned on X; rather we have used our knowledge of the functional relationship to *pool* over values of X. The least squares solution (2.6) amounts to replacing the expectation in (2.16) by averages over the training data.

So both k-nearest neighbors and least squares end up approximating conditional expectations by averages. But they differ dramatically in terms of model assumptions:

- Least squares assumes $f(x)$ is well approximated by a globally linear function.
- k-nearest neighbors assumes $f(x)$ is well approximated by a locally constant function.

Although the latter seems more palatable, we have already seen that we may pay a price for this flexibility.

Many of the more modern techniques described in this book are model based, although far more flexible than the rigid linear model. For example, additive models assume that

$$f(X) = \sum_{j=1}^{p} f_j(X_j). \tag{2.17}$$

This retains the additivity of the linear model, but each coordinate function f_j is arbitrary. It turns out that the optimal estimate for the additive model uses techniques such as k-nearest neighbors to approximate *univariate* conditional expectations *simultaneously* for each of the coordinate functions. Thus the problems of estimating a conditional expectation in high dimensions are swept away in this case by imposing some (often unrealistic) model assumptions, in this case additivity.

Are we happy with the criterion (2.11)? What happens if we replace the L_2 loss function with the L_1: $E|Y - f(X)|$? The solution in this case is the conditional median,

$$\hat{f}(x) = \text{median}(Y|X = x), \tag{2.18}$$

which is a different measure of location, and its estimates are more robust than those for the conditional mean. L_1 criteria have discontinuities in their derivatives, which have hindered their widespread use. Other more resistant loss functions will be mentioned in later chapters, but squared error is analytically convenient and the most popular.

What do we do when the output is a categorical variable G? The same paradigm works here, except we need a different loss function for penalizing prediction errors. An estimate $\hat{G}$ will assume values in $\mathcal{G}$, the set of possible classes. Our loss function can be represented by a $K \times K$ matrix $\mathbf{L}$, where $K = \text{card}(\mathcal{G})$. $\mathbf{L}$ will be zero on the diagonal and nonnegative elsewhere,

where $L(k, \ell)$ is the price paid for classifying an observation belonging to class $\mathcal{G}_k$ as $\mathcal{G}_\ell$. Most often we use the *zero–one* loss function, where all misclassifications are charged a single unit. The expected prediction error is

$$\mathrm{EPE} = \mathrm{E}[L(G, \hat{G}(X))], \tag{2.19}$$

where again the expectation is taken with respect to the joint distribution $\Pr(G, X)$. Again we condition, and can write EPE as

$$\mathrm{EPE} = \mathrm{E}_X \sum_{k=1}^{K} L[\mathcal{G}_k, \hat{G}(X)] \Pr(\mathcal{G}_k|X) \tag{2.20}$$

and again it suffices to minimize EPE pointwise:

$$\hat{G}(x) = \operatorname{argmin}_{g \in \mathcal{G}} \sum_{k=1}^{K} L(\mathcal{G}_k, g) \Pr(\mathcal{G}_k|X = x). \tag{2.21}$$

With the 0–1 loss function this simplifies to

$$\hat{G}(x) = \operatorname{argmin}_{g \in \mathcal{G}} [1 - \Pr(g|X = x)] \tag{2.22}$$

or simply

$$\hat{G}(X) = \mathcal{G}_k \text{ if } \Pr(\mathcal{G}_k|X = x) = \max_{g \in \mathcal{G}} \Pr(g|X = x). \tag{2.23}$$

This reasonable solution is known as the *Bayes classifier*, and says that we classify to the most probable class, using the conditional (discrete) distribution $\Pr(G|X)$. Figure 2.5 shows the Bayes-optimal decision boundary for our simulation example. The error rate of the Bayes classifier is called the *Bayes rate*.

Again we see that the k-nearest neighbor classifier directly approximates this solution—a majority vote in a nearest neighborhood amounts to exactly this, except that conditional probability at a point is relaxed to conditional probability within a neighborhood of a point, and probabilities are estimated by training-sample proportions.

Suppose for a two-class problem we had taken the dummy-variable approach and coded G via a binary Y, followed by squared error loss estimation. Then $\hat{f}(X) = \mathrm{E}(Y|X) = \Pr(G = \mathcal{G}_1|X)$ if $\mathcal{G}_1$ corresponded to $Y = 1$. Likewise for a K-class problem, $\mathrm{E}(Y_k|X) = \Pr(G = \mathcal{G}_k|X)$. This shows that our dummy-variable regression procedure, followed by classification to the largest fitted value, is another way of representing the Bayes classifier. Although this theory is exact, in practice problems can occur, depending on the regression model used. For example, when linear regression is used, $\hat{f}(X)$ need not be positive, and we might be suspicious about using it as an estimate of a probability. We will discuss a variety of approaches to modeling $\Pr(G|X)$ in Chapter 4.

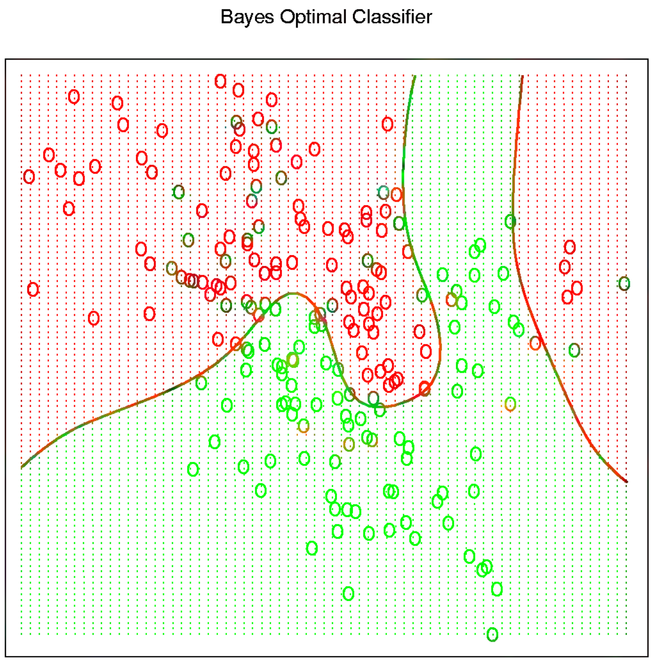

FIGURE 2.5. *The optimal Bayes decision boundary for the simulation example of Figures 2.1, 2.2 and 2.3. Since the generating density is known for each class, this boundary can be calculated exactly (Exercise 2.2).*

2.5 Local Methods in High Dimensions

We have examined two learning techniques for prediction so far: the stable but biased linear model and the less stable but apparently less biased class of k-nearest-neighbor estimates. It would seem that with a reasonably large set of training data, we could always approximate the theoretically optimal conditional expectation by k-nearest-neighbor averaging, since we should be able to find a fairly large neighborhood of observations close to any x and average them. This approach and our intuition breaks down in high dimensions, and the phenomenon is commonly referred to as the *curse of dimensionality* (Bellman, 1961). There are many manifestations of this problem, and we will examine a few here.

Consider the nearest-neighbor procedure for inputs uniformly distributed in a p-dimensional unit hypercube, as in Figure 2.6. Suppose we send out a hypercubical neighborhood about a target point to capture a fraction r of the observations. Since this corresponds to a fraction r of the unit volume, the expected edge length will be $e_p(r) = r^{1/p}$. In ten dimensions $e_{10}(0.01) = 0.63$ and $e_{10}(0.1) = 0.80$, while the entire range for each input is only 1.0.

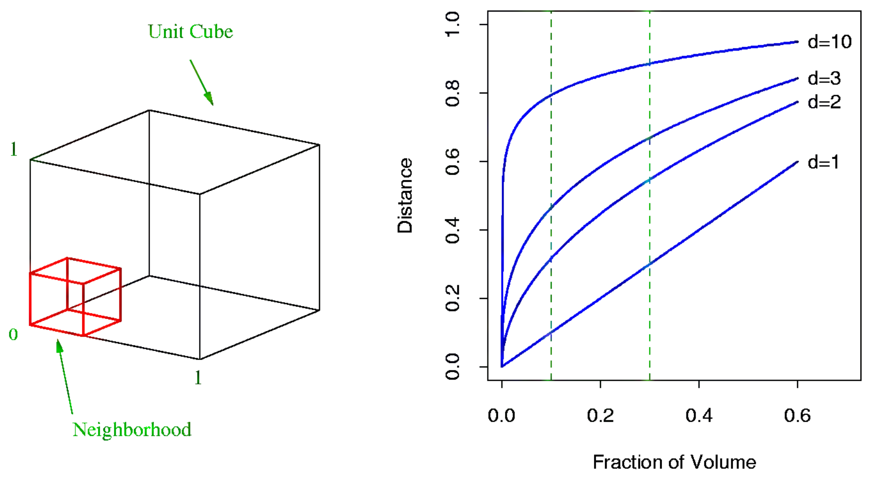

FIGURE 2.6. *The curse of dimensionality is well illustrated by a subcubical neighborhood for uniform data in a unit cube. The figure on the right shows the side-length of the subcube needed to capture a fraction r of the volume of the data, for different dimensions p. In ten dimensions we need to cover* 80% *of the range of each coordinate to capture* 10% *of the data.*

So to capture 1% or 10% of the data to form a local average, we must cover 63% or 80% of the range of each input variable. Such neighborhoods are no longer "local." Reducing r dramatically does not help much either, since the less observations we average, the higher is the variance of our fit.

Another consequence of the sparse sampling in high dimensions is that all sample points are close to an edge of the sample. Consider N data points uniformly distributed in a p-dimensional unit ball centered at the origin. Suppose we consider a nearest-neighbor estimate at the origin. The median distance from the origin to the closest data point is given by the expression

$$d(p,N) = \left(1 - \frac{1}{2}^{1/N}\right)^{1/p} \tag{2.24}$$

(Exercise 2.3). A more complicated expression exists for the mean distance to the closest point. For $N = 5000$, $p = 10$, $d(p,N) \approx 0.52$, more than half way to the boundary. Hence most data points are closer to the boundary of the sample space than to any other data point. The reason that this presents a problem is that prediction is much more difficult near the edges of the training sample. One must extrapolate from neighboring sample points rather than interpolate between them.

Another manifestation of the curse is that the sampling density is proportional to $N^{1/p}$, where p is the dimension of the input space and N is the sample size. Thus if $N_1 = 100$ represents a dense sample for a single input problem, then $N_{10} = 100^{10}$ is the sample size required for the same sampling density with 10 inputs. Thus in high dimensions all feasible training samples sparsely populate the input space.

Let us construct another uniform example. Suppose we have 1000 training features x_i generated uniformly on $[-1, 1]^p$. Assume that the true relationship between X and Y is

$$Y = f(X) = e^{-8||X||^2},$$

without any measurement error. We use the 1-nearest-neighbor rule to predict y_0 at the test-point $x_0 = 0$. Denote the training set by $\mathcal{T}$. We can compute the expected prediction error at x_0 for our procedure, averaging over all such samples of size 1000. Since the problem is deterministic, this is the mean squared error (MSE) for estimating $f(0)$:

$$\begin{aligned} \text{MSE}(x_0) &= \text{E}_{\mathcal{T}}[f(x_0) - \hat{y}_0]^2 \\ &= \text{E}_{\mathcal{T}}[\hat{y}_0 - \text{E}_{\mathcal{T}}(\hat{y}_0)]^2 + [\text{E}_{\mathcal{T}}(\hat{y}_0) - f(x_0)]^2 \\ &= \text{Var}_{\mathcal{T}}(\hat{y}_0) + \text{Bias}^2(\hat{y}_0). \end{aligned} \tag{2.25}$$

Figure 2.7 illustrates the setup. We have broken down the MSE into two components that will become familiar as we proceed: variance and squared bias. Such a decomposition is always possible and often useful, and is known as the *bias–variance decomposition.* Unless the nearest neighbor is at 0, $\hat{y}_0$ will be smaller than $f(0)$ in this example, and so the average estimate will be biased downward. The variance is due to the sampling variance of the 1-nearest neighbor. In low dimensions and with $N = 1000$, the nearest neighbor is very close to 0, and so both the bias and variance are small. As the dimension increases, the nearest neighbor tends to stray further from the target point, and both bias and variance are incurred. By $p = 10$, for more than 99% of the samples the nearest neighbor is a distance greater than 0.5 from the origin. Thus as p increases, the estimate tends to be 0 more often than not, and hence the MSE levels off at 1.0, as does the bias, and the variance starts dropping (an artifact of this example).

Although this is a highly contrived example, similar phenomena occur more generally. The complexity of functions of many variables can grow exponentially with the dimension, and if we wish to be able to estimate such functions with the same accuracy as function in low dimensions, then we need the size of our training set to grow exponentially as well. In this example, the function is a complex interaction of all p variables involved.

The dependence of the bias term on distance depends on the truth, and it need not always dominate with 1-nearest neighbor. For example, if the function always involves only a few dimensions as in Figure 2.8, then the variance can dominate instead.

Suppose, on the other hand, that we know that the relationship between Y and X is linear,

$$Y = X^T\beta + \varepsilon, \tag{2.26}$$

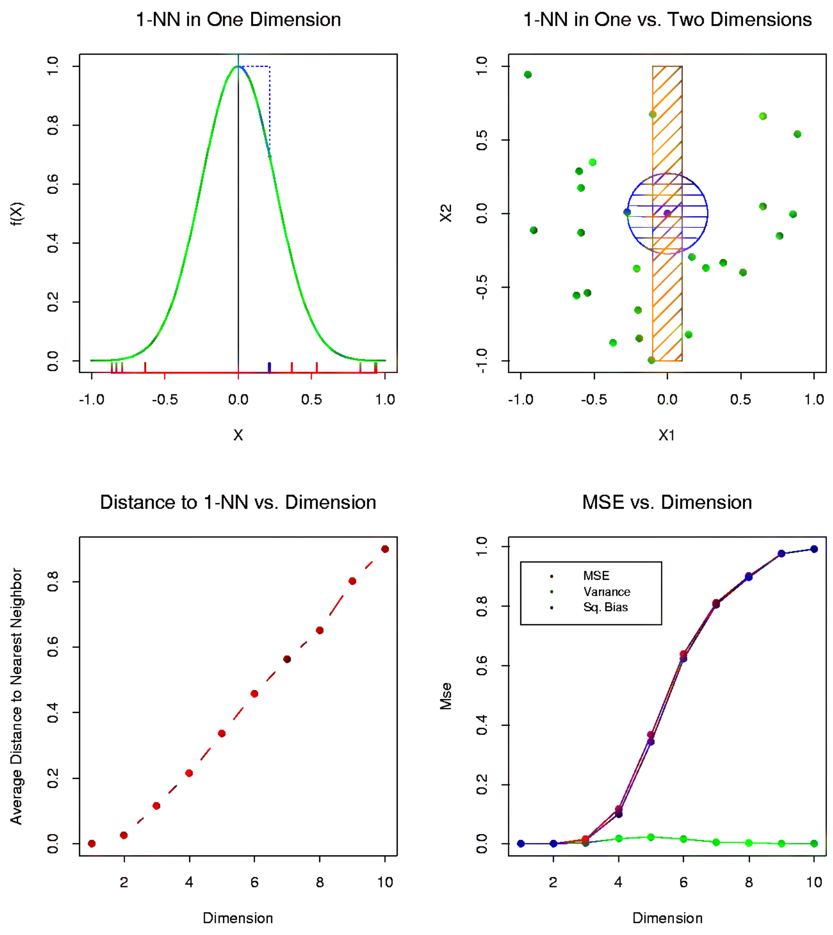

FIGURE 2.7. *A simulation example, demonstrating the curse of dimensionality and its effect on MSE, bias and variance. The input features are uniformly distributed in* $[-1,1]^p$ *for* $p = 1, \dots, 10$ *The top left panel shows the target function (no noise) in* $\mathbb{R}$: $f(X) = e^{-8||X||^2}$, *and demonstrates the error that* 1*-nearest neighbor makes in estimating* $f(0)$. *The training point is indicated by the blue tick mark. The top right panel illustrates why the radius of the* 1*-nearest neighborhood increases with dimension* p. *The lower left panel shows the average radius of the* 1*-nearest neighborhoods. The lower-right panel shows the MSE, squared bias and variance curves as a function of dimension* p.

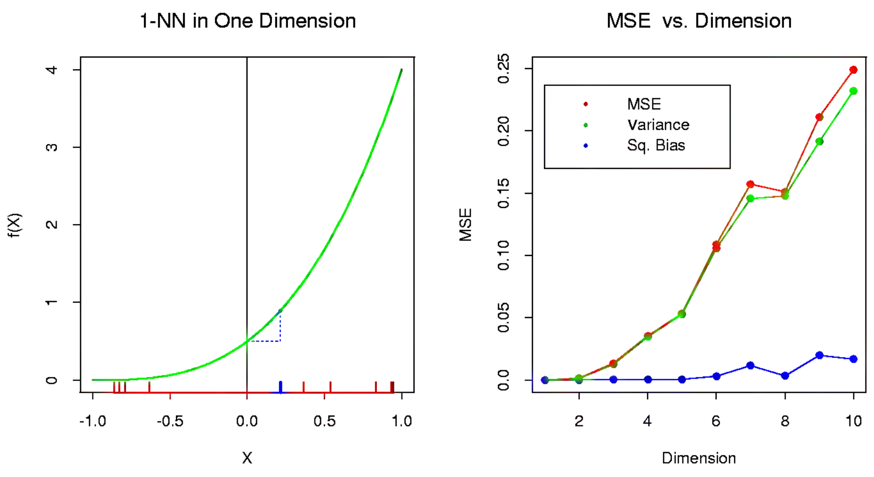

FIGURE 2.8. *A simulation example with the same setup as in Figure 2.7. Here the function is constant in all but one dimension:* $F(X) = \frac{1}{2}(X_1 + 1)^3$. *The variance dominates.*

where $\varepsilon \sim N(0,1)$ and we fit the model by least squares to the training data. For an arbitrary test point x_0, we have $\hat{y}_0 = x_0^T\hat{\beta}$, which can be written as $\hat{y}_0 = x_0^T\beta + \sum_{i=1}^N \ell_i(x_0)\varepsilon_i$, where $\ell_i(x_0)$ is the ith element of $X(X^TX)^{-1}x_0$. Since under this model the least squares estimates are unbiased, we find that

$$\begin{aligned}
\text{EPE}(x_0) &= \text{E}_{y_0|x_0}\text{E}_{\mathcal{T}}(y_0 - \hat{y}_0)^2 \\
&= \text{Var}(y_0|x_0) + \text{E}_{\mathcal{T}}[\hat{y}_0 - \text{E}_{\mathcal{T}}\hat{y}_0]^2 + [\text{E}_{\mathcal{T}}\hat{y}_0 - \text{E}_{\mathcal{T}}y_0]^2 \\
&= \text{Var}(y_0|x_0) + \text{Var}_{\mathcal{T}}(\hat{y}_0) + \text{Bias}^2(\hat{y}_0) \\
&= \sigma^2 + \text{E}_{\mathcal{T}}x_0^T(\mathbf{X}^T\mathbf{X})^{-1}x_0\sigma^2 + 0^2. \qquad (2.27)
\end{aligned}$$

Here we have incurred an additional variance σ^2 in the prediction error, since our target is not deterministic. There is no bias, and the variance depends on x_0, but if N is large and $\mathcal{T}$ were selected at random, then $\mathbf{X}^T\mathbf{X} \to N\text{Cov}(X)$ and

$$\begin{aligned}
\text{E}_{x_0}\text{EPE}(x_0) &\sim \text{E}_{x_0}x_0^T\text{Cov}(X)^{-1}x_0\sigma^2/N + \sigma^2 \\
&= \text{trace}[\text{Cov}(X)^{-1}\text{Cov}(x_0)]\sigma^2/N \\
&= \sigma^2(p/N) + \sigma^2. \qquad (2.28)
\end{aligned}$$

Here we see that the expected EPE increases linearly as a function of p, with slope σ^2/N. If N is large and/or σ^2 is small, this growth in variance is negligible (0 in the deterministic case). By imposing some heavy restrictions on the class of models being fitted, we have avoided the curse of dimensionality.

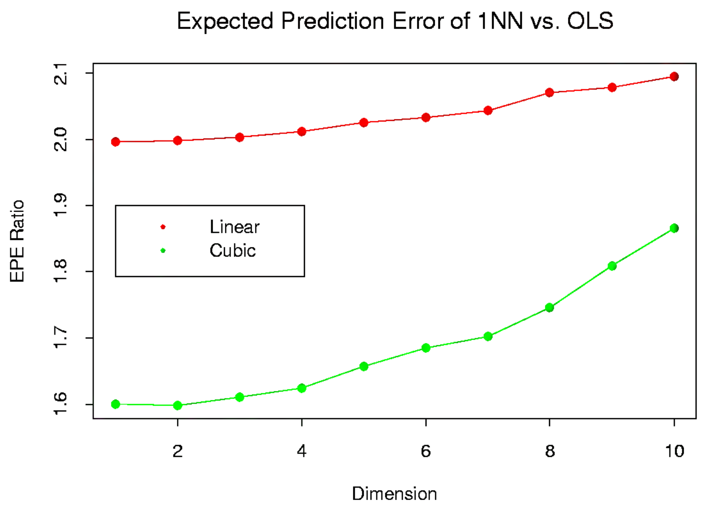

FIGURE 2.9. *The curves show the expected prediction error (at $x_0 = 0$) for 1-nearest neighbor relative to least squares for the model $Y = f(X) + \varepsilon$. For the red curve, $f(x) = x_1$, while for the green curve $f(x) = \frac{1}{2}(x_1 + 1)^3$.*

Figure 2.9 compares 1-nearest neighbor vs. least squares in two situations, both of which have the form $Y = f(X) + \varepsilon$, X uniform as before, and $\varepsilon \sim N(0,1)$. The sample size is $N = 500$. For the red curve, $f(x)$ is linear in the first coordinate, for the green curve, cubic as in Figure 2.8. Shown is the relative EPE of 1-nearest neighbor to least squares, which appears to start at around 2 for the linear case. Least squares is unbiased in this case, and as discussed above the EPE is slightly above $\sigma^2 = 1$. The EPE for 1-nearest neighbor is always above 2, since the variance of $\hat{f}(x_0)$ in this case is at least σ^2, and the ratio increases with dimension as the nearest neighbor strays from the target point. For the cubic case, least squares is biased, which moderates the ratio. Clearly we could manufacture examples where the bias of least squares would dominate the variance, and the 1-nearest neighbor would come out the winner.

By relying on rigid assumptions, the linear model has no bias at all and negligible variance, while the error in 1-nearest neighbor is substantially larger. However, if the assumptions are wrong, all bets are off and the 1-nearest neighbor may dominate. We will see that there is a whole spectrum of models between the rigid linear models and the extremely flexible 1-nearest-neighbor models, each with their own assumptions and biases, which have been proposed specifically to avoid the exponential growth in complexity of functions in high dimensions by drawing heavily on these assumptions.

Before we delve more deeply, let us elaborate a bit on the concept of *statistical models* and see how they fit into the prediction framework.

2.6 Statistical Models, Supervised Learning and Function Approximation

Our goal is to find a useful approximation $\hat{f}(x)$ to the function $f(x)$ that underlies the predictive relationship between the inputs and outputs. In the theoretical setting of Section 2.4, we saw that squared error loss lead us to the regression function $f(x) = \mathrm{E}(Y|X = x)$ for a quantitative response. The class of nearest-neighbor methods can be viewed as direct estimates of this conditional expectation, but we have seen that they can fail in at least two ways:

- if the dimension of the input space is high, the nearest neighbors need not be close to the target point, and can result in large errors;
- if special structure is known to exist, this can be used to reduce both the bias and the variance of the estimates.

We anticipate using other classes of models for $f(x)$, in many cases specifically designed to overcome the dimensionality problems, and here we discuss a framework for incorporating them into the prediction problem.

2.6.1 *A Statistical Model for the Joint Distribution* $\Pr(X, Y)$

Suppose in fact that our data arose from a statistical model

$$Y = f(X) + \varepsilon, \tag{2.29}$$

where the random error ε has $\mathrm{E}(\varepsilon) = 0$ and is independent of X. Note that for this model, $f(x) = \mathrm{E}(Y|X = x)$, and in fact the conditional distribution $\Pr(Y|X)$ depends on X *only* through the conditional mean $f(x)$.

The additive error model is a useful approximation to the truth. For most systems the input–output pairs (X, Y) will not have a deterministic relationship $Y = f(X)$. Generally there will be other unmeasured variables that also contribute to Y, including measurement error. The additive model assumes that we can capture all these departures from a deterministic relationship via the error ε.

For some problems a deterministic relationship does hold. Many of the classification problems studied in machine learning are of this form, where the response surface can be thought of as a colored map defined in $\mathbb{R}^p$. The training data consist of colored examples from the map $\{x_i, g_i\}$, and the goal is to be able to color any point. Here the function is deterministic, and the randomness enters through the x location of the training points. For the moment we will not pursue such problems, but will see that they can be handled by techniques appropriate for the error-based models.

The assumption in (2.29) that the errors are independent and identically distributed is not strictly necessary, but seems to be at the back of our mind when we average squared errors uniformly in our EPE criterion. With such a model it becomes natural to use least squares as a data criterion for model estimation as in (2.1). Simple modifications can be made to avoid the independence assumption; for example, we can have $\mathrm{Var}(Y|X = x) = \sigma(x)$, and now both the mean and variance depend on X. In general the conditional distribution $\Pr(Y|X)$ can depend on X in complicated ways, but the additive error model precludes these.

So far we have concentrated on the quantitative response. Additive error models are typically not used for qualitative outputs G; in this case the target function $p(X)$ *is* the conditional density $\Pr(G|X)$, and this is modeled directly. For example, for two-class data, it is often reasonable to assume that the data arise from independent binary trials, with the probability of one particular outcome being $p(X)$, and the other $1 - p(X)$. Thus if Y is the 0–1 coded version of G, then $\mathrm{E}(Y|X = x) = p(x)$, but the variance depends on x as well: $\mathrm{Var}(Y|X = x) = p(x)[1 - p(x)]$.

2.6.2 Supervised Learning

Before we launch into more statistically oriented jargon, we present the function-fitting paradigm from a machine learning point of view. Suppose for simplicity that the errors are additive and that the model $Y = f(X)+\varepsilon$ is a reasonable assumption. Supervised learning attempts to learn f by example through a *teacher*. One observes the system under study, both the inputs and outputs, and assembles a *training* set of observations $\mathcal{T} = (x_i, y_i),\ i = 1, \ldots, N$. The observed input values to the system x_i are also fed into an artificial system, known as a learning algorithm (usually a computer program), which also produces outputs $\hat{f}(x_i)$ in response to the inputs. The learning algorithm has the property that it can modify its input/output relationship $\hat{f}$ in response to differences $y_i - \hat{f}(x_i)$ between the original and generated outputs. This process is known as *learning by example*. Upon completion of the learning process the hope is that the artificial and real outputs will be close enough to be useful for all sets of inputs likely to be encountered in practice.

2.6.3 Function Approximation

The learning paradigm of the previous section has been the motivation for research into the supervised learning problem in the fields of machine learning (with analogies to human reasoning) and neural networks (with biological analogies to the brain). The approach taken in applied mathematics and statistics has been from the perspective of function approximation and estimation. Here the data pairs $\{x_i, y_i\}$ are viewed as points in a $(p + 1)$-dimensional Euclidean space. The function $f(x)$ has domain equal to the p-dimensional input subspace, and is related to the data via a model such as $y_i = f(x_i) + \varepsilon_i$. For convenience in this chapter we will assume the domain is $\mathbb{R}^p$, a p-dimensional Euclidean space, although in general the inputs can be of mixed type. The goal is to obtain a useful approximation to $f(x)$ for all x in some region of $\mathbb{R}^p$, given the representations in $\mathcal{T}$. Although somewhat less glamorous than the learning paradigm, treating supervised learning as a problem in function approximation encourages the geometrical concepts of Euclidean spaces and mathematical concepts of probabilistic inference to be applied to the problem. This is the approach taken in this book.

Many of the approximations we will encounter have associated a set of parameters θ that can be modified to suit the data at hand. For example, the linear model $f(x) = x^T\beta$ has $\theta = \beta$. Another class of useful approximators can be expressed as *linear basis expansions*

$$f_\theta(x) = \sum_{k=1}^{K} h_k(x)\theta_k, \tag{2.30}$$

where the h_k are a suitable set of functions or transformations of the input vector x. Traditional examples are polynomial and trigonometric expansions, where for example h_k might be x_1^2, $x_1x_2^2$, $\cos(x_1)$ and so on. We also encounter nonlinear expansions, such as the sigmoid transformation common to neural network models,

$$h_k(x) = \frac{1}{1 + \exp(-x^T\beta_k)}. \tag{2.31}$$

We can use least squares to estimate the parameters θ in f_θ as we did for the linear model, by minimizing the residual sum-of-squares

$$\mathrm{RSS}(\theta) = \sum_{i=1}^{N}(y_i - f_\theta(x_i))^2 \tag{2.32}$$

as a function of θ. This seems a reasonable criterion for an additive error model. In terms of function approximation, we imagine our parameterized function as a surface in $p + 1$ space, and what we observe are noisy realizations from it. This is easy to visualize when $p = 2$ and the vertical coordinate is the output y, as in Figure 2.10. The noise is in the output coordinate, so we find the set of parameters such that the fitted surface gets as close to the observed points as possible, where close is measured by the sum of squared vertical errors in $\mathrm{RSS}(\theta)$.

For the linear model we get a simple closed form solution to the minimization problem. This is also true for the basis function methods, if the basis functions themselves do not have any hidden parameters. Otherwise the solution requires either iterative methods or numerical optimization.

While least squares is generally very convenient, it is not the only criterion used and in some cases would not make much sense. A more general

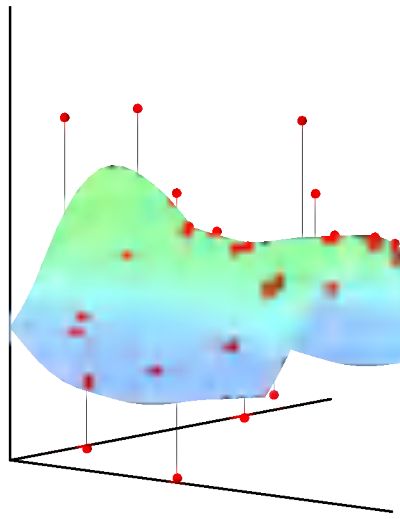

FIGURE 2.10. *Least squares fitting of a function of two inputs. The parameters of $f_\theta(x)$ are chosen so as to minimize the sum-of-squared vertical errors.*

principle for estimation is *maximum likelihood estimation*. Suppose we have a random sample y_i, $i = 1, \ldots, N$ from a density $\Pr_\theta(y)$ indexed by some parameters θ. The log-probability of the observed sample is

$$L(\theta) = \sum_{i=1}^{N} \log \Pr_\theta(y_i). \tag{2.33}$$

The principle of maximum likelihood assumes that the most reasonable values for θ are those for which the probability of the observed sample is largest. Least squares for the additive error model $Y = f_\theta(X) + \varepsilon$, with $\varepsilon \sim N(0, \sigma^2)$, is equivalent to maximum likelihood using the conditional likelihood

$$\Pr(Y|X, \theta) = N(f_\theta(X), \sigma^2). \tag{2.34}$$

So although the additional assumption of normality seems more restrictive, the results are the same. The log-likelihood of the data is

$$L(\theta) = -\frac{N}{2}\log(2\pi) - N\log\sigma - \frac{1}{2\sigma^2}\sum_{i=1}^{N}(y_i - f_\theta(x_i))^2, \tag{2.35}$$

and the only term involving θ is the last, which is $\mathrm{RSS}(\theta)$ up to a scalar negative multiplier.

A more interesting example is the multinomial likelihood for the regression function $\Pr(G|X)$ for a qualitative output G. Suppose we have a model

$\Pr(G = \mathcal{G}_k|X = x) = p_{k,\theta}(x)$, $k = 1, \dots, K$ for the conditional probability of each class given X, indexed by the parameter vector θ. Then the log-likelihood (also referred to as the cross-entropy) is

$$L(\theta) = \sum_{i=1}^{N} \log p_{g_i,\theta}(x_i), \tag{2.36}$$

and when maximized it delivers values of θ that best conform with the data in this likelihood sense.

2.7 Structured Regression Models

We have seen that although nearest-neighbor and other local methods focus directly on estimating the function at a point, they face problems in high dimensions. They may also be inappropriate even in low dimensions in cases where more structured approaches can make more efficient use of the data. This section introduces classes of such structured approaches. Before we proceed, though, we discuss further the need for such classes.

2.7.1 Difficulty of the Problem

Consider the RSS criterion for an arbitrary function f,

$$\text{RSS}(f) = \sum_{i=1}^{N} (y_i - f(x_i))^2. \tag{2.37}$$

Minimizing (2.37) leads to infinitely many solutions: any function $\hat{f}$ passing through the training points (x_i, y_i) is a solution. Any particular solution chosen might be a poor predictor at test points different from the training points. If there are multiple observation pairs $x_i, y_{i\ell}$, $\ell = 1, \dots, N_i$ at each value of x_i, the risk is limited. In this case, the solutions pass through the average values of the $y_{i\ell}$ at each x_i; see Exercise 2.5. The situation is similar to the one we have already visited in Section 2.4; indeed, (2.37) is the finite sample version of (2.11) on page 18. If the sample size N were sufficiently large such that repeats were guaranteed and densely arranged, it would seem that these solutions might all tend to the limiting conditional expectation.

In order to obtain useful results for finite N, we must restrict the eligible solutions to (2.37) to a smaller set of functions. How to decide on the nature of the restrictions is based on considerations outside of the data. These restrictions are sometimes encoded via the parametric representation of f_θ, or may be built into the learning method itself, either implicitly or explicitly. These restricted classes of solutions are the major topic of this book. One thing should be clear, though. Any restrictions imposed on f that lead to a unique solution to (2.37) do not really remove the ambiguity caused by the multiplicity of solutions. There are infinitely many possible restrictions, each leading to a unique solution, so the ambiguity has simply been transferred to the choice of constraint.

In general the constraints imposed by most learning methods can be described as *complexity* restrictions of one kind or another. This usually means some kind of regular behavior in small neighborhoods of the input space. That is, for all input points x sufficiently close to each other in some metric, $\hat{f}$ exhibits some special structure such as nearly constant, linear or low-order polynomial behavior. The estimator is then obtained by averaging or polynomial fitting in that neighborhood.

The strength of the constraint is dictated by the neighborhood size. The larger the size of the neighborhood, the stronger the constraint, and the more sensitive the solution is to the particular choice of constraint. For example, local constant fits in infinitesimally small neighborhoods is no constraint at all; local linear fits in very large neighborhoods is almost a globally linear model, and is very restrictive.

The nature of the constraint depends on the metric used. Some methods, such as kernel and local regression and tree-based methods, directly specify the metric and size of the neighborhood. The nearest-neighbor methods discussed so far are based on the assumption that locally the function is constant; close to a target input x_0, the function does not change much, and so close outputs can be averaged to produce $\hat{f}(x_0)$. Other methods such as splines, neural networks and basis-function methods implicitly define neighborhoods of local behavior. In Section 5.4.1 we discuss the concept of an *equivalent kernel* (see Figure 5.8 on page 133), which describes this local dependence for any method linear in the outputs. These equivalent kernels in many cases look just like the explicitly defined weighting kernels discussed above—peaked at the target point and falling away smoothly away from it.

One fact should be clear by now. Any method that attempts to produce locally varying functions in small isotropic neighborhoods will run into problems in high dimensions—again the curse of dimensionality. And conversely, all methods that overcome the dimensionality problems have an associated—and often implicit or adaptive—metric for measuring neighborhoods, which basically does not allow the neighborhood to be simultaneously small in all directions.

2.8 Classes of Restricted Estimators

The variety of nonparametric regression techniques or learning methods fall into a number of different classes depending on the nature of the restrictions imposed. These classes are not distinct, and indeed some methods fall in several classes. Here we give a brief summary, since detailed descriptions are given in later chapters. Each of the classes has associated with it one or more parameters, sometimes appropriately called *smoothing* parameters, that control the effective size of the local neighborhood. Here we describe three broad classes.

2.8.1 Roughness Penalty and Bayesian Methods

Here the class of functions is controlled by explicitly penalizing $\text{RSS}(f)$ with a roughness penalty

$$\text{PRSS}(f;\lambda) = \text{RSS}(f) + \lambda J(f). \tag{2.38}$$

The user-selected functional $J(f)$ will be large for functions f that vary too rapidly over small regions of input space. For example, the popular *cubic smoothing spline* for one-dimensional inputs is the solution to the penalized least-squares criterion

$$\text{PRSS}(f;\lambda) = \sum_{i=1}^{N}(y_i - f(x_i))^2 + \lambda \int [f''(x)]^2 dx. \tag{2.39}$$

The roughness penalty here controls large values of the second derivative of f, and the amount of penalty is dictated by $\lambda \geq 0$. For $\lambda = 0$ no penalty is imposed, and any interpolating function will do, while for $\lambda = \infty$ only functions linear in x are permitted.

Penalty functionals J can be constructed for functions in any dimension, and special versions can be created to impose special structure. For example, additive penalties $J(f) = \sum_{j=1}^{p} J(f_j)$ are used in conjunction with additive functions $f(X) = \sum_{j=1}^{p} f_j(X_j)$ to create additive models with smooth coordinate functions. Similarly, *projection pursuit regression* models have $f(X) = \sum_{m=1}^{M} g_m(\alpha_m^T X)$ for adaptively chosen directions α_m, and the functions g_m can each have an associated roughness penalty.

Penalty function, or *regularization* methods, express our prior belief that the type of functions we seek exhibit a certain type of smooth behavior, and indeed can usually be cast in a Bayesian framework. The penalty J corresponds to a log-prior, and $\text{PRSS}(f;\lambda)$ the log-posterior distribution, and minimizing $\text{PRSS}(f;\lambda)$ amounts to finding the posterior mode. We discuss roughness-penalty approaches in Chapter 5 and the Bayesian paradigm in Chapter 8.

2.8.2 Kernel Methods and Local Regression

These methods can be thought of as explicitly providing estimates of the regression function or conditional expectation by specifying the nature of the local neighborhood, and of the class of regular functions fitted locally. The local neighborhood is specified by a *kernel function* $K_\lambda(x_0, x)$ which assigns weights to points x in a region around x_0 (see Figure 6.1 on page 166). For example, the Gaussian kernel has a weight function based on the Gaussian density function

$$K_\lambda(x_0, x) = \frac{1}{\lambda} \exp\left[-\frac{||x - x_0||^2}{2\lambda}\right] \tag{2.40}$$

and assigns weights to points that die exponentially with their squared Euclidean distance from x_0. The parameter λ corresponds to the variance of the Gaussian density, and controls the width of the neighborhood. The simplest form of kernel estimate is the Nadaraya–Watson weighted average

$$\hat{f}(x_0) = \frac{\sum_{i=1}^N K_\lambda(x_0, x_i) y_i}{\sum_{i=1}^N K_\lambda(x_0, x_i)}. \tag{2.41}$$

In general we can define a local regression estimate of $f(x_0)$ as $f_{\hat{\theta}}(x_0)$, where $\hat{\theta}$ minimizes

$$\text{RSS}(f_\theta, x_0) = \sum_{i=1}^N K_\lambda(x_0, x_i)(y_i - f_\theta(x_i))^2, \tag{2.42}$$

and f_θ is some parameterized function, such as a low-order polynomial. Some examples are:

- $f_\theta(x) = \theta_0$, the constant function; this results in the Nadaraya–Watson estimate in (2.41) above.
- $f_\theta(x) = \theta_0 + \theta_1 x$ gives the popular local linear regression model.

Nearest-neighbor methods can be thought of as kernel methods having a more data-dependent metric. Indeed, the metric for k-nearest neighbors is

$$K_k(x, x_0) = I(||x - x_0|| \leq ||x_{(k)} - x_0||),$$

where $x_{(k)}$ is the training observation ranked kth in distance from x_0, and $I(S)$ is the indicator of the set S.

These methods of course need to be modified in high dimensions, to avoid the curse of dimensionality. Various adaptations are discussed in Chapter 6.

2.8.3 Basis Functions and Dictionary Methods

This class of methods include the familiar linear and polynomial expansions, but more importantly a wide variety of more flexible models. The model for f is a linear expansion of basis functions

$$f_\theta(x) = \sum_{m=1}^M \theta_m h_m(x), \tag{2.43}$$

where each of the h_m is a function of the input x, and the term linear here refers to the action of the parameters θ. This class covers a wide variety of methods. In some cases the sequence of basis functions is prescribed, such as a basis for polynomials in x of total degree M.

For one-dimensional x, polynomial splines of degree K can be represented by an appropriate sequence of M spline basis functions, determined in turn by $M - K$ *knots*. These produce functions that are piecewise polynomials of degree K between the knots, and joined up with continuity of degree $K - 1$ at the knots. As an example consider linear splines, or piecewise linear functions. One intuitively satisfying basis consists of the functions $b_1(x) = 1$, $b_2(x) = x$, and $b_{m+2}(x) = (x - t_m)_+$, $m = 1, \dots, M - 2$, where t_m is the mth knot, and z_+ denotes positive part. Tensor products of spline bases can be used for inputs with dimensions larger than one (see Section 5.2, and the CART and MARS models in Chapter 9.) The parameter θ can be the total degree of the polynomial or the number of knots in the case of splines.

Radial basis functions are symmetric p-dimensional kernels located at particular centroids,

$$f_\theta(x) = \sum_{m=1}^{M} K_{\lambda_m}(\mu_m, x)\theta_m; \tag{2.44}$$

for example, the Gaussian kernel $K_\lambda(\mu, x) = e^{-||x-\mu||^2/2\lambda}$ is popular.

Radial basis functions have centroids μ_m and scales λ_m that have to be determined. The spline basis functions have knots. In general we would like the data to dictate them as well. Including these as parameters changes the regression problem from a straightforward linear problem to a combinatorially hard nonlinear problem. In practice, shortcuts such as greedy algorithms or two stage processes are used. Section 6.7 describes some such approaches.

A single-layer feed-forward neural network model with linear output weights can be thought of as an adaptive basis function method. The model has the form

$$f_\theta(x) = \sum_{m=1}^{M} \beta_m \sigma(\alpha_m^T x + b_m), \tag{2.45}$$

where $\sigma(x) = 1/(1 + e^{-x})$ is known as the *activation* function. Here, as in the projection pursuit model, the directions α_m and the *bias* terms b_m have to be determined, and their estimation is the meat of the computation. Details are give in Chapter 11.

These adaptively chosen basis function methods are also known as *dictionary* methods, where one has available a possibly infinite set or dictionary $\mathcal{D}$ of candidate basis functions from which to choose, and models are built up by employing some kind of search mechanism.

2.9 Model Selection and the Bias–Variance Tradeoff

All the models described above and many others discussed in later chapters have a *smoothing* or *complexity* parameter that has to be determined:

- the multiplier of the penalty term;
- the width of the kernel;
- or the number of basis functions.

In the case of the smoothing spline, the parameter λ indexes models ranging from a straight line fit to the interpolating model. Similarly a local degree-m polynomial model ranges between a degree-m global polynomial when the window size is infinitely large, to an interpolating fit when the window size shrinks to zero. This means that we cannot use residual sum-of-squares on the training data to determine these parameters as well, since we would always pick those that gave interpolating fits and hence zero residuals. Such a model is unlikely to predict future data well at all.

The k-nearest-neighbor regression fit $\hat{f}_k(x_0)$ usefully illustrates the competing forces that effect the predictive ability of such approximations. Suppose the data arise from a model $Y = f(X) + \varepsilon$, with $\mathrm{E}(\varepsilon) = 0$ and $\mathrm{Var}(\varepsilon) = \sigma^2$. For simplicity here we assume that the values of x_i in the sample are fixed in advance (nonrandom). The expected prediction error at x_0, also known as *test* or *generalization* error, can be decomposed:

$$\begin{aligned}
\mathrm{EPE}_k(x_0) &= \mathrm{E}[(Y - \hat{f}_k(x_0))^2 | X = x_0] \\
&= \sigma^2 + [\mathrm{Bias}^2(\hat{f}_k(x_0)) + \mathrm{Var}_{\mathcal{T}}(\hat{f}_k(x_0))] && (2.46)\\
&= \sigma^2 + \Big[f(x_0) - \frac{1}{k}\sum_{\ell=1}^{k} f(x_{(\ell)})\Big]^2 + \frac{\sigma^2}{k}. && (2.47)
\end{aligned}$$

The subscripts in parentheses (ℓ) indicate the sequence of nearest neighbors to x_0.

There are three terms in this expression. The first term σ^2 is the *irreducible* error—the variance of the new test target— and is beyond our control, even if we know the true $f(x_0)$.

The second and third terms are under our control, and make up the *mean squared error* of $\hat{f}_k(x_0)$ in estimating $f(x_0)$, which is broken down into a bias component and a variance component. The bias term is the squared difference between the true mean $f(x_0)$ and the expected value of the estimate—$[\mathrm{E}_{\mathcal{T}}(\hat{f}_k(x_0)) - f(x_0)]^2$—where the expectation averages the randomness in the training data. This term will most likely increase with k, if the true function is reasonably smooth. For small k the few closest neighbors will have values $f(x_{(\ell)})$ close to $f(x_0)$, so their average should

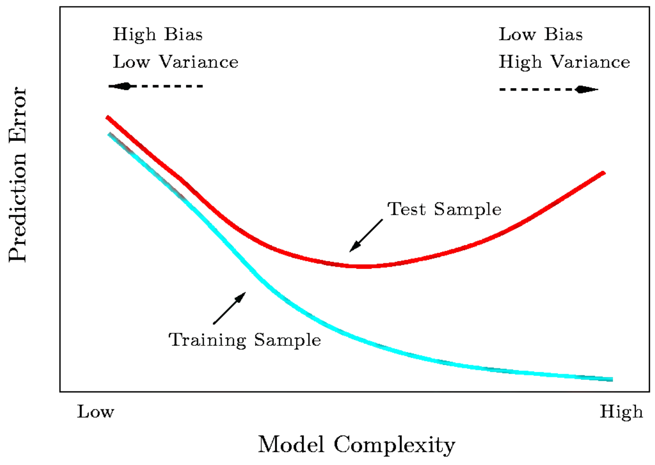

FIGURE 2.11. *Test and training error as a function of model complexity.*

be close to $f(x_0)$. As k grows, the neighbors are further away, and then anything can happen.

The variance term is simply the variance of an average here, and decreases as the inverse of k. So as k varies, there is a *bias–variance tradeoff.*

More generally, as the *model complexity* of our procedure is increased, the variance tends to increase and the squared bias tends to decreases. The opposite behavior occurs as the model complexity is decreased. For k-nearest neighbors, the model complexity is controlled by k.

Typically we would like to choose our model complexity to trade bias off with variance in such a way as to minimize the test error. An obvious estimate of test error is the *training error* $\frac{1}{N}\sum_i(y_i - \hat{y}_i)^2$. Unfortunately training error is not a good estimate of test error, as it does not properly account for model complexity.

Figure 2.11 shows the typical behavior of the test and training error, as model complexity is varied. The training error tends to decrease whenever we increase the model complexity, that is, whenever we fit the data harder. However with too much fitting, the model adapts itself too closely to the training data, and will not generalize well (i.e., have large test error). In that case the predictions $\hat{f}(x_0)$ will have large variance, as reflected in the last term of expression (2.46). In contrast, if the model is not complex enough, it will *underfit* and may have large bias, again resulting in poor generalization. In Chapter 7 we discuss methods for estimating the test error of a prediction method, and hence estimating the optimal amount of model complexity for a given prediction method and training set.

Bibliographic Notes

Some good general books on the learning problem are Duda et al. (2000), Bishop (1995), Ripley (1996), Cherkassky and Mulier (1998) and Vapnik (1996). Parts of this chapter are based on Friedman (1994b).

Exercises

Ex. 2.1 Suppose each of K-classes has an associated target t_k, which is a vector of all zeros, except a one in the kth position. Show that classifying to the largest element of $\hat{y}$ amounts to choosing the closest target, $\min_k ||t_k - \hat{y}||$, if the elements of $\hat{y}$ sum to one.

Ex. 2.2 Show how to compute the Bayes decision boundary for the simulation example in Figure 2.5.

Ex. 2.3 Derive equation (2.24).

Ex. 2.4 The edge effect problem discussed on page 23 is not peculiar to uniform sampling from bounded domains. Consider inputs drawn from a spherical multinormal distribution $X \sim N(0, \mathbf{I}_p)$. The squared distance from any sample point to the origin has a χ^2_p distribution with mean p. Consider a prediction point x_0 drawn from this distribution, and let $a = x_0/||x_0||$ be an associated unit vector. Let $z_i = a^T x_i$ be the projection of each of the training points on this direction.

(a) Show that the z_i are distributed $N(0, 1)$ with expected squared distance from the origin 1, while the target point has expected squared distance p from the origin.

(b) For $p = 10$ show that the expected distance of a test point from the center of the training data is 3.1 standard deviations, while all the training points have expected distance 1 along direction a. So most prediction points see themselves as lying on the edge of the training set.

Ex. 2.5 Consider a regression problem with inputs x_i and outputs y_i, and a parameterized model $f_\theta(x)$ to be fit by least squares. Show that if there are observations with *tied* or *identical* values of x, then the fit can be obtained from a reduced weighted least squares problem.

Ex. 2.6 Suppose we have a sample of N pairs x_i, y_i drawn i.i.d. from the distribution characterized as follows:

$$x_i \sim h(x), \text{ the design density}$$
$$y_i = f(x_i) + \varepsilon_i, \ f \text{ is the regression function}$$
$$\varepsilon_i \sim (0, \sigma^2) \text{ (mean zero, variance } \sigma^2)$$

We construct an estimator for f *linear* in the y_i,

$$\hat{f}(x_0) = \sum_{i=1}^{N} \ell_i(x_0; \mathcal{X}) y_i,$$

where the weights $\ell_i(x_0; \mathcal{X})$ do not depend on the y_i, but do depend on the entire training sequence of x_i, denoted here by $\mathcal{X}$.

(a) Show that linear regression and k-nearest-neighbor regression are members of this class of estimators. Describe explicitly the weights $\ell_i(x_0; \mathcal{X})$ for both these cases.

(b) Decompose the conditional mean-squared error

$$\mathrm{E}_{\mathcal{Y}|\mathcal{X}}(f(x_0) - \hat{f}(x_0))^2$$

into a conditional squared bias and a conditional variance component. Like $\mathcal{X}$, $\mathcal{Y}$ represents the entire training sequence of y_i.

(c) Decompose the (unconditional) mean-squared error

$$\mathrm{E}_{\mathcal{Y},\mathcal{X}}(f(x_0) - \hat{f}(x_0))^2$$

into a squared bias and a variance component.

(d) Establish a relationship between the squared biases and variances in the above two cases.

Ex. 2.7 Compare the classification performance of linear regression and k–nearest neighbor classification on the `zipcode` data. In particular, consider only the `2`'s and `3`'s, and $k = 1, 3, 5, 7$ and 15. Show both the training and test error for each choice. The `zipcode` data are available from the book website `www-stat.stanford.edu/ElemStatLearn`.

3
Linear Methods for Regression

3.1 Introduction

A linear regression model assumes that the regression function $\mathrm{E}(Y|X)$ is linear in the inputs $X_1, \dots, X_p$. Linear models were largely developed in the precomputer age of statistics, but even in today's computer era there are still good reasons to study and use them. They are simple and often provide an adequate and interpretable description of how the inputs affect the output. For prediction purposes they can sometimes outperform fancier nonlinear models, especially in situations with small numbers of training cases, low signal-to-noise ratio or sparse data. Finally, linear methods can be applied to transformations of the inputs and this considerably expands their scope. These generalizations are sometimes called basis-function methods, and are discussed in Chapter 5.

In this chapter we describe linear methods for regression, while in the next chapter we discuss linear methods for classification. On some topics we go into considerable detail, as it is our firm belief that an understanding of linear methods is essential for understanding nonlinear ones. In fact, many nonlinear techniques are direct generalizations of the linear methods discussed here.

3.2 Linear Regression Models and Least Squares

As introduced in Chapter 2, we have a vector of inputs $X = (X_1, X_2, \dots, X_p)$, and want to predict a real-valued output Y. The linear regression model has the form

$$f(X) = \beta_0 + \sum_{j=1}^{p} X_j \beta_j. \tag{3.1}$$

The linear model either assumes that the regression function $\mathrm{E}(Y|X)$ is linear, or that the linear model is a reasonable approximation. Here the β_j's are unknown parameters or coefficients, and the variables X_j can come from different sources:

- quantitative inputs;
- transformations of quantitative inputs, such as log, square-root or square;
- basis expansions, such as $X_2 = X_1^2$, $X_3 = X_1^3$, leading to a polynomial representation;
- numeric or "dummy" coding of the levels of qualitative inputs. For example, if G is a five-level factor input, we might create $X_j,\ j = 1, \dots, 5$, such that $X_j = I(G = j)$. Together this group of X_j represents the effect of G by a set of level-dependent constants, since in $\sum_{j=1}^{5} X_j \beta_j$, one of the X_js is one, and the others are zero.
- interactions between variables, for example, $X_3 = X_1 \cdot X_2$.

No matter the source of the X_j, the model is linear in the parameters.

Typically we have a set of training data $(x_1, y_1) \dots (x_N, y_N)$ from which to estimate the parameters β. Each $x_i = (x_{i1}, x_{i2}, \dots, x_{ip})^T$ is a vector of feature measurements for the ith case. The most popular estimation method is *least squares*, in which we pick the coefficients $\beta = (\beta_0, \beta_1, \dots, \beta_p)^T$ to minimize the residual sum of squares

$$\begin{aligned} \mathrm{RSS}(\beta) &= \sum_{i=1}^{N} (y_i - f(x_i))^2 \\ &= \sum_{i=1}^{N} \Big(y_i - \beta_0 - \sum_{j=1}^{p} x_{ij}\beta_j \Big)^2. \end{aligned} \tag{3.2}$$

From a statistical point of view, this criterion is reasonable if the training observations (x_i, y_i) represent independent random draws from their population. Even if the x_i's were not drawn randomly, the criterion is still valid if the y_i's are conditionally independent given the inputs x_i. Figure 3.1

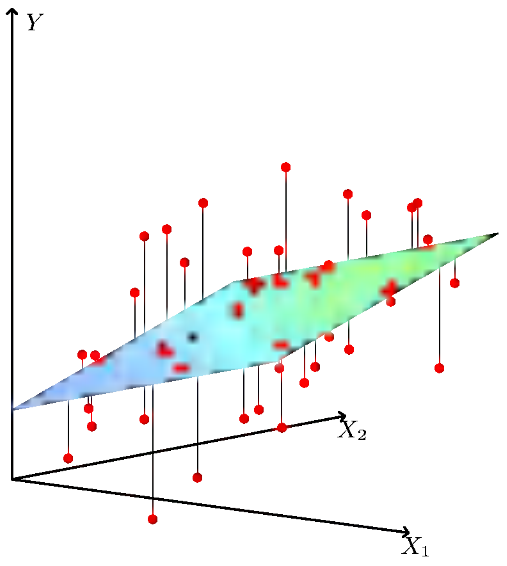

FIGURE 3.1. *Linear least squares fitting with $X \in \mathbb{R}^2$. We seek the linear function of X that minimizes the sum of squared residuals from Y.*

illustrates the geometry of least-squares fitting in the $\mathbb{R}^{p+1}$ dimensional space occupied by the pairs (X, Y). Note that (3.2) makes no assumptions about the validity of model (3.1); it simply finds the best linear fit to the data. Least squares fitting is intuitively satisfying no matter how the data arise; the criterion measures the average lack of fit.

How do we minimize (3.2)? Denote by $\mathbf{X}$ the $N \times (p+1)$ matrix with each row an input vector (with a 1 in the first position), and similarly let $\mathbf{y}$ be the N-vector of outputs in the training set. Then we can write the residual sum-of-squares as

$$\text{RSS}(\beta) = (\mathbf{y} - \mathbf{X}\beta)^T(\mathbf{y} - \mathbf{X}\beta). \tag{3.3}$$

This is a quadratic function in the $p+1$ parameters. Differentiating with respect to β we obtain

$$\begin{aligned} \frac{\partial \text{RSS}}{\partial \beta} &= -2\mathbf{X}^T(\mathbf{y} - \mathbf{X}\beta) \\ \frac{\partial^2 \text{RSS}}{\partial \beta \partial \beta^T} &= -2\mathbf{X}^T\mathbf{X}. \end{aligned} \tag{3.4}$$

Assuming (for the moment) that $\mathbf{X}$ is nonsingular and hence $\mathbf{X}^T\mathbf{X}$ is positive definite, we set the first derivative to zero

$$\mathbf{X}^T(\mathbf{y} - \mathbf{X}\beta) = 0 \tag{3.5}$$

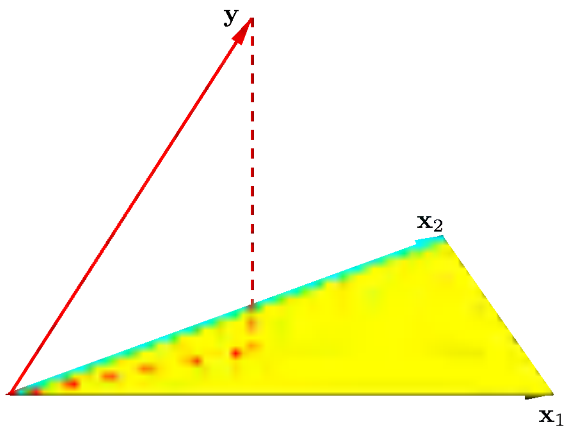

FIGURE 3.2. *The N-dimensional geometry of least squares regression with two predictors. The outcome vector $\mathbf{y}$ is orthogonally projected onto the hyperplane spanned by the input vectors $\mathbf{x}_1$ and $\mathbf{x}_2$. The projection $\hat{\mathbf{y}}$ represents the vector of the least squares predictions*

to obtain the unique solution

$$\hat{\beta} = (\mathbf{X}^T\mathbf{X})^{-1}\mathbf{X}^T\mathbf{y}. \tag{3.6}$$

The predicted values at an input vector x_0 are given by $\hat{f}(x_0) = (1 : x_0^T)\hat{\beta}$; the fitted values at the training inputs are

$$\hat{\mathbf{y}} = \mathbf{X}\hat{\beta} = \mathbf{X}^T(\mathbf{X}^T\mathbf{X})^{-1}\mathbf{X}^T\mathbf{y}, \tag{3.7}$$

where $\hat{y}_i = \hat{f}(x_i)$. The matrix $\mathbf{H} = \mathbf{X}^T(\mathbf{X}^T\mathbf{X})^{-1}\mathbf{X}$ appearing in equation (3.7) is sometimes called the "hat" matrix because it puts the hat on $\mathbf{y}$.

Figure 3.2 shows a different geometrical representation of the the least squares estimate, this time in $\mathbb{R}^N$. We denote the column vectors of $\mathbf{X}$ by $\mathbf{x}_0, \mathbf{x}_1, \dots, \mathbf{x}_p$, with $\mathbf{x}_0 \equiv 1$. For much of what follows, this first column is treated like any other. These vectors span a subspace of $\mathbb{R}^N$, also referred to as the column space of $\mathbf{X}$. We minimize $\text{RSS}(\beta) = \|\mathbf{y} - \mathbf{X}\beta\|^2$ by choosing $\hat{\beta}$ so that the residual vector $\mathbf{y} - \hat{\mathbf{y}}$ is orthogonal to this subspace. This orthogonality is expressed in (3.5), and the resulting estimate $\hat{\mathbf{y}}$ is hence the *orthogonal projection* of $\mathbf{y}$ onto this subspace. The hat matrix $\mathbf{H}$ computes the orthogonal projection, and hence it is also known as a projection matrix.

It might happen that the columns of $\mathbf{X}$ are not linearly independent, so that $\mathbf{X}$ is not of full rank. This would occur, for example, if two of the inputs were perfectly correlated, (e.g., $\mathbf{x}_2 = 3\mathbf{x}_1$). Then $\mathbf{X}^T\mathbf{X}$ is singular and the least squares coefficients $\hat{\beta}$ are not uniquely defined. However, the fitted values $\hat{\mathbf{y}} = \mathbf{X}\hat{\beta}$ are still the projection of $\mathbf{y}$ onto the column space of $\mathbf{X}$; there is just more than one way to express that projection in terms of the column vectors of $\mathbf{X}$. The nonfull rank case occurs most often when one or more qualitative inputs are coded in a redundant fashion. There is usually a natural way to resolve the non-unique representation, by recoding and/or dropping redundant columns in $\mathbf{X}$. Most regression software packages detect these redundancies and automatically implement some strategy for removing them. Rank deficiencies can also occur in signal and image analysis, where the number of inputs p can exceed the number of training cases N. In this case, the features are typically reduced by filtering or else the fitting is controlled by regularization (Section 5.2.3).

Up to now we have made minimal assumptions about the true distribution of the data. In order to pin down the sampling properties of $\hat{\beta}$, we now assume that the observations y_i are uncorrelated and have constant variance σ^2, and that the x_i are fixed (non random). The variance–covariance matrix of the least squares parameter estimates is easily derived from (3.6) and is given by

$$\text{Var}(\hat{\beta}) = (\mathbf{X}^T\mathbf{X})^{-1}\sigma^2. \tag{3.8}$$

Typically one estimates the variance σ^2 by

$$\hat{\sigma}^2 = \frac{1}{N-p-1}\sum_{i=1}^{N}(y_i - \hat{y}_i)^2.$$

The $N-p-1$ rather than N in the denominator makes $\hat{\sigma}^2$ an unbiased estimate of σ^2: $\text{E}(\hat{\sigma}^2) = \sigma^2$.

To draw inferences about the parameters and the model, additional assumptions are needed. We now assume that (3.1) is the correct model for the mean; that is, the conditional expectation of Y is linear in $X_1, \dots, X_p$. We also assume that the deviations of Y around its expectation are additive and Gaussian. Hence

$$\begin{aligned} Y &= \text{E}(Y|X_1, \dots, X_p) + \varepsilon \\ &= \beta_0 + \sum_{j=1}^{p} X_j\beta_j + \varepsilon, \end{aligned} \tag{3.9}$$

where the error ε is a Gaussian random variable with expectation zero and variance σ^2, written $\varepsilon \sim N(0, \sigma^2)$.

Under (3.9), it is easy to show that

$$\hat{\beta} \sim N(\beta, (\mathbf{X}^T\mathbf{X})^{-1}\sigma^2). \tag{3.10}$$

This is a multivariate normal distribution with mean vector and variance–covariance matrix as shown. Also

$$(N-p-1)\hat{\sigma}^2 \sim \sigma^2\chi^2_{N-p-1}, \tag{3.11}$$

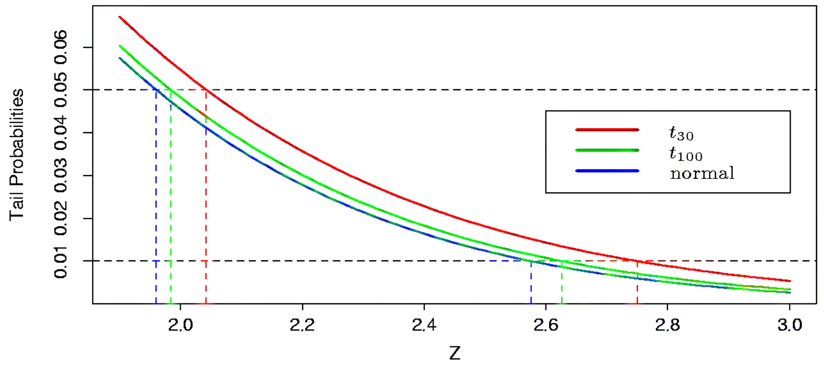

FIGURE 3.3. *The tail probabilities* $\Pr(|Z| > z)$ *for three distributions,* t_{30}*,* t_{100} *and standard normal. Shown are the appropriate quantiles for testing significance at the* $p = 0.05$ *and* 0.01 *levels. The difference between* t *and the standard normal becomes negligible for* N *bigger than about* 100.

a chi-squared distribution with $N-p-1$ degrees of freedom. In addition $\hat{\beta}$ and $\hat{\sigma}^2$ are statistically independent. We use these distributional properties to form tests of hypothesis and confidence intervals for the parameters β_j.

To test the hypothesis that a particular coefficient $\beta_j = 0$, we form the standardized coefficient or *Z-score*

$$z_j = \frac{\hat{\beta}_j}{\hat{\sigma}\sqrt{v_j}}, \tag{3.12}$$

where v_j is the jth diagonal element of $(\mathbf{X}^T\mathbf{X})^{-1}$. Under the null hypothesis that $\beta_j = 0$, z_j is distributed as t_{N-p-1} (a t distribution with $N-p-1$ degrees of freedom), and hence a large (absolute) value of z_j will lead to rejection of this null hypothesis. If σ were known, then z_j would have a standard normal distribution. The difference between the tail quantiles of a t-distribution and a standard normal become negligible as the sample size increases, and so we typically use the normal quantiles (see Figure 3.3).

Often we need to test for the significance of groups of coefficients simultaneously. For example, to test if a categorical variable with k levels can be excluded from a model, we need to test whether the coefficients of the dummy variables used to represent the levels can all be set to zero. Here we use the F statistic,

$$F = \frac{(\mathrm{RSS}_0 - \mathrm{RSS}_1)/(p_1 - p_0)}{\mathrm{RSS}_1/(N - p_1 - 1)}, \tag{3.13}$$

where RSS_1 is the residual sum-of-squares for the least squares fit of the bigger model with p_1+1 parameters, and RSS_0 the same for the nested smaller model with p_0+1 parameters, having p_1-p_0 parameters constrained to be zero. The F statistic measures the change in residual sum-of-squares per additional parameter in the bigger model, and it is normalized by an estimate of σ^2. Under the Gaussian assumptions, and the null hypothesis that the smaller model is correct, the F statistic will have a $F_{p_1-p_0,N-p_1-1}$ distribution. It can be shown (Exercise 3.1) that the z_j in (3.12) are equivalent to the F statistic for dropping the single coefficient β_j from the model. For large N, the quantiles of the $F_{p_1-p_0,N-p_1-1}$ approach those of the $\chi^2_{p_1-p_2}$.

Similarly, we can isolate β_j in (3.10) to obtain a $1-2\alpha$ confidence interval for β_j:

$$(\hat{\beta}_j - z^{(1-\alpha)}v_j\hat{\sigma},\ \ \hat{\beta}_j + z^{(1-\alpha)}v_j\hat{\sigma}). \tag{3.14}$$

Here $z^{(1-\alpha)}$ is the $1-\alpha$ percentile of the normal distribution:

$$\begin{aligned} z^{(1-0.025)} &= 1.96, \\ z^{(1-.05)} &= 1.645, \quad \text{etc.} \end{aligned}$$

Hence the standard practice of reporting $\hat{\beta} \pm 2\cdot \text{se}(\hat{\beta})$ amounts to an approximate 95% confidence interval. Even if the Gaussian error assumption does not hold, this interval will be approximately correct, with its coverage approaching $1-2\alpha$ as the sample size $N\to\infty$.

In a similar fashion we can obtain an approximate confidence set for the entire parameter vector β, namely

$$C_\beta = \{\beta | (\hat{\beta}-\beta)^T\mathbf{X}^T\mathbf{X}(\hat{\beta}-\beta) \le \hat{\sigma}^2{\chi^2_{p+1}}^{(1-\alpha)}\}, \tag{3.15}$$

where $\chi^{2(1-\alpha)}_\ell$ is the $1-\alpha$ percentile of the chi-squared distribution on ℓ degrees of freedom: for example, $\chi^{2(1-0.05)}_5 = 11.1$, $\chi^{2(1-0.1)}_5 = 9.2$. This confidence set for β generates a corresponding confidence interval for the true function $f(x) = x^T\beta$, namely $\{x^T\beta | \beta \in C_\beta\}$ (Exercise 3.2). For an example of such confidence intervals, see Figure 5.4 in Section 5.2.2.

3.2.1 Example: Prostate Cancer

The data for this example come from a study by Stamey et al. (1989). They examined the correlation between the level of prostate-specific antigen and a number of clinical measures in men who were about to receive a radical prostatectomy. The variables are log cancer volume (`lcavol`), log prostate weight (`lweight`), `age`, log of the amount of benign prostatic hyperplasia (`lbph`), seminal vesicle invasion (`svi`), log of capsular penetration (`lcp`), Gleason score (`gleason`), and percent of Gleason scores 4 or 5 (`pgg45`). The correlation matrix of the predictors given in Table 3.1 shows many strong correlations. Figure 1.1 (page 3) of Chapter 1 is a scatterplot matrix showing every pairwise plot between the variables. We see that `svi` is a

TABLE 3.1. *Correlations of predictors in the prostate cancer data.*

	`lcavol`	`lweight`	`age`	`lbph`	`svi`	`lcp`	`gleason`
`lweight`	0.300						
`age`	0.286	0.317					
`lbph`	0.063	0.437	0.287				
`svi`	0.593	0.181	0.129	-0.139			
`lcp`	0.692	0.157	0.173	-0.089	0.671		
`gleason`	0.426	0.024	0.366	0.033	0.307	0.476	
`pgg45`	0.483	0.074	0.276	-0.030	0.481	0.663	0.757

TABLE 3.2. *Linear model fit to the prostate cancer data. The Z score is the coefficient divided by its standard error (3.12). Roughly a Z score larger than two in absolute value is significantly nonzero at the $p = 0.05$ level.*

Term	Coefficient	Std. Error	Z Score
`Intercept`	2.48	0.09	27.66
`lcavol`	0.68	0.13	5.37
`lweight`	0.30	0.11	2.75
`age`	-0.14	0.10	-1.40
`lbph`	0.21	0.10	2.06
`svi`	0.31	0.12	2.47
`lcp`	-0.29	0.15	-1.87
`gleason`	-0.02	0.15	-0.15
`pgg45`	0.27	0.15	1.74

binary variable, and `gleason` is an ordered categorical variable. We see, for example, that both `lcavol` and `lcp` show a strong relationship with the response `lpsa`, and with each other. We need to fit the effects jointly to untangle the relationships between the predictors and the response.

We fit a linear model to the log of prostate-specific antigen, `lpsa`, after first standardizing the predictors to have unit variance. We randomly split the dataset into a training set of size 67 and a test set of size 30. We applied least squares estimation to the training set, producing the estimates, standard errors and Z-scores shown in Table 3.2. The Z-scores are defined in (3.12), and measure the effect of dropping that variable from the model. A Z-score greater than 2 in absolute value is approximately significant at the 5% level. (For our example, we have nine parameters, and the 0.025 tail quantiles of the t_{67-9} distribution are ± 2.002!) The predictor `lcavol` shows the strongest effect, with `lweight` and `svi` also strong. Notice that `lcp` is not significant, once `lcavol` is in the model (when used in a model without `lcavol`, `lcp` is strongly significant). We can also test for the exclusion of a number of terms at once, using the F-statistic (3.13). For example, we consider dropping all the non-significant terms in Table 3.2, namely `age`, `lcp`, `gleason`, and `pgg45`. We get

$$F = \frac{(32.81 - 29.43)/(9-5)}{29.43/(67-9)} = 1.67, \tag{3.16}$$

which has a p-value of 0.17 ($\Pr(F_{4,58} > 1.67) = 0.17$), and hence is not significant.

The mean prediction error on the test data is 0.545. In contrast, prediction using the mean training value of `lpsa` has a test error of 1.050, which is called the "base error rate." Hence the linear model reduces the base error rate by about 50%. We will return to this example later to compare various selection and shrinkage methods.

3.2.2 The Gauss–Markov Theorem

One of the most famous results in statistics asserts that the least squares estimates of the parameters β have the smallest variance among all linear unbiased estimates. We will make this precise here, and also make clear that the restriction to unbiased estimates is not necessarily a wise one. This observation will lead us to consider biased estimates such as ridge regression later in the chapter. We focus on estimation of any linear combination of the parameters $\theta = a^T\beta$; for example, predictions $f(x_0) = x_0^T\beta$ are of this form. The least squares estimate of $a^T\beta$ is

$$\hat{\theta} = a^T\hat{\beta} = a^T(\mathbf{X}^T\mathbf{X})^{-1}\mathbf{X}^T\mathbf{y}. \tag{3.17}$$

Considering $\mathbf{X}$ to be fixed, this is a linear function $\mathbf{c}_0^T\mathbf{y}$ of the response vector $\mathbf{y}$. If we assume that the linear model is correct, $a^T\hat{\beta}$ is unbiased since

$$\begin{aligned} \mathrm{E}(a^T\hat{\beta}) &= \mathrm{E}(a^T(\mathbf{X}^T\mathbf{X})^{-1}\mathbf{X}^T\mathbf{y}) \\ &= a^T(\mathbf{X}^T\mathbf{X})^{-1}\mathbf{X}^T\mathbf{X}\beta \\ &= a^T\beta. \end{aligned} \tag{3.18}$$

The Gauss–Markov theorem states that if we have any other linear estimator $\tilde{\theta} = \mathbf{c}^T\mathbf{y}$ that is unbiased for $a^T\beta$, that is, $\mathrm{E}(\mathbf{c}^T\mathbf{y}) = a^T\beta$, then

$$\mathrm{Var}(a^T\hat{\beta}) \le \mathrm{Var}(\mathbf{c}^T\mathbf{y}). \tag{3.19}$$

The proof (Exercise 3.3) uses the triangle inequality. For simplicity we have stated the result in terms of estimation of a single parameter $a^T\beta$, but with a few more definitions one can state it in terms of the entire parameter vector β (Exercise 3.3).

Consider the mean squared error of an estimator $\tilde{\theta}$ in estimating θ:

$$\begin{aligned} \mathrm{MSE}(\tilde{\theta}) &= \mathrm{E}(\tilde{\theta} - \theta)^2 \\ &= \mathrm{Var}(\tilde{\theta}) + [\mathrm{E}(\tilde{\theta}) - \theta]^2. \end{aligned} \tag{3.20}$$

The first term is the variance, while the second term is the squared bias. The Gauss-Markov theorem implies that the least squares estimator has the smallest mean squared error of all linear estimators with no bias. However, there may well exist a biased estimator with smaller mean squared error. Such an estimator would trade a little bias for a larger reduction in variance. Biased estimates are commonly used. Any method that shrinks or sets to zero some of the least squares coefficients may result in a biased estimate. We discuss many examples, including variable subset selection and ridge regression, later in this chapter. From a more pragmatic point of view, most models are distortions of the truth, and hence are biased; picking the right model amounts to creating the right balance between bias and variance. We go into these issues in more detail in Chapter 7.

Mean squared error is intimately related to prediction accuracy, as discussed in Chapter 2. Consider the prediction of the new response at input x_0,

$$Y_0 = f(x_0) + \varepsilon_0. \tag{3.21}$$

Then the expected prediction error of an estimate $\tilde{f}(x_0) = x_0^T\tilde{\beta}$ is

$$\begin{aligned} \mathrm{E}(Y_0 - \tilde{f}(x_0))^2 &= \sigma^2 + \mathrm{E}(x_0^T\tilde{\beta} - f(x_0))^2 \\ &= \sigma^2 + \mathrm{MSE}(\tilde{f}(x_0)). \end{aligned} \tag{3.22}$$

Therefore, expected prediction error and mean squared error differ only by the constant σ^2, representing the variance of the new observation y_0.

3.3 Multiple Regression from Simple Univariate Regression

The linear model (3.1) with $p > 1$ inputs is called the *multiple linear regression model*. The least squares estimates (3.6) for this model are best understood in terms of the estimates for the *univariate* ($p = 1$) linear model, as we indicate in this section.

Suppose first that we have a univariate model with no intercept, that is,

$$Y = X\beta + \varepsilon. \tag{3.23}$$

The least squares estimate and residuals are

$$\begin{aligned} \hat{\beta} &= \frac{\sum_1^N x_i y_i}{\sum_1^N x_i^2}, \\ r_i &= y_i - x_i\hat{\beta}. \end{aligned} \tag{3.24}$$

In convenient vector notation, we let $\mathbf{y} = (y_1, \dots, y_N)^T$, $\mathbf{x} = (x_1, \dots, x_N)^T$ and define

$$\begin{aligned}\langle \mathbf{x}, \mathbf{y} \rangle &= \sum_{i=1}^{N} x_i y_i, \\ &= \mathbf{x}^T \mathbf{y},\end{aligned}$$

the *inner product* between $\mathbf{x}$ and $\mathbf{y}$.[*] Then we can write

$$\begin{aligned}\hat{\beta} &= \frac{\langle \mathbf{x}, \mathbf{y} \rangle}{\langle \mathbf{x}, \mathbf{x} \rangle}, \\ \mathbf{r} &= \mathbf{y} - \mathbf{x}\hat{\beta}.\end{aligned} \tag{3.25}$$

As we will see, this simple univariate regression provides the building block for multiple least squares regression. Suppose next that the inputs $\mathbf{x}_1, \mathbf{x}_2, \dots, \mathbf{x}_p$ (the columns of the data matrix $\mathbf{X}$) are orthogonal; that is $\langle \mathbf{x}_j, \mathbf{x}_k \rangle = 0$ for all $j \neq k$. Then it is easy to check that the multiple least squares estimates $\hat{\beta}_j$ are equal to $\langle \mathbf{x}_j, \mathbf{y} \rangle / \langle \mathbf{x}_j, \mathbf{x}_j \rangle$—the univariate estimates. In other words, when the inputs are orthogonal, they have no effect on each others parameter estimates in the model.

Orthogonal inputs occur most often with balanced, designed experiments (where orthogonality is enforced), but almost never with observational data. Hence we will have to orthogonalize them in order to carry this idea further. Suppose next that we have an intercept and a single input $\mathbf{x}$. Then the least squares coefficient of $\mathbf{x}$ has the form

$$\hat{\beta}_1 = \frac{\langle \mathbf{x} - \bar{x}\mathbf{1}, \mathbf{y} \rangle}{\langle \mathbf{x} - \bar{x}\mathbf{1}, \mathbf{x} - \bar{x}\mathbf{1} \rangle}, \tag{3.26}$$

where $\bar{x} = \sum_i x_i / N$, and $\mathbf{1} = \mathbf{x}_0$, the vector of N ones. We can view the estimate (3.26) as the result of two applications of the simple regression (3.25). The steps are:

1. regress $\mathbf{x}$ on $\mathbf{1}$ to produce the residual $\mathbf{z} = \mathbf{x} - \bar{x}\mathbf{1}$;
2. regress $\mathbf{y}$ on the residual $\mathbf{z}$ to give the coefficient $\hat{\beta}_1$.

In this procedure, "regress $\mathbf{b}$ on $\mathbf{a}$" means a simple univariate regression of $\mathbf{b}$ on $\mathbf{a}$ with no intercept, producing coefficient $\hat{\gamma} = \langle \mathbf{a}, \mathbf{b} \rangle / \langle \mathbf{a}, \mathbf{a} \rangle$ and residual vector $\mathbf{b} - \hat{\gamma}\mathbf{a}$. We say that $\mathbf{b}$ is adjusted for $\mathbf{a}$, or is "orthogonalized" with respect to $\mathbf{a}$.

Step 1 orthogonalizes $\mathbf{x}$ with respect to $\mathbf{x}_0 = \mathbf{1}$. Step 2 is just a simple univariate regression, using the orthogonal predictors $\mathbf{1}$ and $\mathbf{z}$. Figure 3.4 shows this process for two general inputs $\mathbf{x}_1$ and $\mathbf{x}_2$. The orthogonalization does not change the subspace spanned by $\mathbf{x}_1$ and $\mathbf{x}_2$, it simply produces an orthogonal basis for representing it.

[*]The inner-product notation is suggestive of generalizations of linear regression to different metric spaces, as well as to probability spaces.

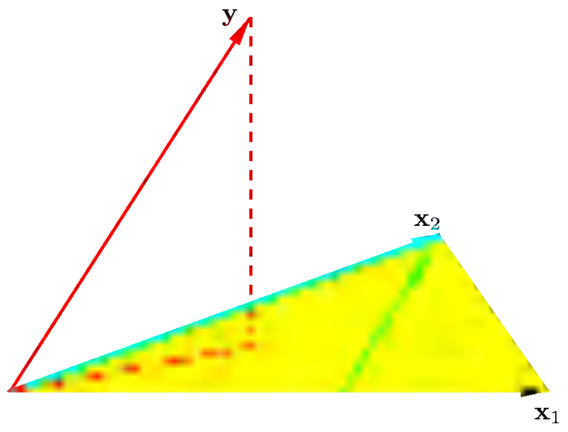

FIGURE 3.4. *Least squares regression by orthogonalization of the inputs. The vector* $\mathbf{x}_2$ *is regressed on the vector* $\mathbf{x}_1$*, leaving the residual vector* $\mathbf{z}$*. The regression of* $\mathbf{y}$ *on* $\mathbf{z}$ *gives the multiple regression coefficient of* $\mathbf{x}_2$*. Adding together the projections of* $\mathbf{y}$ *on each of* $\mathbf{x}_1$ *and* $\mathbf{z}$ *gives the least squares fit* $\hat{\mathbf{y}}$*.*

Algorithm 3.1 *Regression by Successive Orthogonalization.*

```
1. Initialize $\mathbf{z}_0 = \mathbf{x}_0 = \mathbf{1}$.
2. For $j = 1, 2, \ldots, p$
       Regress $\mathbf{x}_j$ on $\mathbf{z}_0, \mathbf{z}_1, \ldots, , \mathbf{z}_{j-1}$ to produce coefficients $\hat{\gamma}_{\ell j} = \langle \mathbf{z}_\ell, \mathbf{x}_j \rangle / \langle \mathbf{z}_\ell, \mathbf{z}_\ell \rangle$, $\ell = 0, \ldots, j-1$ and residual vector $\mathbf{z}_j = \mathbf{x}_j - \sum_{k=0}^{j-1} \hat{\gamma}_{kj} \mathbf{z}_{k-1}$.
3. Regress $\mathbf{y}$ on the residual $\mathbf{z}_p$ to give the estimate $\hat{\beta}_p$.
```

This recipe generalizes to the case of p inputs, as shown in Algorithm 3.1. Note that the inputs $\mathbf{z}_0, \ldots, \mathbf{z}_{j-1}$ in step 2 are orthogonal, hence the simple regression coefficients computed there are in fact also the multiple regression coefficients.

The result of this algorithm is

$$\hat{\beta}_p = \frac{\langle \mathbf{z}_p, \mathbf{y} \rangle}{\langle \mathbf{z}_p, \mathbf{z}_p \rangle}. \tag{3.27}$$

Re-arranging the residual in step 2, we can see that each of the $\mathbf{x}_j$ is a linear combination of the $\mathbf{z}_k$, $k \leq j$. Since the $\mathbf{z}_j$ are all orthogonal, they form a basis for the column space of $\mathbf{X}$, and hence the least squares projection onto this subspace is $\hat{\mathbf{y}}$. Since $\mathbf{x}_p$ alone involves $\mathbf{z}_p$ (with coefficient 1), we see that the coefficient (3.6) is indeed the multiple regression coefficient of $\mathbf{y}$ on $\mathbf{x}_p$. This key result exposes the effect of correlated inputs in multiple regression. Note also that by rearranging the $\mathbf{x}_j$, any one of them could be in the last position, and a similar results holds. Hence stated more generally, we have shown that the jth multiple regression coefficient is the univariate regression coefficient of $\mathbf{y}$ on $\mathbf{x}_{j\cdot 012\ldots(j-1)(j+1)\ldots,p}$, the residual after regressing $\mathbf{x}_j$ on $\mathbf{x}_0, \mathbf{x}_1, \ldots, \mathbf{x}_{j-1}, \mathbf{x}_{j+1}, \ldots, \mathbf{x}_p$:

> *The multiple regression coefficient $\hat{\beta}_j$ represents the additional contribution of $\mathbf{x}_j$ on $\mathbf{y}$, after $\mathbf{x}_j$ has been adjusted for $\mathbf{x}_0, \mathbf{x}_1, \ldots, \mathbf{x}_{j-1}, \mathbf{x}_{j+1}, \ldots, \mathbf{x}_p$.*

If $\mathbf{x}_p$ is highly correlated with some of the other $\mathbf{x}_k$'s, the residual vector $\mathbf{z}_p$ will be close to zero, and from (3.27) the coefficient $\hat{\beta}_p$ will be very unstable. This will be true for all the variables in the correlated set. From (3.27) we also obtain an alternate formula for the variance estimates (3.8),

$$\mathrm{Var}(\hat{\beta}_p) = \frac{\sigma^2}{\langle \mathbf{z}_p, \mathbf{z}_p \rangle} = \frac{\sigma^2}{\|\mathbf{z}_p\|^2}. \tag{3.28}$$

In other words, the precision with which we can estimate $\hat{\beta}_p$ depends on the length of the vector $\mathbf{z}_p$; this represents how much of $\mathbf{x}_p$ is unexplained by the other $\mathbf{x}_k$'s.

Algorithm 3.1 is known as the *Gram–Schmidt* procedure for multiple regression, and is also a useful numerical strategy for computing the estimates. We can obtain from it not just $\hat{\beta}_p$, but also the entire multiple least squares fit, as shown in Exercise 3.4.

We can represent step 2 of Algorithm 3.1 in matrix form:

$$\mathbf{X} = \mathbf{Z}\mathbf{\Gamma}, \tag{3.29}$$

where $\mathbf{Z}$ has as columns the $\mathbf{z}_j$ (in order), and $\mathbf{\Gamma}$ is the upper triangular matrix with entries $\hat{\gamma}_{kj}$. Introducing the diagonal matrix $\mathbf{D}$ with jth diagonal entry $D_{jj} = \|\mathbf{z}_j\|$, we get

$$\begin{aligned} \mathbf{X} &= \mathbf{Z}\mathbf{D}^{-1}\mathbf{D}\mathbf{\Gamma} \\ &= \mathbf{Q}\mathbf{R}, \end{aligned} \tag{3.30}$$

the so-called QR decomposition of $\mathbf{X}$. Here $\mathbf{Q}$ is an $N \times (p+1)$ orthogonal matrix, $\mathbf{Q}^T\mathbf{Q} = \mathbf{I}$, and $\mathbf{R}$ is a $(p+1) \times (p+1)$ upper triangular matrix.

The $\mathbf{QR}$ decomposition represents a convenient orthogonal basis for the column space of $\mathbf{X}$. It is easy to see, for example, that the least squares solution is given by

$$\hat{\beta} = \mathbf{R}^{-1}\mathbf{Q}^T\mathbf{y}, \tag{3.31}$$

$$\hat{\mathbf{y}} = \mathbf{Q}\mathbf{Q}^T\mathbf{y}. \tag{3.32}$$

Equation (3.31) is easy to solve because $\mathbf{R}$ is upper triangular (Exercise 3.4).

3.3.1 Multiple Outputs

Suppose we have multiple outputs $Y_1, Y_2, \ldots, Y_K$ that we wish to predict from our inputs $X_0, X_1, X_2, \ldots, X_p$. We assume a linear model for each output

$$\begin{aligned} Y_k &= \beta_{0k} + \sum_{j=1}^{p} X_j \beta_{jk} + \varepsilon_k && (3.33) \\ &= f_k(X) + \varepsilon_k. && (3.34) \end{aligned}$$

With N training cases we can write the model in matrix notation

$$\mathbf{Y} = \mathbf{X}\mathbf{B} + \mathbf{E}. \qquad (3.35)$$

Here $\mathbf{Y}$ is the $N \times K$ response matrix, with ik entry y_{ik}, $\mathbf{X}$ is the $N \times (p+1)$ input matrix, $\mathbf{B}$ is the $(p+1) \times K$ matrix of parameters and $\mathbf{E}$ is the $N \times K$ matrix of errors. A straightforward generalization of the univariate loss function (3.2) is

$$\begin{aligned} \mathrm{RSS}(\mathbf{B}) &= \sum_{k=1}^{K} \sum_{i=1}^{N} (y_{ik} - f_k(x_i))^2 && (3.36) \\ &= \mathrm{tr}[(\mathbf{Y} - \mathbf{X}\mathbf{B})^T (\mathbf{Y} - \mathbf{X}\mathbf{B})]. && (3.37) \end{aligned}$$

The least squares estimates have exactly the same form as before

$$\hat{\mathbf{B}} = (\mathbf{X}^T\mathbf{X})^{-1}\mathbf{X}^T\mathbf{Y}. \qquad (3.38)$$

Hence the coefficients for the kth outcome are just the least squares estimates in the regression of $\mathbf{y}_k$ on $\mathbf{x}_0, \mathbf{x}_1, \ldots, \mathbf{x}_p$. Multiple outputs do not affect one another's least squares estimates.

If the errors $\varepsilon = (\varepsilon_1, \ldots, \varepsilon_K)$ in (3.33) are correlated, then it might seem appropriate to modify (3.36) in favor of a multivariate version. Specifically, suppose $\mathrm{Cov}(\varepsilon) = \mathbf{\Sigma}$, then the multivariate weighted criterion

$$\mathrm{RSS}(\mathbf{B}; \mathbf{\Sigma}) = \sum_{i=1}^{N} (y_i - f(x_i))^T \mathbf{\Sigma}^{-1} (y_i - f(x_i)) \qquad (3.39)$$

arises naturally from multivariate Gaussian theory. Here $f(x)$ is the vector function $(f_1(x), \ldots, f_K(x))$, and y_i the vector of K responses for observation i. However, it can be shown that again the solution is given by (3.38); K separate regressions that ignore the correlations (Exercise 3.9). If the $\mathbf{\Sigma}_i$ vary among observations, then this is no longer the case, and the solution for $\mathbf{B}$ no longer decouples.

In Section 3.4.6 we pursue the multiple outcome problem, and consider situations where it does pay to combine the regressions.

3.4 Subset Selection and Coefficient Shrinkage

There are two reasons why we are often not satisfied with the least squares estimates (3.6).

- The first is *prediction accuracy*: the least squares estimates often have low bias but large variance. Prediction accuracy can sometimes be improved by shrinking or setting some coefficients to zero. By doing so we sacrifice a little bit of bias to reduce the variance of the predicted values, and hence may improve the overall prediction accuracy.

- The second reason is *interpretation*. With a large number of predictors, we often would like to determine a smaller subset that exhibit the strongest effects. In order to get the "big picture," we are willing to sacrifice some of the small details.

In this section we describe a number of approaches to variable selection and coefficient shrinkage.

3.4.1 Subset Selection

In this approach we retain only a subset of the variables, and eliminate the rest from the model. Least squares regression is used to estimate the coefficients of the inputs that are retained. There are a number of different strategies for choosing the subset. *Best subset regression* finds for each $k \in \{0, 1, 2, \ldots, p\}$ the subset of size k that gives smallest residual sum of squares (3.2). An efficient algorithm—the *leaps and bounds* procedure (Furnival and Wilson, 1974)—makes this feasible for p as large as 30 or 40. Figure 3.5 shows all the subset models for the prostate cancer example. The lower boundary represents the models that are eligible for selection by the best-subsets approach. Note that the best subset of size 2, for example, need not include the variable that was in the best subset of size 1 (for this example all the subsets are nested). The best-subset curve (red lower boundary in Figure 3.5) is necessarily decreasing, so cannot be used to select the subset size k. The question of how to choose k involves the tradeoff between bias and variance, and there are a number of criteria that one may use. Typically we choose the model that minimizes an estimate of the expected prediction error. We defer discussion of this until Chapter 7.

Rather than search through all possible subsets (which becomes infeasible for p much larger than 40), we can seek a good path through them. *Forward stepwise selection* starts with the intercept, and then sequentially adds into the model the predictor that most improves the fit. Suppose our current model has k inputs, represented by parameter estimates $\hat{\beta}$, and we add in a predictor, resulting in estimates $\tilde{\beta}$. The improvement in fit is often based

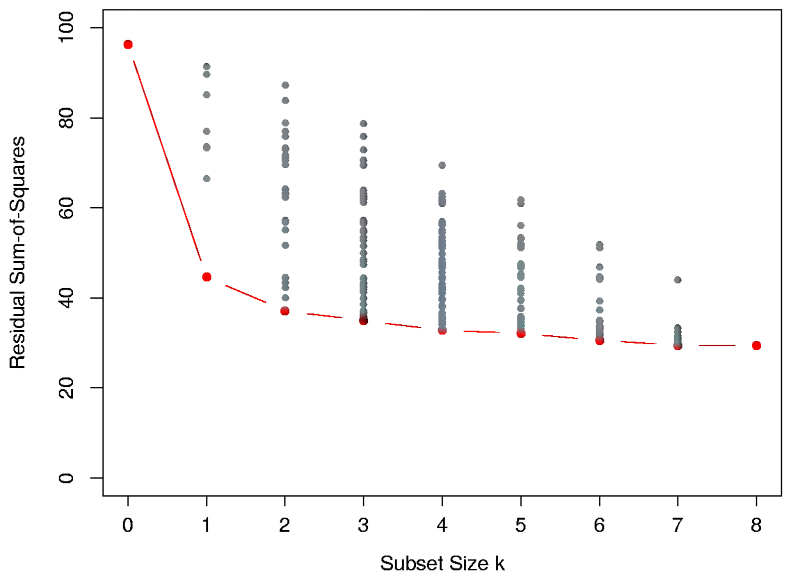

FIGURE 3.5. *All possible subset models for the prostate cancer example. At each subset size is shown the residual sum-of-squares for each model of that size.*

on the F statistic (3.13),

$$F = \frac{\text{RSS}(\hat{\beta}) - \text{RSS}(\tilde{\beta})}{\text{RSS}(\tilde{\beta})/(N-k-2)}. \tag{3.40}$$

A typical strategy adds in sequentially the predictor producing the largest value of F, stopping when no predictor produces an F-ratio greater than the 90th or 95th percentile of the $F_{1,N-k-2}$ distribution.

Backward stepwise selection starts with the full model, and sequentially deletes predictors. Like forward selection, it typically uses an F-ratio like (3.40) to choose the predictor to delete. In this case we drop the predictor producing the smallest value of F at each stage, stopping when each predictor in the model produces a value of F greater than the 90th or 95th percentile when dropped. Backward selection can only be used when $N > p$, while forward stepwise can always be used. There are also hybrid *stepwise selection* strategies that consider both forward and backward moves at each stage, and make the "best" move; these require a parameter to set the threshold between when an "add" move is chosen over a "drop" move.

The F-ratio stopping rule provides only local control of the model search, and does not attempt to find the best model along the sequence of models that it examines. As with all-subsets selection, we can choose the model from the sequence that minimizes an estimate of expected prediction error. This is discussed in Chapter 7, and illustrated in the example below.

TABLE 3.3. *Estimated coefficients and test error results, for different subset and shrinkage methods applied to the prostate data. The blank entries correspond to variables omitted.*

Term	LS	Best Subset	Ridge	Lasso	PCR	PLS
`Intercept`	2.480	2.495	2.467	2.477	2.513	2.452
`lcavol`	0.680	0.740	0.389	0.545	0.544	0.440
`lweight`	0.305	0.367	0.238	0.237	0.337	0.351
`age`	-0.141		-0.029		-0.152	-0.017
`lbph`	0.210		0.159	0.098	0.213	0.248
`svi`	0.305		0.217	0.165	0.315	0.252
`lcp`	-0.288		0.026		-0.053	0.078
`gleason`	-0.021		0.042		0.230	0.003
`pgg45`	0.267		0.123	0.059	-0.053	0.080
Test Error	0.586	0.574	0.540	0.491	0.527	0.636
Std. Error	0.184	0.156	0.168	0.152	0.122	0.172

3.4.2 Prostate Cancer Data Example (Continued)

Table 3.3 shows the coefficients from a number of different selection and shrinkage methods. They are *best-subset selection* using an all-subsets search, *ridge regression*, the *lasso*, *principal components regression* and *partial least squares*. Each method has a complexity parameter, and this was chosen to minimize an estimate of prediction error based on tenfold cross-validation; full details are given in Section 7.10. Briefly, cross-validation works by dividing the training data randomly into ten equal parts. The learning method is fit to nine-tenths of the data, and the prediction error is computed on the remaining one-tenth. This is done in turn for each one-tenth of the data, and the ten prediction error estimates are averaged. Note that we have already divided these data into a training set of size 67 and a test set of size 30. Cross-validation is applied to the training set, since selecting the shrinkage parameter is part of the training process. The test set is there to judge the performance of the selected model.

The estimated prediction error curves are shown in Figure 3.6. Many of the curves are very flat over large ranges near their minimum. Included are estimated standard error bands for each estimated error rate, based on the ten error estimates computed by cross-validation. We have used the "one-standard-error" rule—we pick the most parsimonious model within one standard error of the minimum (Section 7.10, page 216). Such a rule faces up to the fact that the tradeoff curve is estimated with error, and hence takes a conservative approach.

Best-subset selection chose to use the two predictors `lcvol` and `lcweight`. The last two lines of the table give the average prediction error (and its standard error) over the test set.

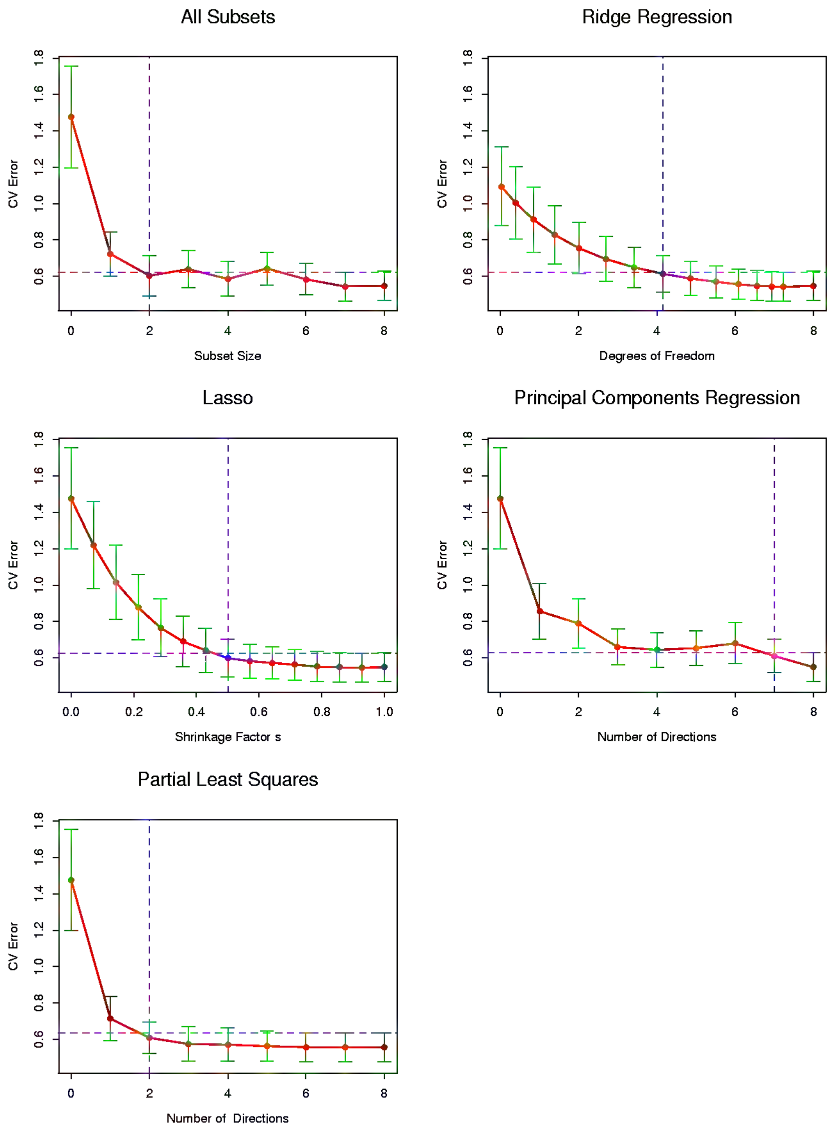

FIGURE 3.6. *Estimated prediction error curves and their standard errors for the various selection and shrinkage methods. Each curve is plotted as a function of the corresponding complexity parameter for that method. The horizontal axis has been chosen so that the model complexity increases as we move from left to right. The prediction error estimates and their standard errors were obtained by tenfold cross-validation; full details are given in Section 7.10. The least complex model within one standard error of the best is chosen.*

3.4.3 Shrinkage Methods

By retaining a subset of the predictors and discarding the rest, subset selection produces a model that is interpretable and has possibly lower prediction error than the full model. However, because it is a discrete process—variables are either retained or discarded—it often exhibits high variance, and so doesn't reduce the prediction error of the full model. Shrinkage methods are more continuous, and don't suffer as much from high variability.

Ridge Regression

Ridge regression shrinks the regression coefficients by imposing a penalty on their size. The ridge coefficients minimize a penalized residual sum of squares,

$$\hat{\beta}^{\text{ridge}} = \underset{\beta}{\operatorname{argmin}} \Big\{ \sum_{i=1}^{N} \big(y_i - \beta_0 - \sum_{j=1}^{p} x_{ij}\beta_j\big)^2 + \lambda \sum_{j=1}^{p} \beta_j^2 \Big\}. \tag{3.41}$$

Here $\lambda \geq 0$ is a complexity parameter that controls the amount of shrinkage: the larger the value of λ, the greater the amount of shrinkage. The coefficients are shrunk toward zero (and each other). The idea of penalizing by the sum-of-squares of the parameters is also used in neural networks, where it is known as *weight decay* (Chapter 11).

An equivalent way to write the ridge problem is

$$\begin{aligned} \hat{\beta}^{\text{ridge}} &= \underset{\beta}{\operatorname{argmin}} \sum_{i=1}^{N} \Big(y_i - \beta_0 - \sum_{j=1}^{p} x_{ij}\beta_j\Big)^2, \\ &\text{subject to } \sum_{j=1}^{p} \beta_j^2 \leq s, \end{aligned} \tag{3.42}$$

which makes explicit the size constraint on the parameters. There is a one-to-one correspondence between the parameters λ in (3.41) and s in (3.42). When there are many correlated variables in a linear regression model, their coefficients can become poorly determined and exhibit high variance. A wildly large positive coefficient on one variable can be canceled by a similarly large negative coefficient on its correlated cousin. By imposing a size constraint on the coefficients, as in (3.42), this phenomenon is prevented from occurring.

The ridge solutions are not equivariant under scaling of the inputs, and so one normally standardizes the inputs before solving (3.41).

In addition, notice that the intercept β_0 has been left out of the penalty term. Penalization of the intercept would make the procedure depend on the origin chosen for Y; that is, adding a constant c to each of the targets y_i would not simply result in a shift of the predictions by the same amount c.

It can be shown (Exercise 3.5) that the solution to (3.41) can be separated into two parts, after reparametrization using *centered* inputs: each x_{ij} gets replaced by $x_{ij} - \bar{x}_j$. We estimate β_0 by $\bar{y} = \sum_1^N y_i/N$. The remaining coefficients get estimated by a ridge regression without intercept, using the centered x_{ij}. Henceforth we assume that this centering has been done, so that the input matrix $\mathbf{X}$ has p (rather than $p+1$) columns.

Writing the criterion in (3.41) in matrix form,

$$\text{RSS}(\lambda) = (\mathbf{y} - \mathbf{X}\beta)^T(\mathbf{y} - \mathbf{X}\beta) + \lambda\beta^T\beta, \tag{3.43}$$

the ridge regression solutions are easily seen to be

$$\hat{\beta}^{\text{ridge}} = (\mathbf{X}^T\mathbf{X} + \lambda\mathbf{I})^{-1}\mathbf{X}^T\mathbf{y}, \tag{3.44}$$

where $\mathbf{I}$ is the $p \times p$ identity matrix. Notice that with the choice of quadratic penalty $\beta^T\beta$, the ridge regression solution is again a linear function of $\mathbf{y}$. The solution adds a positive constant to the diagonal of $\mathbf{X}^T\mathbf{X}$ before inversion. This makes the problem nonsingular, even if $\mathbf{X}^T\mathbf{X}$ is not of full rank, and was the main motivation for ridge regression when it was first introduced in statistics (Hoerl and Kennard, 1970). Traditional descriptions of ridge regression start with definition (3.44). We choose to motivate it via (3.41) and (3.42), as these provide insight into how it works.

Figure 3.7 shows the ridge coefficient estimates for the prostate cancer example, plotted as functions of $\text{df}(\lambda)$, the *effective degrees of freedom* implied by a penalty λ (defined in (3.50) on page 63).

In the case of orthogonal inputs, the ridge estimates are just a scaled version of the least squares estimates, that is, $\hat{\beta}^{\text{ridge}} = \gamma\hat{\beta}$. Here $0 \leq \gamma \leq 1$ is a simple function of λ in equation (3.41); see Section 3.4.5.

Ridge regression can also be derived as the mean or mode of a posterior distribution, with a suitably chosen prior distribution. Suppose $y_i \sim N(\beta_0 + x_i^T\beta, \sigma^2)$, and the parameters β_j are each distributed as $N(0, \tau^2)$, independently of one another. Then the (negative) log-posterior density of β, with τ^2 and σ^2 assumed known, is equal to the expression in curly braces in (3.41), with $\lambda = \sigma^2/\tau^2$ (Exercise 3.6). Thus the ridge estimate is the mode of the posterior distribution; since the distribution is Gaussian, it is also the posterior mean.

The *singular value decomposition* (SVD) of the centered input matrix $\mathbf{X}$ gives us some additional insight into the nature of ridge regression. This decomposition is extremely useful in the analysis of many statistical methods. The SVD of the $N \times p$ matrix $\mathbf{X}$ has the form

$$\mathbf{X} = \mathbf{U}\mathbf{D}\mathbf{V}^T. \tag{3.45}$$

Here $\mathbf{U}$ and $\mathbf{V}$ are $N \times p$ and $p \times p$ orthogonal matrices, with the columns of $\mathbf{U}$ spanning the column space of $\mathbf{X}$, and the columns of $\mathbf{V}$ spanning the row space. $\mathbf{D}$ is a $p \times p$ diagonal matrix, with diagonal entries $d_1 \geq d_2 \geq \cdots \geq d_p \geq 0$ called the singular values of $\mathbf{X}$.

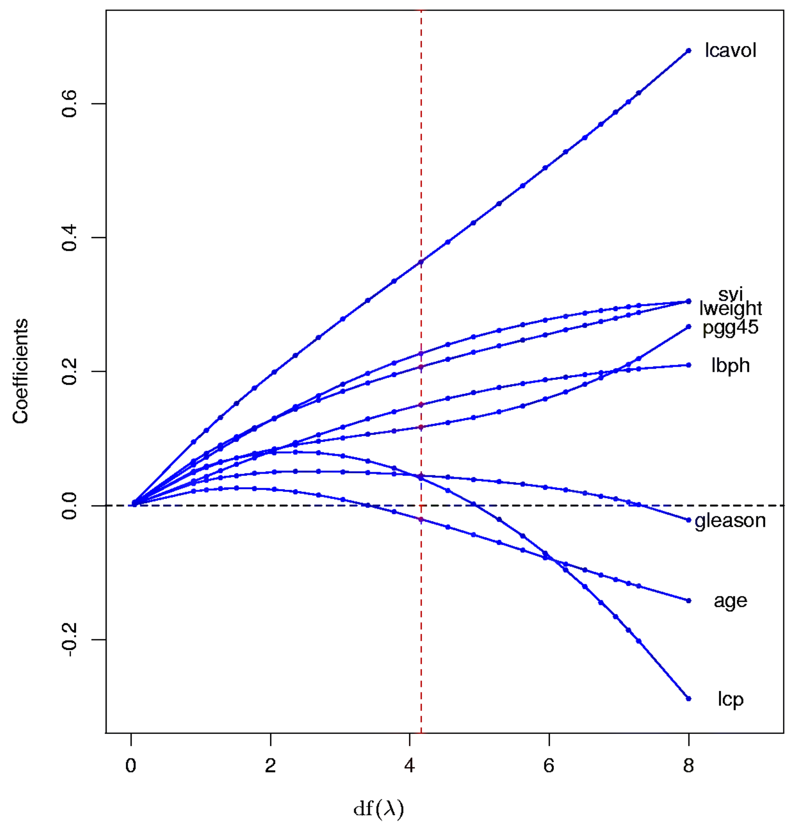

FIGURE 3.7. *Profiles of ridge coefficients for the prostate cancer example, as tuning parameter* λ *is varied. Coefficients are plotted versus* $\text{df}(\lambda)$, *the effective degrees of freedom. A vertical line is drawn at* $\text{df} = 4.16$, *the value chosen by cross-validation.*

Using the singular value decomposition we can write the least squares fitted vector as

$$\begin{aligned}\mathbf{X}\hat{\beta}^{\text{ls}} &= \mathbf{X}(\mathbf{X}^T\mathbf{X})^{-1}\mathbf{X}^T\mathbf{y} \\ &= \mathbf{U}\mathbf{U}^T\mathbf{y}, \end{aligned} \tag{3.46}$$

after some simplification. Note that $\mathbf{U}^T\mathbf{y}$ are the coordinates of $\mathbf{y}$ with respect to the orthonormal basis $\mathbf{U}$. Note also the similarity with (3.32); $\mathbf{Q}$ and $\mathbf{U}$ are generally different bases for the column space of $\mathbf{X}$ (Exercise 3.8).

Now the ridge solutions are

$$\begin{aligned}\mathbf{X}\hat{\beta}^{\text{ridge}} &= \mathbf{X}(\mathbf{X}^T\mathbf{X}+\lambda\mathbf{I})^{-1}\mathbf{X}^T\mathbf{y} \\ &= \mathbf{U}\,\mathbf{D}(\mathbf{D}+\lambda\mathbf{I})^{-1}\mathbf{D}\,\mathbf{U}^T\mathbf{y} \\ &= \sum_{j=1}^{p}\mathbf{u}_j\frac{d_j^2}{d_j^2+\lambda}\mathbf{u}_j^T\mathbf{y}, \end{aligned} \tag{3.47}$$

where the $\mathbf{u}_j$ are the columns of $\mathbf{U}$. Note that since $\lambda \geq 0$, we have $d_j^2/(d_j^2+\lambda) \leq 1$. Like linear regression, ridge regression computes the coordinates of $\mathbf{y}$ with respect to the orthonormal basis $\mathbf{U}$. It then shrinks these coordinates by the factors $d_j^2/(d_j^2+\lambda)$. This means that a greater amount of shrinkage is applied to basis vectors with smaller d_j^2.

What does a small value of d_j^2 mean? The SVD of the centered matrix $\mathbf{X}$ is another way of expressing the *principal components* of the variables in $\mathbf{X}$. The sample covariance matrix is given by $\mathbf{S} = \mathbf{X}^T\mathbf{X}/N$, and from (3.45) we have

$$\mathbf{X}^T\mathbf{X} = \mathbf{V}\mathbf{D}^2\mathbf{V}^T, \tag{3.48}$$

which is the *eigen decomposition* of $\mathbf{X}^T\mathbf{X}$ (and of $\mathbf{S}$, up to a factor N). The eigenvectors v_j are also called the *principal components* (or Karhunen–Loeve) directions of $\mathbf{X}$. The first principal component direction v_1 has the property that $\mathbf{z}_1 = \mathbf{X}v_1$ has the largest sample variance amongst all normalized linear combinations of the columns of $\mathbf{X}$. This sample variance is easily seen to be

$$\text{Var}(\mathbf{z}_1) = \text{Var}(\mathbf{X}v_1) = \frac{d_1^2}{N}, \tag{3.49}$$

and in fact $\mathbf{z}_1 = \mathbf{X}v_1 = \mathbf{u}_1 d_1$. The derived variable $\mathbf{z}_1$ is called the first principal component of $\mathbf{X}$, and hence $\mathbf{u}_1$ is the normalized first principal component. Subsequent principal components $\mathbf{z}_j$ have maximum variance d_j^2/N, subject to being orthogonal to the earlier ones. Conversely the last principal component has *minimum* variance. Hence the small singular values d_j correspond to directions in the column space of $\mathbf{X}$ having small variance, and ridge regression shrinks these directions the most.

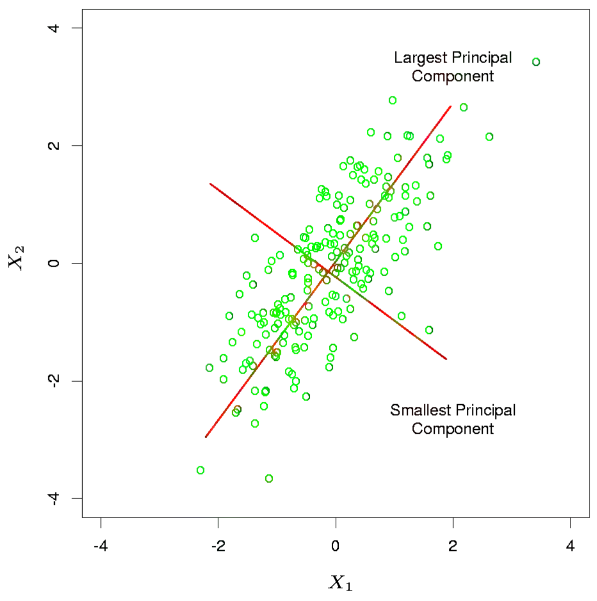

FIGURE 3.8. *Principal components of some input data points. The largest principal component is the direction that maximizes the variance of the projected data, and the smallest principal component minimizes that variance. Ridge regression projects* $\mathbf{y}$ *onto these components, and then shrinks the coefficients of the low-variance components more than the high-variance components.*

Figure 3.8 illustrates the principal components of some data points in two dimensions. If we consider fitting a linear surface over this domain (the Y-axis is sticking out of the page), the configuration of the data allow us to determine its gradient more accurately in the long direction than the short. Ridge regression protects against the potentially high variance of gradients estimated in the short directions. The implicit assumption is that the response will tend to vary most in the directions of high variance of the inputs. This is often a reasonable assumption, but need not hold in general.

In Figure 3.6 we have plotted the estimated prediction error versus the quantity

$$\begin{aligned} \mathrm{df}(\lambda) &= \mathrm{tr}[\mathbf{X}(\mathbf{X}^T\mathbf{X}+\lambda\mathbf{I})^{-1}\mathbf{X}^T], \\ &= \sum_{j=1}^{p}\frac{d_j^2}{d_j^2+\lambda}. \end{aligned} \tag{3.50}$$

This monotone decreasing function is the *effective degrees of freedom* of the ridge regression fit, as described in Section 7.6. Note that $\mathrm{df}(\lambda) = p$

when $\lambda = 0$ (no regularization) and $\mathrm{df}(\lambda) \to 0$ as $\lambda \to \infty$. In Figure 3.6 the minimum occurs at $\mathrm{df}(\lambda) = 4.16$. Table 3.3 shows that ridge regression reduces the test error of the full least squares estimates by a small amount.

The Lasso

The lasso is a shrinkage method like ridge, with subtle but important differences. The lasso estimate is defined by

$$\begin{aligned} \hat{\beta}^{\text{lasso}} &= \underset{\beta}{\operatorname{argmin}} \sum_{i=1}^{N} \Big(y_i - \beta_0 - \sum_{j=1}^{p} x_{ij}\beta_j \Big)^2 \\ &\qquad \text{subject to } \sum_{j=1}^{p} |\beta_j| \le s. \end{aligned} \tag{3.51}$$

Just as in ridge regression, we can reparametrize the constant β_0 by standardizing the predictors; the solution for $\hat{\beta}_0$ is $\bar{y}$, and thereafter we fit a model without an intercept (Exercise 3.11).

Notice the similarity to the ridge regression problem (3.42): the L_2 ridge penalty $\sum_1^p \beta_j^2$ is replaced by the L_1 lasso penalty $\sum_1^p |\beta_j|$. This latter constraint makes the solutions nonlinear in the y_i, and a quadratic programming algorithm is used to compute them. Because of the nature of the constraint, making t sufficiently small will cause some of the coefficients to be exactly zero. Thus the lasso does a kind of continuous subset selection. If t is chosen larger than $t_0 = \sum_1^p |\hat{\beta}_j|$ (where $\hat{\beta}_j = \hat{\beta}_j^{\text{ls}}$, the least squares estimates), then the lasso estimates are the $\hat{\beta}_j$'s. On the other hand, for $t = t_0/2$ say, then the least squares coefficients are shrunk by about 50% on average. However, the nature of the shrinkage is not obvious, and we investigate it further in Section 3.4.5 below. Like the subset size in variable subset selection, or the penalty parameter in ridge regression, t should be adaptively chosen to minimize an estimate of expected prediction error.

In Figure 3.6, for ease of interpretation, we have plotted the lasso prediction error estimates versus the standardized parameter $s = t/\sum_1^p |\hat{\beta}_j|$. A value $\hat{s} \approx 0.50$ was chosen by 10-fold cross-validation; this caused three coefficients to be set to zero (fifth column of Table 3.3). The resulting model has the lowest test error, slightly lower than the full least squares model, but the standard errors of the test error estimates (last line of Table 3.3) are fairly large.

Figure 3.9 shows the lasso coefficients as the standardized tuning parameter $s = t/\sum_1^p |\hat{\beta}_j|$ is varied. At $s = 1.0$ these are the least squares estimates; they decrease to 0 as $s \to 0$. This decrease is not always strictly monotonic, although it is in this example. A vertical line is drawn at $s = 0.5$, the value chosen by cross-validation.

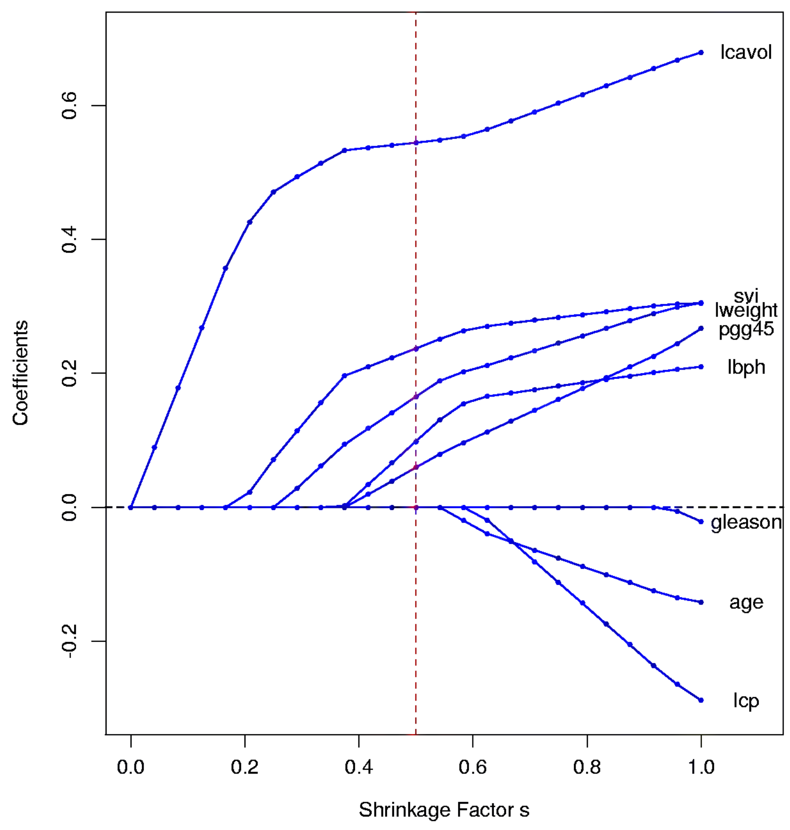

FIGURE 3.9. *Profiles of lasso coefficients, as tuning parameter t is varied. Coefficients are plotted versus $s = t/\sum_1^p |\hat{\beta}_j|$. A vertical line is drawn at $s = 0.5$, the value chosen by cross-validation. Compare Figure 3.7 on page 61; the lasso profiles hit zero, while those for ridge do not.*

3.4.4 Methods Using Derived Input Directions

In many situations we have a large number of inputs, often very correlated. The methods in this section produce a small number of linear combinations Z_m, $m = 1, \dots, M$ of the original inputs X_j, and the Z_m are then used in place of the X_j as inputs in the regression. The methods differ in how the linear combinations are constructed.

Principal Components Regression

In this approach the linear combinations Z_m used are the principal components as defined in Section 3.4.3 above.

Principal component regression forms the derived input columns $\mathbf{z}_m = \mathbf{X}v_m$, and then regresses $\mathbf{y}$ on $\mathbf{z}_1, \mathbf{z}_2, \dots, \mathbf{z}_M$ for some $M \leq p$. Since the $\mathbf{z}_m$s are orthogonal, this regression is just a sum of univariate regressions:

$$\hat{\mathbf{y}}^{\text{pcr}} = \bar{y} + \sum_{m=1}^{M} \hat{\theta}_m \mathbf{z}_m, \tag{3.52}$$

where $\hat{\theta}_m = \langle \mathbf{z}_m, \mathbf{y} \rangle / \langle \mathbf{z}_m, \mathbf{z}_m \rangle$. Since the $\mathbf{z}_m$ are each linear combinations of the original $\mathbf{x}_j$, we can express the solution (3.52) in terms of coefficients of the $\mathbf{x}_j$ (Exercise 3.12):

$$\hat{\beta}^{\text{pcr}}(M) = \sum_{m=1}^{M} \hat{\theta}_m v_m. \tag{3.53}$$

As with ridge regression, principal components depend on the scaling of the inputs, so typically we first standardize them. Note that if $M = p$, we would just get back the usual least squares estimates, since the columns of $\mathbf{Z} = \mathbf{UD}$ span the column space of $\mathbf{X}$. For $M < p$ we get a reduced regression. We see that principal components regression is very similar to ridge regression: both operate via the principal components of the input matrix. Ridge regression shrinks the coefficients of the principal components (Figure 3.10), shrinking more depending on the size of the corresponding eigenvalue; principal components regression discards the $p - M$ smallest eigenvalue components. Figure 3.10 illustrates this.

In Figure 3.6 we see that cross-validation suggests seven terms; the resulting model has about the same test error as ridge regression in Table 3.3.

Partial Least Squares

This technique also constructs a set of linear combinations of the inputs for regression, but unlike principal components regression it uses $\mathbf{y}$ (in addition to $\mathbf{X}$) for this construction. We assume that $\mathbf{y}$ is centered and each $\mathbf{x}_j$ is standardized to have mean 0 and variance 1. PLS begins by computing the univariate regression coefficient $\hat{\varphi}_{1j}$ of $\mathbf{y}$ on each $\mathbf{x}_j$, that

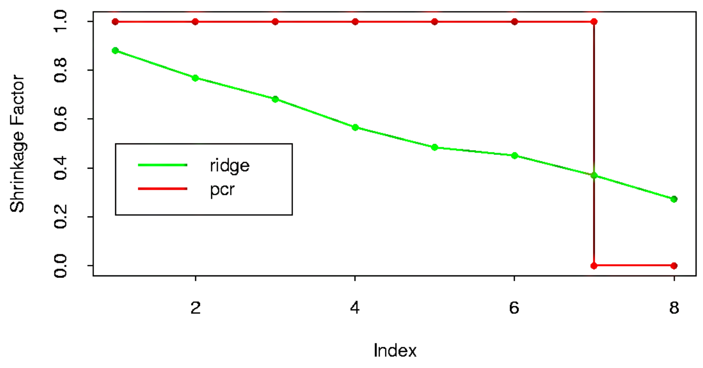

FIGURE 3.10. *Ridge regression shrinks the regression coefficients of the principal components, using shrinkage factors $d_j^2/(d_j^2+\lambda)$ as in (3.47). Principal component regression truncates them. Shown are the shrinkage and truncation patterns corresponding to Figure 3.6, as a function of the principal component index.*

is, $\hat{\varphi}_{1j} = \langle \mathbf{x}_j, \mathbf{y} \rangle$. From this we construct the derived input $\mathbf{z}_1 = \sum \hat{\varphi}_{1j}\mathbf{x}_j$, which is the first partial least squares direction. Hence in the construction of each $\mathbf{z}_m$, the inputs are weighted by the strength of their univariate effect on $\mathbf{y}$. The outcome $\mathbf{y}$ is regressed on $\mathbf{z}_1$ giving coefficient $\hat{\theta}_1$, and then we orthogonalize $\mathbf{x}_1, \ldots, \mathbf{x}_p$ with respect to $\mathbf{z}_1$. We continue this process, until $M \leq p$ directions have been obtained. In this manner, partial least squares produces a sequence of derived inputs or directions $\mathbf{z}_1, \mathbf{z}_2, \ldots, \mathbf{z}_M$. As with principal-component regression, if we were to construct all $M = p$ directions, we would get back a solution equivalent to the usual least squares estimates; using $M < p$ directions produces a reduced regression. The procedure is described fully in Algorithm 3.2.

In the prostate cancer example, cross-validation chose $M = 2$ PLS directions in Figure 3.6. This produced the model given in the rightmost column of Table 3.3.

What optimization problem is partial least squares solving? Since it uses the response $\mathbf{y}$ to construct its directions, its solution is a nonlinear function of $\mathbf{y}$. It can be shown that partial least squares seeks directions that have high variance *and* have high correlation with the response, in contrast to principal components regression (Stone and Brooks, 1990; Frank and Friedman, 1993). In particular, the mth principal component direction v_m solves:

$$\max_{\substack{||\alpha||=1 \\ v_\ell^T \mathbf{S}\alpha = 0,\, \ell=1,\ldots,m-1}} \mathrm{Var}(\mathbf{X}\alpha), \tag{3.54}$$

where $\mathbf{S}$ is the sample covariance matrix of the $\mathbf{x}_j$. The conditions $v_\ell^T \mathbf{S}\alpha = 0$ ensures that $\mathbf{z}_m = \mathbf{X}\alpha$ is uncorrelated with all the previous linear combi-

Algorithm 3.2 *Partial Least Squares.*

```
1. Standardize each $\mathbf{x}_j$ to have mean zero and variance one. Set $\hat{\mathbf{y}}^{(0)} = \mathbf{1}\bar{y}$, and $\mathbf{x}_j^{(0)} = \mathbf{x}_j$, $j = 1, \dots, p$.

2. For $m = 1, 2, \dots, p$

    • $\mathbf{z}_m = \sum_{j=1}^{p} \hat{\varphi}_{mj} \mathbf{x}_j^{(m-1)}$, where $\hat{\varphi}_{mj} = \langle \mathbf{x}_j^{(m-1)}, \mathbf{y} \rangle$.
    • $\hat{\theta}_m = \langle \mathbf{z}_m, \mathbf{y} \rangle / \langle \mathbf{z}_m, \mathbf{z}_m \rangle$.
    • $\hat{\mathbf{y}}^{(m)} = \hat{\mathbf{y}}^{(m-1)} + \hat{\theta}_m \mathbf{z}_m$.
    • Orthogonalize each $\mathbf{x}_j^{(m-1)}$ with respect to $\mathbf{z}_m$: $\mathbf{x}_j^{(m)} = \mathbf{x}_j^{(m-1)} - [\langle \mathbf{z}_m, \mathbf{x}_j^{(m-1)} \rangle / \langle \mathbf{z}_m, \mathbf{z}_m \rangle] \mathbf{z}_m$, $j = 1, 2, \dots, p$.

3. Output the sequence of fitted vectors $\hat{\mathbf{y}}^{(m)}$, $m = 1, \dots, p$. The corresponding sequence of PLS coefficients on the original $\mathbf{x}_j$ are given by $\hat{\beta}_j^{\text{pls}}(m) = \sum_{\ell=1}^{m} \hat{\varphi}_{\ell j} \hat{\theta}_\ell$.
```

nations $\mathbf{z}_\ell = \mathbf{X} v_\ell$. The mth PLS direction $\hat{\varphi}_m$ solves:

$$\max_{\substack{||\alpha||=1 \\ \hat{\varphi}_\ell^T \mathbf{S} \alpha = 0, \ell = 1, \dots, m-1}} \text{Corr}^2(\mathbf{y}, \mathbf{X}\alpha) \text{Var}(\mathbf{X}\alpha). \tag{3.55}$$

Further analysis reveals that the variance aspect tends to dominate, and so partial least squares behaves much like ridge regression and principal components regression. We discuss this further in the next section.

If the input matrix $\mathbf{X}$ is orthogonal, then partial least squares finds the least squares estimates after $m = 1$ steps. Subsequent steps have no effect since the $\hat{\varphi}_{mj}$ are zero for $m > 1$ (Exercise 3.13). It can also be shown that the sequence of PLS coefficients for $m = 1, 2, \dots, p$ represents the conjugate gradient sequence for computing the least squares solutions (Exercise 3.16).

3.4.5 Discussion: A Comparison of the Selection and Shrinkage Methods

There are some simple settings where we can understand better the relationship between the methods described above. Consider an example with two correlated inputs X_1 and X_2, with correlation ρ. We assume that with the true regression coefficients are $\beta_1 = 4$ and $\beta_2 = 2$. Figure 3.11 shows the coefficient profiles for the different methods, as their tuning parameters are varied. The top panel has $\rho = 0.5$, the bottom panel $\rho = -0.5$. The tuning parameters for ridge and lasso vary over a continuous range, while best subset, PLS and PCR take just two discrete steps to the least squares solution. In the top panel, starting at the origin, ridge regression

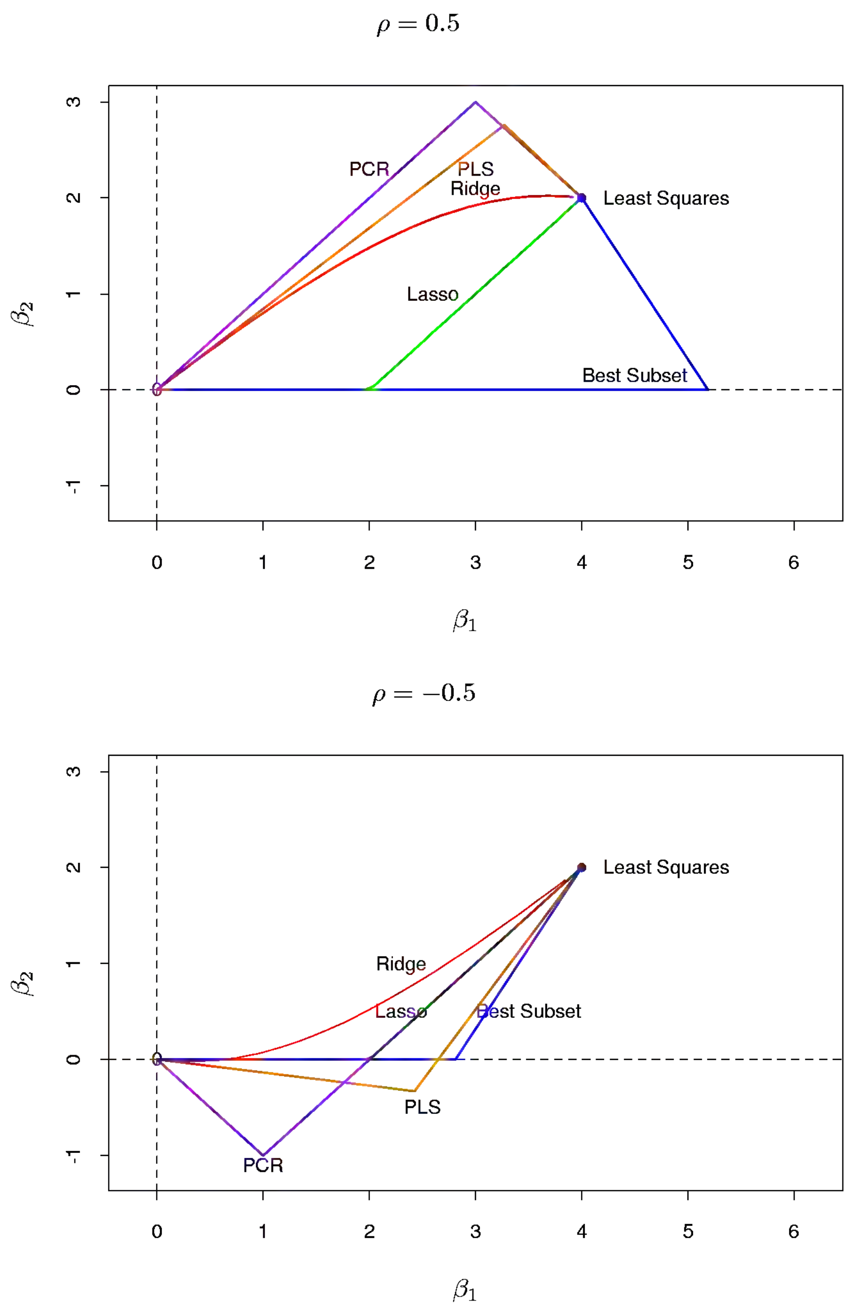

FIGURE 3.11. *Coefficient profiles from different methods for a simple problem: two inputs with correlation* ± 0.5*, and the true regression coefficients* $\beta = (4, 2)$*.*

shrinks the coefficients together until it finally converges to least squares. PLS and PCR show similar behavior to ridge, although are discrete and more extreme. Best subset overshoots the solution and then backtracks. The behavior of the lasso is intermediate to the other methods. When the correlation is negative (lower panel), again PLS and PCR roughly track the ridge path, while all of the methods are more similar to one another.

We can gain further insight into these methods by taking a Bayesian point of view. Suppose we adopt a Gaussian prior as discussed earlier on page 60:

$$\beta \sim N(0, \tau I). \tag{3.56}$$

We saw that the ridge regression estimate $\hat{\beta}^{\text{ridge}}$ is the posterior mode (and mean). This reveals an interesting point: the prior (3.56) is a function only of the length of β and not its direction. Therefore, ridge regression's shrinkage of low-variance directions is not due to a prior distribution that favors high-variance directions; this shrinkage achieves variance reduction to account for the correlation present in the input matrix $\mathbf{X}$.

Recall that ridge regression shrinks all directions, but shrinks low-variance directions more. Principal components regression leaves M high-variance directions alone, and discards the rest. Hence its implicit prior puts more probability on M high-variance directions and zero probability on $p - M$ low-variance directions. Interestingly, it can be shown that partial least squares also tends to shrink the low-variance directions, but can actually inflate some of the higher variance directions. This can make PLS a little unstable, and cause it to have slightly higher prediction error compared to ridge regression. A full study is given in Frank and Friedman (1993). These authors conclude that for minimizing prediction error, ridge regression is generally preferable to variable subset selection, principal components regression and partial least squares. However the improvement over the latter two methods was only slight.

To summarize so far, PLS, PCR and ridge regression tend to behave similarly. Ridge regression may be preferred because it shrinks smoothly, rather than in discrete steps.

We now focus on ridge regression, the lasso and subset regression. In the case of an orthonormal input matrix $\mathbf{X}$ the three procedures have explicit solutions. Each method applies a simple transformation to the least squares estimate $\hat{\beta}_j$, as detailed in Table 3.4. Ridge regression does a proportional shrinkage. Best subset keeps the M largest coefficients, while lasso translates each by a constant factor, truncating at zero. This is called "soft thresholding," and is used in the context of wavelet-based smoothing in Section 5.9. Note that the threshold parameter γ in the lasso formula is a one-to-one transformation of the bound t appearing in the definition (3.51).

Back to the nonorthogonal case; some pictures help understand their relationship. Figure 3.12 depicts the lasso (left) and ridge regression (right)

TABLE 3.4. *Estimators of β_j in the case of orthonormal columns of $\mathbf{X}$. λ, M and γ are constants chosen by the corresponding techniques.* sign *denotes the sign of its argument (± 1), and x_+ denotes "positive part" of x.*

Estimator	Formula
Best subset (size M)	$\hat{\beta}_j \cdot I(\mathrm{rank}(\lvert\hat{\beta}_j\rvert) \le M)$
Ridge	$\hat{\beta}_j/(1+\lambda)$
Lasso	$\mathrm{sign}(\hat{\beta}_j)(\lvert\hat{\beta}_j\rvert - \gamma)_+$

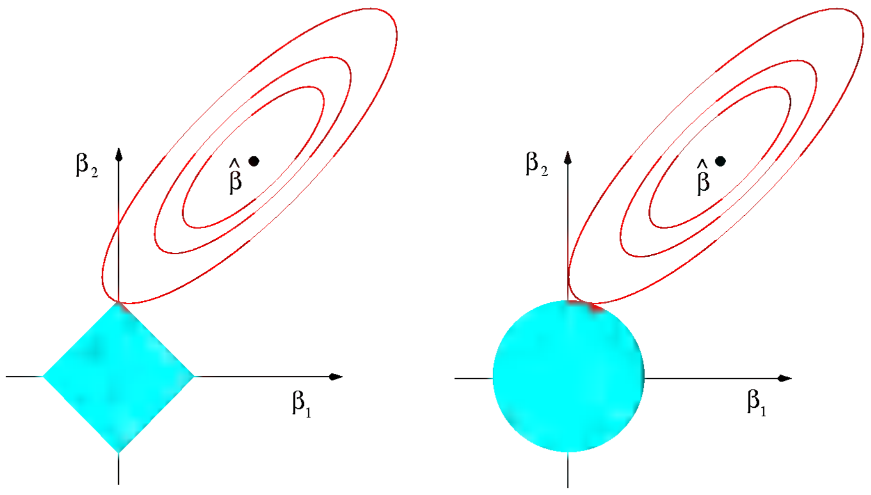

FIGURE 3.12. *Estimation picture for the lasso (left) and ridge regression (right). Shown are contours of the error and constraint functions. The solid blue areas are the constraint regions $|\beta_1| + |\beta_2| \le t$ and $\beta_1^2 + \beta_2^2 \le t^2$, respectively, while the red ellipses are the contours of the least squares error function.*

With $\mathbf{\Sigma}$ replaced by the estimate $\mathbf{Y}^T\mathbf{Y}/N$, one can show (Exercise 3.19) that the solution is given by a CCA of $\mathbf{Y}$ and $\mathbf{X}$:

$$\hat{\mathbf{B}}^{\text{rr}}(m) = \hat{\mathbf{B}}\mathbf{U}_m\mathbf{U}_m^-, \tag{3.62}$$

where $\mathbf{U}_m$ is the $K \times m$ sub-matrix of $\mathbf{U}$ consisting of the first m columns, and $\mathbf{U}$ is the $K \times M$ matrix of *left* canonical vectors $u_1, u_2, \dots, u_M$. $\mathbf{U}_m^-$ is its generalized inverse. Writing the solution as

$$\hat{\mathbf{B}}^{\text{rr}}(M) = (\mathbf{X}^T\mathbf{X})^{-1}\mathbf{X}^T(\mathbf{Y}\mathbf{U}_m)\mathbf{U}_m^-, \tag{3.63}$$

we see that reduced-rank regression performs a linear regression on the pooled response matrix $\mathbf{Y}\mathbf{U}_m$, and then maps the coefficients (and hence the fits as well) back to the original response space. The reduced-rank fits are given by

$$\begin{aligned}\hat{\mathbf{Y}}^{\text{rr}}(m) &= \mathbf{X}(\mathbf{X}^T\mathbf{X})^{-1}\mathbf{X}^T\mathbf{Y}\mathbf{U}_m\mathbf{U}_m^- \\ &= \mathbf{H}\mathbf{Y}\mathbf{P}_m,\end{aligned} \tag{3.64}$$

where $\mathbf{H}$ is the usual linear regression projection operator, and $\mathbf{P}_m$ is the rank-m CCA response projection operator. Although a better estimate of $\mathbf{\Sigma}$ would be $(\mathbf{Y}-\mathbf{X}\hat{\mathbf{B}})^T(\mathbf{Y}-\mathbf{X}\hat{\mathbf{B}})/(N-pK)$, one can show that the solution remains the same (Exercise 3.20).

Reduced-rank regression borrows strength among responses by truncating the CCA. Breiman and Friedman (1997) explored with some success shrinkage of the canonical variates between $\mathbf{X}$ and $\mathbf{Y}$, a smooth version of *reduced rank* regression. Their proposal has the form (compare (3.62))

$$\hat{\mathbf{B}}^{\text{c+w}} = \hat{\mathbf{B}}\mathbf{U}\mathbf{\Lambda}\mathbf{U}^{-1}, \tag{3.65}$$

where $\mathbf{\Lambda}$ is a diagonal shrinkage matrix (the "c+w" stands for "Curds and Whey", the name they gave to their procedure). Based on optimal prediction in the population setting, they show that $\mathbf{\Lambda}$ has diagonal entries

$$\lambda_m = \frac{c_m^2}{c_m^2 + \frac{p}{N}(1 - c_m^2)}, \; m = 1, \dots, M, \tag{3.66}$$

where c_m is the mth canonical correlation coefficient. Note that as the ratio of the number of input variables to sample size p/N gets small, the shrinkage factors approach 1. Breiman and Friedman (1997) proposed modified versions of $\mathbf{D}$ based on training data and cross-validation, but the general form is the same. Here the fitted response has the form

$$\hat{\mathbf{Y}}^{\text{c+w}} = \mathbf{H}\mathbf{Y}\mathbf{S}^{\text{c+w}}, \tag{3.67}$$

where $\mathbf{S}^{\text{c+w}} = \mathbf{U}\mathbf{\Lambda}\mathbf{U}^{-1}$ is the response shrinkage operator.

Breiman and Friedman (1997) also suggested shrinking in both the Y space and X space. This leads to hybrid shrinkage models of the form

$$\hat{\mathbf{Y}}^{\text{ridge,c+w}} = \mathbf{A}_\lambda \mathbf{Y}\mathbf{S}^{\text{c+w}}, \tag{3.68}$$

where $\mathbf{A}_\lambda = \mathbf{X}(\mathbf{X}^T\mathbf{X}+\lambda\mathbf{I})^{-1}\mathbf{X}^T$ is the ridge regression shrinkage operator, as in (3.46) on page 62. Their paper and the discussions thereof contain many more details.

3.5 Computational Considerations

Least squares fitting is usually done via the Cholesky decomposition of the matrix $\mathbf{X}^T\mathbf{X}$ or a QR decomposition of $\mathbf{X}$. With N observations and p features, the Cholesky decomposition requires $p^3+Np^2/2$ operations, while the QR decomposition requires Np^2 operations. Depending on the relative size of N and p, the Cholesky can sometimes be faster; on the other hand, it can be less numerically stable (Lawson and Hansen, 1974). Computation of the lasso requires quadratic programming; see for example Murray et al. (1981).

Bibliographic Notes

Linear regression is discussed in many statistics books, for example Seber (1984), Weisberg (1980) and Mardia et al. (1979). Ridge regression was introduced by Hoerl and Kennard (1970), while the lasso was proposed by Tibshirani (1996). Partial least squares was introduced by Wold (1975). Comparisons of shrinkage methods may be found in Copas (1983) and Frank and Friedman (1993).

Exercises

Ex. 3.1 Show that the F statistic (3.13) for dropping a single coefficient from a model is equal to the square of the corresponding z-score (3.12).

Ex. 3.2 Given data on two variables X and Y, consider fitting a cubic polynomial regression model $f(X) = \sum_{j=0}^{3} \beta_j X^j$. In addition to plotting the fitted curve, you would like a 95% confidence band about the curve. Consider the following two approaches:

1. At each point x_0, form a 95% confidence interval for the linear function $a^T\beta = \sum_{j=0}^{3} \beta_j x_0^j$.

2. Form a 95% confidence set for β as in (3.15), which in turn generates confidence intervals for $f(x_0)$.

How do these approaches differ? Which band is likely to be wider? Conduct a small simulation experiment to compare the two methods.

Ex. 3.3

(a) Prove the Gauss-Markov theorem: the least squares estimate of a parameter $a^T\beta$ has variance no bigger than that of any other linear unbiased estimate of $a^T\beta$ (Section 3.2.2).

(b) The matrix inequality $\mathbf{B} \preceq \mathbf{A}$ holds if $\mathbf{A} - \mathbf{B}$ is positive semidefinite. Show that if $\hat{\mathbf{V}}$ is the variance-covariance matrix of the least squares estimate of β and $\tilde{\mathbf{V}}$ is the variance-covariance matrix of any other unbiased estimate, then $\hat{\mathbf{V}} \preceq \tilde{\mathbf{V}}$.

Ex. 3.4 Show how the vector of least squares coefficients can be obtained from a single pass of the Gram–Schmidt procedure (Algorithm 3.1). Represent your solution in terms of the QR decomposition of $\mathbf{X}$.

Ex. 3.5 Consider the ridge regression problem (3.41). Show that this problem is equivalent to the problem

$$\hat{\beta}^c = \underset{\beta^c}{\operatorname{argmin}}\Big\{\sum_{i=1}^{N}\big[y_i - \beta_0^c - \sum_{j=1}^{p}(x_{ij} - \bar{x}_j)\beta_j^c\big]^2 + \lambda\sum_{j=1}^{p}\beta_j^{c2}\Big\}. \qquad (3.69)$$

Give the correspondence between β^c and the original β in (3.41). Characterize the solution to this modified criterion.

Ex. 3.6 Show that the ridge regression estimate is the mean (and mode) of the posterior distribution, under a Gaussian prior $\beta \sim N(0, \tau\mathbf{I})$, and Gaussian sampling model $\mathbf{y} \sim N(\mathbf{X}\beta, \sigma^2\mathbf{I})$. Find the relationship between the regularization parameter λ in the ridge formula, and the variances τ and σ^2.

Ex. 3.7 Assume $y_i \sim N(\beta_0 + x_i^T\beta, \sigma^2), i = 1, 2, \dots, N$, and the parameters β_j are each distributed as $N(0, \tau^2)$, independently of one another. Assuming σ^2 and τ^2 are known, show that the (minus) log-posterior density of β is proportional to $\sum_{i=1}^N(y_i - \beta_0 - \sum_j x_{ij}\beta_j)^2 + \lambda\sum_{j=1}^p \beta_j^2$ where $\lambda = \sigma^2/\tau^2$.

Ex. 3.8 Consider the QR decomposition of the uncentered $N \times (p+1)$ matrix $\mathbf{X}$, and the SVD of the $N \times p$ centered matrix $\tilde{\mathbf{X}}$. Show that $\mathbf{Q}_2$ and $\mathbf{U}$ span the same subspace, where $\mathbf{Q}_2$ is the sub-matrix of $\mathbf{Q}$ with the first column removed. Under what circumstances will they be the same, up to sign flips?

Ex. 3.9 Show that the solution to the multivariate linear regression problem (3.39) is given by (3.38). What happens if the covariance matrices $\mathbf{\Sigma}_i$ are different for each observation?

Ex. 3.10 Show that the ridge regression estimates can be obtained by ordinary least squares regression on an augmented data set. We augment the centered matrix $\mathbf{X}$ with p additional rows $\sqrt{\lambda}\mathbf{I}$, and augment $\mathbf{y}$ with p zeros. By introducing artificial data having response value zero, the fitting procedure is forced to shrink the coefficients toward zero. This is related to the idea of *hints* due to Abu-Mostafa (1995), where model constraints are implemented by adding artificial data examples that satisfy them.

Ex. 3.11 Consider the lasso problem (3.51). Show that this problem is equivalent to the problem

$$\hat{\beta}^c = \underset{\beta^c}{\operatorname{argmin}}\Big\{\sum_{i=1}^{N}\big[y_i - \beta_0^c - \sum_{j=1}^{p}(x_{ij} - \bar{x}_j)\beta_j^c\big]^2 + \lambda\sum_{j=1}^{p}|\beta_j^c|\Big\}. \qquad (3.70)$$

Give the correspondence between β^c and the original β in (3.51). Characterize the solution to this modified criterion.

Ex. 3.12 Derive the expression (3.53), and show that $\hat{\beta}^{\text{pcr}}(p) = \hat{\beta}^{\text{ls}}$.

Ex. 3.13 Show that in the orthogonal case, PLS stops after $m = 1$ steps, because subsequent $\hat{\varphi}_{mj}$ in step 2 in Algorithm 3.2 are zero.

Ex. 3.14 Derive the entries in Table 3.4, the explicit forms for estimators in the orthogonal case.

Ex. 3.15 Repeat the analysis of Table 3.3 on the spam data discussed in Chapter 1.

Ex. 3.16 Read about conjugate gradient algorithms (Murray et al., 1981, for example) and establish a connection between these algorithms and partial least squares.

Ex. 3.17 Show that $\|\hat{\beta}^{\text{ridge}}\|$ increases as its tuning parameter $\lambda \to 0$. Does the same property hold for the lasso and partial least squares estimates? For the latter, consider the "tuning parameter" to be the successive steps in the algorithm.

Ex. 3.18 Consider the canonical-correlation problem (3.60). Show that the leading pair of canonical variates u_1 and v_1 solve the problem

$$\max_{\substack{u^T(\mathbf{Y}^T\mathbf{Y})u=1 \\ v^T(\mathbf{X}^T\mathbf{X})v=1}} u^T(\mathbf{Y}^T\mathbf{X})v, \qquad (3.71)$$

a generalized SVD problem. Show that the solution is given by $u_1 = (\mathbf{Y}^T\mathbf{Y})^{-\frac{1}{2}}u_1^*$, and $v_1 = (\mathbf{X}^T\mathbf{X})^{-\frac{1}{2}}v_1^*$, where u_1^* and v_1^* are the leading left and right singular vectors in

$$(\mathbf{Y}^T\mathbf{Y})^{-\frac{1}{2}}(\mathbf{Y}^T\mathbf{X})(\mathbf{X}^T\mathbf{X})^{-\frac{1}{2}} = \mathbf{U}^*\mathbf{D}^*\mathbf{V}^{*T}. \tag{3.72}$$

Show that the entire sequence $u_m,\ v_m,\ m = 1, \ldots, \min(K, p)$ is also given by (3.72).

Ex. 3.19 Show that the solution to the reduced-rank regression problem (3.61), with $\mathbf{\Sigma}$ estimated by $\mathbf{Y}^T\mathbf{Y}/N$, is given by (3.62). Hint: transform $\mathbf{Y}$ to $\mathbf{Y}^* = \mathbf{Y}\mathbf{\Sigma}^{-\frac{1}{2}}$, and solved in terms of the canonical vectors u_m^*. Show that $\mathbf{U}_m = \mathbf{\Sigma}^{-\frac{1}{2}}\mathbf{U}_m^*$, and a generalized inverse is $\mathbf{U}_m^- = \mathbf{U}_m^{*\,T}\mathbf{\Sigma}^{\frac{1}{2}}$.

Ex. 3.20 Show that the solution in Exercise 3.19 does not change if $\mathbf{\Sigma}$ is estimated by the more natural quantity $(\mathbf{Y} - \mathbf{X}\hat{\mathbf{B}})^T(\mathbf{Y} - \mathbf{X}\hat{\mathbf{B}})/(N - pK)$.

4 Linear Methods for Classification

4.1 Introduction

In this chapter we revisit the classification problem and focus on linear methods for classification. Since our predictor $G(x)$ takes values in a discrete set $\mathcal{G}$, we can always divide the input space into a collection of regions labeled according to the classification. We saw in Chapter 2 that the boundaries of these regions can be rough or smooth, depending on the prediction function. For an important class of procedures, these *decision boundaries* are linear; this is what we will mean by linear methods for classification.

There are several different ways in which linear decision boundaries can be found. In Chapter 2 we fit linear regression models to the class indicator variables, and classify to the largest fit. Suppose there are K classes, for convenience labelled $1, 2, \ldots, K$, and the fitted linear model for the kth indicator response variable is $\hat{f}_k(x) = \hat{\beta}_{k0} + \hat{\beta}_k^T x$. The decision boundary between class k and ℓ is that set of points for which $\hat{f}_k(x) = \hat{f}_\ell(x)$, that is, the set $\{x : (\hat{\beta}_{k0} - \hat{\beta}_{\ell 0}) + (\hat{\beta}_k - \hat{\beta}_\ell)^T x = 0\}$, an affine set or hyperplane* Since the same is true for any pair of classes, the input space is divided into regions of constant classification, with piecewise hyperplanar decision boundaries. This regression approach is a member of a class of methods that model *discriminant functions* $\delta_k(x)$ for each class, and then classify x to the class with the largest value for its discriminant function. Methods

*Strictly speaking, a hyperplane passes through the origin, while an affine set need not. We sometimes ignore the distinction and refer in general to hyperplanes.

that model the posterior probabilities $\Pr(G = k|X = x)$ are also in this class. Clearly, if either the $d_k(x)$ or $\Pr(G = k|X = x)$ are linear in x, then the decision boundaries will be linear.

Actually, all we require is that some monotone transformation of d_k or $\Pr(G = k|X = x)$ be linear for the decision boundaries to be linear. For example, if there are two classes, a popular model for the posterior probabilities is

$$\begin{aligned} \Pr(G = 1|X = x) &= \frac{\exp(\beta_0 + \beta^T x)}{1 + \exp(\beta_0 + \beta^T x)}, \\ \Pr(G = 2|X = x) &= \frac{1}{1 + \exp(\beta_0 + \beta^T x)}. \end{aligned} \tag{4.1}$$

Here the monotone transformation is the *logit* transformation: $\log[p/(1-p)]$, and in fact we see that

$$\log \frac{\Pr(G = 1|X = x)}{\Pr(G = 2|X = x)} = \beta_0 + \beta^T x. \tag{4.2}$$

The decision boundary is the set of points for which the *log-odds* are zero, and this is a hyperplane defined by $\{x|\beta_0 + \beta^T x = 0\}$. We discuss two very popular but different methods that result in linear log-odds or logits: linear discriminant analysis and linear logistic regression. Although they differ in their derivation, the essential difference between them is in the way the linear function is fit to the training data.

A more direct approach is to explicitly model the boundaries between the classes as linear. For a two-class problem in a p-dimensional input space, this amounts to modeling the decision boundary as a hyperplane—in other words, a normal vector and a cut-point. We will look at two methods that explicitly look for "separating hyperplanes." The first is the well-known *perceptron* model of Rosenblatt (1958), with an algorithm that finds a separating hyperplane in the training data, if one exists. The second method, due to Vapnik (1996), finds an *optimally separating hyperplane* if one exists, else finds a hyperplane that minimizes some measure of overlap in the training data. We treat the separable case here, and defer treatment of the nonseparable case to Chapter 12.

While this entire chapter is devoted to linear decision boundaries, there is considerable scope for generalization. For example, we can expand our variable set $X_1, \ldots, X_p$ by including their squares and cross-products $X_1^2, X_2^2, \ldots,$ $X_1X_2, \ldots$, thereby adding $p(p+1)/2$ additional variables. Linear functions in the augmented space map down to quadratic functions in the original space —hence linear decision boundaries to quadratic decision boundaries. Figure 4.1 illustrates the idea. The data are the same: the left plot uses linear decision boundaries in the two-dimensional space shown, while the right plot uses linear decision boundaries in the augmented five-dimensional space described above. This approach can be used with any basis transfor-

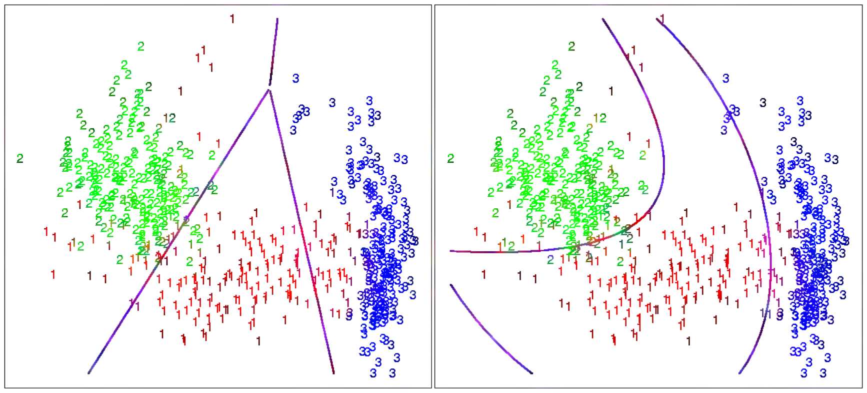

FIGURE 4.1. *The left plot shows some data from three classes, with linear decision boundaries found by linear discriminant analysis. The right plot shows quadratic decision boundaries. These were obtained by finding linear boundaries in the five-dimensional space $X_1, X_2, X_{12}, X_1^2, X_2^2$. Linear inequalities in this space are quadratic inequalities in the original space.*

mation $h(X)$ where $h : \mathbb{R}^p \mapsto \mathbb{R}^q$ with $q > p$, and will be explored in later chapters.

4.2 Linear Regression of an Indicator Matrix

Here each of the response categories are coded via an indicator variable. Thus if $\mathcal{G}$ has K classes, there will be K such indicators Y_k, $k = 1, \dots, K$, with $Y_k = 1$ if $G = k$ else 0. These are collected together in a vector $Y = (Y_1, \dots, Y_K)$, and the N training instances of these form an $N \times K$ *indicator response matrix* $\mathbf{Y}$. $\mathbf{Y}$ is a matrix of 0's and 1's, with each row having a single 1. We fit a linear regression model to each of the columns of $\mathbf{Y}$ simultaneously, and the fit is given by

$$\hat{\mathbf{Y}} = \mathbf{X}(\mathbf{X}^T\mathbf{X})^{-1}\mathbf{X}^T\mathbf{Y}. \tag{4.3}$$

Chapter 3 has more details on linear regression. Note that we have a coefficient vector for each response column $\mathbf{y}_k$, and hence a $(p+1) \times K$ coefficient matrix $\hat{\mathbf{B}} = (\mathbf{X}^T\mathbf{X})^{-1}\mathbf{X}^T\mathbf{Y}$. Here $\mathbf{X}$ is the model matrix with $p+1$ columns corresponding to the p inputs, and a leading column of 1's for the intercept.

A new observation with input x is classified as follows:

- compute the fitted output $\hat{f}(x) = [(1, x)\hat{\mathbf{B}}]^T$, a K vector;
- identify the largest component and classify accordingly:

$$\hat{G}(x) = \text{argmax}_{k \in \mathcal{G}} \hat{f}_k(x). \tag{4.4}$$

What is the rationale for this approach? One rather formal justification is to view the regression as an estimate of conditional expectation. For the random variable Y_k, $E(Y_k|X = x) = \Pr(G = k|X = x)$, so conditional expectation of each of the Y_k seems a sensible goal. The real issue is: how good an approximation to conditional expectation is the rather rigid linear regression model? Alternatively, are the $\hat{f}_k(x)$ reasonable estimates of the posterior probabilities $\Pr(G = k|X = x)$, and more importantly, does this matter?

It is quite straightforward to verify that $\sum_{k\in\mathcal{G}} \hat{f}_k(x) = 1$ for any x, as long as there is an intercept in the model (column of 1's in $\mathbf{X}$). However, the $\hat{f}_k(x)$ can be negative or greater than 1, and typically some are. This is a consequence of the rigid nature of linear regression, especially if we make predictions outside the hull of the training data. These violations in themselves do not guarantee that this approach will not work, and in fact on many problems it gives similar results to more standard linear methods for classification. If we allow linear regression onto basis expansions $h(X)$ of the inputs, this approach can lead to consistent estimates of the probabilities. As the size of the training set N grows bigger, we adaptively include more basis elements so that linear regression onto these basis functions approaches conditional expectation. We discuss such approaches in Chapter 5.

A more simplistic viewpoint is to construct *targets* t_k for each class, where t_k is the kth column of the $K \times K$ identity matrix. Our prediction problem is to try and reproduce the appropriate target for an observation. With the same coding as before, the response vector y_i (ith row of $\mathbf{Y}$) for observation i has the value $y_i = t_k$ if $g_i = k$. We might then fit the linear model by least squares:

$$\min_{\mathbf{B}} \sum_{i=1}^{N} ||y_i - [(1, x_i)\mathbf{B}]^T||^2. \tag{4.5}$$

The criterion is a sum-of-squared Euclidean distances of the fitted vectors from their targets. A new observation is classified by computing its fitted vector $\hat{f}(x)$ and classifying to the closest target:

$$\hat{G}(x) = \operatorname*{argmin}_k ||\hat{f}(x) - t_k||^2. \tag{4.6}$$

This is exactly the same as the previous approach:

- The sum-of-squared-norm criterion is exactly the criterion for multiple response linear regression, just viewed slightly differently. Since a squared norm is itself a sum of squares, the components decouple and can be rearranged as a separate linear model for each element. Note that this is only possible because there is nothing in the model that binds the different responses together.

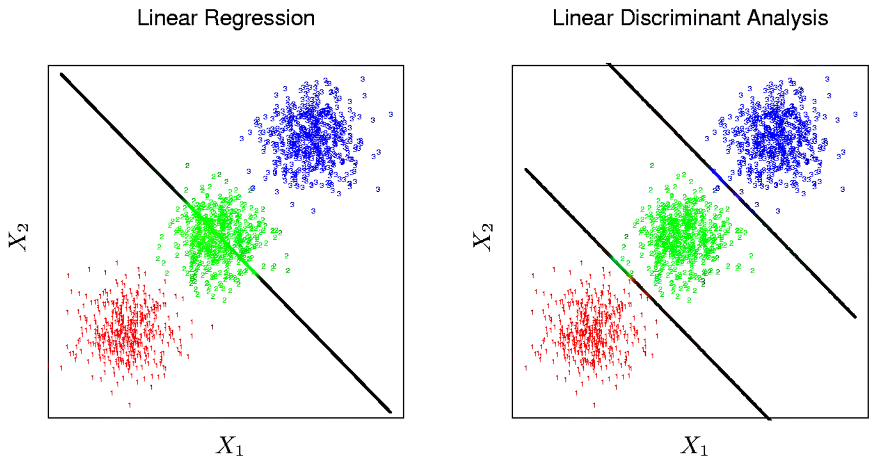

FIGURE 4.2. *The data come from three classes in* $\mathbb{R}^2$ *and are easily separated by linear decision boundaries. The right plot shows the boundaries found by linear discriminant analysis. The left plot shows the boundaries found by linear regression of the indicator response variables. The middle class is completely masked (never dominates).*

- The closest target classification rule (4.6) is easily seen to be exactly the same as the maximum fitted component criterion (4.4), but does require that the fitted values sum to 1.

There is a serious problem with the regression approach when the number of classes $K \geq 3$, especially prevalent when K is large. Because of the rigid nature of the regression model, classes can be *masked* by others. Figure 4.2 illustrates an extreme situation when $K = 3$. The three classes are perfectly separated by linear decision boundaries, yet linear regression misses the middle class completely.

In Figure 4.3 we have projected the data onto the line joining the three centroids (there is no information in the orthogonal direction in this case), and we have included and coded the three response variables Y_1, Y_2 and Y_3. The three regression lines (left panel) are included, and we see that the line corresponding to the middle class is horizontal and its fitted values are never dominant! Thus, observations from class 2 are classified either as class 1 or class 3. The right panel uses quadratic regression rather than linear regression. For this simple example a quadratic rather than linear fit (for the middle class at least) would solve the problem. However, it can be seen that if there were four rather than three classes lined up like this, a quadratic would not come down fast enough, and a cubic would be needed as well. A loose but general rule is that if $K \geq 3$ classes are lined up, polynomial terms up to degree $K - 1$ might be needed to resolve them. Note also that these are polynomials along the derived direction

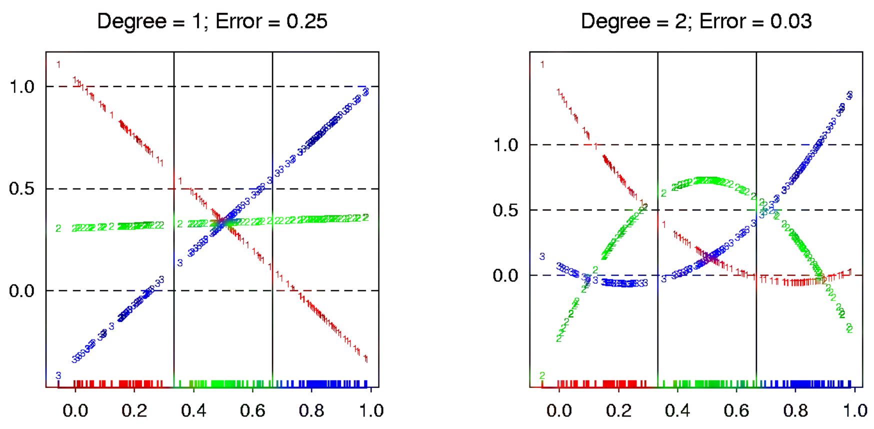

FIGURE 4.3. *The effects of masking on linear regression in* $\mathbb{R}$ *for a three-class problem. The* rug plot *at the base indicates the positions and class membership of each observation. The three curves in each panel are the fitted regressions to the three-class indicator variables; for example, for the red class,* y_{red} *is* 1 *for the red observations, and* 0 *for the green and blue. The fits are linear and quadratic polynomials. Above each plot is the training error rate. The Bayes error rate is* 0.025 *for this problem, as is the LDA error rate.*

passing through the centroids, which can have arbitrary orientation. So in p-dimensional input space, one would need general polynomial terms and cross-products of total degree $K-1$, $O(p^{K-1})$ terms in all, to resolve such worst-case scenarios.

The example is extreme, but for large K and small p such maskings naturally occur. As a more realistic illustration, Figure 4.4 is a projection of the training data for a vowel recognition problem onto an informative two-dimensional subspace. There are $K = 11$ classes in $p = 10$ dimensions. This is a difficult classification problem, and the best methods achieve around 40% errors on the test data. The main point here is summarized in Table 4.1; linear regression has an error rate of 67%, while a close relative, linear discriminant analysis, has an error rate of 56%. It seems that masking has hurt in this case. While all the other methods in this chapter are based on linear functions of x as well, they use them in such a way that avoids this masking problem.

4.3 Linear Discriminant Analysis

Decision theory for classification (Section 2.4) tells us that we need to know the class posteriors $\Pr(G|X)$ for optimal classification. Suppose $f_k(x)$ is the class-conditional density of X in class $G = k$, and let π_k be the prior probability of class k, with $\sum_{k=1}^{K} \pi_k = 1$. A simple application of Bayes

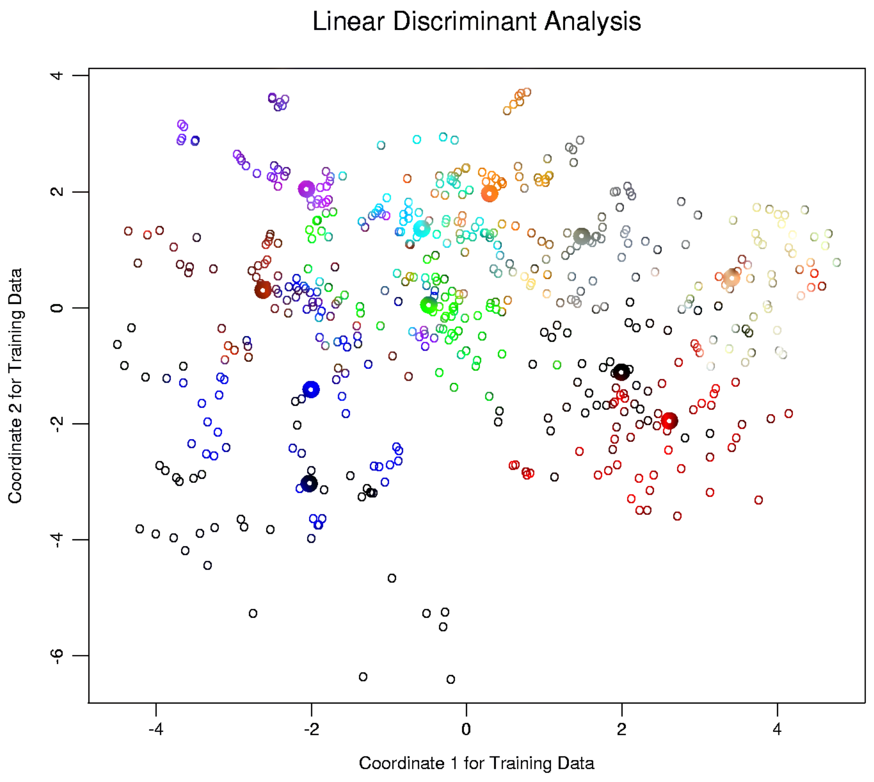

FIGURE 4.4. *A two-dimensional plot of the vowel training data. There are eleven classes with $X \in \mathbb{R}^{10}$, and this is the best view in terms of a LDA model (Section 4.3.3). The heavy circles are the projected mean vectors for each class. The class overlap is considerable.*

TABLE 4.1. *Training and test error rates using a variety of linear techniques on the vowel data. There are eleven classes in ten dimensions, of which three account for* 90% *of the variance (via a principal components analysis). We see that linear regression is hurt by masking, increasing the test and training error by over* 10%.

Technique	Error Rates	
	Training	Test
Linear regression	0.48	0.67
Linear discriminant analysis	0.32	0.56
Quadratic discriminant analysis	0.01	0.53
Logistic regression	0.22	0.51

theorem gives us

$$\Pr(G = k|X = x) = \frac{f_k(x)\pi_k}{\sum_{\ell=1}^K f_\ell(x)\pi_\ell}. \tag{4.7}$$

We see that in terms of ability to classify, having the $f_k(x)$ is almost equivalent to having the quantity $\Pr(G = k|X = x)$.

Many techniques are based on models for the class densities:

- linear and quadratic discriminant analysis use Gaussian densities;
- more flexible mixtures of Gaussians allow for nonlinear decision boundaries (Section 6.8);
- general nonparametric density estimates for each class density allow the most flexibility (Section 6.6.2);
- *Naive Bayes* models are a variant of the previous case, and assume that each of the class densities are products of marginal densities; that is, they assume that the inputs are conditionally independent in each class (Section 6.6.3).

Suppose that we model each class density as multivariate Gaussian

$$f_k(x) = \frac{1}{(2\pi)^{p/2}|\mathbf{\Sigma}_k|^{1/2}} e^{-\frac{1}{2}(x-\mu_k)^T \mathbf{\Sigma}_k^{-1}(x-\mu_k)}. \tag{4.8}$$

Linear discriminant analysis (LDA) arises in the special case when we assume that the classes have a common covariance matrix $\mathbf{\Sigma}_k = \mathbf{\Sigma}\ \forall k$. In comparing two classes k and ℓ, it is sufficient to look at the log-ratio, and we see that

$$\begin{aligned}\log \frac{\Pr(G = k|X = x)}{\Pr(G = \ell|X = x)} &= \log \frac{f_k(x)}{f_\ell(x)} + \log \frac{\pi_k}{\pi_\ell} \\ &= \log \frac{\pi_k}{\pi_\ell} - \frac{1}{2}(\mu_k + \mu_\ell)^T \mathbf{\Sigma}^{-1}(\mu_k - \mu_\ell) \\ &\quad + x^T \mathbf{\Sigma}^{-1}(\mu_k - \mu_\ell),\end{aligned} \tag{4.9}$$

an equation linear in x. The equal covariance matrices cause the normalization factors to cancel, as well as the quadratic part in the exponents. This linear log-odds function implies that the decision boundary between classes k and ℓ—the set where $\Pr(G = k|X = x) = \Pr(G = \ell|X = x)$—is linear in x; in p dimensions a hyperplane. This is of course true for any pair of classes, so all the decision boundaries are linear. If we divide $\mathbb{R}^p$ into regions that are classified as class 1, class 2, etc., these regions will be separated by hyperplanes. Figure 4.5 (left panel) shows an idealized example with three classes and $p = 2$. Here the data do arise from three Gaussian distributions with a common covariance matrix. We have included in the

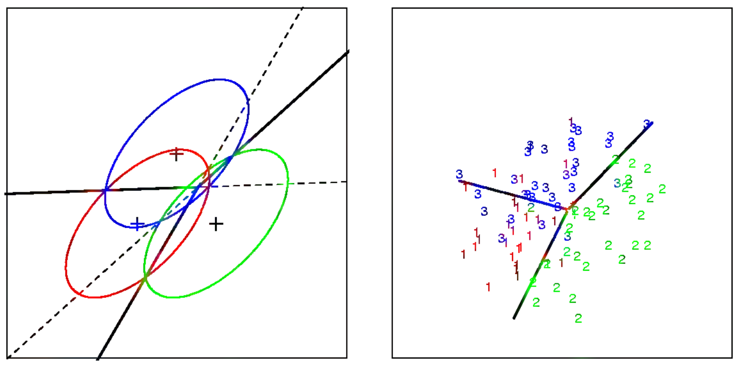

FIGURE 4.5. *The left panel shows three Gaussian distributions, with the same covariance and different means. Included are the contours of constant density enclosing 95% of the probability in each case. The Bayes decision boundaries between each pair of classes are shown (broken straight lines), and the Bayes decision boundaries separating all three classes are the thicker solid lines (a subset of the former). On the right we see a sample of* 30 *drawn from each Gaussian distribution, and the fitted LDA decision boundaries.*

figure the contours corresponding to 95% highest probability density, as well as the class centroids. Notice that the the decision boundaries are not the perpendicular bisectors of the line segments joining the centroids. This would be the case if the covariance $\mathbf{\Sigma}$ were spherical $\sigma^2\mathbf{I}$, and the class priors were equal.

From (4.9) we see that the *linear discriminant functions*

$$\delta_k(x) = x^T\mathbf{\Sigma}^{-1}\mu_k - \frac{1}{2}\mu_k^T\mathbf{\Sigma}^{-1}\mu_k + \log\pi_k \tag{4.10}$$

are an equivalent description of the decision rule, with $G(x) = \text{argmax}_k\delta_k(x)$.

In practice we do not know the parameters of the Gaussian distributions, and will need to estimate them using our training data:

- $\hat{\pi}_k = N_k/N$, where N_k is the number of class-k observations;
- $\hat{\mu}_k = \sum_{g_i=k} x_i/N_k$;
- $\hat{\mathbf{\Sigma}} = \sum_{k=1}^K \sum_{g_i=k}(x_i - \mu_k)(x_i - \mu_k)^T/(N - K)$.

Figure 4.5(right panel) shows the estimated decision boundaries based on a sample of size 30 each from three Gaussian distributions. Figure 4.1 on page 81 is another example, but here the classes are not Gaussian.

With two classes there is a simple correspondence between linear discriminant analysis and classification by linear least squares, as in (4.5).

The LDA rule classifies to class 2 if

$$x^T\hat{\mathbf{\Sigma}}^{-1}(\hat{\mu}_2-\hat{\mu}_1) > \frac{1}{2}\hat{\mu}_2^T\hat{\mathbf{\Sigma}}\hat{\mu}_2 - \frac{1}{2}\hat{\mu}_1^T\hat{\mathbf{\Sigma}}\hat{\mu}_1 + \log(N_1/N) - \log(N_2/N), \tag{4.11}$$

and class 1 otherwise. Suppose we code the targets in the two classes as $+1$ and -1, respectively. It is easy to show that the coefficient vector from least squares is proportional to the LDA direction given in (4.11) (Exercise 4.2). [In fact, this correspondence occurs for any (distinct) coding of the targets; see Exercise 4.2]. However unless $N_1 = N_2$ the intercepts are different and hence the resulting decision rules are different.

Since this derivation of the LDA direction via least squares does not use a Gaussian assumption for the features, the applicability the LDA direction extends beyond the realm of Gaussian data. However the derivation of the particular intercept or cut-point given in (4.11) *does* require Gaussian data. Thus it makes sense to instead choose the cut-point that empirically minimizes training error for a given dataset. This is something we have found to work well in practice, but have not seen it mentioned in the literature.

With more than two classes, LDA is not the same as linear regression of the class indicator matrix, and it avoids the masking problems associated with that approach (Hastie et al., 1994). A correspondence between regression and LDA can be established through the notion of *optimal scoring*, discussed in Section 12.5.

Getting back to the general discriminant problem (4.8), if the $\mathbf{\Sigma}_k$ are not assumed to be equal, then the convenient cancellations in (4.9) do not occur; in particular the pieces quadratic in x remain. We then get *quadratic discriminant functions* (QDA),

$$\delta_k(x) = -\frac{1}{2}\log|\mathbf{\Sigma}_k| - \frac{1}{2}(x-\mu_k)^T\mathbf{\Sigma}_k^{-1}(x-\mu_k) + \log\pi_k. \tag{4.12}$$

The decision boundary between each pair of classes k and ℓ is described by a quadratic equation $\{x : \delta_k(x) = \delta_\ell(x)\}$.

Figure 4.6 shows an example (from Figure 4.1 on page 81) where the three classes are Gaussian mixtures (Section 6.8) and the decision boundaries are approximated by quadratic equations in x. Here we illustrate two popular ways of fitting these quadratic boundaries. The right plot uses QDA as described here, while the left plot uses LDA in the enlarged five-dimensional quadratic polynomial space. The differences are generally small; QDA is the preferred approach, with the LDA method a convenient substitute. [†]

[†]For this figure and many similar figures in the book we compute the decision boundaries by an exhaustive contouring method. We compute the decision rule on a fine lattice of points, and then use contouring algorithms to compute the boundaries.

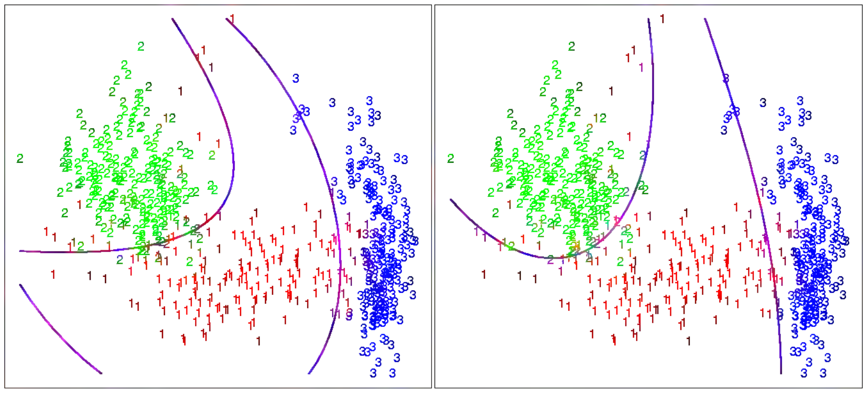

FIGURE 4.6. *Two methods for fitting quadratic boundaries. The left plot shows the quadratic decision boundaries for the data in Figure 4.1 (obtained using LDA in the five-dimensional space $x_1, x_2, x_{12}, x_1^2, x_2^2$). The right plot shows the quadratic decision boundaries found by QDA. The differences are small, as is usually the case.*

The estimates for QDA are similar to those for LDA, except that separate covariance matrices must be estimated for each class. When p is large this can mean a dramatic increase in parameters. Since the decision boundaries are functions of the parameters of the densities, counting the number of parameters must be done with care. For LDA, it seems that there $(K-1) \times (p+1)$ parameters, since we only need the differences $\delta_k(x) - \delta_K(x)$ between the discriminant functions where K is some pre-chosen class (here we have chosen the last), and each difference requires $p+1$ parameters.[‡] Likewise for QDA there will be $(K-1) \times p(p+2)/2$ parameters. Both LDA and QDA perform well on an amazingly large and diverse set of classification tasks. For example, in the STATLOG project (Michie et al., 1994) LDA was among the top 3 classifiers for 7 of the 22 datasets, QDA among the top 3 for 4 datasets, and one of the pair were in the top 3 for 10 datasets. Both techniques are widely used, and entire books are devoted to LDA. It seems that whatever exotic tools are the rage of the day, we should always have available these two simple tools. The question arises why LDA and QDA have such a good track record. The reason is not likely to be that the data are approximately Gaussian, and in addition for LDA that the covariances are approximately equal. More likely a reason is that the data can only support simple decision boundaries such as linear or quadratic, and the estimates provided via the Gaussian models are stable. This is a bias

[‡]Although we fit the covariance matrix $\hat{\mathbf{\Sigma}}$ to compute the LDA discriminant functions, a much reduced function of it is all that is required to estimate the $O(p)$ parameters needed to compute the decision boundaries.

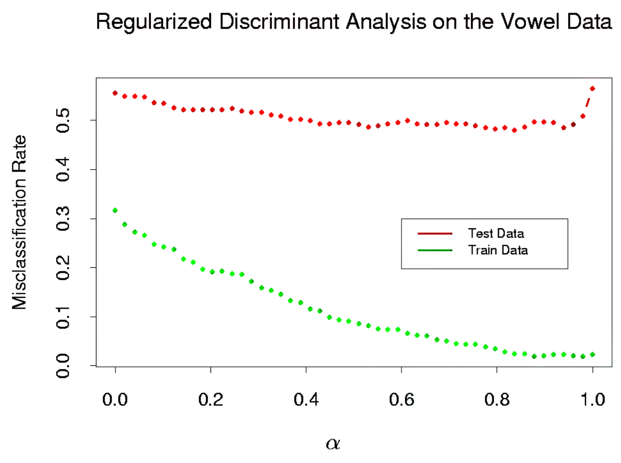

FIGURE 4.7. *Test and training errors for the vowel data, using regularized discriminant analysis with a series of values of $\alpha \in [0, 1]$. The optimum for the test data occurs around $\alpha = 0.9$, close to quadratic discriminant analysis.*

variance tradeoff—we can put up with the bias of a linear decision boundary because it can be estimated with much lower variance than more exotic alternatives. This argument is less believable for QDA, since it can have many parameters itself, although perhaps fewer than the non-parametric alternatives.

4.3.1 Regularized Discriminant Analysis

Friedman (1989) proposed a compromise between LDA and QDA, which allows one to shrink the separate covariances of QDA toward a common covariance as in LDA. These methods are very similar in flavor to ridge regression. The regularized covariance matrices have the form

$$\hat{\mathbf{\Sigma}}_k(\alpha) = \alpha\hat{\mathbf{\Sigma}}_k + (1-\alpha)\hat{\mathbf{\Sigma}}, \tag{4.13}$$

where $\hat{\mathbf{\Sigma}}$ is the pooled covariance matrix as used in LDA. Here $\alpha \in [0, 1]$ allows a continuum of models between LDA and QDA, and needs to be specified. In practice α can be chosen based on the performance of the model on validation data, or by cross-validation.

Figure 4.7 shows the results of RDA applied to the vowel data. Both the training and test error improve with increasing α, although the test error increases sharply after $\alpha = 0.9$. The large discrepancy between the training and test error is partly due to the fact that there are many repeat measurements on a small number of individuals, different in the training and test set.

Similar modifications allow $\hat{\mathbf{\Sigma}}$ itself to be shrunk toward the scalar covariance,

$$\hat{\mathbf{\Sigma}}(\gamma) = \gamma\hat{\mathbf{\Sigma}} + (1-\gamma)\hat{\sigma}^2\mathbf{I} \tag{4.14}$$

for $\gamma \in [0,1]$. Replacing $\hat{\mathbf{\Sigma}}$ in (4.13) by $\hat{\mathbf{\Sigma}}(\gamma)$ leads to a a more general family of covariances $\hat{\mathbf{\Sigma}}(\alpha,\gamma)$ indexed by a pair of parameters.

In Chapter 12, we discuss other regularized versions of LDA, which are more suitable when the data arise from digitized analog signals and images. In these situations the features are high-dimensional and correlated, and the LDA coefficients can be regularized to be smooth or sparse in the original domain of the signal. This leads to better generalization and allows for easier interpretation of the coefficients.

4.3.2 Computations for LDA

As a lead-in to the next topic, we briefly digress on the computations required for LDA and especially QDA. Their computations are simplified by diagonalizing $\hat{\mathbf{\Sigma}}$ or $\hat{\mathbf{\Sigma}}_k$. For the latter, suppose we compute the eigendecomposition for each $\hat{\mathbf{\Sigma}}_k = \mathbf{U}_k\mathbf{D}_k\mathbf{U}_k^T$, where $\mathbf{U}_k$ is $p\times p$ orthonormal, and $\mathbf{D}_k$ a diagonal matrix of positive eigenvalues $d_{k\ell}$. Then the ingredients for $\delta_k(x)$ (4.12) are

- $(x-\hat{\mu}_k)^T\hat{\mathbf{\Sigma}}_k^{-1}(x-\hat{\mu}_k) = [\mathbf{U}_k^T(x-\mu_k)]^T\mathbf{D}_k^{-1}[\mathbf{U}_k^T(x-\mu_k)]$;
- $\log|\hat{\mathbf{\Sigma}}_k| = \sum_\ell \log d_{k\ell}$.

In light of the computational steps outlined above, the LDA classifier can be implemented by the following pair of steps:

- *Sphere* the data with respect to the common covariance estimate $\hat{\mathbf{\Sigma}}$: $X^* \leftarrow \mathbf{D}^{-\frac{1}{2}}\mathbf{U}^TX$, where $\hat{\mathbf{\Sigma}} = \mathbf{UDU}^T$. The common covariance estimate of X^* will now be the identity.
- Classify to the closest class centroid in the transformed space, modulo the effect of the class prior probabilities π_k.

4.3.3 Reduced-Rank Linear Discriminant Analysis

So far we have discussed LDA as a restricted Gaussian classifier. Part of its popularity is due to an additional restriction that allows us to view informative low-dimensional projections of the data.

The K centroids in p-dimensional input space span at most a $K-1$ dimensional subspace, and if p is much larger than K, this will be a considerable drop in dimension. Moreover, in locating the closest centroid, we can ignore distances orthogonal to this subspace, since they will contribute equally to each class. Thus we might just as well project the X^* onto this centroid-spanning subspace H_{K-1}, and make distance comparisons there. Thus there is a fundamental dimension reduction in LDA, namely that we need only consider the data in a subspace of dimension at most $K - 1$. If $K = 3$, for instance, this could allow us to view the data in a two-dimensional plot, color-coding the classes. In doing so we would not have relinquished any of the information needed for LDA classification.

What if $K > 3$? We might then ask for a $L < K-1$ dimensional subspace $H_L \subseteq H_{K-1}$ optimal for LDA in some sense. Fisher defined optimal to mean that the projected centroids were spread out as much as possible in terms of variance. This amounts to finding principal component subspaces of the centroids themselves (principal components are described briefly in Section 3.4.4, and in more detail in Section 14.5.1). Figure 4.4 shows such an optimal two-dimensional subspace for the vowel data. Here there are eleven classes, each a different vowel sound, in a ten-dimensional input space. The centroids require the full space in this case, since $K - 1 = p$, but we have shown an optimal two-dimensional subspace. The dimensions are ordered, so we can compute additional dimensions in sequence. Figure 4.8 shows four additional pairs of coordinates, also known as *canonical* or *discriminant* variables.

In summary then, finding the sequences of optimal subspaces for LDA involves the following steps:

- compute the $K \times p$ matrix of class centroids $\mathbf{M}$ and the common covariance matrix $\mathbf{W}$ (for *within-class* covariance);
- compute $\mathbf{M}^* = \mathbf{M}\mathbf{W}^{-\frac{1}{2}}$ using the eigen-decomposition of $\mathbf{W}$;
- compute $\mathbf{B}^*$, the covariance matrix of $\mathbf{M}^*$ ($\mathbf{B}$ for *between-class* covariance), and its eigen-decomposition $\mathbf{B}^* = \mathbf{V}^*\mathbf{D}_B\mathbf{V}^{*T}$. The columns v_ℓ^* of $\mathbf{V}^*$ in sequence from first to last define the coordinates of the optimal subspaces.

Combining all these operations the ℓth *discriminant variable* is given by $Z_\ell = v_\ell^T X$ with $v_\ell = \mathbf{W}^{-\frac{1}{2}} v_\ell^*$.

Fisher arrived at this decomposition via a different route, without referring to Gaussian distributions at all. He posed the problem:

Find the linear combination $Z = a^T X$ such that the between-class variance is maximized relative to the within-class variance.

Again, the between class variance is the variance of the class means of Z, and the within class variance is the pooled variance about the means. Figure 4.9 shows why this criterion makes sense. Although the direction joining the centroids separates the means as much as possible (i.e., maximizes the between-class variance), there is considerable overlap between the projected classes due to the nature of the covariances. By taking the

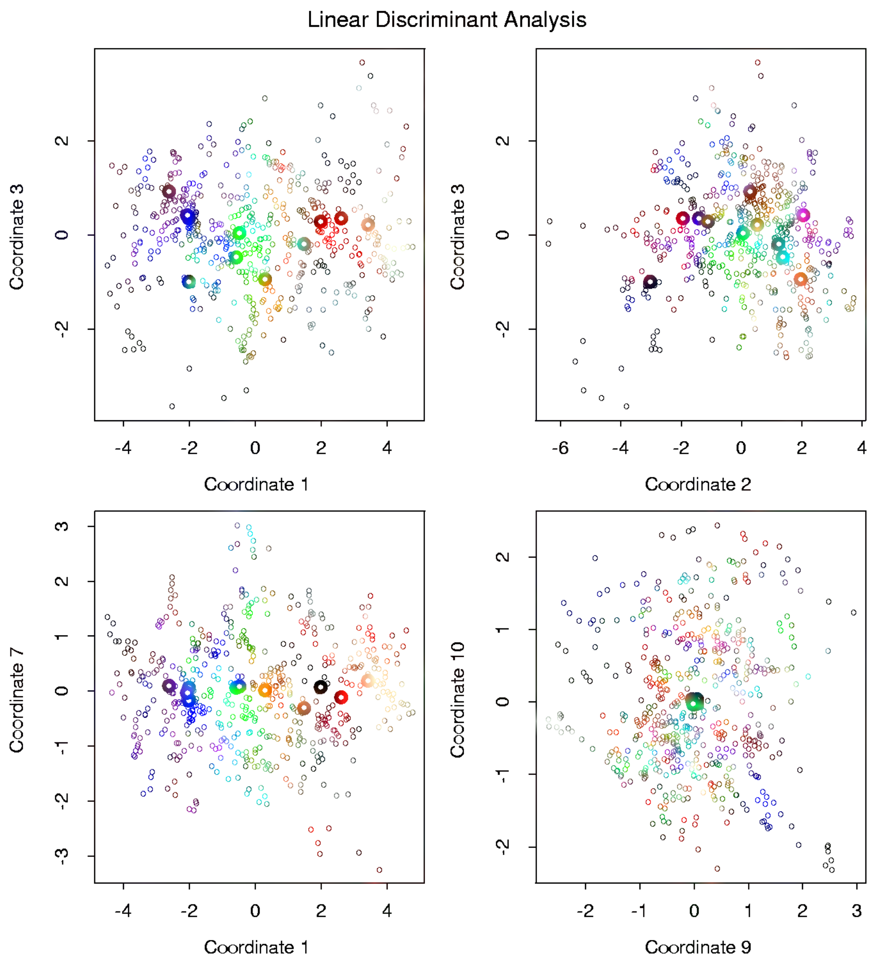

FIGURE 4.8. *Four projections onto pairs of canonical variates. Notice that as the rank of the canonical variates increases, the centroids become less spread out. In the lower right panel they appear to be superimposed, and the classes most confused.*

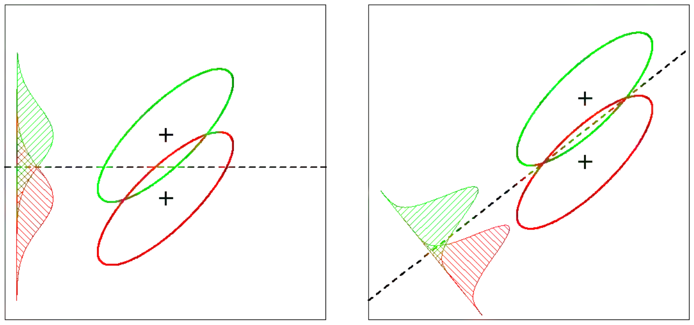

FIGURE 4.9. *Although the line joining the centroids defines the direction of greatest centroid spread, the projected data overlap because of the covariance (left panel). The discriminant direction minimizes this overlap for Gaussian data (right panel).*

covariance into account as well, a direction with minimum overlap can be found.

The between-class variance of Z is $a^T\mathbf{B}a$ and the within-class variance $a^T\mathbf{W}a$, where $\mathbf{W}$ is defined earlier, and $\mathbf{B}$ is the covariance matrix of the class centroid matrix $\mathbf{M}$. Note that $\mathbf{B}+\mathbf{W}=\mathbf{T}$, where $\mathbf{T}$ is the *total* covariance matrix of X, ignoring class information.

Fisher's problem therefore amounts to maximizing the *Rayleigh quotient*,

$$\max_a \frac{a^T\mathbf{B}a}{a^T\mathbf{W}a}, \tag{4.15}$$

or equivalently

$$\max_a a^T\mathbf{B}a \text{ subject to } a^T\mathbf{W}a = 1. \tag{4.16}$$

This is a generalized eigenvalue problem, with a given by the largest eigenvalue of $\mathbf{W}^{-1}\mathbf{B}$. It is not hard to show (Exercise 4.1) that the optimal a_1 is identical to v_1 defined above. Similarly one can find the next direction a_2, orthogonal in $\mathbf{W}$ to a_1, such that $a_2^T\mathbf{B}a_2/a_2^T\mathbf{W}a_2$ is maximized; the solution is $a_2 = v_2$, and so on. The a_ℓ are referred to as *discriminant coordinates*, not to be confused with discriminant functions. They are also referred to as *canonical variates*, since an alternative derivation of these results is through a canonical correlation analysis of the indicator response matrix $\mathbf{Y}$ on the predictor matrix $\mathbf{X}$. This line is pursued in Section 12.5.

To summarize the developments so far:

- Gaussian classification with common covariances leads to linear decision boundaries. Classification can be achieved by sphering the data with respect to $\mathbf{W}$, and classifying to the closest centroid (modulo $\log\pi_k$) in the sphered space.

- Since only the relative distances to the centroids count, one can confine the data to the subspace spanned by the centroids in the sphered space.
- This subspace can be further decomposed into successively optimal subspaces in term of centroid separation. This decomposition is identical to the decomposition due to Fisher.

The reduced subspaces have been motivated as a data reduction (for viewing) tool. Can they also be used for classification, and what is the rationale? Clearly they can, as in our original derivation; we simply limit the distance-to-centroid calculations to the chosen subspace. One can show that this is a Gaussian classification rule with the additional restriction that the centroids of the Gaussians lie in a L-dimensional subspace of $\mathbb{R}^p$. Fitting such a model by maximum likelihood, and then constructing the posterior probabilities using Bayes' theorem amounts to the classification rule described above (Exercise 4.8).

Gaussian classification dictates the $\log \pi_k$ correction factor in the distance calculation. The reason for this correction can be seen in Figure 4.9. The misclassification rate is based on the area of overlap between the two densities. If the π_k are equal (implicit in that figure), then the optimal cut-point is midway between the projected means. If the π_k are not equal, moving the cut-point toward the *smaller* class will improve the error rate. As mentioned earlier for two classes, one can derive the linear rule using LDA (or any other method), and then choose the cut-point to minimize misclassification error over the training data.

As an example of the benefit of the reduced-rank restriction, we return to the vowel data. There are 11 classes and 10 variables, and hence 10 possible dimensions for the classifier. We can compute the training and test error in each of these hierarchical subspaces; Figure 4.10 shows the results. Figure 4.11 shows the decision boundaries for the classifier based on the two-dimensional LDA solution.

There is a close connection between Fisher's reduced rank discriminant analysis and regression of an indicator response matrix. It turns out that LDA amounts to the regression followed by an eigen-decomposition of $\hat{\mathbf{Y}}^T\mathbf{Y}$. In the case of two classes, there is a single discriminant variable that is identical up to a scalar multiplication to either of the columns of $\hat{\mathbf{Y}}$. These connections are developed in Chapter 12. A related fact is that if one transforms the original predictors $\mathbf{X}$ to $\hat{\mathbf{Y}}$, then LDA using $\hat{\mathbf{Y}}$ is identical to LDA in the original space (Exercise 4.3).

4.4 Logistic Regression

The logistic regression model arises from the desire to model the posterior probabilities of the K classes via linear functions in x, while at the same

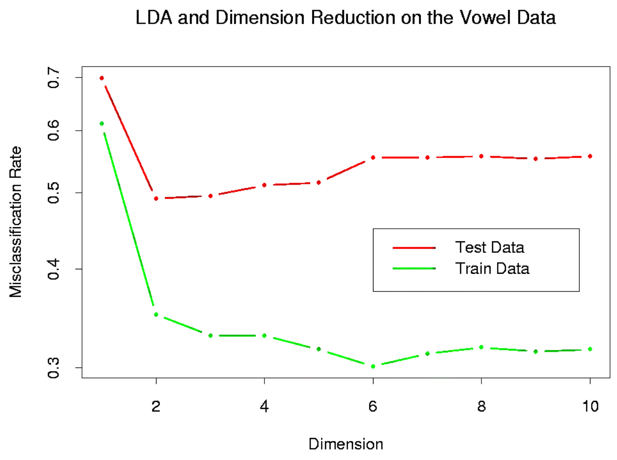

FIGURE 4.10. *Training and test error rates for the vowel data, as a function of the dimension of the discriminant subspace. In this case the best error rate is for dimension 2. Figure 4.11 shows the decision boundaries in this space.*

time ensuring that they sum to one and remain in $[0, 1]$. The model has the form

$$\begin{aligned}
\log \frac{\Pr(G=1|X=x)}{\Pr(G=K|X=x)} &= \beta_{10} + \beta_1^T x \\
\log \frac{\Pr(G=2|X=x)}{\Pr(G=K|X=x)} &= \beta_{20} + \beta_2^T x \\
&\vdots \\
\log \frac{\Pr(G=K-1|X=x)}{\Pr(G=K|X=x)} &= \beta_{(K-1)0} + \beta_{K-1}^T x.
\end{aligned} \tag{4.17}$$

The model is specified in terms of $K-1$ log-odds or logit transformations (reflecting the constraint that the probabilities sum to one). Although the model uses the last class as the denominator in the odds-ratios, the choice of denominator is arbitrary in that the estimates are equivariant under this choice. A simple calculation shows that

$$\begin{aligned}
\Pr(G=k|X=x) &= \frac{\exp(\beta_{k0} + \beta_k^T x)}{1 + \sum_{\ell=1}^{K-1} \exp(\beta_{\ell 0} + \beta_\ell^T x)}, \quad k = 1, \ldots, K-1, \\
\Pr(G=K|X=x) &= \frac{1}{1 + \sum_{\ell=1}^{K-1} \exp(\beta_{\ell 0} + \beta_\ell^T x)},
\end{aligned} \tag{4.18}$$

and they clearly sum to one. To emphasize the dependence on the entire parameter set $\theta = \{\beta_{10}, \beta_1, \ldots, \beta_{(K-1)0}, \beta_{K-1}\}$, we denote the probabilities $\Pr(G=k|X=x) = p_k(x;\theta)$.

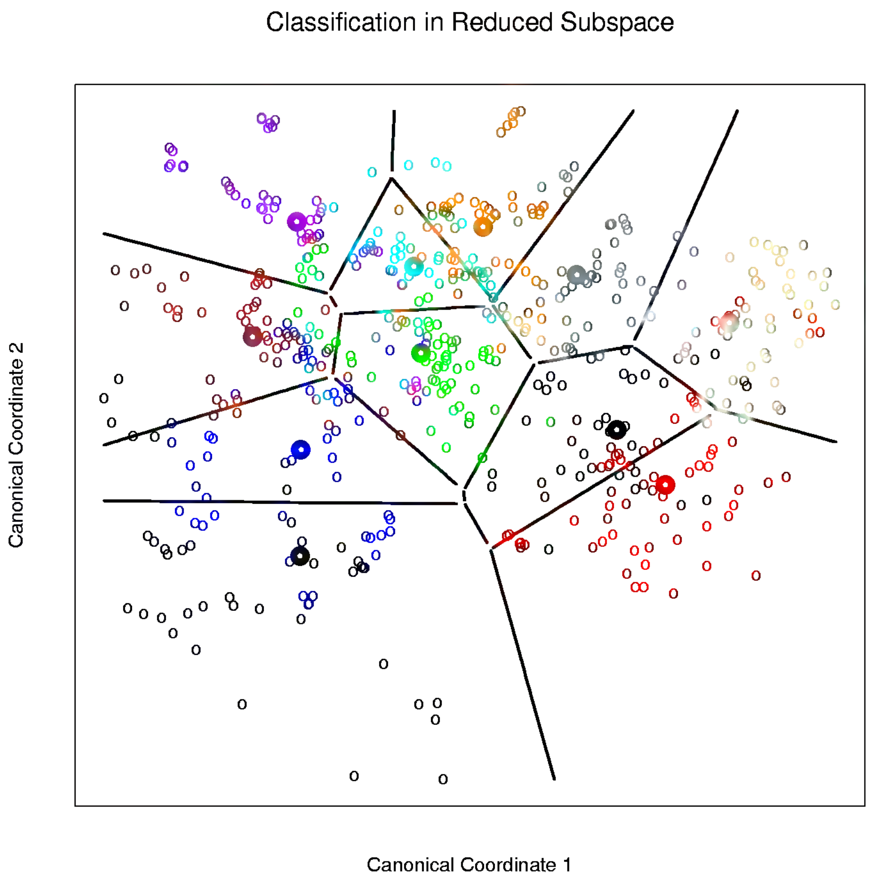

FIGURE 4.11. *Decision boundaries for the vowel training data, in the two-dimensional subspace spanned by the first two canonical variates. Note that in any higher-dimensional subspace, the decision boundaries are higher-dimensional affine planes, and could not be represented as lines.*

When $K = 2$, this model is especially simple, since there is only a single linear function. It is widely used in biostatistical applications where binary responses (two classes) occur quite frequently. For example, patients survive or die, have heart disease or not, or a condition is present or absent.

4.4.1 Fitting Logistic Regression Models

Logistic regression models are usually fit by maximum likelihood, using the conditional likelihood of G given X. Since $\Pr(G|X)$ completely specifies the conditional distribution, the *multinomial* distribution is appropriate. The log-likelihood for N observations is

$$\ell(\theta) = \sum_{i=1}^{N} \log p_{g_i}(x_i; \theta), \tag{4.19}$$

where $p_k(x_i; \theta) = \Pr(G = k|X = x_i; \theta)$.

We discuss in detail the two-class case, since the algorithms simplify considerably. It is convenient to code the two-class g_i via a $0/1$ response y_i, where $y_i = 1$ when $g_i = 1$, and $y_i = 0$ when $g_i = 2$. Let $p_1(x; \theta) = p(x; \theta)$, and $p_2(x; \theta) = 1 - p(x; \theta)$. The log-likelihood can be written

$$\begin{aligned} \ell(\beta) &= \sum_{i=1}^{N} \Big\{ y_i \log p(x_i; \beta) + (1 - y_i) \log(1 - p(x_i; \beta)) \Big\} \\ &= \sum_{i=1}^{N} \Big\{ y_i \beta^T x_i + \log(1 + e^{\beta^T x_i}) \Big\}. \end{aligned} \tag{4.20}$$

Here $\beta = \{\beta_{10}, \beta_1\}$, and we assume that the vector of inputs x_i includes the constant term 1 to accommodate the intercept.

To maximize the log-likelihood, we set its derivatives to zero. These *score* equations are

$$\frac{\partial \ell(\beta)}{\partial \beta} = \sum_{i=1}^{N} x_i (y_i - p(x_i; \beta)) = 0, \tag{4.21}$$

which are $p+1$ equations *nonlinear* in β. Notice that since the first component of x_i is 1, the first score equation specifies that $\sum_{i=1}^{N} y_i = \sum_{i=1}^{N} p(x_i; \beta)$; the *expected* number of class ones matches the observed number (and hence also class twos.)

To solve the score equations (4.21), we use the Newton-Raphson algorithm, which requires the second-derivative or Hessian matrix

$$\frac{\partial^2 \ell(\beta)}{\partial \beta \partial \beta^T} = -\sum_{i=1}^{N} x_i {x_i}^T p(x_i; \beta)(1 - p(x_i; \beta)). \tag{4.22}$$

Starting with β^{old}, a single Newton-Raphson update is

$$\beta^{\text{new}} = \beta^{\text{old}} - \left(\frac{\partial^2 \ell(\beta)}{\partial\beta\partial\beta^T}\right)^{-1} \frac{\partial \ell(\beta)}{\partial\beta}, \tag{4.23}$$

where the derivatives are evaluated at β^{old}.

It is convenient to write the score and Hessian in matrix notation. Let $\mathbf{y}$ denote the vector of y_i values, $\mathbf{X}$ the $N \times (p+1)$ matrix of x_i values, $\mathbf{p}$ the vector of fitted probabilities with ith element $p(x_i;\beta^{\text{old}})$ and $\mathbf{W}$ a $N \times N$ diagonal matrix of weights with ith diagonal element $p(x_i;\beta^{\text{old}})(1-p(x_i;\beta^{\text{old}}))$. Then $\frac{\partial\ell(\beta)}{\partial\beta} = \mathbf{X}^T(\mathbf{y}-\mathbf{p})$ and $\frac{\partial^2\ell(\beta)}{\partial\beta\partial\beta^T} = -\mathbf{X}^T\mathbf{W}\mathbf{X}$.

The Newton-Raphson step is thus

$$\begin{aligned}\beta^{\text{new}} &= \beta^{\text{old}} + (\mathbf{X}^T\mathbf{W}\mathbf{X})^{-1}\mathbf{X}^T(\mathbf{y}-\mathbf{p}) \\ &= (\mathbf{X}^T\mathbf{W}\mathbf{X})^{-1}\mathbf{X}^T\mathbf{W}\left(\mathbf{X}\beta^{\text{old}} + \mathbf{W}^{-1}(\mathbf{y}-\mathbf{p})\right) \\ &= (\mathbf{X}^T\mathbf{W}\mathbf{X})^{-1}\mathbf{X}^T\mathbf{W}\mathbf{z}. \end{aligned}\tag{4.24}$$

In the second and third line we have re-expressed the Newton-Raphson step as a weighted least squares step, with the response

$$\mathbf{z} = \mathbf{X}\beta^{\text{old}} + \mathbf{W}^{-1}(\mathbf{y}-\mathbf{p}), \tag{4.25}$$

sometimes known as the *adjusted response*. These equations get solved repeatedly, since at each iteration $\mathbf{p}$ changes, and hence so does $\mathbf{W}$ and $\mathbf{z}$. This algorithm is referred to as *iteratively reweighted least squares* or IRLS, since each iteration solves the weighted least squares problem:

$$\beta^{\text{new}} \leftarrow \arg\min_{\beta} (\mathbf{z}-\mathbf{X}\beta)^T\mathbf{W}(\mathbf{z}-\mathbf{X}\beta). \tag{4.26}$$

It seems that $\beta = 0$ is a good starting value for the iterative procedure, although convergence is never guaranteed. Typically the algorithm does converge, since the log-likelihood is concave, but overshooting can occur. In the rare cases that the log-likelihood decreases, step size halving will guarantee convergence.

For the multiclass case ($K \geq 3$) the Newton algorithm can also be expressed as an iteratively reweighted least squares algorithm, but with a *vector* of $K-1$ responses and a nondiagonal weight matrix per observation. The latter precludes any simplified algorithms, and in this case it is numerically more convenient to work with the expanded vector θ directly (Exercise 4.4).

Logistic regression models are used mostly as a data analysis and inference tool, where the goal is to understand the role of the input variables in *explaining* the outcome. Typically many models are fit in a search for a parsimonious model involving a subset of the variables, possibly with some interactions terms. The following example illustrates some of the issues involved.

TABLE 4.2. *Results from a logistic regression fit to the South African heart disease data.*

	Coefficient	Std. Error	Z Score
`(Intercept)`	−4.130	0.964	−4.285
`sbp`	0.006	0.006	1.023
`tobacco`	0.080	0.026	3.034
`ldl`	0.185	0.057	3.219
`famhist`	0.939	0.225	4.178
`obesity`	-0.035	0.029	−1.187
`alcohol`	0.001	0.004	0.136
`age`	0.043	0.010	4.184

4.4.2 Example: South African Heart Disease

Here we present an analysis of binary data to illustrate the traditional statistical use of the logistic regression model. The data in Figure 4.12 are a subset of the Coronary Risk-Factor Study (CORIS) baseline survey, carried out in three rural areas of the Western Cape, South Africa (Rousseauw et al., 1983). The aim of the study was to establish the intensity of ischemic heart disease risk factors in that high-incidence region. The data represent white males between 15 and 64, and the response variable is the presence or absence of myocardial infarction (MI) at the time of the survey (the overall prevalence of MI was 5.1% in this region). There are 160 cases in our data set, and a sample of 302 controls. These data are described in more detail in Hastie and Tibshirani (1987).

We fit this model by maximum likelihood, giving the results shown in Table 4.2.

This summary includes Z scores for each of the coefficients in the model (coefficients divided by their standard errors); a nonsignificant Z score suggests a coefficient can be dropped from the model. Each of these correspond formally to a test of the null hypothesis that the coefficient in question is zero, while all the others are not (also known as the Wald test). A Z score greater than approximately 2 in absolute value is significant at the 5% level.

There are some surprises in this table of coefficients, which must be interpreted with caution. Systolic blood pressure (`sbp`) is not significant! Nor is `obesity`, and its sign is negative. This confusion is a result of the correlation between the set of predictors. On their own, both `sbp` and `obesity` are significant, and with positive sign. However, in the presence of many other correlated variables, they are no longer needed (and can even get a negative sign).

At this stage the analyst might do some model selection; find a subset of the variables that are sufficient for explaining their joint effect on the prevalence of `chd`. One way to proceed by is to drop the least significant co-

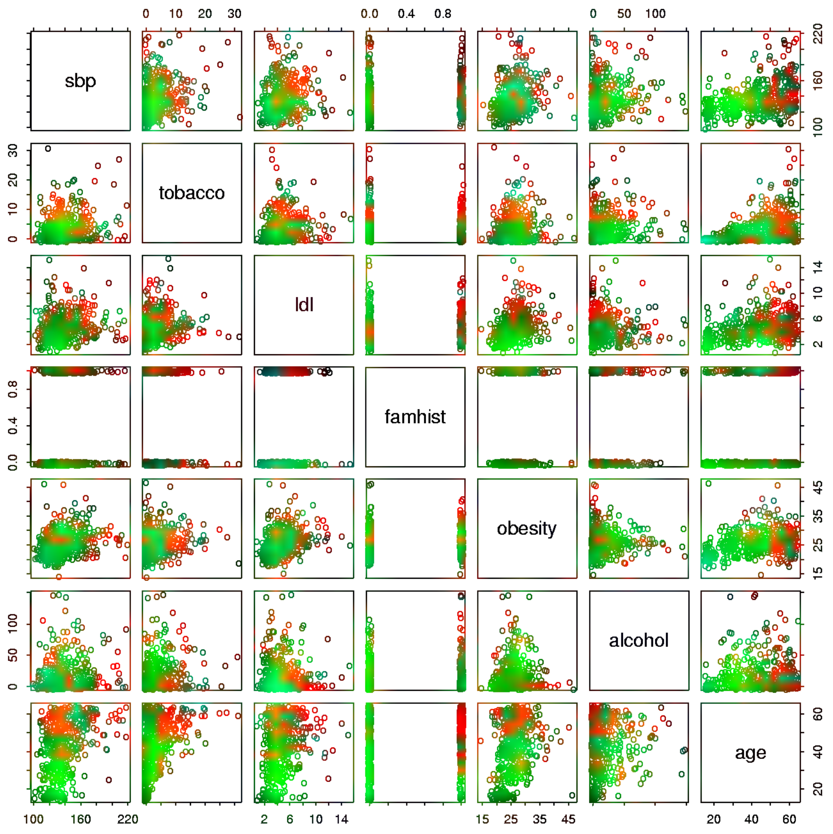

FIGURE 4.12. *A scatterplot matrix of the South African heart disease data. Each plot shows a pair of risk factors, and the cases and controls are color coded (red is a case). The variable* family history of heart disease (`famhist`) *is binary (yes or no).*

TABLE 4.3. *Results from stepwise logistic regression fit to South African Heart Disease data*

	Coefficient	Std. Error	Z score
`(Intercept)`	-4.204	0.498	-8.45
`tobacco`	0.081	0.026	3.16
`ldl`	0.168	0.054	3.09
`famhist`	0.924	0.223	4.14
`age`	0.044	0.010	4.52

efficient, and refit the model. This is done repeatedly until no further terms can be dropped from the model. This gave the model shown in Table 4.3.

A better but more time-consuming strategy is to refit each of the models with one variable removed, and then perform an *analysis of deviance* to decide which variable to exclude. The residual deviance of a fitted model is minus twice its log-likelihood, and the deviance between two models is the difference of their individual residual deviances (in analogy to sums-of-squares). This strategy gave the same final model as above.

How does one interpret a coefficient of 0.081 (Std. Error = 0.026) for `tobacco`, for example? Tobacco is measured in total lifetime usage in kilograms, with a median of $1.0kg$ for the controls and $4.1kg$ for the cases. Thus an increase of $1kg$ in lifetime tobacco usage accounts for an increase in the odds of coronary heart disease of $\exp(0.081) = 1.084$ or 8.4%. Incorporating the standard error we get an approximate 95% confidence interval of $\exp(0.081 \pm 2 \times 0.026) = (1.03, 1.14)$.

We return to these data in Chapter 5, where we see that some of the variables have nonlinear effects, and when modeled appropriately, are not excluded from the model.

4.4.3 Quadratic Approximations and Inference

The maximum-likelihood parameter estimates $\hat\beta$ satisfy a self-consistency relationship: they are the coefficients of a weighted least squares fit, where the responses are

$$z_i = x_i^T\hat\beta + \frac{(y_i - \hat p_i)}{\hat p_i(1-\hat p_i)}, \tag{4.27}$$

and the weights are $w_i = \hat p_i(1-\hat p_i)$, both depending on $\hat\beta$ itself. Apart from providing a convenient algorithm, this connection with least squares has more to offer:

- The weighted residual sum-of-squares is the familiar Pearson chi-square statistic

$$\sum_{i=1}^{N} \frac{(y_i - \hat{p}_i)^2}{\hat{p}_i(1-\hat{p}_i)}, \tag{4.28}$$

  a quadratic approximation to the deviance.

- Asymptotic likelihood theory says that if the model is correct, then $\hat{\beta}$ is consistent (i.e., converges to the *true* β).

- A central limit theorem then shows that the distribution of $\hat{\beta}$ converges to $N(\beta, (\mathbf{X}^T\mathbf{W}\mathbf{X})^{-1})$. This and other asymptotics can be derived directly from the weighted least squares fit by mimicking normal theory inference.

- Model building can be costly for logistic regression models, because each model fitted requires iteration. Popular shortcuts are the *Rao score test* which tests for inclusion of a term, and the *Wald test* which can be used to test for exclusion of a term. Neither of these require iterative fitting, and are based on the maximum-likelihood fit of the current model. It turns out that both of these amount to adding or dropping a term from the weighted least squares fit, using the *same* weights. Such computations can be done efficiently, without recomputing the entire weighted least squares fit.

Software implementations can take advantage of these connections. For example, the generalized linear modeling software in S-PLUS (which includes logistic regression as part of the binomial family of models) exploits them fully. GLM (generalized linear model) objects can be treated as linear model objects, and all the tools available for linear models can be applied automatically.

4.4.4 Logistic Regression or LDA?

In Section 4.3 we find that the log-posterior odds between class k and K are linear functions of x (4.9):

$$\begin{aligned}
\log\frac{\Pr(G=k|X=x)}{\Pr(G=K|X=x)} &= \log\frac{\pi_k}{\pi_K} - \frac{1}{2}(\mu_k+\mu_K)^T\mathbf{\Sigma}^{-1}(\mu_k-\mu_K) \\
&\quad + x^T\mathbf{\Sigma}^{-1}(\mu_k-\mu_K) \\
&= \alpha_{k0} + \alpha_k^T x.
\end{aligned} \tag{4.29}$$

This linearity is a consequence of the Gaussian assumption for the class densities, as well as the assumption of a common covariance matrix. The linear logistic model (4.17) by construction has linear logits:

$$\log \frac{\Pr(G = k|X = x)}{\Pr(G = K|X = x)} = \beta_{k0} + \beta_k^T x. \tag{4.30}$$

It seems that the models are the same. Although they have exactly the same form, the difference lies in the way the linear coefficients are estimated. The logistic regression model is more general, in that it makes less assumptions. We can write the *joint density* of X and G as

$$\Pr(X, G = k) = \Pr(X)\Pr(G = k|X), \tag{4.31}$$

where $\Pr(X)$ denotes the marginal density of the inputs X. For both LDA and logistic regression, the second term on the right has the logit-linear form

$$\Pr(G = k|X = x) = \frac{e^{\beta_{k0}+\beta_k^T x}}{1 + \sum_{\ell=1}^{K-1} e^{\beta_{\ell 0}+\beta_\ell^T x}}, \tag{4.32}$$

where we have again arbitrarily chosen the last class as the reference.

The logistic regression model leaves the marginal density of X as an arbitrary density function $\Pr(X)$, and fits the parameters of $\Pr(G|X)$ by maximizing the *conditional likelihood*—the multinomial likelihood with probabilities the $\Pr(G = k|X)$. Although $\Pr(X)$ is totally ignored, we can think of this marginal density as being estimated in a fully nonparametric and unrestricted fashion, using the empirical distribution function which places mass $1/N$ at each observation.

With LDA we fit the parameters by maximizing the full log-likelihood, based on the joint density

$$\Pr(X, G = k) = \phi(X; \mu_k, \mathbf{\Sigma})\pi_k, \tag{4.33}$$

where ϕ is the Gaussian density function. Standard normal theory leads easily to the estimates $\hat\mu_k$,$\hat{\mathbf{\Sigma}}$, and $\hat\pi_k$ given in Section 4.3. Since the linear parameters of the logistic form (4.29) are functions of the Gaussian parameters, we get their maximum-likelihood estimates by plugging in the corresponding estimates. However, unlike in the conditional case, the marginal density $\Pr(X)$ does play a role here. It is a mixture density

$$\Pr(X) = \sum_{k=1}^{K} \pi_k \phi(X; \mu_k, \mathbf{\Sigma}), \tag{4.34}$$

which also involves the parameters.

What role can this additional component/restriction play? By relying on the additional model assumptions, we have more information about the parameters, and hence can estimate them more efficiently (lower variance).

If in fact the true $f_k(x)$ are Gaussian, then in the worst case ignoring this marginal part of the likelihood constitutes a loss of efficiency of about 30% asymptotically in the error rate (Efron, 1975). Paraphrasing: with 30% more data, the conditional likelihood will do as well.

For example, observations far from the decision boundary (which are down-weighted by logistic regression) play a role in estimating the common covariance matrix. This is not all good news, because it also means that LDA is not robust to gross outliers.

From the mixture formulation, it is clear that even observations without class labels have information about the parameters. Often it is expensive to generate class labels, but unclassified observations come cheaply. By relying on strong model assumptions, such as here, we can use both types of information.

The marginal likelihood can be thought of as a regularizer, requiring in some sense that class densities be *visible* from this marginal view. For example, if the data in a two-class logistic regression model can be perfectly separated by a hyperplane, the maximum likelihood estimates of the parameters are undefined (i.e., infinite; see Exercise 4.5). The LDA coefficients for the same data will be well defined, since the marginal likelihood will not permit these degeneracies.

In practice these assumptions are never correct, and often some of the components of X are qualitative variables. It is generally felt that logistic regression is a safer, more robust bet than the LDA model, relying on fewer assumptions. It is our experience that the models give very similar results, even when LDA is used in inappropriately, such as with qualitative predictors.

4.5 Separating Hyperplanes

We have seen that linear discriminant analysis and logistic regression both estimate linear decision boundaries in similar but slightly different ways. For the rest of this chapter we describe separating hyperplane classifiers. These procedures construct linear decision boundaries that explicitly try to separate the data into different classes as well as possible. They provide the basis for support vector classifiers, discussed in Chapter 12. The mathematical level of this section is somewhat higher than that of the previous sections.

Figure 4.13 shows 20 data points in two classes in $\mathbb{R}^2$. These data can be separated by a linear boundary. Included in the figure (blue lines) are two of the infinitely many possible *separating hyperplanes*. The orange line is the least squares solution to the problem, obtained by regressing the $-1/1$ response Y on X (with intercept); the line is given by

$$\{x : \hat\beta_0 + \hat\beta_1 x_1 + \hat\beta_2 x_2 = 0\}. \tag{4.35}$$

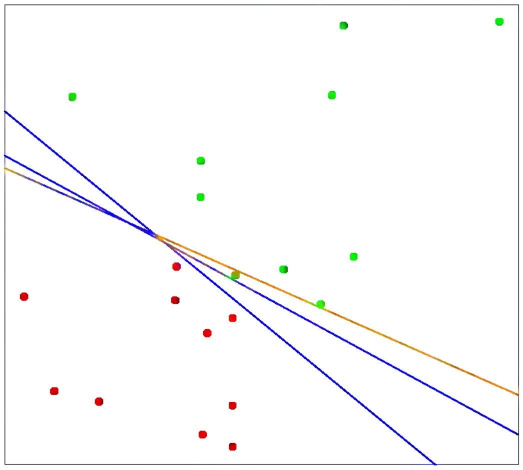

FIGURE 4.13. *A toy example with two classes separable by a hyperplane. The orange line is the least squares solution, which misclassifies one of the training points. Also shown are two blue separating hyperplanes found by the* perceptron learning algorithm *with different random starts.*

This least squares solution does not do a perfect job in separating the points, and makes one error. This is the same boundary found by LDA, in light of its equivalence with linear regression in the two-class case (Section 4.3 and Exercise 4.2).

Classifiers such as (4.35), that compute a linear combination of the input features and return the sign, were called *perceptrons* in the engineering literature in the late 1950s (Rosenblatt, 1958). Perceptrons set the foundations for the neural network models of the 1980s and 1990s.

Before we continue, let us digress slightly and review some vector algebra. Figure 4.14 depicts a hyperplane or *affine set* L defined by the equation $f(x) = \beta_0 + \beta^T x = 0$; since we are in $\mathbb{R}^2$ this is a line.

Here we list some properties:

1. For any two points x_1 and x_2 lying in L, $\beta^T(x_1 - x_2) = 0$, and hence $\beta^* = \beta/||\beta||$ is the vector normal to the surface of L.

2. For any point x_0 in L, $\beta^T x_0 = -\beta_0$.

3. The signed distance of any point x to L is given by

$$\begin{aligned} \beta^{*T}(x - x_0) &= \frac{1}{||\beta||}(\beta^T x + \beta_0) \\ &= \frac{1}{||f'(x)||} f(x). \end{aligned} \tag{4.36}$$

Hence $f(x)$ is proportional to the signed distance from x to the hyperplane defined by $f(x) = 0$.

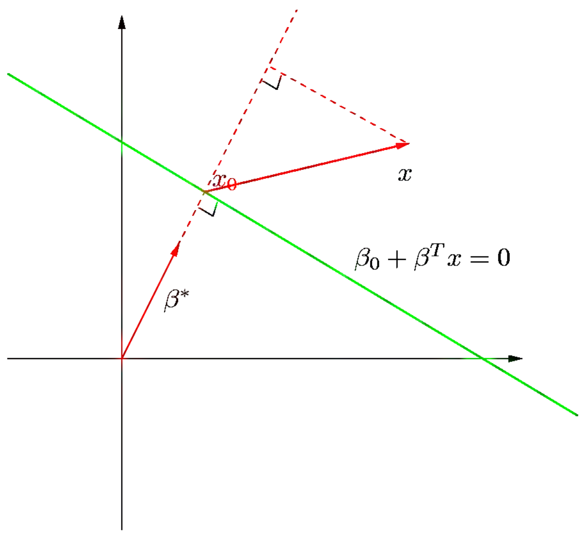

FIGURE 4.14. *The linear algebra of a hyperplane (affine set).*

4.5.1 Rosenblatt's Perceptron Learning Algorithm

The *perceptron learning algorithm* tries to find a separating hyperplane by minimizing the distance of misclassified points to the decision boundary. If a response $y_i = 1$ is misclassified, then $x_i^T\beta + \beta_0 < 0$, and the opposite for a misclassified response with $y_i = -1$. The goal is to minimize

$$D(\beta, \beta_0) = -\sum_{i \in \mathcal{M}} y_i(x_i^T\beta + \beta_0), \tag{4.37}$$

where $\mathcal{M}$ indexes the set of misclassified points. The quantity is non-negative and proportional to the distance of the misclassified points to the decision boundary defined by $\beta^T x + \beta_0 = 0$. The gradient (assuming $\mathcal{M}$ is fixed) is given by

$$\partial\frac{D(\beta, \beta_0)}{\partial\beta} = -\sum_{i \in \mathcal{M}} y_i x_i, \tag{4.38}$$

$$\partial\frac{D(\beta, \beta_0)}{\partial\beta_0} = -\sum_{i \in \mathcal{M}} y_i. \tag{4.39}$$

The algorithm in fact uses *stochastic gradient descent* to minimize this piecewise linear criterion. This means that rather than computing the sum of the gradient contributions of each observation followed by a step in the negative gradient direction, a step is taken after each observation is visited. Hence each of the misclassified observations are visited in some sequence, and the parameters β are updated via

$$\begin{pmatrix}\beta\\ \beta_0\end{pmatrix} \leftarrow \begin{pmatrix}\beta\\ \beta_0\end{pmatrix} + \rho\begin{pmatrix}y_i x_i\\ y_i\end{pmatrix}. \tag{4.40}$$

Here ρ is the learning rate, which in this case can be taken to be 1 without loss in generality. If the classes are linearly separable, it can be shown that the algorithm converges to a separating hyperplane in a finite number of steps (Exercise 4.6). Figure 4.13 shows two solutions to a toy problem, each started at a different random guess.

There are a number of problems with this algorithm, summarized in Ripley (1996):

- When the data are separable, there are many solutions, and which one is found depends on the starting values.
- The "finite" number of steps can be very large. The smaller the gap, the longer the time to find it.
- When the data are not separable, the algorithm will not converge, and cycles develop. The cycles can be long and therefore hard to detect.

The second problem can often be eliminated by seeking a hyperplane not in the original space, but in a much enlarged space obtained by creating many basis-function transformations of the original variables. This is analogous to driving the residuals in a polynomial regression problem down to zero by making the degree sufficiently large. Perfect separation cannot always be achieved: for example, if observations from two different classes share the same input. It may not be desirable either, since the resulting model is likely to be overfit and will not generalize well. We return to this point at the end of the next section.

A rather elegant solution to the first problem is to add additional constraints to the separating hyperplane.

4.5.2 Optimal Separating Hyperplanes

The *optimal separating hyperplane* separates the two classes and maximizes the distance to the closest point from either class (Vapnik, 1996). Not only does this provide a unique solution to the separating hyperplane problem, but by maximizing the margin between the two classes on the training data, this leads to better classification performance on test data.

We need to generalize criterion (4.37). Consider the optimization problem

$$\begin{gathered}\max_{\beta,\beta_0,||\beta||=1} C\\ \text{subject to } y_i(x_i^T\beta+\beta_0)\geq C,\ i=1,\ldots,N.\end{gathered} \tag{4.41}$$

The set of conditions ensure that all the points are at least a signed distance C from the decision boundary defined by β and β_0, and we seek the largest such C and associated parameters. We can get rid of the $||\beta|| = 1$ constraint by replacing the conditions with

$$\frac{1}{||\beta||} y_i(x_i^T\beta + \beta_0) \geq C, \tag{4.42}$$

(which redefines β_0) or equivalently

$$y_i(x_i^T\beta + \beta_0) \geq C||\beta||. \tag{4.43}$$

Since for any β and β_0 satisfying these inequalities, any positively scaled multiple satisfies them too, we can arbitrarily set $||\beta|| = 1/C$. Thus (4.41) is equivalent to

$$\begin{gathered} \min_{\beta,\beta_0} \frac{1}{2}||\beta||^2 \\ \text{subject to } y_i(x_i^T\beta + \beta_0) \geq 1,\ i = 1, \dots, N. \end{gathered} \tag{4.44}$$

In light of (4.36), the constraints define an empty slab or margin around the linear decision boundary of thickness $1/||\beta||$. Hence we choose β and β_0 to maximize its thickness. This is a convex optimization problem (quadratic criterion with linear inequality constraints). The Lagrange (primal) function is

$$L_P = \min_{\beta,\beta_0} \frac{1}{2}||\beta||^2 + \sum_{i=1}^N \alpha_i[y_i(x_i^T\beta + \beta_0) - 1]. \tag{4.45}$$

Setting the derivatives to zero, we obtain:

$$\beta = \sum_{i=1}^N \alpha_i y_i x_i, \tag{4.46}$$

$$0 = \sum_{i=1}^N \alpha_i y_i, \tag{4.47}$$

and substituting these in (4.45) we obtain the so-called Wolfe dual

$$L_D = \sum_{i=1}^N \alpha_i - \frac{1}{2}\sum_{i=1}^N\sum_{k=1}^N \alpha_i\alpha_k y_i y_k x_i^T x_k \quad \text{subject to} \quad \alpha_i \geq 0. \tag{4.48}$$

The solution is obtained by maximizing L_D in the positive orthant, a simpler convex optimization problem, for which standard software can be used.

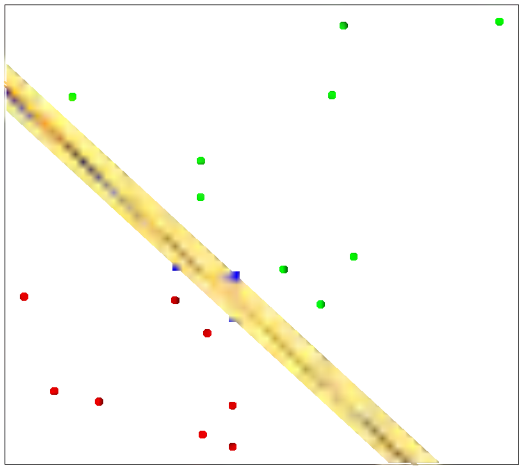

FIGURE 4.15. *The same data as in Figure 4.13. The shaded region delineates the maximum margin separating the two classes. There are three support points indicated, which lie on the boundary of the margin, and the optimal separating hyperplane (blue line) bisects the slab. Included in the figure is the boundary found using logistic regression (red line), which is very close to the optimal separating hyperplane (see Section 12.3.3).*

In addition the solution must satisfy the Karush–Kuhn–Tucker conditions, which include (4.46), (4.47), (4.48) and

$$\alpha_i[y_i(x_i^T\beta+\beta_0)-1]=0\ \forall i. \tag{4.49}$$

From these we can see that

- if $\alpha_i > 0$, then $y_i(x_i^T\beta+\beta_0) = 1$, or in other words, x_i is on the boundary of the slab;
- if $y_i(x_i^T\beta+\beta_0) > 1$, x_i is not on the boundary of the slab, and $\alpha_i = 0$.

From (4.46) we see that the solution vector β is defined in terms of a linear combination of the *support points* x_i—those points defined to be on the boundary of the slab via $\alpha_i = 0$. Figure 4.15 shows the optimal separating hyperplane for our toy example; there are three support points. Likewise, β_0 is obtained by solving (4.49) for any of the support points.

The optimal separating hyperplane produces a function $\hat{f}(x) = x^T\hat{\beta}+\hat{\beta}_0$ for classifying new observations:

$$\hat{G}(x) = \text{sign}\hat{f}(x). \tag{4.50}$$

Although none of the training observations fall in the margin (by construction), this will not necessarily be the case for test observations. The intuition is that a large margin on the training data will lead to good separation on the test data.

The description of the solution in terms of support points seems to suggest that the optimal hyperplane focuses more on the points that count, and is more robust to model misspecification. The LDA solution, on the other hand, depends on all of the data, even points far away from the decision boundary. Note, however, that the identification of these support points required the use of all the data. Of course, if the classes are really Gaussian, then LDA is optimal, and separating hyperplanes will pay a price for focusing on the (noisier) data at the boundaries of the classes.

Included in Figure 4.15 is the logistic regression solution to this problem, fit by maximum likelihood. Both solutions are similar in this case. When a separating hyperplane exists, logistic regression will always find it, since the log-likelihood can be driven to 0 in this case (Exercise 4.5). The logistic regression solution shares some other qualitative features with the separating hyperplane solution. The coefficient vector is defined by a weighted least squares fit of a zero-mean linearized response on the input features, and the weights are larger for points near the decision boundary than for those further away.

When the data are not separable, there will be no feasible solution to this problem, and an alternative formulation is needed. Again one can enlarge the space using basis transformations, but this can lead to artificial separation through over-fitting. In Chapter 12 we discuss a more attractive alternative known as the *support vector machine*, which allows for overlap, but minimizes a measure of the extent of this overlap.

Bibliographic Notes

Good general texts on classification include Duda et al. (2000), Hand (1981), McLachlan (1992) and Ripley (1996). Mardia et al. (1979) have a concise discussion of linear discriminant analysis. Michie et al. (1994) compare a large number of popular classifiers on benchmark datasets. Linear separating hyperplanes are discussed in Vapnik (1996). Our account of the perceptron learning algorithm follows Ripley (1996).

Exercises

Ex. 4.1 Show how to solve the generalized eigenvalue problem $\max a^T\mathbf{B}a$ subject to $a^T\mathbf{W}a = 1$ by transforming to a standard eigenvalue problem.

Ex. 4.2 Suppose we have features $x \in \mathbb{R}^p$, a two-class response, with class sizes N_1, N_2, and the target coded as $-N/N_1, N/N_2$.

(a) Show that the LDA rule classifies to class 2 if

$$x^T\hat{\mathbf{\Sigma}}^{-1}(\hat{\mu}_2 - \hat{\mu}_1) > \frac{1}{2}\hat{\mu}_2^T\hat{\mathbf{\Sigma}}\hat{\mu}_2 - \frac{1}{2}\hat{\mu}_1^T\hat{\mathbf{\Sigma}}\hat{\mu}_1 + \log(N_1/N) - \log(N_2/N),$$

and class 1 otherwise.

(b) Consider minimization of the least squares criterion

$$\sum_{i=1}^{N}(y_i - \beta_0 - \beta^T x_i)^2. \tag{4.51}$$

Show that the solution $\hat{\beta}$ satisfies

$$\left[(N-2)\hat{\mathbf{\Sigma}} + \frac{N_1 N_2}{N}\hat{\mathbf{\Sigma}}_B\right]\beta = N(\hat{\mu}_2 - \hat{\mu}_1) \tag{4.52}$$

(after simplification),where $\hat{\mathbf{\Sigma}}_B = (\hat{\mu}_2 - \hat{\mu}_1)(\hat{\mu}_2 - \hat{\mu}_1)^T$.

(c) Hence show that $\hat{\mathbf{\Sigma}}_B\beta$ is in the direction $(\hat{\mu}_2 - \hat{\mu}_1)$ and thus

$$\hat{\beta} \propto \hat{\mathbf{\Sigma}}^{-1}(\hat{\mu}_2 - \hat{\mu}_1). \tag{4.53}$$

Therefore the least squares regression coefficient is identical to the LDA coefficient, up to a scalar multiple.

(d) Show that this result holds for any (distinct) coding of the two classes.

(e) Find the solution $\hat{\beta}_0$, and hence the predicted values $\hat{f} = \hat{\beta}_0 + \hat{\beta}^T x$. Consider the following rule: classify to class 2 if $\hat{y}_i > 0$ and class 1 otherwise. Show this is not the same as the LDA rule unless the classes have equal numbers of observations.

(Fisher, 1936; Ripley, 1996)

Ex. 4.3 Suppose we transform the original predictors $\mathbf{X}$ to $\hat{\mathbf{Y}}$ via linear regression. In detail, let $\hat{\mathbf{Y}} = \mathbf{X}(\mathbf{X}^T\mathbf{X})^{-1}\mathbf{X}^T\mathbf{Y} = \mathbf{X}\hat{\mathbf{B}}$, where $\mathbf{Y}$ is the indicator response matrix. Similarly for any input $x \in \mathbb{R}^p$, we get a transformed vector $\hat{y} = \hat{\mathbf{B}}x \in \mathbb{R}^K$. Show that LDA using $\hat{\mathbf{Y}}$ is identical to LDA in the original space.

Ex. 4.4 Consider the multilogit model with K classes (4.17). Let β be the $(p+1)(K-1)$-vector consisting of all the coefficients. Define a suitably enlarged version of the input vector x to accommodate this vectorized coefficient matrix. Derive the Newton-Raphson algorithm for maximizing the multinomial log-likelihood, and describe how you would implement this algorithm.

Ex. 4.5 Consider a two-class logistic regression problem with $x \in \mathbb{R}$. Characterize the maximum-likelihood estimates of the slope and intercept parameter if the sample x_i for the two classes are separated by a point $x_0 \in \mathbb{R}$. Generalize this result to (a) $x \in \mathbb{R}^p$ (see Figure 4.15), and (b) more than two classes.

Ex. 4.6 Suppose we have N points x_i in $\mathbb{R}^p$ in general position, with class labels $y_i \in \{-1, 1\}$. Prove that the perceptron learning algorithm converges to a separating hyperplane in a finite number of steps:

(a) Denote a hyperplane by $f(x) = \beta_1^T x + \beta_0 = 0$, or in more compact notation $\beta^T x^* = 0$, where $x^* = (x, 1)$ and $\beta = (\beta_1, \beta_0)$. Let $z_i = x_i^* / ||x_i^*||$. Show that separability implies the existence of a β_{opt} such that $y_i \beta_{\text{opt}}^T z_i \geq 1 \ \forall i$

(b) Given a current β_{old}, the perceptron algorithm identifies a point z_i that is misclassified, and produces the update $\beta_{\text{new}} \leftarrow \beta_{\text{old}} + y_i z_i$. Show that $||\beta_{\text{new}} - \beta_{\text{opt}}||^2 \leq ||\beta_{\text{old}} - \beta_{\text{opt}}||^2 - 1$, and hence that the algorithm converges to a separating hyperplane in no more than $||\beta_{\text{start}} - \beta_{\text{opt}}||^2$ steps (Ripley, 1996).

Ex. 4.7 Consider the criterion

$$D^*(\beta, \beta_0) = -\sum_{i=1}^{N} y_i (x_i^T \beta + \beta_0), \tag{4.54}$$

a generalization of (4.37) where we sum over all the observations. Consider minimizing D^* subject to $||\beta|| = 1$. Describe this criterion in words. Does it solve the optimal separating hyperplane problem?

Ex. 4.8 Consider the multivariate Gaussian model $X|G = k \sim N(\mu_k, \mathbf{\Sigma})$, with the additional restriction that $\text{rank}\{\mu_k\}_1^K = L < \max(K - 1, p)$. Derive the constrained MLEs for the μ_k and $\mathbf{\Sigma}$. Show that the Bayes classification rule is equivalent to classifying in the reduced subspace computed by LDA (Hastie and Tibshirani, 1996b).

Ex. 4.9 Write a computer program to perform a quadratic discriminant analysis by fitting a separate Gaussian model per class. Try it out on the vowel data, and compute the misclassification error for the test data. The data can be found in the book website `www-stat.stanford.edu/ElemStatLearn`.

5 Basis Expansions and Regularization

5.1 Introduction

We have already made use of models linear in the input features, both for regression and classification. Linear regression, linear discriminant analysis, logistic regression and separating hyperplanes all rely on a linear model. It is extremely unlikely that the true function $f(X)$ is actually linear in X. In regression problems, $f(X) = \text{E}(Y|X)$ will typically be nonlinear and nonadditive in X, and representing $f(X)$ by a linear model is usually a convenient, and sometimes a necessary, approximation. Convenient because a linear model is easy to interpret, and is the first-order Taylor approximation to $f(X)$. Sometimes necessary, because with N small and/or p large, a linear model might be all we are able to fit to the data without overfitting. Likewise in classification, a linear, Bayes-optimal decision boundary implies that some monotone transformation of $\Pr(Y = 1|X)$ is linear in X. This is inevitably an approximation.

In this chapter and the next we discuss popular methods for moving beyond linearity. The core idea in this chapter is to augment/replace the vector of inputs X with additional variables, which are transformations of X, and then use linear models in this new space of derived input features.

Denote by $h_m(X) : \mathbb{R}^p \mapsto \mathbb{R}$ the mth transformation of X, $m = 1, \dots, M$. We then model

$$f(X) = \sum_{m=1}^{M} \beta_m h_m(X), \tag{5.1}$$

a *linear basis expansion* in X. The beauty of this approach is that once the basis functions h_m have been determined, the models are linear in these new variables, and the fitting proceeds as before.

Some simple and widely used examples of the h_m are the following:

- $h_m(X) = X_m,\ m = 1, \dots, p$ recovers the original linear model.
- $h_m(X) = X_j^2$ or $h_m(X) = X_j X_k$ allows us to augment the inputs with polynomial terms to achieve higher-order Taylor expansions. Note, however, that the number of variables grows exponentially in the degree of the polynomial. A full quadratic model in p variables requires $O(p^2)$ square and cross-product terms, or more generally $O(p^d)$ for a degree-d polynomial.
- $h_m(X) = \log(X_j),\ \sqrt{X_j}, \dots$ permits other nonlinear transformations of single inputs. More generally one can use similar functions involving several inputs, such as $h_m(X) = ||X||$.
- $h_m(X) = I(L_m \leq X_k < U_m)$, an indicator for a region of X_k. By breaking the range of X_k up into M_k such nonoverlapping regions results in a model with a piecewise constant contribution for X_k.

Sometimes the problem at hand will call for particular basis functions h_m, such as logarithms or power functions. More often, however, we use the basis expansions as a device to achieve more flexible representations for $f(X)$. Polynomials are an example of the latter, although they are limited by their global nature—tweaking the coefficients to achieve a functional form in one region can cause the function to flap about madly in remote regions. In this chapter we consider more useful families of *piecewise-polynomials* and *splines* that allow for local polynomial representations. We also discuss the *wavelet* bases, especially useful for modeling signals and images. These methods produce a *dictionary* $\mathcal{D}$ consisting of typically a very large number $|\mathcal{D}|$ of basis functions, far more than we can afford to fit to our data. Along with the dictionary we require a method for controlling the complexity of our model, using basis functions from the dictionary. There are three common approaches:

- Restriction methods, where we decide before-hand to limit the class of functions. Additivity is an example, where we assume that our model has the form

$$\begin{aligned} f(X) &= \sum_{j=1}^{p} f_j(X_j) \\ &= \sum_{j=1}^{p} \sum_{m=1}^{M_j} \beta_{jm} h_{jm}(X_j). \end{aligned} \tag{5.2}$$

The size of the model is limited by the number of basis functions M_j used for each component function f_j.

- Selection methods, which adaptively scan the dictionary and include only those basis functions h_m that contribute significantly to the fit of the model. Here the variable selection techniques discussed in Chapter 3 are useful. The stagewise greedy approaches such as CART, MARS and boosting fall into this category as well.

- Regularization methods where we use the entire dictionary but restrict the coefficients. Ridge regression is a simple example of a regularization approach, while the lasso is both a regularization and selection method. Here we discuss these and more sophisticated methods for regularization.

5.2 Piecewise Polynomials and Splines

We assume until Section 5.7 that X is one-dimensional. A piecewise polynomial function $f(X)$ is obtained by dividing the domain of X into contiguous intervals, and representing f by a separate polynomial in each interval. Figure 5.1 shows two simple piecewise polynomials. The first is piecewise constant, with three basis functions:

$$h_1(X) = I(X < \xi_1), \quad h_2(X) = I(\xi_1 \le X < \xi_2), \quad h_3(X) = I(\xi_2 \le X).$$

Since these are positive over disjoint regions, the least squares estimate of the model $f(X) = \sum_{m=1}^{3} \beta_m h_m(X)$ amounts to $\hat{\beta}_m = \bar{Y}_m$, the mean of Y in the mth region.

The top right panel shows a piecewise linear fit. Three additional basis functions are needed: $h_{m+3} = h_m(X)X,\ m = 1, \ldots, 3$. Except in special cases, we would typically prefer the third panel, which is also piecewise linear, but restricted to be continuous at the two knots. These continuity restrictions lead to linear constraints on the parameters; for example, $f(\xi_1^-) = f(\xi_1^+)$ implies that $\beta_1 + \xi_1\beta_4 = \beta_2 + \xi_1\beta_5$. In this case, since there are two restrictions, we expect to *get back* two parameters, leaving four free parameters.

A more direct way to proceed in this case is to use a basis that incorporates the constraints:

$$h_1(X) = 1, \quad h_2(X) = X, \quad h_3(X) = (X - \xi_1)_+, \quad h_4(X) = (X - \xi_2)_+,$$

where t_+ denotes the positive part. The function h_3 is shown in the lower right panel of Figure 5.1. We often prefer smoother functions, and these can be achieved by increasing the order of the local polynomial. Figure 5.2 shows a series of piecewise-cubic polynomials fit to the same data, with

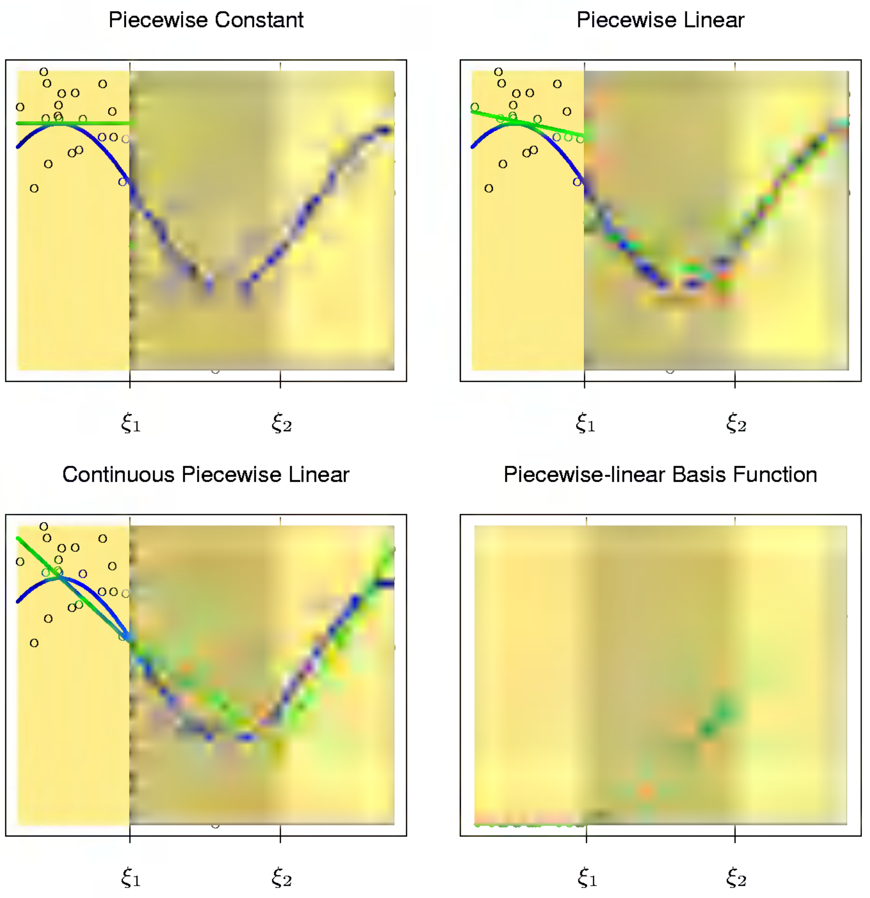

FIGURE 5.1. *The top left panel shows a piecewise constant function fit to some artificial data. The broken vertical lines indicate the positions of the two* knots *ξ_1 and ξ_2. The blue curve represents the true function, from which the data were generated with Gaussian noise. The remaining two panels show piecewise linear functions fit to the same data—the top right unrestricted, and the lower left restricted to be continuous at the knots. The lower right panel shows a piecewise-linear basis function, $h_3(X) = (X - \xi_1)_+$, continuous at ξ_1. The black points indicate the sample evaluations $h_3(x_i)$, $i = 1, \dots, N$.*

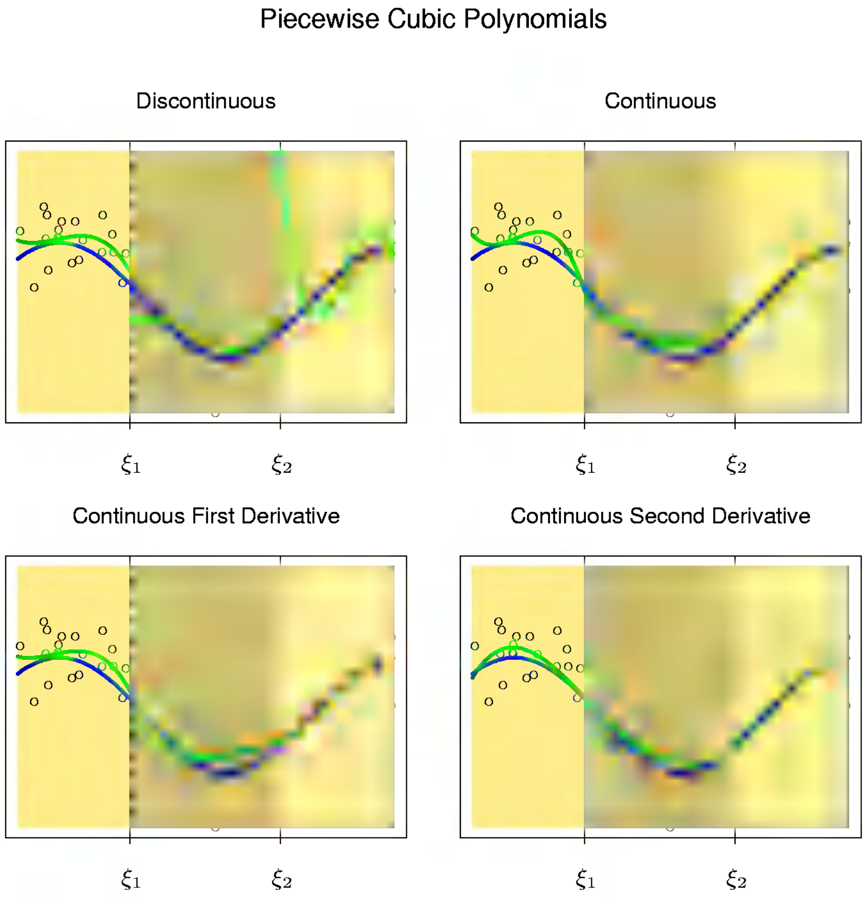

FIGURE 5.2. *A series of piecewise-cubic polynomials, with increasing orders of continuity.*

increasing orders of continuity at the knots. The function in the lower right panel is continuous, and has continuous first and second derivatives at the knots. It is known as a *cubic spline*. Enforcing one more order of continuity would lead to a global cubic polynomial. It is not hard to show (Exercise 5.1) that the following basis represents a cubic spline with knots at ξ_1 and ξ_2:

$$\begin{aligned} h_1(X) &= 1, & h_3(X) &= X^2, & h_5(X) &= (X-\xi_1)^3_+, \\ h_2(X) &= X, & h_4(X) &= X^3, & h_6(X) &= (X-\xi_2)^3_+. \end{aligned} \tag{5.3}$$

There are six basis functions corresponding to a six-dimensional linear space of functions. A quick check confirms the parameter count: (3 regions)×(4 parameters per region) −(2 knots)×(3 constraints per knot)= 6.

More generally, an order-M spline with knots ξ_j, $j = 1, \dots, K$ is a piecewise-polynomial of order M, and has continuous derivatives up to order $M - 2$. A cubic spline has $M = 4$. In fact the piecewise-constant function in Figure 5.1 is an order-1 spline, while the continuous piecewise linear function is an order-2 spline. Likewise the general form for the truncated-power basis set would be

$$\begin{aligned} h_j(X) &= X^{j-1},\ j = 1, \dots, M, \\ h_{M+\ell}(X) &= (X - \xi_\ell)_+^{M-1},\ \ell = 1, \dots, K. \end{aligned}$$

It is claimed that cubic splines are the lowest-order spline for which the knot-discontinuity is not visible to the human eye. There is seldom any good reason to go beyond cubic-splines, unless one is interested in smooth derivatives. In practice the most widely used orders are $M = 1, 2$ and 4.

These fixed-knot splines are also known as *regression splines.* One needs to select the order of the spline, the number of knots and their placement. One simple approach is to parameterize a family of splines by the number of basis functions or degrees of freedom, and have the observations x_i determine the positions of the knots. For example, the expression `bs(x,df=7)` in S-PLUS generates a basis matrix of cubic-spline functions evaluated at the N observations in `x`, with the $7 - 3 = 4$* interior knots at the appropriate percentiles of `x` (25, 50 and 75th in this case.) One can be more explicit, however; `bs(x, degree=1, knots = c(0.2, 0.4, 0.6))` generates a basis for linear splines, with three interior knots, and returns an $N \times 4$ matrix.

Since the space of spline functions of a particular order and knot sequence is a vector space, there are many equivalent bases for representing them (just as there are for ordinary polynomials.) While the truncated power basis is conceptually simple, it is not too attractive numerically: powers of large numbers can lead to severe rounding problems. The *B-spline* basis, described in the Appendix to this chapter, allows for efficient computations even when the number of knots K is large.

5.2.1 Natural Cubic Splines

We know that the behavior of polynomials fit to data tends to be erratic near the boundaries, and extrapolation can be dangerous. These problems are exacerbated with splines. The polynomials fit beyond the boundary knots behave even more wildly than the corresponding global polynomials in that region. This can be conveniently summarized in terms of the pointwise variance of spline functions fit by least squares (see the example in the next section for details on these variance calculations). Figure 5.3 compares

*A cubic spline with four knots is eight-dimensional. The `bs()` function omits by defaults the constant term in the basis, since terms like this are typically included with other terms in the model

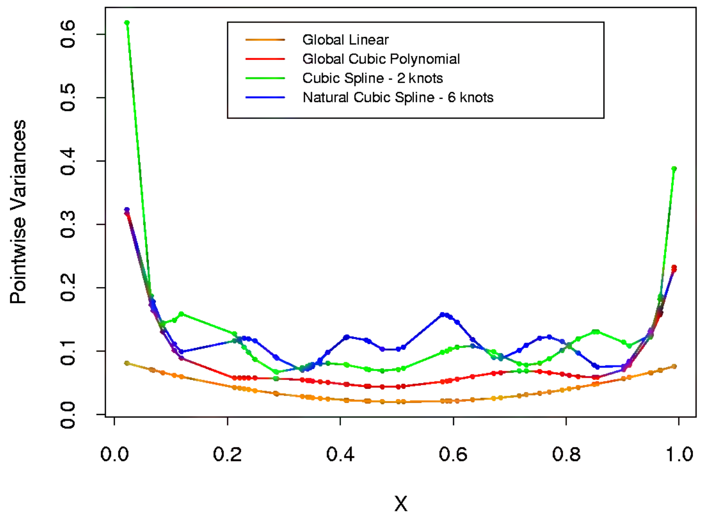

FIGURE 5.3. *Pointwise variance curves for four different models, with X consisting of* 50 *points drawn at random from* $U[0,1]$*, and an assumed error model with constant variance. The linear and cubic polynomial fits have two and four degrees of freedom respectively, while the cubic spline and natural cubic spline each have six degrees of freedom. The cubic spline has two knots at* 0.33 *and* 0.66*, while the natural spline has boundary knots at* 0.1 *and* 0.9*, and four interior knots uniformly spaced between them.*

the pointwise variances for a variety of different models. The explosion of the variance near the boundaries is clear, and inevitably is worst for cubic splines.

A *natural cubic spline* adds additional constraints, namely that the function is linear beyond the boundary knots. This frees up four degrees of freedom (two constraints each in both boundary regions), which can be spent more profitably by sprinkling more knots in the interior region. This tradeoff is illustrated in terms of variance in Figure 5.3. There will be a price paid in bias near the boundaries, but assuming the function is linear near the boundaries (where we have less information anyway) is often considered reasonable.

A natural cubic spline with K knots is represented by K basis functions. One can start from a basis for cubic splines, and derive the reduced basis by imposing the boundary constraints. For example, starting from the truncated power series basis described in Section 5.2, we arrive at (Exercise 5.4):

$$N_1(X) = 1, \quad N_2(X) = X, \quad N_{k+2}(X) = d_k(X) - d_{K-1}(X), \qquad (5.4)$$

where

$$d_k(X) = \frac{(X-\xi_k)^3_+ - (X-\xi_K)^3_+}{\xi_K - \xi_k}. \tag{5.5}$$

Each of these basis functions can be seen to have zero second and third derivative for $X \geq \xi_K$.

5.2.2 Example: South African Heart Disease (Continued)

In Section 4.4.2 we fit linear logistic regression models to the South African heart disease data. Here we explore nonlinearities in the functions using natural splines. The functional form of the model is

$$\text{logit}[\Pr(\texttt{chd}|X)] = \theta_0 + h_1(X_1)^T\theta_1 + h_2(X_2)^T\theta_2 + \cdots + h_p(X_p)^T\theta_p, \tag{5.6}$$

where each of the θ_j are vectors of coefficients multiplying their associated vector of natural spline basis functions h_j.

We use four natural spline bases for each term in the model. For example, with X_1 representing `sbp`, $h_1(X_1)$ is a basis consisting of four basis functions. This actually implies three rather than two interior knots (chosen at uniform quantiles of `sbp`), plus two boundary knots at the extremes of the data, since we exclude the constant term from each of the h_j.

Since `famhist` is a two-level factor, it is coded by a simple binary or dummy variable, and is associated with a single coefficient in the fit of the model.

More compactly we can combine all p vectors of basis functions (and the constant term) into one big vector $h(X)$, and then the model is simply $h(X)^T\theta$, with total number of parameters $\text{df} = 1 + \sum_{j=1}^p \text{df}_j$, the sum of the parameters in each component term. Each basis function is evaluated at each of the N samples, resulting in a $N \times \text{df}$ basis matrix $\mathbf{H}$. At this point the model is like any other linear logistic model, and the algorithms described in Section 4.4.1 apply.

We carried out a backward stepwise deletion process, dropping terms from this model while preserving the group structure of each term, rather than dropping one coefficient at a time. The AIC statistic (Section 7.5) was used to drop terms, and all the terms remaining in the final model would cause AIC to increase if deleted from the model (see Table 5.1). Figure 5.4 shows a plot of the final model selected by the stepwise regression. The functions displayed are $\hat{f}_j(X_j) = h_j(X_j)^T\hat{\theta}_j$ for each variable X_j. The covariance matrix $\text{Cov}(\hat{\theta}) = \mathbf{\Sigma}$ is estimated by $\hat{\mathbf{\Sigma}} = (\mathbf{H}^T\mathbf{W}\mathbf{H})^{-1}$, where $\mathbf{W}$ is the diagonal weight matrix from the logistic regression. Hence $v_j(X_j) = \text{Var}[\hat{f}_j(X_j)] = h_j(X_j)^T\hat{\mathbf{\Sigma}}_{jj}h_j(X_j)$ is the pointwise variance function of $\hat{f}_j$, where $\text{Cov}(\hat{\theta}_j) = \hat{\mathbf{\Sigma}}_{jj}$ is the appropriate sub-matrix of $\hat{\mathbf{\Sigma}}$. The shaded region in each panel is defined by $\hat{f}_j(X_j) \pm 2\sqrt{v_j(X_j)}$.

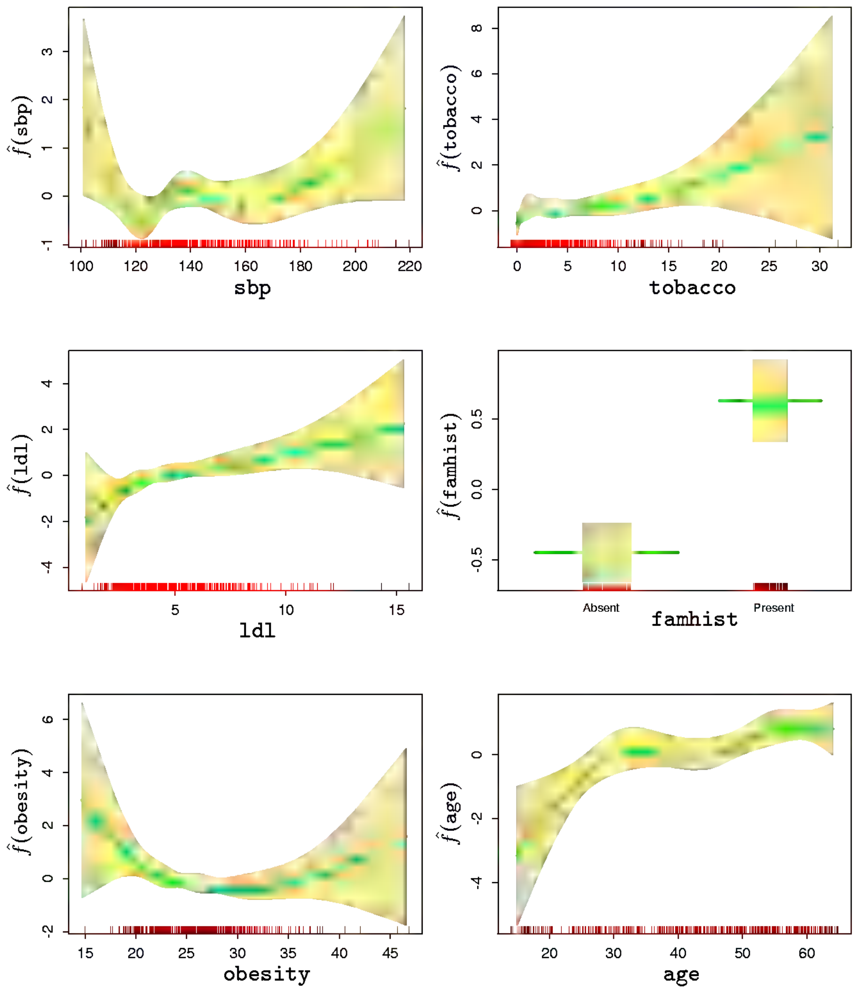

FIGURE 5.4. *Fitted natural-spline functions for each of the terms in the final model selected by the stepwise procedure. Included are pointwise standard-error bands. The* rug plot *at the base of each figure indicates the location of each of the sample values for that variable (jittered to break ties).*

TABLE 5.1. *Final logistic regression model, after stepwise deletion of natural splines terms. The column labeled "LRT" is the likelihood-ratio test statistic when that term is deleted from the model, and is the change in deviance from the full model (labeled "none").*

Terms	Df	Deviance	AIC	LRT	P-value
`none`		458.09	502.09		
`sbp`	4	467.16	503.16	9.076	0.059
`tobacco`	4	470.48	506.48	12.387	0.015
`ldl`	4	472.39	508.39	14.307	0.006
`famhist`	1	479.44	521.44	21.356	0.000
`obesity`	4	466.24	502.24	8.147	0.086
`age`	4	481.86	517.86	23.768	0.000

The AIC statistic is slightly more generous than the likelihood-ratio test (deviance test). Both `sbp` and `obesity` are included in this model, while they were not in the linear model. The figure explains why, since their contributions are inherently nonlinear. These effects at first may come as a surprise, but an explanation lies in the nature of the retrospective data. These measurements were made sometime after the patients suffered a heart attack, and in many cases they had already benefited from a healthier diet and lifestyle, hence the apparent *increase* in risk at low values for `obesity` and `sbp`. Table 5.1 shows a summary of the selected model.

5.2.3 Example: Phoneme Recognition

In this example we use splines to reduce flexibility rather than increase it; the application comes under the general heading of *functional* modeling. In the top panel of Figure 5.5 are displayed a sample of 15 log-periodograms for each of the two phonemes "aa" and "ao" measured at 256 frequencies. The goal is to use such data to classify a spoken phoneme. These two phonemes were chosen because they are difficult to separate.

The input feature is a vector x of length 256, which we can think of as a vector of evaluations of a function $X(f)$ over a grid of frequencies f. In reality there is a continuous analog signal which is a function of frequency, and we have a sampled version of it.

The gray lines in the lower panel of Figure 5.5 show the coefficients of a linear logistic regression model fit by maximum likelihood to a training sample of 1000 drawn from the total of 695 "aa"s and 1022 "ao"s. The coefficients are also plotted as a function of frequency, and in fact we can think of the model in terms of its continuous counterpart

$$\log \frac{\Pr(\text{aa}|X)}{\Pr(\text{ ao }|X)} = \int X(f)\beta(f)df, \tag{5.7}$$

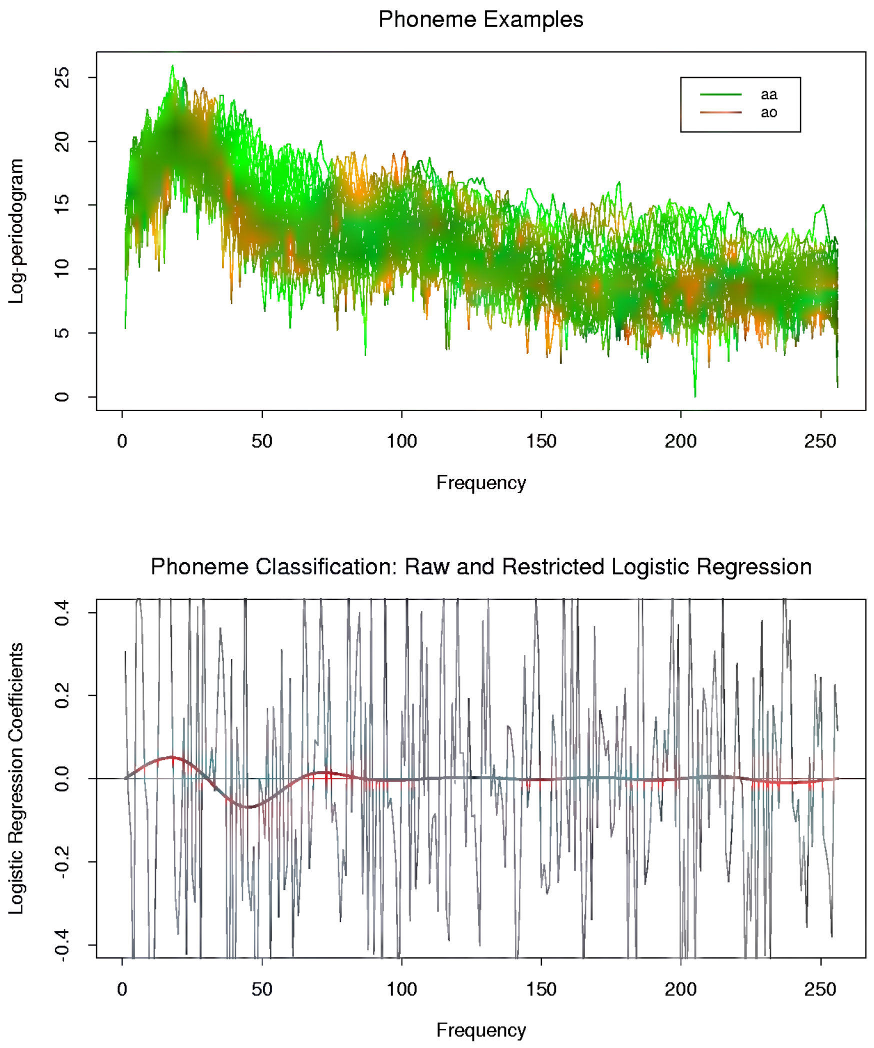

FIGURE 5.5. *The top panel displays the log-periodogram as a function of frequency for* 15 *examples each of the phonemes "aa" and "ao" sampled from a total of* 695 *"aa"s and* 1022 *"ao"s. Each log-periodogram is measured at* 256 *uniformly spaced frequencies. The lower panel shows the coefficients (as a function of frequency) of a logistic regression fit to the data by maximum likelihood, using the* 256 *log-periodogram values as inputs. The coefficients are restricted to be smooth in the red curve, and are unrestricted in the jagged gray curve.*

which we approximate by

$$\sum_{j=1}^{256} X(f_j)\beta(f_j) = \sum_{j=1}^{256} x_j\beta_j. \tag{5.8}$$

The coefficients compute a contrast functional, and will have appreciable values in regions of frequency where the log-periodograms differ between the two classes.

The gray curves are very rough. Since the input signals have fairly strong positive autocorrelation, this results in negative autocorrelation in the coefficients. In addition the sample size effectively provides only four observations per coefficient.

Applications such as this permit a natural regularization. We force the coefficients to vary smoothly as a function of frequency. The red curve in the lower panel of Figure 5.5 shows such a smooth coefficient curve fit to these data. We see that the lower frequencies offer the most discriminatory power. Not only does the smoothing allow easier interpretation of the contrast, it also produces a more accurate classifier:

	Raw	Regularized
Training error	0.080	0.185
Test error	0.255	0.158

The smooth red curve was obtained through a very simple use of natural cubic splines. We can represent the coefficient function as an expansion of splines $\beta(f) = \sum_{m=1}^{M} h_m(f)\theta_m$. In practice this means that $\beta = \mathbf{H}\theta$ where, $\mathbf{H}$ is a $p \times M$ basis matrix of natural cubic splines, defined on the set of frequencies. Here we used $M = 12$ basis functions, with knots uniformly placed over the integers $1, 2, \dots, 256$ representing the frequencies. Since $x^T\beta = x^T\mathbf{H}\theta$, we can simply replace the input features x by their *filtered* versions $x^* = \mathbf{H}^T x$, and fit θ by linear logistic regression on the x^*. The red curve is thus $\hat{\beta}(f) = h(f)^T\hat{\theta}$.

5.3 Filtering and Feature Extraction

In the previous example, we constructed a $p \times M$ basis matrix $\mathbf{H}$, and then transformed our features x into new features $x^* = \mathbf{H}^T x$. These filtered versions of the features were then used as inputs into a learning procedure: in the previous example, this was linear logistic regression.

Preprocessing of high-dimensional features is a very general and powerful method for improving the performance of a learning algorithm. The preprocessing need not be linear as it was above, but can be a general (nonlinear) function of the form $x^* = g(x)$. The derived features x^* can then be used as inputs into any (linear or nonlinear) learning procedure.

For example, for signal or image recognition a popular approach is to first transform the raw features via a wavelet transform $x^* = \mathbf{H}^T x$ (Section 5.9) and then use the features x^* as inputs into a neural network (Chapter 11). Wavelets are effective in capturing discrete jumps or edges, and the neural network is powerful tool for constructing nonlinear functions of these features for predicting the target variable. By using domain knowledge to construct appropriate features, one can often improve upon a learning method that has only the raw features x at its disposal.

5.4 Smoothing Splines

Here we discuss a spline basis method that avoids the knot selection problem completely by using a maximal set of knots. The complexity of the fit is controlled by regularization. Consider the following problem: among all functions $f(x)$ with two continuous derivatives, find one that minimizes the penalized residual sum of squares

$$\mathrm{RSS}(f, \lambda) = \sum_{i=1}^{N} \{y_i - f(x_i)\}^2 + \lambda \int \{f''(t)\}^2 dt, \tag{5.9}$$

where λ is a fixed *smoothing parameter*. The first term measures closeness to the data, while the second term penalizes curvature in the function, and λ establishes a tradeoff between the two. Two special cases are:

$\lambda = 0:$ f can be any function that interpolates the data.

$\lambda = \infty:$ the simple least squares line fit, since no second derivative can be tolerated.

These vary from very rough to very smooth, and the hope is that $\lambda \in (0, \infty)$ indexes an interesting class of functions in between.

The criterion (5.9) is defined on an infinite-dimensional function space—in fact, a Sobolev space of functions for which the second term is defined. Remarkably, it can be shown that (5.9) has an explicit, finite-dimensional, unique minimizer which is a natural cubic spline with knots at the unique values of the x_i, $i = 1, \dots, N$ (Exercise 5.7). At face value it seems that the family is still over-parametrized, since there are as many as N knots, which implies N degrees of freedom. However, the penalty term translates to a penalty on the spline coefficients, which are shrunk some of the way toward the linear fit.

Since the solution is a natural spline, we can write it as

$$f(x) = \sum_{j=1}^{N} N_j(x)\theta_j, \tag{5.10}$$

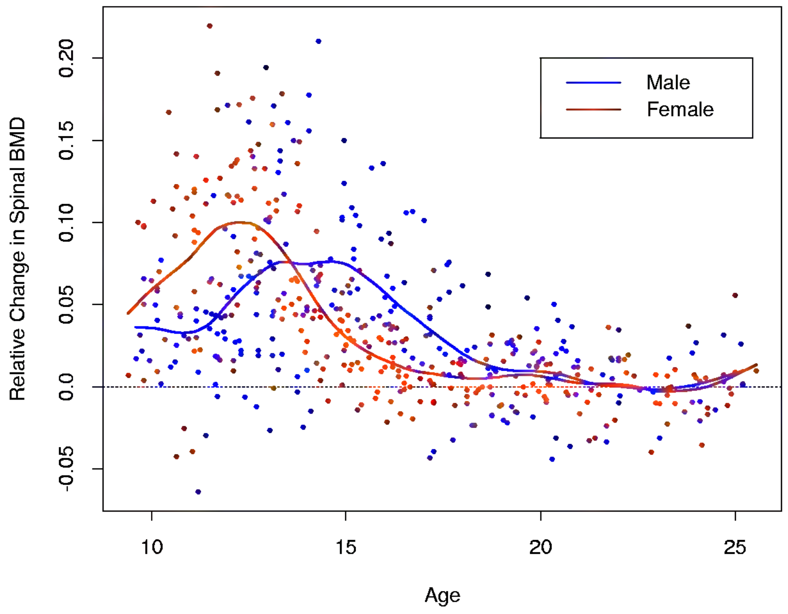

FIGURE 5.6. *The response is the relative change in bone mineral density measured at the spine in adolescents, as a function of age. A separate smoothing spline was fit to the males and females, with* $\lambda \approx 0.00022$. *This choice corresponds to about* 12 *degrees of freedom.*

where the $N_j(x)$ are an N-dimensional set of basis functions for representing this family of natural splines (Section 5.2.1 and Exercise 5.4). The criterion thus reduces to

$$\text{RSS}(\theta, \lambda) = (\mathbf{y} - \mathbf{N}\theta)^T(\mathbf{y} - \mathbf{N}\theta) + \lambda\theta^T\mathbf{\Omega}_N\theta, \tag{5.11}$$

where $\{\mathbf{N}\}_{ij} = N_j(x_i)$ and $\{\mathbf{\Omega}_N\}_{jk} = \int N_j''(t)N_k''(t)dt$. The solution is easily seen to be

$$\hat{\theta} = (\mathbf{N}^T\mathbf{N} + \lambda\mathbf{\Omega}_N)^{-1}\mathbf{N}^T\mathbf{y}, \tag{5.12}$$

a generalized ridge regression. The fitted smoothing spline is given by

$$\hat{f}(x) = \sum_{j=1}^{N} N_j(x)\hat{\theta}_j. \tag{5.13}$$

Efficient computational techniques for smoothing splines are discussed in the Appendix to this chapter.

Figure 5.6 shows a smoothing spline fit to some data on bone mineral density (BMD) in adolescents. The response is relative change in spinal BMD over two consecutive visits, typically about one year apart. The data are color coded by gender, and two separate curves were fit. This simple summary reinforces the evidence in the data that the growth spurt for females precedes that for males by about two years. In both cases the smoothing parameter λ was approximately 0.00022; this choice is discussed in the next section.

5.4.1 Degrees of Freedom and Smoother Matrices

We have not yet indicated how λ is chosen for the smoothing spline. Later in this chapter we describe automatic methods using techniques such as cross-validation. In this section we discuss intuitive ways of prespecifying the amount of smoothing.

A smoothing spline with prechosen λ is an example of a *linear smoother* (as in linear operator). This is because the estimated parameters in (5.12) are a linear combination of the y_i. Denote by $\hat{\mathbf{f}}$ the N-vector of fitted values $\hat{f}(x_i)$ at the training predictors x_i. Then

$$\begin{aligned} \hat{\mathbf{f}} &= \mathbf{N}(\mathbf{N}^T\mathbf{N} + \lambda\boldsymbol{\Omega}_N)^{-1}\mathbf{N}^t\mathbf{y} \\ &= \mathbf{S}_\lambda \mathbf{y}. \end{aligned} \tag{5.14}$$

Again the fit is linear in $\mathbf{y}$, and the finite linear operator $\mathbf{S}_\lambda$ is known as the *smoother matrix*. One consequence of this linearity is that the recipe for producing $\hat{\mathbf{f}}$ from $\mathbf{y}$ does not depend on $\mathbf{y}$ itself; $\mathbf{S}_\lambda$ depends only on the x_i and λ.

Linear operators are familiar in more traditional least squares fitting as well. Suppose $\mathbf{B}_\xi$ is a $N \times M$ matrix of M cubic-spline basis functions evaluated at the N training points x_i, with knot sequence ξ, and $M \ll N$. Then the vector of fitted spline values is given by

$$\begin{aligned} \hat{\mathbf{f}} &= \mathbf{B}_\xi(\mathbf{B}_\xi^T\mathbf{B}_\xi)^{-1}\mathbf{B}_\xi^T\mathbf{y} \\ &= \mathbf{H}_\xi \mathbf{y}. \end{aligned} \tag{5.15}$$

Here the linear operator $\mathbf{H}_\xi$ is a projection operator, also known as the *hat* matrix in statistics. There are some important similarities and differences between $\mathbf{H}_\xi$ and $\mathbf{S}_\lambda$:

- Both are symmetric, positive semidefinite matrices.
- $\mathbf{H}_\xi\mathbf{H}_\xi = \mathbf{H}_\xi$ (idempotent), while $\mathbf{S}_\lambda\mathbf{S}_\lambda \preceq \mathbf{S}_\lambda$, meaning that the right-hand side exceeds the left-hand side by a positive semidefinite matrix. This is a consequence of the *shrinking* nature of $\mathbf{S}_\lambda$, which we discuss further below.
- $\mathbf{H}_\xi$ has rank M, while $\mathbf{S}_\lambda$ has rank N.

The expression $M = \text{trace}(\mathbf{H}_\xi)$ gives the dimension of the projection space, which is also the number of basis functions, and hence the number of parameters involved in the fit. By analogy we define the *effective degrees of freedom* of a smoothing spline to be

$$\text{df}_\lambda = \text{trace}(\mathbf{S}_\lambda), \tag{5.16}$$

the sum of the diagonal elements of $\mathbf{S}_\lambda$. This very useful definition allows us a more intuitive way to parameterize the smoothing spline, and indeed many other smoothers as well, in a consistent fashion. For example, in Figure 5.6 we specified $\text{df}_\lambda = 12$ for each of the curves, and the corresponding $\lambda \approx 0.00022$ was derived numerically by solving $\text{trace}(\mathbf{S}_\lambda) = 12$. There are many arguments supporting this definition of degrees of freedom, and we cover some of them here.

Since $\mathbf{S}_\lambda$ is symmetric (and positive semidefinite), it has a real eigen-decomposition. Before we proceed, it is convenient to rewrite $\mathbf{S}_\lambda$ in the *Reinsch* form

$$\mathbf{S}_\lambda = (\mathbf{I} + \lambda\mathbf{K})^{-1}, \tag{5.17}$$

where $\mathbf{K}$ does not depend on λ (Exercise 5.9). Since $\hat{\mathbf{f}} = \mathbf{S}_\lambda\mathbf{y}$ solves

$$\min_{\mathbf{f}} (\mathbf{y} - \mathbf{f})^T(\mathbf{y} - \mathbf{f}) + \lambda\mathbf{f}^T\mathbf{K}\mathbf{f}, \tag{5.18}$$

$\mathbf{K}$ is known as the *penalty matrix*, and indeed a quadratic form in $\mathbf{K}$ has a representation in terms of a weighted sum of squared (divided) second differences. The eigen-decomposition of $\mathbf{S}_\lambda$ is

$$\mathbf{S}_\lambda = \sum_{k=1}^{N} \rho_k(\lambda)\mathbf{u}_k\mathbf{u}_k^T \tag{5.19}$$

with

$$\rho_k(\lambda) = \frac{1}{1 + \lambda d_i}, \tag{5.20}$$

and d_k the corresponding eigenvalue of $\mathbf{K}$.

Figure 5.7 (top) shows the results of applying a cubic smoothing spline to some air pollution data (128 observations). Two fits are given: a *smoother* fit corresponding to a larger penalty λ and a *rougher* fit for a smaller penalty. The lower panels represent the eigenvalues (lower left) and some eigenvectors (lower right) of the corresponding smoother matrices. Some of the highlights of the eigenrepresentation are the following:

- The eigenvectors are not affected by changes in λ, and hence the whole family of smoothing splines (for a particular sequence $\mathbf{x}$) indexed by λ have the same eigenvectors.

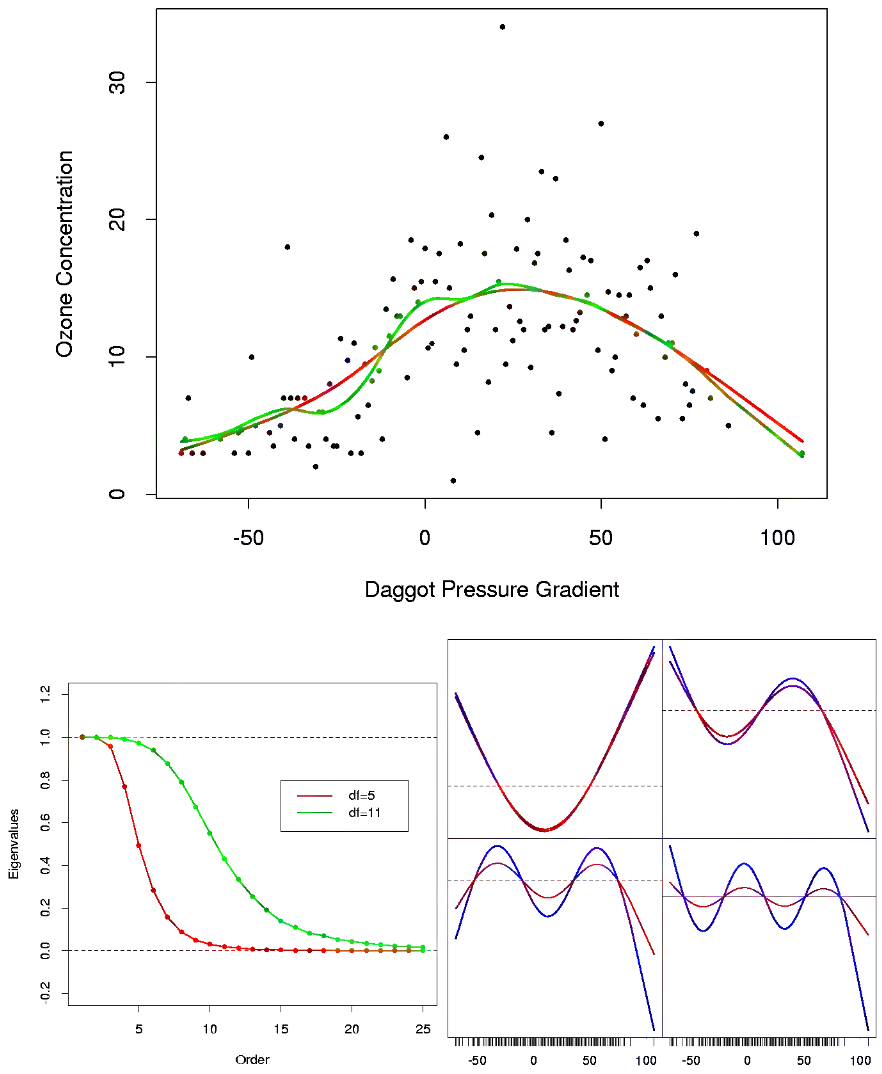

FIGURE 5.7. *[Top] Smoothing spline fit of ozone concentration versus Daggot pressure gradient. The two fits correspond to different values of the smoothing parameter, chosen to achieve* 5 *and* 11 *effective degrees of freedom, defined by* $df_\lambda = \text{trace}(\mathbf{S}_\lambda)$. *[Lower left] First* 25 *eigenvalues for the two smoothing-spline matrices. The first two are exactly* 1*, and all are* ≥ 0. *[Lower right] third to sixth eigenvectors of the spline smoother matrices. In each case,* $\mathbf{u}_k$ *is plotted against* $\mathbf{x}$*, and as such is viewed as a function of* x. *The* rug *at the base of the plots indicate the occurrence of data points. The damped functions represent the smoothed versions of these functions (using the* 5*df smoother).*

- $\mathbf{S}_\lambda \mathbf{y} = \sum_{k=1}^N \mathbf{u}_k \rho_k(\lambda) \langle \mathbf{u}_k, \mathbf{y} \rangle$, and hence the smoothing spline operates by decomposing $\mathbf{y}$ w.r.t. the (complete) basis $\{\mathbf{u}_k\}$, and differentially shrinking the contributions using $\rho_k(\lambda)$. This is to be contrasted with a basis-regression method, where the components are either left alone, or shrunk to zero—that is, a projection matrix such as $\mathbf{H}_\xi$ above has M eigenvalues equal to 1, and the rest are 0. For this reason smoothing splines are referred to as *shrinking* smoothers, while regression splines are *projection* smoothers (see Figure 3.10 on page 67).

- The sequence of $\mathbf{u}_k$, ordered by decreasing $\rho_k(\lambda)$, appear to increase in complexity. Indeed, they have the zero-crossing behavior of polynomials of increasing degree. Since $\mathbf{S}_\lambda \mathbf{u}_k = \rho_k(\lambda)\mathbf{u}_k$, we see how each of the eigenvectors themselves are shrunk by the smoothing spline: the higher the complexity, the more they are shrunk. If the domain of X is periodic, then the $\mathbf{u}_k$ are sines and cosines at different frequencies.

- The first two eigenvalues are *always* one, and they correspond to the two-dimensional eigenspace of functions linear in x (Exercise 5.11), which are never shrunk.

- The eigenvalues $\rho_k(\lambda) = 1/(1 + \lambda d_k)$ are an inverse function of the eigenvalues d_k of the penalty matrix $\mathbf{K}$, moderated by λ; λ controls the rate at which the $\rho_k(\lambda)$ decrease to zero. $d_1 = d_2 = 0$ and again linear functions are not penalized.

- One can reparametrize the smoothing spline using the basis vectors $\mathbf{u}_k$ (the *Demmler–Reinsch* basis). In this case the smoothing spline solves

$$\min_{\boldsymbol{\theta}} \|\mathbf{y} - \mathbf{U}\boldsymbol{\theta}\|^2 + \lambda \boldsymbol{\theta}^T \mathbf{D} \boldsymbol{\theta}, \qquad (5.21)$$

  where $\mathbf{U}$ has columns $\mathbf{u}_k$ and $\mathbf{D}$ is a diagonal matrix with elements d_k.

- $\text{df}_\lambda = \text{trace}(\mathbf{S}_\lambda) = \sum_{k=1}^N \rho_k(\lambda)$. For projection smoothers, all the eigenvalues are 1, each one corresponding to a dimension of the projection subspace.

Figure 5.8 depicts a smoothing spline matrix, with the rows ordered with x. The banded nature of this representation suggests that a smoothing spline is a local fitting method, much like the locally weighted regression procedures in Chapter 6. The right panel shows in detail selected rows of $\mathbf{S}$, which we call the *equivalent kernels*. As $\lambda \to 0$, $\text{df}_\lambda \to N$, and $\mathbf{S}_\lambda \to \mathbf{I}$, the N-dimensional identity matrix. As $\lambda \to \infty$, $\text{df}_\lambda \to 2$, and $\mathbf{S}_\lambda \to \mathbf{H}$, the hat matrix for linear regression on $\mathbf{x}$.

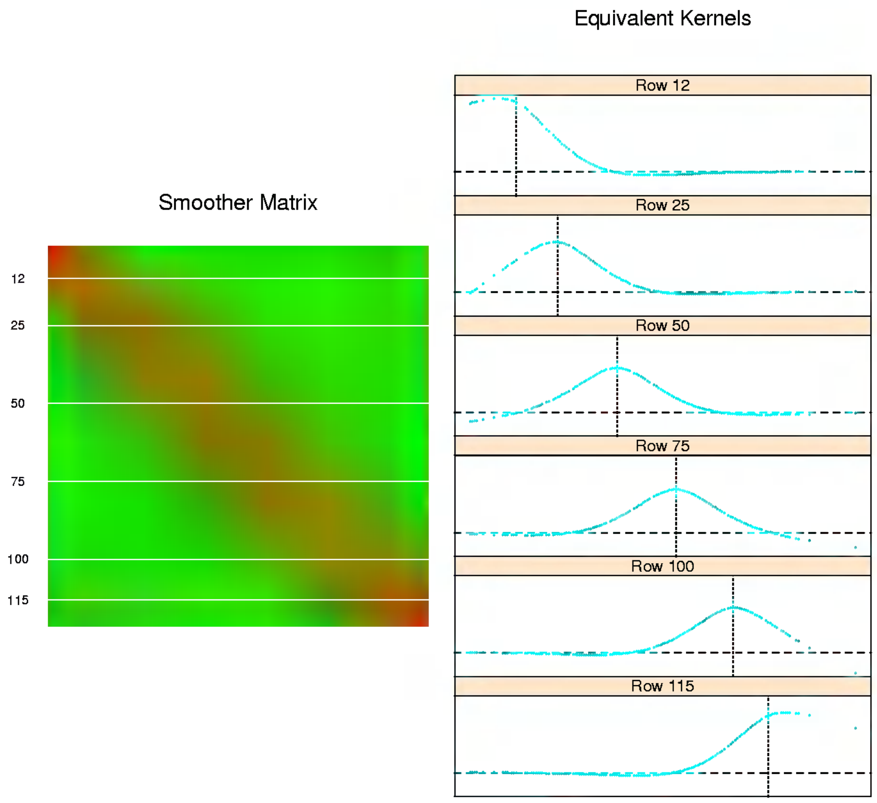

FIGURE 5.8. *The smoother matrix for a smoothing spline is nearly banded, indicating an equivalent kernel with local support. The left panel represents the elements of* **S** *as an image. The right panel shows the equivalent kernel or weighting function in detail for the indicated rows.*

5.5 Automatic Selection of the Smoothing Parameters

The smoothing parameters for regression splines encompass the degree of the splines, and the number and placement of the knots. For smoothing splines, we have only the penalty parameter λ to select, since the knots are at all the unique training X's, and cubic degree is almost always used in practice.

Selecting the placement and number of knots for regression splines can be a combinatorially complex task, unless some simplifications are enforced. The MARS procedure in Chapter 9 uses a greedy algorithm with some additional approximations to achieve a practical compromise. We will not discuss this further here.

5.5.1 Fixing the Degrees of Freedom

Since $\text{df}_\lambda = \text{trace}(\mathbf{S}_\lambda)$ is monotone in λ for smoothing splines, we can invert the relationship and specify λ by fixing df. In practice this can be achieved by simple numerical methods. So, for example, in S-PLUS one can use `smooth.spline(x,y,df=6)` to specify the amount of smoothing. This encourages a more traditional mode of model selection, where we might try a couple of different values of df, and select one based on approximate F-tests, residual plots and other more subjective criteria. Using df in this way provides a uniform approach to compare many different smoothing methods. It is particularly useful in *generalized additive models* (Chapter 9), where several smoothing methods can be simultaneously used in one model.

5.5.2 The Bias–Variance Tradeoff

Figure 5.9 shows the effect of the choice of df_λ when using a smoothing spline on a simple example:

$$\begin{aligned} Y &= f(X) + \varepsilon, \\ f(X) &= \frac{\sin(12(X+0.2))}{X+0.2}, \end{aligned} \tag{5.22}$$

with $X \sim U[0,1]$ and $\varepsilon \sim N(0,1)$. Our training sample consists of $N = 100$ pairs x_i, y_i drawn independently from this model.

The fitted splines for three different values of df_λ are shown. The yellow shaded region in the figure represents the pointwise standard error of $\hat{f}_\lambda$, that is, we have shaded the region between $\hat{f}_\lambda(x) \pm 2 \cdot \text{se}(\hat{f}_\lambda(x))$. Since $\hat{\mathbf{f}} = \mathbf{S}_\lambda \mathbf{y}$,

$$\begin{aligned} \text{Cov}(\hat{\mathbf{f}}) &= \mathbf{S}_\lambda \text{Cov}(\mathbf{y}) \mathbf{S}_\lambda^T \\ &= \mathbf{S}_\lambda \mathbf{S}_\lambda^T. \end{aligned} \tag{5.23}$$

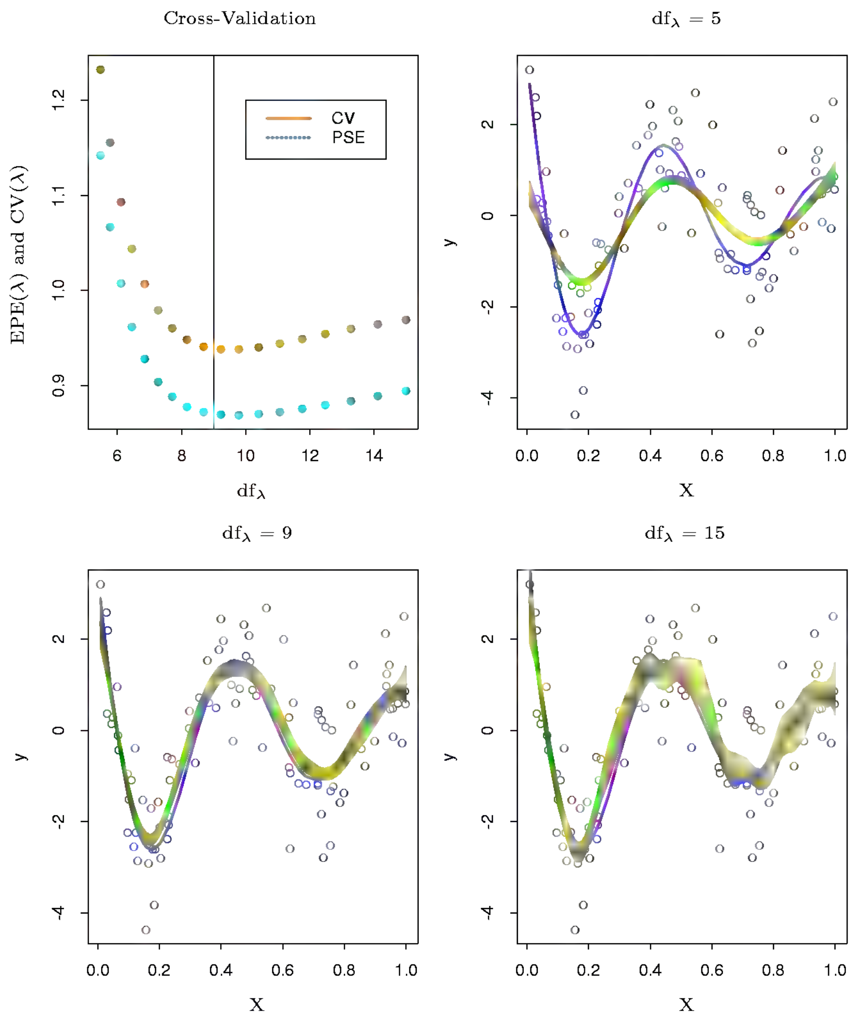

FIGURE 5.9. *The top left panel shows the* EPE(λ) *and* CV(λ) *curves for a realization from a nonlinear additive error model (5.22). The remaining panels show the data, the true functions (in purple), and the fitted curves (in green) with yellow shaded* $\pm 2\times$ *standard error bands, for three different values of* df_λ.

The diagonal contains the pointwise variances at the training x_i. The bias is given by

$$\begin{aligned}\text{Bias}(\hat{\mathbf{f}}) &= \mathbf{f} - \text{E}(\hat{\mathbf{f}}) \\ &= \mathbf{f} - \mathbf{S}_\lambda \mathbf{f}, \end{aligned} \tag{5.24}$$

where $\mathbf{f}$ is the (unknown) vector of evaluations of the true f at the training X's. The expectations and variances are with respect to repeated draws of samples of size $N = 100$ from the model (5.22). In a similar fashion $\text{Var}(\hat{f}_\lambda(x_0))$ and $\text{Bias}(\hat{f}_\lambda(x_0)$ can be computed at any point x_0 (Exercise 5.10). The three fits displayed in the figure give a visual demonstration of the bias-variance tradeoff associated with selecting the smoothing parameter.

$\text{df}_\lambda = 5$: The spline under fits, and clearly *trims down the hills and fills in the valleys*. This leads to a bias that is most dramatic in regions of high curvature. The standard error band is very narrow, so we estimate a badly biased version of the true function with great reliability!

$\text{df}_\lambda = 9$: Here the fitted function is close to the true function, although a slight amount of bias seems evident. The variance has not increased appreciably.

$\text{df}_\lambda = 15$: The fitted function is somewhat wiggly, but close to the true function. The wiggliness also accounts for the increased width of the standard error bands—the curve is starting to follow some individual points too closely.

Note that in these figures we are seeing a single realization of data and hence fitted spline $\hat{f}$ in each case, while the bias involves an expectation $\text{E}(\hat{f})$. We leave it as an exercise (5.10) to compute similar figures where the bias is shown as well. The middle curve seems "just right," in that it has achieved a good compromise between bias and variance.

The integrated squared prediction error (EPE) combines both bias and variance in a single summary:

$$\begin{aligned}\text{EPE}(\hat{f}_\lambda) &= \text{E}(Y - \hat{f}_\lambda(X))^2 \\ &= \text{Var}(Y) + \text{E}\left[\text{Bias}^2(\hat{f}_\lambda(X)) + \text{Var}(\hat{f}_\lambda(X))\right] \\ &= \sigma^2 + \text{MSE}(\hat{f}_\lambda). \end{aligned} \tag{5.25}$$

Note that this is averaged both over the training sample (giving rise to $\hat{f}_\lambda$), and the values of the (independently chosen) prediction points (X, Y). EPE is a natural quantity of interest, and does create a tradeoff between bias and variance. The blue points in the top left panel of Figure 5.9 suggest that $\text{df}_\lambda = 9$ is spot on!

Since we don't know the true function, we do not have access to EPE, and need an estimate. This topic is discussed in some detail in Chapter 7, and techniques such as K-fold cross-validation, GCV and C_p are all in common use. In Figure 5.9 we include the N-fold (leave-one-out) cross-validation curve:

$$\begin{aligned}\mathrm{CV}(\hat{f}_\lambda) &= \sum_{i=1}^{N}(y_i - \hat{f}_\lambda^{(-i)}(x_i))^2 && (5.26)\\ &= \sum_{i=1}^{N}\left(\frac{y_i - \hat{f}_\lambda(x_i)}{1 - S_\lambda(i,i)}\right)^2, && (5.27)\end{aligned}$$

which can (remarkably) be computed for each value of λ from the original fitted values and the diagonal elements $S_\lambda(i,i)$ of $\mathbf{S}_\lambda$ (Exercise 5.13).

The EPE and CV curves have a similar shape, but the entire CV curve is above the EPE curve. For some realizations this is reversed, and overall the CV curve is approximately unbiased as an estimate of the EPE curve.

5.6 Nonparametric Logistic Regression

The smoothing spline problem (5.9) in Section 5.4 is posed in a regression setting. It is typically straightforward to transfer this technology to other domains. Here we consider logistic regression with a single quantitative input X. The model is

$$\log\frac{\Pr(Y=1|X=x)}{\Pr(Y=0|X=x)} = f(x), \tag{5.28}$$

which implies

$$\Pr(Y=1|X=x) = \frac{e^{f(x)}}{1+e^{f(x)}}. \tag{5.29}$$

Fitting $f(x)$ in a smooth fashion leads to a smooth estimate of the conditional probability $\Pr(Y=1|x)$, which can be used for classification or risk scoring.

We construct the penalized log-likelihood criterion

$$\begin{aligned}\ell(f;\lambda) &= \sum_{i=1}^{N}[y_i \log p(x_i) + (1-y_i)\log(1-p(x_i))] - \frac{1}{2}\lambda\int\{f''(t)\}^2 dt\\ &= \sum_{i=1}^{N}\left[y_i f(x_i) + \log(1+e^{f(x_i)})\right] - \frac{1}{2}\lambda\int\{f''(t)\}^2 dt, && (5.30)\end{aligned}$$

where we have abbreviated $p(x) = \Pr(Y = 1|x)$. The first term in this expression is the log-likelihood based on the binomial distribution (c.f. Chapter 4, page 98). Arguments similar to those used in Section 5.4 show that the optimal f is a finite-dimensional natural spline with knots at the unique values of x. This means that we can represent $f(x) = \sum_{j=1}^{N} N_j(x)\theta_j$. We compute the first and second derivatives

$$\begin{aligned} \frac{\partial \ell(\theta)}{\partial \theta} &= \mathbf{N}^T(\mathbf{y} - \mathbf{p}) - \lambda \boldsymbol{\Omega}\theta, &(5.31)\\ \frac{\partial^2 \ell(\theta)}{\partial \theta \partial \theta^T} &= -\mathbf{N}^T\mathbf{W}\mathbf{N} - \lambda \boldsymbol{\Omega}, &(5.32)\end{aligned}$$

where $\mathbf{p}$ is the N-vector with elements $p(x_i)$, and $\mathbf{W}$ is a diagonal matrix of weights $p(x_i)(1 - p(x_i))$. The first derivative (5.31) is nonlinear in θ, so we need to use an iterative algorithm as in Section 4.4.1. Using Newton–Raphson as in (4.23) and (4.24) for linear logistic regression, the update equation can be written

$$\begin{aligned} \theta^{\text{new}} &= (\mathbf{N}^T\mathbf{W}\mathbf{N} + \lambda\boldsymbol{\Omega})^{-1}\mathbf{N}^T\mathbf{W}\left(\mathbf{N}\theta^{\text{old}} + \mathbf{W}^{-1}(\mathbf{y} - \mathbf{p})\right)\\ &= (\mathbf{N}^T\mathbf{W}\mathbf{N} + \lambda\boldsymbol{\Omega})^{-1}\mathbf{N}^T\mathbf{W}\mathbf{z}. &(5.33)\end{aligned}$$

We can also express this update in terms of the fitted values

$$\begin{aligned} \mathbf{f}^{\text{new}} &= \mathbf{N}(\mathbf{N}^T\mathbf{W}\mathbf{N} + \lambda\boldsymbol{\Omega})^{-1}\mathbf{N}^T\mathbf{W}\left(\mathbf{f}^{\text{old}} + \mathbf{W}^{-1}(\mathbf{y} - \mathbf{p})\right)\\ &= \mathbf{S}_{\lambda,w}\mathbf{z}. &(5.34)\end{aligned}$$

Referring back to (5.12) and (5.14), we see that the update fits a weighted smoothing spline to the working response $\mathbf{z}$ (Exercise 5.12).

The form of (5.34) is suggestive. It is tempting to replace $\mathbf{S}_{\lambda,w}$ by any nonparametric (weighted) regression operator, and obtain general families of nonparametric logistic regression models. Although here x is one-dimensional, this procedure generalizes naturally to higher-dimensional x. These extensions are at the heart of *generalized additive models*, which we pursue in Chapter 9.

5.7 Multidimensional Splines

So far we have focussed on one-dimensional spline models. Each of the approaches have multidimensional analogs. Suppose $X \in \mathbb{R}^2$, and we have a basis of functions $h_{1k}(X_1)$, $k = 1, \ldots, M_1$ for representing functions of coordinate X_1, and likewise a set of M_2 functions $H_{2k}(X_2)$ for coordinate X_2. Then the $M_1 \times M_2$ dimensional *tensor product basis* defined by

$$g_{jk}(X) = h_{1j}(X_1)h_{2k}(X_2),\ j = 1, \ldots, M_1,\ k = 1, \ldots, M_2 \qquad (5.35)$$

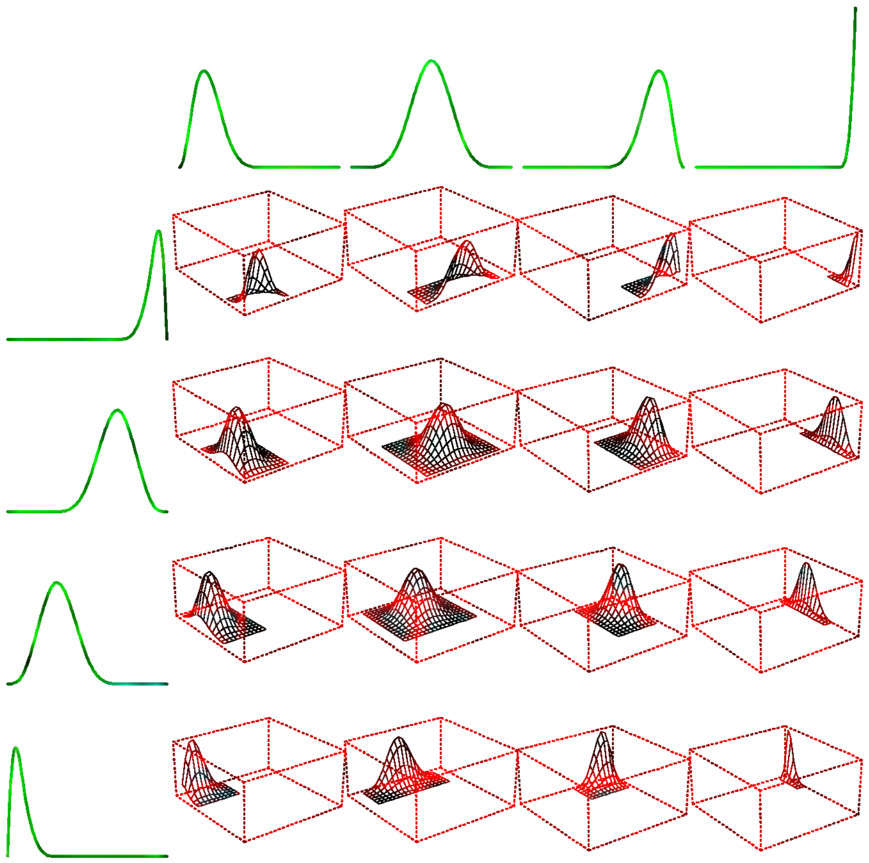

FIGURE 5.10. *A tensor product basis of B-splines, showing some selected pairs. Each two-dimensional function is the tensor product of the corresponding one dimensional marginals.*

can be used for representing a two-dimensional function:

$$g(X) = \sum_{j=1}^{M_1} \sum_{k=1}^{M_2} \theta_{jk} g_{jk}(X). \tag{5.36}$$

Figure 5.10 illustrates a tensor product basis using B-splines. The coefficients can be fit by least squares, as before. This can generalized to d dimensions, but note that the dimension of the basis grows exponentially fast—yet another manifestation of the curse of dimensionality. The MARS procedure discussed in Chapter 9 is a greedy forward algorithm for including only those tensor products that are deemed necessary by least squares.

Figure 5.11 illustrates the difference between additive and tensor product (natural) splines on the simulated classification example from Chapter 2. A logistic regression model $\text{logit}[\Pr(T|x)] = h(x)^T\theta$ is fit to the binary response, and the estimated decision boundary is the contour $h(x)^T\hat{\theta} = 0$. The tensor product basis can achieve more flexibility at the decision boundary, but introduces some spurious structure along the way.

One-dimensional smoothing splines (via regularization) generalize to higher dimensions as well. Suppose we have pairs y_i, x_i with $x_i \in \mathbb{R}^d$, and we seek a d-dimensional regression function $f(x)$. The idea is to set up the problem

$$\min_f \sum_{i=1}^N \{y_i - f(x_i)\}^2 + \lambda J[f], \tag{5.37}$$

where J is an appropriate penalty functional for stabilizing a function f in $\mathbb{R}^d$. For example, a natural generalization of the one-dimensional roughness penalty (5.9) for functions on $\mathbb{R}^2$ is

$$J[f] = \int\int_{\mathbb{R}^2} \left[\left(\frac{\partial^2 f(x)}{\partial x_1^2}\right)^2 + 2\left(\frac{\partial^2 f(x)}{\partial x_1 \partial x_2}\right)^2 + \left(\frac{\partial^2 f(x)}{\partial x_2^2}\right)^2\right] dx_1 dx_2. \tag{5.38}$$

Optimizing (5.37) with this penalty leads to a smooth two-dimensional surface, known as a thin-plate spline. It shares many properties with the one-dimensional cubic smoothing spline:

- as $\lambda \to 0$, the solution approaches an interpolating function [the one with smallest penalty (5.38)];
- as $\lambda \to \infty$, the solution approaches the least squares plane;
- for intermediate values of λ, the solution can be represented as a linear expansion of basis functions, whose coefficients are obtained by a form of generalized ridge regression.

The solution has the form

$$f(x) = \beta_0 + \beta^T x + \sum_{j=1}^N \alpha_j h_j(x), \tag{5.39}$$

where $h_j(x) = \eta(||x - x_j||)$, and $\eta(z) = z^2 \log z^2$. These h_j are examples of *radial basis functions*, which are discussed in more detail in the next section. The coefficients are found by plugging (5.39) into (5.37), which reduces to a finite-dimensional penalized least squares problem. For the penalty to be finite, the coefficients α_j have to satisfy a set of linear constraints; see Exercise 5.14.

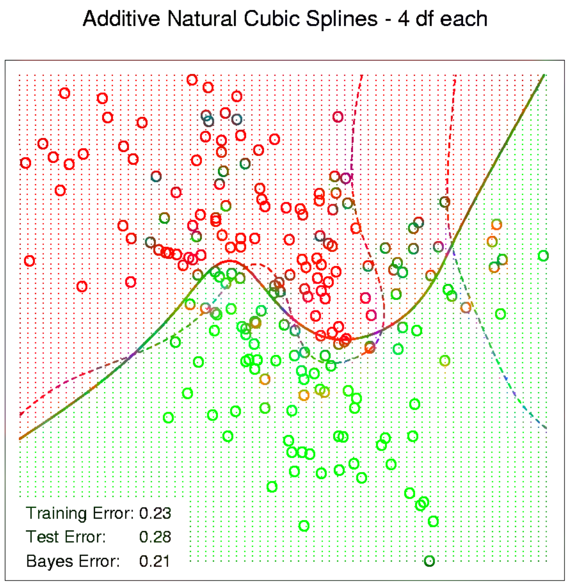

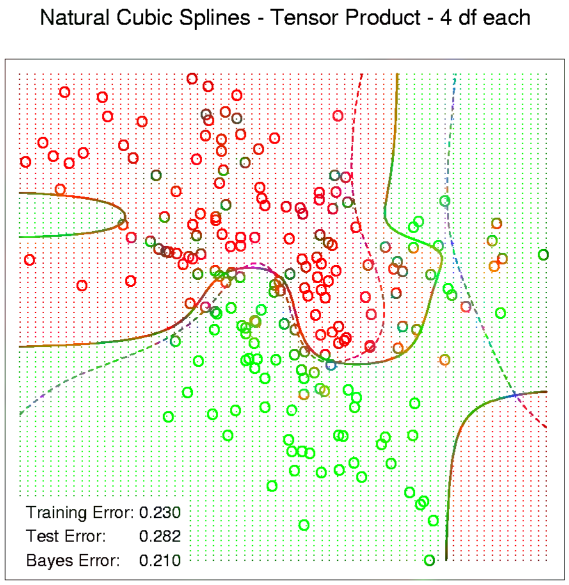

FIGURE 5.11. *The simulation example of Figure 2.1. The upper panel shows the decision boundary of an additive logistic regression model, using natural splines in each of the two coordinates (total df* $= 1 + (4 - 1) + (4 - 1) = 7$*). The lower panel shows the results of using a tensor product of natural spline bases in each coordinate (total df* $= 4 \times 4 = 16$*). The broken purple boundary is the Bayes decision boundary for this problem.*

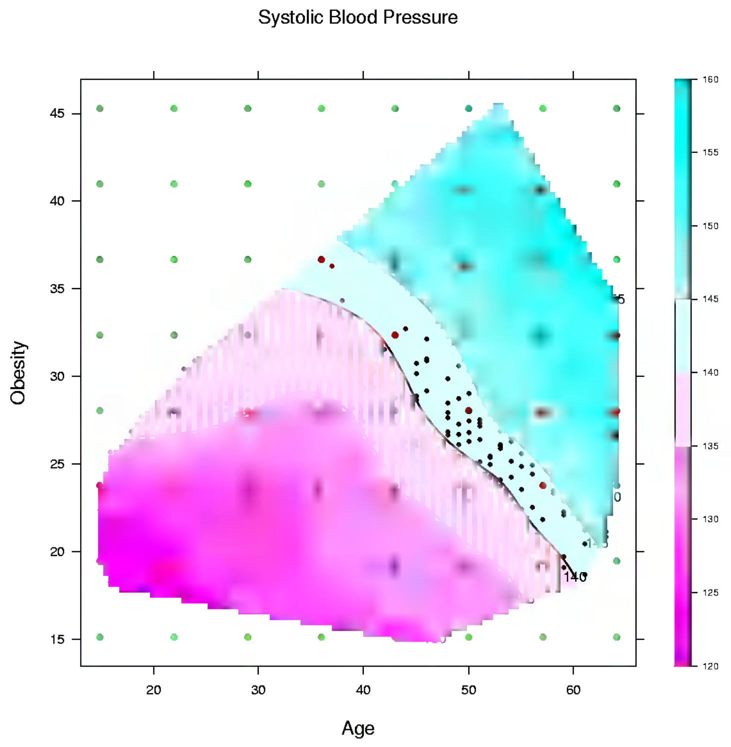

FIGURE 5.12. *A thin-plate spline fit to the heart disease data, displayed as a contour plot. The response is* `systolic blood pressure`*, modeled as a function of* `age` *and* `obesity`*. The data points are indicated, as well as the lattice of points used as knots. Care should be taken to use knots from the lattice inside the convex hull of the data (red), and ignore those outside (green).*

Thin-plate splines are defined more generally for arbitrary dimension d, for which an appropriately more general J is used.

There are a number of hybrid approaches that are popular in practice, both for computational and conceptual simplicity. Unlike one-dimensional smoothing splines, the computational complexity for thin-plate splines is $O(N^3)$, since there is not in general any sparse structure that can be exploited. However, as with univariate smoothing splines, we can get away with substantially less than the N knots prescribed by the solution (5.39). In practice, it is usually sufficient to work with a lattice of knots covering the domain. The penalty is computed for the reduced expansion just as before. Using K knots reduces the computations to $O(NK^2 + K^3)$. Figure 5.12 shows the result of fitting a thin-plate spline to some heart disease risk factors, representing the surface as a contour plot. Indicated are the location of the input features, as well as the knots used in the fit. Note that λ was specified via $\text{df}_\lambda = \text{trace}(S_\lambda) = 15$.

More generally one can represent $f \in \mathbb{R}^d$ as an expansion in any arbitrarily large collection of basis functions, and control the complexity by applying a regularizer such as (5.38). For example, we could construct a basis by forming the tensor products of all pairs of univariate smoothing-spline basis functions as in (5.35), using, for example, the univariate B-splines recommended in Section 5.9.2 as ingredients. This leads to an exponential growth in basis functions as the dimension increases, and typically we have to reduce the number of functions per coordinate accordingly.

The additive spline models discussed in Chapter 9 are a restricted class of multidimensional splines. They can be represented in this general formulation as well; that is, there exists a penalty $J[f]$ that guarantees that the solution has the form $f(X) = \alpha + f_1(X_1) + \cdots + f_d(X_d)$ and that each of the functions f_j are univariate splines. In this case the penalty is somewhat degenerate, and it is more natural to *assume* that f is additive, and then simply impose an additional penalty on each of the component functions:

$$\begin{aligned} J[f] &= J(f_1 + f_2 + \cdots + f_d) \\ &= \sum_{j=1}^{d} \int f_j''(t_j)^2 dt_j. \end{aligned} \tag{5.40}$$

These are naturally extended to ANOVA spline decompositions,

$$f(X) = \alpha + \sum_j f_j(X_j) + \sum_{j<k} f_{jk}(X_j, X_k) + \cdots , \tag{5.41}$$

where each of the components are splines of the required dimension. There are many choices to be made:

- The maximum order of interaction—we have shown up to order 2 above.
- Which terms to include—not all main effects and interactions are necessarily needed.
- What representation to use—some choices are:
  - regression splines with a relatively small number of basis functions per coordinate, and their tensor products for interactions;
  - a complete basis as in smoothing splines, and include appropriate regularizers for each term in the expansion.

In many cases when the number of potential dimensions (features) is large, automatic methods are more desirable. The MARS and MART procedures (Chapters 9 and 10 respectively), both fall into this category.

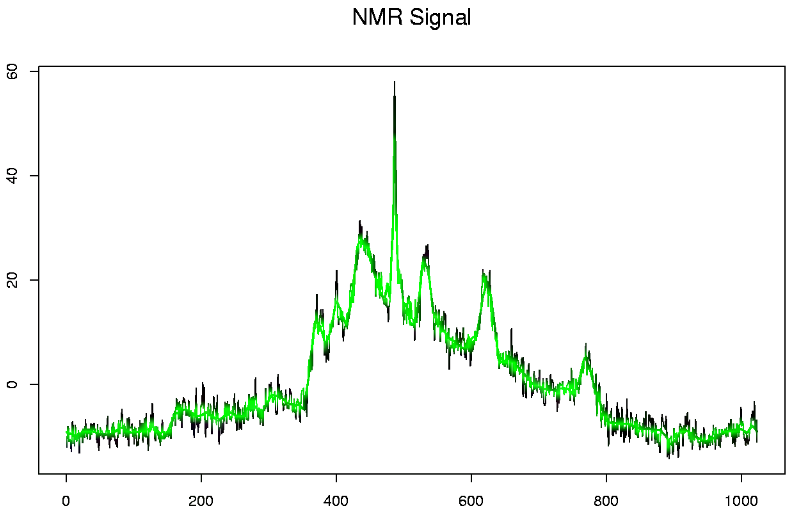

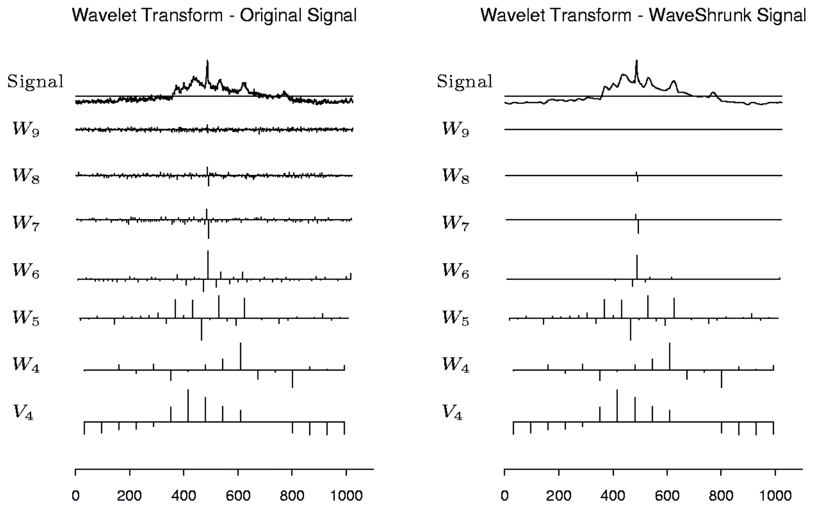

FIGURE 5.14. *The top panel shows a NMR signal, with the wavelet-shrunk version superimposed in green. The lower left panel represents the wavelet transform of the original signal, down to V_4, using the* symmlet-8 *basis. Each coefficient is represented by the height (positive or negative) of the vertical bar. The lower right panel represents the wavelet coefficients after being shrunken using the* `waveshrink` *function in S-PLUS, which implements the* SureShrink *method of wavelet adaptation of Donoho and Johnstone.*

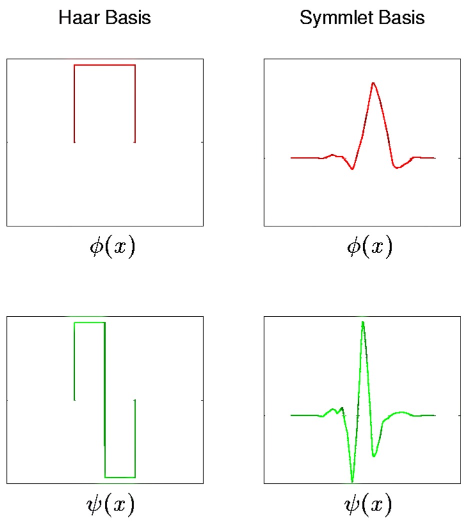

FIGURE 5.15. *The* Haar *and* symmlet *father (scaling) wavelet* $\phi(x)$ *and mother wavelet* $\psi(x)$.

generated by the *mother wavelet* $\psi(x) = \phi(2x) - \psi(2x-1)$ form an orthonormal basis for W_0 for the Haar family. Likewise $\psi_{j,k} = 2^{j/2}\psi(2^j x - k)$ form a basis for W_j.

Now $V_{j+1} = V_j \oplus W_j = V_{j-1} \oplus W_{j-1} \oplus W_j$, so besides representing a function by its level-j detail and level-j rough components, the latter can be broken down to level-$(j-1)$ detail and rough, and so on. Finally we get a representation of the form $V_J = V_0 \oplus W_0 \oplus W_1 \cdots \oplus W_{J-1}$. Figure 5.13 on page 149 shows particular wavelets $\psi_{j,k}(x)$.

Notice that since these spaces are orthogonal, all the basis functions are orthonormal. In fact, if the domain is discrete with $N = 2^J$ (time) points, this is as far as we can go. There are 2^j basis elements at level j, and adding up, we have a total of $2^J - 1$ elements in the W_j, and one in V_0. This structured orthonormal basis allows for a *multiresolution analysis*, which we illustrate in the next section.

While helpful for understanding the construction above, the Haar basis is often too coarse for practical purposes. Fortunately, many clever wavelet bases have been invented. Figures 5.13 and 5.15 include the *Daubechies symmlet-8* basis. This basis has smoother elements than the corresponding Haar basis, but there is a tradeoff:

- Each wavelet has a support covering 15 consecutive time intervals, rather than one for the Haar basis. More generally, the symmlet-p family has a support of $2p-1$ consecutive intervals. The wider the support, the more time the wavelet has to die to zero, and so it can achieve this more smoothly. Note that the effective support seems to be much narrower.

- The symmlet-p wavelet $\phi(x)$ has p vanishing moments; that is,

$$\int \phi(x)x^j dx = 0, \; j = 1, \dots, p.$$

One implication is that any degree-p polynomial over the $N = 2^J$ times points is reproduced exactly in V_0 (Exercise 5.17). In this sense V_0 is equivalent to the null space of the smoothing-spline penalty. The Haar wavelets have one vanishing moment, and V_0 can reproduce any constant function.

The symmlet-p scaling functions are one of many families of wavelet generators. The operations are similar to those for the Haar basis:

- If V_0 is spanned by $\phi(x-k)$, then $V_1 \supset V_0$ is spanned by $\phi_{1,k}(x) = \sqrt{2}\phi(2x-k)$ and $\phi(x) = \sum_{k \in \mathcal{Z}} h(k)\phi_{1,k}(x)$, for some filter coefficients $h(k)$.
- W_0 is spanned by $\psi(x) = \sum_{k \in \mathcal{Z}} g(k)\phi_{1,k}(x)$, with filter coefficients $g(k) = (-1)^\ell h(1-k)$.

5.9.2 Adaptive Wavelet Filtering

Wavelets are particularly useful when the data are measured on a uniform lattice, such as a discretized signal, image, or a time series. We will focus on the one-dimensional case, and having $N = 2^J$ lattice-points is convenient. Suppose $\mathbf{y}$ is the response vector, and $\mathbf{W}$ is the $N \times N$ orthonormal wavelet basis matrix evaluated at the N uniformly spaced observations. Then $\mathbf{y}^* = \mathbf{W}^T\mathbf{y}$ is called the *wavelet transform* of $\mathbf{y}$ (and is the full least squares regression coefficient). A popular method for adaptive wavelet fitting is known as *SURE shrinkage* [Stein Unbiased Risk Estimation, (Donoho and Johnstone, 1994)]:

$$\min_{\boldsymbol{\theta}} ||\mathbf{y} - \mathbf{W}\boldsymbol{\theta}||_2^2 + 2\lambda||\boldsymbol{\theta}||_1, \tag{5.67}$$

which is the same as the lasso criterion in Chapter 3. Because $\mathbf{W}$ is orthonormal, this leads to the simple solution:

$$\hat{\theta}_j = \text{sign}(y_j^*)(|y_j^*| - \lambda)_+. \tag{5.68}$$

The least squares coefficients are translated toward zero, and truncated at zero. The fitted function (vector) is then given by the *inverse wavelet transform* $\hat{\mathbf{f}} = \mathbf{W}\hat{\boldsymbol{\theta}}$.

A simple choice for λ is $\lambda = \sigma\sqrt{2\log N}$, where σ is an estimate of the standard deviation of the noise. We can give some motivation for this choice. Since $\mathbf{W}$ is an orthonormal transformation, if the elements of $\mathbf{y}$ are white noise (independent Gaussian variates with mean 0 and variance σ^2), then so are $\mathbf{y}^*$. Furthermore if random variables $Z_1, Z_2, \ldots, Z_N$ are white noise, the expected maximum of $|Z_j|, j = 1, \ldots, N$ is approximately $\sigma\sqrt{2\log N}$. Hence all coefficients below $\sigma\sqrt{2\log N}$ are likely to be noise and are set to zero.

The space $\mathbf{W}$ could be any basis of orthonormal functions: polynomials, natural splines or cosinusoids. For example what makes wavelets special is the particular form of basis functions used, which allows for a representation *localized in time and in frequency.*

Let's look again at the NMR signal of Figure 5.14. The wavelet transform was computed using a *symmlet*−8 basis. Notice that the coefficients do not descend all the way to V_0, but stop at V_4 which has 16 basis functions. As we ascend to each level of detail, the coefficients get smaller, except in locations where spiky behavior is present. The wavelet coefficients represent characteristics of the signal localized in time (the basis functions at each level are translations of each other) and localized in frequency. Each dilation increases the detail by a factor of two, and in this sense corresponds to doubling the frequency in a traditional Fourier representation. In fact, a more mathematical understanding of wavelets reveals that the wavelets at a particular scale have a Fourier transform that is restricted to a limited range or octave of frequencies.

The shrinking/truncation in the right panel was achieved using the SURE approach described in the introduction to this section. The orthonormal $N \times N$ basis matrix $\mathbf{W}$ has columns, which are the wavelet basis functions evaluated at the N time points. In particular, in this case there will be 16 columns corresponding to the $\phi_{4,k}(x)$, and the remainder devoted to the $\psi_{j,k}(x)$, $j = 4, \ldots, 11$. In practice λ depends on the noise variance, and has to be estimated from the data (such as the variance of the coefficients at the highest level).

Notice the similarity between the SURE criterion (5.67) on page 153, and the smoothing spline criterion (5.21) on page 132:

- Both are hierarchically structured from coarse to fine detail, although wavelets are also localized in time within each resolution level.

- The splines build in a bias toward smooth functions by imposing differential shrinking constants d_k. Early versions of SURE shrinkage treated all scales equally. The `S+wavelets` function `waveshrink()` has many options, some of which allow for differential shrinkage.

- The spline L_2 penalty cause pure shrinkage, while the SURE L_1 penalty does shrinkage and selection.

More generally smoothing splines achieve compression of the original signal by imposing smoothness, while wavelets impose sparsity. Figure 5.16 compares a wavelet fit (using SURE shrinkage) to a smoothing spline fit (using cross-validation) on two examples different in nature. For the NMR data in the left panel, the smoothing spline introduces detail everywhere in order to capture the detail in the isolated spikes; the wavelet fit nicely localizes the spikes. In the right panel, the true function is smooth, and the noise is relatively high. The wavelet fit has let in some additional and unnecessary wiggles—a price it pays in variance for the additional adaptivity.

The wavelet transform is not performed by matrix multiplication as in $\mathbf{y}^* = \mathbf{W}^T\mathbf{y}$. In fact, using clever pyramidal schemes $\mathbf{y}^*$ can be obtained in $O(N)$ computations, which is even faster than the $N\log(N)$ of the fast Fourier transform (FFT). While the general construction is beyond the scope of this book, it is easy to see for the Haar basis (Exercise 5.18). Likewise, the inverse wavelet transform $\mathbf{W}\hat{\boldsymbol{\theta}}$ is also $O(N)$.

This has been a very brief glimpse of this vast and growing field. There is a very large mathematical and computational base built on wavelets. Modern image compression is often performed using two-dimensional wavelet representations.

Bibliographic Notes

Splines and B-splines are discussed in detail in de Boor (1978). Green and Silverman (1994) and Wahba (1990) give a thorough treatment of smoothing splines and thin-plate splines; the latter also covers reproducing kernel Hilbert spaces. See also Girosi et al. (1995) and Evgeniou et al. (2001) for connections between many nonparametric regression techniques using RKHS approaches. Modelling functional data, as in Section 5.2.3, is covered in detail in Ramsay and Silverman (1997).

Daubechies (1992) is a classic and mathematical treatment of wavelets. Other useful sources are Chui (1992) and Wickerhauser (1994). Donoho and Johnstone (1994) developed the SURE shrinkage and selection technology from a statistical estimation framework; see also Vidakovic (1999). Bruce and Gao (1996) is a useful applied introduction, which also describes the wavelet software in S-PLUS.

Exercises

Ex. 5.1 Show that the truncated power basis functions in (5.3) represent a basis for a cubic spline with the two knots as indicated.

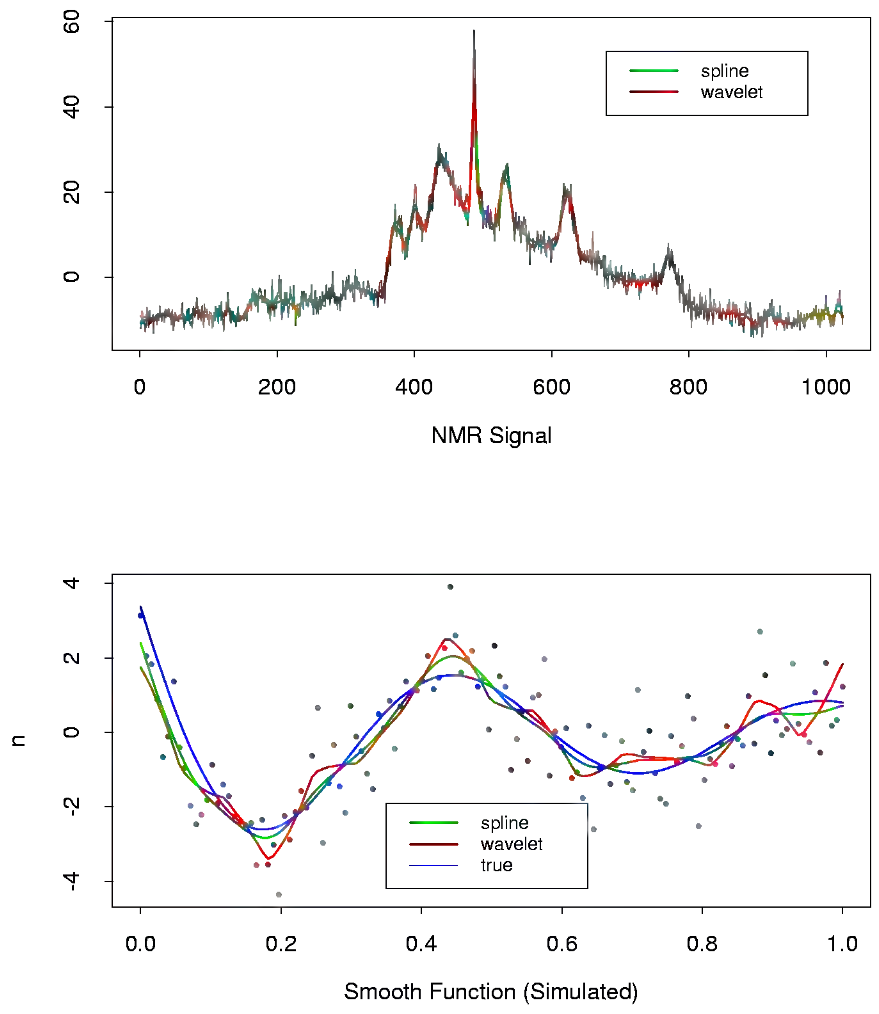

FIGURE 5.16. *Wavelet smoothing compared with smoothing splines on two examples. Each panel compares the SURE-shrunk wavelet fit to the cross-validated smoothing spline fit.*

Ex. 5.2 Suppose that $B_{i,m}(x)$ is an order M B-spline defined in Section 5.9.2.

(a) Show by induction that $B_{i,m}(x) = 0$ for $x \notin [\tau_i, \tau_{i+m}]$. This shows, for example, that the support of cubic B-splines is at most 5 knots.

(b) Show by induction that $B_{i,m}(x) > 0$ for $x \in (\tau_i, \tau_{i+m})$. B-splines are positive in the interior of their support.

(c) Show, using induction, that $\sum_{i=1}^{K+m} B_{i,m}(x) = 1 \, \forall x \in [\xi_0, \xi_{K+1}]$.

(d) Show that $B_{i,m}$ is a piecewise polynomial of order m, with breaks only at the knots τ_j.

(e) Show that an order-M B-spline basis function is the density function of a convolution of M uniform random variables.

Ex. 5.3 Write a program to reproduce Figure 5.3 on page 121.

Ex. 5.4 Consider the truncated power series representation for cubic splines with K interior knots. Let

$$f(X) = \sum_{j=0}^{3} \beta_j X^j + \sum_{k=1}^{K} \theta_k (X - \xi_k)_+^3. \tag{5.69}$$

Prove that the natural boundary conditions for natural cubic splines (Section 5.2.1) imply the following linear constraints on the coefficients:

$$\begin{aligned} \beta_2 = 0, \qquad & \textstyle\sum_{k=1}^{K} \theta_k = 0, \\ \beta_3 = 0, \qquad & \textstyle\sum_{k=1}^{K} \xi_k \theta_k = 0. \end{aligned} \tag{5.70}$$

Hence derive the basis (5.4) and (5.5).

Ex. 5.5 Write a program to classify the `phoneme` data using a quadratic discriminant analysis (Section 4.3). Since there are many correlated features, you should filter them using a smooth basis of natural cubic splines (Section 5.2.3). Decide beforehand on a series of five different choices for the number and position of the knots, and use tenfold cross-validation to make the final selection. The `phoneme` data are available from the book website `www-stat.stanford.edu/ElemStatLearn`.

Ex. 5.6 Suppose you wish to fit a periodic function, with a known period T. Describe how you could modify the truncated power series basis to achieve this goal.

Ex. 5.7 *Derivation of smoothing splines* (Green and Silverman, 1994). Suppose that $N \geq 2$, and that g is the natural cubic spline interpolant to the pairs $\{x_i, z_i\}_1^N$, with $a < x_1 < \cdots < x_N < b$. This is a natural spline with a knot at every x_i; being an N-dimensional space of functions, we can determine the coefficients such that it interpolates the sequence z_i exactly. Let $\tilde{g}$ be any other differentiable function on $[a,b]$ that interpolates the N pairs.

(a) Let $h(x) = \tilde{g}(x) - g(x)$. Use the boundary conditions on g and integration by parts to show that

$$\int_a^b g''(x)h''(x)dx = -\sum_{j=1}^{N-1} g'''(x_j^+)\{h(x_{j+1} - h(x_j)\}. \tag{5.71}$$

(b) Use the fact that g is a natural cubic spline to argue that this expression is zero, and hence that

$$\int_a^b \tilde{g}''(t)^2 dt \geq \int_a^b g''(t)^2 dt.$$

(c) Show that equality can only hold if h is identically zero in $[a,b]$.

(d) Consider the penalized least squares problem

$$\min_f \left[\sum_{i=1}^N (y_i - f(x_i))^2 + \lambda \int_a^b f''(t)^2 dt\right].$$

Use (b) to argue that the minimizer must be a cubic spline with knots at each of the x_i.

Ex. 5.8 In the appendix to this chapter we show how the smoothing spline computations could be more efficiently carried out using a $(N+4)$ dimensional basis of B-splines. Describe a slightly simpler scheme using a $(N+2)$ dimensional B-spline basis defined on the $N-2$ interior knots.

Ex. 5.9 Derive the Reinsch form $\mathbf{S}_\lambda = (\mathbf{I} + \lambda\mathbf{K})^{-1}$ for the smoothing spline.

Ex. 5.10 Derive an expression for $\text{Var}(\hat{f}_\lambda(x_0))$ and $\text{bias}(\hat{f}_\lambda(x_0))$. Using the example (5.22), create a version of Figure 5.9 where the mean and several (pointwise) quantiles of $\hat{f}_\lambda(x)$ are shown.

Ex. 5.11 Prove that for a smoothing spline the null space of $\mathbf{K}$ is spanned by functions linear in X.

Ex. 5.12 Characterize the solution to the following problem,

$$\min_f \text{RSS}(f,\lambda) = \sum_{i=1}^N w_i\{y_i - f(x_i)\}^2 + \lambda \int \{f''(t)\}^2 dt, \tag{5.72}$$

where the $w_i \geq 0$ are observation weights.

Characterize the solution to the smoothing spline problem (5.9) when the training data have ties in X.

Ex. 5.13 You have fitted a smoothing spline $\hat{f}_\lambda$ to a sample of N pairs (x_i, y_i). Suppose you augment your original sample with the pair $x_0, \hat{f}_\lambda(x_0)$, and refit; describe the result. Use this to derive the N-fold cross-validation formula (5.26).

Ex. 5.14 Derive the constraints on the α_j in the thin-plate spline expansion (5.39) to guarantee that the penalty $J(f)$ is finite. How else could one ensure that the penalty was finite?

Ex. 5.15 This exercise derives some of the results quoted in Section 5.8.1. Suppose $K(x,y)$ satisfying the conditions (5.45) and let $f(x) \in \mathcal{H}_K$. Show that

(a) $\langle K(\cdot, x_i), f\rangle_{\mathcal{H}_K} = f(x_i)$.

(b) $\langle K(\cdot, x_i), K(\cdot, x_j)\rangle_{\mathcal{H}_K} = K(x_i, x_j)$.

(c) If $g(x) = \sum_{i=1}^N \alpha_i K(x, x_i)$, then

$$J(g) = \sum_{i=1}^N \sum_{j=1}^N K(x_i, x_j)\alpha_i\alpha_j.$$

Suppose that $\tilde{g}(x) = g(x) + \rho(x)$, with $\rho(x) \in \mathcal{H}_K$, and orthogonal in $\mathcal{H}_K$ to each of $K(x, x_i)$, $i = 1, \dots, N$. Show that

(d)

$$\sum_{i=1}^N L(y_i, \tilde{g}(x_i)) + \lambda J(\tilde{g}) \geq \sum_{i=1}^N L(y_i, g(x_i)) + \lambda J(g) \tag{5.73}$$

with equality iff $\rho(x) = 0$.

Ex. 5.16 Consider the ridge regression problem (5.53), and assume $M \geq N$. Assume you have a kernel K that computes the inner product $K(x,y) = \sum_{m=1}^M h_m(x)h_m(y)$.

(a) Derive (5.62) on page 147 in the text. How would you compute the matrices $\mathbf{V}$ and $\mathbf{D}_\gamma$, given K? Hence show that (5.63) is equivalent to (5.53).

(b) Show that

$$\begin{aligned} \mathbf{f} &= \mathbf{H}\hat{\boldsymbol{\beta}} \\ &= \mathbf{K}(\mathbf{K} + \lambda\mathbf{I})^{-1}\mathbf{y}, \end{aligned} \tag{5.74}$$

where $\mathbf{H}$ is the $N \times M$ matrix of evaluations $h_m(x_i)$, and $\mathbf{K} = \mathbf{H}\mathbf{H}^T$ the $N \times N$ matrix of inner-products $h(x_i)^T h(x_j)$;

(c) Show that

$$\begin{aligned}\hat{f}(x) &= h(x)^T\hat{\boldsymbol{\beta}} \\ &= \sum_{i=1}^{N} K(x, x_i)\hat{\boldsymbol{\alpha}}_i \end{aligned} \tag{5.75}$$

and $\hat{\boldsymbol{\alpha}} = (\mathbf{K} + \lambda\mathbf{I})^{-1}\mathbf{y}$.

(d) How would you modify your solution if $M < N$?

Ex. 5.17 The scaling function $\phi(x)$ of the the symmlet-p wavelet basis has vanishing moments up to order p. Show that this implies that polynomials of degree p are represented exactly in V_0, defined on page 150.

Ex. 5.18 Show that the Haar wavelet transform of a signal of length $N = 2^J$ can be computed in $O(N)$ computations.

Computational Considerations for Splines

In this appendix, we describe the B-spline basis for representing polynomial splines. We also discuss their use in the computations of smoothing splines.

Appendix: B-splines

Before we can get started, we need to augment the knot sequence defined in Section 5.2. Let $\xi_0 < \xi_1$ and $\xi_K < \xi_{K+1}$ be two *boundary* knots, which typically define the domain over which we wish to evaluate our spline. We now define the augmented knot sequence τ such that

- $\tau_1 \le \tau_2 \le \cdots \le \tau_M \le \xi_0$;
- $\tau_{j+M} = \xi_j,\ j = 1, \cdots, K$;
- $\xi_{K+1} \le \tau_{K+M+1} \le \tau_{K+M+2} \le \cdots \le \tau_{K+2M}$.

The actual values of these additional knots beyond the boundary are arbitrary, and it is customary to make them all the same and equal to ξ_0 and ξ_{K+1}, respectively.

Denote by $B_{i,m}(x)$ the ith B-spline basis function of order m for the knot-sequence τ, $m \le M$. They are defined recursively in terms of divided differences as follows:

$$B_{i,1} = \begin{cases} 1 & \text{if } \tau_i \le x < \tau_{i+1} \\ 0 & \text{otherwise} \end{cases} \tag{5.76}$$

for $i = 1, \ldots, K + 2M - 1$. These are also known as Haar basis functions.

$$B_{i,m}(x) = \frac{x-\tau_i}{\tau_{i+m-1}-\tau_i}B_{i,m-1} + \frac{\tau_{i+m}-x}{\tau_{i+m}-\tau_{i+1}}B_{i+1,m-1}(x) \quad (5.77)$$

for $i = 1, \ldots, K+2M-m$.

Thus with $M = 4$, $B_{i,4}$, $i = 1, \cdots, K+4$ are the $K+4$ cubic B-spline basis functions for the knot sequence ξ. This recursion can be continued and will generate the B-spline basis for any order spline. Figure 5.17 shows the sequence of B-splines up to order four with knots at the points $0.0, 0.1, \ldots, 1.0$. Since we have created some duplicate knots, some care has to be taken to avoid division by zero. If we adopt the convention that $B_{i,1} = 0$ if $\tau_i = \tau_{i+1}$, then by induction $B_{i,m} = 0$ if $\tau_i = \tau_{i+1} = \ldots = \tau_{i+m}$.

To fully understand the properties of these functions, and to show that they do indeed span the space of cubic splines for the knot sequence, requires additional mathematical machinery including the properties of divided differences. Exercises 5.2–5.2 explore these issues.

The scope of B-splines is in fact bigger than advertised here, and has to do with knot duplication. If we duplicate an interior knot in the construction of the τ sequence above, and then generate the B-spline sequence as before, the resulting basis spans the space of piecewise polynomials with one less continuous derivative at the duplicated knot. In general, if in addition to the repeated boundary knots, we include the interior knot ξ_j $1 \leq r_j \leq M$ times, then the lowest-order derivative to be discontinuous at $x = \xi_j$ will be order $M - r_j$. Thus for cubic splines with no repeats, $r_j = 1$, $j = 1, \ldots, K$, and at each interior knot the third derivatives $(4-1)$ are discontinuous. Repeating the jth knot three times leads to a discontinuous 1st derivative; repeating it four times leads to a discontinuous zeroeth derivative, i.e., the function is discontinuous at $x = \xi_j$. This is exactly what happens at the boundary knots; we repeat the knots M times, so the spline becomes discontinuous at the boundary knots (i.e., undefined beyond the boundary).

The local support of B-splines has important computational implications, especially when the number of knots K is large. Least squares computations with N observations and $K+M$ variables (basis functions) take $O(N(K+M)^2 + (K+M)^3)$ flops (floating point operations.) If K is some appreciable fraction of N, this leads to $O(N^3)$ algorithms which becomes unacceptable for large N. If the N observations are sorted, the $N \times (K+M)$ regression matrix consisting of the $K+M$ B-spline basis functions evaluated at the N points has many zeros, which can be exploited to reduce the computational complexity back to $O(N)$. We take this up further in the next section.

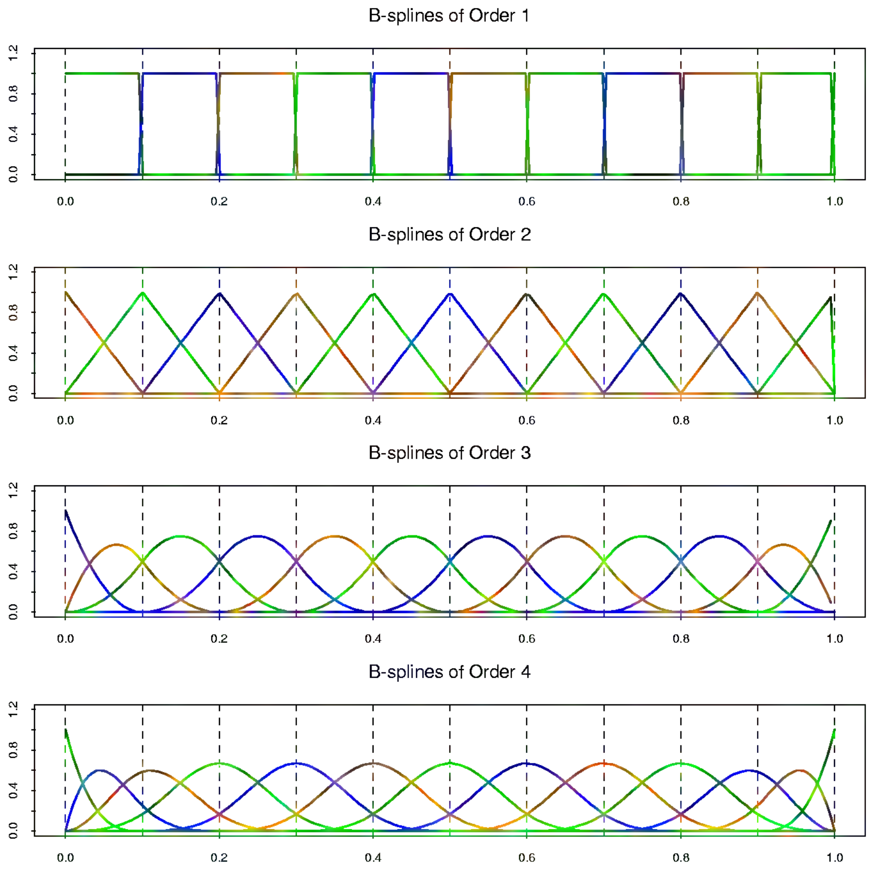

FIGURE 5.17. *The sequence of B-splines up to order four with ten knots evenly spaced from* 0 *to* 1*. The B-splines have* local support*; they are nonzero on an interval spanned by $M + 1$ knots.*

Computations for Smoothing Splines

Although natural splines (Section 5.2.1) provide a basis for smoothing splines, it is computationally more convenient to operate in the larger space of unconstrained B-splines. We write $f(x) = \sum_1^{N+4} \gamma_j B_j(x)$, where γ_j are coefficients and the B_j are the cubic B-spline basis functions. The solution looks the same as before,

$$\hat{\boldsymbol{\gamma}} = (\mathbf{B}^T\mathbf{B} + \lambda\boldsymbol{\Omega}_B)^{-1}\mathbf{B}^T\mathbf{y}, \tag{5.78}$$

except now the $N \times N$ matrix $\mathbf{N}$ is replaced by the $(N+4) \times N$ matrix $\mathbf{B}$, and similarly the $(N+4) \times (N+4)$ penalty matrix $\boldsymbol{\Omega}_B$ replaces the $N \times N$ dimensional $\boldsymbol{\Omega}_N$. Although at face value it seems that there are no boundary derivative constraints, it turns out that the penalty term automatically imposes them by giving effectively infinite weight to any non zero derivative beyond the boundary. In practice, $\hat{\gamma}$ is restricted to a linear subspace for which the penalty is always finite.

Since the columns of $\mathbf{B}$ are the evaluated B-splines, in order from left to right and evaluated at the *sorted* values of X, and the cubic B-splines have local support, $\mathbf{B}$ is lower 4-banded. Consequently the matrix $\mathbf{M} = (\mathbf{B^TB} + \lambda\boldsymbol{\Omega})$ is 4-banded and hence its Cholesky decomposition $\mathbf{M} = \mathbf{LL^T}$ can be computed easily. One then solves $\mathbf{LL}^T\boldsymbol{\gamma} = \mathbf{B}^T\mathbf{y}$ by back-substitution to give $\boldsymbol{\gamma}$ and hence the solution $\hat{f}$ in $O(N)$ operations.

In practice, when N is large, it is unnecessary to use all N interior knots, and any reasonable *thinning* strategy will save in computations and have negligible effect on the fit. For example, the `smooth.spline` function in S-PLUS uses an approximately logarithmic strategy: if $N < 50$ all knots are included, but even at $N = 5,000$ only 204 knots are used.

6
Kernel Methods

In this chapter we describe a class of regression techniques that achieve flexibility in estimating the regression function $f(X)$ over the domain $\mathbb{R}^p$ by fitting a different but simple model separately at each query point x_0. This is done by using only those observations close to the target point x_0 to fit the simple model, and in such a way that the resulting estimated function $\hat{f}(X)$ is *smooth* in $\mathbb{R}^p$. This localization is achieved via a weighting function or *kernel* $K_\lambda(x_0, x_i)$, which assigns a weight to x_i based on its distance from x_0. The kernels K_λ are typically indexed by a parameter λ that dictates the width of the neighborhood. These *memory-based* methods require in principle little or no training; all the work gets done at evaluation time. The only parameter that needs to be determined from the training data is λ. The model, however, is the entire training data set.

We also discuss more general classes of kernel-based techniques, which tie in with structured methods in other chapters, and are useful for density estimation and classification.

6.1 One-Dimensional Kernel Smoothers

In Chapter 2, we motivated the k–nearest-neighbor average

$$\hat{f}(x) = \text{Ave}(y_i|x_i \in N_k(x)) \tag{6.1}$$

as an estimate of the regression function $\text{E}(Y|X = x)$. Here $N_k(x)$ is the set of k points nearest to x in squared distance, and Ave denotes the average

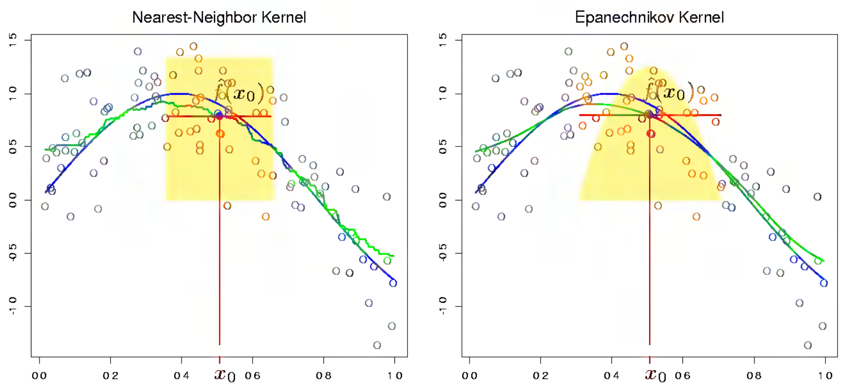

FIGURE 6.1. *In each panel* 100 *pairs* x_i, y_i *are generated at random from the blue curve with Gaussian errors:* $Y = \sin(4X)+\varepsilon$, $X \sim U[0,1]$, $\varepsilon \sim N(0,1/3)$. *In the left panel the green curve is the result of a* 30*-nearest-neighbor running-mean smoother. The red point is the fitted constant* $\hat{f}(x_0)$*, and the orange shaded circles indicate those observations contributing to the fit at* x_0*. The solid orange region indicates the weights assigned to observations. In the right panel, the green curve is the kernel-weighted average, using an Epanechnikov kernel with (half) window width* $\lambda = 0.2$.

(mean). The idea is to relax the definition of conditional expectation, as illustrated in the left panel of Figure 6.1, and compute an average in a neighborhood of the target point. In this case we have used the 30-nearest neighborhood—the fit at x_0 is the average of the 30 pairs whose x_i values are closest to x_0. The green curve is traced out as we apply this definition at different values x_0. The green curve is bumpy, since $\hat{f}(x)$ is discontinuous in x. As we move x_0 from left to right, the k-nearest neighborhood remains constant, until a point x_i to the right of x_0 becomes closer than the furthest point $x_{i'}$ in the neighborhood to the left of x_0, at which time x_i replaces $x_{i'}$. The average in (6.1) changes in a discrete way, leading to a discontinuous $\hat{f}(x)$.

This discontinuity is ugly and unnecessary. Rather than give all the points in the neighborhood equal weight, we can assign weights that die off smoothly with distance from the target point. The right panel shows an example of this, using the so-called Nadaraya–Watson kernel-weighted average

$$\hat{f}(x_0) = \frac{\sum_{i=1}^{N} K_\lambda(x_0, x_i) y_i}{\sum_{i=1}^{N} K_\lambda(x_0, x_i)}, \tag{6.2}$$

with the *Epanechnikov* quadratic kernel

$$K_\lambda(x_0, x) = D\left(\frac{|x - x_0|}{\lambda}\right), \tag{6.3}$$

with

$$D(t) = \begin{cases} \frac{3}{4}(1-t^2) & \text{if } |t| \le 1; \\ 0 & \text{otherwise.} \end{cases} \tag{6.4}$$

The fitted function is now continuous, and quite smooth in the right panel of Figure 6.1. As we move the target from left to right, points enter the neighborhood initially with weight zero, and then their contribution slowly increases (see Exercise 6.1).

In the right panel we used a metric window size $\lambda = 0.2$ for the kernel fit, which does not change as we move the target point x_0, while the size of the 30-nearest-neighbor smoothing window adapts to the local density of the x_i. One can, however, also use such adaptive neighborhoods with kernels, but we need to use a more general notation. Let $h_\lambda(x_0)$ be a width function (indexed by λ) that determines the width of the neighborhood at x_0. Then more generally we have

$$K_\lambda(x_0, x) = D\left(\frac{|x - x_0|}{h_\lambda(x_0)}\right). \tag{6.5}$$

In (6.3), $h_\lambda(x_0) = \lambda$ is constant. For k-nearest neighborhoods, the neighborhood size k replaces λ, and we have $h_k(x_0) = |x_0 - x_{[k]}|$ where $x_{[k]}$ is the kth closest x_i to x_0.

There are a number of details that one has to attend to in practice:

- The smoothing parameter λ, which determines the width of the local neighborhood, has to be determined. Large λ implies lower variance (averages over more observations) but higher bias (we essentially assume the true function is constant within the window).

- Metric window widths (constant $h_\lambda(x)$) tend to keep the bias of the estimate constant, but the variance is inversely proportional to the local density. Nearest-neighbor window widths exhibit the opposite behavior; the variance stays constant and the absolute bias varies inversely with local density.

- Issues arise with nearest-neighbors when there are ties in the x_i. With most smoothing techniques one can simply reduce the data set by averaging the y_i at tied values of X, and supplementing these new observations at the unique values of x_i with an additional weight w_i (which multiples the kernel weight).

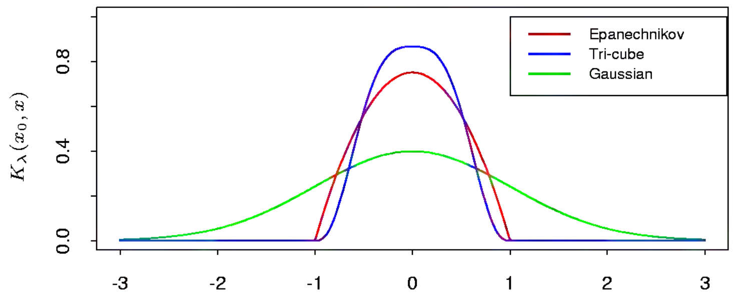

FIGURE 6.2. *A comparison of three popular kernels for local smoothing. Each has been calibrated to integrate to 1. The tri-cube kernel is compact and has two continuous derivatives at the boundary of its support, while the Epanechnikov kernel has none. The Gaussian kernel is continuously differentiable, but has infinite support.*

- This leaves a more general problem to deal with: observation weights w_i. Operationally we simply multiply them by the kernel weights before computing the weighted average. With nearest neighborhoods, it is now natural to insist on neighborhoods with a total weight content k (relative to $\sum w_i$). In the event of overflow (the last observation needed in a neighborhood has a weight w_j which causes the sum of weights to exceed the budget k), then fractional parts can be used.

- Boundary issues arise. The metric neighborhoods tend to contain less points on the boundaries, while the nearest-neighborhoods get wider.

- The Epanechnikov kernel has compact support (needed when used with nearest-neighbor window size). Another popular compact kernel is based on the tri-cube function

$$D(t) = \begin{cases} (1 - t^3)^3 & \text{if } |t| \leq 1; \\ 0 & \text{otherwise} \end{cases} \tag{6.6}$$

  This is flatter on the top (like the nearest-neighbor box) and is differentiable at the boundary of its support. The Gaussian density function $D(t) = \phi(t)$ is a popular noncompact kernel, with the standard-deviation playing the role of the window size. Figure 6.2 compares the three.

6.1.1 Local Linear Regression

We have progressed from the raw moving average to a smoothly varying locally weighted average by using kernel weighting. The smooth kernel fit still has problems, however, as exhibited in Figure 6.3(left panel). Locally-weighted averages can be badly biased on the boundaries of the domain,

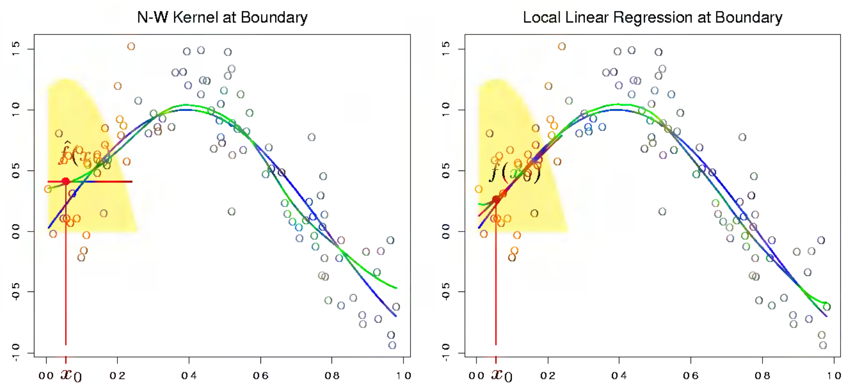

FIGURE 6.3. *The locally weighted average has bias problems at or near the boundaries of the domain. The true function is approximately linear here, but most of the observations in the neighborhood have a higher mean than the target point, so despite weighting, their mean will be biased upwards. By fitting a locally weighted linear regression (right panel), this bias is removed to first order*

because of the asymmetry of the kernel in that region. By fitting straight lines rather than constants locally, we can remove this bias exactly to first order; see Figure 6.3 (right panel). Actually, this bias can be present in the interior of the domain as well, if the X values are not equally spaced (for the same reasons, but usually less severe). Again locally weighted linear regression will make a first-order correction.

Locally weighted regression solves a separate weighted least squares problem at each target point x_0:

$$\min_{\alpha(x_0),\beta(x_0)} \sum_{i=1}^{N} K_\lambda(x_0, x_i)\left[y_i - \alpha(x_0) - \beta(x_0)x_i\right]^2. \tag{6.7}$$

The estimate is then $\hat{f}(x_0) = \hat{\alpha}(x_0) + \hat{\beta}(x_0)x_0$. Notice that although we fit an entire linear model to the data in the region, we only use it to evaluate the fit at the single point x_0.

Define the vector-valued function $b(x)^T = (1, x)$. Let $\mathbf{B}$ be the $N \times 2$ regression matrix with ith row $b(x_i)^T$, and $\mathbf{W}(x_0)$ the $N \times N$ diagonal matrix with ith diagonal element $K_\lambda(x_0, x_i)$. Then

$$\begin{aligned} \hat{f}(x_0) &= b(x_0)^T(\mathbf{B}^T\mathbf{W}(x_0)\mathbf{B})^{-1}\mathbf{B}^T\mathbf{W}(x_0)\mathbf{y} & (6.8)\\ &= \sum_{i=1}^{N} l_i(x_0)y_i. & (6.9) \end{aligned}$$

Equation (6.8) gives an explicit expression for the local linear regression estimate, and (6.9) highlights the fact that the estimate is *linear* in the

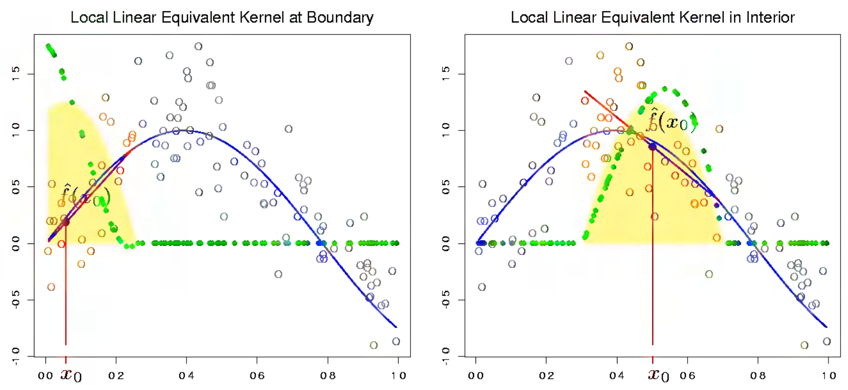

FIGURE 6.4. *The green points show the equivalent kernel $l_i(x_0)$ for local regression. These are the weights in $\hat{f}(x_0) = \sum_{i=1}^N l_i(x_0)y_i$, plotted against their corresponding x_i. For display purposes, these have been rescaled, since in fact they sum to 1. Since the orange shaded region is the (rescaled) equivalent kernel for the Nadaraya–Watson local average, we see how local regression automatically modifies the weighting kernel to correct for biases due to asymmetry in the smoothing window.*

y_i (the $l_i(x_0)$ do not involve $\mathbf{y}$). These weights $l_i(x_0)$ combine the weighting kernel $K_\lambda(x_0, \cdot)$ and the least squares operations, and are sometimes referred to as the *equivalent kernel*. Figure 6.4 illustrates the effect of local linear regression on the equivalent kernel. Historically, the bias in the Nadaraya–Watson and other local average kernel methods were corrected by modifying the kernel. These modifications were based on theoretical asymptotic mean-square-error considerations, and besides being tedious to implement, are only approximate for finite sample sizes. Local linear regression *automatically* modifies the kernel to correct the bias *exactly* to first order, a phenomenon dubbed as *automatic kernel carpentry*. Consider the following expansion for $\mathrm{E}\hat{f}(x_0)$, using the linearity of local regression and a series expansion of the true function f around x_0,

$$\begin{aligned}\mathrm{E}\hat{f}(x_0) &= \sum_{i=1}^N l_i(x_0)f(x_i)\\ &= f(x_0)\sum_{i=1}^N l_i(x_0) + f'(x_0)\sum_{i=1}^N (x_i - x_0)l_i(x_0)\\ &\qquad + \frac{f''(x_0)}{2}\sum_{i=1}^N (x_i - x_0)^2 l_i(x_0) + R, \end{aligned} \tag{6.10}$$

where the remainder term R involves third– and higher–order derivatives of f, and is typically small under suitable smoothness assumptions. It can

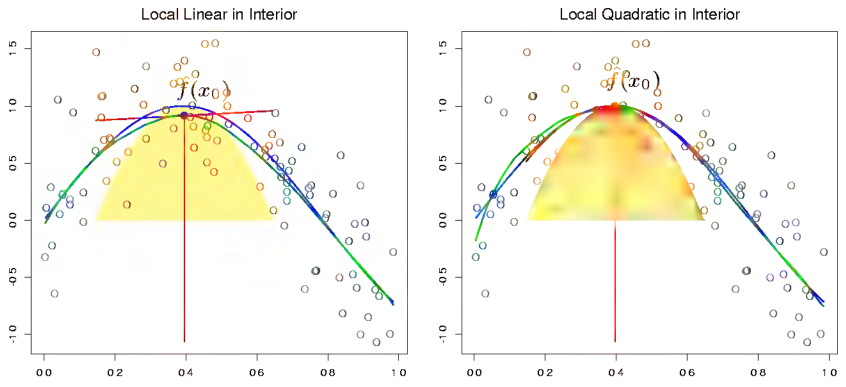

FIGURE 6.5. *Local linear fits exhibit bias in regions of curvature of the true function. Local quadratic fits tend to eliminate this bias.*

be shown (Exercise 6.2) that for local linear regression, $\sum_{i=1}^N l_i(x_0) = 1$ and $\sum_{i=1}^N (x_i - x_0)l_i(x_0) = 0$. Hence the middle term equals $f(x_0)$, and since the bias is $\mathrm{E}\hat{f}(x_0) - f(x_0)$, we see that it depends only on quadratic and higher–order terms in the expansion of f.

6.1.2 Local Polynomial Regression

Why stop at local linear fits? We can fit local polynomial fits of any degree d,

$$\min_{\alpha(x_0),\beta_j(x_0),\, j=1,\ldots,d} \sum_{i=1}^N K_\lambda(x_0, x_i)\left[y_i - \alpha(x_0) - \sum_{j=1}^d \beta_j(x_0)x_i^j\right]^2 \tag{6.11}$$

with solution $\hat{f}(x_0) = \hat{\alpha}(x_0) + \sum_{j=1}^d \hat{\beta}_j(x_0)x_0^j$. In fact, an expansion like (6.10) will tell us that the bias will only have components of degree $d+1$ and higher (Exercise 6.2). Figure 6.5 illustrates local quadratic regression. Local linear fits tend to be biased in regions of curvature of the true function, a phenomenon referred to as *trimming the hills* and *filling the valleys*. Local quadratic regression is generally able to correct this bias.

There is of course a price to be paid for this bias reduction, and that is increased variance. The fit in the right panel of Figure 6.5 is slightly more wiggly, especially in the tails. Assuming the model $y_i = f(x_i) + \varepsilon_i$, with ε_i independent and identically distributed with mean zero and variance σ^2, $\mathrm{Var}(\hat{f}(x_0)) = \sigma^2||l(x_0)||^2$, where $l(x_0)$ is the vector of equivalent kernel weights at x_0. It can be shown (Exercise 6.3) that $||l(x_0)||$ increases with d, and so there is a bias–variance tradeoff in selecting the polynomial degree. Figure 6.6 illustrates these variance curves for degree zero, one and two

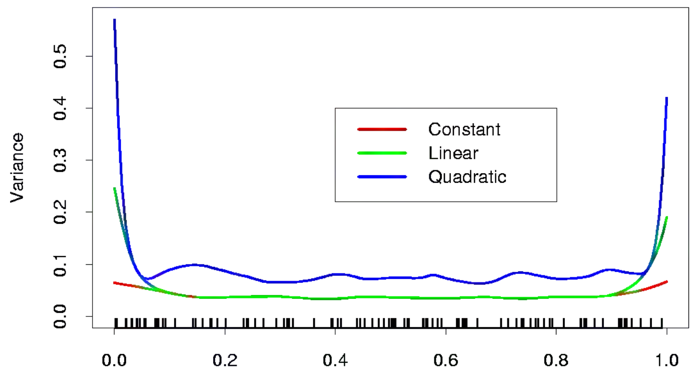

FIGURE 6.6. *The variances functions* $||l(x)||^2$ *for local constant, linear and quadratic regression, for a metric bandwidth* ($\lambda = 0.2$) *tri-cube kernel.*

local polynomials. To summarize some collected wisdom on this issue:

- Local linear fits can help bias dramatically at the boundaries at a modest cost in variance. Local quadratic fits do little at the boundaries for bias, but increase the variance a lot.

- Local quadratic fits tend to be most helpful in reducing bias due to curvature in the interior of the domain.

- Asymptotic analysis suggest that local polynomials of odd degree dominate those of even degree. This is largely due to the fact that asymptotically the MSE is dominated by boundary effects.

While it may be helpful to tinker, and move from local linear fits at the boundary to local quadratic fits in the interior, we do not recommend such strategies. Usually the application will dictate the degree of the fit. For example, if we are interested in extrapolation, then the boundary is of more interest, and local linear fits are probably more reliable.

6.2 Selecting the Width of the Kernel

In each of the kernels K_λ, λ is a parameter that controls its width:

- For the Epanechnikov or tri-cube kernel with metric width, λ is the radius of the support region.

- For the Gaussian kernel, λ is the standard deviation.

- λ is the number k of nearest neighbors in k-nearest neighborhoods, often expressed as a fraction or *span* k/N of the total training sample.

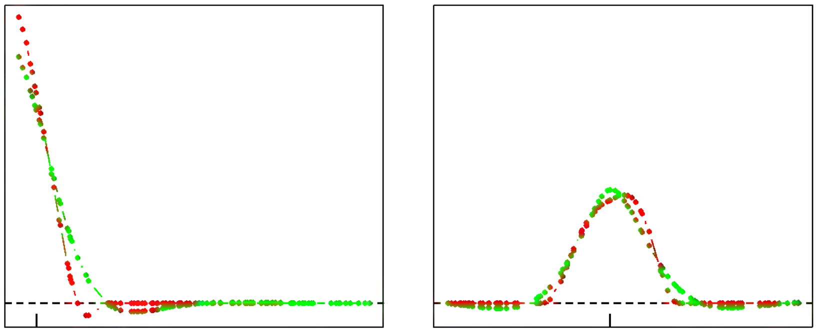

FIGURE 6.7. *Equivalent kernels for a local linear regression smoother (tri-cube kernel; red) and a smoothing spline (green), with matching degrees of freedom. The vertical spikes indicates the target points.*

There is a natural bias–variance tradeoff as we change the width of the averaging window, which is most explicit for local averages:

- If the window is narrow, $\hat{f}(x_0)$ is an average of a small number of y_i close to x_0, and its variance will be relatively large—close to that of an individual y_i. The bias will tend to be small, again because each of the $E(y_i) = f(x_i)$ should be close to $f(x_0)$.
- If the window is wide, the variance of $\hat{f}(x_0)$ will be small relative to the variance of any y_i, because of the effects of averaging. The bias will be higher, because we are now using observations x_i further from x_0, and there is no guarantee that $f(x_i)$ will be close to $f(x_0)$.

Similar arguments apply to local regression estimates, say local linear: as the width goes to zero, the estimates approach a piecewise-linear function that interpolates the training data; as the width gets infinitely large, the fit approaches the global linear least-squares fit to the data.

The discussion in Chapter 5 on selecting the regularization parameter for smoothing splines applies here, and will not be repeated. Local regression smoothers are linear estimators; the smoother matrix in $\hat{\mathbf{f}} = \mathbf{S}_\lambda \mathbf{y}$ is built up from the equivalent kernels (6.8), and has ijth entry $\{\mathbf{S}_\lambda\}_{ij} = l_i(x_j)$. Leave-one-out cross-validation is particularly simple (Exercise 6.7), as is generalized cross-validation, C_p (Exercise 6.10), and k-fold cross-validation. The effective degrees of freedom is again defined as trace$(\mathbf{S}_\lambda)$, and can be used to calibrate the amount of smoothing. Figure 6.7 compares the equivalent kernels for a smoothing spline and local linear regression. The local regression smoother has a span of 40%, which results in df $=$ trace$(\mathbf{S}_\lambda) = 5.86$. The smoothing spline was calibrated to have the same df, and their equivalent kernels are qualitatively quite similar.

6.3 Local Regression in $\mathbb{R}^p$

Kernel smoothing and local regression generalize very naturally to two or more dimensions. The Nadaraya–Watson kernel smoother fits a constant locally with weights supplied by a p-dimensional kernel. Local linear regression will fit a hyperplane locally in X, by weighted least squares, with weights supplied by a p-dimensional kernel. It is simple to implement and is generally preferred to the local constant fit for its superior performance on the boundaries.

Let $b(X)$ be a vector of polynomial terms in X of maximum degree d. For example, with $d = 1$ and $p = 2$ we get $b(X) = (1, X_1, X_2)$; with $d = 2$ we get $b(X) = (1, X_1, X_2, X_1^2, X_2^2, X_1 X_2)$; and trivially with $d = 0$ we get $b(X) = 1$. At each $x_0 \in \mathbb{R}^p$ solve

$$\min_{\beta(x_0)} \sum_{i=1}^{N} K_\lambda(x_0, x_i)(y_i - b(x_i)^T \beta(x_0))^2 \tag{6.12}$$

to produce the fit $\hat{f}(x_0) = b(x_0)^T \hat{\beta}(x_0)$. Typically the kernel will be a radial function, such as the radial Epanechnikov or tri-cube kernel

$$K_\lambda(x_0, x) = d\left(\frac{||x - x_0||}{\lambda}\right), \tag{6.13}$$

where $||\cdot||$ is the Euclidean norm. Since the Euclidean norm depends on the units in each coordinate, it makes most sense to standardize each predictor, for example, to unit standard deviation, prior to smoothing.

While boundary effects are a problem in one-dimensional smoothing, they are a much bigger problem in two or higher dimensions, since the fraction of points on the boundary is larger. In fact, one of the manifestations of the curse of dimensionality is that the fraction of points close to the boundary increases to one as the dimension grows. Directly modifying the kernel to accommodate two-dimensional boundaries becomes very messy, especially for irregular boundaries. Local polynomial regression seamlessly performs boundary correction to the desired order in any dimensions. Figure 6.8 illustrates local linear regression on some measurements from an astronomical study with an unusual predictor design (star shaped). Here the boundary is extremely irregular, and the fitted surface must also interpolate over regions of increasing data sparsity as we approach the boundary.

Local regression becomes less useful in dimensions much higher than two or three. We have discussed in some detail the problems of dimensionality, for example, in Chapter 2. It is impossible to simultaneously maintain localness ($\Rightarrow$ low bias) and a sizeable sample in the neighborhood ($\Rightarrow$ low variance) as the dimension increases, without the total sample size increasing exponentially in p. Visualization of $\hat{f}(X)$ also becomes difficult in higher dimensions, and this is often one of the primary goals of smoothing.

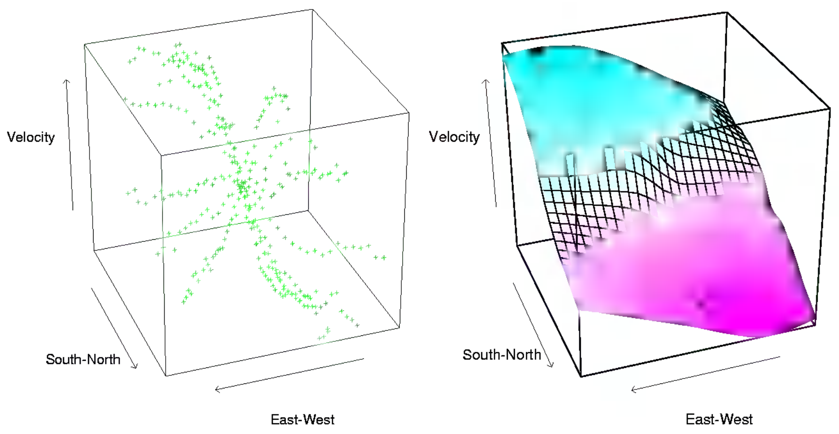

FIGURE 6.8. *The left panel shows three-dimensional data, where the response is the velocity measurements on a galaxy, and the two predictors record positions on the celestial sphere. The unusual "star" shaped design indicates the way the measurements were made, and results in an extremely irregular boundary. The right panel shows the results of local linear regression smoothing in* $\mathbb{R}^2$, *using a nearest-neighbor window with* 15% *of the data.*

Although the scatter-cloud and wire-frame pictures in Figure 6.8 look attractive, it is quite difficult to interpret the results except at a gross level. From a data analysis perspective, conditional plots are far more useful.

Figure 6.9 shows an analysis of some environmental data with three predictors. The *trellis* display here shows ozone as a function of radiation, conditioned on the other two variables, temperature and wind speed. However, conditioning on the value of a variable really implies local to that value (as in local regression). Above each of the panels in Figure 6.9 is an indication of the range of values present in that panel for each of the conditioning values. In the panel itself the data subsets are displayed (response versus remaining variable), and a one-dimensional local linear regression is fit to the data. Although this is not quite the same as looking at slices of a fitted three-dimensional surface, it is probably more useful in terms of understanding the joint behavior of the data.

6.4 Structured Local Regression Models in $\mathbb{R}^p$

When the dimension to sample-size ratio is unfavorable, local regression does not help us much, unless we are willing to make some structural assumptions about the model. Much of this book is about structured regression and classification models. Here we focus on some approaches directly related to kernel methods.

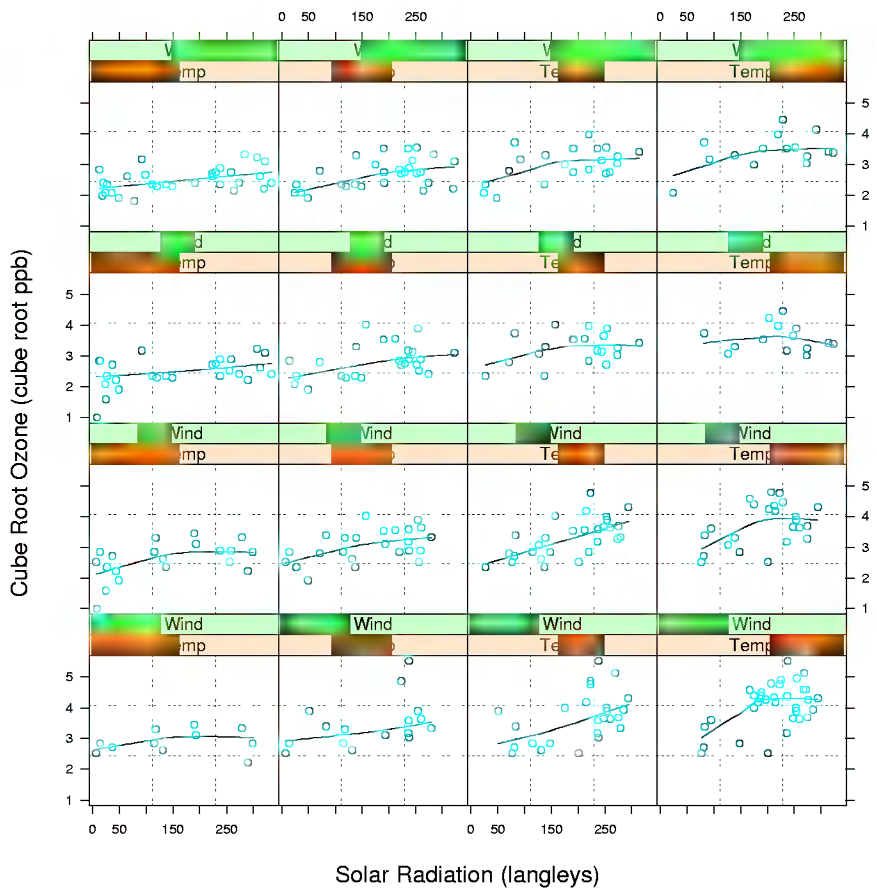

FIGURE 6.9. *Three-dimensional smoothing example. The response is (cube-root) of ozone concentration, and the three predictors are temperature, wind speed and radiation. The* trellis *display shows ozone as a function of radiation, conditioned on intervals of temperature and wind speed (indicated by darker green or orange shaded bars). Each panel contains about 40% of the range of each of the conditioned variables. The curve in each panel is a univariate local linear regression, fit to the data in the panel.*

6.4.1 Structured Kernels

One line of approach is to modify the kernel. The default spherical kernel (6.13) gives equal weight to each coordinate, and so a natural default strategy is to standardize each variable to unit standard deviation. A more general approach is to use a positive semidefinite matrix $\mathbf{A}$ to weigh the different coordinates:

$$K_{\lambda,A}(x_0, x) = d\left(\frac{(x - x_0)^T\mathbf{A}(x - x_0)}{\lambda}\right). \tag{6.14}$$

Entire coordinates or directions can be downgraded or omitted by imposing appropriate restrictions on $\mathbf{A}$. For example, if $\mathbf{A}$ is diagonal, then we can increase or decrease the influence of individual predictors X_j by increasing or decreasing A_{jj}. Often the predictors are many and highly correlated, such as those arising from digitized analog signals or images. The covariance function of the predictors can be used to tailor a metric $\mathbf{A}$ that focuses less, say, on high-frequency contrasts (Exercise 6.4). Proposals have been made for learning the parameters for multidimensional kernels. For example, the projection-pursuit regression model discussed in Chapter 11 is of this flavor, where low-rank versions of $\mathbf{A}$ imply ridge functions for $\hat{f}(X)$. More general models for $\mathbf{A}$ are cumbersome, and we favor instead the structured forms for the regression function discussed next.

6.4.2 Structured Regression Functions

We are trying to fit a regression function $E(Y|X) = f(X_1, X_2, \ldots, X_p)$ in $\mathbb{R}^p$, in which every level of interaction is potentially present. It is natural to consider analysis-of-variance (ANOVA) decompositions of the form

$$f(X_1, X_2, \ldots, X_p) = \alpha + \sum_j g_j(X_j) + \sum_{k<\ell} g_{k\ell}(X_k, X_\ell) + \cdots \tag{6.15}$$

and then introduce structure by eliminating some of the higher-order terms. Additive models assume only main effect terms: $f(X) = \alpha + \sum_{j=1}^p g_j(X_j)$; second-order models will have terms with interactions of order at most two, and so on. In Chapter 9, we describe iterative *backfitting* algorithms for fitting such low-order interaction models. In the additive model, for example, if all but the kth term is assumed known, then we can estimate g_k by local regression of $Y - \sum_{j\neq k} g_j(X_j)$ on X_k. This is done for each function in turn, repeatedly, until convergence. The important detail is that at any stage, one-dimensional local regression is all that is needed. The same ideas can be used to fit low-dimensional ANOVA decompositions.

An important special case of these structured models are the class of *varying coefficient models*. Suppose, for example, that we divide the p predictors in X into a set $(X_1, X_2, \ldots, X_q)$ with $q < p$, and the remainder of

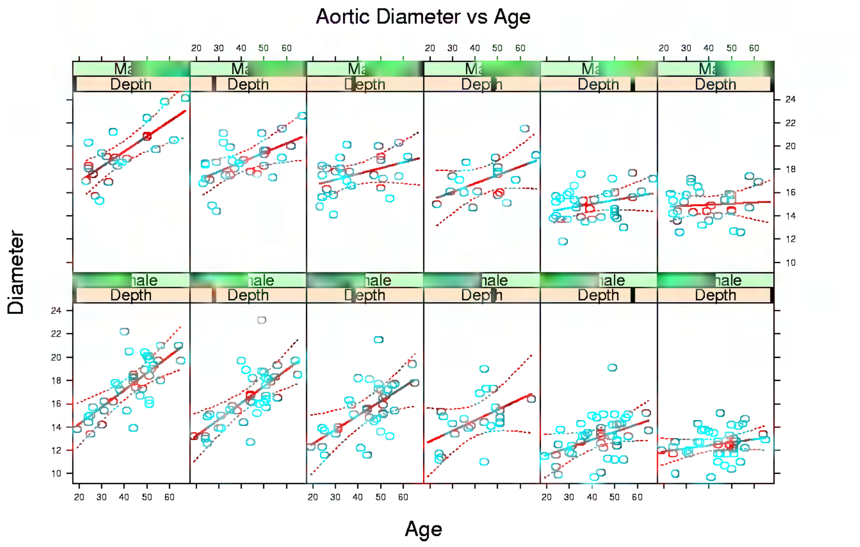

FIGURE 6.10. *In each panel the* `aorta diameter` *is modeled as a linear function of* `age`. *The coefficients of this model vary with* `gender` *and* `depth` *down the* `aorta` *(left is near the top, right is low down). There is a clear trend in the coefficients of the linear model.*

the variables we collect in the vector Z. We then assume the conditionally linear model

$$f(X) = \alpha(Z) + \beta_1(Z)X_1 + \cdots + \beta_q(Z)X_q. \tag{6.16}$$

For given Z, this is a linear model, but each of the coefficients can vary with Z. It is natural to fit such a model by locally weighted least squares:

$$\min_{\alpha(z_0),\beta(z_0)} \sum_{i=1}^{N} K_\lambda(z_0, z_i)\left(y_i - \alpha(z_0) - x_{1i}\beta_1(z_0) - \cdots - x_{qi}\beta_q(z_0)\right)^2. \tag{6.17}$$

Figure 6.10 illustrates the idea on measurements of the human aorta. A longstanding claim has been that the aorta thickens with `age`. Here we model the `diameter` of the aorta as a linear function of `age`, but allow the coefficients to vary with `gender` and `depth` down the aorta. We used a local regression model separately for males and females. While the aorta clearly does thicken with age at the higher regions of the aorta, the relationship fades with distance down the aorta. Figure 6.11 shows the intercept and slope as a function of depth.

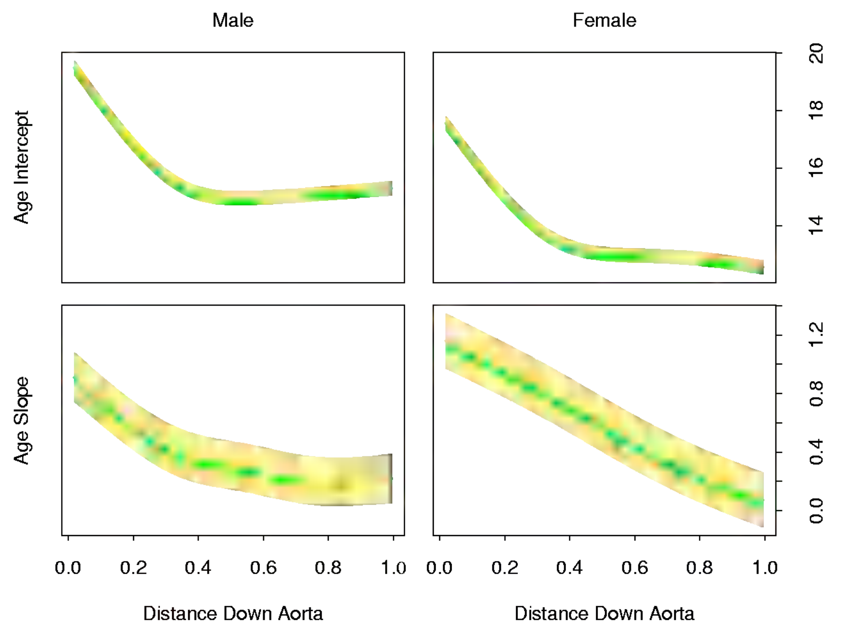

FIGURE 6.11. *The intercept and slope of* `age` *as a function of* `distance` *down the aorta, separately for males and females. The yellow bands indicate one standard error.*

6.5 Local Likelihood and Other Models

The concept of local regression and varying coefficient models is extremely broad: any parametric model can be made local if the fitting method accommodates observation weights. Here are some examples:

- Associated with each observation y_i is a parameter $\theta_i = \theta(x_i) = x_i^T\beta$ linear in the covariate(s) x_i, and inference for β is based on the log-likelihood $l(\beta) = \sum_{i=1}^N l(y_i, x_i^T\beta)$. We can model $\theta(X)$ more flexibly by using the likelihood local to x_0 for inference of $\theta(x_0) = x_0^T\beta(x_0)$:

$$l(\beta(x_0)) = \sum_{i=1}^N K_\lambda(x_0, x_i) l(y_i, x_i^T\beta(x_0)).$$

  Many likelihood models, in particular the family of generalized linear models including logistic and log-linear models, involve the covariates in a linear fashion. Local likelihood allows a relaxation from a globally linear model to one that is locally linear.

- As above, except different variables are associated with θ from those used for defining the local likelihood:

$$l(\theta(z_0)) = \sum_{i=1}^{N} K_\lambda(z_0, z_i) l(y_i, \eta(x_i, \theta(z_0))).$$

  For example, $\eta(x, \theta) = x^T\theta$ could be a linear model in x. This will fit a varying coefficient model $\theta(z)$ by maximizing the local likelihood.

- Autoregressive time series models of order k have the form $y_t = \beta_0 + \beta_1 y_{t-1} + \beta_2 y_{t-2} + \cdots + \beta_k y_{t-k} + \varepsilon_t$. Denoting the *lag set* by $z_t = (y_{t-1}, y_{t-2}, \ldots, y_{t-k})$, the model looks like a standard linear model $y_t = z_t^T\beta + \varepsilon_t$, and is typically fit by least squares. Fitting by local least squares with a kernel $K(z_0, z_t)$ allows the model to vary according the short-term history of the series. This is to be distinguished from the more traditional dynamic linear models that vary by windowing time.

As an illustration of local likelihood, we consider the local version of the multi-class linear logistic regression model (4.32) of Chapter 4. The data consist of features x_i and an associated categorical response $g_i \in \{1, 2, \ldots, J\}$, and the linear model has the form

$$\Pr(G = j|X = x) = \frac{e^{\beta_{j0}+\beta_j^T x}}{1 + \sum_{k=1}^{J-1} e^{\beta_{k0}+\beta_k^T x}}. \tag{6.18}$$

The local log-likelihood for this J class model can be written

$$\sum_{i=1}^{N} K_\lambda(x_0, x_i)\Bigg\{\beta_{g_i0}(x_0) + \beta_{g_i}(x_0)^T(x_i - x_0) \\ - \log\left[1 + \sum_{k=1}^{J-1} \exp\left(\beta_{k0}(x_0) + \beta_k(x_0)^T(x_i - x_0)\right)\right]\Bigg\}. \tag{6.19}$$

Notice that

- we have used g_i as a subscript in the first line to pick out the appropriate numerator;
- $\beta_{J0} = 0$ and $\beta_J = 0$ by the definition of the model;
- we have centered the local regressions at x_0, so that the fitted posterior probabilities at x_0 are simply

$$\hat{\Pr}(G = j|X = x_0) = \frac{e^{\hat\beta_{j0}(x_0)}}{1 + \sum_{k=1}^{J-1} e^{\hat\beta_{k0}(x_0)}}. \tag{6.20}$$

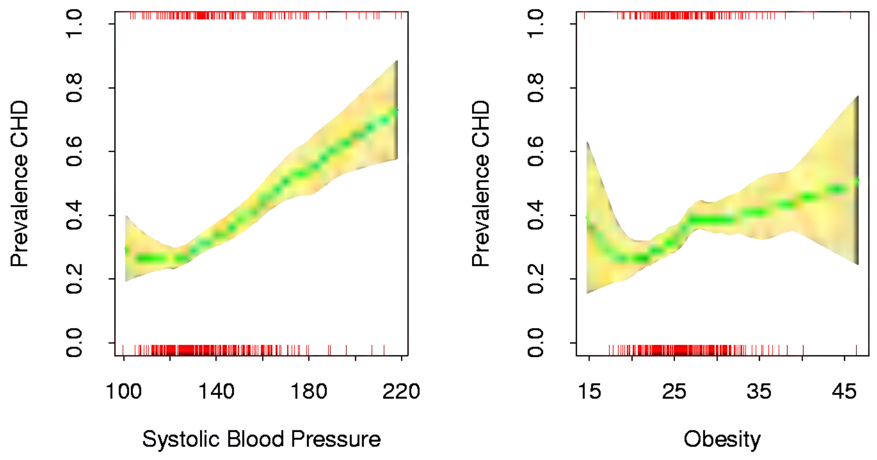

FIGURE 6.12. *Each plot shows the binary response CHD (coronary heart disease) as a function of a risk factor for the South African heart disease data. For each plot we have computed the fitted prevalence of CHD using a local linear logistic regression model. The unexpected increase in the prevalence of CHD at the lower ends of the ranges is because these are retrospective data, and some of the subjects had already undergone treatment to reduce their blood pressure and weight. The shaded region in the plot indicates an estimated pointwise standard error band.*

This model can be used for flexible multi-class classification in moderately low dimensions, although successes have been reported with the high-dimensional ZIP-code classification problem. Generalized additive models (Chapter 9) using kernel smoothing methods are closely related, and avoid dimensionality problems by assuming an additive structure for the regression function.

As a simple illustration we fit a two-class local linear logistic model to the heart disease data of Chapter 4. Figure 6.12 shows the univariate local logistic models fit to two of the risk factors (separately). This is a useful screening device for detecting nonlinearities, when the data themselves have little visual information to offer. In this case an unexpected anomaly is uncovered in the data, which may have gone unnoticed with traditional methods.

Since `CHD` is a binary indicator, we could estimate the conditional prevalence $\Pr(G = j|x_0)$ by simply smoothing this binary response directly without resorting to a likelihood formulation. This amounts to fitting a locally constant logistic regression model (Exercise 6.5). In order to enjoy the bias-correction of local-linear smoothing, it is more natural to operate on the unrestricted logit scale.

Typically with logistic regression, we compute parameter estimates as well as their standard errors. This can be done locally as well, and so

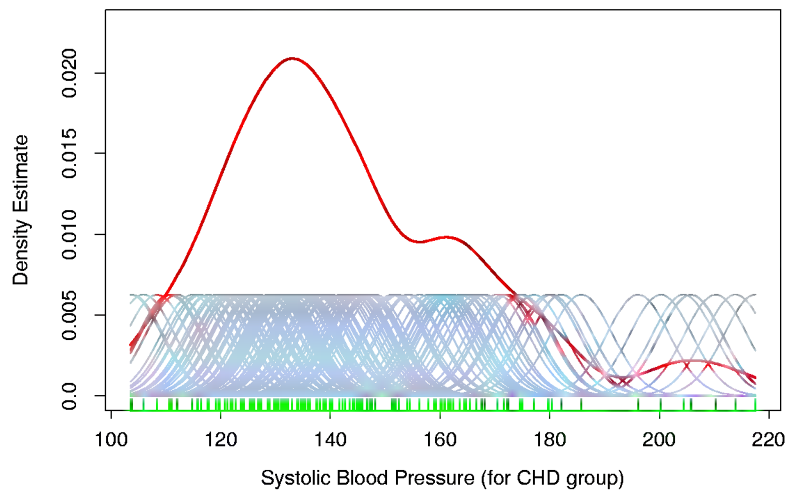

FIGURE 6.13. *A kernel density estimate for systolic blood pressure (for the CHD group). The density estimate at each point is the average contribution from each of the kernels at that point. We have scaled the kernels down by a factor of 10 to make the graph readable.*

we can produce, as shown in the plot, estimated pointwise standard-error bands about our fitted prevalence.

6.6 Kernel Density Estimation and Classification

Kernel density estimation is an unsupervised learning procedure, which historically precedes kernel regression. It also leads naturally to a simple family of procedures for nonparametric classification.

6.6.1 Kernel Density Estimation

Suppose we have a random sample $x_1, \ldots, x_N$ drawn from a probability density $f_X(x)$, and we wish to estimate f_X at a point x_0. For simplicity we assume for now that $X \in \mathbb{R}$. Arguing as before, a natural local estimate has the form

$$\hat{f}_X(x_0) = \frac{\#x_i \in \mathcal{N}(x_0)}{N\lambda}, \tag{6.21}$$

where $\mathcal{N}(x_0)$ is a small metric neighborhood around x_0 of width λ. This estimate is bumpy, and the smooth *Parzen* estimate is preferred

$$\hat{f}_X(x_0) = \frac{1}{N\lambda}\sum_{i=1}^{N} K_\lambda(x_0, x_i), \tag{6.22}$$

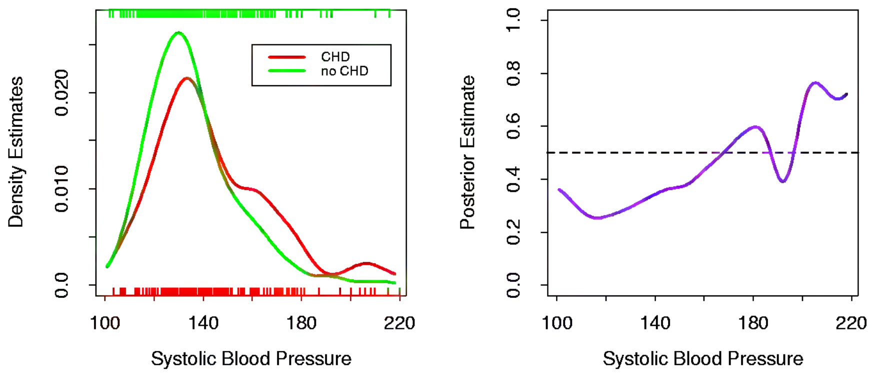

FIGURE 6.14. *The left panel shows the two separate density estimates for systolic blood pressure in the CHD versus no-CHD groups, using a Gaussian kernel density estimate in each. The right panel shows the estimated posterior probabilities for CHD, using (6.25).*

because it counts observations close to x_0 with weights that decrease with distance from x_0. In this case a popular choice for K_λ is the Gaussian kernel $K_\lambda(x_0, x) = \phi(|x - x_0|/\lambda)$. Figure 6.13 shows a Gaussian kernel density fit to the sample values for `systolic blood pressure` for the `CHD` group. Letting ϕ_λ denote the Gaussian density with mean zero and standard-deviation λ, then (6.22) has the form

$$\begin{aligned} \hat{f}_X(x) &= \frac{1}{N}\sum_{i=1}^{N}\phi_\lambda(x - x_i) \\ &= (\hat{F} \star \phi_\lambda)(x), \end{aligned} \tag{6.23}$$

the convolution of the sample empirical distribution $\hat{F}$ with ϕ_λ. The distribution $\hat{F}(x)$ puts mass $1/N$ at each of the observed x_i, and is jumpy; in $\hat{f}_X(x)$ we have smoothed $\hat{F}$ by adding independent Gaussian noise to each observation x_i.

The Parzen density estimate is the equivalent of the local average, and improvements have been proposed along the lines of local regression (on the log scale for densities; see Loader (1999)). We will not pursue these here. In $\mathbb{R}^p$ the natural generalization of the Gaussian density estimate amounts to using the Gaussian product kernel in (6.23),

$$\hat{f}_X(x_0) = \frac{1}{N(2\lambda^2\pi)^{\frac{p}{2}}}\sum_{i=1}^{N} e^{-\frac{1}{2}(||x_i - x_0||/\lambda)^2}. \tag{6.24}$$

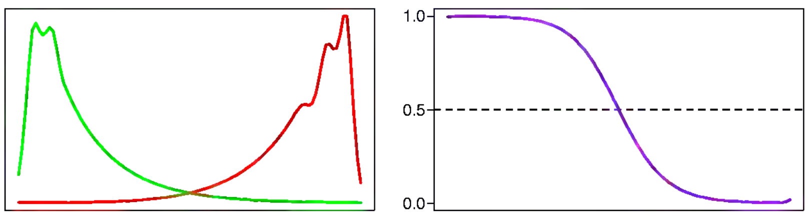

FIGURE 6.15. *The population class densities may have interesting structure (left) that disappears when the posterior probabilities are formed (right).*

6.6.2 Kernel Density Classification

One can use nonparametric density estimates for classification in a straightforward fashion using Bayes' theorem. Suppose for a J class problem we fit nonparametric density estimates $\hat{f}_j(X)$, $j = 1, \dots, J$ separately in each of the classes, and we also have estimates of the class priors $\hat{\pi}_j$ (usually the sample proportions). Then

$$\hat{\Pr}(G = j|X = x_0) = \frac{\hat{\pi}_j \hat{f}_j(x_0)}{\sum_{k=1}^{J} \hat{\pi}_k \hat{f}_k(x_0)}. \tag{6.25}$$

Figure 6.14 uses this method to estimate the prevalence of CHD for the heart risk factor study, and should be compared with the left panel of Figure 6.12. The main difference occurs in the region of high SBP in the right panel of Figure 6.14. In this region the data are sparse for both classes, and since the Gaussian kernel density estimates use metric kernels, the density estimates are low and of poor quality (high variance) in these regions. The local logistic regression method (6.20) uses the tri-cube kernel with k-NN bandwidth; this effectively widens the kernel in this region, and makes use of the local linear assumption to smooth out the estimate (on the logit scale).

If classification is the ultimate goal, then learning the separate class densities well may be unnecessary, and can in fact be misleading. Figure 6.15 shows an example where the densities are both multimodal, but the posterior ratio is quite smooth. In learning the separate densities from data, one might decide to settle for a rougher, high-variance fit to capture these features, which are irrelevant for the purposes of estimating the posterior probabilities. In fact, if classification is the ultimate goal, then we need only to estimate the posterior well near the decision boundary (for two classes, this is the set $\{x|\Pr(G = 1|X = x) = \frac{1}{2}\}$).

6.6.3 The Naive Bayes Classifier

This is a technique that has remained popular over the years, despite its name (also known as "Idiot's Bayes"!) It is especially appropriate when the dimension p of the feature space is high, making density estimation unattractive. The naive Bayes model assumes that given a class $G = j$, the features X_k are independent:

$$f_j(X) = \prod_{k=1}^{p} f_{jk}(X_k). \tag{6.26}$$

While this assumption is generally not true, it does simplify the estimation dramatically:

- The individual class-conditional marginal densities f_{jk} can each be estimated separately using one-dimensional kernel density estimates. This is in fact a generalization of the original naive Bayes procedures, which used univariate Gaussians to represent these marginals.

- If a component X_j of X is discrete, then an appropriate histogram estimate can be used. This provides a seamless way of mixing variable types in a feature vector.

Despite these rather optimistic assumptions, naive Bayes classifiers often outperform far more sophisticated alternatives. The reasons are related to Figure 6.15: although the individual class density estimates may be biased, this bias might not hurt the posterior probabilities as much, especially near the decision regions. In fact, the problem may be able to withstand considerable bias for the savings in variance such a "naive" assumption earns.

Starting from (6.26) we can derive the logit-transform (using class J as the base):

$$\begin{aligned}
\text{logit}\frac{\Pr(G=\ell|X)}{\Pr(G=J|X)} &= \log\frac{\pi_\ell f_\ell(X)}{\pi_J f_J(X)} \\
&= \log\frac{\pi_\ell \prod_{k=1}^{p} f_{\ell k}(X_k)}{\pi_J \prod_{k=1}^{p} f_{Jk}(X_k)} \\
&= \log\frac{\pi_\ell}{\pi_J} + \sum_{k=1}^{p}\log\frac{f_{\ell k}(X_k)}{f_{Jk}(X_k)} \\
&= \beta_{0\ell} + \sum_{k=1}^{J} g_k(X_k).
\end{aligned} \tag{6.27}$$

This has the form of a *generalized additive model*, which is described in more detail in Chapter 9. The models are fit in quite different ways though; their differences are explored in Exercise 6.9. The relationship between naive Bayes and generalized additive models is analogous to that between linear discriminant analysis and logistic regression (Section 4.4.4).

6.7 Radial Basis Functions and Kernels

In Chapter 5, functions are represented as expansions in basis functions: $f(x) = \sum_{j=1}^{M} \beta_j h_j(x)$. The art of flexible modeling using basis expansions consists of picking an appropriate family of basis functions, and then controlling the complexity of the representation by selection, regularization, or both. Some of the families of basis functions have elements that are defined locally; for example, B-splines are defined locally in $\mathbb{R}$. If more flexibility is desired in a particular region, then that region needs to be represented by more basis functions (which in the case of B-splines translates to more knots). Tensor products of $\mathbb{R}$-local basis functions deliver basis functions local in $\mathbb{R}^p$. Not all basis functions are local—for example, the truncated power bases for splines, or the sigmoidal basis functions $\sigma(\alpha_0 + \alpha x)$ used in neural-networks (see Chapter 11). The composed function $f(x)$ can nevertheless show local behavior, because of the particular signs and values of the coefficients causing cancellations of global effects. For example, the truncated power basis has an equivalent B-spline basis for the same space of functions; the cancellation is exact in this case.

Kernel methods achieve flexibility by fitting simple models in a region local to the target point x_0. Localization is achieved via a weighting kernel K_λ, and individual observations receive weights $K_\lambda(x_0, x_i)$.

Radial basis functions combine these ideas, by treating the kernel functions $K_\lambda(\xi, x)$ as basis functions. This leads to the model

$$\begin{aligned} f(x) &= \sum_{j=1}^{M} K_{\lambda_j}(\xi, x)\beta_j \\ &= \sum_{j=1}^{M} D\left(\frac{||x-\xi_j||}{\lambda_j}\right)\beta_j, \end{aligned} \tag{6.28}$$

where each basis element is indexed by a location or *prototype* parameter ξ_j and a scale parameter λ_j. A popular choice for D is the standard Gaussian density function. There are several approaches to learning the parameters $\{\lambda_j, \xi_j, \beta_j\}$, $j = 1, \dots, M$. For simplicity we will focus on least squares methods for regression, and use the Gaussian kernel.

- Optimize the sum-of-squares with respect to all the parameters:

$$\min_{\{\lambda_j,\xi_j,\beta_j\}_1^M} \sum_{i=1}^{N} \left(y_i - \beta_0 - \sum_{j=1}^{M} \beta_j \exp\left\{ -\frac{(x_i-\xi_j)^T(x_i-\xi_j)}{\lambda_j^2} \right\} \right)^2. \tag{6.29}$$

  This model is commonly referred to as an RBF network, an alternative to the sigmoidal neural network discussed in Chapter 11; the ξ_j

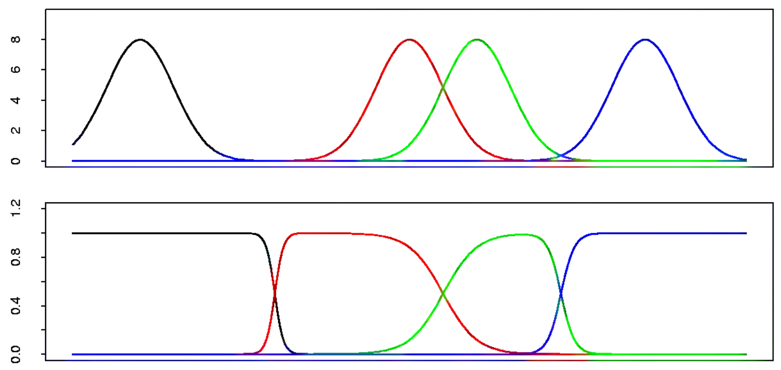

FIGURE 6.16. *Gaussian radial basis functions in* $\mathbb{R}$ *with fixed width can leave holes (top panel). Renormalized Gaussian radial basis functions avoid this problem, and produce basis functions similar in some respects to B-splines.*

and λ_j playing the role of the weights. This criterion is nonconvex with multiple local minima, and the algorithms for optimization are similar to those used for neural networks.

- Estimate the $\{\lambda_j, \xi_j\}$ separately from the β_j. Given the former, the estimation of the latter is a simple least squares problem. Often the kernel parameters λ_j and ξ_j are chosen in an unsupervised way using the X distribution alone. One of the methods is to fit a Gaussian mixture density model to the training x_i, which provides both the centers ξ_j and the scales λ_j. Other even more adhoc approaches use clustering methods to locate the prototypes ξ_j, and treat $\lambda_j = \lambda$ as a hyper-parameter. The obvious drawback of these approaches is that the conditional distribution $\Pr(Y|X)$ and in particular $E(Y|X)$ is having no say in where the action is concentrated. On the positive side, they are much simpler to implement.

While it would seem attractive to reduce the parameter set and assume a constant value for $\lambda_j = \lambda$, this can have an undesirable side effect of creating *holes*—regions of $\mathbb{R}^p$ where none of the kernels has appreciable support, as illustrated in Figure 6.16 (upper panel). *Renormalized* radial basis functions,

$$h_j(x) = \frac{D(||x - \xi_j||/\lambda)}{\sum_{k=1}^{M} D(||x - \xi_k||/\lambda)}, \tag{6.30}$$

avoid this problem (lower panel).

The Nadaraya–Watson kernel regression estimator (6.2) in $\mathbb{R}^p$ can be viewed as an expansion in renormalized radial basis functions,

$$\begin{aligned} \hat{f}(x_0) &= \textstyle\sum_{i=1}^N y_i \frac{K_\lambda(x_0,x_i)}{\sum_{i=1}^N K_\lambda(x_0,x_i)} \\ &= \textstyle\sum_{i=1}^N y_i h_i(x_0) \end{aligned} \tag{6.31}$$

with a basis function h_i located at every observation and coefficients y_i; that is, $\xi_i = x_i$, $\hat{\beta}_i = y_i$, $i = 1, \dots, N$.

6.8 Mixture Models for Density Estimation and Classification

The mixture model is a useful tool for density estimation, and can be viewed as a kind of kernel method. The Gaussian mixture model has the form

$$f(x) = \sum_{m=1}^{M} \alpha_m \phi(x; \mu_m, \mathbf{\Sigma}_m) \tag{6.32}$$

with mixing proportions α_m, $\sum_m \alpha_m = 1$, and each Gaussian density has a mean μ_m and covariance matrix $\mathbf{\Sigma}_m$. In general, mixture models can use any component densities in place of the Gaussian in (6.32): the Gaussian mixture model is by far the most popular.

The parameters are usually fit by maximum likelihood, using the EM algorithm as described in Chapter 8. Some special cases arise:

- If the covariance matrices are constrained to be scalar: $\mathbf{\Sigma}_m = \sigma_m \mathbf{I}$, then (6.32) has the form of a radial basis expansion.
- If in addition $\sigma_m = \sigma > 0$ is fixed, and $M \uparrow N$, then the maximum likelihood estimate for (6.32) approaches the kernel density estimate (6.22) where $\hat{\alpha}_m = 1/N$ and $\hat{\mu}_m = x_m$.

Using Bayes' theorem, separate mixture densities in each class lead to flexible models for $\Pr(G|X)$; this is taken up in some detail in Chapter 12.

Figure 6.17 shows an application of mixtures to the heart disease risk-factor study. In the top row are histograms of `Age` for the `no CHD` and `CHD` groups separately, and then combined on the right. Using the combined data, we fit a two-component mixture of the form (6.32) with the (scalars) $\mathbf{\Sigma}_1$ and $\mathbf{\Sigma}_2$ not constrained to be equal. Fitting was done via the EM algorithm (Chapter 8): note that the procedure does not use knowledge of the `CHD` labels. The resulting estimates were

$$\begin{aligned} &\hat{\mu}_1 = 36.4, \quad &\hat{\Sigma}_1 = 157.7, \quad &\hat{\alpha}_1 = 0.7, \\ &\hat{\mu}_2 = 58.0, \quad &\hat{\Sigma}_2 = 15.6, \quad &\hat{\alpha}_2 = 0.3. \end{aligned}$$

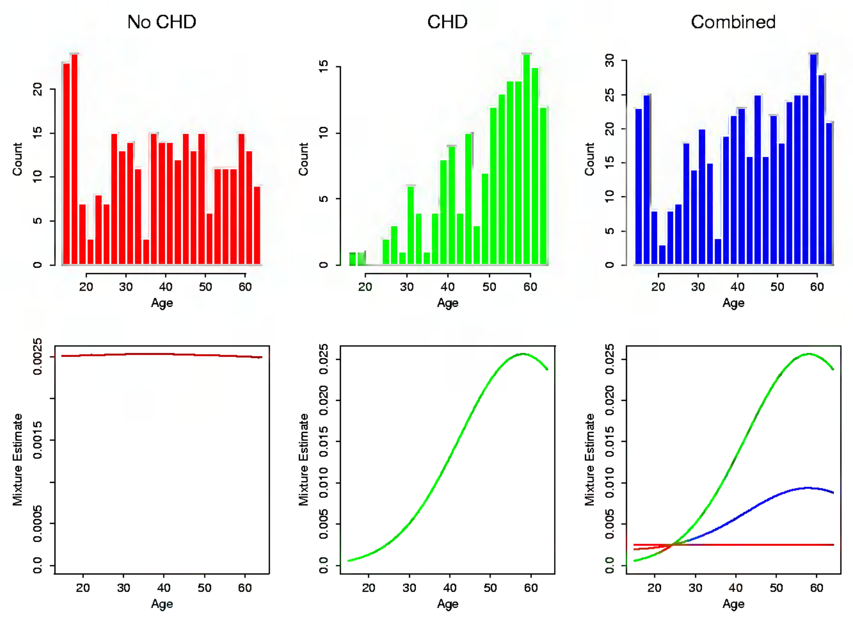

FIGURE 6.17. *Application of mixtures to the heart disease risk-factor study. Top row: histograms of* `Age` *for the* `no CHD` *and* `CHD` *groups separately, and combined. Bottom row: estimated component densities from a Gaussian mixture model, (left, middle); bottom right: estimated component densities (green and red) along with the estimated mixture density (blue). The red density has a very large standard deviation, and is approximating a uniform density.*

The component densities $\phi(\hat{\mu}_1, \hat{\Sigma}_1)$ and $\phi(\hat{\mu}_2, \hat{\Sigma}_2)$ are shown in the lower-left and middle panels. The lower right panel shows these component densities (green and red) along with the estimated mixture density (blue).

The mixture model also provides an estimate of the probability that observation i belongs to component m,

$$\hat{r}_{im} = \frac{\hat{\alpha}_m \phi(x_i; \hat{\mu}_m, \hat{\Sigma}_m)}{\sum_{k=1}^{M} \hat{\alpha}_k \phi(x_i; \hat{\mu}_k, \hat{\Sigma}_k)}, \tag{6.33}$$

where x_i is `Age` in our example. Suppose we threshold each value $\hat{r}_{i2}$ and hence define $\hat{\delta}_i = I(\hat{r}_{i2} > 0.5)$. Then we can compare the classification of each observation by `CHD` and the mixture model:

		Mixture model	
		$\hat{\delta} = 0$	$\hat{\delta} = 1$
CHD	No	232	70
	Yes	76	84

Although the mixture model did not use the `CHD` labels, it has done a fair job in discovering the two `CHD` subpopulations. Linear logistic regression, using the CHD as a response, achieves the same error rate (32%) when fit to these data using maximum-likelihood (Section 4.4).

6.9 Computational Considerations

Kernel and local regression and density estimation are *memory-based* methods: the model is the entire training data set, and the fitting is done at evaluation or prediction time. For many real-time applications, this can make this class of methods infeasible.

The computational cost to fit at a single observation x_0 is $O(N)$ flops, except in oversimplified cases (such as square kernels). By comparison, an expansion in M basis functions costs $O(M)$ for one evaluation, and typically $M \sim O(\log N)$. Basis function methods have an initial cost of at least $O(NM^2 + M^3)$.

The smoothing parameter(s) λ for kernel methods are typically determined off-line, for example using cross-validation, at a cost of $O(N^2)$ flops.

Popular implementations of local regression, such as the `loess` function in S-PLUS and the `locfit` procedure (Loader, 1999), use triangulation schemes to reduce the computations. They compute the fit exactly at M carefully chosen locations ($O(NM)$), and then use blending techniques to interpolate the fit elsewhere ($O(M)$ per evaluation).

Bibliographic Notes

There is a vast literature on kernel methods which we will not attempt to summarize. Rather we will point to a few good references that themselves have extensive bibliographies. Loader (1999) gives excellent coverage of local regression and likelihood, and also describes state-of-the-art software for fitting these models. Fan and Gijbels (1996) cover these models from a more theoretical aspect. Hastie and Tibshirani (1990) discuss local regression in the context of additive modeling. Silverman (1986) gives a good overview of density estimation, as does Scott (1992).

Exercises

Ex. 6.1 Show that the Nadaraya–Watson kernel smooth with fixed metric bandwidth λ and a Gaussian kernel is differentiable. What can be said for the Epanechnikov kernel? What can be said for the Epanechnikov kernel with adaptive nearest-neighbor bandwidth $\lambda(x_0)$?

Ex. 6.2 Show that $\sum_{i=1}^{N}(x_i - x_0)l_i(x_0) = 0$ for local linear regression. Define $b_j(x_0) = \sum_{i=1}^{N}(x_i - x_0)^j l_i(x_0)$. Show that $b_0(x_0) = 1$ for local polynomial regression of any degree (including local constants). Show that $b_j(x_0) = 0$ for all $j \in \{0, 1, \ldots, k\}$ for local polynomial regression of degree k. What are the implications of this on the bias?

Ex. 6.3 Show that $||l(x)||$ (Section 6.1.2) increases with the degree of the local polynomial.

Ex. 6.4 Suppose that the p predictors X arise from sampling relatively smooth analog curves at p uniformly spaced abscissa values. Denote by $\text{Cov}(X|Y) = \mathbf{\Sigma}$ the conditional covariance matrix of the predictors, and assume this does not change much with Y. Discuss the nature of *Mahalanobis* choice $\mathbf{A} = \mathbf{\Sigma}^{-1}$ for the metric in (6.14). How does this compare with $\mathbf{A} = \mathbf{I}$? How might you construct a kernel $\mathbf{A}$ that (a) downweighs high-frequency components in the distance metric; (b) ignores them completely?

Ex. 6.5 Show that fitting a locally constant multinomial logit model of the form (6.19) amounts to smoothing the binary response indicators for each class separately using a Nadaraya–Watson kernel smoother with kernel weights $K_\lambda(x_0, x_i)$.

Ex. 6.6 Suppose that all you have is software for fitting local regression, but you can specify exactly which monomials are included in the fit. How could you use this software to fit a varying-coefficient model in some of the variables?

Ex. 6.7 Derive an expression for the leave-one-out cross-validated residual sum-of-squares for local polynomial regression.

Ex. 6.8 Suppose that for continuous response Y and predictor X, we model the joint density of X, Y using a multivariate Gaussian kernel estimator. Note that the kernel in this case would be the product kernel $\phi_\lambda(X)\phi_\lambda(Y)$. Show that the conditional mean $E(Y|X)$ derived from this estimate is a Nadaraya–Watson estimator. Extend this result to classification by providing a suitable kernel for the estimation of the joint distribution of a continuous X and discrete Y.

Ex. 6.9 Explore the differences between the naive Bayes model (6.27) and a generalized additive logistic regression model, in terms of (a) model assumptions and (b) estimation. If all the variables X_k are discrete, what can you say about the corresponding GAM?

Ex. 6.10 Suppose we have N samples generated from the model $y_i = f(x_i) + \varepsilon_i$, with ε_i independent and identically distributed with mean zero and variance σ^2, the x_i assumed fixed (non random). We estimate f using a linear smoother (local regression, smoothing spline, etc.) with smoothing parameter λ. Thus the vector of fitted values is given by $\hat{\mathbf{f}} = \mathbf{S}_\lambda \mathbf{y}$. Consider the *in-sample* prediction error

$$\mathrm{PE}(\lambda) = \mathrm{E}\frac{1}{N}\sum_{i=1}^{N}(y_i^* - \hat{f}_\lambda(x_i))^2 \tag{6.34}$$

for predicting new responses at the N input values. Show that the average squared residual on the training data, $\mathrm{ASR}(\lambda)$, is a biased estimate (optimistic) for $\mathrm{PE}(\lambda)$, while

$$C_\lambda = \mathrm{ASR}(\lambda) + \frac{2\sigma^2}{N}\mathrm{trace}(\mathbf{S}_\lambda) \tag{6.35}$$

is unbiased.

Ex. 6.11 Show that for the Gaussian mixture model (6.32) the likelihood is maximized at $+\infty$, and describe how.

Ex. 6.12 Write a computer program to perform a local linear discriminant analysis. At each query point x_0, the training data receive weights $K_\lambda(x_0, x_i)$ from a weighting kernel, and the ingredients for the linear decision boundaries (see Section 4.3) are computed by weighted averages. Try out your program on the `zipcode` data, and show the training and test errors for a series of five pre-chosen values of λ. The `zipcode` data are available from the book website `www-stat.stanford.edu/ElemStatLearn`.

7 Model Assessment and Selection

7.1 Introduction

The *generalization* performance of a learning method relates to its prediction capability on independent test data. Assessment of this performance is extremely important in practice, since it guides the choice of learning method or model, and gives us a measure of the quality of the ultimately chosen model.

In this chapter we describe and illustrate the key methods for performance assessment, and show how they are used to select models. We begin the chapter with a discussion of the interplay between bias, variance and model complexity.

7.2 Bias, Variance and Model Complexity

Figure 7.1 illustrates the important issue in assessing the ability of a learning method to generalize. This is the same as Figure 2.11; because it is so important, we display it here again. Consider first the case of a quantitative or interval scale response. We have a target variable Y, a vector of inputs X, and a prediction model $\hat{f}(X)$ that has been estimated from a training sample. The loss function for measuring errors between Y and

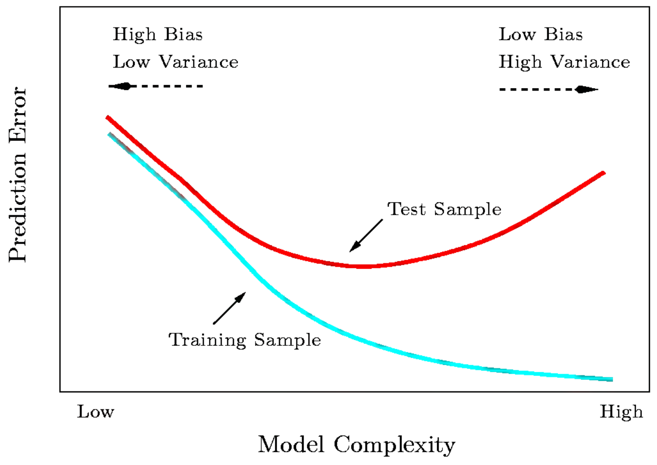

FIGURE 7.1. *Behavior of test sample and training sample error as the model complexity is varied.*

$\hat{f}(X)$ is denoted by $L(Y, \hat{f}(X))$. Typical choices are

$$L(Y, \hat{f}(X)) = \begin{cases} (Y - \hat{f}(X))^2 & \text{squared error} \\ |Y - \hat{f}(X)| & \text{absolute error.} \end{cases} \tag{7.1}$$

Test error, also referred to as *generalization error*, is the expected prediction error over an independent test sample

$$\text{Err} = \text{E}[L(Y, \hat{f}(X))], \tag{7.2}$$

where both X and Y are drawn randomly from their joint distribution (population). Note that this expectation averages anything that is random, including the randomness in the training sample that produced $\hat{f}$. *Training error* is the average loss over the training sample

$$\overline{\text{err}} = \frac{1}{N}\sum_{i=1}^{N} L(y_i, \hat{f}(x_i)). \tag{7.3}$$

We would like to know the test error of our estimated model $\hat{f}$. As the model becomes more and more complex, it is able to adapt to more complicated underlying structures (a decrease in bias), but the estimation error increases (an increase in variance). In between there is an optimal model complexity that gives minimum test error.

Unfortunately training error is not a good estimate of the test error, as seen in Figure 7.1. Training error consistently decreases with model complexity, typically dropping to zero if we increase the model complexity enough. However, a model with zero training error is overfit to the training data and will typically generalize poorly.

The story is similar for a qualitative or categorical response G taking one of K values in a set $\mathcal{G}$, labelled for convenience as $1, 2, \ldots, K$. Typically we model the probabilities $p_k(X) = \Pr(G = k|X)$ (or some monotone transformations $f_k(X)$), and then $\hat{G}(X) = \arg\max_k \hat{p}_k(X)$. In some cases, such as 1-nearest neighbor classification (Chapters 2 and 13) we produce $\hat{G}(X)$ directly. Typical loss functions are

$$\begin{aligned} L(G, \hat{G}(X)) &= I(G \neq \hat{G}(X)) \quad \text{0–1 loss,} & (7.4) \\ L(G, \hat{p}(X)) &= -2\sum_{k=1}^{K} I(G = k)\log \hat{p}_k(X) \\ &= -2\log \hat{p}_G(X) \quad \text{log-likelihood.} & (7.5) \end{aligned}$$

The log-likelihood is sometimes referred to as *cross-entropy* loss or *deviance*.

Again, test error is given by $\text{Err} = \text{E}[L(G, \hat{G}(X))]$, the expected misclassification rate, or $\text{Err} = \text{E}[L(G, \hat{p}(X))]$. Training error is the sample analogue, for example,

$$\overline{\text{err}} = \frac{-2}{N}\sum_{i=1}^{N} \log \hat{p}_{g_i}(x_i), \tag{7.6}$$

the sample log-likelihood for the model.

The log-likelihood can be used as a loss-function for general response densities, such as the Poisson, gamma, exponential, log-normal and others. If $\Pr_{\theta(X)}(Y)$ is the density of Y, indexed by a parameter $\theta(X)$ that depends on the predictor X, then

$$L(Y, \theta(X)) = -2 \cdot \log \Pr_{\theta(X)}(Y). \tag{7.7}$$

The "2" in the definition makes the log-likelihood loss for the Gaussian distribution match squared-error loss.

For ease of exposition, for the remainder of this chapter we will use Y and $f(X)$ to represent all of the above situations, since we focus mainly on the quantitative response (squared-error loss) setting. For the other situations, the appropriate translations are obvious.

In this chapter we describe a number of methods for estimating the test error curve for a model. Typically our model will have a tuning parameter or parameters α and so we can write our predictions as $\hat{f}_\alpha(x)$. The tuning parameter varies the complexity of our model, and we wish to find the value of α that minimizes error, that is, produces the minimum of the test error curve in Figure 7.1. Having said this, for brevity we will often suppress the dependence of $\hat{f}(x)$ on α.

It is important to note that there are in fact two separate goals that we might have in mind:

Model selection: estimating the performance of different models in order to choose the (approximate) best one.

Model assessment: having chosen a final model, estimating its prediction error (generalization error) on new data.

If we are in a data-rich situation, the best approach for both problems is to randomly divide the dataset into three parts: a training set, a validation set, and a test set. The training set is used to fit the models; the validation set is used to estimate prediction error for model selection; the test set is used for assessment of the generalization error of the final chosen model. Ideally, the test set should be kept in a "vault," and be brought out only at the end of the data analysis. Suppose instead that we use the test set repeatedly, choosing the model with smallest test set error. Then the test set error of the final chosen model will underestimate the true test error, sometimes substantially.

It is difficult to give a general rule on how to choose the number of observations in each of the three parts, as this depends on the signal-to-noise ratio in the data and the training sample size. A typical split might be 50% for training, and 25% each for validation and testing:

Train
Validation
Test

The methods in this chapter are designed for situations where there is insufficient data to split it into three parts. Again it is too difficult to give a general rule on how much training data is enough; among other things, this depends on the signal-to-noise ratio of the underlying function, and the complexity of the models being fit to the data.

The methods of this chapter approximate the validation step either analytically (AIC, BIC, MDL, SRM) or by efficient sample re-use (cross-validation and the bootstrap). Besides their use in model selection, we also examine to what extent each method provides a reliable estimate of test error of the final chosen model.

Before jumping into these topics, we first explore in more detail the nature of test error and the bias–variance tradeoff.

7.3 The Bias–Variance Decomposition

As in Chapter 2, if we assume that $Y = f(X) + \varepsilon$ where $\mathrm{E}(\varepsilon) = 0$ and $\mathrm{Var}(\varepsilon) = \sigma_\varepsilon^2$, we can derive an expression for the expected prediction error of a regression fit $\hat{f}(X)$ at an input point $X = x_0$, using squared-error loss:

$$\begin{aligned} \text{Err}(x_0) &= E[(Y - \hat{f}(x_0))^2 | X = x_0] \\ &= \sigma_\varepsilon^2 + [E\hat{f}(x_0) - f(x_0)]^2 + E[\hat{f}(x_0) - E\hat{f}(x_0)]^2 \\ &= \sigma_\varepsilon^2 + \text{Bias}^2(\hat{f}(x_0)) + \text{Var}(\hat{f}(x_0)) \\ &= \text{Irreducible Error} + \text{Bias}^2 + \text{Variance}. \end{aligned} \tag{7.8}$$

The first term is the variance of the target around its true mean $f(x_0)$, and cannot be avoided no matter how well we estimate $f(x_0)$, unless $\sigma_\varepsilon^2 = 0$. The second term is the squared bias, the amount by which the average of our estimate differs from the true mean; the last term is the variance; the expected squared deviation of $\hat{f}(x_0)$ around its mean. Typically the more complex we make the model $\hat{f}$, the lower the (squared) bias but the higher the variance.

For the k-nearest-neighbor regression fit, these expressions have the simple form

$$\begin{aligned} \text{Err}(x_0) &= E[(Y - \hat{f}_k(x_0))^2 | X = x_0] \\ &= \sigma_\varepsilon^2 + \Big[f(x_0) - \frac{1}{k}\sum_{\ell=1}^{k} f(x_{(\ell)})\Big]^2 + \sigma_\varepsilon^2/k. \end{aligned} \tag{7.9}$$

Here we assume for simplicity that training inputs x_i are fixed, and the randomness arises from the y_i. The number of neighbors k is inversely related to the model complexity. For small k, the estimate $\hat{f}_k(x)$ can potentially adapt itself better to the underlying $f(x)$. As we increase k, the bias—the squared difference between $f(x_0)$ and the average of $f(x)$ at the k-nearest neighbors—will typically increase, while the variance decreases.

For a linear model fit $\hat{f}_p(x) = \hat{\beta}^T x$, where the parameter vector β with p components is fit by least squares, we have

$$\begin{aligned} \text{Err}(x_0) &= E[(Y - \hat{f}_p(x_0))^2 | X = x_0] \\ &= \sigma_\varepsilon^2 + [f(x_0) - E\hat{f}_p(x_0)]^2 + ||\mathbf{h}(x_0)||^2\sigma_\varepsilon^2. \end{aligned} \tag{7.10}$$

Here $\mathbf{h}(x_0)$ is the N-vector of linear weights that produce the fit $\hat{f}_p(x_0) = x_0^T(\mathbf{X}^T\mathbf{X})^{-1}\mathbf{X}^T\mathbf{y}$, and hence $\text{Var}[\hat{f}_p(x_0)] = ||\mathbf{h}(x_0)||^2\sigma_\varepsilon^2$. While this variance changes with x_0, its average (over the sample values x_i) is $(p/N)\sigma_\varepsilon^2$, and hence

$$\frac{1}{N}\sum_{i=1}^{N}\text{Err}(x_i) = \sigma_\varepsilon^2 + \frac{1}{N}\sum_{i=1}^{N}[f(x_i) - E\hat{f}(x_i)]^2 + \frac{p}{N}\sigma_\varepsilon^2, \tag{7.11}$$

the *in-sample* error. Here model complexity is directly related to the number of parameters p.

The test error $\text{Err}(x_0)$ for a ridge regression fit $\hat{f}_\alpha(x_0)$ is identical in form to (7.10), except the linear weights in the variance term are different: $\mathbf{h}(x_0) = \mathbf{X}(\mathbf{X}^T\mathbf{X} + \alpha\mathbf{I})^{-1}x_0$. The bias term will also be different.

For a linear model family such as ridge regression, we can break down the bias more finely. Let β_* denote the parameters of the best-fitting linear approximation to f:

$$\beta_* = \arg\min_\beta \text{E}\left(f(X) - \beta^T X\right)^2. \tag{7.12}$$

Here the expectation is taken with respect to the distribution of the input variables X. Then we can write the squared bias as

$$\begin{aligned}\left[f(x_0) - E\hat{f}_\alpha(x_0)\right]^2 &= \left[f(x_0) - \beta_*^T x_0\right]^2 + \left[\beta_*^T x - \text{E}\hat{\beta}_\alpha^T x_0\right]^2 \\ &= [\text{Model Bias}]^2 + [\text{Estimation Bias}]^2. \quad (7.13)\end{aligned}$$

The first term on the right-hand side is the squared *model bias*, the error between the best-fitting linear approximation and the true function. The second term is the squared *estimation bias*, the error between the average estimate $\text{E}(\hat{\beta}^T x_0)$ and the best fitting linear approximation.

For linear models fit by ordinary least squares, the estimation bias is zero. For restricted fits, such as ridge regression, it is positive, and we trade it off with the benefits of a reduced variance. The model bias can only be reduced by enlarging the class of linear models to a richer collection of models, by including interactions and transformations of the variables in the model.

Figure 7.2 shows the bias–variance tradeoff schematically. In the case of linear models, the model space is the set of all linear predictions from p inputs and the black dot labeled "closest fit" is $\beta_*^T x$. The blue-shaded region indicates the error σ_ε with which we see the truth in the training sample.

Also shown is the variance of the least squares fit, indicated by the large yellow circle centered at the black dot labelled "closest fit in population'. Now if we were to fit a model with fewer predictors, or regularize the coefficients by shrinking them toward zero (say), we would get the "shrunken fit" shown in the figure. This fit has an additional estimation bias, due to the fact that it is not the closest fit in the model space. On the other hand, it has smaller variance. If the decrease in variance exceeds the increase in (squared) bias, then this is worthwhile.

7.3.1 Example: Bias–Variance Tradeoff

Figure 7.3 shows the bias–variance tradeoff for two simulated examples. There are 50 observations and 20 predictors, uniformly distributed in the hypercube $[0,1]^{20}$. The situations are as follows:

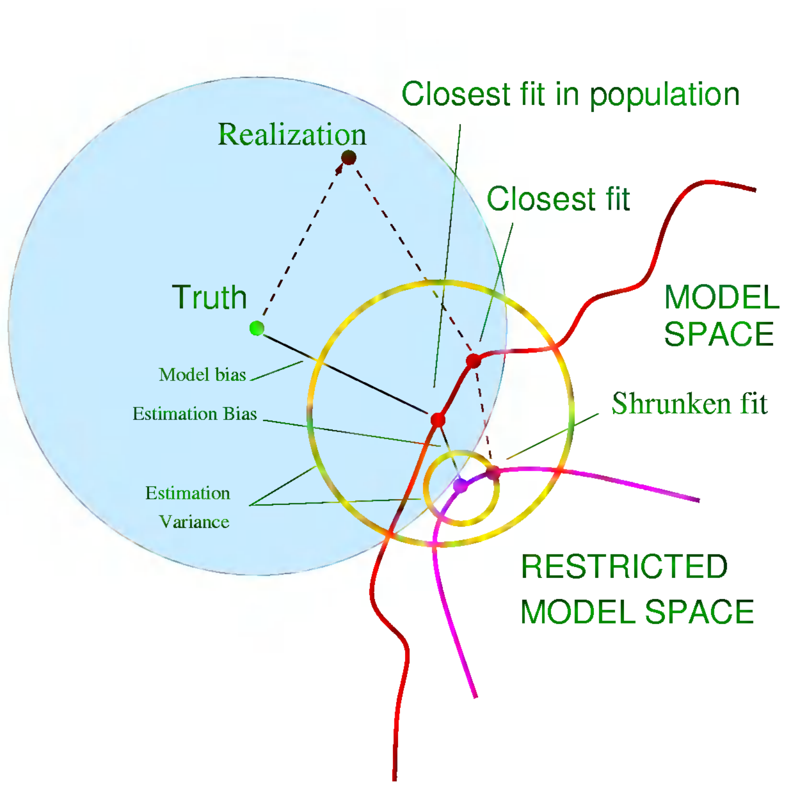

FIGURE 7.2. *Schematic of the behavior of bias and variance. The model space is the set of all possible predictions from the model, with the "closest fit" labeled with a black dot. The model bias from the truth is shown, along with the variance, indicated by the large yellow circle centered at the black dot labelled "closest fit in population". A shrunken or regularized fit is also shown, having additional estimation bias, but smaller prediction error due to its decreased variance.*

Left panels: Y is 0 if $X_1 \le 1/2$ and 1 if $X_1 > 1/2$, and we apply k-nearest neighbors.

Right panels: Y is 1 if $\sum_{j=1}^{10} X_j$ is greater than 5 and 0 otherwise, and we use best subset linear regression of size p.

The top row is regression with squared error loss; the bottom row is classification with 0–1 loss. The figures show the prediction error (red), squared bias (green) and variance (blue), all computed for a large test sample.

In the regression problems, bias and variance add to produce the prediction error curves, with minima at about $k = 5$ for k-nearest neighbors, and $p \ge 10$ for the linear model. For classification loss (bottom figures), some interesting phenomena can be seen. The bias and variance curves are the same as in the top figures, and prediction error now refers to misclassification rate. We see that prediction error is no longer the sum of squared bias and variance. For the k-nearest neighbor classifier, prediction error decreases or stays the same as the number of neighbors is increased to 20, despite the fact that the squared bias is rising. For the linear model classifier the minimum occurs for $p \ge 10$ as in regression, but the improvement over the $p = 1$ model is more dramatic. We see that bias and variance seem to interact in determining prediction error.

Why does this happen? There is a simple explanation for the first phenomenon. Suppose at a given input point, the true probability of class 1 is 0.9 while the expected value of our estimate is 0.6. Then the squared bias—$(0.6 - 0.9)^2$—is considerable, but the prediction error is zero since we make the correct decision. In other words, estimation errors that leave us on the right side of the decision boundary don't hurt. Exercise 7.2 demonstrates this phenomenon analytically, and also shows the interaction effect between bias and variance.

The overall point is that the bias–variance tradeoff behaves differently for 0–1 loss than it does for squared error loss. This in turn means that the best choices of tuning parameters may differ substantially in the two settings. One should base the choice of tuning parameter on an estimate of prediction error, as described in the following sections.

7.4 Optimism of the Training Error Rate

Typically, the training error rate

$$\overline{\text{err}} = \frac{1}{N}\sum_{i=1}^{N} L(y_i, \hat{f}(x_i)) \tag{7.14}$$

will be less than the true error $\text{Err} = \text{E}[L(Y, \hat{f}(X))]$, because the same data is being used to fit the method and assess its error. A fitting method

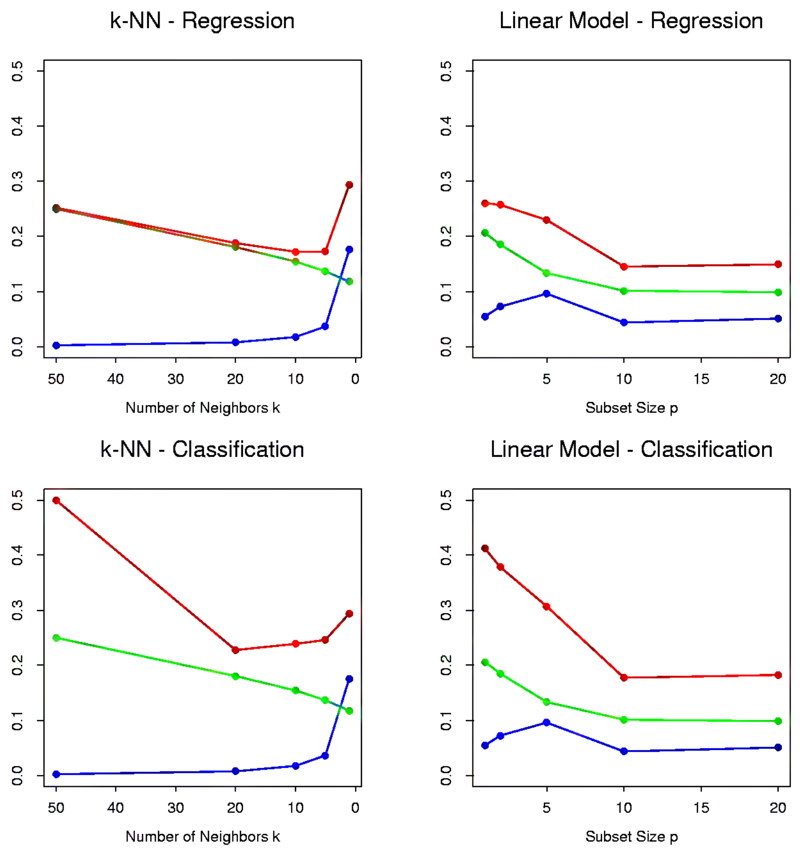

FIGURE 7.3. *Prediction error (red), squared bias (green) and variance (blue) for a simulated example. The top row is regression with squared error loss; the bottom row is classification with* 0–1 *loss. The models are k-nearest neighbors (left) and best subset regression of size p (right). The variance and bias curves are the same in regression and classification, but the prediction error curve is different.*

typically adapts to the training data, and hence the apparent or training error $\overline{\text{err}}$ will be an overly optimistic estimate of the generalization error Err.

Part of the discrepancy is due to where the evaluation points occur. Err is a kind of *extra-sample* error, since the test feature vectors don't need to coincide with the training feature vectors. The nature of the optimism in $\overline{\text{err}}$ is easiest to understand when we focus not on Err but on the *in-sample* error

$$\text{Err}_{\text{in}} = \frac{1}{N}\sum_{i=1}^{N} \text{E}_{Y^{\text{new}}} L(Y_i^{\text{new}}, \hat{f}(x_i)). \tag{7.15}$$

The Y^{new} notation indicates that we observe N new response values at each of the training points $x_i,\ i = 1, 2, \ldots, N$. We define the *optimism* as the expected difference between Err_{in} and the training error $\overline{\text{err}}$:

$$\text{op} \equiv \text{Err}_{\text{in}} - \text{E}_{\mathbf{y}}(\overline{\text{err}}). \tag{7.16}$$

This is typically positive since $\overline{\text{err}}$ is usually biased downward as an estimate of prediction error.

For squared error, 0–1, and other loss functions, one can show quite generally that

$$\text{op} = \frac{2}{N}\sum_{i=1}^{N} \text{Cov}(\hat{y}_i, y_i), \tag{7.17}$$

where Cov indicates covariance. Thus the amount by which $\overline{\text{err}}$ underestimates the true error depends on how strongly y_i affects its own prediction. The harder we fit the data, the greater $\text{Cov}(\hat{y}_i, y_i)$ will be, thereby increasing the optimism. Exercise 7.4 proves this result for squared error loss where $\hat{y}_i$ is the fitted value from the regression. For 0–1 loss, $\hat{y}_i \in \{0, 1\}$ is the classification at x_i, and for entropy loss, $\hat{y}_i \in [0, 1]$ is the fitted probability of class 1 at x_i.

In summary, we have the important relation

$$\text{Err}_{\text{in}} = \text{E}_{\mathbf{y}}(\overline{\text{err}}) + \frac{2}{N}\sum_{i=1}^{N} \text{Cov}(\hat{y}_i, y_i). \tag{7.18}$$

This expression simplifies if $\hat{y}_i$ is obtained by a linear fit with d inputs or basis functions. For example,

$$\sum_{i=1}^{N} \text{Cov}(\hat{y}_i, y_i) = d\sigma_\varepsilon^2 \tag{7.19}$$

for the additive error model $Y = f(X) + \varepsilon$, and so

$$\text{Err}_{\text{in}} = \text{E}\,\overline{\text{err}} + 2 \cdot \frac{d}{N}\sigma_\varepsilon^2. \tag{7.20}$$

The optimism increases linearly with the number d of inputs or basis functions we use, but decreases as the training sample size increases. Versions of (7.20) hold approximately for other error models, such as binary data and entropy loss.

An obvious way to estimate prediction error is to estimate the optimism and then add it to the training error rate $\overline{\text{err}}$. The methods described in the next section—AIC, BIC and others—work in this way, for a special class of estimates that are linear in their parameters.

In contrast, the cross-validation and bootstrap methods, described later in the chapter, are direct estimates of the extra-sample error Err. These general tools can be used with any loss function, and with nonlinear, adaptive fitting techniques.

In-sample error is not usually of direct interest since future values of the features are not likely to coincide with with their training set values. But for comparison between models, in-sample error is convenient and often leads to effective model selection. The reason is that the relative (not absolute) size of the error is what matters.

7.5 Estimates of In-Sample Prediction Error

The general form of the in-sample estimates is

$$\widehat{\text{Err}_{\text{in}}} = \overline{\text{err}} + \widehat{\text{op}}, \tag{7.21}$$

where $\widehat{\text{op}}$ is an estimate of the optimism.

Using expression (7.20), applicable when d parameters are fit under squared error loss, leads to the so-called C_p statistic,

$$C_p = \overline{\text{err}} + 2 \cdot \frac{d}{N}\hat{\sigma}_\varepsilon^2. \tag{7.22}$$

Here $\hat{\sigma}_\varepsilon^2$ is an estimate of the noise variance, obtained from the mean-squared error of a low-bias model. Using this criterion we adjust the training error by a factor proportional to the number of basis functions used.

The *Akaike information criterion* is a similar but more generally applicable estimate of Err_{in} when a log-likelihood loss function is used. It relies on a relationship similar to (7.20) that holds asymptotically as $N \to \infty$:

$$-2 \cdot \text{E}[\log \text{Pr}_{\hat{\theta}}(Y)] \approx -\frac{2}{N} \cdot \text{E}[\text{loglik}] + 2 \cdot \frac{d}{N}. \tag{7.23}$$

Here $\text{Pr}_\theta(Y)$ is a family of densities for Y (containing the "true" density), $\hat{\theta}$ is the maximum-likelihood estimate of θ, and "loglik" is the maximized log-likelihood:

$$\text{loglik} = \sum_{i=1}^{N} \log \text{Pr}_{\hat{\theta}}(y_i). \tag{7.24}$$

For example, for the logistic regression model, using the binomial log-likelihood, we have

$$\mathrm{AIC} = -2 \cdot \mathrm{loglik} + 2 \cdot \frac{d}{N}. \tag{7.25}$$

For the Gaussian model (with variance $\sigma_\varepsilon^2 = \hat{\sigma}_\varepsilon^2$ assumed known), the AIC statistic is equivalent to C_p, and so we refer to them collectively as AIC.

To use AIC for model selection, we simply choose the model giving smallest AIC over the set of models considered. For nonlinear and other complex models, we need to replace d by some measure of model complexity. We discuss this in Section 7.6.

Given a set of models $f_\alpha(x)$ indexed by a tuning parameter α, denote by $\overline{\mathrm{err}}(\alpha)$ and $d(\alpha)$ the training error and number of parameters for each model. Then for this set of models we define

$$\mathrm{AIC}(\alpha) = \overline{\mathrm{err}}(\alpha) + 2 \cdot \frac{d(\alpha)}{N}\hat{\sigma}_\varepsilon^2. \tag{7.26}$$

The function $\mathrm{AIC}(\alpha)$ provides an estimate of the test error curve, and we find the tuning parameter $\hat{\alpha}$ that minimizes it. Our final chosen model is $f_{\hat{\alpha}}(x)$. Note that if the basis functions are chosen adaptively, (7.19) no longer holds. For example, if we have a total of p inputs, and we choose the best-fitting linear model with $d < p$ inputs, the optimism will exceed $(2d/N)\sigma_\varepsilon^2$. Put another way, by choosing the best-fitting model with d inputs, the *effective number of parameters* fit is more than d.

Figure 7.4 shows AIC in action for the phoneme recognition example of Section 5.2.3 on page 124. The input vector is the log-periodogram of the spoken vowel, quantized to 256 uniformly spaced frequencies. A linear logistic regression model is used to predict the phoneme class, with coefficient function $\beta(f) = \sum_{m=1}^M h_m(f)\theta_m$, an expansion in M spline basis functions. For any given M, a basis of natural cubic splines is used for the h_m, with knots chosen uniformly over the range of frequencies (so $d(\alpha) = d(M) = M$). Using AIC to select the number of basis functions will approximately minimize $\mathrm{Err}(M)$ for both entropy and 0–1 loss.

The simple formula

$$(2/N)\sum_{i=1}^N \mathrm{Cov}(\hat{y}_i, y_i) = (2d/N)\sigma_\varepsilon^2$$

holds exactly for linear models with additive errors and squared error loss, and approximately for linear models and log-likelihoods. In particular, the formula does not hold in general for 0–1 loss (Efron, 1986), although many authors nevertheless use it in that context (right panel of Figure 7.4).

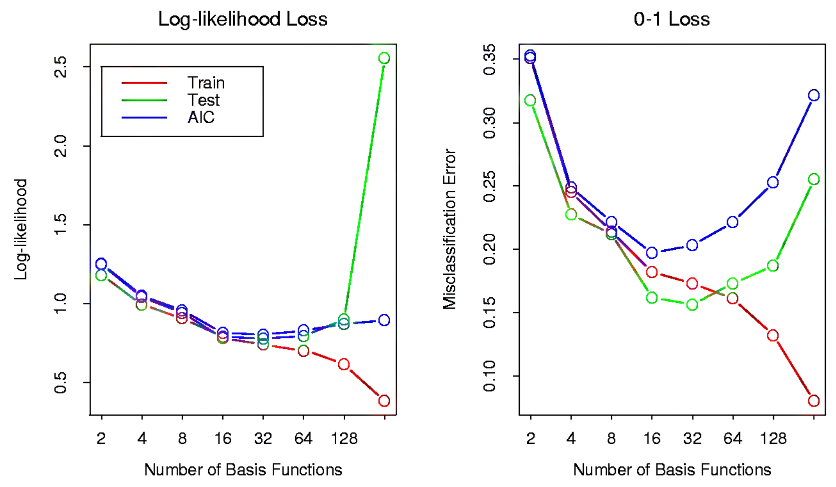

FIGURE 7.4. *AIC used for model selection for the phoneme recognition example of Section 5.2.3. The logistic regression coefficient function* $\beta(f) = \sum_{m=1}^{M} h_m(f)\theta_m$ *is modeled as an expansion in M spline basis functions. In the left panel we see the AIC statistic used to estimate* $\mathrm{Err}_{\mathrm{in}}$ *using log-likelihood loss. Included is an estimate of* Err *based on an independent test sample. It does well except for the extremely over-parametrized case ($M = 256$ parameters for $N = 1000$ observations). In the right panel the same is done for 0–1 loss. Although the AIC formula does not strictly apply here, it does a reasonable job in this case.*

7.6 The Effective Number of Parameters

The concept of "number of parameters" can be generalized, especially to models where regularization is used in the fitting. Suppose we stack the outcomes $y_1, y_2, \dots, y_N$ into a vector $\mathbf{y}$, and similarly for the predictions $\hat{\mathbf{y}}$. Then a linear fitting method is one for which we can write

$$\hat{\mathbf{y}} = \mathbf{S}\mathbf{y}, \tag{7.27}$$

where $\mathbf{S}$ is an $N \times N$ matrix depending on the input vectors x_i but not on the y_i. Linear fitting methods include linear regression on the original features or on a derived basis set, and smoothing methods that use quadratic shrinkage, such as ridge regression and cubic smoothing splines. Then the *effective number of parameters* is defined as

$$d(\mathbf{S}) = \mathrm{trace}(\mathbf{S}), \tag{7.28}$$

the sum of the diagonal elements of $\mathbf{S}$. Note that if $\mathbf{S}$ is an orthogonal-projection matrix onto a basis set spanned by M features, then $\mathrm{trace}(\mathbf{S}) =$

M. It turns out that trace($\mathbf{S}$) is exactly the correct quantity to replace d as the number of parameters in the C_p statistic (7.22) (Exercise 7.4 and 7.5). We motivate $d = \text{trace}(\mathbf{S})$ in some detail in Section 5.4.1 on page 129.

For models like neural networks, in which we minimize an error function $R(w)$ with weight decay penalty (regularization) $\alpha \sum_m w_m^2$, the effective number of parameters has the form

$$d(\alpha) = \sum_{m=1}^{M} \frac{\theta_m}{\theta_m + \alpha}, \tag{7.29}$$

where the θ_m are the eigenvalues of the Hessian matrix $\partial^2 R(w)/\partial w \partial w^T$. Expression (7.29) follows from (7.28) if we make a quadratic approximation to the error function at the solution (Bishop, 1995).

7.7 The Bayesian Approach and BIC

The Bayesian information criterion (BIC), like AIC, is applicable in settings where the fitting is carried out by maximization of a log-likelihood. The generic form of BIC is

$$\text{BIC} = -2 \cdot \text{loglik} + (\log N) \cdot d. \tag{7.30}$$

The BIC statistic (times 1/2) is also known as the Schwartz criterion (Schwartz, 1979).

Under the Gaussian model, assuming the variance σ_ε^2 is known, $-2\cdot\text{loglik}$ equals (up to a constant) $\sum_i (y_i - \hat{f}(x_i))^2/\sigma_\varepsilon^2$, which is $N \cdot \overline{\text{err}}/\sigma_\varepsilon^2$ for squared error loss. Hence we can write

$$\text{BIC} = \frac{N}{\sigma_\varepsilon^2}\Big[\overline{\text{err}} + (\log N) \cdot \frac{d}{N}\Big]. \tag{7.31}$$

Therefore BIC is proportional to AIC (C_p), with the factor 2 replaced by $\log N$. Assuming $N > e^2 \approx 7.4$, BIC tends to penalize complex models more heavily, giving preference to simpler models in selection. As with AIC, σ_ε^2 is typically estimated by the mean squared error of a low-bias model. For classification problems, use of the multinomial log-likelihood leads to a similar relationship with the AIC, using cross-entropy as the error measure. Note however that the misclassification error measure does not arise in the BIC context, since it does not correspond to the log-likelihood of the data under any probability model.

Despite its similarity with AIC, BIC is motivated in quite a different way. It arises in the Bayesian approach to model selection, which we now describe.

Suppose we have a set of candidate models $\mathcal{M}_m, m = 1, \ldots, M$ and corresponding model parameters θ_m, and we wish to choose a best model from among them. Assuming we have a prior distribution $\Pr(\theta_m|\mathcal{M}_m)$ for the parameters of each model $\mathcal{M}_m$, the posterior probability of a given model is

$$\begin{aligned}\Pr(\mathcal{M}_m|\mathbf{Z}) &\propto \Pr(\mathcal{M}_m)\cdot\Pr(\mathbf{Z}|\mathcal{M}_m) \\ &\propto \Pr(\mathcal{M}_m)\cdot\int\Pr(\mathbf{Z}|\theta_m,\mathcal{M}_m)\Pr(\theta_m|\mathcal{M}_m)d\theta_m,\end{aligned}\tag{7.32}$$

where $\mathbf{Z}$ represents the training data $\{x_i, y_i\}_1^N$. To compare two models $\mathcal{M}_m$ and $\mathcal{M}_\ell$, we form the posterior odds

$$\frac{\Pr(\mathcal{M}_m|\mathbf{Z})}{\Pr(\mathcal{M}_\ell|\mathbf{Z})}=\frac{\Pr(\mathcal{M}_m)}{\Pr(\mathcal{M}_\ell)}\cdot\frac{\Pr(\mathbf{Z}|\mathcal{M}_m)}{\Pr(\mathbf{Z}|\mathcal{M}_\ell)}.\tag{7.33}$$

If the odds are greater than one we choose model m, otherwise we choose model ℓ. The rightmost quantity

$$\mathrm{BF}(\mathbf{Z})=\frac{\Pr(\mathbf{Z}|\mathcal{M}_m)}{\Pr(\mathbf{Z}|\mathcal{M}_\ell)}\tag{7.34}$$

is called the *Bayes factor*, the contribution of the data toward the posterior odds.

Typically we assume that the prior over models is uniform, so that $\Pr(\mathcal{M}_m)$ is constant. We need some way of approximating $\Pr(\mathbf{Z}|\mathcal{M}_m)$. A so-called Laplace approximation to the integral followed by some other simplifications (Ripley, 1996, page 64) to (7.32) gives

$$\log\Pr(\mathbf{Z}|\mathcal{M}_m)=\log\Pr(\mathbf{Z}|\hat{\theta}_m,\mathcal{M}_m)-\frac{d_m}{2}\cdot\log N+O(1).\tag{7.35}$$

Here $\hat{\theta}_m$ is a maximum likelihood estimate and d_m is the number of free parameters in model $\mathcal{M}_m$. If we define our loss function to be

$$-2\log\Pr(\mathbf{Z}|\hat{\theta}_m,\mathcal{M}_m),$$

this is equivalent to the BIC criterion of equation (7.30).

Therefore, choosing the model with minimum BIC is equivalent to choosing the model with largest (approximate) posterior probability. But this framework gives us more. If we compute the BIC criterion for a set of M, models, giving BIC_m, $m=1,2,\ldots,M$, then we can estimate the posterior probability of each model $\mathcal{M}_m$ as

$$\frac{e^{-2\cdot\mathrm{BIC}_m}}{\sum_{\ell=1}^M e^{-2\cdot\mathrm{BIC}_\ell}}.\tag{7.36}$$

Thus we can estimate not only the best model, but also assess the relative merits of the models considered.

For model selection purposes, there is no clear choice between AIC and BIC. BIC is asymptotically consistent as a selection criterion. What this means is that given a family of models, including the true model, the probability that BIC will select the correct model approaches one as the sample size $N \to \infty$. This is not the case for AIC, which tends to choose models which are too complex as $N \to \infty$. On the other hand, for finite samples, BIC often chooses models that are too simple, because of its heavy penalty on complexity.

7.8 Minimum Description Length

The minimum description length (MDL) approach gives a selection criterion formally identical to the BIC approach, but is motivated from an optimal coding viewpoint. We first review the theory of coding for data compression, and then apply it to model selection.

We think of our datum z as a message that we want to encode and send to someone else (the "receiver"). We think of our model as a way of encoding the datum, and will choose the most parsimonious model, that is the shortest code, for the transmission.

Suppose first that the possible messages we might want to transmit are $z_1, z_2, \ldots, z_m$. Our code uses a finite alphabet of length A: for example, we might use a binary code $\{0, 1\}$ of length $A = 2$. Here is an example with four possible messages and a binary coding:

Message	z_1	z_2	z_3	z_4
Code	0	10	110	111

(7.37)

This code is known as an instantaneous prefix code: no code is the prefix of any other, and the receiver (who knows all of the possible codes), knows exactly when the message has been completely sent. We restrict our discussion to such instantaneous prefix codes.

One could use the coding in (7.37) or we could permute the codes, for example use codes $110, 10, 111, 0$ for z_1, z_2, z_3, z_4. How do we decide which to use? It depends on how often we will be sending each of the messages. If, for example, we will be sending z_1 most often, it makes sense to use the shortest code 0 for z_1. Using this kind of strategy—shorter codes for more frequent messages—the average message length will be shorter.

In general, if messages are sent with probabilities $\Pr(z_i), i = 1, 2, \ldots, 4$, a famous theorem due to Shannon says we should use code lengths $l_i = -\log_2 \Pr(z_i)$ and the average message length satisfies

$$\mathrm{E}(\text{length}) \geq -\sum \Pr(z_i) \log_2 (\Pr(z_i)). \tag{7.38}$$

The right-hand side above is also called the entropy of the distribution $\Pr(z_i)$. The inequality is an equality when the probabilities satisfy $p_i =$

A^{-l_i}. In our example, if $\Pr(z_i) = 1/2, 1/4, 1/8, 1/8$, respectively, then the coding shown in (7.37) is optimal and achieves the entropy lower bound.

In general the lower bound cannot be achieved, but procedures like the Huffmann coding scheme can get close to the bound. Note that with an infinite set of messages, the entropy is replaced by $-\int \Pr(z)\log_2 \Pr(z)dz$.

From this result we glean the following:

> *To transmit a random variable z having probability density function $\Pr(z)$, we require about $-\log_2 \Pr(z)$ bits of information.*

We henceforth change notation from $\log_2 \Pr(z)$ to $\log \Pr(z) = \log_e \Pr(z)$; this is for convenience, and just introduces an unimportant additive constant.

Now we apply this result to the problem of model selection. We have a model M with parameters θ, and data $\mathbf{Z} = (\mathbf{X}, \mathbf{y})$ consisting of both inputs and outputs. Let the (conditional) probability of the outputs under the model be $\Pr(\mathbf{y}|\theta, M, \mathbf{X})$, assume the receiver knows all of the inputs, and we wish to transmit the outputs. Then the message length required to transmit the outputs is

$$\text{length} = -\log \Pr(\mathbf{y}|\theta, M, \mathbf{X}) - \log \Pr(\theta|M), \tag{7.39}$$

the log-probability of the target values given the inputs. The second term is the average code length for transmitting the model parameters θ, while the first term is the average code length for transmitting the discrepancy between the model and actual target values. For example suppose we have a single target y with $y \sim N(\theta, \sigma^2)$, parameter $\theta \sim N(0, 1)$ and no input (for simplicity). Then the message length is

$$\text{length} = \text{constant} + \log \sigma + \frac{(y-\theta)^2}{\sigma^2} + \frac{\theta^2}{2}. \tag{7.40}$$

Note that the smaller σ, is the shorter the message length, since y is more concentrated around θ.

The MDL principle says that we should choose the model that minimizes (7.39). We recognize (7.39) as the (negative) log-posterior distribution, and hence minimizing description length is equivalent to maximizing posterior probability. Hence the BIC criterion, derived as approximation to log-posterior probability, can also be viewed as a device for (approximate) model choice by minimum description length.

Note that we have ignored the precision with which a random variable z is coded. With a finite code length we cannot code a continuous variable exactly. However, if we code z within a tolerance δz, the message length needed is the log of the probability in the interval $[z, z+\delta z]$ which is well approximated by $\delta z \Pr(z)$ if δz is small. Since $\log \delta z \Pr(z) = \log \delta z + \log \Pr(z)$, this means we can just ignore the constant $\log \delta z$ and use $\log \Pr(z)$ as our measure of message length, as we did above.

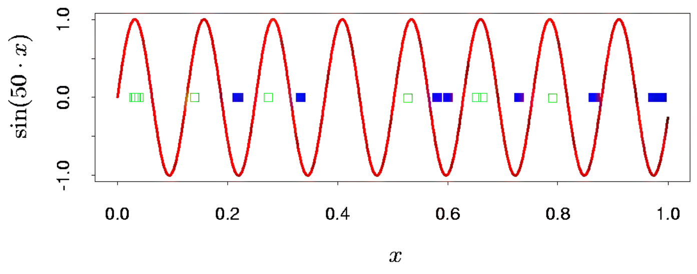

FIGURE 7.5. *The solid curve is the function* $\sin(50x)$ *for* $x \in [0, 1]$. *The blue (solid) and green (hollow) points illustrate how the associated indicator function* $I(\sin(\alpha x) > 0)$ *can shatter (separate) an arbitrarily large number of points by choosing an appropriately high frequency* α.

The preceding view of MDL for model selection says that we should choose the model with highest posterior probability. However many Bayesians would instead do inference by sampling from the posterior distribution.

7.9 Vapnik–Chernovenkis Dimension

A difficulty in using estimates of in-sample error is the need to specify the number of parameters (or the complexity) d used in the fit. Although the effective number of parameters introduced in Section 7.6 is useful for some nonlinear models, it is not fully general. The Vapnik–Chernovenkis (VC) theory provides such a general measure of complexity, and gives associated bounds on the optimism. Here we give a brief review of this theory.

Suppose we have a class of functions $\{f(x, \alpha)\}$ indexed by a parameter vector α, with $x \in \mathbb{R}^p$. Assume for now that f is an indicator function, that is, takes the values 0 or 1. If $\alpha = (\alpha_0, \alpha_1)$ and f is the linear indicator function $I(\alpha_0 + \alpha_1 x > 0)$, then it seems reasonable to say that the complexity of the class f is the number of parameters $p + 1$. But what about $f(x, \alpha) = I(\sin \alpha \cdot x)$ where α is any real number? The function $\sin(50 \cdot x)$ is shown in Figure 7.5. This is a very wiggly function that gets even rougher as the frequency α increases, but it has only one parameter: despite this, it doesn't seem reasonable to conclude that it has less complexity than the linear indicator function $I(\alpha_0 + \alpha_1 x)$ in $p = 1$ dimension.

The Vapnik–Chernovenkis dimension is a way of measuring the complexity of a class of functions by assessing how wiggly its members can be.

> *The* VC dimension *of the class* $\{f(x, \alpha)\}$ *is defined to be the largest number of points (in some configuration) that can be* shattered *by members of* $\{f(x, \alpha)\}$.

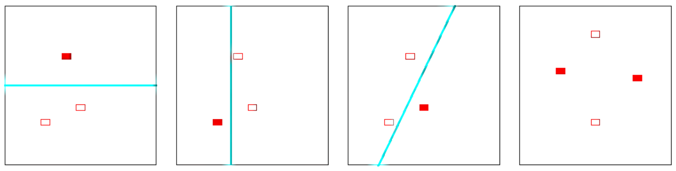

FIGURE 7.6. *The first three panels show that the class of lines in the plane can shatter three points. The last panel shows that this class cannot shatter four points, as no line will put the hollow points on one side and the solid points on the other. Hence the VC dimension of the class of straight lines in the plane is three. Note that a class of nonlinear curves could shatter four points, and hence has VC dimension greater than three.*

A set of points is said to be shattered by a class of functions if, no matter how we we assign a binary label to each point, a member of the class can perfectly separate them.

Figure 7.6 shows that the VC dimension of linear indicator functions in the plane is 3 but not 4, since no four points can be shattered by a set of lines. In general, a linear indicator function in p dimensions has VC dimension $p+1$, which is also the number of free parameters. On the other hand, it can be shown that the family $\sin(\alpha x)$ has infinite VC dimension, as Figure 7.5 suggests. By appropriate choice of α, any set of points can be shattered by this class (Exercise 7.7).

So far we have discussed the VC dimension only of indicator functions, but this can be extended to real-valued functions. The VC dimension of a class of real-valued functions $\{g(x, \alpha)\}$ is defined to be the VC dimension of the indicator class $\{I(g(x, \alpha) - \beta > 0)\}$, where β takes values over the range of g.

One can use the VC dimension in constructing an estimate of in-sample prediction error; different types of results are available. Using the concept of VC dimension, one can prove results about the optimism of the training error when using a class of functions. An example of such a result is the following. If we fit N training points using a class of functions $\{f(x, \alpha)\}$ having VC dimension h, then with probability at least $1 - \eta$ over training sets:

$$\begin{aligned}
\text{Err} &\le \overline{\text{err}} + \frac{\epsilon}{2}\left(1 + \sqrt{1 + \frac{4 \cdot \overline{\text{err}}}{\epsilon}}\right) \quad \text{(binary classification)} \\
\text{Err} &\le \frac{\overline{\text{err}}}{(1 - c\sqrt{\epsilon})_+} \quad \text{(regression)} \qquad (7.41) \\
&\text{where} \quad \epsilon = a_1 \frac{h[\log(a_2 N/h) + 1] - \log(\eta/4)}{N}.
\end{aligned}$$

These bounds hold simultaneously for all members $f(x, \alpha)$, and are taken from Cherkassky and Mulier (1998), pages 108–110. They recommend the value $c = 1$. For regression they suggest $a_1 = a_2 = 1$, and for classification they make no recommendation, with $a_1 = 4$ and $a_2 = 2$ corresponding to worst-case scenarios. The bounds suggest that the optimism increases with h and decreases with N in qualitative agreement with the AIC correction d/N given is (7.20). However, the results in (7.41) are stronger: rather than giving the expected optimism for each fixed function $f(x, \alpha)$, they give probabilistic upper bounds for all functions $f(x, \alpha)$, and hence allow for searching over the class.

Vapnik's *structural risk minimization* approach fits a nested sequence of models of increasing VC dimensions $h_1 < h_2 < \cdots$, and then chooses the model with the smallest value of the upper bound.

We note that upper bounds like the ones in (7.41) are often very loose, but that doesn't rule them out as good criteria for model selection, where the relative (not absolute) size of the test error is important. The main drawback of this approach is the difficulty in calculating the VC dimension of a class of functions. Often only a crude upper bound for VC dimension is obtainable, and this may not be adequate. An example in which the structural risk minimization program can be successfully carried out is the support vector classifier, discussed in Section 12.2.

7.9.1 Example (Continued)

Figure 7.7 shows the results when AIC, BIC and SRM are used to select the model size for the examples of Figure 7.3. For the examples labeled `KNN`, the model index α refers to neighborhood size, while for those labeled `REG` α refers to subset size. Using each selection method (e.g., AIC) we estimated the best model $\hat{\alpha}$ and found its true prediction error $\text{Err}(\hat{\alpha})$ on a test set. For the same training set we computed the prediction error of the best and worst possible model choices: $\min_\alpha \text{Err}(\alpha)$ and $\max_\alpha \text{Err}(\alpha)$. The boxplots show the distribution of the quantity

$$100 \times \frac{\text{Err}(\hat{\alpha}) - \min_\alpha \text{Err}(\alpha)}{\max_\alpha \text{Err}(\alpha) - \min_\alpha \text{Err}(\alpha)},$$

which represents the error in using the chosen model relative to the best model. For linear regression the model complexity was measured by the number of features; this is also the VC dimension of the linear classifier. For k-nearest neighbors, we used the quantity N/k. This is a rough estimate of complexity; we do not know if it corresponds to the VC dimension. We used $a_1 = a_2 = 1$ for the constants in (7.41); the results for SRM changed with different constants, and this choice gave the most favorable results. For misclassification error we used $\hat{\sigma}_\varepsilon^2 = [N/(N - d)] \cdot \overline{\text{err}}(\alpha)$ for the least restrictive model ($k = 5$ for KNN, since $k = 1$ results in zero training error). The AIC criterion seems to work well in all four scenarios, despite the lack of theoretical support with 0–1 loss. BIC is less successful in the regression/KNN case. SRM performs poorly overall.

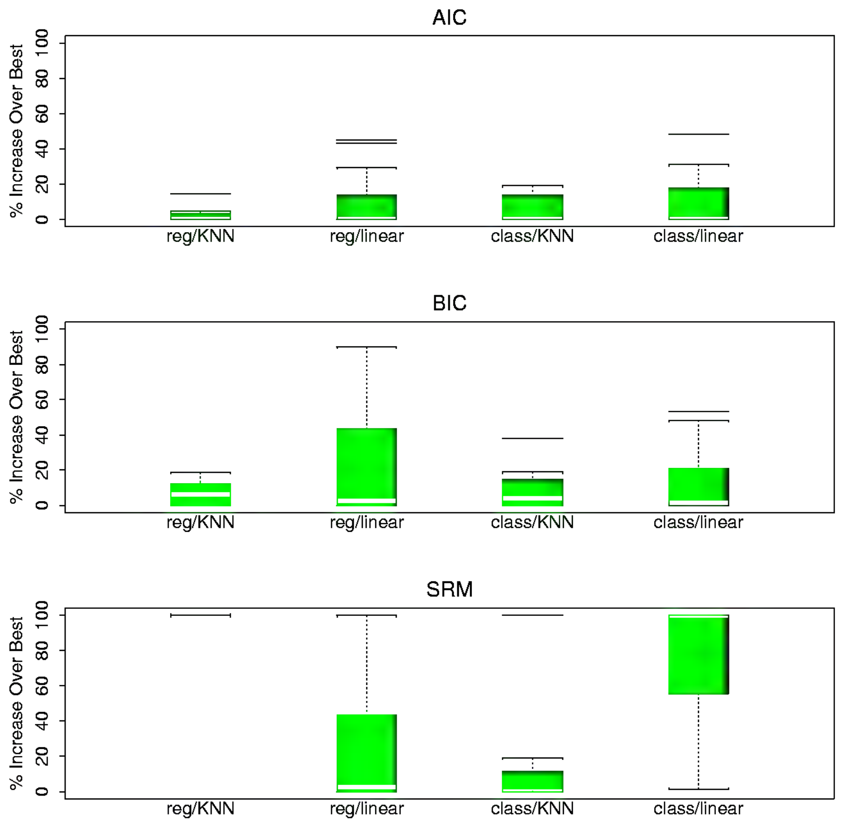

FIGURE 7.7. *Boxplots show the distribution of the relative error* $100 \times [\text{Err}(\hat{\alpha}) - \min_\alpha \text{Err}(\alpha)]/[\max_\alpha \text{Err}(\alpha) - \min_\alpha \text{Err}(\alpha)]$ *over the four scenarios of Figure 7.3. This is the error in using the chosen model relative to the best model. There are* 20 *training sets represented in each boxplot.*

7.10 Cross-Validation

Probably the simplest and most widely used method for estimating prediction error is cross-validation. This method directly estimates the extra-sample error $\text{Err} = \text{E}[L(Y, \hat{f}(X))]$, which is the generalization error when the method $\hat{f}(X)$ is applied to an independent test sample from the joint distribution of X and Y.

Ideally if we had enough data, we would set aside a validation set and use it to assess the performance of our prediction model. Since data are often scarce, this is usually not possible. To finesse the problem, K-fold cross-validation uses part of the available data to fit the model, and a different part to test it. We split the data into K roughly equal-sized parts; for example, when $K = 5$, the scenario looks like this:

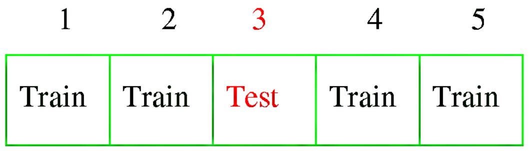

For the kth part (third above), we fit the model to the other $K-1$ parts of the data, and calculate the prediction error of the fitted model when predicting the kth part of the data. We do this for $k = 1, 2, \ldots, K$ and combine the K estimates of prediction error.

Here are more details. Let $\kappa : \{1, \ldots, N\} \mapsto \{1, \ldots, K\}$ be an indexing function that indicates the partition to which observation i is allocated by the randomization. Denote by $\hat{f}^{-k}(x)$ the fitted function, computed with the kth part of the data removed. Then the cross-validation estimate of prediction error is

$$\text{CV} = \frac{1}{N}\sum_{i=1}^{N} L(y_i, \hat{f}^{-\kappa(i)}(x_i)). \tag{7.42}$$

Typical choices of K are 5 or 10 (see below). The case $K = N$ is known as *leave-one-out* cross-validation. In this case $\kappa(i) = i$, and for the ith observation the fit is computed using all the data except the ith.

Given a set of models $f(x, \alpha)$ indexed by a tuning parameter α, denote by $\hat{f}^{-k}(x, \alpha)$ the αth model fit with the kth part of the data removed. Then for this set of models we define

$$\text{CV}(\alpha) = \frac{1}{N}\sum_{i=1}^{N} L(y_i, \hat{f}^{-\kappa(i)}(x_i, \alpha)). \tag{7.43}$$

The function $\text{CV}(\alpha)$ provides an estimate of the test error curve, and we find the tuning parameter $\hat{\alpha}$ that minimizes it. Our final chosen model is $f(x, \hat{\alpha})$, which we then fit to all the data.

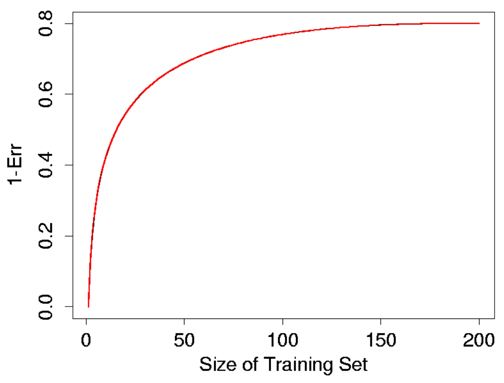

FIGURE 7.8. *Hypothetical learning curve for a classifier on a given task; a plot of* $1 - \text{Err}$ *versus the size of the training set* N*. With a dataset of* 200 *observations, fivefold cross-validation would use training sets of size* 160*, which would behave much like the full set. However, with a dataset of* 50 *observations fivefold cross-validation would use training sets of size* 40*, and this would result in a considerable overestimate of prediction error.*

What value should we choose for K? With $K = N$, CV is approximately unbiased for the true prediction error, but can have high variance because the N "training sets" are so similar to one another. The computational burden is also considerable, requiring N applications of the learning method. In certain special problems, this computation can be done quickly—see Exercise 7.3 and 5.13.

On the other hand, with $K = 5$ say, CV has lower variance. But bias could be a problem, depending on how the performance of the learning method varies with the size of the training set. Figure 7.8 shows a hypothetical "learning curve" for a classifier on a given task, a plot of $1 - \text{Err}$ versus the size of the training set N. The performance of the classifier improves as the training set size increases to 100 observations; increasing the number further to 200 brings only a small benefit. If our training set had 200 observations, fivefold cross-validation would estimate the performance of our classifier over training sets of size 160, which from Figure 7.8 is virtually the same as the performance for training set size 200. Thus cross-validation would not suffer from much bias. However if the training set had 50 observations, fivefold cross-validation would estimate the performance of our classifier over training sets of size 40, and from the figure that would be an underestimate of $1 - \text{Err}$. Hence as an estimate of Err, cross-validation would be biased upward.

To summarize, if the learning curve has a considerable slope at the given training set size, five- or tenfold cross-validation will overestimate the true prediction error. Whether this bias is a drawback in practice depends on the objective. On the other hand, leave-one-out cross-validation has low

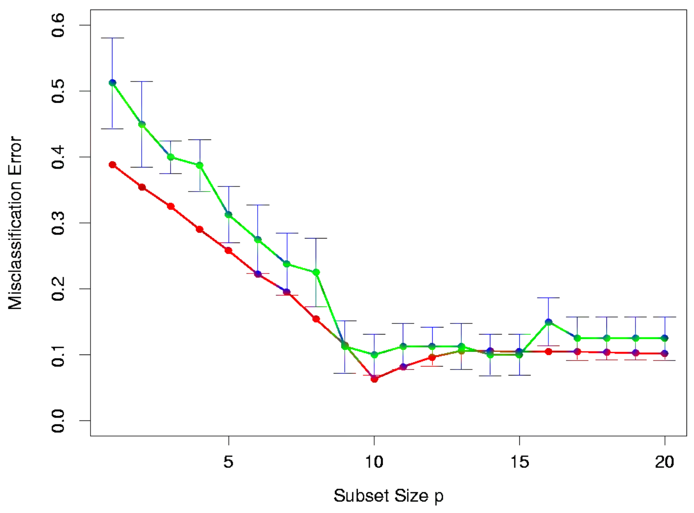

FIGURE 7.9. *Prediction error (red) and tenfold cross-validation curve (green) estimated from a single training set, from the scenario in the bottom right panel of Figure 7.3.*

bias but can have high variance. Overall, five- or tenfold cross-validation are recommended as a good compromise.

Figure 7.9 shows the prediction error and tenfold cross-validation curve estimated from a single training set, from the scenario in the bottom right panel of Figure 7.3. This is a two-class classification problem, using a linear model with best subsets regression of subset size p. Standard error bars are shown, which are the standard errors of the individual misclassification error rates for each of the ten parts. Both curves have minima at $p = 10$, although the CV curve is rather flat beyond 10. Often a "one-standard error" rule is used with cross-validation, in which we choose the most parsimonious model whose error is no more than one standard error above the error of the best model. Here it looks like a model with about $p = 9$ predictors would be chosen, while the true model uses $p = 10$.

Generalized cross-validation provides a convenient approximation to leave-one out cross-validation, for linear fitting under squared-error loss. As defined in Section 7.6, a linear fitting method is one for which we can write

$$\hat{\mathbf{y}} = \mathbf{S}\mathbf{y}. \tag{7.44}$$

Now for many linear fitting methods,

$$\frac{1}{N}\sum_{i=1}^{N}[y_i - \hat{f}^{-i}(x_i)]^2 = \frac{1}{N}\sum_{i=1}^{N}\left[\frac{y_i - \hat{f}(x_i)}{1 - S_{ii}}\right]^2, \tag{7.45}$$

where S_{ii} is the *ith* diagonal element of $\mathbf{S}$ (see Exercise 7.3). The GCV approximation is

$$\text{GCV} = \frac{1}{N}\sum_{i=1}^{N}\Big[\frac{y_i - \hat{f}(x_i)}{1 - \text{trace}(\mathbf{S})/N}\Big]^2. \tag{7.46}$$

The quantity trace($\mathbf{S}$) is the effective number of parameters, as defined in Section 7.6.

GCV can have a computational advantage in some settings, where the trace of $\mathbf{S}$ can be computed more easily than th individual elements S_{ii}. In smoothing problems, GCV can also alleviate the tendency of cross-validation to undersmooth. The similarity between GCV and AIC can be seen from the approximation $1/(1-x)^2 \approx 1 + 2x$ (Exercise 7.6).

7.11 Bootstrap Methods

The bootstrap is a general tool for assessing statistical accuracy. First we describe the bootstrap in general, and then show how it can be used to estimate extra-sample prediction error.

Suppose we have a model fit to a set of training data. We denote the training set by $\mathbf{Z} = (z_1, z_2, \ldots, z_N)$ where $z_i = (x_i, y_i)$. The basic idea is to randomly draw datasets with replacement from the training data, each sample the same size as the original training set. This is done B times ($B = 100$ say), producing B bootstrap datasets, as shown in Figure 7.10. Then we refit the model to each of the bootstrap datasets, and examine the behavior of the fits over the B replications.

In the figure, $S(\mathbf{Z})$ is any quantity computed from the data $\mathbf{Z}$, for example, the prediction at some input point. From the bootstrap sampling we can estimate any aspect of the distribution of $S(\mathbf{Z})$, for example, its variance,

$$\widehat{\text{Var}}[S(\mathbf{Z})] = \frac{1}{B-1}\sum_{b=1}^{B}(S(\mathbf{Z}^{*b}) - \bar{S}^*)^2, \tag{7.47}$$

where $\bar{S}^* = \sum_b S(\mathbf{Z}^{*b})/B$. Note that $\widehat{\text{Var}}[S(\mathbf{Z})]$ can be thought of as a Monte-Carlo estimate of the variance of $S(\mathbf{Z})$ under sampling from the empirical distribution function $\hat{F}$ for the data $(z_1, z_2, \ldots, z_N)$.

How can we apply the bootstrap to estimate prediction error? One approach would be to fit the model in question on a set of bootstrap samples, and then keep track of how well it predicts the original training set. If $\hat{f}^{*b}(x_i)$ is the predicted value at x_i, from the model fitted to the bth bootstrap dataset, our estimate is

$$\widehat{\text{Err}}_{\text{boot}} = \frac{1}{B}\frac{1}{N}\sum_{b=1}^{B}\sum_{i=1}^{N}L(y_i, \hat{f}^{*b}(x_i)). \tag{7.48}$$

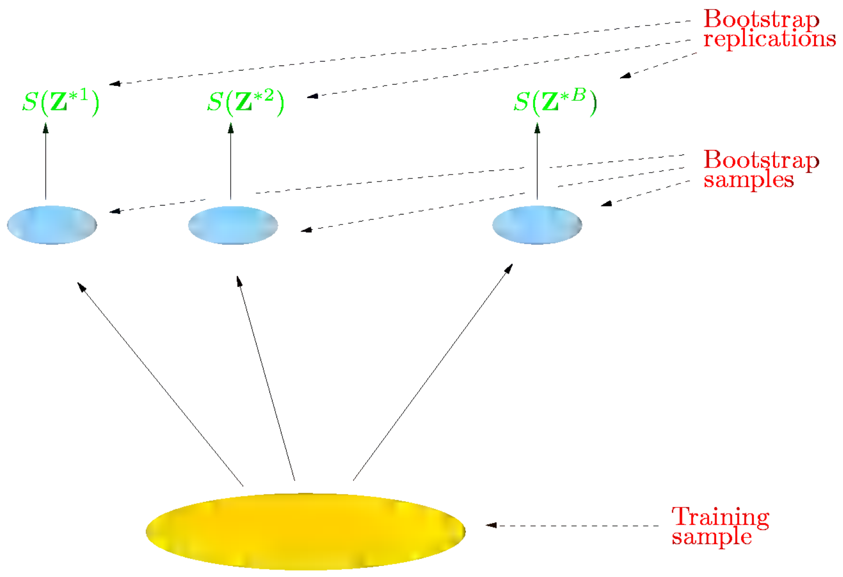

FIGURE 7.10. *Schematic of the bootstrap process. We wish to assess the statistical accuracy of a quantity $S(\mathbf{Z})$ computed from our dataset. B training sets $\mathbf{Z}^{*b}$, $b = 1, \ldots, B$ each of size N are drawn with replacement from the original dataset. The quantity of interest $S(\mathbf{Z})$ is computed from each bootstrap training set, and the values $S(\mathbf{Z}^{*1}), \ldots, S(\mathbf{Z}^{*B})$ are used to assess the statistical accuracy of $S(\mathbf{Z})$.*

However it is easy to see that $\widehat{\text{Err}}_{\text{boot}}$ does not provide a good estimate in general. The reason is that the bootstrap datasets are acting as the training samples, while the original training set is acting as the test sample, and these two samples have observations in common. This overlap can make overfit predictions look unrealistically good, and is the reason that cross-validation explicitly uses non-overlapping data for the training and test samples. Consider for example a 1-nearest neighbor classifier applied to a two-class classification problem with the same number of observations in each class, in which the features and class labels are in fact independent. Then the true error rate is 0.5. But the contributions to the bootstrap estimate $\widehat{\text{Err}}_{\text{boot}}$ will be zero unless the observation i does not appear in the bootstrap sample b. In this latter case it will have the correct expectation 0.5. Now

$$\begin{aligned}\Pr\{\text{observation } i \in \text{bootstrap sample } b\} &= 1 - \left(1 - \frac{1}{N}\right)^N \\ &\approx 1 - e^{-1} \\ &= 0.632. \qquad (7.49)\end{aligned}$$

Hence the expectation of $\widehat{\text{Err}}_{\text{boot}}$ is about $0.5 \times 0.368 = 0.184$, far below the correct error rate 0.5.

By mimicking cross-validation, a better bootstrap estimate can be obtained. For each observation, we only keep track of predictions from bootstrap samples not containing that observation. The leave-one-out bootstrap estimate of prediction error is defined by

$$\widehat{\text{Err}}^{(1)} = \frac{1}{N}\sum_{i=1}^{N}\frac{1}{|C^{-i}|}\sum_{b\in C^{-i}} L(y_i, \hat{f}^{*b}(x_i)). \tag{7.50}$$

Here C^{-i} is the set of indices of the bootstrap samples b that do *not* contain observation i, and $|C^{-i}|$ is the number of such samples. In computing $\widehat{\text{Err}}^{(1)}$, we either have to choose B large enough to ensure that all of the $|C^{-i}|$ are greater than zero, or we can just leave out the terms in (7.50) corresponding to $|C^{-i}|$'s that are zero.

The leave-one out bootstrap solves the overfitting problem suffered by $\widehat{\text{Err}}_{\text{boot}}$, but has the training-set-size bias mentioned in the discussion of cross-validation. The average number of distinct observations in each bootstrap sample is about $0.632 \cdot N$, so its bias will roughly behave like that of twofold cross-validation. Thus if the learning curve has considerable slope at sample size $N/2$, the leave-one out bootstrap will be biased upward as an estimate of the true error.

The ".632 estimator" is designed to alleviate this bias. It is defined by

$$\widehat{\text{Err}}^{(.632)} = .368 \cdot \overline{\text{err}} + .632 \cdot \widehat{\text{Err}}^{(1)}. \tag{7.51}$$

The derivation of the .632 estimator is complex; intuitively it pulls the leave-one out bootstrap estimate down toward the training error rate, and hence reduces its upward bias. The use of the constant .632 relates to (7.49).

The .632 estimator works well in "light fitting" situations, but can break down in overfit ones. Here is an example due to Breiman et al. (1984). Suppose we have two equal-size classes, with the targets independent of the class labels, and we apply a one-nearest neighbor rule. Then $\overline{\text{err}} = 0$, $\widehat{\text{Err}}^{(1)} = 0.5$ and so $\widehat{\text{Err}}^{(.632)} = .632 \times 0.5 = .316$. However the true error rate is 0.5.

One can improve the .632 estimator by taking into account the amount of overfitting. First we define γ to be the *no-information error rate* : this is the error rate of our prediction rule if the inputs and class labels were independent. An estimate of γ is obtained by evaluating the prediction rule on all possible combinations of targets y_i and predictors $x_{i'}$

$$\hat{\gamma} = \frac{1}{N^2}\sum_{i=1}^{N}\sum_{i'=1}^{N} L(y_i, \hat{f}(x_{i'})). \tag{7.52}$$

For example, consider the dichotomous classification problem: let $\hat{p}_1$ be the observed proportion of responses y_i equaling 1, and let $\hat{q}_1$ be the observed proportion of predictions $\hat{f}(x_{i'})$ equaling 1. Then

$$\hat{\gamma} = \hat{p}_1(1 - \hat{q}_1) + (1 - \hat{p}_1)\hat{q}_1. \tag{7.53}$$

With a rule like 1-nearest neighbors for which $\hat{q}_1 = \hat{p}_1$ the value of $\hat{\gamma}$ is $2\hat{p}_1(1-\hat{p}_1)$. The multi-category generalization of (7.53) is $\hat{\gamma} = \sum_\ell \hat{p}_\ell(1-\hat{q}_\ell)$.

Using this, the *relative overfitting rate* is defined to be

$$\hat{R} = \frac{\widehat{\mathrm{Err}}^{(1)} - \overline{\mathrm{err}}}{\hat{\gamma} - \overline{\mathrm{err}}}, \tag{7.54}$$

a quantity that ranges from 0 if there is no overfitting ($\widehat{\mathrm{Err}}^{(1)} = \overline{\mathrm{err}}$) to 1 if the overfitting equals the no-information value $\hat{\gamma} - \overline{\mathrm{err}}$. Finally, we define the ".632+" estimator by

$$\begin{aligned} \widehat{\mathrm{Err}}^{(.632+)} &= (1 - \hat{w}) \cdot \overline{\mathrm{err}} + \hat{w} \cdot \widehat{\mathrm{Err}}^{(1)} \\ \text{with } \hat{w} &= \frac{.632}{1 - .368\hat{R}}. \end{aligned} \tag{7.55}$$

The weight w ranges from .632 if $\hat{R} = 0$ to 1 if $\hat{R} = 1$, so $\widehat{\mathrm{Err}}^{(.632+)}$ ranges from $\widehat{\mathrm{Err}}^{(.632)}$ to $\widehat{\mathrm{Err}}^{(1)}$. Again, the derivation of (7.55) is complicated: roughly speaking, it produces a compromise between the leave-one-out bootstrap and the training error rate that depends on the amount of overfitting. For the 1-nearest-neighbor problem with class labels independent of the inputs, $\hat{w} = \hat{R} = 1$, so $\widehat{\mathrm{Err}}^{(.632+)} = \widehat{\mathrm{Err}}^{(1)}$, which has the correct expectation of 0.5. In other problems with less overfitting, $\widehat{\mathrm{Err}}^{(.632+)}$ will lie somewhere between $\overline{\mathrm{err}}$ and $\widehat{\mathrm{Err}}^{(1)}$.

7.11.1 Example (Continued)

Figure 7.11 shows the results of fivefold cross-validation and the .632+ bootstrap estimate in the same four problems of Figures 7.7. As in that figure, Figure 7.11 shows boxplots of $100 \cdot [\mathrm{Err}_{\hat{\alpha}} - \min_\alpha \mathrm{Err}(\alpha)]/[\max_\alpha \mathrm{Err}(\alpha) - \min_\alpha \mathrm{Err}(\alpha)]$, the error in using the chosen model relative to the best model. There are 20 different training sets represented in each boxplot. Both measures perform well overall, perhaps the same or slightly worse that the AIC in Figure 7.7.

Our conclusion is that for these particular problems and fitting methods, minimization of either AIC, cross-validation or bootstrap yields a model fairly close to the best available. Note that for the purpose of model selection, any of the measures could be biased and it wouldn't affect things, as long as the bias did not change the relative performance of the methods. For example, the addition of a constant to any of the measures would not

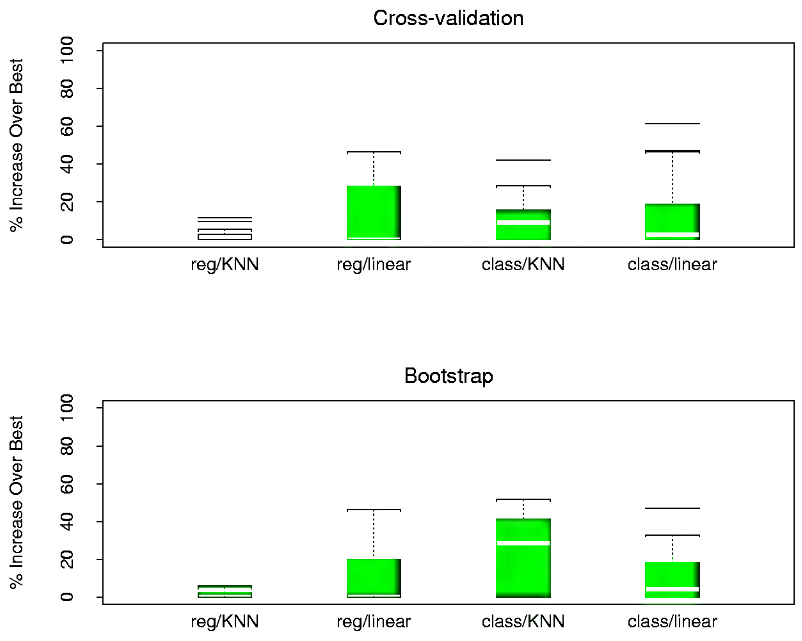

FIGURE 7.11. *Boxplots show the distribution of the relative error* $100 \cdot [\mathrm{Err}_{\hat{\alpha}} - \min_\alpha \mathrm{Err}(\alpha)]/[\max_\alpha \mathrm{Err}(\alpha) - \min_\alpha \mathrm{Err}(\alpha)]$ *over the four scenarios of Figure 7.3. This is the error in using the chosen model relative to the best model. There are* 20 *training sets represented in each boxplot.*

change the resulting chosen model. However, for many adaptive, nonlinear techniques (like trees), estimation of the effective number of parameters is very difficult. This makes methods like AIC impractical and leaves us with cross-validation or bootstrap as the methods of choice.

A different question is: how well does each method estimate test error? On the average the AIC criterion overestimated prediction error of its chosen model by 38%, 37%, 51%, and 30%, respectively, over the four scenarios, with BIC performing similarly. In contrast, cross-validation overestimated the error by 1%, 4%, 0%, and 4%, with the bootstrap doing about the same. Hence the extra work involved in computing a cross-validation or bootstrap measure is worthwhile, if an accurate estimate of test error is required. With other fitting methods like trees, cross-validation and bootstrap can underestimate the true error by 10%, because the search for best tree is strongly affected by the validation set. In these situations only a separate test set will provide an unbiased estimate of test error.

Bibliographic Notes

Key references for cross-validation are Stone (1974), Stone (1977) and Allen (1977). The AIC was proposed by Akaike (1973), while the BIC was introduced by Schwartz (1979). Madigan and Raftery (1994) give an overview of Bayesian model selection. The MDL criterion is due to Rissanen (1983). Cover and Thomas (1991) contains a good description of coding theory and complexity. VC dimension is described in Vapnik (1996). Stone (1977) showed that the AIC and leave-one out cross-validation are asymptotically equivalent. Generalized cross-validation is described by Golub et al. (1979) and Wahba (1980); a further discussion of the topic may be found in the monograph by Wahba (1990). See also Hastie and Tibshirani (1990), Chapter 3. The bootstrap is due to Efron (1979); see Efron and Tibshirani (1993) for an overview. Efron (1983) proposes a number of bootstrap estimates of prediction error, including the optimism and .632 estimates. Efron (1986) compares CV, GCV and bootstrap estimates of error rates. The use of cross-validation and the bootstrap for model selection is studied by Breiman and Spector (1992), Breiman (1992), Shao (1996) and Zhang (1993). The .632+ estimator was proposed by Efron and Tibshirani (1997).

Exercises

Ex. 7.1 Derive the estimate of in-sample error (7.20).

Ex. 7.2 For 0–1 loss with $\Pr(Y=1|x_0)=f(x_0)$, show that

$$\begin{aligned}\mathrm{Err}(x_0) &= \Pr(Y \neq \hat{f}(x_0))|X=x_0] \\ &\approx \sigma_\varepsilon^2 + \Phi\Big(\frac{\mathrm{sign}[(\hat{f}(x_0)-1/2)(1/2-f(x_0))]}{\sqrt{\mathrm{Var}(\hat{f}(x_0))}}\Big), \end{aligned} \qquad (7.56)$$

where $\hat{f}(x_0)$ is an estimate of $f(x_0)$. In the above,

$$\Phi(t) = \frac{1}{\sqrt{2\pi}}\int_{-\infty}^{t}\exp(-t^2/2)dt,$$

the cumulative distribution function of the Gaussian distribution. This is an increasing function, with value zero at $t=-\infty$ and value 1 at $t=+\infty$.

We can think of $\mathrm{sign}[(\hat{f}(x_0)-1/2)(1/2-f(x_0))]$ as a kind of bias term, and it depends only on which side of boundary (1/2) that $\hat{f}(x_0)$ lies. Notice also that the bias and variance combine in a multiplicative rather than additive fashion. If the $\hat{f}(x_0)$ is on the same side of 1/2 as $f(x_0)$, then the bias is negative and decreasing the variance will decrease the misclassification error. On the other hand, if $\hat{f}(x_0)$ is on the opposite side of 1/2 to

$f(x_0)$, then the bias is positive and it pays to increase the variance! Such an increase will improve the chance that $\hat{f}(x_0)$ falls on the correct side of 1/2 (Friedman, 1997).

Ex. 7.3 Let $\hat{\mathbf{f}} = \mathbf{S}\mathbf{y}$ be a linear smoothing of $\mathbf{y}$.

(a) If S_{ii} is the ith diagonal element of $\mathbf{S}$, show that for $\mathbf{S}$ arising from least squares projections and cubic smoothing splines, the cross-validated residual can be written as

$$y_i - \hat{f}^{-i}(x_i) = \frac{y_i - \hat{f}(x_i)}{1 - S_{ii}}. \tag{7.57}$$

(b) Use this result to show that $|y_i - \hat{f}^{-i}(x_i)| \geq |y_i - \hat{f}(x_i)|$.

(c) Find general conditions on any smoother $\mathbf{S}$ to make result (7.57) hold.

Ex. 7.4 Consider the in-sample prediction error (7.15) and the training error $\overline{\text{err}}$ in the case of squared-error loss:

$$\begin{aligned}\text{Err}_{\text{in}} &= \frac{1}{N}\sum_{i=1}^{N} \text{E}_{Y^{\text{new}}}(Y_i^{\text{new}} - \hat{f}(x_i))^2 \\ \overline{\text{err}} &= \frac{1}{N}\sum_{i=1}^{N}(y_i - \hat{f}(x_i))^2.\end{aligned}$$

Add and subtract $f(x_i)$ and $\text{E}\hat{f}(x_i)$ in each expression and expand. Hence establish that the optimism in the training error is

$$\frac{2}{N}\sum_{i=1}^{N}\text{Cov}(\hat{y}_i, y_i),$$

as given in (7.17).

Ex. 7.5 For a linear smoother $\hat{\mathbf{y}} = \mathbf{S}\mathbf{y}$, show that

$$\sum_{i=1}^{N}\text{Cov}(\hat{y}_i, y_i) = \text{trace}(\mathbf{S})\sigma_\varepsilon^2, \tag{7.58}$$

which justifies its use as the effective number of parameters.

Ex. 7.6 Use the approximation $1/(1-x)^2 \approx 1+2x$ to expose the relationship between C_p/AIC (7.22) and GCV (7.46), the main difference being the model used to estimate the noise variance σ_ε^2.

Ex. 7.7 Show that the set of functions $\{I(\sin(\alpha x) > 0)\}$ can shatter the following points on the line:

$$z^1 = 10^{-1}, \dots , z^\ell = 10^{-\ell}, \tag{7.59}$$

for any ℓ. Hence the VC dimension of the class $\{I(\sin(\alpha x) > 0)\}$ is infinite.

Ex. 7.8 For the prostrate data of Chapter 3, carry out a best-subset linear regression analysis, as in Table 3.3 (third column from left). Compute the AIC, BIC, five- and tenfold cross-validation, and bootstrap .632 estimates of prediction error. Discuss the results.

8
Model Inference and Averaging

8.1 Introduction

For most of this book, the fitting (learning) of models has been achieved by minimizing a sum of squares for regression, or by minimizing cross-entropy for classification. In fact, both of these minimizations are instances of the maximum likelihood approach to fitting.

In this chapter we provide a general exposition of the maximum likelihood approach, as well as the Bayesian method for inference. The bootstrap, introduced in Chapter 7, is discussed in this context, and its relation to maximum likelihood and Bayes is described. Finally, we present some related techniques for model averaging and improvement, including committee methods, bagging, stacking and bumping.

8.2 The Bootstrap and Maximum Likelihood Methods

8.2.1 A Smoothing Example

The bootstrap method provides a direct computational way of assessing uncertainty, by sampling from the training data. Here we illustrate the bootstrap in a simple one-dimensional smoothing problem, and show its connection to maximum likelihood.

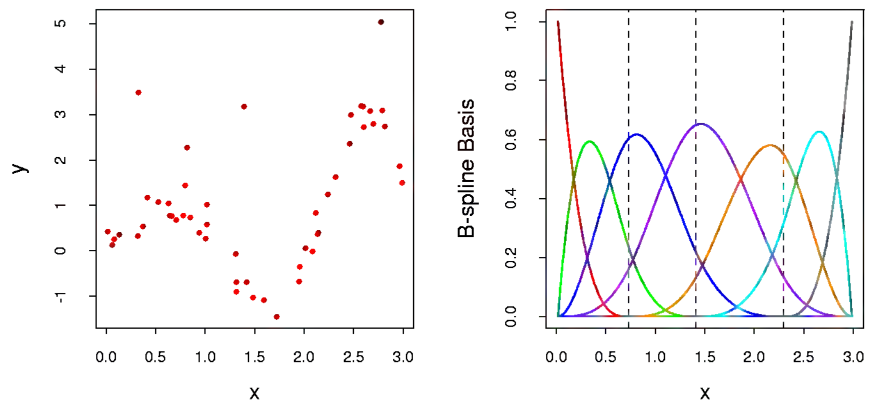

FIGURE 8.1. *Left panel: data for smoothing example. Right panel: set of seven B-spline basis functions. The broken vertical lines indicate the placement of the three knots.*

Denote the training data by $\mathbf{Z} = \{z_1, z_2, \dots, z_N\}$, with $z_i = (x_i, y_i)$, $i = 1, 2, \dots, N$. Here x_i is a one-dimensional input, and y_i the outcome, either continuous or categorical. As an example, consider the $N = 50$ data points shown in the left panel of Figure 8.1.

Suppose we decide to fit a cubic spline to the data, with three knots placed at the quartiles of the X values. This is a seven-dimensional linear space of functions, and can be represented, for example, by a linear expansion of B-spline basis functions (see Section 5.9.2):

$$\mu(x) \quad = \quad \sum_{j=1}^{7} \beta_j h_j(x). \tag{8.1}$$

Here the $h_j(x)$, $j = 1, 2, \dots, 7$ are the seven functions shown in the right panel of Figure 8.1. We can think of $\mu(x)$ as representing the conditional mean $\mathrm{E}(Y|X = x)$.

Let $\mathbf{H}$ be the $N \times 7$ matrix with ijth element $h_j(x_i)$. The usual estimate of β, obtained by minimizing the squared error over the training set, is given by

$$\hat{\beta} = (\mathbf{H}^T\mathbf{H})^{-1}\mathbf{H}^T\mathbf{y}. \tag{8.2}$$

The corresponding fit $\hat{\mu}(x) = \sum_{j=1}^{7} \hat{\beta}_j h_j(x)$ is shown in the top left panel of Figure 8.2.

The estimated covariance matrix of $\hat{\beta}$ is

$$\widehat{\mathrm{Var}}(\hat{\beta}) = (\mathbf{H}^T\mathbf{H})^{-1}\hat{\sigma}^2, \tag{8.3}$$

where we have estimated the noise variance by $\hat{\sigma}^2 = \sum_{i=1}^{N}(y_i - \hat{\mu}(x_i))^2/N$. Letting $h(x)^T = (h_1(x), h_2(x), \dots, h_7(x))$, the standard error of a predic-

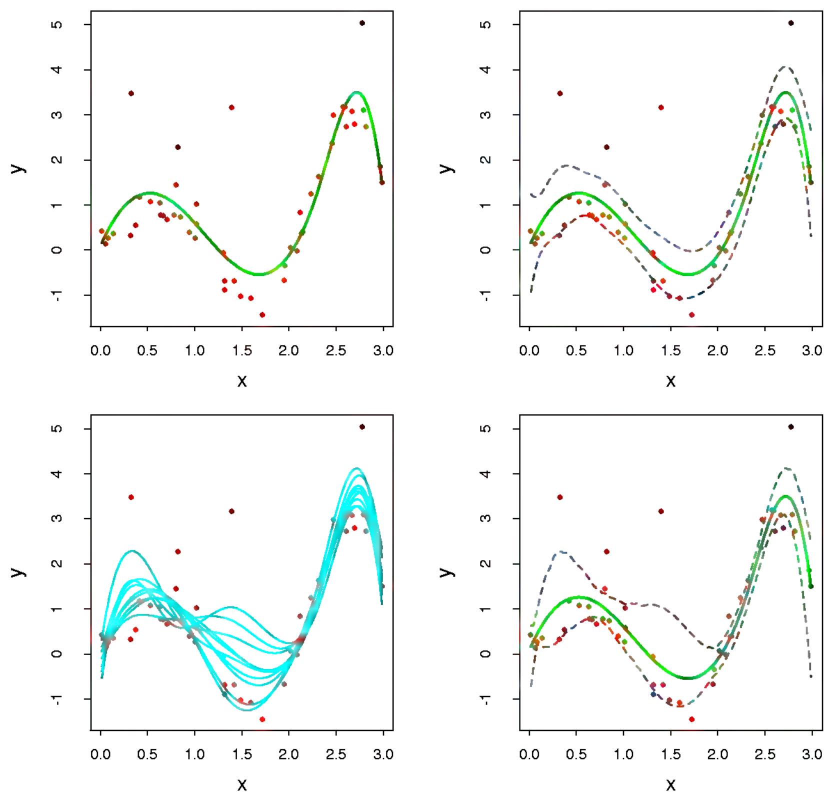

FIGURE 8.2. *Top left: B-spline smooth of data. Top right: B-spline smooth plus and minus* $1.96\times$ *standard error bands. Bottom left: ten bootstrap replicates of the B-spline smooth. Bottom right: B-spline smooth with* 95% *standard error bands computed from the bootstrap distribution.*

tion $\hat{\mu}(x) = h(x)^T\hat{\beta}$ is

$$\widehat{\text{se}}[\hat{\mu}(x)] = [h(x)^T(\mathbf{H}^T\mathbf{H})^{-1}h(x)]^{\frac{1}{2}}\hat{\sigma}. \tag{8.4}$$

In the top right panel of Figure 8.2 we have plotted $\hat{\mu}(x) \pm 1.96 \cdot \widehat{\text{se}}[\hat{\mu}(x)]$. Since 1.96 is the 97.5% point of the standard normal distribution, these represent approximate $100 - 2 \times 2.5\% = 95\%$ pointwise confidence bands for $\mu(x)$.

Here's how we could apply the bootstrap in this example. We draw B datasets each of size $N = 50$ with replacement from our training data, the sampling unit being the pair $z_i = (x_i, y_i)$. To each bootstrap dataset $\mathbf{Z}^*$ we fit a cubic spline $\hat{\mu}^*(x)$; the fits from ten such samples are shown in the bottom left panel of Figure 8.2. Using $B = 200$ bootstrap samples, we can form a 95% pointwise confidence band from the percentiles at each x: we find the $2.5\% \times 200 =$ fifth largest and smallest values at each x. These are plotted in the bottom right panel of Figure 8.2. The bands look similar to those in the top right, being a little wider at the endpoints.

There is actually a close connection between the least squares estimates (8.2) and (8.3), the bootstrap, and maximum likelihood. Suppose we further assume that the model errors are Gaussian,

$$\begin{aligned} Y &= \mu(X) + \varepsilon; \quad \varepsilon \sim N(0, \sigma^2), \\ \mu(x) &= \sum_{j=1}^{7} \beta_j h_j(x). \end{aligned} \tag{8.5}$$

The bootstrap method described above, in which we sample with replacement from the training data, is called the *nonparametric bootstrap*. This really means that the method is "model-free," since it uses the raw data, not a specific parametric model, to generate new datasets. Consider a variation of the bootstrap, called the *parametric bootstrap*, in which we simulate new responses by adding Gaussian noise to the predicted values:

$$y_i^* = \hat{\mu}(x_i) + \varepsilon_i^*; \quad \varepsilon_i^* \sim N(0, \hat{\sigma}^2); \quad i = 1, 2, \ldots, N. \tag{8.6}$$

This process is repeated B times, where $B = 200$ say. The resulting bootstrap datasets have the form $(x_1, y_1^*), \ldots, (x_N, y_N^*)$ and we recompute the B-spline smooth on each. The confidence bands from this method will exactly equal the least squares bands in the top right panel, as the number of bootstrap samples goes to infinity. A function estimated from a bootstrap sample $\mathbf{y}^*$ is given by $\hat{\mu}^*(x) = h(x)^T(\mathbf{H}^T\mathbf{H})^{-1}\mathbf{H}^T\mathbf{y}^*$, and has distribution

$$\hat{\mu}^*(x) \sim N(\hat{\mu}(x), h(x)^T(\mathbf{H}^T\mathbf{H})^{-1}h(x)\hat{\sigma}^2). \tag{8.7}$$

Notice that the mean of this distribution is the least squares estimate, and the standard deviation is the same as the approximate formula (8.4).

8.2.2 Maximum Likelihood Inference

It turns out that the parametric bootstrap agrees with least squares in the previous example because the model (8.5) has additive Gaussian errors. In general, the parametric bootstrap agrees not with least squares but with maximum likelihood, which we now review.

We begin by specifying a probability density or probability mass function for our observations

$$z_i \sim g_\theta(z). \tag{8.8}$$

In this expression θ represents one or more unknown parameters that govern the distribution of Z. This is called a *parametric model* for Z. As an example, if Z has a normal distribution with mean μ and variance σ^2, then

$$\theta = (\mu, \sigma^2), \tag{8.9}$$

and

$$g_\theta(z) = \frac{1}{\sqrt{2\pi}\sigma} e^{-\frac{1}{2}(z-\mu)^2/\sigma^2}. \tag{8.10}$$

Maximum likelihood is based on the *likelihood function*, given by

$$L(\theta; \mathbf{Z}) = \prod_{i=1}^{N} g_\theta(z_i), \tag{8.11}$$

the probability of the observed data under the model g_θ. The likelihood is defined only up to a positive multiplier, which we have taken to be one. We think of $L(\theta; \mathbf{Z})$ as a function of θ, with our data $\mathbf{Z}$ fixed.

Denote the logarithm of $L(\theta; \mathbf{Z})$ by

$$\begin{aligned} \ell(\theta; \mathbf{Z}) &= \sum_{i=1}^{N} \ell(\theta; z_i) \\ &= \sum_{i=1}^{N} \log g_\theta(z_i), \end{aligned} \tag{8.12}$$

which we will sometimes abbreviate as $\ell(\theta)$. This expression is called the log-likelihood, and each value $\ell(\theta; z_i) = \log g_\theta(z_i)$ is called a log-likelihood component. The method of maximum likelihood chooses the value $\theta = \hat{\theta}$ to maximize $\ell(\theta; \mathbf{Z})$.

The likelihood function can be used to assess the precision of $\hat{\theta}$. We need a few more definitions. The *score function* is defined by

$$\dot{\ell}(\theta; \mathbf{Z}) = \sum_{i=1}^{N} \dot{\ell}(\theta; z_i), \tag{8.13}$$

where $\dot{\ell}(\theta; z_i) = \partial\ell(\theta; z_i)/\partial\theta$. Assuming that the likelihood takes its maximum in the interior of the parameter space, $\dot{\ell}(\hat{\theta}; \mathbf{Z}) = 0$. The *information matrix* is

$$\mathbf{I}(\theta) = -\sum_{i=1}^{N} \frac{\partial^2\ell(\theta; z_i)}{\partial\theta\partial\theta^T}. \tag{8.14}$$

When $\mathbf{I}(\theta)$ is evaluated at $\theta = \hat{\theta}$, it is often called the *observed information.* The *Fisher information* (or expected information) is

$$\mathbf{i}(\theta) = \mathrm{E}_\theta[\mathbf{I}(\theta)]. \tag{8.15}$$

Finally, let θ_0 denote the true value of θ.

A standard result says that the sampling distribution of the maximum likelihood estimator has a limiting normal distribution

$$\hat{\theta} \to N(\theta_0, \mathbf{i}(\theta_0)^{-1}), \tag{8.16}$$

as $N \to \infty$. Here we are independently sampling from $g_{\theta_0}(z)$. This suggests that the sampling distribution of $\hat{\theta}$ may be approximated by

$$N(\hat{\theta}, \mathbf{i}(\hat{\theta})^{-1}) \text{ or } N(\hat{\theta}, \mathbf{I}(\hat{\theta})^{-1}), \tag{8.17}$$

where $\hat{\theta}$ represents the maximum likelihood estimate from the observed data.

The corresponding estimates for the standard errors of $\hat{\theta}_j$ are obtained from

$$\sqrt{\mathbf{i}(\hat{\theta})^{-1}_{jj}} \qquad \text{and} \qquad \sqrt{\mathbf{I}(\hat{\theta})^{-1}_{jj}}. \tag{8.18}$$

Confidence points for θ_j can be constructed from either approximation in (8.17). Such a confidence point has the form

$$\hat{\theta}_j - z^{(1-\alpha)} \cdot \sqrt{\mathbf{i}(\hat{\theta})^{-1}_{jj}} \qquad \text{or} \qquad \hat{\theta}_j - z^{(1-\alpha)} \cdot \sqrt{\mathbf{I}(\hat{\theta})^{-1}_{jj}},$$

respectively, where $z^{(1-\alpha)}$ is the $1-\alpha$ percentile of the standard normal distribution. More accurate confidence intervals can be derived from the likelihood function, by using the chi-squared approximation

$$2[\ell(\hat{\theta}) - \ell(\theta_0)] \sim \chi^2_p, \tag{8.19}$$

where p is the number of components in θ. The resulting $1-2\alpha$ confidence interval is the set of all θ such that $2[\ell(\hat{\theta})-\ell(\theta_0)] \le \chi_p^{2^{(1-2\alpha)}}$, where $\chi_p^{2^{(1-2\alpha)}}$ is the $1-2\alpha$ percentile of the chi-squared distribution with p degrees of freedom.

Let's return to our smoothing example to see what maximum likelihood yields. The parameters are $\theta = (\beta, \sigma^2)$. The log-likelihood is

$$\ell(\theta) = -\frac{N}{2} \log \sigma^2 2\pi - \frac{1}{2\sigma^2} \sum_{i=1}^{N} (y_i - h(x_i)^T \beta)^2. \tag{8.20}$$

The maximum likelihood estimate is obtained by setting $\partial\ell/\partial\beta = 0$ and $\partial\ell/\partial\sigma^2 = 0$, giving

$$\begin{aligned} \hat{\beta} &= (\mathbf{H}^T\mathbf{H})^{-1}\mathbf{H}^T\mathbf{y}, \\ \hat{\sigma}^2 &= \frac{1}{N} \sum (y_i - \hat{\mu}(x_i))^2, \end{aligned} \tag{8.21}$$

which are the same as the usual estimates given in (8.2) and below (8.3).

The information matrix for $\theta = (\beta, \sigma^2)$ is block-diagonal, and the block corresponding to β is

$$\mathbf{I}(\beta) = (\mathbf{H}^T\mathbf{H})/\sigma^2, \tag{8.22}$$

so that the estimated variance $(\mathbf{H}^T\mathbf{H})^{-1}\hat{\sigma}^2$ agrees with the least squares estimate (8.3).

8.2.3 Bootstrap versus Maximum Likelihood

In essence the bootstrap is a computer implementation of nonparametric or parametric maximum likelihood. The advantage of the bootstrap over the maximum likelihood formula is that it allows us to compute maximum likelihood estimates of standard errors and other quantities in settings where no formulas are available.

In our example, suppose that we adaptively choose by cross-validation the number and position of the knots that define the B-splines, rather than fix them in advance. Denote by λ the collection of knots and their positions. Then the standard errors and confidence bands should account for the adaptive choice of λ, but there is no way to do this analytically. With the bootstrap, we compute the B-spline smooth with an adaptive choice of knots for each bootstrap sample. The percentiles of the resulting curves capture the variability from both the noise in the targets as well as that from $\hat{\lambda}$. In this particular example the confidence bands (not shown) don't look much different than the fixed λ bands. But in other problems, where more adaptation is used, this can be an important effect to capture.

8.3 Bayesian Methods

In the Bayesian approach to inference, we specify a sampling model $\Pr(\mathbf{Z}|\theta)$ (density or probability mass function) for our data given the parameters, and a prior distribution for the parameters $\Pr(\theta)$ reflecting our knowledge about θ before we see the data. We then compute the posterior distribution

$$\Pr(\theta|\mathbf{Z}) = \frac{\Pr(\mathbf{Z}|\theta)\cdot\Pr(\theta)}{\int \Pr(\mathbf{Z}|\theta)\cdot\Pr(\theta)d\mathbf{Z}}, \tag{8.23}$$

which represents our updated knowledge about θ after we see the data. To understand this posterior distribution, one might draw samples from it or summarize by computing its mean or mode. The Bayesian approach differs from the standard ("frequentist") method for inference in its use of a prior distribution to express the uncertainty present before seeing the data, and to allow the uncertainly remaining after seeing the data to be expressed in the form of a posterior distribution.

The posterior distribution also provides the basis for predicting the values of a future observation z^{new}, via the *predictive distribution*:

$$\Pr(z^{\text{new}}|\mathbf{Z}) = \int \Pr(z^{\text{new}}|\theta)\cdot\Pr(\theta|\mathbf{Z})d\theta. \tag{8.24}$$

In contrast, the maximum likelihood approach would use $\Pr(z^{\text{new}}|\hat{\theta})$, the data density evaluated at the maximum likelihood estimate, to predict future data. Unlike the predictive distribution (8.24), this does not account for the uncertainty in estimating θ.

Let's walk through the Bayesian approach in our smoothing example. We start with the parametric model given by equation (8.5), and assume for the moment that σ^2 is known. We assume that the observed feature values $x_1, x_2, \dots, x_N$ are fixed, so that the randomness in the data comes solely from y varying around its mean $\mu(x)$.

The second ingredient we need is a prior distribution. Distributions on functions are fairly complex entities: one approach is to use a Gaussian process prior in which we specify the prior covariance between any two function values $\mu(x)$ and $\mu(x')$ (Wahba, 1990; Neal, 1996).

Here we take a simpler route: by considering a finite B-spline basis for $\mu(x)$, we can instead provide a prior for the coefficients β, and this implicitly defines a prior for $\mu(x)$. We choose a Gaussian prior centered at zero

$$\beta \sim N(0, \tau\mathbf{\Sigma}) \tag{8.25}$$

with the choices of the prior correlation matrix $\mathbf{\Sigma}$ and variance τ to be discussed below. The implicit process prior for $\mu(x)$ is hence Gaussian, with covariance kernel

$$\begin{aligned} K(x,x') &= \text{cov}[\mu(x),\mu(x')] \\ &= \tau\cdot h(x)^T\mathbf{\Sigma}h(x'). \end{aligned} \tag{8.26}$$

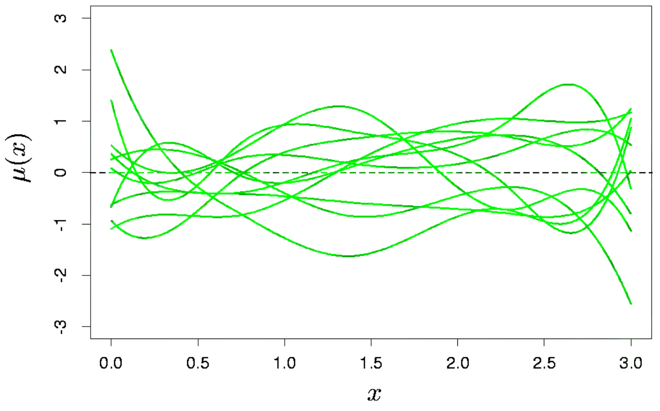

FIGURE 8.3. *Smoothing example: Ten draws from the Gaussian prior distribution for the function $\mu(x)$.*

The posterior distribution for β is also Gaussian, with mean and covariance

$$\begin{aligned} \mathrm{E}(\beta|\mathbf{Z}) &= \left(\mathbf{H}^T\mathbf{H} + \frac{1}{\tau}\mathbf{\Sigma}^{-1}\right)^{-1}\mathbf{H}^T\mathbf{y}, \\ \mathrm{cov}(\beta|\mathbf{Z}) &= \left(\mathbf{H}^T\mathbf{H} + \frac{1}{\tau}\mathbf{\Sigma}^{-1}\right)^{-1}\sigma^2, \end{aligned} \tag{8.27}$$

with the corresponding posterior values for $\mu(x)$,

$$\begin{aligned} \mathrm{E}(\mu(x)|\mathbf{Z}) &= h(x)^T\left(\mathbf{H}^T\mathbf{H} + \frac{1}{\tau}\mathbf{\Sigma}^{-1}\right)^{-1}\mathbf{H}^T\mathbf{y}, \\ \mathrm{cov}[\mu(x),\mu(x')|\mathbf{Z}] &= h(x)^T\left(\mathbf{H}^T\mathbf{H} + \frac{1}{\tau}\mathbf{\Sigma}^{-1}\right)^{-1}h(x')\sigma^2. \end{aligned} \tag{8.28}$$

How do we choose the prior correlation matrix $\mathbf{\Sigma}$? In some settings the prior can be chosen from subject matter knowledge about the parameters. Here we are willing to say the function $\mu(x)$ should be smooth, and have guaranteed this by expressing μ in a smooth low-dimensional basis of B-splines. Hence we can take the prior correlation matrix to be the identity $\mathbf{\Sigma} = \mathbf{I}$. When the number of basis functions is large, this might not be sufficient, and additional smoothness can be enforced by imposing restrictions on $\mathbf{\Sigma}$; this is exactly the case with smoothing splines (Section 5.8.1).

Figure 8.3 shows ten draws from the corresponding prior for $\mu(x)$. To generate posterior values of the function $\mu(x)$, we generate values θ' from its posterior (8.27), giving corresponding posterior value $\mu'(x) = \sum_1^7 \beta'_j h_j(x)$. Ten such posterior curves are shown in Figure 8.4. Two different values were used for the prior variance τ, 1 and 1000. Notice how similar the right panel looks to the bootstrap distribution in the bottom left panel

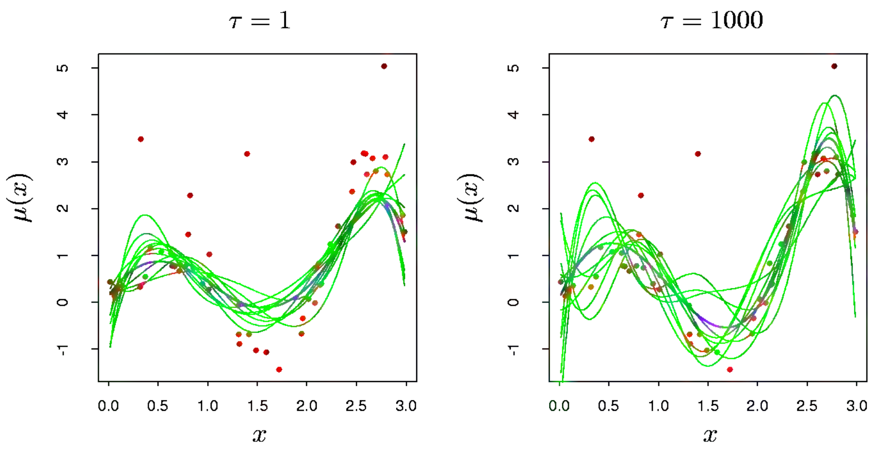

FIGURE 8.4. *Smoothing example: Ten draws from the posterior distribution for the function $\mu(x)$, for two different values of the prior variance τ. The purple curves are the posterior means.*

of Figure 8.2 on page 227. This similarity is no accident. As $\tau \to \infty$, the posterior distribution (8.27) and the bootstrap distribution (8.7) coincide. On the other hand, for $\tau = 1$, the posterior curves $\mu(x)$ in the left panel of Figure 8.4 are smoother than the bootstrap curves, because we have imposed more prior weight on smoothness.

The distribution (8.25) with $\tau \to \infty$ is called a *noninformative prior* for θ. In Gaussian models, maximum likelihood and parametric bootstrap analyses tend to agree with Bayesian analyses that use a noninformative prior for the free parameters. These tend to agree, because with a constant prior, the posterior distribution is proportional to the likelihood. This correspondence also extends to the nonparametric case, where the nonparametric bootstrap approximates a noninformative Bayes analysis; Section 8.4 has the details.

We have, however, done some things that are not proper from a Bayesian point of view. We have used a noninformative (constant) prior for σ^2 and replaced it with the maximum likelihood estimate $\hat{\sigma}^2$ in the posterior. A more standard Bayesian analysis would also put a prior on σ (typically $g(\sigma) \propto 1/\sigma$), calculate a joint posterior for $\mu(x)$ and σ, and then integrate out σ, rather than just extract the maximum of the posterior distribution ("MAP" estimate).

8.4 Relationship Between the Bootstrap and Bayesian Inference

Consider first a very simple example, in which we observe a single observation z from a normal distribution

$$z \sim N(\theta, 1). \tag{8.29}$$

To carry out a Bayesian analysis for θ, we need to specify a prior. The most convenient and common choice would be $\theta \sim N(0, \tau)$ giving posterior distribution

$$\theta|z \sim N\left(z, \frac{1}{1+1/\tau}\right). \tag{8.30}$$

Now the larger we take τ, the more concentrated the posterior becomes around the maximum likelihood estimate $\hat{\theta} = z$. In the limit as $\tau \to \infty$ we obtain a noninformative (constant) prior, and the posterior distribution is

$$\theta|z \sim N(z, 1). \tag{8.31}$$

This is the same as a parametric bootstrap distribution in which we generate bootstrap values z^* from the maximum likelihood estimate of the sampling density $N(z, 1)$.

There are three ingredients that make this correspondence work:

1. The choice of noninformative prior for θ.

2. The dependence of the log-likelihood $\ell(\theta; \mathbf{Z})$ on the data $\mathbf{Z}$ only through the maximum likelihood estimate $\hat{\theta}$. Hence we can write the log-likelihood as $\ell(\theta; \hat{\theta})$.

3. The symmetry of the log-likelihood in θ and $\hat{\theta}$, that is, $\ell(\theta; \hat{\theta}) = \ell(\hat{\theta}; \theta) + \text{constant}$.

Properties (2) and (3) essentially only hold for the Gaussian distribution. However, they also hold approximately for the multinomial distribution, leading to a correspondence between the nonparametric bootstrap and Bayes inference, which we outline next.

Assume that we have a discrete sample space with L categories. Let w_j be the probability that a sample point falls in category j, and $\hat{w}_j$ the observed proportion in category j. Let $w = (w_1, w_2, \ldots, w_L), \hat{w} = (\hat{w}_1, \hat{w}_2, \ldots, \hat{w}_L)$. Denote our estimator by $S(\hat{w})$; take as a prior distribution for w a symmetric Dirichlet distribution with parameter a:

$$w \sim \text{Di}_L(a1), \tag{8.32}$$

that is, the prior probability mass function is proportional to $\prod_{\ell=1}^{L} w_\ell^{a-1}$. Then the posterior density of w is

$$w \sim \mathrm{Di}_L(a1 + N\hat{w}), \tag{8.33}$$

where N is the sample size. Letting $a \to 0$ to obtain a noninformative prior gives

$$w \sim \mathrm{Di}_L(N\hat{w}). \tag{8.34}$$

Now the bootstrap distribution, obtained by sampling with replacement from the data, can be expressed as sampling the category proportions from a multinomial distribution. Specifically,

$$N\hat{w}^* \sim \mathrm{Mult}(N, \hat{w}), \tag{8.35}$$

where $\mathrm{Mult}(N, \hat{w})$ denotes a multinomial distribution, having probability mass function $\binom{N}{N\hat{w}_1^*, \ldots, N\hat{w}_L^*} \prod \hat{w}_\ell^{N\hat{w}_\ell^*}$. This distribution is similar to the posterior distribution above, having the same support, same mean, and nearly the same covariance matrix. Hence the bootstrap distribution of $S(\hat{w}^*)$ will closely approximate the posterior distribution of $S(w)$.

In this sense, the bootstrap distribution represents an (approximate) nonparametric, noninformative posterior distribution for our parameter. But this bootstrap distribution is obtained painlessly—without having to formally specify a prior and without having to sample from the posterior distribution. Hence we might think of the bootstrap distribution as a "poor man's" Bayes posterior. By perturbing the data, the bootstrap approximates the Bayesian effect of perturbing the parameters, and is typically much simpler to carry out.

8.5 The EM Algorithm

The EM algorithm is a popular tool for simplifying difficult maximum likelihood problems. We first describe it in the context of a simple mixture model.

8.5.1 Two-Component Mixture Model

In this section we describe a simple mixture model for density estimation, and the associated EM algorithm for carrying out maximum likelihood estimation. This has a natural connection to Gibbs sampling methods for Bayesian inference. Mixture models are discussed and demonstrated in several other parts of the book, in particular Sections 6.8, 12.7 and 13.2.3.

The left panel of Figure 8.5 shows a histogram of the 20 fictitious data points in Table 8.1.

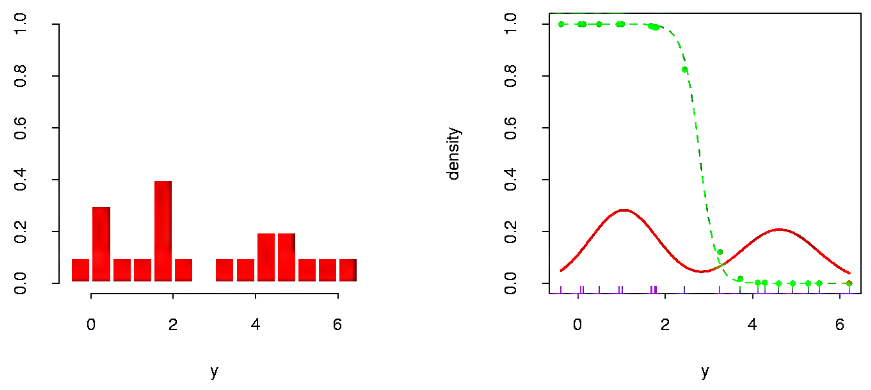

FIGURE 8.5. *Mixture example. Left panel: histogram of data. Right panel: maximum likelihood fit of Gaussian densities (solid red) and responsibility (dotted green) of the left component density for observation y, as a function of y.*

TABLE 8.1. *20 fictitious data points used in the two-component mixture example in Figure 8.5.*

-0.39	0.12	0.94	1.67	1.76	2.44	3.72	4.28	4.92	5.53
0.06	0.48	1.01	1.68	1.80	3.25	4.12	4.60	5.28	6.22

We would like to model the density of the data points, and due to the apparent bi-modality, a Gaussian distribution would not be appropriate. There seems to be two separate underlying regimes, so instead we model Y as a mixture of two normal distributions:

$$\begin{aligned} Y_1 &\sim N(\mu_1, \sigma_1^2), \\ Y_2 &\sim N(\mu_2, \sigma_2^2), \\ Y &= (1-\Delta)\cdot Y_1 + \Delta \cdot Y_2, \end{aligned} \tag{8.36}$$

where $\Delta \in \{0, 1\}$ with $\Pr(\Delta = 1) = \pi$. This *generative* representation is explicit: generate a $\Delta \in \{0, 1\}$ with probability π, and then depending on the outcome, deliver either Y_1 or Y_2. Let $\phi_\theta(x)$ denote the normal density with parameters $\theta = (\mu, \sigma^2)$. Then the density of Y is

$$g_Y(y) = (1-\pi)\phi_{\theta_1}(y) + \pi\phi_{\theta_2}(y). \tag{8.37}$$

Now suppose we wish to fit this model to the data in Figure 8.5 by maximum likelihood. The parameters are

$$\theta = (\pi, \theta_1, \theta_2) = (\pi, \mu_1, \sigma_1^2, \mu_2, \sigma_2^2). \tag{8.38}$$

The log-likelihood based on the N training cases is

$$\ell(\theta; \mathbf{Z}) = \sum_{i=1}^{N} \log[(1-\pi)\phi_{\theta_1}(y_i) + \pi\phi_{\theta_2}(y_i)]. \tag{8.39}$$

Algorithm 8.1 *EM algorithm for two-component Gaussian mixture.*

1. Take initial guesses for the parameters $\hat\mu_1, \hat\sigma_1^2, \hat\mu_2, \hat\sigma_2^2, \hat\pi$ (see text).

2. *Expectation Step*: compute the responsibilities

$$\hat\gamma_i = \frac{\hat\pi\phi_{\hat\theta_2}(y_i)}{(1-\hat\pi)\phi_{\hat\theta_1}(y_i) + \hat\pi\phi_{\hat\theta_2}(y_i)},\ i = 1, 2, \ldots, N. \tag{8.42}$$

3. *Maximization Step*: compute the weighted means and variances:

$$\hat\mu_1 = \frac{\sum_{i=1}^N (1-\hat\gamma_i)y_i}{\sum_{i=1}^N (1-\hat\gamma_i)}, \qquad \hat\sigma_1^2 = \frac{\sum_{i=1}^N (1-\hat\gamma_i)(y_i-\hat\mu_1)^2}{\sum_{i=1}^N (1-\hat\gamma_i)},$$

$$\hat\mu_2 = \frac{\sum_{i=1}^N \hat\gamma_i y_i}{\sum_{i=1}^N \hat\gamma_i}, \qquad \hat\sigma_2^2 = \frac{\sum_{i=1}^N \hat\gamma_i(y_i-\hat\mu_1)^2}{\sum_{i=1}^N \hat\gamma_i},$$

and the mixing probability $\hat\pi = \sum_{i=1}^N \hat\gamma_i/N$.

4. Iterate steps 2 and 3 until convergence.

Direct maximization of $\ell(\theta; \mathbf{Z})$ is quite difficult numerically, because of the sum of terms inside the logarithm. There is, however, a simpler approach. We consider unobserved latent variables Δ_i taking values 0 or 1 as in (8.36): if $\Delta_i = 1$ then Y_i comes from model 2, otherwise it comes from model 1. Suppose we knew the values of the Δ_i's. Then the log-likelihood would be

$$\ell_0(\theta; \mathbf{Z}, \boldsymbol\Delta) = \sum_{i=1}^N \left[(1-\Delta_i)\log\phi_{\theta_1}(y_i) + \Delta_i \log\phi_{\theta_2}(y_i)\right] \tag{8.40}$$

and the maximum likelihood estimates of μ_1 and σ_1^2 would be the sample mean and variance for those data with $\Delta_i = 0$, and similarly those for μ_2 and σ_2^2 would be the sample mean and variance of the data with $\Delta_i = 1$.

Since the values of the Δ_i's are actually unknown, we proceed in an iterative fashion, substituting for each Δ_i in (8.40) its expected value

$$\gamma_i(\theta) = \mathrm{E}(\Delta_i|\theta, \mathbf{Z}) = \Pr(\Delta_i = 1|\theta, \mathbf{Z}), \tag{8.41}$$

also called the *responsibility* of model 2 for observation i. We use a procedure called the EM algorithm, given in Algorithm 8.1 for the special case of Gaussian mixtures. In the *expectation* step, we do a soft assignment of each observation to each model: the current estimates of the parameters are used to assign responsibilities according to the relative density of the training points under each model. In the *maximization* step, these responsibilities

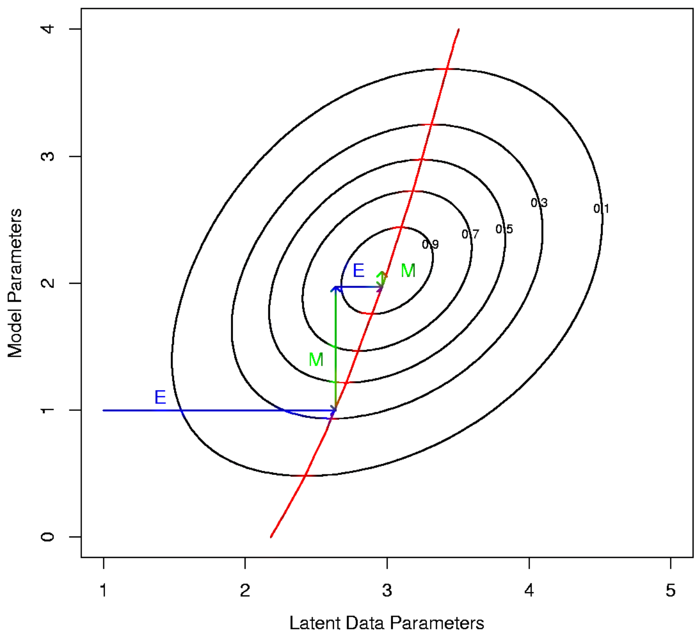

FIGURE 8.7. *Maximization–maximization view of the EM algorithm. Shown are the contours of the (augmented) observed data log-likelihood $F(\theta', \tilde{P})$. The E step is equivalent to maximizing the log-likelihood over the parameters of the latent data distribution. The M step maximizes it over the parameters of the log-likelihood. The red curve corresponds to the observed data log-likelihood, a* profile *obtained by maximizing $F(\theta', \tilde{P})$ for each value of θ'.*

The EM algorithm can be viewed as a joint maximization method for F over θ' and $\tilde{P}(\mathbf{Z}^m)$, by fixing one argument and maximizing over the other. The maximizer over $\tilde{P}(\mathbf{Z}^m)$ for fixed θ' can be shown to be

$$\tilde{P}(\mathbf{Z}^m) = \Pr(\mathbf{Z}^m|\mathbf{Z}, \theta') \tag{8.49}$$

(Exercise 8.3). This is the distribution computed by the E step, for example (8.42) in the mixture example. In the M step, we maximize $F(\theta', \tilde{P})$ over θ' with $\tilde{P}$ fixed: this is the same as maximizing the first term $\mathrm{E}_{\tilde{P}}[\ell_0(\theta'; \mathbf{T})|\mathbf{Z}, \theta]$ since the second term does not involve θ'.

Finally, since $F(\theta', \tilde{P})$ and the observed data log-likelihood agree when $\tilde{P}(\mathbf{Z}^m) = \Pr(\mathbf{Z}^m|\mathbf{Z}, \theta')$, maximization of the former accomplishes maximization of the latter. Figure 8.7 shows a schematic view of this process. This view of the EM algorithm leads to alternative maximization procedures. For example, one does not need to maximize with respect to all of the latent data parameters at once, but could instead maximize over one of them at a time, alternating with the M step.

Algorithm 8.3 *Gibbs sampler.*

```
1. Take some initial values $U_k^{(0)}, k = 1, 2, \ldots, K$.
2. Repeat for $t = 1, 2, \ldots, .$ :
     For $k = 1, 2, \ldots, K$ generate $U_k^{(t)}$ from
         $\Pr(U_k^{(t)} | U_1^{(t)}, \ldots, U_{k-1}^{(t)}, U_{k+1}^{(t-1)}, \ldots, U_K^{(t-1)})$.
3. Continue step 2 until the joint distribution of $(U_1^{(t)}, U_2^{(t)}, \ldots, U_K^{(t)})$
   does not change.
```

8.6 MCMC for Sampling from the Posterior

Having defined a Bayesian model, one would like to draw samples from the resulting posterior distribution, in order to make inferences about the parameters. Except for simple models, this is often a difficult computational problem. In this section we discuss the *Markov chain Monte Carlo* (MCMC) approach to posterior sampling. We will see that Gibbs sampling, an MCMC procedure, is closely related to the EM algorithm: the main difference is that it samples from the conditional distributions rather than maximizing over them.

Consider first the following abstract problem. We have random variables $U_1, U_2, \ldots, U_K$ and we wish to draw a sample from their joint distribution. Suppose this is difficult to do, but it is easy to simulate from the conditional distributions $\Pr(U_j | U_1, U_2, \ldots, U_{j-1}, U_{j+1}, \ldots, U_K)$, $j = 1, 2, \ldots, K$. The Gibbs sampling procedure alternatively simulates from each of these distributions and when the process stabilizes, provides a sample from the desired joint distribution. The procedure is defined Algorithm 8.3.

Under regularity conditions it can be shown that this procedure eventually stabilizes, and the resulting random variables are indeed a sample from the joint distribution of $U_1, U_2, \ldots, U_K$. This occurs despite the fact that the samples $(U_1^{(t)}, U_2^{(t)}, \ldots, U_K^{(t)})$ are clearly not independent for different t. More formally, Gibbs sampling produces a Markov chain whose stationary distribution is the true joint distribution, and hence the term "Markov chain Monte Carlo." It is not surprising that the true joint distribution is stationary under this process, as the successive steps leave the marginal distributions of the U_k's unchanged.

Note that we don't need to know the explicit form of the conditional densities, but just need to be able to sample from them. After the procedure reaches stationarity, the marginal density of any subset of the variables can be approximated by a density estimate applied to the sample values. However if the explicit form of the conditional density $\Pr(U_k, | U_\ell, \ell \neq k)$ is available, a better estimate of say the marginal density of U_k can be

Algorithm 8.4 *Gibbs sampling for mixtures.*

1. Take some initial values $\theta^{(0)} = (\mu_1^{(0)}, \mu_2^{(0)})$.

2. Repeat for $t = 1, 2, \ldots,$.

   (a) For $i = 1, 2, \ldots, N$ generate $\Delta_i^{(t)} \in \{0, 1\}$ with $\Pr(\Delta_i^{(t)} = 1) = \hat{\gamma}_i(\theta^{(t)})$, from equation (8.42).

   (b) Set

$$\begin{aligned} \hat{\mu}_1 &= \frac{\sum_{i=1}^N (1 - \Delta_i^{(t)}) \cdot y_i}{\sum_{i=1}^N (1 - \Delta_i^{(t)})}, \\ \hat{\mu}_2 &= \frac{\sum_{i=1}^N \Delta_i^{(t)} \cdot y_i}{\sum_{i=1}^N \Delta_i^{(t)}}, \end{aligned}$$

   and generate $\mu_1^{(t)} \sim N(\hat{\mu}_1, \hat{\sigma}_1^2)$ and $\mu_2^{(t)} \sim N(\hat{\mu}_2, \hat{\sigma}_2^2)$.

3. Continue step 2 until the joint distribution of $(\boldsymbol{\Delta}^{(t)}, \mu_1^{(t)}, \mu_2^{(t)})$ doesn't change

obtained from (Exercise 8.4).

$$\widehat{\Pr}_{U_k}(u) = \frac{1}{(M - m + 1)} \sum_{t=m}^{M} \Pr(u | U_\ell^{(t)}, \ell \neq k). \tag{8.50}$$

Here we have averaged over the last $M - m + 1$ members of the sequence, to allow for an initial "burn-in" period before stationarity is reached.

Now getting back to Bayesian inference, our goal is to draw a sample from the joint posterior of the parameters given the data $\mathbf{Z}$. Gibbs sampling will be helpful if it is easy to sample from the conditional distribution of each parameter given the other parameters and $\mathbf{Z}$. An example—the Gaussian mixture problem—is detailed next.

There is a close connection between Gibbs sampling from a posterior and the EM algorithm in exponential family models. The key is to consider the latent data $\mathbf{Z}^m$ from the EM procedure to be another parameter for the Gibbs sampler. To make this explicit for the Gaussian mixture problem, we take our parameters to be $(\theta, \mathbf{Z}^m)$. For simplicity we fix the variances σ_1^2, σ_2^2 and mixing proportion π at their maximum likelihood values so that the only unknown parameters in θ are the means μ_1 and μ_2. The Gibbs sampler for the mixture problem is given in Algorithm 8.4. We see that steps 2(a) and 2(b) are the same as the E and M steps of the EM procedure, except that we sample rather than maximize. In step 2(a), rather than compute the maximum likelihood responsibilities $\gamma_i = \text{E}(\Delta_i | \theta, \mathbf{Z})$,

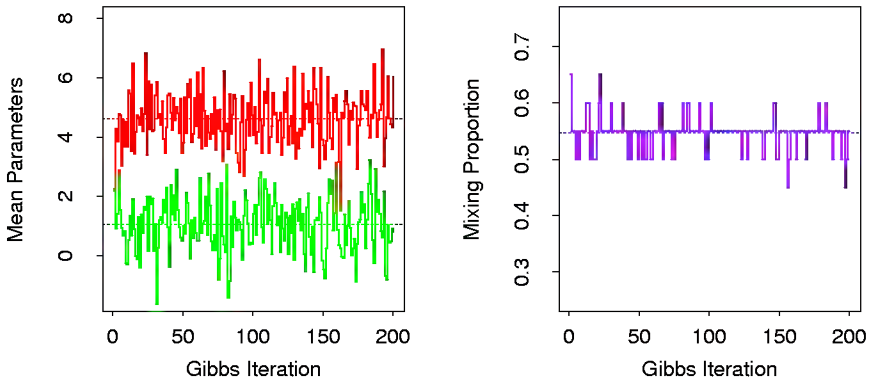

FIGURE 8.8. *Mixture example. Left panel:* 200 *values of the two mean parameters from Gibbs sampling; horizontal lines are drawn at the maximum likelihood estimates* $\hat{\mu}_1$, $\hat{\mu}_2$. *Right panel: proportion of values with* $\Delta_i = 1$, *for each of the* 200 *Gibbs sampling iterations; a horizontal line is drawn at* $\sum_i \hat{\gamma}_i/N$.

the Gibbs sampling procedure simulates the latent data Δ_i from the distributions $\Pr(\Delta_i|\theta, \mathbf{Z})$. In step 2(b), rather than compute the maximizers of the posterior $\Pr(\mu_1, \mu_2, \boldsymbol{\Delta}|\mathbf{Z})$ we simulate from the conditional distribution $\Pr(\mu_1, \mu_2|\boldsymbol{\Delta}, \mathbf{Z})$.

Figure 8.8 shows 200 iterations of Gibbs sampling, with the mean parameters μ_1 (lower) and μ_2 (upper) shown in the left panel, and the proportion of class 2 observations $\sum_i \Delta_i/N$ on the right. Horizontal broken lines have been drawn at the maximum likelihood estimate values $\hat{\mu}_1, \hat{\mu}_2$ and $\sum_i \hat{\gamma}_i/N$ in each case. The values seem to stabilize quite quickly, and are distributed evenly around the maximum likelihood values.

The above mixture model was simplified, in order to make the clear connection between Gibbs sampling and the EM algorithm. More realistically, one would put a prior distribution on the variances σ_1^2, σ_2^2 and mixing proportion π, and include separate Gibbs sampling steps in which we sample from their posterior distributions, conditional on the other parameters. One can also incorporate proper (informative) priors for the mean parameters. These priors must not be improper as this will lead to a degenerate posterior, with all the mixing weight on one component.

Gibbs sampling is just one of a number of recently developed procedures for sampling from posterior distributions. It uses conditional sampling of each parameter given the rest, and is useful when the structure of the problem makes this sampling easy to carry out. Other methods do not require such structure, for example the *Metropolis–Hastings* algorithm. These and other computational Bayesian methods have been applied to sophisticated learning algorithms such as Gaussian process models and neural networks. Details may be found in the references given in the Bibliographic Notes at the end of this chapter.

8.7 Bagging

Earlier we introduced the bootstrap as a way of assessing the accuracy of a parameter estimate or a prediction. Here we show how to use the bootstrap to improve the estimate or prediction itself. In Section 8.4 we investigated the relationship between the bootstrap and Bayes approaches, and found that the bootstrap mean is approximately a posterior average. Bagging further exploits this connection.

Consider first the regression problem. Suppose we fit a model to our training data $\mathbf{Z} = \{(x_1, y_1), (x_2, y_2), \ldots, (x_N, y_N)\}$, obtaining the prediction $\hat{f}(x)$ at input x. Bootstrap aggregation or *bagging* averages this prediction over a collection of bootstrap samples, thereby reducing its variance. For each bootstrap sample $\mathbf{Z}^{*b}$, $b = 1, 2, \ldots, B$, we fit our model, giving prediction $\hat{f}^{*b}(x)$. The bagging estimate is defined by

$$\hat{f}_{\text{bag}}(x) = \frac{1}{B} \sum_{b=1}^{B} \hat{f}^{*b}(x). \tag{8.51}$$

Denote by $\hat{\mathcal{P}}$ the empirical distribution putting equal probability $1/N$ on each of the data points (x_i, y_i). In fact the "true" bagging estimate is defined by $\mathrm{E}_{\hat{\mathcal{P}}} \hat{f}^*(x)$, where $\mathbf{Z}^* = (x_1^*, y_1^*), (x_2^*, y_2^*), \ldots, (x_N^*, y_N^*)$ and each $(x_i^*, y_i^*) \sim \hat{\mathcal{P}}$. Expression (8.51) is a Monte Carlo estimate of the true bagging estimate, approaching it as $B \to \infty$.

The bagged estimate (8.51) will differ from the original estimate $\hat{f}(x)$ only when the latter is a nonlinear or adaptive function of the data. For example, to bag the B-spline smooth of Section 8.2.1, we average the curves in the bottom left panel of Figure 8.2 at each value of x. The B-spline smoother is linear in the data if we fix the inputs; hence if we sample using the parametric bootstrap in equation (8.6), then $\hat{f}_{\text{bag}}(x) \to \hat{f}(x)$ as $B \to \infty$ (Exercise 8.5). Hence bagging just reproduces the original smooth in the top left panel of Figure 8.2. The same is approximately true if we were to bag using the nonparametric bootstrap.

A more interesting example is a regression tree, where $\hat{f}(x)$ denotes the tree's prediction at input vector x (regression trees are described in Chapter 9). Each bootstrap tree will typically involve different features than the original, and might have a different number of terminal nodes. The bagged estimate is the average prediction at x from these B trees.

Now suppose our tree produces a classifier $\hat{G}(x)$ for a K-class response. Here it is useful to consider an underlying indicator-vector function $\hat{f}(x)$, with value a single one and $K-1$ zeroes, such that $\hat{G}(x) = \arg\max_k \hat{f}(x)$. Then the bagged estimate $\hat{f}_{\text{bag}}(x)$ (8.51) is a K-vector $(p_1, p_2, \ldots, p_K)$, with p_k equal to the proportion of trees predicting class k at x. Treating these as estimates of the class probabilities, our predicted class is the one with the most "votes" from the B trees, $\hat{G}_{\text{bag}}(x) = \arg\max_k \hat{f}_{\text{bag}}(x)$.

For many classifiers $\hat{G}(x)$, (including trees), there is already an underlying function $\hat{f}(x)$ that estimates the class probabilities at x. An alternative bagging strategy is to average these instead, rather than the indicator vectors, and this tends to produce bagged estimates with lower variance, especially for small B (see Figure 8.10).

8.7.1 Example: Trees with Simulated Data

We generated a sample of size $N = 30$, with two classes and $p = 5$ features, each having a standard Gaussian distribution with pairwise correlation 0.95. The response Y was generated according to $\Pr(Y = 1|x_1 \leq 0.5) = 0.2$, $\Pr(Y = 1|x_1 > 0.5) = 0.8$. The Bayes error is 0.2. A test sample of size 2000 was also generated from the same population. We fit classification trees to the training sample and to each of 200 bootstrap samples (classification trees are described in Chapter 9). No pruning was used. Figure 8.9 shows the original tree and five bootstrap trees. Notice how the trees are all different, with different splitting features and cutpoints. The test error for the original tree and the bagged tree is shown in Figure 8.10. In this example the trees have high variance due to the correlation in the predictors. Bagging succeeds in smoothing out this variance and hence reducing the test error.

Bagging can dramatically reduce the variance of unstable procedures like trees, leading to improved prediction. A simple argument shows why bagging helps under squared-error loss, in short because averaging reduces variance and leaves bias unchanged.

Assume our training observations (x_i, y_i), $i = 1, \ldots, N$ are independently drawn from a distribution $\mathcal{P}$, and consider the ideal aggregate estimator $f_{\text{ag}}(x) = \text{E}_{\mathcal{P}}\hat{f}^*(x)$. Here x is fixed and the bootstrap dataset $\mathbf{Z}^*$ consists of observations x_i^*, y_i^*, $i = 1, 2, \ldots, N$ sampled from $\mathcal{P}$. Note that $f_{\text{ag}}(x)$ is a bagging estimate, drawing bootstrap samples from the actual population $\mathcal{P}$ rather than the data. It is not an estimate that we can use in practice, but is convenient for analysis. We can write

$$\begin{aligned}
\text{E}_{\mathcal{P}}[Y - \hat{f}^*(x)]^2 &= \text{E}_{\mathcal{P}}[Y - f_{\text{ag}}(x) + f_{\text{ag}}(x) - \hat{f}^*(x)]^2 \\
&= \text{E}_{\mathcal{P}}[Y - f_{\text{ag}}(x)]^2 + \text{E}_{\mathcal{P}}[\hat{f}^*(x) - f_{\text{ag}}(x)]^2 \\
&\geq \text{E}_{\mathcal{P}}[Y - f_{\text{ag}}(x)]^2. \qquad (8.52)
\end{aligned}$$

The extra error on the right-hand side comes from the variance of $\hat{f}^*(x)$ around its mean $f_{\text{ag}}(x)$. Therefore true population aggregation never increases mean squared error. This suggests that bagging—drawing samples from the training data— will often decrease mean-squared error.

The above argument does not hold for classification under 0-1 loss, because of the nonadditivity of bias and variance. In that setting, bagging a good classifier can make it better, but bagging a bad classifier can make it

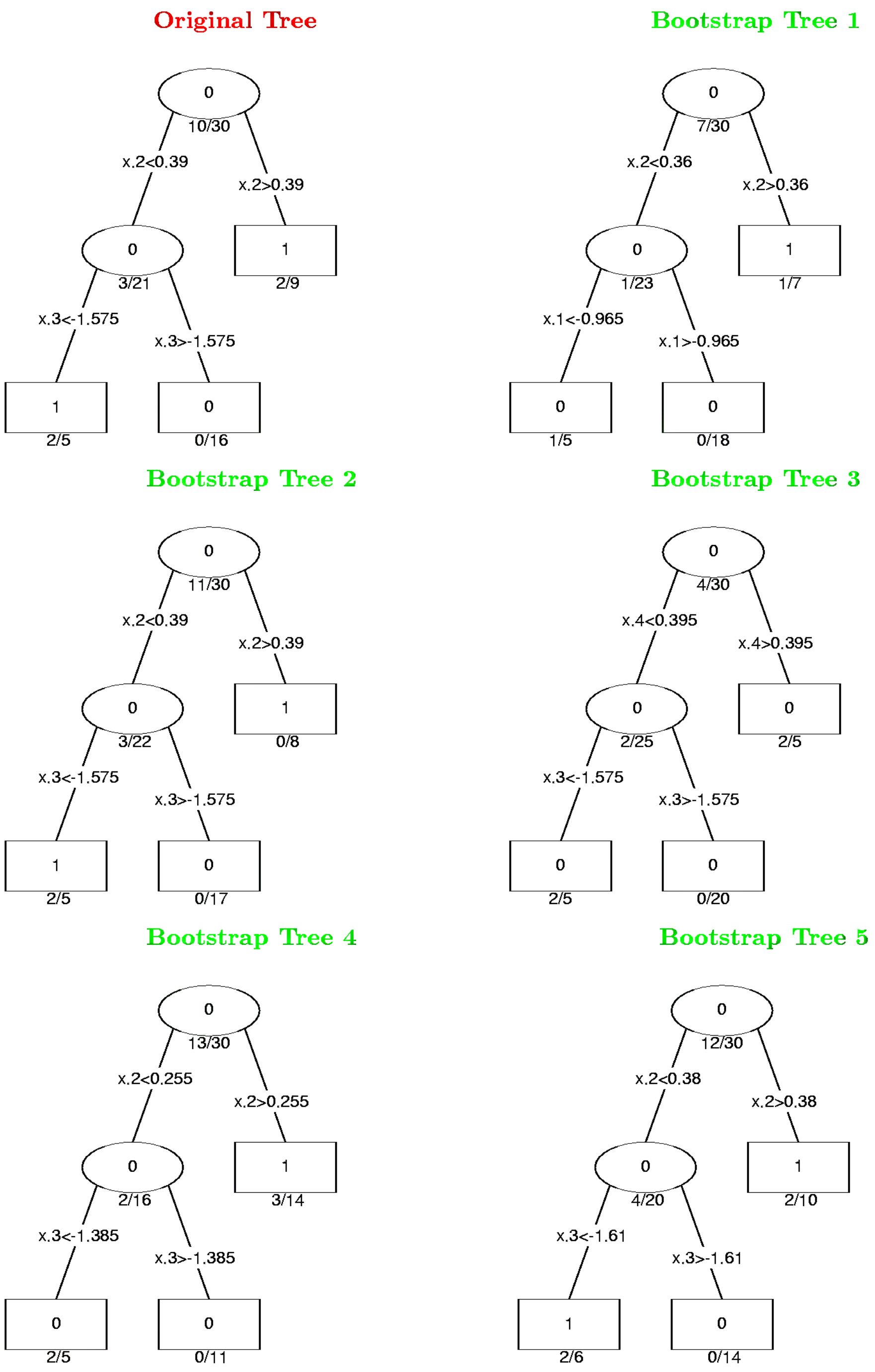

FIGURE 8.9. *Bagging trees on simulated dataset. Top left panel shows original tree. Five trees grown on bootstrap samples are shown.*

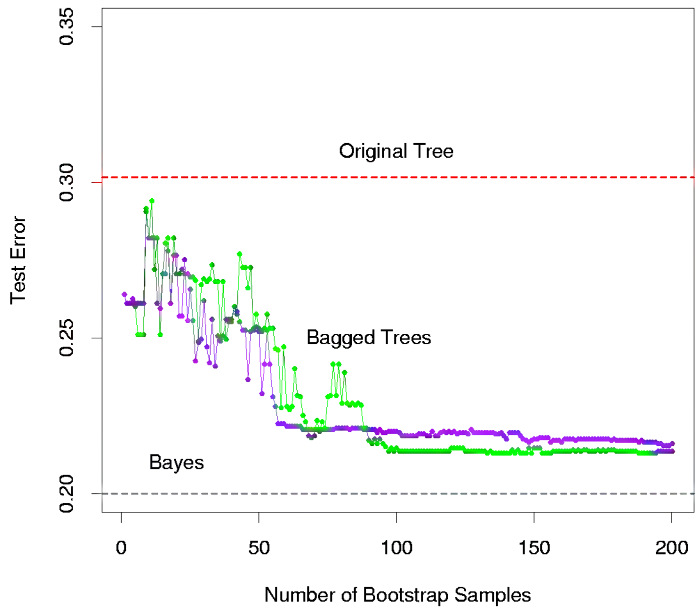

FIGURE 8.10. *Error curves for the bagging example of Figure 8.9. Shown is the test error of the original tree and bagged trees as a function of the number of bootstrap samples. The green points correspond to majority vote, while the purple points average the probabilities.*

worse. Here is a simple example, using a randomized rule. Suppose $Y = 1$ for all x, and the classifier $\hat{G}(x)$ predicts $Y = 1$ (for all x) with probability 0.4 and predicts $Y = 0$ (for all x) with probability 0.6. Then the misclassification error of $\hat{G}(x)$ is 0.6 but that of the bagged classifier is 1.0.

Note that when we bag a model, any simple structure in the model is lost. As an example, a bagged tree is no longer a tree. For interpretation of the model this is clearly a drawback. More stable procedures like nearest neighbors are typically not affected much by bagging. Unfortunately, the unstable models most helped by bagging are unstable because of the emphasis on interpretability, and this is lost in the bagging process.

Figure 8.11 shows an example where bagging doesn't help. The 100 data points shown have two features and two classes, separated by the gray linear boundary $x_1 + x_2 = 1$. We choose as our classifier $\hat{G}(x)$ a single axis-oriented split, choosing the split along either x_1 or x_2 that produces the largest decrease in training misclassification error.

The decision boundary obtained from bagging the 0-1 decision rule over $B = 50$ bootstrap samples is shown by the blue curve in the left panel. It does a poor job of capturing the true boundary. The single split rule, derived from the training data, splits near 0 (the middle of the range of x_1 or x_2), and hence has little contribution away from the center. Averaging

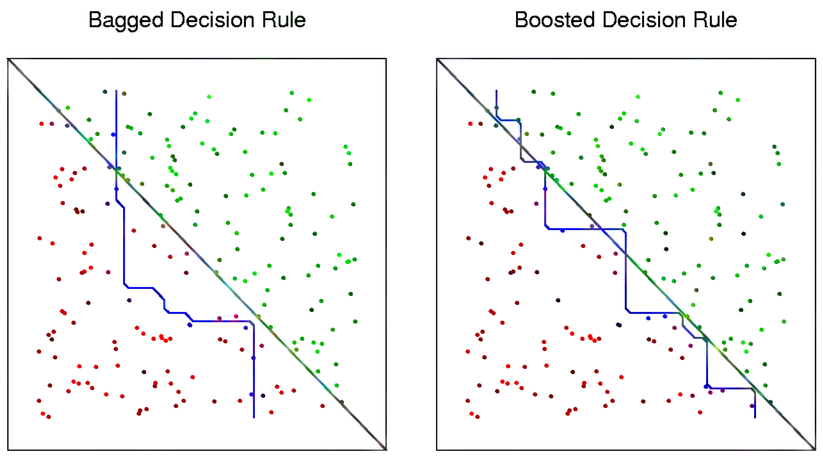

FIGURE 8.11. *Data with two features and two classes, separated by a linear boundary. Left panel: decision boundary estimated from bagging the decision rule from a single split, axis-oriented classifier. Right panel: decision boundary from boosting the decision rule of the same classifier. The test error rates are* 0.166, *and* 0.065 *respectively. Boosting is described in Chapter 10.*

the probabilities rather than the classifications does not help here. Bagging estimates the expected class probabilities from the single split rule, that is, averaged over many replications. In a stylized version of the above model, its error can be shown to be 0.5 for all x_1, x_2 (Exercise 8.1). Note that the expected class probabilities computed by bagging cannot be realized on any single replication, in the same way that a woman cannot have 2.4 children. In this sense, bagging increases somewhat the space of models of the individual base classifier. However it doesn't help in this and many other examples where a greater enlargement of the model class is needed. "Boosting" is a way of doing this and is described in Chapter 10. The decision boundary in the right panel is the result of the boosting procedure, and it roughly captures the diagonal boundary.

8.8 Model Averaging and Stacking

In Section 8.4 we viewed bootstrap values of an estimator as approximate posterior values of a corresponding parameter, from a kind of nonparametric Bayesian analysis. Viewed in the way, the bagged estimate (8.51) is an approximate posterior Bayesian mean. In contrast, the training sample estimate $\hat{f}(x)$ corresponds to the mode of the posterior. Since the posterior mean (not mode) minimizes squared-error loss, it is not surprising that bagging can often reduce mean squared-error.

Here we discuss Bayesian model averaging more generally. We have a set of candidate models $\mathcal{M}_m$, $m = 1, \ldots, M$ for our training set $\mathbf{Z}$. These models may be of the same type with different parameter values (e.g., subsets in linear regression), or different models for the same task (e.g., neural networks and regression trees).

Suppose ζ is some quantity of interest, for example, a prediction $f(x)$ at some fixed feature value x. The posterior distribution of ζ is

$$\Pr(\zeta|\mathbf{Z}) = \sum_{m=1}^{M} \Pr(\zeta|\mathcal{M}_m, \mathbf{Z})\Pr(\mathcal{M}_m|\mathbf{Z}), \tag{8.53}$$

with posterior mean

$$\mathrm{E}(\zeta|\mathbf{Z}) = \sum_{m=1}^{M} \mathrm{E}(\zeta|\mathcal{M}_m, \mathbf{Z})\Pr(\mathcal{M}_m|\mathbf{Z}). \tag{8.54}$$

This Bayesian prediction is a weighted average of the individual predictions, with weights proportional to the posterior probability of each model.

This formulation leads to a number of different model-averaging strategies. *Committee methods* take a simple unweighted average of the predictions from each model, essentially giving equal probability to each model. More ambitiously, the development in Section 7.7 shows the BIC criterion can be used to estimate posterior model probabilities. This is applicable in cases where the different models arise from the same parametric model, with different parameter values. The BIC gives weight to each model depending on how well it fits and how many parameters it uses. One can also carry out the Bayesian recipe in full. If each model $\mathcal{M}_m$ has parameters θ_m, we write

$$\begin{aligned}\Pr(\mathcal{M}_m|\mathbf{Z}) &\propto \Pr(\mathcal{M}_m)\cdot\Pr(\mathbf{Z}|\mathcal{M}_m)\\ &\propto \Pr(\mathcal{M}_m)\cdot\int \Pr(\mathbf{Z}|\theta_m, \mathcal{M}_m)\Pr(\theta_m|\mathcal{M}_m)d\theta_m.\end{aligned} \tag{8.55}$$

In principle one can specify priors $\Pr(\theta_m|\mathcal{M}_m)$ and numerically compute the posterior probabilities from (8.55), to be used as model-averaging weights. However, we have seen no real evidence that this is worth all of the effort, relative to the much simpler BIC approximation.

How can we approach model averaging from a frequentist viewpoint? Given predictions $\hat{f}_1(x), \hat{f}_2(x), \ldots, \hat{f}_M(x)$, under squared-error loss, we can seek the weights $w = (w_1, w_2, \ldots, w_M)$ such that

$$\hat{w} = \operatorname*{argmin}_{w} \mathrm{E}_{\mathcal{P}}\Big[Y - \sum_{m=1}^{M} w_m \hat{f}_m(x)\Big]^2. \tag{8.56}$$

Here the input value x is fixed and the N observations in the dataset $\mathbf{Z}$ (and the target Y) are distributed according to $\mathcal{P}$. The solution is the population linear regression of Y on $\hat{F}(x)^T \equiv [\hat{f}_1(x), \hat{f}_2(x), \dots, \hat{f}_M(x)]$:

$$\hat{w} = \mathrm{E}_{\mathcal{P}}[\hat{F}(x)\hat{F}(x)^T]^{-1}\mathrm{E}_{\mathcal{P}}[\hat{F}(x)Y]. \tag{8.57}$$

Now the full regression has smaller error than any single model

$$\mathrm{E}_{\mathcal{P}}\Big[Y - \sum_{m=1}^{M} \hat{w}_m \hat{f}_m(x)\Big]^2 \leq \mathrm{E}_{\mathcal{P}}\Big[Y - \hat{f}_m(x)\Big]^2 \ \forall m \tag{8.58}$$

so combining models never makes things worse, at the population level.

Of course the population linear regression (8.57) is not available, and it is natural to replace it with the linear regression over the training set. But there are simple examples where this does not work well. For example, if $\hat{f}_m(x),\ m = 1, 2, \dots, M$ represent the prediction from the best subset of inputs of size m among M total inputs, then linear regression would put all of the weight on the largest model, that is, $\hat{w}_M = 1,\ \hat{w}_m = 0,\ m < M$. The problem is that we have not put each of the models on the same footing by taking into account their complexity (the number of inputs m in this example).

Stacked generalization, or *stacking*, is a way of doing this. Let $\hat{f}_m^{-i}(x)$ be the prediction at x, using model m, applied to the dataset with the ith training observation removed. The stacking estimate of the weights is obtained from the least squares linear regression of y_i on $\hat{f}_m^{-i}(x_i),\ m = 1, 2, \dots, M$. In detail the stacking weights are given by

$$\hat{w}^{\text{st}} = \underset{w}{\operatorname{argmin}} \sum_{i=1}^{N} \Big[y_i - \sum_{m=1}^{M} w_m \hat{f}_m^{-i}(x_i)\Big]^2. \tag{8.59}$$

The final prediction is $\sum_m \hat{w}_m^{\text{st}} \hat{f}_m(x)$. By using the cross-validated predictions $\hat{f}_m^{-i}(x)$, stacking avoids giving unfairly high weight to models with higher complexity. Better results can be obtained by restricting the weights to be nonnegative, and to sum to 1. This seems like a reasonable restriction if we interpret the weights as posterior model probabilities as in equation (8.54), and it leads to a tractable quadratic programming problem.

There is a close connection between stacking and model selection via leave-one-out cross-validation (Section 7.10). If we restrict the minimization in (8.59) to weight vectors w that have one unit weight and the rest zero, this leads to a model choice $\hat{m}$ with smallest leave-one-out cross-validation error. Rather than choose a single model, stacking combines them with estimated optimal weights. This will often lead to better prediction, but less interpretability than the choice of only one of the M models.

The stacking idea is actually more general than described above. One can use any learning method, not just linear regression, to combine the models as in (8.59); the weights could also depend on the input location x. In this way, learning methods are "stacked" on top of one another, to improve prediction performance.

8.9 Stochastic Search: Bumping

The final method described in this chapter does not involve averaging or combining models, but rather is a technique for finding a better single model. *Bumping* uses bootstrap sampling to move randomly through model space. For problems where fitting method finds many local minima, bumping can help the method to avoid getting stuck in poor solutions.

As in bagging, we draw bootstrap samples and fit a model to each. But rather than average the predictions, we choose the model estimated from a bootstrap sample that best fits the training data. In detail, we draw bootstrap samples $\mathbf{Z}^{*1}, \dots, \mathbf{Z}^{*B}$ and fit our model to each, giving predictions $\hat{f}^{*b}(x)$, $b = 1, 2, \dots, B$ at input point x. We then choose the model that produces the smallest prediction error, averaged over the *original training set*. For squared error, for example, we choose the model obtained from bootstrap sample $\hat{b}$, where

$$\hat{b} = \arg\min_b \sum_{i=1}^{N} [y_i - \hat{f}^{*b}(x_i)]^2. \tag{8.60}$$

The corresponding model predictions are $\hat{f}^{*\hat{b}}(x)$. By convention we also include the original training sample in the set of bootstrap samples, so that the method is free to pick the original model if it has the lowest training error.

By perturbing the data, bumping tries to move the fitting procedure around to good areas of model space. For example, if a few data points are causing the procedure to find a poor solution, any bootstrap sample that omits those data points should procedure a better solution.

For another example, consider the classification data in Figure 8.12, the notorious *exclusive or (XOR)* problem. There are two classes (green and red) and two input features, with the features exhibiting a pure interaction. By splitting the data at $x_1 = 0$ and then splitting each resulting strata at $x_2 = 0$, (or vice versa) a tree-based classifier could achieve perfect discrimination. However, the greedy, short-sighted CART algorithm (Section 9.2) tries to find the best split on either feature, and then splits the resulting strata. Because of the balanced nature of the data, all initial splits on x_1 or x_2 appear to be useless, and the procedure essentially generates a random split at the top level. The actual split found for these data is shown in the left panel of Figure 8.12. By bootstrap sampling from the data, bumping breaks the balance in the classes, and with a reasonable number of

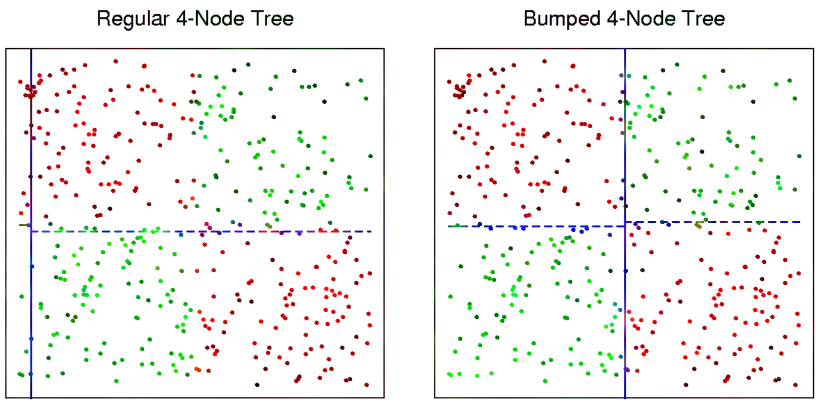

FIGURE 8.12. *Data with two features and two classes (green and red), displaying a pure interaction. The left panel shows the partition found by three splits of a standard, greedy, tree-growing algorithm. The vertical blue line near the left edge is the first split, and the broken lines are the two subsequent splits. The algorithm has no idea where to make a good initial split, and makes a poor choice. The right panel shows the near-optimal splits found by bumping the tree-growing algorithm* 20 *times.*

bootstrap samples (here 20), it will by chance produce at least one tree with initial split near either $x_1 = 0$ or $x_2 = 0$. Using just 20 bootstrap samples, bumping found the near optimal splits shown in the right panel of Figure 8.12. This shortcoming of the greedy tree-growing algorithm is exacerbated if we add a number of noise features that are independent of the class label. Then the tree-growing algorithm cannot distinguish x_1 or x_2 from the others, and gets seriously lost.

Since bumping compares different models on the training data, one must ensure that the models have roughly the same complexity. In the case of trees, this would mean growing trees with the same number of terminal nodes on each bootstrap sample. Bumping can also help in problems where it is difficult to optimize the fitting criterion, perhaps because of a lack of smoothness. The trick is to optimize a different, more convenient criterion over the bootstrap samples, and then choose the model producing the best results for the desired criterion on the training sample.

Bibliographic Notes

There are many books on classical statistical inference: Cox and Hinkley (1974) and Silvey (1975) give nontechnical accounts. The bootstrap is due to Efron (1979) and is described more fully in Efron and Tibshirani (1993) and Hall (1992). A good modern book on Bayesian inference is Gelman et al. (1995). A lucid account of the application of Bayesian methods to neural networks is given in Neal (1996). The statistical application of Gibbs sampling is due to Geman and Geman (1984), and Gelfand and Smith (1990), with related work by Tanner and Wong (1987). Markov chain Monte Carlo methods, including Gibbs sampling and the Metropolis–Hastings algorithm, are discussed in Spiegelhalter et al. (1996). The EM algorithm is due to Dempster et al. (1977); as the discussants in that paper make clear, there was much related, earlier work. The view of EM as a joint maximization scheme for a penalized complete-data log-likelihood was elucidated by Neal and Hinton (1998); they credit Csiszar and Tusnády (1984) and Hathaway (1986) as having noticed this connection earlier. Bagging was proposed by Breiman (1996a). Stacking is due to Wolpert (1992); Breiman (1996b) contains an accessible discussion for statisticians. Leblanc and Tibshirani (1996) describe variations on stacking based on the bootstrap. Model averaging in the Bayesian framework has been recently advocated by Madigan and Raftery (1994). Bumping was proposed by Tibshirani and Knight (1999).

Exercises

Ex. 8.1 Consider the unit square and partition it into nine smaller squares of equal size by two lines cutting each axis at values 1/3 and 2/3, respectively. Below the line $x_1 + x_2 = 1$ is class 1; the rest is class 2.

We consider a single split classifier, that yields splits at one of the four lines (two on x_1 at 1/3 and 2/3, and similarly for x_2), with all four splits having equal probability.

(a) Analyze the effects of bagging the decision rule and the probability estimates, and show that the former has an error rate of 0.5, while the latter has the Bayes error rate of zero.

(b) Calculate the bias and variance of the single split probability estimates, and their bagged versions. Hence determine whether the positive effect of bagging is to reduce bias or variance.

Ex. 8.2 Let $r(y)$ and $q(y)$ be probability density functions. Jensen's inequality states that for a random variable X and a convex function $\phi(x)$, $\mathrm{E}[\phi(X)] \geq \phi[\mathrm{E}(X)]$. Use Jensen's inequality to show that

$$\mathrm{E}_q \log[r(Y)/q(Y)] \tag{8.61}$$

is maximized as a function of $r(y)$ when $r(y) = q(y)$. Hence show that $R(\theta, \theta) \geq R(\theta', \theta)$ as stated below equation (8.46).

Ex. 8.3 Consider the maximization of the log-likelihood (8.48), over distributions $\tilde{P}(\mathbf{Z}^m)$ such that $\tilde{P}(\mathbf{Z}^m) \geq 0$ and $\sum_{\mathbf{Z}^m} \tilde{P}(\mathbf{Z}^m) = 1$. Use Lagrange multipliers to show that the solution is the conditional distribution $\tilde{P}(\mathbf{Z}^m) = \Pr(\mathbf{Z}^m|\mathbf{Z}, \theta')$, as in (8.49).

Ex. 8.4 Justify the estimate (8.50), using the relationship

$$\Pr(A) = \int \Pr(A|B)d(\Pr(B)).$$

Ex. 8.5 Consider the bagging method of Section 8.7. Let our estimate $\hat{f}(x)$ be the B-spline smoother $\hat{\mu}(x)$ of Section 8.2.1. Consider the parametric bootstrap of equation (8.6), applied to this estimator. Show that if we bag $\hat{f}(x)$, using the parametric bootstrap to generate the bootstrap samples, the bagging estimate $\hat{f}_{\text{bag}}(x)$ converges to the original estimate $\hat{f}(x)$ as $B \to \infty$.

Ex. 8.6 Suggest generalizations of each of the loss functions in Figure 10.4 to more than two classes, and design an appropriate plot to compare them.

Ex. 8.7 Consider the bone mineral density data of Figure 5.6.

(a) Fit a cubic smooth spline to the relative change in spinal BMD, as a function of age. Use cross-validation to estimate the optimal amount of smoothing. Construct pointwise 90% confidence bands for the underlying function.

(b) Compute the posterior mean and covariance for the true function via (8.28), and compare the posterior bands to those obtained in (a).

(c) Compute 100 bootstrap replicates of the fitted curves, as in the bottom left panel of Figure 8.2. Compare the results to those obtained in (a) and (b).

9
Additive Models, Trees, and Related Methods

In this chapter we begin our discussion of some specific methods for supervised learning. These techniques each assume a (different) structured form for the unknown regression function, and by doing so they finesse the curse of dimensionality. Of course, they pay the possible price of misspecifying the model, and so in each case there is a tradeoff that has to be made. They take off where Chapters 3–6 left off. We describe five related techniques: generalized additive models, trees, multivariate adaptive regression splines, the patient rule induction method, and hierarchical mixtures of experts.

9.1 Generalized Additive Models

Regression models play an important role in many data analyses, providing prediction and classification rules, and data analytic tools for understanding the importance of different inputs.

Although attractively simple, the traditional linear model often fails in these situations: in real life, effects are often not linear. In earlier chapters we described techniques that used predefined basis functions to achieve nonlinearities. This section describes more automatic flexible statistical methods that may be used to identify and characterize nonlinear regression effects. These methods are called "generalized additive models."

In the regression setting, a generalized additive model has the form

$$\mathrm{E}(Y|X_1, X_2, \dots, X_p) = \alpha + f_1(X_1) + f_2(X_2) + \cdots + f_p(X_p). \tag{9.1}$$

As usual $X_1, X_2, \dots, X_p$ represent predictors and Y is the outcome; the f_j's are unspecified smooth ("nonparametric") functions. If we were to model each function using an expansion of basis functions (as in Chapter 5), the resulting model could then be fit by simple least squares. Our approach here is different: we fit each function using a scatterplot smoother (e.g., a cubic smoothing spline or kernel smoother), and provide an algorithm for simultaneously estimating all p functions (Section 9.1.1).

For two-class classification, recall the logistic regression model for binary data discussed in Section 4.4. We relate the mean of the binary response $\mu(X) = \Pr(Y = 1|X)$ to the predictors via a linear regression model and the *logit* link function:

$$\log\left(\frac{\mu(X)}{1-\mu(X)}\right) = \alpha + \beta_1 X_1 + \cdots + \beta_p X_p. \tag{9.2}$$

The *additive* logistic regression model replaces each linear term by a more general functional form

$$\log\left(\frac{\mu(X)}{1-\mu(X)}\right) = \alpha + f_1(X_1) + \cdots + f_p(X_p), \tag{9.3}$$

where again each f_j is an unspecified smooth function. While the nonparametric form for the functions f_j makes the model more flexible, the additivity is retained and allows us to interpret the model in much the same way as before. The additive logistic regression model is an example of a generalized additive model. In general, the conditional mean $\mu(X)$ of a response Y is related to an additive function of the predictors via a *link* function g:

$$g[\mu(X)] = \alpha + f_1(X_1) + \cdots + f_p(X_p). \tag{9.4}$$

Examples of classical link functions are the following:

- $g(\mu) = \mu$ is the identity link, used for linear and additive models for Gaussian response data.
- $g(\mu) = \text{logit}(\mu)$ as above, or $g(\mu) = \text{probit}(\mu)$, the *probit* link function, for modeling binomial probabilities. The probit function is the inverse Gaussian cumulative distribution function: $\text{probit}(\mu) = \Phi^{-1}(\mu)$.
- $g(\mu) = \log(\mu)$ for log-linear or log-additive models for Poisson count data.

All three of these arise from exponential family sampling models, which in addition include the gamma and negative-binomial distributions. These families generate the well-known class of generalized linear models, which are all extended in the same way to generalized additive models.

The functions f_j are estimated in a flexible manner, using an algorithm whose basic building block is a scatterplot smoother. The estimated function $\hat{f}_j$ can then reveal possible nonlinearities in the effect of X_j. Not all of the functions f_j need to be nonlinear. We can easily mix in linear and other parametric forms with the nonlinear terms, a necessity when some of the inputs are qualitative variables (factors). The nonlinear terms are not restricted to main effects either; we can have nonlinear components in two or more variables, or separate curves in X_j for each level of the factor X_k. Thus each of the following would qualify:

- $g(\mu) = X^T\beta + \alpha_k + f(Z)$—a *semiparametric* model, where X is a vector of predictors to be modeled linearly, α_k the effect for the kth level of a qualitative input V, and the effect of predictor Z is modeled nonparametrically.
- $g(\mu) = f(X) + g_k(Z)$—again k indexes the levels of a qualitative input V. and thus creates an interaction term $g(V, Z) = g_k(Z)$ for the effect of V and Z.
- $g(\mu) = f(X) + g(Z, W)$ where g is a nonparametric function in two features.

Additive models can replace linear models in a wide variety of settings, for example an additive decomposition of time series,

$$Y_t = S_t + T_t + \varepsilon_t, \tag{9.5}$$

where S_t is a seasonal component, T_t is a trend and ε is an error term.

9.1.1 *Fitting Additive Models*

In this section we describe a modular algorithm for fitting additive models and their generalizations. The building block is the scatterplot smoother for fitting nonlinear effects in a flexible way. For concreteness we use as our scatterplot smoother the cubic smoothing spline described in Chapter 5.

The additive model has the form

$$Y = \alpha + \sum_{j=1}^{p} f_j(X_j) + \varepsilon, \tag{9.6}$$

where the error term ε has mean zero. Given observations x_i, y_i, a criterion like the penalized sum of squares (5.9) of Section 5.4 can be specified for this problem,

$$\text{PRSS}(\alpha, f_1, f_2, \dots, f_p) = \sum_{i=1}^{N}\Big\{y_i - \alpha - \sum_{j=1}^{p} f_j(x_{ij})\Big\}^2 + \sum_{j=1}^{p}\lambda_j \int f_j''(t_j)^2 dt_j, \tag{9.7}$$

Algorithm 9.1 *The backfitting algorithm for additive models.*

```
1. Initialize: $\hat{\alpha} = \frac{1}{N}\sum_1^N y_i$, $\hat{f}_j \equiv 0, \forall i, j$.
2. Cycle: $j = 1, 2, \ldots, p, \ldots, 1, 2, \ldots, p, \ldots,$
       $\hat{f}_j \leftarrow \mathcal{S}_j\Big[\{y_i - \hat{\alpha} - \sum_{k \neq j} \hat{f}_k(x_{ik})\}_1^N\Big],$
       $\hat{f}_j \leftarrow \hat{f}_j - \frac{1}{N}\sum_{i=1}^N \hat{f}_j(x_{ij}).$
   until the functions $\hat{f}_j$ change less than a prespecified threshold.
```

where the $\lambda_j \geq 0$ are tuning parameters. It can be shown that the minimizer of (9.7) is an additive cubic spline model; each of the functions f_j is a cubic spline in the component X_j, with knots at each of the unique values of x_{ij}, $i = 1, \ldots, N$. However, without further restrictions on the model, the solution is not unique. The constant α is not identifiable, since we can add or subtract any constants to each of the functions f_j, and adjust α accordingly. The standard convention is to assume that $\sum_1^N f_j(x_{ij}) = 0$ $\forall j$—the functions average zero over the data. It is easily seen that $\hat{\alpha} = \text{ave}(y_i)$ in this case. If in addition to this restriction, the matrix of input values (having ijth entry x_{ij}) is nonsingular, then (9.7) is a strictly convex criterion and the minimizer is unique. If the matrix is singular, then the *linear part* of the components f_j cannot be uniquely determined (while the nonlinear parts can!)(Buja et al., 1989).

Furthermore, a simple iterative procedure exists for finding the solution. We set $\hat{\alpha} = \text{ave}(y_i)$, and it never changes. We apply a cubic smoothing spline $\mathcal{S}_k$ to the targets $\{y_i - \hat{\alpha} - \sum_{j \neq k} \hat{f}_j(x_{ij})\}_1^N$, as a function of x_{ik}, to obtain a new estimate $\hat{f}_k$. This is done for each predictor in turn, using the current estimates of the other functions $\hat{f}_j$ when computing $y_i - \hat{\alpha} - \sum_{j \neq k} \hat{f}_j(x_{ij})$. The process is continued until the estimates $\hat{f}_j$ stabilize. This procedure, given in detail in Algorithm 9.1, is known as "backfitting" and the resulting fit is analogous to a multiple regression for linear models.

In principle, the second step in (2) of Algorithm 9.1 is not needed, since the smoothing spline fit to a mean-zero response has mean zero (Exercise 9.1). In practice, machine rounding can cause slippage, and the adjustment is advised.

This same algorithm can accommodate other fitting methods in exactly the same way, by specifying appropriate smoothing operators $\mathcal{S}_j$:

- other univariate regression smoothers such as local polynomial regression and kernel methods;

- linear regression operators yielding polynomial fits, piecewise constant fits, parametric spline fits, series and Fourier fits;
- more complicated operators such as surface smoothers for second or higher-order interactions or periodic smoothers for seasonal effects.

If we consider the operation of smoother $\mathcal{S}_j$ only at the training points, it can be represented by an $N \times N$ operator matrix $\mathbf{S}_j$ (see Section 5.4.1). Then the degrees of freedom for the jth term are (approximately) computed as $\text{df}_j = \text{trace}[\mathbf{S}_j] - 1$, by analogy with degrees of freedom for smoothers discussed in Chapters 5 and 6.

For a large class of linear smoothers $\mathbf{S}_j$, backfitting is equivalent to a Gauss–Seidel algorithm for solving a certain linear system of equations. Details are given in Exercise 9.2.

For the logistic regression model and other generalized additive models, the appropriate criterion is a penalized log-likelihood. To maximize it, the backfitting procedure is used in conjunction with a likelihood maximizer. The usual Newton–Raphson routine for maximizing log-likelihoods in generalized linear models can be recast as an IRLS (iteratively reweighted least squares) algorithm. This involves repeatedly fitting a weighted linear regression of a working response variable on the covariates; each regression yields a new value of the parameter estimates, which in turn give new working responses and weights, and the process is iterated (see Section 4.4.1). In the generalized additive model, the weighted linear regression is simply replaced by a weighted backfitting algorithm. We describe the algorithm in more detail for logistic regression below, and more generally in Chapter 6 of Hastie and Tibshirani (1990).

9.1.2 Example: Additive Logistic Regression

Probably the most widely used model in medical research is the logistic model for binary data. In this model the outcome Y can be coded as 0 or 1, with 1 indicating an event (like death or relapse of a disease) and 0 indicating no event. We wish to model $\Pr(Y = 1|X)$, the probability of an event given values of the prognostic factors $X = (X_1, \ldots, X_p)$. The goal is usually to understand the roles of the prognostic factors, rather than to classify new individuals. Logistic models are also used in applications where one is interested in estimating the class probabilities, for use in risk screening. Apart from medical applications, credit risk screening is a popular application.

The generalized additive logistic model has the form

$$\log \frac{\Pr(Y = 1|X)}{\Pr(Y = 0|X)} = \alpha + f_1(X_1) + \cdots + f_p(X_p). \tag{9.8}$$

The functions $f_1, f_2, \ldots, f_p$ are estimated by a backfitting algorithm within a Newton–Raphson procedure, shown in Algorithm 9.2.

Algorithm 9.2 *Local scoring algorithm for the additive logistic regression model.*

```
1. Compute starting values: $\hat{\alpha} = \log[\bar{y}/(1-\bar{y})]$, where $\bar{y} = \text{ave}(y_i)$, the
   sample proportion of ones, and set $\hat{f}_j \equiv 0 \ \forall j$.

2. Define $\hat{\eta}_i = \hat{\alpha} + \sum_j \hat{f}_j(x_{ij})$ and $\hat{p}_i = 1/[1+\exp(-\hat{\eta}_i)]$.
   Iterate:
   (a) Construct the working target variable
           $z_i = \hat{\eta}_i + \frac{(y_i - \hat{p}_i)}{\hat{p}_i(1-\hat{p}_i)}.$
   (b) Construct weights $w_i = \hat{p}_i(1-\hat{p}_i)$
   (c) Fit an additive model to the targets $z_i$ with weights $w_i$, us-
       ing a weighted backfitting algorithm. This gives new estimates
       $\hat{\alpha}, \hat{f}_j, \ \forall j$

3. Continue step 2. until the change in the functions falls below a pre-
   specified threshold.
```

The additive model fitting in step (2) of Algorithm 9.2 requires a weighted scatterplot smoother. Most smoothing procedures can accept observation weights (Exercise 5.12); see Chapter 3 of Hastie and Tibshirani (1990) for further details.

The additive logistic regression model can be generalized further to handle more than two classes, using the multilogit formulation as outlined in 4.4. While the formulation is a straightforward extension of (9.8), the algorithms for fitting such models are more complex. See Yee and Wild (1996) for details, and the `VGAM` software currently available from:

`http://www.stat.auckland.ac.nz/PEOPLE/yee.`

Example: Predicting Email Spam

We apply a generalized additive model to the `spam` data introduced in Chapter 1. The data consists of information from 4601 email messages, in a study to screen email for "spam" (i.e., junk email). The data is publicly available at `ftp.ics.uci.edu`, and was donated by George Forman from Hewlett-Packard laboratories, Palo Alto, California.

The response variable is binary, with values `email` or `spam`, and there are 57 predictors as described below:

- 48 quantitative predictors—the percentage of words in the email that match a given word. Examples include `business`, `address`, `internet`,

TABLE 9.1. *Test data confusion matrix for the additive logistic regression model fit to the spam training data. The overall test error rate is* 5.3%.

	Predicted Class	
True Class	`email` (0)	`spam` (1)
`email` (0)	58.5%	2.5%
`spam` (1)	2.7%	36.2%

`free`, and **`george`**. The idea was that these could be customized for individual users.

- 6 quantitative predictors—the percentage of characters in the email that match a given character. The characters are **`ch;`**, **`ch(`**, **`ch[`**, **`ch!`**, **`ch$`**, and **`ch#`**.
- The average length of uninterrupted sequences of capital letters: **`CAPAVE`**.
- The length of the longest uninterrupted sequence of capital letters: **`CAPMAX`**.
- The sum of the length of uninterrupted sequences of capital letters: **`CAPTOT`**.

We coded `spam` as 1 and `email` as zero. A test set of size 1536 was randomly chosen, leaving 3065 observations in the training set. A generalized additive model was fit, using a cubic smoothing spline with a nominal four degrees of freedom for each predictor. What this means is that for each predictor X_j, the smoothing-spline parameter λ_j was chosen so that trace$[\mathbf{S}_j(\lambda_j)]-1 = 4$, where $\mathbf{S}_j(\lambda)$ is the smoothing spline operator matrix constructed using the observed values $x_{ij},\ i = 1, \dots, N$. This is a convenient way of specifying the amount of smoothing in such a complex model.

The test error rates are shown in Table 9.1; the overall error rate is 5.3%. By comparison, a linear logistic regression has a test error rate of 7.6%. Table 9.2 shows the predictors that are highly significant in the additive model.

For ease of interpretation, in Table 9.2 the contribution for each variable is decomposed into a linear component and the remaining nonlinear component. The top block of predictors are positively correlated with spam, while the bottom block is negatively correlated. The linear component is a weighted least squares linear fit of the fitted curve on the predictor, while the nonlinear part is the residual. The linear component of an estimated function is summarized by the coefficient, standard error and Z-score; the latter is the coefficient divided by its standard error, and is considered significant if it exceeds the appropriate quantile of a standard normal distribution. The column labeled *nonlinear P-value* is a test of nonlinearity

TABLE 9.2. *Significant predictors from the additive model fit to the spam training data. The coefficients represent the linear part of $\hat{f}_j$, along with their standard errors and Z-score. The nonlinear P-value is for a test of nonlinearity of $\hat{f}_j$.*

Name	Num.	df	Coefficient	Std. Error	Z Score	Nonlinear P-value
			Positive effects			
`our`	6	3.9	0.566	0.114	4.970	0.052
`over`	7	3.9	0.244	0.195	1.249	0.004
`remove`	8	4.0	0.949	0.183	5.201	0.093
`internet`	9	4.0	0.524	0.176	2.974	0.028
`free`	17	3.9	0.507	0.127	4.010	0.065
`business`	18	3.8	0.779	0.186	4.179	0.194
`hpl`	27	3.8	0.045	0.250	0.181	0.002
`ch!`	53	4.0	0.674	0.128	5.283	0.164
`ch$`	54	3.9	1.419	0.280	5.062	0.354
`CAPMAX`	57	3.8	0.247	0.228	1.080	0.000
`CAPTOT`	58	4.0	0.755	0.165	4.566	0.063
			Negative effects			
`hp`	26	3.9	-1.404	0.224	-6.262	0.140
`george`	28	3.7	-5.003	0.744	-6.722	0.045
`1999`	38	3.8	-0.672	0.191	-3.512	0.011
`re`	46	3.9	-0.620	0.133	-4.649	0.597
`edu`	47	4.0	-1.183	0.209	-5.647	0.000

of the estimated function. Note, however, that the effect of each predictor is fully adjusted for the entire effects of the other predictors, not just for their linear parts. The predictors shown in the table were judged significant by at least one of the tests (linear or nonlinear) at the $p = 0.01$ level (two-sided).

Figure 9.1 shows the estimated functions for the significant predictors appearing in Table 9.2. Many of the nonlinear effects appear to account for a strong discontinuity at zero. For example, the probability of `spam` drops significantly as the frequency of `george` increases from zero, but then does not change much after that. This suggests that one might replace each of the frequency predictors by an indicator variable for a zero count, and resort to a linear logistic model. This gave a test error rate of 7.4%; including the linear effects of the frequencies as well dropped the test error to 6.6%. It appears that the nonlinearities in the additive model have an additional predictive power.

It is more serious to classify a genuine `email` message as `spam`, since then a good email would be filtered out and would not reach the user. We can alter the balance between the class error rates by changing the losses (see Section 2.4). If we assign a loss L_{01} for predicting a true class 0 as class 1, and L_{10} for predicting a true class 1 as class 0, then the estimated Bayes

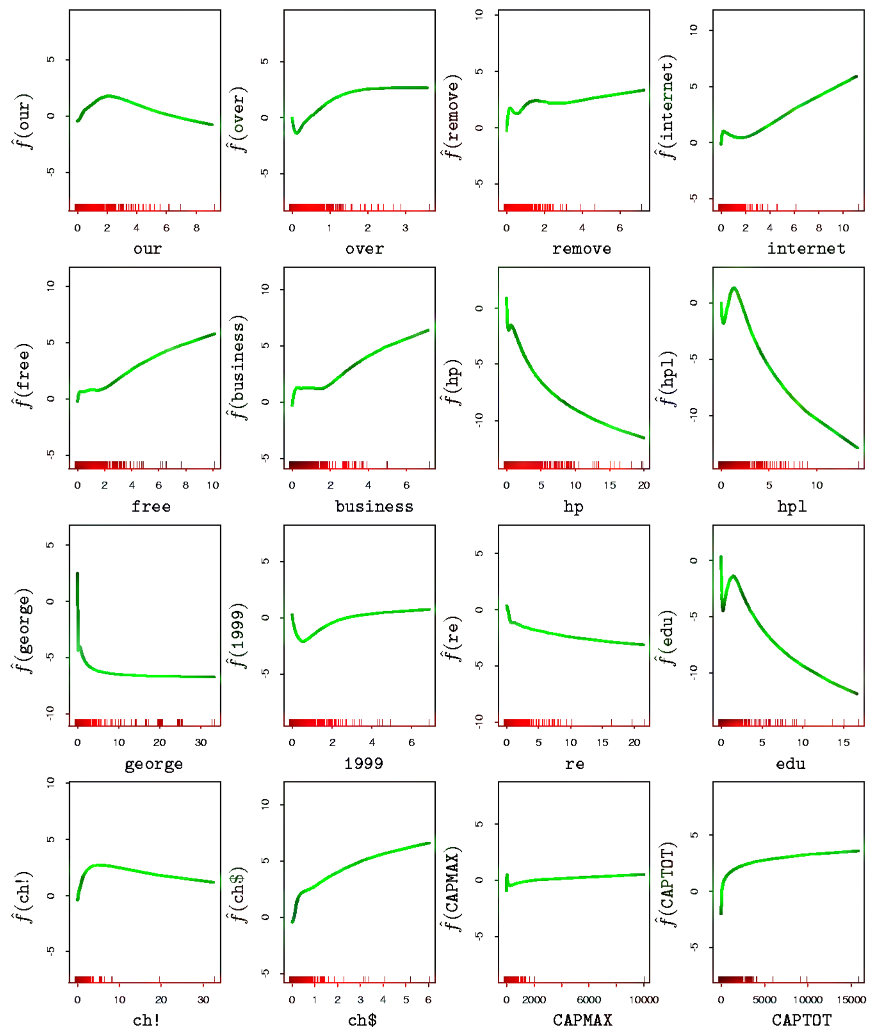

FIGURE 9.1. *Spam analysis: estimated functions for significantly predictors. The* rug plot *along the bottom of each frame indicate the observed values of the corresponding predictor. For many of the predictors the nonlinearity picks up the discontinuity at zero.*

rule predicts class 1 if its probability is greater than $L_{01}/(L_{01}+L_{10})$. For example, if we take $L_{01}=10, L_{10}=1$ then the (true) class 0 and class 1 error rates change to 0.8% and 8.7%.

More ambitiously, we can encourage the model to fit better data in the class 0 by using weights L_{01} for the class 0 observations and L_{10} for the class 1 observations. As above, we then use the estimated Bayes rule to predict. This gave error rates of 1.2% and 8.0% in (true) class 0 and class 1, respectively. We discuss below the issue of unequal losses further, in the context of tree-based models.

After fitting an additive model, one should check whether the inclusion of some interactions can significantly improve the fit. This can be done "manually," by inserting products of some or all of the significant inputs, or automatically via the MARS procedure (Section 9.4).

This example uses the additive model in an automatic fashion. As a data analysis tool, additive models are often used in a more interactive fashion, adding and dropping terms to determine their effect. By calibrating the amount of smoothing in terms of df_j, one can move seamlessly between linear models ($\text{df}_j = 1$) and partially linear models, where some terms are modeled more flexibly. See Hastie and Tibshirani (1990) for more details.

9.1.3 Summary

Additive models provide a useful extension of linear models, making them more flexible while still retaining much of their interpretability. The familiar tools for modelling and inference in linear models are also available for additive models, seen for example in Table 9.2. The backfitting procedure for fitting these models is simple and modular, allowing one to choose a fitting method appropriate for each input variable. As a result they have become widely used in the statistical community.

However additive models can have limitations for large data-mining applications. The backfitting algorithm fits all predictors, which is not feasible or desirable when a large number are available. The BRUTO procedure (Hastie and Tibshirani, 1990, Chapter 9) combines backfitting with selection of inputs, but is not designed for large data-mining problems. For these problems a forward stagewise approach such as boosting (Chapter 10) is more effective, and also allows for interactions to be included in the model.

9.2 Tree-Based Methods

9.2.1 Background

Tree-based methods partition the feature space into a set of rectangles, and then fit a simple model (like a constant) in each one. They are conceptually simple yet powerful. We first describe a popular method for tree-based regression and classification called CART, and later contrast it with C4.5, a major competitor.

Let's consider a regression problem with continuous response Y and inputs X_1 and X_2, each taking values in the unit interval. The top left panel of Figure 9.2 shows a partition of the feature space by lines that are parallel to the coordinate axes. In each partition we can model Y with a different constant. However, there is a problem: although each partitioning line has a simple description like $X_1 = c$, some of the resulting regions are complicated to describe.

To simplify matters, we restrict attention to recursive binary partitions like that in the top right panel of Figure 9.2. We first split the space into two regions, and model the response by the mean of Y in each region. We choose the variable and split-point to achieve the best fit. Then one or both of these regions are split into two more regions, and this process is continued, until some stopping rule is applied. For example, in the top right panel of Figure 9.2, we first split at $X_1 = t_1$. Then the region $X_2 \leq t_1$ is split at $X_2 = t_2$ and the region $X_1 > t_2$ is split at $X_1 = t_3$. Finally, the region $X_1 > t_3$ is split at $X_2 = t_4$. The result of this process is a partition into the five regions $R_1, R_2, \dots, R_5$ shown in the figure. The corresponding regression model predicts Y with a constant c_m in region R_m, that is,

$$\hat{f}(X) = \sum_{m=1}^{5} c_m I\{(X_1, X_2) \in R_m\}. \tag{9.9}$$

This same model can be represented by the binary tree in the bottom left panel of Figure 9.2. The full dataset sits at the top of the tree. Observations satisfying the condition at each junction are assigned to the left branch, and the others to the right branch. The terminal nodes or leaves of the tree correspond to the regions $R_1, R_2, \dots, R_5$. The bottom right panel of Figure 9.2 is a perspective plot of the regression surface from this model. For illustration, we chose the node means $c_1 = -5, c_2 = -7, c_3 = 0, c_4 = 2, c_5 = 4$ to make this plot.

A key advantage of the recursive binary tree is its interpretability. The feature space partition is fully described by a single tree. With more than two inputs, partitions like that in the top right panel of Figure 9.2 are difficult to draw, but the binary tree representation works in the same way. This representation is also popular among medical scientists, perhaps because it mimics the way that a doctor thinks. The tree stratifies the population into strata of high and low outcome, on the basis of patient characteristics.

9.2.2 *Regression Trees*

We now turn to the question of how to grow a regression tree. Our data consists of p inputs and a response, for each of N observations: that is,

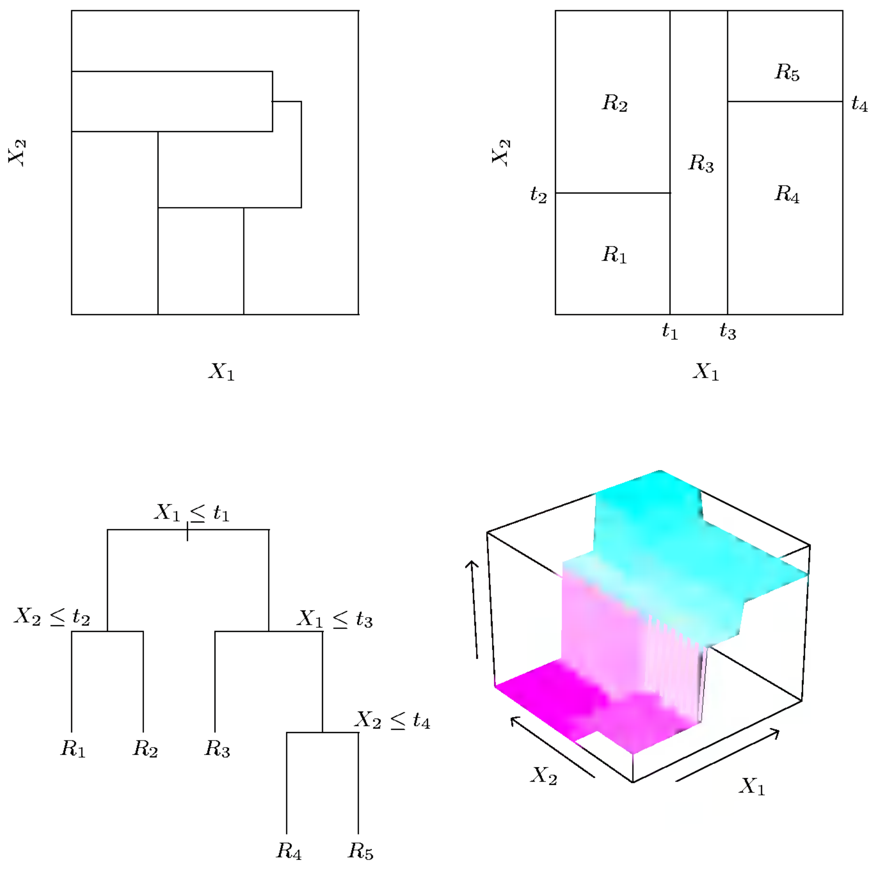

FIGURE 9.2. *Partitions and CART. Top right panel shows a partition of a two-dimensional feature space by recursive binary splitting, as used in CART, applied to some fake data. Top left panel shows a general partition that cannot be obtained from recursive binary splitting. Bottom left panel shows the tree corresponding to the partition in the top right panel, and a perspective plot of the prediction surface appears in the bottom right panel.*

(x_i, y_i) for $i = 1, 2, \ldots, N$, with $x_i = (x_{i1}, x_{i2}, \ldots, x_{ip})$. The algorithm needs to automatically decide on the splitting variables and split points, and also what topology (shape) the tree should have. Suppose first that we have a partition into M regions $R_1, R_2, \ldots, R_M$, and we model the response as a constant c_m in each region:

$$f(x) = \sum_{m=1}^{M} c_m I(x \in R_m). \tag{9.10}$$

If we adopt as our criterion minimization of the sum of squares $\sum(y_i - f(x_i))^2$, it is easy to see that the best $\hat{c}_m$ is just the average of y_i in region R_m:

$$\hat{c}_m = \operatorname{ave}(y_i | x_i \in R_m). \tag{9.11}$$

Now finding the best binary partition in terms of minimum sum of squares is generally computationally infeasible. Hence we proceed with a greedy algorithm. Starting with all of the data, consider a splitting variable j and split point s, and define the pair of half-planes

$$R_1(j, s) = \{X | X_j \leq s\} \text{ and } R_2(j, s) = \{X | X_j > s\}. \tag{9.12}$$

Then we seek the splitting variable j and split point s that solve

$$\min_{j,\, s}\Big[\min_{c_1} \sum_{x_i \in R_1(j,s)} (y_i - c_1)^2 + \min_{c_2} \sum_{x_i \in R_2(j,s)} (y_i - c_2)^2\Big]. \tag{9.13}$$

For any choice j and s, the inner minimization is solved by

$$\hat{c}_1 = \operatorname{ave}(y_i | x_i \in R_1(j, s)) \text{ and } \hat{c}_2 = \operatorname{ave}(y_i | x_i \in R_2(j, s)). \tag{9.14}$$

For each splitting variable, the determination of the split point s can be done very quickly and hence by scanning through all of the inputs, determination of the best pair (j, s) is feasible.

Having found the best split, we partition the data into the two resulting regions and repeat the splitting process on each of the two regions. Then this process is repeated on all of the resulting regions.

How large should we grow the tree? Clearly a very large tree might overfit the data, while a small tree might not capture the important structure. Tree size is a tuning parameter governing the model's complexity, and the optimal tree size should be adaptively chosen from the data. One approach would be to split tree nodes only if the decrease in sum-of-squares due to the split exceeds some threshold. This strategy is too short-sighted, however, since a seemingly worthless split might lead to a very good split below it.

The preferred strategy is to grow a large tree T_0, stopping the splitting process only when some minimum node size (say 5) is reached. Then this large tree is pruned using *cost-complexity pruning*, which we now describe.

We define a subtree $T \subset T_0$ to be any tree that can be obtained by pruning T_0, that is, collapsing any number of its internal (non-terminal) nodes. We index terminal nodes by m, with node m representing region R_m. Let $|T|$ denote the number of terminal nodes in T. Letting

$$\begin{aligned} \hat{c}_m &= \frac{1}{N_m} \sum_{x_i \in R_m} y_i, \\ Q_m(T) &= \frac{1}{N_m} \sum_{x_i \in R_m} (y_i - \hat{c}_m)^2, \end{aligned} \tag{9.15}$$

we define the cost complexity criterion

$$C_\alpha(T) = \sum_{m=1}^{|T|} N_m Q_m(T) + \alpha |T|. \tag{9.16}$$

The idea is to find, for each α, the subtree $T_\alpha \subseteq T_0$ to minimize $C_\alpha(T)$. The tuning parameter $\alpha \geq 0$ governs the tradeoff between tree size and its goodness of fit to the data. Large values of α result in smaller trees T_α, and conversely for smaller values of α. As the notation suggests, with $\alpha = 0$ the solution is the full tree T_0. We discuss how to adaptively choose α below.

For each α one can show that there is a unique smallest subtree T_α that minimizes $C_\alpha(T)$. To find T_α we use *weakest link pruning*: we successively collapse the internal node that produces the smallest per-node increase in $\sum_m N_m Q_m(T)$, and continue until we produce the single-node (root) tree. This gives a (finite) sequence of subtrees, and one can show this sequence must contains T_α. See Breiman et al. (1984) or Ripley (1996) for details. Estimation of α is achieved by five- or tenfold cross-validation: we choose the value $\hat{\alpha}$ to minimize the cross-validated sum of squares. Our final tree is $T_{\hat{\alpha}}$.

9.2.3 *Classification Trees*

If the target is a classification outcome taking values $1, 2, \ldots, K$, the only changes needed in the tree algorithm pertain to the criteria for splitting nodes and pruning the tree. For regression we used the squared-error node impurity measure $Q_m(T)$ defined in (9.15), but this is not suitable for classification. In a node m, representing a region R_m with N_m observations, let

$$\hat{p}_{mk} = \frac{1}{N_m} \sum_{x_i \in R_m} I(y_i = k),$$

the proportion of class k observations in node m. We classify the observations in node m to class $k(m) = \arg\max_k \hat{p}_{km}$, the majority class in node

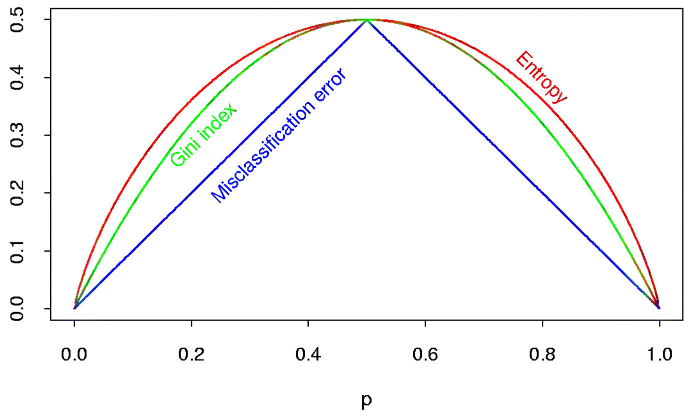

FIGURE 9.3. *Node impurity measures for two-class classification, as a function of the proportion p in class 2. Cross-entropy has been scaled to pass through* $(0.5, 0.5)$.

m. Different measures $Q_m(T)$ of node impurity include the following:

$$\begin{aligned}
&\text{Misclassification error:} && \frac{1}{N_m}\sum_{i\in R_m} I(y_i \neq k(m)) = 1-\hat{p}_{mk(m)}.\\
&\text{Gini index:} && \sum_{k\neq k'}\hat{p}_{mk}\hat{p}_{mk'} = \sum_{k=1}^{K}\hat{p}_{mk}(1-\hat{p}_{mk}).\\
&\text{Cross-entropy or deviance:} && -\sum_{k=1}^{K}\hat{p}_{mk}\log\hat{p}_{mk}.
\end{aligned} \tag{9.17}$$

For two classes, if p is the proportion in the second class, these three measures are $1 - \max(p, 1-p)$, $2p(1-p)$ and $-p\log p - (1-p)\log(1-p)$, respectively. They are shown in Figure 9.3. All three are similar, but cross-entropy and the Gini index are differentiable, and hence more amenable to numerical optimization.

In addition, cross-entropy and the Gini index are more sensitive to changes in the node probabilities than the misclassification rate. For example, in a two-class problem with 400 observations in each class (denote this by $(400, 400)$), suppose one split created nodes $(300, 100)$ and $(100, 300)$, while the other created nodes $(200, 400)$ and $(200, 0)$. Both splits produce a misclassification rate of 0.25, but the second split produces a pure node and is probably preferable. Both the Gini index and cross-entropy are lower for the second split. For this reason, either the Gini index or cross-entropy should be used when growing the tree. To guide cost-complexity pruning, any of the three measures can be used, but typically it is the misclassification rate.

The Gini index can be interpreted in two interesting ways. Rather than classify observations to the majority class in the node, we could classify them to class k with probability $\hat{p}_{mk}$. Then the training error rate of this rule in the node is $\sum_{k\neq k'}\hat{p}_{mk}\hat{p}_{mk'}$—the Gini index. Similarly, if we code each observation as 1 for class k and zero otherwise, the variance over the node of this 0-1 response is $\hat{p}_{mk}(1-\hat{p}_{mk})$. Summing over classes k again gives the Gini index.

9.2.4 Other Issues

Categorical Predictors

When splitting a predictor having q possible unordered values, there are 2^{q-1} possible partitions of the q values into two groups, and the computations become prohibitive for large q. However, with a binary 0-1 outcome, this computation can be greatly simplified. We simply order the predictor classes according to the proportion falling in outcome class 1. Then we split this predictor as if it were an ordered predictor. One can show this gives the optimal split, in terms squared error or Gini index, among all possible 2^{q-1} splits. This result also holds for a quantitative outcome—the categories are ordered by increasing mean of the outcome (Breiman et al., 1984).

The Loss Matrix

In classification problems, the consequences of misclassifying observations are more serious in some classes than others. For example it is probably worse to predict that a person will not have a heart attack when he/she actually will, than vice versa. To account for this, we define a $K \times K$ loss matrix $\mathbf{L}$, with $L_{kk'}$ being the loss incurred for classifying a class k observation as class k'. Typically no loss is incurred for correct classifications, that is, $L_{kk} = 0\ \forall k$. To incorporate the losses into the modeling process, we could modify the Gini index to $\sum_{k \neq k'} L_{kk'} \hat{p}_{mk} \hat{p}_{mk'}$; this would be the expected loss incurred by the randomized rule. This works for the multiclass case, but in the two-class case has no effect, since the coefficient of $\hat{p}_{mk}\hat{p}_{mk'}$ is $L_{kk'} + L_{k'k'}$. For two classes a better approach is to weight the observations in class k by $L_{kk'}$. This can be used in the multiclass case only if, as a function of k, $L_{kk'}$ doesn't depend on k'. Observation weighting can be used with the deviance as well. The effect of observation weighting is to alter the prior probability on the classes. In a terminal node, the empirical Bayes rule implies that we classify to class $k(m) = \arg\min_k \sum_\ell L_{\ell k} \hat{p}_{m\ell}$.

Missing Predictor Values

Suppose our data has some missing predictor values in some or all of the variables. We might discard any observation with some missing values, but this could lead to serious depletion of the training set. Alternatively we might try to fill in (impute) the missing values, with say the mean of that predictor over the nonmissing observations. For tree-based models, there are two better approaches. The first is applicable to categorical predictors: we simply make a new category for "missing." From this we might discover that observations with missing values for some measurement behave differently than those with nonmissing values. The second more general approach is the construction of surrogate variables. When considering a predictor for a split, we use only the observations for which that predictor is not missing. Having chosen the best (primary) predictor and split point, we form a list of surrogate predictors and split points. The first surrogate is the predictor and corresponding split point that best mimics the split of the training data achieved by the primary split. The second surrogate is the predictor and corresponding split point that does second best, and so on. When sending observations down the tree either in the training phase or during prediction, we use the surrogate splits in order, if the primary spitting predictor is missing. Surrogate splits exploit correlations between predictors to try and alleviate the effect of missing data. The higher the correlation between the missing predictor and the other predictors, the smaller the loss of information due to the missing value. The general problem of missing data is discussed in Section 9.6,

Why Binary Splits?

Rather than splitting each node into just two groups at each stage (as above), we might consider multiway splits into more than two groups. While this can sometimes be useful, it is not a good general strategy. The problem is that multiway splits fragment the data too quickly, leaving insufficient data at the next level down. Hence we would want to use such splits only when needed. Since multiway splits can be achieved by a series of binary splits, the latter are preferred.

Other Tree Building Procedures

The discussion above focuses on the CART (classification and regression tree) implementation of trees. The other popular methodology is ID3 and its later versions, C4.5 and C5.0 (Quinlan, 1993). Early versions of the program were limited to categorical predictors, and used a top-down rule with no pruning. With more recent developments, C5.0 has become quite similar to CART. The most significant feature unique to C5.0 is a scheme for deriving rule sets. After a tree is grown, the splitting rules that define the terminal nodes can sometimes be simplified: that is, one or more condition can be dropped without changing the subset of observations that fall in the node. We end up with a simplified set of rules defining each terminal node; these no longer follow a tree structure, but their simplicity might make them more attractive to the user.

Linear Combination Splits

Rather than restricting splits to be of the form $X_j \leq s$, one can allow splits along linear combinations of the form $\sum a_j X_j \leq s$. The weights a_j and split point s are optimized to minimize the relevant criterion (such as the

Gini index). While this can improve the predictive power of the tree, it can hurt interpretability. Computationally, the discreteness of the split point search precludes the use of a smooth optimization for the weights. A better way to incorporate linear combination splits is in the hierarchical mixtures of experts (HME) model, the topic of Section 9.5.

Instability of Trees

One major problem with trees is their high variance. Often a small change in the data can result in a very different series of splits, making interpretation somewhat precarious. The major reason for this instability is the hierarchical nature of the process: the effect of an error in the top split is propagated down to all of the splits below it. One can alleviate this to some degree by trying to use a more stable split criterion, but the inherent instability is not removed. It is the price to be paid for estimating a simple, tree-based structure from the data. *Bagging* (Section 8.7) averages many trees to reduce this variance.

Lack of Smoothness

Another limitation of trees is the lack of smoothness of the prediction surface, as can be seen in the bottom right panel of Figure 9.2. In classification with 0/1 loss, this doesn't hurt much, since bias in estimation of the class probabilities has a limited effect. However, this can degrade performance in the regression setting, where we would normally expect the underlying function to be smooth. The MARS procedure, described in Section 9.4, can be viewed as a modification of CART designed to alleviate this lack of smoothness.

Difficulty in Capturing Additive Structure

Another problem with trees is their difficulty in modeling additive structure. In regression, suppose for example that $Y = c_1 I(X_1 < t_1) + c_2 I(X_2 < t_2) + \varepsilon$ where ε is zero-mean noise. Then a binary tree might make its first split on X_1 near t_1. At the next level down it would have to split both nodes on X_2 at t_2 in order to capture the additive structure. This might happen with sufficient data, but the model is given no special encouragement to find such structure. If there were ten rather than two additive effects, it would take many fortuitous splits to recreate the structure, and the data analyst would be hard pressed to recognize it in the estimated tree. The "blame" here can again be attributed to the binary tree structure, which has both advantages and drawbacks. Again the MARS method (Section 9.4) gives up this tree structure in order to capture additive structure.

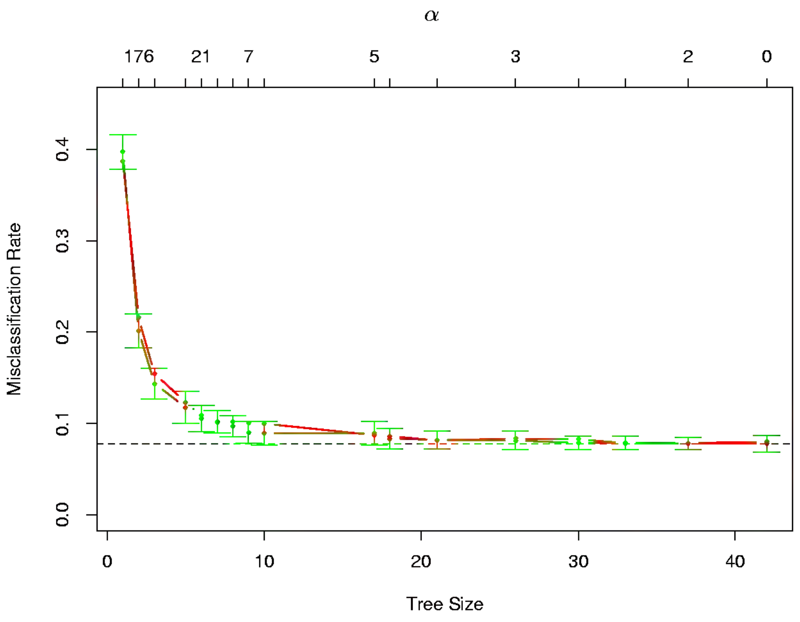

FIGURE 9.4. *Results for* `spam` *example. The green curve is the tenfold cross-validation estimate of misclassification rate as a function of tree size, with* $\pm$ *two standard error bars. The minimum occurs at a tree size with about* 17 *terminal nodes. The red curve is the test error, which tracks the CV error quite closely. The cross-validation was indexed by values of* α*, shown above. The tree sizes shown below refer to* $|T_\alpha|$*, the size of the original tree indexed by* α*.*

9.2.5 Spam Example (Continued)

We applied the classification tree methodology to the `spam` example introduced earlier. We used the deviance measure to grow the tree and misclassification rate to prune it. Figure 9.4 shows the tenfold cross-validation error rate as a function of the size of the pruned tree, along with ± 2 standard errors of the mean, from the ten replications. The test error curve is shown in red. Note that the cross-validation error rates are indexed by a sequence of values of α and *not* tree size; for trees grown in different folds, a value of α might imply different sizes. The sizes shown at the base of the plot refer to $|T_\alpha|$, the sizes of the pruned *original* tree.

The error flattens out at around 17 terminal nodes, giving the pruned tree in Figure 9.5. Of the 13 distinct features chosen by the tree, 11 overlap with the 16 significant features in the additive model (Table 9.2). The overall error rate show in Table 9.3 is about 50% higher than for the additive model in Table 9.1.

Consider the rightmost branches of the tree. We branch to the right with a `spam` warning if more than 5.5% of the characters are the $ sign.

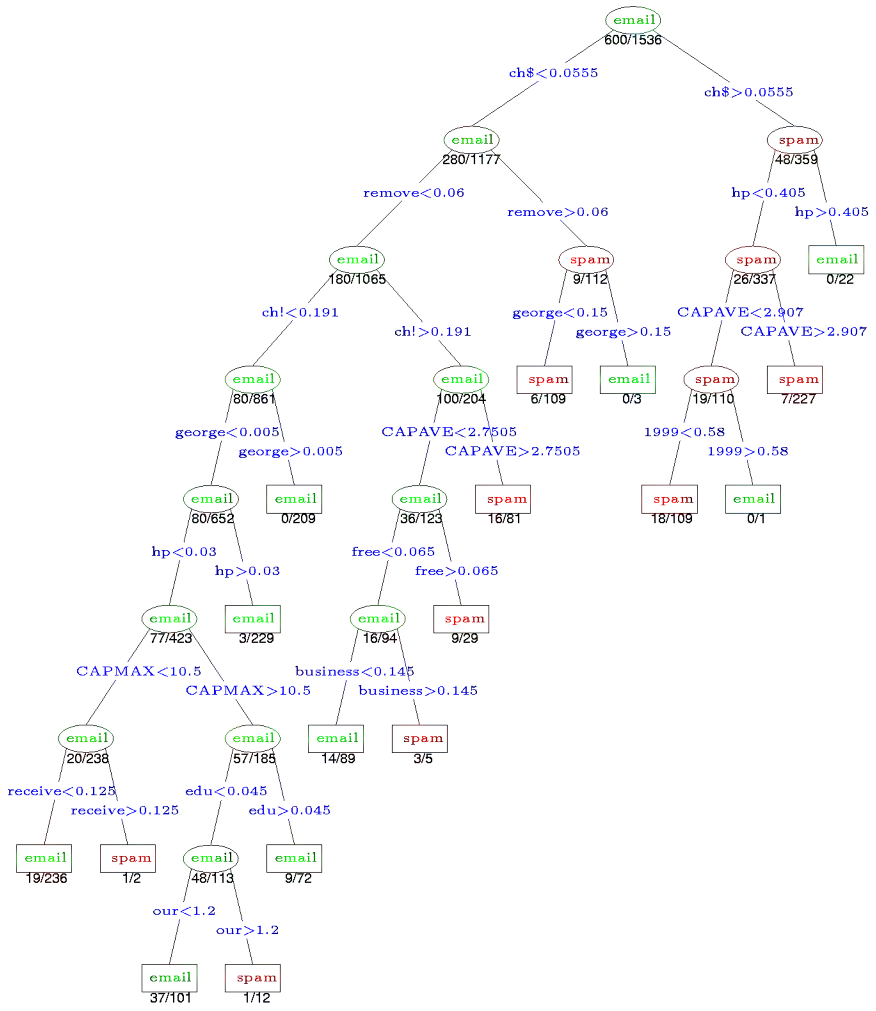

FIGURE 9.5. *The pruned tree for the* `spam` *example. The split variables are shown in blue on the branches, and the classification is shown in every node. The numbers under the terminal nodes indicate misclassification rates on the test data.*

TABLE 9.3. *Spam data: confusion rates for the 17-node tree (chosen by cross-validation) on the test data. Overall error rate is 8.7%.*

	Predicted	
True	`email`	`spam`
`email`	57.3%	4.0%
`spam`	5.3%	33.4%

However, if in addition the phrase `hp` occurs frequently, then this is likely to be company business and we classify as `email`. All of the 22 cases in the test set satisfying these criteria were correctly classified. If the second condition is not met, and in addition the average length of repeated capital letters `CAPAVE` is larger than 2.9, then we classify as `spam`. Of the 227 test cases, only seven were misclassified.

In medical classification problems, the terms *sensitivity* and *specificity* are used to characterize a rule. They are defined as follows:

Sensitivity: probability of predicting disease given true state is disease.

Specificity: probability of predicting non-disease given true state is non-disease.

If we think of `spam` and `email` as presence and absence of disease, respectively, then from Table 9.3 we have

$$\begin{aligned} \textit{Sensitivity} &= 100 \times \frac{33.4}{33.4+5.3} = 86.3\%, \\ \textit{Specificity} &= 100 \times \frac{57.3}{57.3+4.0} = 93.4\%. \end{aligned}$$

In this analysis we have used equal losses. As before let $L_{kk'}$ be the loss associated with predicting a class k object as class k'. By varying the relative sizes of the losses L_{01} and L_{10}, we increase the sensitivity and decrease the specificity of the rule, or vice versa. In this example, we want to avoid marking good `email` as `spam`, and thus we want the specificity to be very high. We can achieve this by setting $L_{01} > 1$ say, with $L_{10} = 1$. The Bayes' rule in each terminal node classifies to class 1 (`spam`) if the proportion of `spam` is $\geq L_{10}/(L_{10} + L_{01})$, and class zero otherwise. The receiver operating characteristic curve (ROC) is a commonly used summary for assessing the tradeoff between sensitivity and specificity. It is a plot of the sensitivity versus specificity as we vary the parameters of a classification rule. Varying the loss L_{01} between 0.1 and 10, and applying Bayes' rule to the 17-node tree selected in Figure 9.4, produced the ROC curve shown in Figure 9.6. We see that in order to achieve a specificity of close to 100%, the sensitivity has to drop to about 50%. The area under the curve is a commonly used quantitative summary; extending the curve linearly in each direction so that it is defined over $[0, 100]$, the area is approximately 0.95. For comparison, we have included the ROC curve for the GAM model fit to these data in Section 9.2; it gives a better classification rule for any loss, with an area of 0.98.

Rather than just modifying the Bayes rule in the nodes, it is better to take full account of the unequal losses in growing the tree, as was done in Section 9.2. With just two classes 0 and 1, losses may be incorporated into the tree-growing process by using weight $L_{k,1-k}$ for an observation in

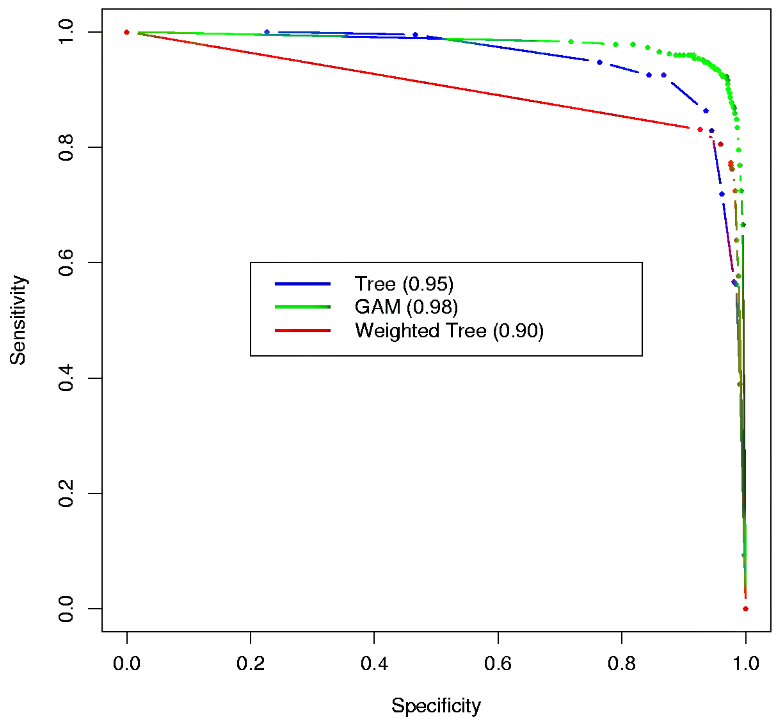

FIGURE 9.6. *ROC curves for the classification rules fit to the* `spam` *data. Curves that are closer to the northeast corner represent better classifiers. In this case the GAM classifier dominates the trees. The weighted tree achieves better sensitivity for higher specificity than the unweighted tree. The numbers in the legend represent the area under the curve.*

class k. Here we chose $L_{01} = 5$, $L_{10} = 1$ and fit the same size tree as before ($|T_\alpha| = 17$). This tree has higher sensitivity at high values of the specificity than the original tree, but does more poorly at the other extreme. Its top few splits are the same as the original tree, and then it departs from it. For this application the tree grown using $L_{01} = 5$ is clearly better than the original tree.

9.3 PRIM—Bump Hunting

Tree-based methods (for regression) partition the feature space into box-shaped regions, to try to make the response averages in each box as different as possible. The splitting rules defining the boxes are related to each through a binary tree, facilitating their interpretation.

The patient rule induction method (PRIM) also finds boxes in the feature space, but seeks boxes in which the response average is high. Hence it looks for maxima in the target function, an exercise known as *bump hunting*. (If minima rather than maxima are desired, one simply works with the negative response values.)

PRIM also differs from tree-based partitioning methods in that the box definitions are not described by a binary tree. This makes interpretation of the collection of rules more difficult; however, by removing the binary tree constraint, the individual rules are often simpler.

The main box construction method in PRIM works from the top down, starting with a box containing all of the data. The box is compressed along one face by a small amount, and the observations then falling outside the box are *peeled* off. The face chosen for compression is the one resulting in the largest box mean, after the compression is performed. Then the process is repeated, stopping when the current box contains some minimum number of data points.

This process is illustrated in Figure 9.7. There are 200 data points uniformly distributed over the unit square. The color-coded plot indicates the response Y taking the value 1 (red) when $0.5 < X_1 < 0.8$ and $0.4 < X_2 < 0.6$. and zero (blue) otherwise. The panels shows the successive boxes found by the top-down peeling procedure, peeling off a proportion $\alpha = 0.1$ of the remaining data points at each stage.

Figure 9.8 shows the mean of the response values in the box, as the box is compressed.

After the top-down sequence is computed, PRIM reverses the process, expanding along any edge, if such an expansion increases the box mean. This is called *pasting*. Since the top-down procedure is greedy at each step, such an expansion is often possible.

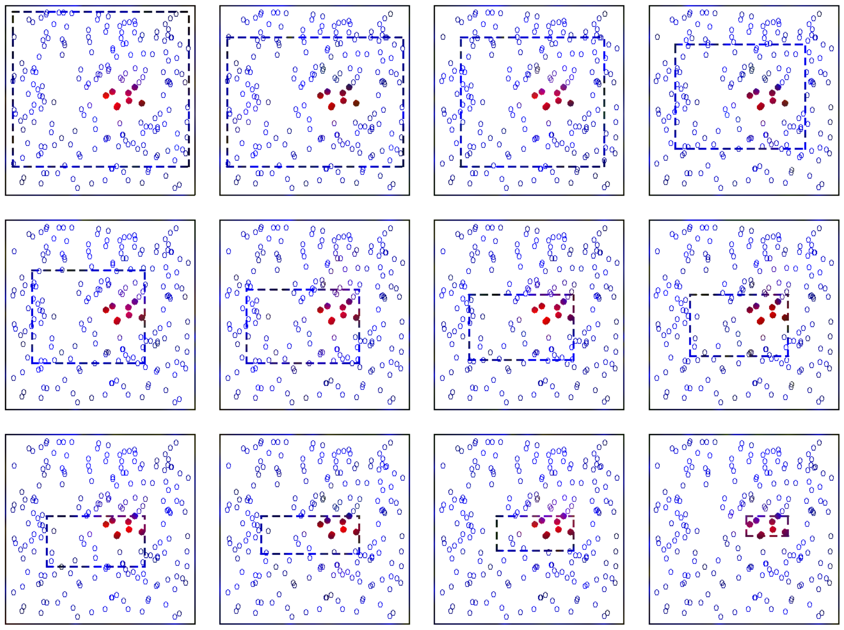

FIGURE 9.7. *Illustration of PRIM algorithm. There are two classes, indicated by the blue (class* 0*) and red (class* 1*) points. The procedure starts with a rectangle (shown in orange) surrounding all of the data, and then peels away points along one edge by a prespecified amount in order to maximize the mean of the points remaining in the box. Starting at the top left panel, the sequence of peelings is shown, until a pure red region is isolated in the bottom right panel.*

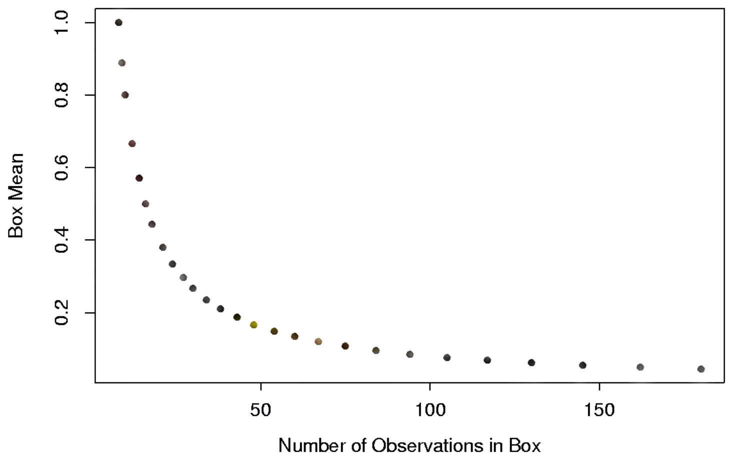

FIGURE 9.8. *Box mean as a function of number of observations in the box.*

Algorithm 9.3 *Patient rule-induction method.*

1. Start with all of the training data, and a maximal box containing all of the data.
2. Consider shrinking the box by compressing one face, so as to peel off the proportion α of observations having either the highest values of a predictor X_j, or the lowest. Choose the peeling that produces the highest response mean in the remaining box. (Typically $\alpha = 0.05$ or 0.10.)
3. Repeat step 2 until some minimal number of observations (say 10) remain in the box.
4. Expand the box along any face, as long as the resulting box mean increases.
5. Steps 1–4 give a sequence of boxes, with different numbers of observations in each box. Use cross-validation to choose a member of the sequence. Call the box B_1.
6. Remove the data in box B_1 from the dataset and repeat steps 2–5 to obtain a second box, and continue to get as many boxes as desired.

The result of these steps is a sequence of boxes, with different numbers of observation in each box. Cross-validation, combined with the judgment of the data analyst, is used to choose the optimal box size.

Denote by B_1 the indices of the observations in the box found in step 1. The PRIM procedure then removes the observations in B_1 from the training set, and the two-step process—top down peeling, followed by bottom-up pasting—is repeated on the remaining dataset. This entire process is repeated several times, producing a sequence of boxes $B_1, B_2, \dots, B_k$. Each box is defined by a set of rules involving a subset of predictors like

$$(a_1 \le X_1 \le b_1) \text{ and } (b_1 \le X_3 \le b_2).$$

A summary of the PRIM procedure is given Algorithm 9.3.

PRIM can handle a categorical predictor by considering all partitions of the predictor, as in CART. Missing values are also handled in a manner similar to CART. PRIM is designed for regression (quantitative response variable); a two-class outcome can be handled simply by coding it as 0 and 1. There is no simple way to deal with $k > 2$ classes simultaneously: one approach is to run PRIM separately for each class versus a baseline class.

An advantage of PRIM over CART is its patience. Because of its binary splits, CART fragments the data quite quickly. Assuming splits of equal size, with N observations it can only make $\log_2(N) - 1$ splits before running out of data. If PRIM peels off a proportion α of training points at each stage, it can perform approximately $-\log(N)/\log(1-\alpha)$ peeling steps before running out of data. For example, if $N = 128$ and $\alpha = 0.10$, then $\log_2(N) - 1 = 6$ while $-\log(N)/\log(1-\alpha) \approx 46$. Taking into account that there must be an integer number of observations at each stage, PRIM in fact can peel only 29 times. In any case, the ability of PRIM to be more patient should help the top-down greedy algorithm find a better solution.

9.3.1 Spam Example (Continued)

We applied PRIM to the `spam` data, with the response coded as 1 for `spam` and 0 for `email`.

The first two boxes found by PRIM are summarized below:

Rule 1	Global Mean	Box Mean	Box Support
Training	0.3931	0.9607	0.1413
Test	0.3958	1.0000	0.1536

$$\text{Rule 1} \left\{ \begin{array}{rcl} \texttt{ch!} & > & 0.029 \\ \texttt{CAPAVE} & > & 2.331 \\ \texttt{your} & > & 0.705 \\ \texttt{1999} & < & 0.040 \\ \texttt{CAPTOT} & > & 79.50 \\ \texttt{edu} & < & 0.070 \\ \texttt{re} & < & 0.535 \\ \texttt{ch;} & < & 0.030 \end{array} \right.$$

Rule 2	Remain Mean	Box Mean	Box Support
Training	0.2998	0.9560	0.1043
Test	0.2862	0.9264	0.1061

$$\text{Rule 2} \left\{ \begin{array}{rcl} \texttt{remove} & > & 0.010 \\ \texttt{george} & < & 0.110 \end{array} \right.$$

The box support is the proportion of observations falling in the box. The first box is purely `spam`, and contains about 15% of the test data. The second box contains 10.6% of the test observations, 92.6% of which are `spam`. Together the two boxes contain 26% of the data and are about 97% `spam`. The next few boxes (not shown) are quite small, containing only about 3% of the data.

The predictors are listed in order of importance. Interestingly the top splitting variables in the CART tree (Figure 9.5) do not appear in PRIM's first box.

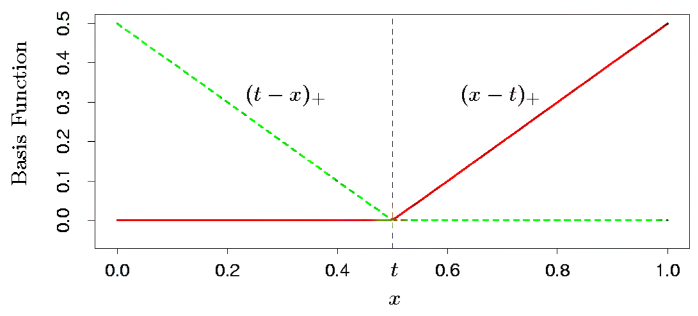

FIGURE 9.9. *The basis functions $(x-t)_+$ (solid red) and $(t-x)_+$ (broken green) used by MARS.*

9.4 MARS: Multivariate Adaptive Regression Splines

MARS is an adaptive procedure for regression, and is well suited for high-dimensional problems (i.e., a large number of inputs). It can be viewed as a generalization of stepwise linear regression or a modification of the CART method to improve the latter's performance in the regression setting. We introduce MARS from the first point of view, and later make the connection to CART.

MARS uses expansions in piecewise linear basis functions of the form $(x-t)_+$ and $(t-x)_+$. The "+" means positive part, so

$$(x-t)_+ = \begin{cases} x-t, & \text{if } x > t, \\ 0, & \text{otherwise,} \end{cases} \quad \text{and} \quad (t-x)_+ = \begin{cases} t-x, & \text{, if } x < t, \\ 0, & \text{otherwise.} \end{cases}$$

As an example, the functions $(x-0.5)_+$ and $(0.5-x)_+$ are shown in Figure 9.9.

Each function is piecewise linear, with a *knot* at the value t. In the terminology of Chapter 5, these are linear splines. We call the two functions a *reflected pair* in the discussion below. The idea is to form reflected pairs for each input X_j with knots at each observed value x_{ij} of that input. Therefore, the collection of basis functions is

$$\mathcal{C} = \{(X_j - t)_+, \ (t - X_j)_+\}_{\substack{t \in \{x_{1j}, x_{2j}, \dots, x_{Nj}\} \\ j = 1, 2, \dots, p.}} \tag{9.18}$$

If all of the input values are distinct, there are $2Np$ basis functions altogether. Note that although each basis function depends only on a single X_j, for example, $h(X) = (X_j - t)_+$, it is considered as a function over the entire input space $\mathbb{R}^p$.

The model-building strategy is like a forward stepwise linear regression, but instead of using the original inputs, we are allowed to use functions from the set $\mathcal{C}$ and their products. Thus the model has the form

$$f(X) = \beta_0 + \sum_{m=1}^{M} \beta_m h_m(X), \tag{9.19}$$

where each $h_m(X)$ is a function in $\mathcal{C}$, or a product of two or more such functions.

Given a choice for the h_m, the coefficients β_m are estimated by minimizing the residual sum-of-squares, that is, by standard linear regression. The real art, however, is in the construction of the functions $h_m(x)$. We start with only the constant function $h_0(X) = 1$ in our model, and all functions in the set $\mathcal{C}$ are candidate functions. This is depicted in Figure 9.10.

At each stage we consider as a new basis function pair all products of a function h_m in the model set $\mathcal{M}$ with one of the reflected pairs in $\mathcal{C}$. We add to the model $\mathcal{M}$ the term of the form

$$\hat{\beta}_{M+1} h_\ell(X) \cdot (X_j - t)_+ + \hat{\beta}_{M+2} h_\ell(X) \cdot (t - X_j)_+, \; h_\ell \in \mathcal{M},$$

that produces the largest decrease in training error. Here $\hat{\beta}_{M+1}$ and $\hat{\beta}_{M+2}$ are coefficients estimated by least squares, along with all the other $M+1$ coefficients in the model. Then the winning products are added to the model and the process is continued until the model set $\mathcal{M}$ contains some preset maximum number of terms.

For example, at the first stage we consider adding to the model a function of the form $\beta_1(X_j - t)_+ + \beta_2(t - X_j)_+$; $t \in \{x_{ij}\}$, since multiplication by the constant function just produces the function itself. Suppose the best choice is $\hat{\beta}_1(X_2 - x_{72})_+ + \hat{\beta}_2(x_{72} - X_2)_+$. Then this pair of basis functions is added to the set $\mathcal{M}$, and at the next stage we consider including a pair of products the form

$$h_m(X) \cdot (X_j - t)_+ \quad \text{and} \quad h_m(X) \cdot (t - X_j)_+, \; t \in \{x_{ij}\},$$

where for h_m we have the choices

$$\begin{aligned} h_0(X) &= 1, \\ h_1(X) &= (X_2 - x_{72})_+, \text{ or} \\ h_2(X) &= (x_{72} - X_2)_+. \end{aligned}$$

The third choice produces functions such as $(X_1 - x_{51})_+ \cdot (x_{72} - X_2)_+$, depicted in Figure 9.11.

At the end of this process we have a large model of the form (9.19). This model typically overfits the data, and so a backward deletion procedure is applied. The term whose removal causes the smallest increase in residual squared error is deleted from the model at each stage, producing an estimated best model $\hat{f}_\lambda$ of each size (number of terms) λ. One could use

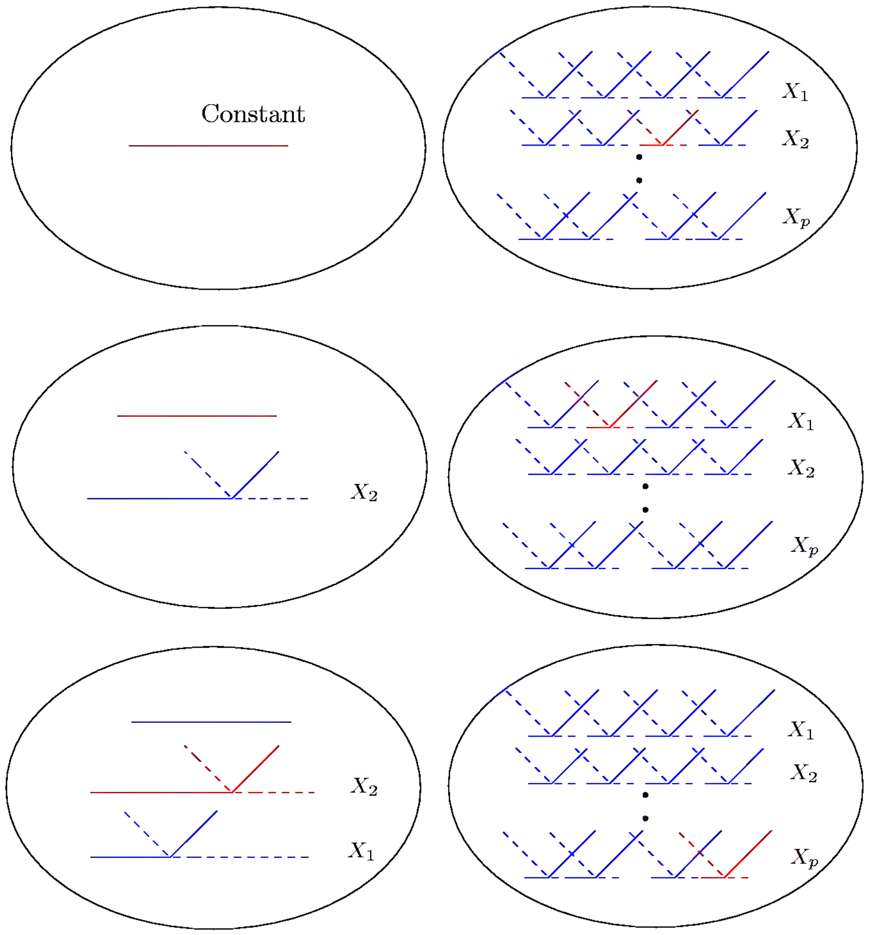

FIGURE 9.10. *Schematic of the MARS forward model-building procedure. On the left are the basis functions currently in the model: initially, this is the constant function $h(X) = 1$. On the right are all candidate basis functions to be considered in building the model. These are pairs of piecewise linear basis functions as in Figure 9.9, with knots t at all unique observed values x_{ij} of each predictor X_j. At each stage we consider all products of a candidate pair with a basis function in the model. The product that decreases the residual error the most is added into the current model. Above we illustrate the first three steps of the procedure, with the selected functions shown in red.*

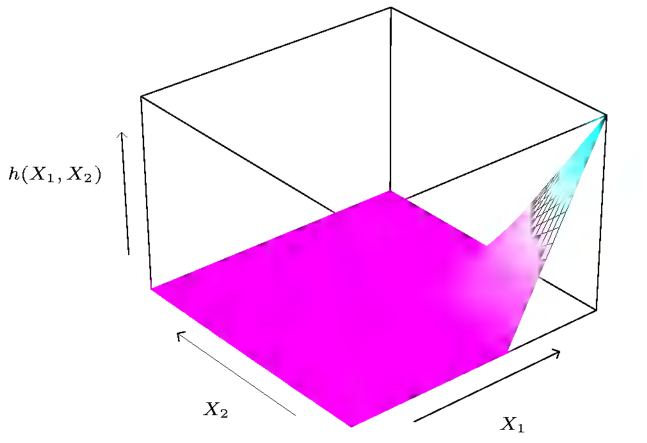

FIGURE 9.11. *The function $h(X_1, X_2) = (X_1 - x_{51})_+ \cdot (x_{72} - X_2)_+$, resulting from multiplication of two piecewise linear MARS basis functions.*

cross-validation to estimate the optimal value of λ, but for computational savings the MARS procedure instead uses generalized cross-validation. This criterion is defined as

$$\text{GCV}(\lambda) = \frac{\sum_{i=1}^{N}(y_i - \hat{f}_\lambda(x_i))^2}{(1 - M(\lambda)/N)^2}. \tag{9.20}$$

The value $M(\lambda)$ is the effective number of parameters in the model: this accounts both for the number of terms in the models, plus the number of parameters used in selecting the optimal positions of the knots. Some mathematical and simulation results suggest that one should pay a price of three parameters for selecting a knot in a piecewise linear regression.

Thus if there are r linearly independent basis functions in the model, and K knots were selected in the forward process, the formula is $M(\lambda) = r+cK$, where $c = 3$. (When the model is restricted to be additive—details below—a penalty of $c = 2$ is used). Using this, we choose the model along the backward sequence that minimizes GCV(λ).

Why these piecewise linear basis functions, and why this particular model strategy? A key property of the functions of Figure 9.9 is their ability to operate locally; they are zero over part of their range. When they are multiplied together, as in Figure 9.11, the result is nonzero only over the small part of the feature space where both component functions are nonzero. As a result, the regression surface is built up parsimoniously, using nonzero components locally—only where they are needed. This is important, since one should "spend" parameters carefully in high dimensions, as they can run out quickly. The use of other basis functions such as polynomials, would produce a nonzero product everywhere, and would not work as well.

The second important advantage of the piecewise linear basis function concerns computation. Consider the product of a function in $\mathcal{M}$ with each of the N reflected pairs for an input X_j. This appears to require the fitting of N single-input linear regression models, each of which uses $O(N)$ operations, making a total of $O(N^2)$ operations. However, we can exploit the simple form of the piecewise linear function. We first fit the reflected pair with rightmost knot. As the knot is moved successively one position at a time to the left, the basis functions differ by zero over the left part of the domain, and by a constant over the right part. Hence after each such move we can update the fit in $O(1)$ operations. This allows us to try every knot in only $O(N)$ operations.

The forward modeling strategy in MARS is hierarchical, in the sense that multiway products are built up from products involving terms already in the model. For example, a four-way product can only be added to the model if one of its three-way components is already in the model. The philosophy here is that a high-order interaction will likely only exist if some of its lower-order "footprints" exist as well. This need not be true, but is a reasonable working assumption and avoids the search over an exponentially growing space of alternatives.

There is one restriction put on the formation of model terms: each input can appear at most once in a product. This prevents the formation of higher-order powers of an input, which increase or decrease too sharply near the boundaries of the feature space. Such powers can be approximated in a more stable way with piecewise linear functions.

A useful option in the MARS procedure is to set an upper limit on the order of interaction. For example, one can set a limit of two, allowing pairwise products of piecewise linear functions, but not three- or higher-way products. This can aid in the interpretation of the final model. An upper limit of one results in an additive model.

9.4.1 Spam Example (Continued)

We applied MARS to the "spam" data analyzed earlier in this chapter. To enhance interpretability, we restricted MARS to second-degree interactions. Although the target is a two-class variable, we used the squared-error loss function nonetheless (see Section 9.4.3). Figure 9.12 shows the test error misclassification rate as a function of the rank (number of independent basis functions) in the model. The error rate levels off at about 5.5%, which is slightly higher than that of the generalized additive model (5.3%) discussed earlier. GCV chose a model size of 60, which is roughly the smallest model giving optimal performance. The leading interactions found by MARS involved inputs (`ch$, remove`), (`ch$, free`) and (`hp, crl-tot`). However, these interactions give no improvement in performance over the generalized additive model.

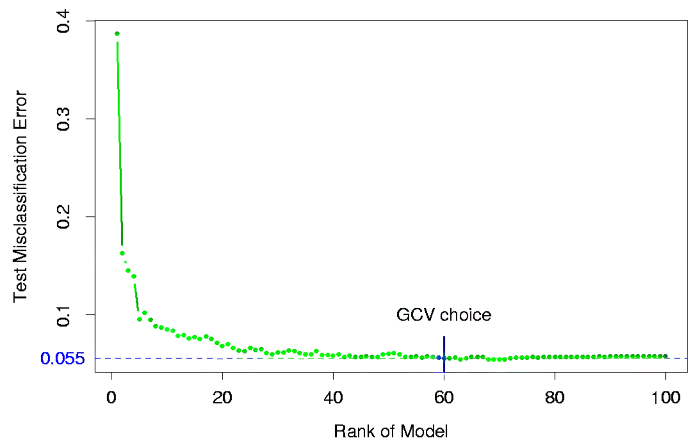

FIGURE 9.12. *Spam data: test error misclassification rate for the MARS procedure, as a function of the rank (number of independent basis functions) in the model.*

9.4.2 Example (Simulated Data)

Here we examine the performance of MARS in three contrasting scenarios. There are $N = 100$ observations, and the predictors $X_1, X_2, \dots, X_p$ and errors ε have independent standard normal distributions.

Scenario 1: The data generation model is

$$Y = (X_1 - 1)_+ + (X_1 - 1)_+ \cdot (X_2 - .8)_+ + 0.12 \cdot \varepsilon. \tag{9.21}$$

The noise standard deviation 0.12 was chosen so that the signal-to-noise ratio was about 5. We call this the tensor-product scenario; the product term gives a surface that looks like that of Figure 9.11.

Scenario 2: This is the same as scenario 1, but with $p = 20$ total predictors; that is, there are 18 inputs that are independent of the response.

Scenario 3: This has the structure of a neural network:

$$\begin{aligned} \ell_1 &= X_1 + X_2 + X_3 + X_4 + X_5, \\ \ell_2 &= X_6 - X_7 + X_8 - X_9 + X_{10}, \\ \sigma(t) &= 1/(1 + e^{-t}), \\ Y &= \sigma(\ell_1) + \sigma(\ell_2) + 0.12 \cdot \varepsilon. \end{aligned} \tag{9.22}$$

Scenarios 1 and 2 are ideally suited for MARS, while scenario 3 contains high-order interactions and may be difficult for MARS to approximate. We ran five simulations from each model, and recorded the results.

In scenario 1, MARS typically uncovered the correct model almost perfectly. In scenario 2, it found the correct structure but also found a few extraneous terms involving other predictors.

TABLE 9.4. *Proportional decrease in model error (R^2) when MARS is applied to three different scenarios.*

Scenario	Mean (S.E)
1: Tensor product $p = 2$	0.97 (0.01)
2: Tensor product $p = 20$	0.96 (0.01)
3: Neural network	0.79 (0.01)

Let $\mu(x)$ be the true mean of Y, and let

$$\begin{aligned} \text{MSE}_0 &= \text{ave}_{x \in \text{Test}}(\bar{y} - \mu(x))^2, \\ \text{MSE} &= \text{ave}_{x \in \text{Test}}(\hat{f}(x) - \mu(x))^2. \end{aligned} \tag{9.23}$$

These represent the mean-square error of the constant model and the fitted MARS model, estimated by averaging at the 1000 test values of x. Table 9.4 shows the proportional decrease in model error or R^2 for each scenario:

$$R^2 = \frac{\text{MSE}_0 - \text{MSE}}{\text{MSE}_0}. \tag{9.24}$$

The values shown are means and standard error over the five simulations. The performance of MARS is degraded only slightly by the inclusion of the useless inputs in scenario 2; it performs substantially worse in scenario 3.

9.4.3 Other Issues

MARS for Classification

The MARS method and algorithm can be extended to handle classification problems. Several strategies have been suggested.

For two classes, one can code the output as 0/1 and treat the problem as a regression; we did this for the `spam` example. For more than two classes, one can use the indicator response approach described in Section 4.2. One codes the K response classes via 0/1 indicator variables, and then performs a multiresponse MARS regression. For the latter we use a common set of basis functions for all response variables. Classification is made to the class with the largest predicted response value. There are, however, potential masking problems with this approach, as described in Section 4.2. A generally superior approach is the "optimal scoring" method discussed in Section 12.5.

Stone et al. (1997) developed a hybrid of MARS called PolyMARS specifically designed to handle classification problems. It uses the multiple logistic framework described in Section 4.4. It grows the model in a forward stagewise fashion like MARS, but at each stage uses a quadratic approximation to the multinomial log-likelihood to search for the next basis-function pair. Once found, the enlarged model is fit by maximum likelihood, and the process is repeated.

Relationship of MARS to CART

Although they might seem quite different, the MARS and CART strategies actually have strong similarities. Suppose we take the MARS procedure and make the following changes:

- Replace the piecewise linear basis functions by step functions $I(x-t > 0)$ and $I(x - t \leq 0)$.
- When a model term is involved in a multiplication by a candidate term, it gets replaced by the interaction, and hence is not available for further interactions.

With these changes, the MARS forward procedure is the same as the CART tree-growing algorithm. Multiplying a step function by a pair of reflected step functions is equivalent to splitting a node at the step. The second restriction implies that a node may not be split more than once, and leads to the attractive binary-tree representation of the CART model. On the other hand, it is this restriction that makes it difficult for CART to model additive structures. MARS foregoes the tree structure and gains the ability to capture additive effects.

Mixed Inputs

Mars can handle "mixed" predictors—quantitative and qualitative—in a natural way, much like CART does. MARS considers all possible binary partitions of the categories for a qualitative predictor into two groups. Each such partition generates a pair of piecewise constant basis functions—indicator functions for the two sets of categories. This basis pair is now treated as any other, and is used in forming tensor products with other basis functions already in the model.

9.5 Hierarchical Mixtures of Experts

The hierarchical mixtures of experts (HME) procedure can be viewed as a variant of tree-based methods. The main difference is that the tree splits are not hard decisions but rather soft probabilistic ones. At each node an observation goes left or right with probabilities depending on its input values. This has some computational advantages since the resulting parameter optimization problem is smooth, unlike the discrete split point search in the tree-based approach. The soft splits might also help in prediction accuracy and provide a useful alternative description of the data.

There are other differences between HMEs and the CART implementation of trees. In an HME, a linear (or logistic regression) model is fit in each terminal node, instead of a constant as in CART. The splits can be multiway, not just binary, and the splits are probabilistic functions of a

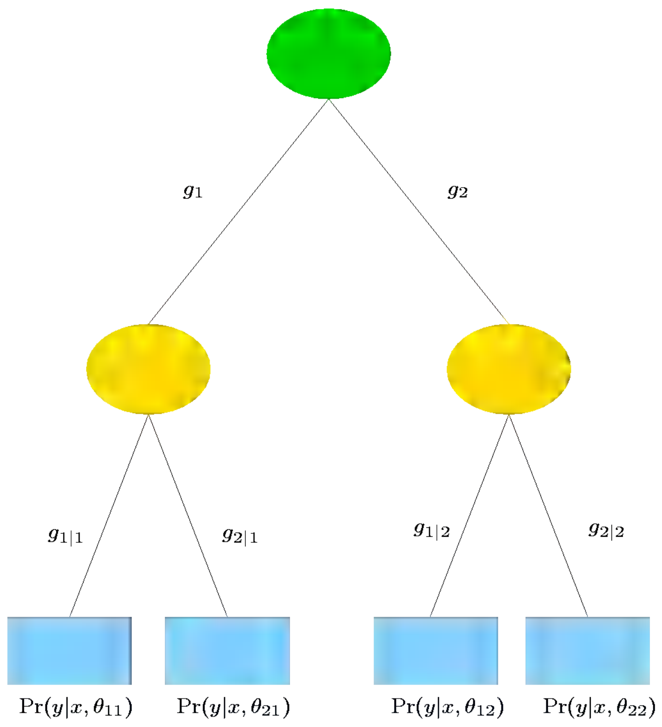

FIGURE 9.13. *A two-level hierarchical mixture of experts (HME) model.*

linear combination of inputs, rather than a single input as in the standard use of CART. However, the relative merits of these choices are not clear, and most were discussed at the end of Section 9.2.

A simple two-level HME model in shown in Figure 9.13. It can be thought of as a tree with soft splits at each non-terminal node. However, the inventors of this methodology use a different terminology. The terminal nodes are called *experts*, and the non-terminal nodes are called *gating networks*. The idea is that each expert provides an opinion (prediction) about the response, and these are combined together by the gating networks. As we will see, the model is formally a mixture model, and the two-level model in the figure can be extend to multiple levels, hence the name *hierarchical mixtures of experts*.

Consider the regression or classification problem, as described earlier in the chapter. The data is $(x_i, y_i), i = 1, 2, \ldots, N$, with y_i either a continuous or binary-valued response, and x_i a vector-valued input. For ease of notation we assume that the first element of x_i is one, to account for intercepts.

Here is how an HME is defined. The top gating network has the output

$$g_j(x, \gamma_j) = \frac{e^{\gamma_j^T x}}{\sum_{k=1}^K e^{\gamma_k^T x}}, \ j = 1, 2, \ldots, K, \tag{9.25}$$

where each γ_j is a vector of unknown parameters. This represents a soft K-way split ($K = 2$ in Figure 9.13.) Each $g_j(x, \gamma_j)$ is the probability of assigning an observation with feature vector x to the jth branch. Notice that with $K = 2$ groups, if we take the coefficient of one of the elements of x to be $+\infty$, then we get a logistic curve with infinite slope. In this case, the gating probabilities are either 0 or 1, corresponding to a hard split on that input.

At the second level, the gating networks have a similar form:

$$g_{\ell|j}(x, \gamma_{j\ell}) = \frac{e^{\gamma_{j\ell}^T x}}{\sum_{k=1}^K e^{\gamma_{jk}^T x}}, \quad \ell = 1, 2, \dots, K. \tag{9.26}$$

This is the probability of assignment to the ℓth branch, given assignment to the jth branch at the level above.

At each expert (terminal node), we have a model for the response variable of the form

$$Y \sim \Pr(y|x, \theta_{j\ell}). \tag{9.27}$$

This differs according to the problem.

Regression: The Gaussian linear regression model is used, with $\theta_{j\ell} = (\beta_{j\ell}, \sigma_{j\ell}^2)$:

$$Y = \beta_{j\ell}^T x + \varepsilon \text{ and } \varepsilon \sim N(0, \sigma_{j\ell}^2). \tag{9.28}$$

Classification: The linear logistic regression model is used:

$$\Pr(Y = 1|x, \theta_{j\ell}) = \frac{1}{1 + e^{-\theta_{j\ell}^T x}}. \tag{9.29}$$

Denoting the collection of all parameters by $\Psi = \{\gamma_j, \gamma_{j\ell}, \theta_{j\ell}\}$, the total probability that $Y = y$ is

$$\Pr(y|x, \Psi) = \sum_{j=1}^K g_j(x, \gamma_j) \sum_{\ell=1}^K g_{\ell|j}(x, \gamma_{j\ell}) \Pr(y|x, \theta_{j\ell}). \tag{9.30}$$

This is a mixture model, with the mixture probabilities determined by the gating network models.

To estimate the parameters, we maximize the log-likelihood of the data, $\sum_i \log \Pr(y_i|x_i, \Psi)$, over the parameters in Ψ. The most convenient method for doing this is the EM algorithm, which we describe for mixtures in Section 8.5. We define latent variables Δ_j, all of which are zero except for a single one. We interpret these as the branching decisions made by the top level gating network. Similarly we define latent variables $\Delta_{\ell|j}$ to describe the gating decisions at the second level.

In the E-step, the EM algorithm computes the expectations of the Δ_j and $\Delta_{\ell|j}$ given the current values of the parameters. These expectations are then used as observation weights in the M-step of the procedure, to estimate the parameters in the expert networks. The parameters in the internal nodes are estimated by a version of multiple logistic regression. The expectations of the Δ_j or $\Delta_{\ell|j}$ are probability profiles, and these are used as the response vectors for these logistic regressions.

The hierarchical mixtures of experts approach is a promising competitor to CART trees. By using *soft splits* rather than hard decision rules it can capture situations where the transition from low to high response is gradual. The log-likelihood is a smooth function of the unknown weights and hence is amenable to numerical optimization. The model is similar to CART with linear combination splits, but the latter is more difficult to optimize. On the other hand, to our knowledge there are no methods for finding a good tree topology for the HME model, as there are in CART. Typically one uses a fixed tree of some depth, possibly the output of the CART procedure. The emphasis in the research on HMEs has been on prediction rather than interpretation of the final model. A close cousin of the HME is the *latent class model* (Lin et al., 2000), which typically has only one layer; here the nodes or latent classes are interpreted as groups of subjects that show similar response behavior.

9.6 Missing Data

It is quite common to have observations with missing values for one or more input features. The usual approach is to impute (fill-in) the missing values in some way.

However, the first issue in dealing with the problem is determining whether missing data mechanism has distorted the observed data. Roughly speaking, data are missing at random if the mechanism resulting in its omission is independent of its (unobserved) value. A more precise definition is given in Little and Rubin (1987). Suppose $\mathbf{y}$ is the response vector and $\mathbf{X}$ is the $N \times p$ matrix of inputs (some of which are missing). Denote by $\mathbf{X}_{\text{obs}}$ the observed entries in $\mathbf{X}$ and let $\mathbf{Z} = (\mathbf{y}, \mathbf{X})$, $\mathbf{Z}_{\text{obs}} = (\mathbf{y}, \mathbf{X}_{\text{obs}})$. Finally, if $\mathbf{R}$ is an indicator matrix with ijth entry 1 if x_{ij} is missing and zero otherwise, then the data said to be *missing at random* (MAR) if the distribution of $\mathbf{R}$ depends on the data $\mathbf{Z}$ only through $\mathbf{Z}_{\text{obs}}$:

$$\Pr(\mathbf{R}|\mathbf{Z}, \theta) = \Pr(\mathbf{R}|\mathbf{Z}_{\text{obs}}, \theta). \tag{9.31}$$

Here θ are any parameters in the distribution of $\mathbf{R}$. Data are said to be *missing completely at random* (MCAR) if the distribution of $\mathbf{R}$ doesn't depend on the observed or missing data:

$$\Pr(\mathbf{R}|\mathbf{Z}, \theta) = \Pr(\mathbf{R}|\theta). \tag{9.32}$$

MCAR is a stronger assumption than MAR: most imputation methods rely on MCAR for their validity.

For example, if a patient's measurement was not taken because the doctor felt he was too sick, that observation would not be MAR or MCAR. In this case the missing data mechanism causes our observed training data to give a distorted picture of the true population, and data imputation is dangerous in this instance. Often the determination of whether features are MCAR must be made from information about the data collection process. For categorical features, one way to diagnose this problem is to code "missing" as an addition class. Then we fit our model to the training data and see if class "missing" is predictive of the response.

Assuming the features are missing completely at random, there are a number of ways of proceeding:

1. Discard observations with any missing values.

2. Rely on the learning algorithm to deal with missing values in its training phase.

3. Impute all missing values before training.

Approach (1) can be used if the relative amount of missing data is small, but otherwise should be avoided. Regarding (2), CART is one learning algorithm that deals effectively with missing values, through *surrogate splits* (Section 9.2.4). MARS and PRIM use similar approaches. In generalized additive modelling, all observations missing for a given input feature are omitted when the partial residuals are smoothed against that feature in the backfitting algorithm, and their fitted values are set to zero. Since the fitted curves have mean zero (when the model includes an intercept), this amounts to assigning the average fitted value to the missing observations.

For most learning methods, the imputation approach (3) is necessary. The simplest tactic is to impute the missing value with the mean or median of the nonmissing values for that feature. (Note that the above procedure for generalized additive models is analogous to this.)

If the features have at least some moderate degree of dependence, one can do better by estimating a predictive model for each feature given the other features and then imputing each missing value by its prediction from the model. In choosing the learning method for imputation of the features, one must remember that this choice is distinct from the method used for predicting $\mathbf{y}$ from $\mathbf{X}$. Thus a flexible, adaptive method will often be preferred, even for the eventual purpose of carrying out a linear regression of $\mathbf{y}$ on $\mathbf{X}$. In addition if there any many missing feature values in the training set, the learning method must itself be able to deal with missing feature values. CART therefore is an ideal choice for this imputation "engine."

After imputation, missing values are typically treated as if they were actually observed. This ignores the uncertainty due to the imputation, which will itself introduces additional uncertainty into estimates and predictions from the response model. One can measure this additional uncertainty by doing multiple imputations and hence creating many different training sets. The predictive model for $\mathbf{y}$ can be fit to each training set, and the variation across training sets can be assessed. If CART was used for the imputation engine, the multiple imputations could be done by sampling from the values in the corresponding terminal nodes.

9.7 Computational Considerations

With N observations and p predictors, additive model fitting requires some number mp of applications of a one-dimensional smoother or regression method. The required number of cycles m of the backfitting algorithm is usually less than 20 and often less than 10, and depends on the amount of correlation in the inputs. With cubic smoothing splines, for example, $N \log N$ operations are needed for an initial sort and N operations for the spline fit. Hence the total operations for an additive model fit is $pN \log N + mpN$.

Trees require $pN \log N$ operations for an initial sort for each predictor, and typically another $pN \log N$ operations for the split computations. If the splits occurred near the edges of the predictor ranges, this number could increase to N^2p.

MARS requires $Nm^2 + pmN$ operations to add a basis function to a model with m terms already present, from a pool of p predictors. Hence to build an M-term model requires $NM^3 + pM^2N$ computations, which can be quite prohibitive if M is a reasonable fraction of M.

Each of the components of an HME are typically inexpensive to fit at each M-step: Np^2 for the regressions, and Np^2K^2 for a K-class logistic regression. The EM algorithm, however, can take a long time to converge, and so sizable HME models are considered costly to fit.

Bibliographic Notes

The most comprehensive source for generalized additive models is the text of that name by Hastie and Tibshirani (1990). Different applications of this work in medical problems are discussed in Hastie et al. (1989) and Hastie and Herman (1990), and the software implementation in Splus is described in Chambers and Hastie (1991). Green and Silverman (1994) discuss penalization and spline models in a variety of settings. Efron and Tibshirani (1991) give an exposition of modern developments in statistics (including generalized additive models), for a nonmathematical audience. Classification and regression trees date back at least as far as Morgan and Sonquist

(1963). We have followed the modern approaches of Breiman et al. (1984) and Quinlan (1993). The PRIM method is due Friedman and Fisher (1999), while MARS is introduced in Friedman (1991), with an additive precursor in Friedman and Silverman (1989). Hierarchical mixtures of experts were proposed in Jordan and Jacobs (1994); see also Jacobs et al. (1991).

Exercises

Ex. 9.1 Show that a smoothing spline fit of y_i to x_i preserves the *linear part* of the fit. In other words, if $y_i = \hat{y}_i + r_i$, where $\hat{y}_i$ represents the linear regression fits, and $\mathbf{S}$ is the smoothing matrix, then $\mathbf{Sy} = \hat{\mathbf{y}} + \mathbf{Sr}$. Show that the same is true for local linear regression (Section 6.1.1). Hence argue that the adjustment step in the second line of (2) in Algorithm 9.1 is unnecessary.

Ex. 9.2 Let $\mathbf{A}$ be a known $k \times k$ matrix, $\mathbf{b}$ be a known k-vector, and $\mathbf{z}$ be an unknown k-vector. A Gauss–Seidel algorithm for solving the linear system of equations $\mathbf{Az} = \mathbf{b}$ works by successively solving for element z_j in the jth equation, fixing all other z_j's at their current guesses. This process is repeated for $j = 1, 2, \dots, k, 1, 2, \dots, k, \dots,$ until convergence (Golub and Van Loan, 1983).

(a) Consider an additive model with N observations and p terms, with the jth term to be fit by a linear smoother $\mathbf{S}_j$. Consider the following system of equations:

$$\begin{pmatrix} \mathbf{I} & \mathbf{S}_1 & \mathbf{S}_1 & \cdots & \mathbf{S}_1 \\ \mathbf{S}_2 & \mathbf{I} & \mathbf{S}_2 & \cdots & \mathbf{S}_2 \\ \vdots & \vdots & \vdots & \ddots & \vdots \\ \mathbf{S}_p & \mathbf{S}_p & \mathbf{S}_p & \cdots & \mathbf{I} \end{pmatrix} \begin{pmatrix} \mathbf{f}_1 \\ \mathbf{f}_2 \\ \vdots \\ \mathbf{f}_p \end{pmatrix} = \begin{pmatrix} \mathbf{S}_1\mathbf{y} \\ \mathbf{S}_2\mathbf{y} \\ \vdots \\ \mathbf{S}_p\mathbf{y} \end{pmatrix}. \tag{9.33}$$

Here each $\mathbf{f}_j$ is an N-vector of evaluations of the jth function at the data points, and $\mathbf{y}$ is an N-vector of the response values. Show that backfitting is a block-wise Gauss–Seidel algorithm for solving this system of equations.

(b) The Gauss–Seidel procedure converges if the matrix $\mathbf{A}$ is positive definite. For a simple case $p = 2$, and assuming each $\mathbf{S}_j$ is symmetric with eigenvalues in $[0, 1)$, show that backfitting converges (the next exercise asks for a direct proof).

Ex. 9.3 *Backfitting with two terms.* Let $\mathbf{S}_1$ and $\mathbf{S}_2$ be symmetric smoothing operators (matrices) with eigenvalues in $[0, 1)$. Consider a backfitting algorithm with response vector $\mathbf{y}$ and smoothers $\mathbf{S}_1, \mathbf{S}_2$. Show that with any starting values, the algorithm converges and give a formula for the final iterates.

Ex. 9.4 *Backfitting equations.* Consider a backfitting procedure with orthogonal projections, and let $\mathbf{D}$ be the overall regression matrix whose columns span $V = \mathcal{L}_{\text{col}}(\mathbf{S}_1) \oplus \mathcal{L}_{\text{col}}(\mathbf{S}_2) \oplus \cdots, \oplus \mathcal{L}_{\text{col}}(\mathbf{S}_p)$, where $\mathcal{L}_{\text{col}}(\mathbf{S})$ denotes the column space of a matrix S. Show that the estimating equations

$$\begin{pmatrix} \mathbf{I} & \mathbf{S}_1 & \mathbf{S}_1 & \cdots & \mathbf{S}_1 \\ \mathbf{S}_2 & \mathbf{I} & \mathbf{S}_2 & \cdots & \mathbf{S}_2 \\ \vdots & \vdots & \vdots & \ddots & \vdots \\ \mathbf{S}_p & \mathbf{S}_p & \mathbf{S}_p & \cdots & \mathbf{I} \end{pmatrix} \begin{pmatrix} \mathbf{f}_1 \\ \mathbf{f}_2 \\ \vdots \\ \mathbf{f}_p \end{pmatrix} = \begin{pmatrix} \mathbf{S}_1\mathbf{y} \\ \mathbf{S}_2\mathbf{y} \\ \vdots \\ \mathbf{S}_p\mathbf{y} \end{pmatrix}$$

are equivalent to the least squares normal equations $\mathbf{D}^T\mathbf{D}\beta = \mathbf{D}^T\mathbf{y}$ where β is the vector of coefficients.

Ex. 9.5 Suppose the same smoother $\mathbf{S}$ is used to estimate both terms in a two-term additive model (i.e., both variables are identical). Assume that $\mathbf{S}$ is symmetric with eigenvalues in $[0, 1)$. Show that the backfitting residual converges to $(\mathbf{I} + \mathbf{S})^{-1}(\mathbf{I} - \mathbf{S})\mathbf{y}$, and that the residual sum of squares converges upward. Can the residual sum of squares converge upward in less structured situations? How does this fit compare to the fit with a single term fit by $\mathbf{S}$? [*Hint*: Use the eigen-decomposition of $\mathbf{S}$ to help with this comparison.]

Ex. 9.6 *Degrees of freedom of a tree.* Given data y_i with mean $f(x_i)$ and variance σ^2, and a fitting operation $\mathbf{y} \to \hat{\mathbf{y}}$, let's define the degrees of freedom of a fit by $\sum_i \text{var}(\hat{y}_i)/\sigma^2$.

Consider a fit $\hat{\mathbf{y}}$ estimated by a regression tree, fit to a set of predictors $X_1, X_2, \ldots, X_p$.

(a) In terms of the number of terminal nodes m, give a rough formula for the degrees of freedom of the fit.

(b) Generate 100 observations with predictors $X_1, X_2, \ldots, X_{10}$ as independent standard Gaussian variates and fix these values.

(c) Generate response values also as standard Gaussian ($\sigma^2 = 1$), independent of the predictors. Fit regression trees to the data of fixed size 1,5 and 10 terminal nodes and hence estimate the degrees of freedom of each fit. [Do ten simulations of the response and average the results, to get a good estimate of degrees of freedom.]

(d) Compare your estimates of degrees of freedom in (a) and (c) and discuss.

(e) If the regression tree fit were a linear operation, we could write $\hat{\mathbf{y}} = \mathbf{S}\mathbf{y}$ for some matrix $\mathbf{S}$. Then the degrees of freedom would be $(1/\sigma^2)\text{trace}(\mathbf{S})$.

Suggest a way to compute an approximate **S** matrix for a regression tree, compute it and compare the resulting degrees of freedom to those in (a) and (c).

Ex. 9.7 Consider the ozone data of Figure 6.9.

(a) Fit an additive model to the cube root of ozone concentration. as a function of temperature, wind speed, and radiation. Compare your results to those obtained via the trellis display in Figure 6.9.

(b) Fit trees, MARS, and PRIM to the same data, and compare the results to those found in (a) and in Figure 6.9.

10
Boosting and Additive Trees

10.1 Boosting Methods

Boosting is one of the most powerful learning ideas introduced in the last ten years. It was originally designed for classification problems, but as will be seen in this chapter, it can profitably be extended to regression as well. The motivation for boosting was a procedure that combines the outputs of many "weak" classifiers to produce a powerful "committee." From this perspective boosting bears a resemblance to bagging and other committee-based approaches (Section 8.8). However we shall see that the connection is at best superficial and that boosting is fundamentally different.

We begin by describing the most popular boosting algorithm due to Freund and Schapire (1997) called "AdaBoost.M1." Consider a two class problem, with the output variable coded as $Y \in \{-1, 1\}$. Given a vector of predictor variables X, a classifier $G(X)$ produces a prediction taking one of the two values $\{-1, 1\}$. The error rate on the training sample is

$$\overline{\text{err}} = \frac{1}{N} \sum_{i=1}^{N} I(y_i \neq G(x_i)),$$

and the expected error rate on future predictions is $\text{E}_{XY} I(Y \neq G(X))$.

A weak classifier is one whose error rate is only slightly better than random guessing. The purpose of boosting is to sequentially apply the weak classification algorithm to repeatedly modified versions of the data, thereby producing a sequence of weak classifiers $G_m(x), m = 1, 2, \dots, M$. The predictions from all of them are then combined through a weighted

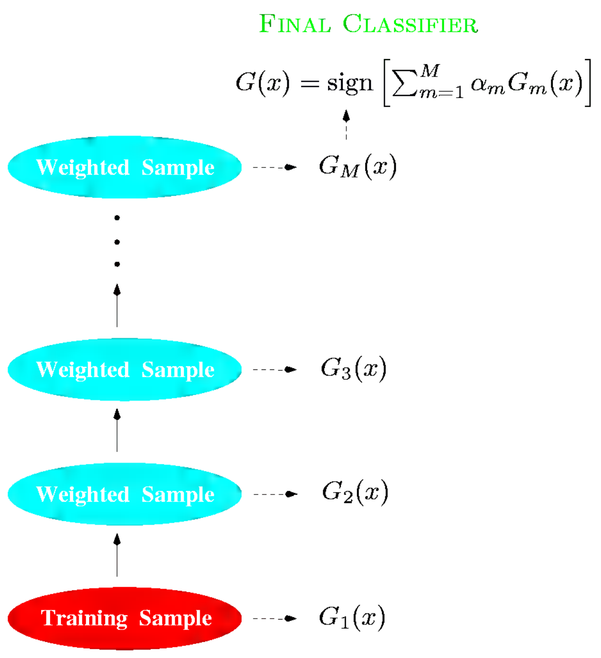

FIGURE 10.1. *Schematic of AdaBoost. Classifiers are trained on weighted versions of the dataset, and then combined to produce a final prediction.*

majority vote to produce the final prediction:

$$G(x) = \text{sign}\left(\sum_{m=1}^{M} \alpha_m G_m(x)\right). \tag{10.1}$$

Here $\alpha_1, \alpha_2, \ldots, \alpha_M$ are computed by the boosting algorithm and weigh the contribution of each respective $G_m(x)$. Their effect is to give higher influence to the more accurate classifiers in the sequence. Figure 10.1 shows a schematic of the AdaBoost procedure.

The data modifications at each boosting step consist of applying weights $w_1, w_2, \ldots, w_N$ to each of the training observations (x_i, y_i), $i = 1, 2, \ldots, N$. Initially all of the weights are set to $w_i = 1/N$, so that the first step simply trains the classifier on the data in the usual manner. For each successive iteration $m = 2, 3, \ldots, M$ the observation weights are individually modified and the classification algorithm is reapplied to the weighted observations. At step m, those observations that were misclassified by the classifier $G_{m-1}(x)$ induced at the previous step have their weights increased, whereas the weights are decreased for those that were classified correctly. Thus as iterations proceed, observations that are difficult to correctly classify receive ever-increasing influence. Each successive classifier is thereby forced

Algorithm 10.1 *AdaBoost.M1.*

```
1. Initialize the observation weights $w_i = 1/N,\ i = 1, 2, \ldots, N$.
2. For $m = 1$ to $M$:
    (a) Fit a classifier $G_m(x)$ to the training data using weights $w_i$.
    (b) Compute
        $$\text{err}_m = \frac{\sum_{i=1}^N w_i I(y_i \neq G_m(x_i))}{\sum_{i=1}^N w_i}.$$
    (c) Compute $\alpha_m = \log((1 - \text{err}_m)/\text{err}_m)$.
    (d) Set $w_i \leftarrow w_i \cdot \exp[\alpha_m \cdot I(y_i \neq G_m(x_i))],\ i = 1, 2, \ldots, N$.
3. Output $G(x) = \text{sign}\left[\sum_{m=1}^M \alpha_m G_m(x)\right]$.
```

to concentrate on those training observations that are missed by previous ones in the sequence.

Algorithm 10.1 shows the details of the AdaBoost.M1 algorithm. The current classifier $G_m(x)$ is induced on the weighted observations at line 2a. The resulting weighted error rate is computed at line 2b. Line 2c calculates the weight α_m given to $G_m(x)$ in producing the final classifier $G(x)$ (line 3). The individual weights of each of the observations are updated for the next iteration at line 2c. Observations misclassified by $G_m(x)$ have their weights scaled by a factor $\exp(\alpha_m)$, increasing their relative influence for inducing the next classifier $G_{m+1}(x)$ in the sequence.

The AdaBoost.M1 algorithm is known as "Discrete AdaBoost" in Friedman et al. (2000), because the base classifier $G_m(x)$ returns a discrete class label. If the base classifier instead returns a real-valued prediction (e.g., a probability mapped to the interval $[-1, 1]$), AdaBoost can be modified appropriately (see "Real AdaBoost" in Friedman et al. (2000)).

The power of AdaBoost to dramatically increase the performance of even a very weak classifier is illustrated in Figure 10.2. The features $X_1, \ldots, X_{10}$ are standard independent Gaussian, and the deterministic target Y is defined by

$$Y = \begin{cases} 1 & \text{if } \sum X_j^2 > \chi^2_{10}(0.5), \\ \text{-1} & \text{otherwise.} \end{cases} \tag{10.2}$$

Here $\chi^2_{10}(0.5) = 9.34$ is the median of a chi-squared random variable with 10 degrees of freedom (sum of squares of 10 standard Gaussians). There are 2000 training cases, with approximately 1000 cases in each class, and 10,000 test observations. Here the weak classifier is just a "stump": a two–terminal node classification tree. Applying this classifier alone to the training data

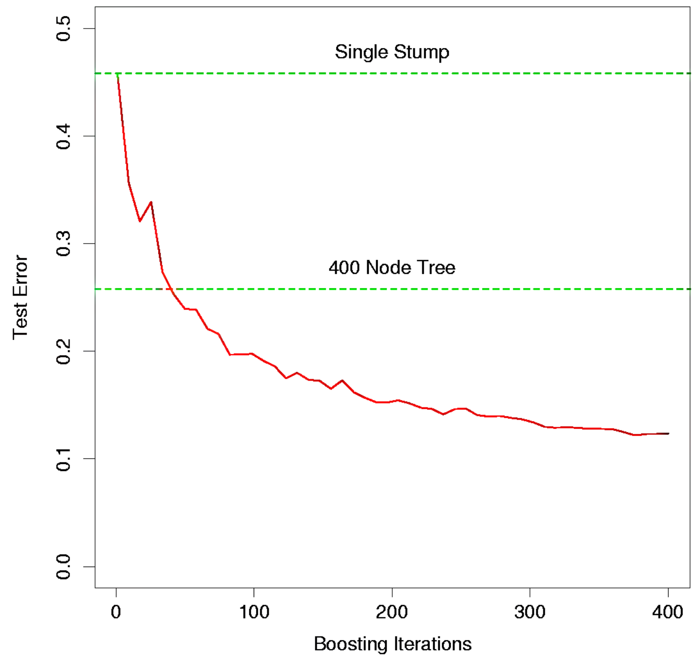

FIGURE 10.2. *Simulated data (10.2): test error rate for boosting with stumps, as a function of the number of iterations. Also shown are the test error rate for a single stump, and a* 400 *node classification tree.*

set yields a very poor test set error rate of 46%, compared to 50% for random guessing. However, as boosting iterations proceed the error rate steadily decreases, reaching 12.2% after 400 iterations. Thus, boosting this simple very weak classifier reduces its prediction error rate by more than a factor of eight. It also outperforms a single large classification tree (error rate 26%). Since its introduction, much has been written to explain the success of AdaBoost in producing accurate classifiers. Most of this work has centered on using classification trees as the "base learner" $G(x)$, where improvements are often most dramatic. In fact, Breiman (NIPS Workshop, 1996) referred to AdaBoost with trees as the "best off-the-shelf classifier in the world" (see also Breiman (1998)). This is especially the case for data-mining applications as discussed more fully in Section 10.7 later in this chapter.

10.1.1 Outline of this Chapter

Here is an outline of the developments in this chapter:

- We show that AdaBoost fits an additive model in a base learner, optimizing a novel exponential loss function. This loss function is very similar to the (negative) binomial log-likelihood (Sections 10.2–10.4).

- The population minimizer of the exponential loss function is shown to be the log-odds of the class probabilities (Section 10.5).
- We describe loss functions for regression and classification that are more robust than squared error or exponential loss (Section 10.6).
- It is argued that decision trees are an ideal base learner for data mining applications of boosting (Sections 10.7 and 10.9).
- Using a gradient approach, we develop a class of techniques ("MART") for boosting trees with any loss function (Section 10.10).
- The importance of "slow learning" is emphasized, and implemented by shrinkage of each new term that enters the model (Section 10.12).
- We draw a connection between forward stagewise shrinkage and an L_1 penalty for the model parameters (the "lasso"). We argue that L_1 penalties may be superior to the L_2 penalties used by methods such as the support vector machine (Section 10.12.2).
- Tools for interpretation of the fitted model are described (Section 10.13).

10.2 Boosting Fits an Additive Model

The success of boosting is really not very mysterious. The key lies in expression (10.1). Boosting is a way of fitting an additive expansion in a set of elementary "basis" functions. Here the basis functions are the individual classifiers $G_m(x) \in \{-1, 1\}$. More generally, basis function expansions take the form

$$f(x) = \sum_{m=1}^{M} \beta_m b(x; \gamma_m), \tag{10.3}$$

where $\beta_m, m = 1, 2, \ldots, M$ are the expansion coefficients, and $b(x; \gamma) \in \mathbb{R}$ are usually simple functions of the multivariate argument x, characterized by a set of parameters γ. We discuss basis expansions in some detail in Chapter 5.

Additive expansions like this form the basis of many of the learning techniques covered in this book:

- In single hidden layer neural networks (Chapter 11), $b(x; \gamma) = \sigma(\gamma_0 + \gamma_1^t x)$, where $\sigma(\cdot)$ is a sigmoidal function and γ parameterizes a linear combination of the input variables.

- In signal processing, wavelets (Section 5.9.1) are a popular choice with γ parameterizing the location and scale shifts of a "mother" wavelet.
- MARS (Section 9.4) uses truncated power spline basis functions where γ parameterizes the variables and values for the knots.
- For trees, γ parameterizes the split variables and split points at the internal nodes, and the predictions at the terminal nodes.

Typically these models are fit by minimizing a loss function averaged over the training data, such as squared-error or a likelihood-based loss function,

$$\min_{\{\beta_m,\gamma_m\}_1^M} \sum_{i=1}^{N} L\left(y_i, \sum_{m=1}^{M} \beta_m b(x_i;\gamma_m)\right). \tag{10.4}$$

For many loss functions $L(y, f(x))$ and/or basis functions $b(x;\gamma)$ this requires computationally intensive numerical optimization techniques. However, a simple alternative often can be found when it is feasible to rapidly solve the subproblem of fitting just a single basis function,

$$\min_{\beta,\gamma} \sum_{i=1}^{N} L\left(y_i, \beta b(x_i;\gamma)\right). \tag{10.5}$$

10.3 Forward Stagewise Additive Modeling

Forward stagewise modeling approximates the solution to (10.4) by sequentially adding new basis functions to the expansion without adjusting the parameters and coefficients of those that have already been added. This is outlined in Algorithm 10.2. At each iteration m, one solves for the optimal basis function $b(x;\gamma_m)$ and corresponding coefficient β_m to add to the current expansion $f_{m-1}(x)$. This produces $f_m(x)$, and the process is repeated. Previously added terms are not modified.

For squared-error loss

$$L(y, f(x)) = (y - f(x))^2, \tag{10.6}$$

one has

$$\begin{aligned} L(y_i, f_{m-1}(x_i) + \beta b(x_i;\gamma)) &= (y_i - f_{m-1}(x_i) - \beta b(x_i;\gamma))^2 \\ &= (r_{im} - \beta b(x_i;\gamma))^2, \end{aligned} \tag{10.7}$$

where $r_{im} = y_i - f_{m-1}(x_i)$ is simply the error (residual) of the current model on the ith observation. Thus, for squared-error loss, the term $\beta_m b(x;\gamma_m)$ that best fits the current residuals is added to the expansion at each step. This idea is the basis for "least squares" regression boosting discussed in Section 10.10.2. However, as we show near the end of the next section, squared-error loss is generally not a good choice for classification: hence the need to consider other loss criteria.

Algorithm 10.2 *Forward stagewise additive modeling.*

```
1. Initialize $f_0(x) = 0$.
2. For $m = 1$ to $M$:
    (a) Compute
        $$(\beta_m, \gamma_m) = \arg\min_{\beta,\gamma} \sum_{i=1}^{N} L(y_i, f_{m-1}(x_i) + \beta b(x_i; \gamma)).$$
    (b) Set $f_m(x) = f_{m-1}(x) + \beta_m b(x; \gamma_m)$.
```

10.4 Exponential Loss and AdaBoost

We now show that AdaBoost.M1 (Algorithm 10.1) is equivalent to forward stagewise additive modeling (Algorithm 10.2) using the loss function

$$L(y, f(x)) = \exp(-y\, f(x)). \tag{10.8}$$

The appropriateness of this criterion is addressed in the next section.

For AdaBoost the basis functions are the individual classifiers $G_m(x) \in \{-1, 1\}$. Using the exponential loss function, one must solve

$$(\beta_m, G_m) = \arg\min_{\beta,G} \sum_{i=1}^{N} \exp[-y_i(f_{m-1}(x_i) + \beta\, G(x))]$$

for the classifier G_m and corresponding coefficient β_m to be added at each step. This can be expressed as

$$(\beta_m, G_m) = \arg\min_{\beta,G} \sum_{i=1}^{N} w_i^{(m)} \exp(-\beta\, y_i\, G(x_i)) \tag{10.9}$$

with $w_i^{(m)} = \exp(-y_i\, f_{m-1}(x_i))$. Since each $w_i^{(m)}$ depends neither on β nor $G(x)$, it can be regarded as a weight that is applied to each observation. This weight depends on $f_{m-1}(x_i)$, and so the individual weight values change with each iteration m.

The solution to (10.9) can be obtained in two steps. First, for any value of $\beta > 0$, the solution to (10.9) for $G_m(x)$ is

$$G_m = \arg\min_{G} \sum_{i=1}^{N} w_i^{(m)} I(y_i \neq G(x_i)), \tag{10.10}$$

which is the classifier that minimizes the weighted error rate in predicting y. This can be easily seen by expressing the criterion in (10.9) as

$$e^{-\beta} \cdot \sum_{y_i = G(x_i)} w_i^{(m)} + e^{\beta} \cdot \sum_{y_i \neq G(x_i)} w_i^{(m)},$$

which in turn can be written as

$$\left(e^{\beta}-e^{-\beta}\right)\cdot\sum_{i=1}^{N}w_i^{(m)}I(y_i\neq G(x_i))+e^{-\beta}\cdot\sum_{i=1}^{N}w_i^{(m)}. \tag{10.11}$$

Plugging this G_m into (10.9) and solving for β one obtains

$$\beta_m=\frac{1}{2}\log\frac{1-\text{err}_m}{\text{err}_m}, \tag{10.12}$$

where err_m is the minimized weighted error rate

$$\text{err}_m=\frac{\sum_{i=1}^{N}w_i^{(m)}I(y_i\neq G_m(x_i))}{\sum_{i=1}^{N}w_i^{(m)}}. \tag{10.13}$$

The approximation is then updated

$$f_m(x)=f_{m-1}(x)+\beta_m G_m(x),$$

which causes the weights for the next iteration to be

$$w_i^{(m+1)}=w_i^{(m)}\cdot e^{-\beta_m y_i G_m(x_i)}. \tag{10.14}$$

Using the fact that $y_iG_m(x_i)=2\cdot I(y_i\neq G(x_i))-1$, (10.14) becomes

$$w_i^{(m+1)}=w_i^{(m)}\cdot e^{\alpha_m I(y_i\neq G(x_i))}\cdot e^{-\beta_m}, \tag{10.15}$$

where $\alpha_m=2\beta_m$ is the quantity defined at line 2c of AdaBoost.M1 (Algorithm 10.1). The factor $e^{-\beta_m}$ in (10.15) multiplies all weights by the same value, so it has no effect. Thus (10.15) is equivalent to line 2(d) of Algorithm 10.1. One can view line 2(a) of the algorithm as a method for solving the minimization in (10.10). Hence we conclude that AdaBoost.M1 minimizes the exponential loss criterion (10.8) via a forward-stagewise additive modeling approach.

Figure 10.3 shows the training-set misclassification error rate and average exponential loss for the simulated data problem (10.2) of Figure 10.2. The training-set misclassification error levels off at around 250 iterations, but the exponential loss keeps decreasing because it is more sensitive to changes in the estimated class probabilities.

10.5 Why Exponential Loss?

The AdaBoost.M1 algorithm was originally motivated from a very different perspective than presented in the previous section. Its equivalence to forward stagewise additive modeling based on exponential loss was only

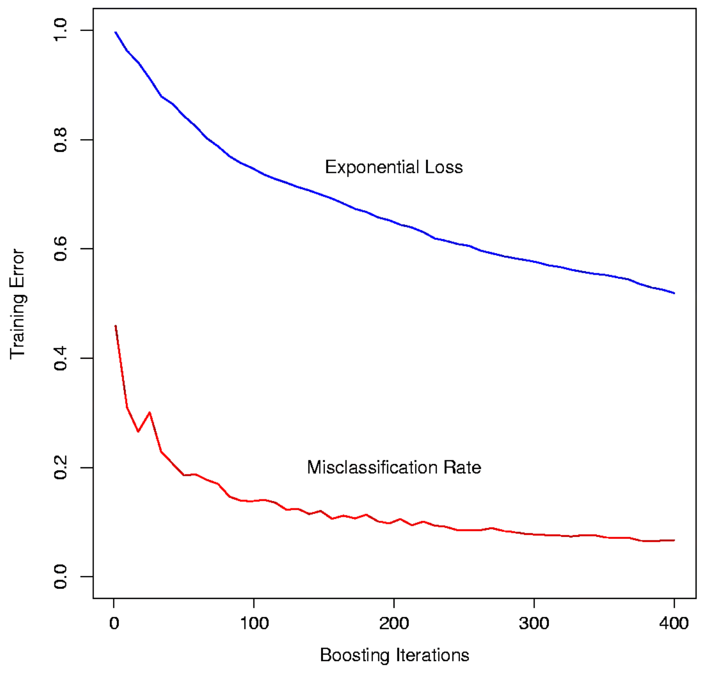

FIGURE 10.3. *Simulated data, boosting with stumps: misclassification error rate on the training set, and average exponential loss:* $(1/N)\sum_{i=1}^{N}\exp(-y_i f(x_i))$.

recently discovered. By studying the properties of the exponential loss criterion, one can gain insight into the procedure and discover ways it might be improved.

The principal attraction of exponential loss in the context of additive modeling is computational; it leads to the simple modular reweighting AdaBoost algorithm. However, it is of interest to inquire about its statistical properties. What does it estimate and how well is it being estimated? The first question is answered by seeking its population minimizer.

It is easy to show (Friedman et al., 2000) that

$$f^*(x) = \arg\min_{f(x)} \mathrm{E}_{Y|x}(e^{-Yf(x)}) = \frac{1}{2}\log\frac{\Pr(Y=1|x)}{\Pr(Y=-1|x)}, \tag{10.16}$$

or equivalently

$$\Pr(Y=1|x) = \frac{1}{1+e^{-2f^*(x)}}.$$

Thus, the additive expansion produced by AdaBoost is estimating one-half the log-odds of $P(Y=1|x)$. This justifies using its sign as the classification rule in (10.1).

Another loss criterion with the same population minimizer is the binomial negative log-likelihood or *deviance* (also known as cross-entropy), interpreting f as the logit transform. Let

$$p(x) = \Pr(Y = 1 \mid x) = \frac{e^{f(x)}}{e^{-f(x)} + e^{f(x)}} = \frac{1}{1 + e^{-2f(x)}} \tag{10.17}$$

and define $Y' = (Y + 1)/2 \in \{0, 1\}$. Then the binomial log-likelihood loss function is

$$l(Y, p(x)) = Y' \log p(x) + (1 - Y') \log(1 - p(x)),$$

or equivalently the deviance is

$$-l(Y, f(x)) = \log\left(1 + e^{-2Yf(x)}\right). \tag{10.18}$$

Since the population maximizer of log-likelihood is at the true probabilities $p(x) = \Pr(Y = 1 \mid x)$, we see from (10.17) that the population minimizers of the deviance $\mathrm{E}_{Y|x}[-l(Y, f(x))]$ and $\mathrm{E}_{Y|x}[e^{-Yf(x)}]$ are the same. Thus, using either criterion leads to the same solution at the population level. Note that e^{-Yf} itself is not a proper log-likelihood, since it is not the logarithm of any probability mass function of $Y \in \{-1, 1\}$.

10.6 Loss Functions and Robustness

In this section we examine the different loss functions for classification and regression more closely, and characterize them in terms of their robustness to extreme data.

Robust Loss Functions for Classification

Although both the exponential (10.8) and binomial deviance (10.18) yield the same solution when applied to the population joint distribution, the same is not true for finite data sets. Both criteria are monotone decreasing functions of the "margin" $yf(x)$. In classification (with a $-1/1$ response) the margin plays a role analogous to the residuals $y - f(x)$ in regression. The classification rule $G(x) = \mathrm{sign}[f(x)]$ implies that observations with positive margin $y_i f(x_i) > 0$ are classified correctly whereas those with negative margin $y_i f(x_i) < 0$ are misclassified. The decision boundary is defined by $f(x) = 0$. The goal of the classification algorithm is to produce positive margins as frequently as possible. Any loss criterion used for classification should penalize negative margins more heavily than positive ones since positive margin observations are already correctly classified.

Figure 10.4 shows both the exponential (10.8) and binomial deviance criteria as a function of the margin $y \cdot f(x)$. Also shown is misclassification loss $L(y, f(x)) = I(y \cdot f(x) < 0)$, which gives unit penalty for negative margin values, and no penalty at all for positive ones. Both the exponential

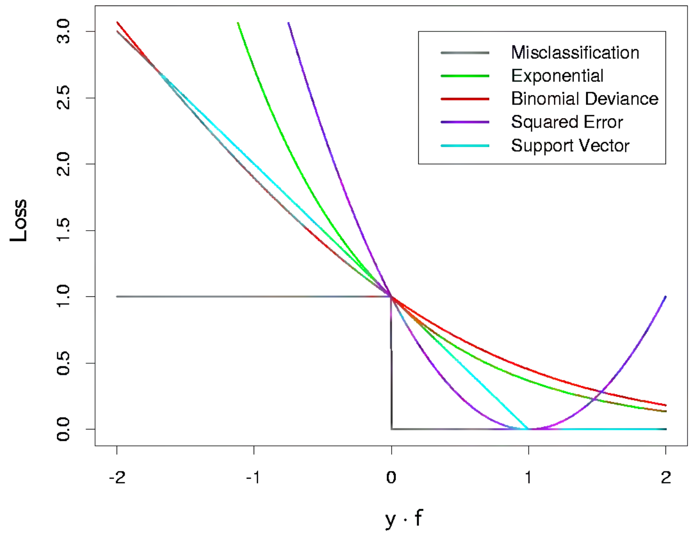

FIGURE 10.4. *Loss functions for two-class classification. The response is* $y = \pm 1$*; the prediction is* f*, with class prediction* $\text{sign}(f)$*. The losses are misclassification:* $I(\text{sign}(f) \neq y)$*; exponential:* $\exp(-yf)$*; binomial deviance:* $\log(1+\exp(-2yf))$*; squared error:* $(y-f)^2$*; and support vector:* $(1-yf)\cdot I(yf > 1)$ *(see Section 12.3). Each function has been scaled so that it passes through the point* $(0,1)$.

and deviance loss can be viewed as monotone continuous approximations to misclassification loss. They continuously penalize increasingly negative margin values more heavily than they reward increasingly positive ones. The difference between them is in degree. The penalty associated with binomial deviance increases linearly for large increasingly negative margin, whereas the exponential criterion increases the influence of such observations exponentially.

At any point in the training process the exponential criterion concentrates much more influence on observations with large negative margins. Binomial deviance concentrates relatively less influence on such observations, more evenly spreading the influence among all of the data. It is therefore far more robust in noisy settings where the Bayes error rate is not close to zero, and especially in situations where there is misspecification of the class labels in the training data. The performance of AdaBoost has been empirically observed to dramatically degrade in such situations.

Also shown in the figure is squared-error loss. The minimizer of the corresponding risk on the population is

$$f^*(x) = \arg\min_{f(x)} \mathrm{E}_{Y|x}(Y - f(x))^2 = \mathrm{E}(Y \mid x) = 2 \cdot \Pr(Y = 1 \mid x) - 1.$$

As before the classification rule is $G(x) = \text{sign}[f(x)]$. Squared-error loss is not a good surrogate for misclassification error. As seen in Figure 10.4, it is not a monotone decreasing function of increasing margin $yf(x)$. For margin values $y_i f(x_i) > 1$ it increases quadratically, thereby placing increasing influence (error) on observations that are correctly classified with increasing certainty, thereby reducing the relative influence of those incorrectly classified $y_i f(x_i) < 0$. Thus, if class assignment is the goal, a monotone decreasing criterion serves as a better surrogate loss function.

With K-class classification, the response Y takes values in the unordered set $\mathcal{G} = \{\mathcal{G}_1, \dots, \mathcal{G}_k\}$ (see Sections 2.4 and 4.4). We now seek a classifier $G(x)$ taking values in $\mathcal{G}$. It is sufficient to know the class conditional probabilities $p_k(x) = \Pr(Y = \mathcal{G}_k|x), k = 1, 2, \dots, K$, for then the Bayes classifier is

$$G(x) = \mathcal{G}_k \text{ where } k = \arg\max_{\ell} p_\ell(x). \tag{10.19}$$

In principal, though, we need not learn the $p_k(x)$, but simply which one is largest. However, in data mining applications the interest is often more in the class probabilities $p_\ell(x),\ \ell = 1, \dots, K$ themselves, rather than in performing a class assignment. As in Section 4.4, the logistic model generalizes naturally to K classes,

$$p_k(x) = \frac{e^{f_k(x)}}{\sum_{l=1}^{K} e^{f_l(x)}}, \tag{10.20}$$

which ensures that $0 \le p_k(x) \le 1$ and that they sum to one. Note that here we have K different functions, one per class. There is a redundancy in the functions $f_k(x)$, since adding an arbitrary $h(x)$ to each leaves the model unchanged. Traditionally one of them is set to zero: for example, $f_K(x) = 0$, as in (4.17). Here we prefer to retain the symmetry, and impose the constraint $\sum_{k=1}^{K} f_k(x) = 0$. The binomial deviance extends naturally to the K-class *multinomial deviance* loss function:

$$\begin{aligned} L(y, p(x)) &= -\sum_{k=1}^{K} I(y = \mathcal{G}_k) \log p_k(x) \\ &= -\sum_{k=1}^{K} I(y = \mathcal{G}_k) f_k(x) + \log\left(\sum_{\ell=1}^{K} e^{f_\ell(x)}\right). \end{aligned} \tag{10.21}$$

As in the two-class case, the criterion (10.21) penalizes incorrect predictions only linearly in their degree of incorrectness. We know of no natural generalization of the exponential criterion for K classes.

Robust Loss Functions for Regression

In the regression setting, analogous to the relationship between exponential loss and binomial log-likelihood is the relationship between squared-error

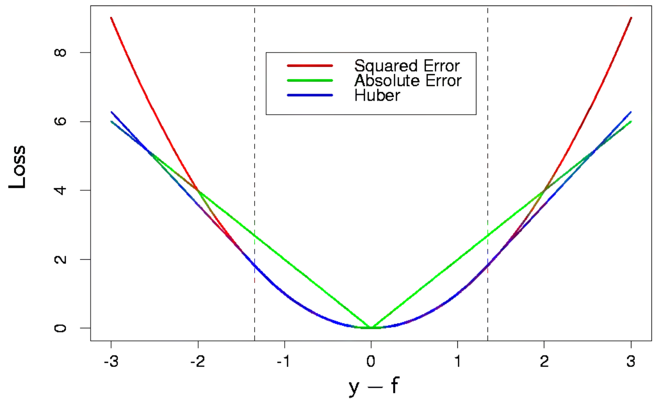

FIGURE 10.5. *A comparison of three loss functions for regression, plotted as a function of the margin $y-f$. The Huber loss function combines the good properties of squared-error loss near zero and absolute error loss when $|y-f|$ is large.*

loss $L(y, f(x)) = (y - f(x))^2$ and absolute loss $L(y, f(x)) = |\,y - f(x)\,|$. The population solutions are $f(x) = \mathrm{E}(Y|x)$ for squared-error loss, and $f(x) = \mathrm{median}(Y|x)$ for absolute loss; for symmetric error distributions these are the same. However, on finite samples squared-error loss places much more emphasis on observations with large absolute residuals $|\,y_i - f(x_i)\,|$ during the fitting process. It is thus far less robust, and its performance severely degrades for long-tailed error distributions and especially for grossly mismeasured y-values ("outliers"). Other more robust criteria, such as absolute loss perform much better in these situations. In the statistical robustness literature, a variety of regression loss criteria have been proposed that provide strong resistance (if not absolute immunity) to gross outliers while being nearly as efficient as least squares for Gaussian errors. They are often better than either for error distributions with moderately heavy tails. One such criterion is the Huber loss criterion used for M-regression (Huber, 1964)

$$L(y, f(x)) = \begin{cases} [y - f(x)]^2, & \text{for } |\,y - f(x)\,| \le \delta, \\ \delta(|\,y - f(x)\,| - \delta/2), & \text{otherwise.} \end{cases} \tag{10.22}$$

Figure 10.5 compares these three loss functions.

Thus absolute loss in regression is analogous to binomial deviance in classification: it increases linearly for extreme margins. Exponential loss is even more severe than squared-error loss, penalizing exponentially rather than quadratically.

These considerations suggest than when robustness is a concern, as is especially the case in data mining applications (see Section 10.7), squared-error loss for regression and exponential loss for classification are not the best criteria from a statistical perspective. However, they both lead to the elegant modular boosting algorithms in the context of forward stagewise additive modeling. For squared-error loss one simply fits the base learner to the residuals from the current model $y_i - f_{m-1}(x_i)$ at each step. For exponential loss one performs a weighted fit of the base learner to the output values y_i, with weights $w_i = \exp(-y_i f(x_i))$. Using other more robust criteria directly in their place does not give rise to such simple feasible boosting algorithms. However, in Section 10.10.2 we show how one can derive simple elegant boosting algorithms based on any differentiable loss criterion, thereby producing highly robust boosting procedures for data mining.

10.7 "Off-the-Shelf" Procedures for Data Mining

Predictive learning is an important aspect of data mining. As can be seen from this book, a wide variety of methods have been developed for predictive learning from data. For each particular method there are situations for which it is particularly well suited, and others where it performs badly compared to the best that can be done with that data. We have attempted to characterize appropriate situations in our discussions of each of the respective methods. However, it is seldom known in advance which procedure will perform best or even well for any given problem. Table 10.1 summarizes some of the characteristics of a number of learning methods.

Industrial and commercial data mining applications tend to be especially challenging in terms of the requirements placed on learning procedures. Data sets are often very large in terms of number of observations and number of variables measured on each of them. Thus, computational considerations play an important role. Also, the data are usually *messy*: the inputs tend to be mixtures of quantitative, binary, and categorical variables, the latter often with many levels. There are generally many missing values, complete observations being rare. Distributions of numeric predictor and response variables are often long-tailed and highly skewed. In addition they usually contain a substantial fraction of gross mismeasurements (outliers). The predictor variables are generally measured on very different scales.

In data mining applications, usually only a small fraction of the large number of predictor variables that have been included in the analysis are actually relevant to prediction. Also, unlike many applications such as pattern recognition, there is seldom reliable domain knowledge to help create especially relevant features and/or filter out the irrelevant ones, the inclusion of which dramatically degrades the performance of many methods.

In addition, data mining applications generally require interpretable models. It is not enough to simply produce predictions. It is also desirable to have information providing qualitative understanding of the relationship between joint values of the input variables and the resulting predicted response value. Thus, *black box* methods such as neural networks, which can

TABLE 10.1. *Some characteristics of different learning methods. Key:* 🟢*= good,* 🟡*=fair, and* 🔴*=poor.*

Characteristic	Neural nets	SVM	Trees	MARS	k-NN, kernels
Natural handling of data of "mixed" type	🔴	🔴	🟢	🟢	🔴
Handling of missing values	🔴	🔴	🟢	🟢	🟢
Robustness to outliers in input space	🔴	🔴	🟢	🔴	🟢
Insensitive to monotone transformations of inputs	🔴	🔴	🟢	🔴	🔴
Computational scalability (large N)	🔴	🔴	🟢	🟢	🔴
Ability to deal with irrelevant inputs	🔴	🔴	🟢	🟢	🔴
Ability to extract linear combinations of features	🟢	🟢	🔴	🔴	🟡
Interpretability	🔴	🔴	🟡	🟢	🔴
Predictive power	🟢	🟢	🔴	🟡	🟢

be quite useful in purely predictive settings such as pattern recognition, are far less useful for data mining.

These requirements of speed, interpretability and the messy nature of the data sharply limit the usefulness of most learning procedures as off-the-shelf methods for data mining. An "off-the-shelf" method is one that can be directly applied to the data without requiring a great deal of time consuming data preprocessing or careful tuning of the learning procedure.

Of all the well-known learning methods, decision trees come closest to meeting the requirements for serving as an off-the-shelf procedure for data mining. They are relatively fast to construct and they produce interpretable models. As discussed in Section 9.2, they naturally incorporate mixtures of numeric and categorical predictor variables and missing values. They are invariant under (strictly monotone) transformations of the individual predictors. As a result, scaling and/or more general transformations are not an issue, and they are immune to the effects of predictor outliers. They perform internal feature selection as an integral part of the procedure. They are thereby resistant, if not completely immune, to the inclusion of many irrelevant predictor variables. These properties of decision trees are largely the reason that they have emerged as the most popular learning method for data mining.

Trees have one aspect that prevents them from being the ideal tool for predictive learning, namely inaccuracy. They seldom provide predictive accuracy comparable to the best that can be achieved with the data at hand. As seen in Section 10.1, boosting decision trees improves their accuracy, often dramatically. At the same time it maintains most of their desirable properties for data mining. Some advantages of trees that are sacrificed by boosting are speed, interpretability, and, for AdaBoost, robustness against overlapping class distributions and especially mislabeling of the training data. A multiple additive regression tree (MART) is a generalization of tree boosting that attempts to mitigate these problems, so as to produce an accurate and effective off-the-shelf procedure for data mining.

10.8 Example—Spam Data

Before we go into the details of MART, we demonstrate its abilities on a two-class classification problem. The spam data are introduced in Chapter 1, and used as an example for many of the procedures in Chapter 9 (Sections 9.1.2, 9.2.5, 9.3.1 and 9.4.1).

Applying MART to this data resulted in a test error rate of 4.0%, using the same test set as was used in Section 9.1.2. By comparison, an additive logistic regression achieved 5.3%, a CART tree fully grown and pruned by cross-validation 8.7%, and MARS 5.5%. The standard error of these estimates is around 0.6%.

In Section 10.13 below we develop a relative importance measure for each predictor, as well as a partial dependence plot describing a predictor's contribution to the fitted model. We now illustrate these for the spam data.

Figure 10.6 displays the relative importance spectrum for all 57 predictor variables. Clearly some predictors are more important than others in separating `spam` from `email`. The left panel of The frequencies of the character strings `!`, `$`, `hp`, and `remove` are estimated to be the four most relevant predictor variables. At the other end of the spectrum, the character strings `857`, `415`, `table`, and `spam` have virtually no relevance.

The quantity being modeled here is the log-odds of `spam` versus `email`

$$f(x) = \log \frac{\Pr(\texttt{spam}|x)}{\Pr(\texttt{email}|x)} \tag{10.23}$$

(see Section 10.13 below). Figure 10.7 shows the partial dependence of the log-odds on selected important predictors, two positively associated with `spam` (`!` and `remove`), and two negatively associated (`edu` and `hp`). These particular dependencies are seen to be generally monotonic.There is a general agreement with the corresponding functions found by the additive logistic regression model; see Figure 9.1.

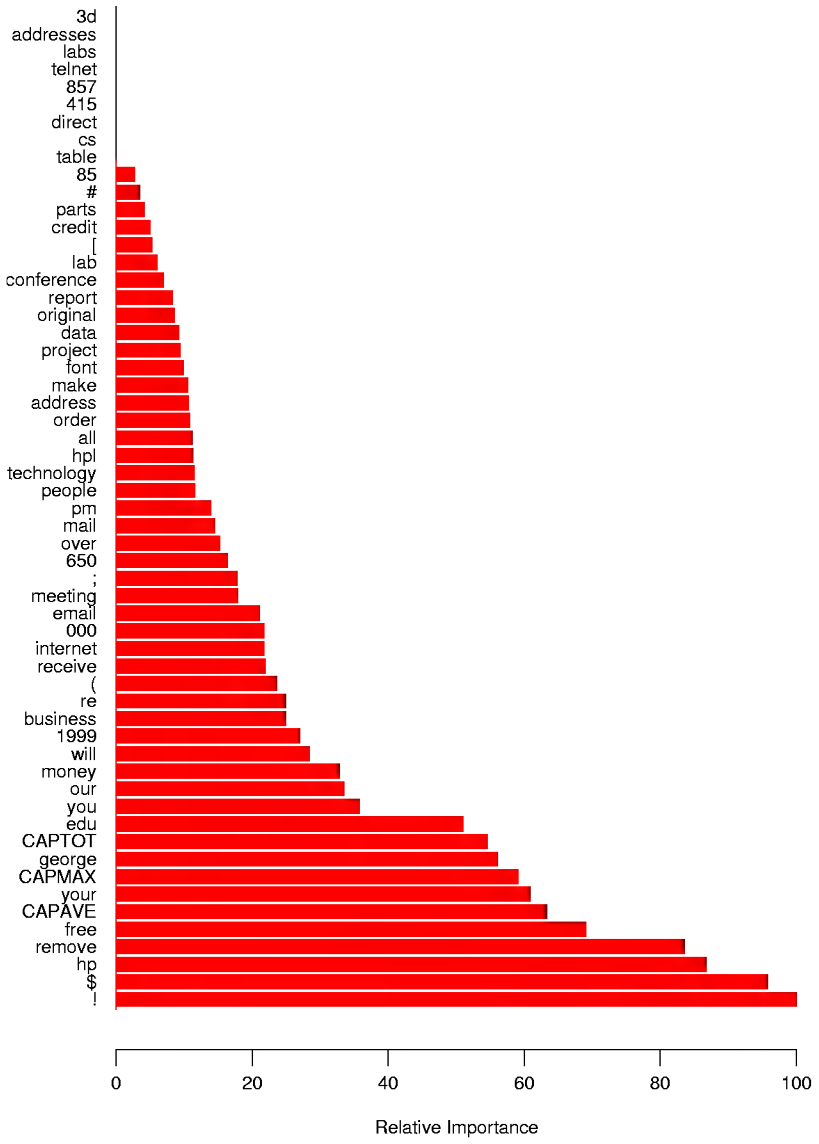

FIGURE 10.6. *Predictor variable importance spectrum for the* `spam` *data. The variable names are written on the vertical axis.*

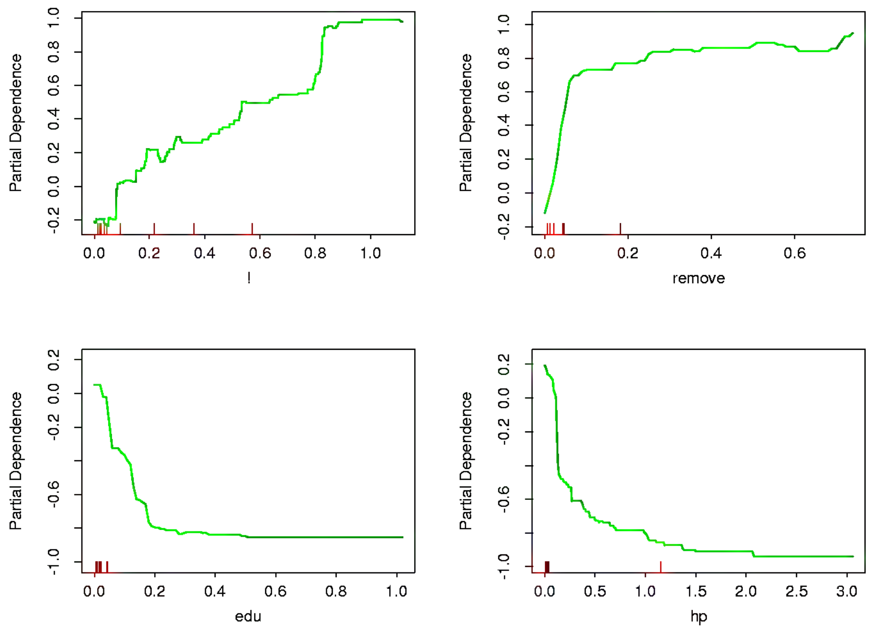

FIGURE 10.7. *Partial dependence of log-odds of* `spam` *on four important predictors. The red ticks at the base of the plots are deciles of the input variable.*

Running MART on these data with $J = 2$ terminal node trees produces a purely additive (main effects) model for the log-odds, with a corresponding error rate of 4.6%, as compared to 4.0% for the full MART model. (Since there are 1536 observations in the test set, the standard error of these rates is approximately $\sqrt{0.04(1-0.04)/1536} = 0.005$ or 0.5%). This slightly higher error rate suggests that there may be interactions among some of the important predictor variables. This can be diagnosed through two-variable partial dependence plots. Figure 10.8 shows one of the several such plots displaying strong interaction effects.

One sees that for very low frequencies of `hp`, the log-odds of `spam` are greatly increased. For high frequencies of `hp`, the log-odds of `spam` tend to be much lower and roughly constant as a function of `!`. As the frequency of `hp` decreases, the functional relationship with `!` strengthens.

10.9 Boosting Trees

Regression and classification trees are discussed in detail in Section 9.2. They partition the space of all joint predictor variable values into disjoint regions $R_j, j = 1, 2, \dots, J$, as represented by the terminal nodes of the tree.

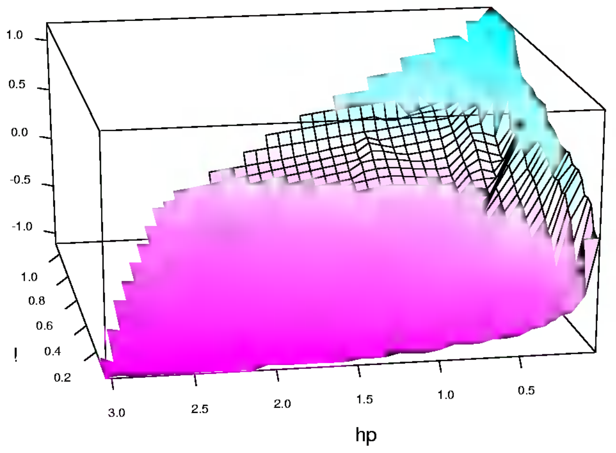

FIGURE 10.8. *Partial dependence of the log-odds of* `spam` *vs.* `email` *as a function of joint frequencies of* `hp` *and* `!`.

A constant γ_j is assigned to each such region and the predictive rule is

$$x \in R_j \Rightarrow f(x) = \gamma_j.$$

Thus a tree can be formally expressed as

$$T(x;\Theta) = \sum_{j=1}^{J} \gamma_j I(x \in R_j), \tag{10.24}$$

with parameters $\Theta = \{R_j, \gamma_j\}_1^J$. J is usually treated as a meta-parameter. The parameters are found by minimizing the empirical risk

$$\hat{\Theta} = \arg\min_{\Theta} \sum_{j=1}^{J} \sum_{x_i \in R_j} L(y_i, \gamma_j). \tag{10.25}$$

This is a formidable combinatorial optimization problem, and we usually settle for approximate suboptimal solutions. It is useful to divide the optimization problem into two parts:

Finding γ_j given R_j: Given the R_j, estimating the γ_j is typically trivial, and often $\hat{\gamma}_j = \bar{y}_j$, the mean of the y_i falling in region R_j. For misclassification loss, $\hat{\gamma}_j$ is the modal class of the observations falling in region R_j.

Finding R_j: This is the difficult part, for which approximate solutions are found. Note also that finding the R_j entails estimating the γ_j as well. A typical strategy is to use a greedy, top-down recursive partitioning algorithm to find the R_j. In addition, it is sometimes necessary to approximate (10.25) by a smoother and more convenient criterion for optimizing the R_j:

$$\tilde{\Theta} = \arg\min_{\Theta} \sum_{i=1}^{N} \tilde{L}(y_i, T(x_i, \Theta)). \tag{10.26}$$

Then given the $\hat{R}_j = \tilde{R}_j$, the γ_j can be estimated more precisely using the original criterion.

In Section 9.2 we described such a strategy for classification trees. The Gini index replaced misclassification loss in the growing of the tree (identifying the R_j).

The boosted tree model is a sum of such trees,

$$f_M(x) = \sum_{m=1}^{M} T(x; \Theta_m), \tag{10.27}$$

induced in a forward stagewise manner (Algorithm 10.2). At each step in the forward stagewise procedure one must solve

$$\hat{\Theta}_m = \arg\min_{\Theta_m} \sum_{i=1}^{N} L\left(y_i, f_{m-1}(x_i) + T(x_i; \Theta_m)\right) \tag{10.28}$$

for the region set and constants $\Theta_m = \{R_{jm}, \gamma_{jm}\}_1^{J_m}$ of the next tree, given the current model $f_{m-1}(x)$.

Given the regions R_{jm}, finding the optimal constants γ_{jm} in each region is typically straightforward:

$$\hat{\gamma}_{jm} = \arg\min_{\gamma_{jm}} \sum_{x_i \in R_{jm}} L\left(y_i, f_{m-1}(x_i) + \gamma_{jm}\right). \tag{10.29}$$

Finding the regions is difficult, and even more difficult than for a single tree. For a few special cases, the problem simplifies.

For squared-error loss, the solution to (10.28) is no harder than for a single tree. It is simply the regression tree that best predicts the current residuals $y_i - f_{m-1}(x_i)$, and $\hat{\gamma}_{jm}$ is the mean of the these residuals in each corresponding region.

For two-class classification and exponential loss, this stagewise approach gives rise to the AdaBoost method for boosting classification trees (Algorithm 10.1). In particular, if the trees $T(x; \Theta_m)$ are restricted to be scaled classification trees, then we showed in Section 10.4 that the solution to (10.28) is the tree that minimizes the weighted error rate $\sum_{i=1}^{N} w_i^{(m)} I(y_i \neq T(x_i; \Theta_m))$ with weights $w_i^{(m)} = e^{-y_i f_{m-1}(x_i)}$. By a scaled classification tree, we mean $\beta_m T(x; \Theta_m)$, with the restriction that $\gamma_{jm} \in \{-1, 1\}$).

Without this restriction, (10.28) still simplifies for exponential loss to a weighted exponential criterion for the new tree:

$$\hat{\Theta}_m = \arg\min_{\Theta_m} \sum_{i=1}^{N} w_i^{(m)} \exp[-y_i T(x_i; \Theta_m)]. \tag{10.30}$$

It is straightforward to implement a greedy recursive-partitioning algorithm using this weighted exponential loss as a splitting criterion. Note that given the R_{jm}, the solution to (10.29) is the weighted log-odds in each corresponding region

$$\hat{\gamma}_{jm} = \log \frac{\sum_{x_i \in R_{jm}} w_i^{(m)} I(y_i = 1)}{\sum_{x_i \in R_{jm}} w_i^{(m)} I(y_i = -1)}. \tag{10.31}$$

This requires a specialized tree-growing algorithm; in practice, we prefer the approximation presented below that uses a weighted least squares regression tree.

Using loss criteria such as the absolute error or the Huber loss (10.22) in place of squared-error loss for regression, and the deviance (10.21) in place of exponential loss for classification, will serve to robustify boosting trees. Unfortunately, unlike their nonrobust counterparts, these robust criteria do not give rise to simple fast boosting algorithms.

For more general loss criteria the solution to (10.29), given the R_{jm}, is typically straightforward since it is a simple "location" estimate. For absolute loss it is just the median of the residuals in each respective region. For the other criteria fast iterative algorithms exist for solving (10.29), and usually their faster "single-step" approximations are adequate. The problem is tree induction. Simple fast algorithms do not exist for solving (10.28) for these more general loss criteria, and approximations like (10.26) become essential.

10.10 Numerical Optimization

Fast approximate algorithms for solving (10.28) with any differentiable loss criterion can be derived by analogy to numerical optimization. The loss in using $f(x)$ to predict y on the training data is

$$L(f) = \sum_{i=1}^{N} L(y_i, f(x_i)). \tag{10.32}$$

The goal is to minimize $L(f)$ with respect to f, where here $f(x)$ is constrained to be a sum of trees (10.27). Ignoring this constraint, minimizing (10.32) can be viewed as a numerical optimization

$$\hat{\mathbf{f}} = \arg\min_{\mathbf{f}} L(\mathbf{f}), \tag{10.33}$$

where the "parameters" $\mathbf{f} \in \mathbb{R}^N$ are the values of the approximating function $f(x_i)$ at each of the N data points x_i:

$$\mathbf{f} = \{f(x_1), f(x_2)), \ldots, f(x_N)\}.$$

Numerical optimization procedures solve (10.33) as a sum of component vectors

$$\mathbf{f}_M = \sum_{m=0}^{M} \mathbf{f}_m\,, \quad \mathbf{f}_m \in \mathbb{R}^N,$$

where $\mathbf{f}_0$ is an initial guess, and each successive $\mathbf{f}_m$ is induced based on the current parameter vector $\mathbf{f}_{m-1}$, which is the sum of the previously induced vectors. Numerical optimization methods differ in their prescriptions for computing each increment vector $\mathbf{f}_m$ ("step").

10.10.1 Steepest Descent

Steepest descent chooses $\mathbf{f}_m = -\rho_m \mathbf{g}_m$ where ρ_m is a scalar and $\mathbf{g}_m \in \mathbb{R}^N$ is the gradient of $L(\mathbf{f})$ evaluated at $\mathbf{f} = \mathbf{f}_{m-1}$. The components of the gradient $\mathbf{g}_m$ are

$$g_{im} = \left[\frac{\partial L(y_i, f(x_i))}{\partial f(x_i)}\right]_{f(x_i)=f_{m-1}(x_i)} \tag{10.34}$$

The *step length* ρ_m is the solution to

$$\rho_m = \arg\min_{\rho} L(\mathbf{f}_{m-1} - \rho \mathbf{g}_m). \tag{10.35}$$

The current solution is then updated

$$\mathbf{f}_m = \mathbf{f}_{m-1} - \rho_m \mathbf{g}_m$$

and the process repeated at the next iteration. Steepest descent can be viewed as a very greedy strategy, since $-\mathbf{g}_m$ is the local direction in $\mathbb{R}^N$ for which $L(\mathbf{f})$ is most rapidly decreasing at $\mathbf{f} = \mathbf{f}_{m-1}$.

10.10.2 Gradient Boosting

Forward stagewise boosting (Algorithm 10.2) is also a very greedy strategy. At each step the solution tree is the one that maximally reduces (10.28), given the current model f_{m-1} and its fits $f_{m-1}(x_i)$. Thus, the tree predictions $T(x_i; \Theta_m)$ are analogous to the components of the negative gradient (10.34). The principal difference between them is that the tree components $\mathbf{t}_m = (T(x_1; \Theta_m), \ldots, T(x_N; \Theta_m)$ are not independent. They are constrained to be the predictions of a J_m-terminal node decision tree, whereas the negative gradient is the unconstrained maximal descent direction.

TABLE 10.2. *Gradients for commonly used loss functions*

Setting	Loss Function	$-\partial L(y_i, f(x_i))/\partial f(x_i)$
Regression	$\frac{1}{2}[y_i - f(x_i)]^2$	$y_i - f(x_i)$
Regression	$\|y_i - f(x_i)\|$	$\text{sign}[y_i - f(x_i)]$
Regression	Huber	$y_i - f(x_i)$ for $\|y_i - f(x_i)\| \leq \delta_m$
		$\delta_m \text{sign}[y_i - f(x_i)]$ for $\|y_i - f(x_i)\| > \delta_m$
		where $\delta_m = \alpha$th-quantile$\{\|y_i - f(x_i)\|\}$
Classification	Deviance	kth component: $I(y_i = \mathcal{G}_k) - p_k(x_i)$

The solution to (10.29) in the stagewise approach is analogous to the line search (10.35) in steepest descent. The difference is that (10.29) performs a separate line search for those components of $\mathbf{t}_m$ that correspond to each separate terminal region $\{T(x_i; \Theta_m)\}_{x_i \in R_{jm}}$.

If minimizing loss on the training data (10.32) were the only goal, steepest descent would be the preferred strategy. The gradient (10.34) is trivial to calculate for any differentiable loss function $L(y, f(x))$, whereas solving (10.28) is difficult for the robust criteria discussed in Section 10.6. Unfortunately the gradient (10.34) is defined only at the training data points x_i, whereas the ultimate goal is to generalize $f_M(x)$ to new data not represented in the training set.

A possible resolution to this dilemma is to induce a tree $T(x; \Theta_m)$ at the mth iteration whose predictions $\mathbf{t}_m$ are as close as possible to the negative gradient. Using squared error to measure closeness, this leads us to

$$\tilde{\Theta}_m = \arg\min_{\Theta} \sum_{i=1}^{N} \left(-g_{im} - T(x_i; \Theta)\right)^2. \tag{10.36}$$

That is, one fits the tree T to the negative gradient values (10.34) by least squares. As noted in Section 10.10 fast algorithms exist for least squares decision tree induction. Although the solution regions $\tilde{R}_{jm}$ to (10.36) will not be identical to the regions R_{jm} that solve (10.28), it is generally similar enough to serve the same purpose. In any case, the forward stagewise boosting procedure, and top-down decision tree induction, are themselves approximation procedures. After constructing the tree (10.36), the corresponding constants in each region are given by (10.29).

Table 10.2 summarizes the gradients for commonly used loss functions. For squared error loss, the negative gradient is just the ordinary residual $-g_{im} = y_i - f_{m-1}(x_i)$, so that (10.36) on its own is equivalent standard least squares boosting. With absolute error loss, the negative gradient is

Algorithm 10.3 *Gradient tree boosting for multiple additive regression trees.*

```
1. Initialize $f_0(x) = \arg\min_\gamma \sum_{i=1}^N L(y_i, \gamma)$.
2. For $m = 1$ to $M$:
    (a) For $i = 1, 2, \dots, N$ compute
            $r_{im} = -\left[\frac{\partial L(y_i, f(x_i))}{\partial f(x_i)}\right]_{f=f_{m-1}}$.
    (b) Fit a regression tree to the targets $r_{im}$ giving terminal regions
        $R_{jm},\ j = 1, 2, \dots, J_m$.
    (c) For $j = 1, 2, \dots, J_m$ compute
            $\gamma_{jm} = \arg\min_\gamma \sum_{x_i \in R_{jm}} L\left(y_i, f_{m-1}(x_i) + \gamma\right)$.
    (d) Update $f_m(x) = f_{m-1}(x) + \sum_{j=1}^{J_m} \gamma_{jm} I(x \in R_{jm})$.
3. Output $\hat{f}(x) = f_M(x)$.
```

the *sign* of the residual, so at each iteration (10.36) fits the tree to the sign of the current residuals by least squares. For Huber M-regression, the negative gradient is a compromise between these two (see the table).

For classification the loss function is the multinomial deviance (10.21), and K least squares trees are constructed at each iteration. Each tree T_{km} is fit to its respective negative gradient vector $\mathbf{g}_{km}$,

$$\begin{aligned} -g_{ikm} &= \frac{\partial L\left(y_i, f_{1m}(x_i), \dots, f_{1m}(x_i)\right)}{\partial f_{km}(x_i)} \\ &= I(y_i = \mathcal{G}_k) - p_k(x_i), \end{aligned} \tag{10.37}$$

with $p_k(x)$ given by (10.20). Although K separate trees are built at each iteration, they are related through (10.20).

10.10.3 MART

Algorithm 10.3 presents the generic gradient tree-boosting algorithm for regression. Specific algorithms are obtained by inserting different loss criteria $L(y, f(x))$. This approach is referred to as "multiple additive regression trees," or MART. The first line of the algorithm initializes to the optimal constant model, which is just a single terminal node tree. The components of the negative gradient computed at line 2(a) are referred to as generalized or *pseudo* residuals, r. Gradients for commonly used loss functions are summarized in Table 10.2.

The algorithm for classification is similar. Lines 2(a)–(d) are repeated K times at each iteration m, once for each class using (10.37). The result at line 3 is K different (coupled) tree expansions $f_{kM}(x), k = 1, 2, \dots, K$. These produce probabilities via (10.20) or do classification as in (10.19). Details are given in Exercise 10.5.

Tuning parameters associated with the MART procedure are the number of iterations M and the sizes of each of the constituent trees J_m, $m = 1, 2, \dots, M$.

10.11 Right-Sized Trees for Boosting

Historically, boosting was considered to be a technique for combining models, here trees. As such, the tree building algorithm was regarded as a primitive that produced models to be combined by the boosting procedure. In this scenario, the optimal size of each tree is estimated separately in the usual manner when it is built (Section 9.2). A very large (oversized) tree is first induced, and then a bottom-up procedure is employed to prune it to the estimated optimal number of terminal nodes. This approach assumes implicitly that each tree is the last one in the expansion (10.27). Except perhaps for the very last tree, this is clearly a very poor assumption. The result is that trees tend to be much too large, especially during the early iterations. This substantially degrades performance and increases computation.

The simplest strategy for avoiding this problem is to restrict all trees to be the same size, $J_m = J \ \forall m$. At each iteration a J-terminal node regression tree is induced. Thus J becomes a meta-parameter of the entire boosting procedure, to be adjusted to maximize estimated performance for the data at hand.

One can get an idea of useful values for J by considering the properties of the "target" function

$$\eta = \arg\min_f \mathrm{E}_{XY} L(Y, f(X)). \tag{10.38}$$

Here the expected value is over the population joint distribution of (X, Y). The target function $\eta(x)$ is the one with minimum prediction risk on future data. This is the function we are trying to approximate.

One relevant property of $\eta(X)$ is the degree to which the coordinates variables $X = (X_1, X_2, \dots, X_p)$ interact with one another. This is captured by its ANOVA (analysis of variance) expansion

$$\eta(X) = \sum_j \eta_j(X_j) + \sum_{jk} \eta_{jk}(X_j, X_k) + \sum_{jkl} \eta_{jkl}(X_j, X_k, X_l) + \cdots . \tag{10.39}$$

The first sum in (10.39) is over functions of only a single predictor variable X_j. The particular functions $\eta_j(X_j)$ are those that jointly best approximate $\eta(X)$ under the loss criterion being used. Each such $\eta_j(X_j)$ is called the "main effect" of X_j. The second sum is over those two-variable functions that when added to the main effects best fit $\eta(X)$. These are called the second-order interactions of each respective variable pair (X_j, X_k). The third sum represents third-order interactions, and so on. For many problems encountered in practice, low-order interaction effects tend to dominate. When this is the case, models that produce strong higher-order interaction effects, such as large decision trees, suffer in accuracy.

The interaction level of tree-based approximations is limited by the tree size J. Namely, no interaction effects of level greater that $J-1$ are possible. Since boosted models are additive in the trees (10.27), this limit extends to them as well. Setting $J = 2$ (single split "decision stump") produces boosted models with only main effects; no interactions are permitted. With $J = 3$, two-variable interaction effects are also allowed, and so on. This suggests that the value chosen for J should reflect the level of dominant interactions of $\eta(x)$. This is of course generally unknown, but in most situations it will tend to be low. Figure 10.9 illustrates the effect of interaction order (choice of J) on the simulation example (10.2). The generative function is additive (sum of quadratic monomials), so boosting models with $J > 2$ incurs unnecessary variance and hence the higher test error. Figure 10.10 compares the coordinate functions found by boosted stumps with the true functions.

Although in many applications $J = 2$ will be insufficient, it is unlikely that $J > 10$ will be required. Experience so far indicates that $4 \le J \le 8$ works well in the context of boosting, with results being fairly insensitive to particular choices in this range. One can fine tune the value for J by trying several different values and choosing the one that produces the lowest risk on a validation sample. However, this seldom provides significant improvement over using $J \simeq 6$.

10.12 Regularization

Besides the size of the constituent trees, J, the other meta-parameter of the MART procedure is the number of boosting iterations M. Each iteration usually reduces the training risk $L(f_M)$, so that for M large enough this risk can be made arbitrarily small. However, fitting the training data too well

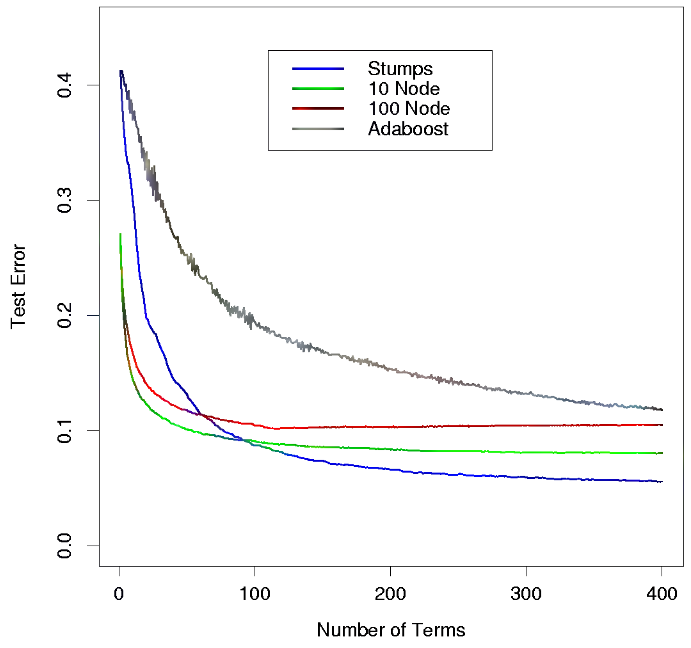

FIGURE 10.9. *Boosting with different sized trees, applied to the example (10.2) used in Figure 10.2. Since the generative model is additive, stumps perform the best. The boosting algorithm used the binomial deviance loss in Algorithm 10.3; shown for comparison is the AdaBoost algorithm 10.1.*

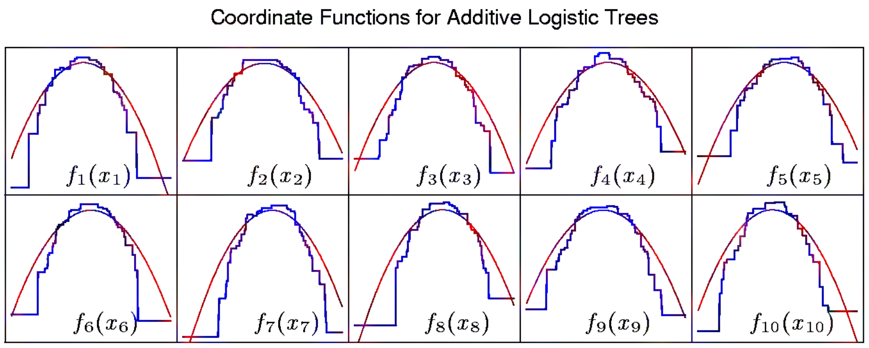

FIGURE 10.10. *Coordinate functions estimated by boosting stumps for the simulated example used in Figure 10.9. The true quadratic functions are shown for comparison.*

can lead to overfitting, which degrades the risk on future predictions. Thus, there is an optimal number M^* minimizing future risk that is application dependent. A convenient way to estimate M^* is to monitor prediction risk as a function of M on a validation sample. The value of M that minimizes this risk is taken to be an estimate of M^*. This is analogous to the early stopping strategy often used with neural networks (Section 11.4).

10.12.1 Shrinkage

Controlling the value of M is not the only possible regularization strategy. As with ridge regression and neural networks, shrinkage techniques can be employed as well (see Sections 3.4.3 and 11.5). The simplest implementation of shrinkage in the context of boosting is to scale the contribution of each tree by a factor $0 < \nu < 1$ when it is added to the current approximation. That is, line 2(d) of Algorithm 10.3 is replaced by

$$f_m(x) = f_{m-1}(x) + \nu \cdot \sum_{j=1}^{J} \hat{\gamma}_{jm} I(x \in R_{jm}). \tag{10.40}$$

The parameter ν can be regarded as controlling the learning rate of the boosting procedure. Smaller values of ν (more shrinkage) result in larger training risk for the same number of iterations M. Thus, both ν and M control prediction risk on the training data. However, these parameters do not operate independently. Smaller values of ν lead to larger values of M for the same training risk, so that there is a tradeoff between them.

Empirically it has been found (Friedman, 2001) that smaller values of ν favor better test error, and require correspondingly larger values of M. In fact, the best strategy appears to be to set ν to be very small ($\nu < 0.1$) and then choose M by early stopping. This yields dramatic improvements (over no shrinkage $\nu = 1$) for regression and for probability estimation. The corresponding improvements in misclassification risk via (10.19) are less, but still substantial. The price paid for these improvements is computational: smaller values of ν give rise to larger values of M, and computation is proportional to the latter. However, as seen below, many iterations are generally computationally feasible even on very large data sets. This is partly due to the fact that small trees are induced at each step with no pruning.

Figure 10.12.1 shows test error curves for the simulated example (10.2) of Figure 10.2. MART was trained using binomial deviance, using either stumps or six terminal-node trees, and with or without shrinkage. The benefits of shrinkage is evident, especially when the binomial deviance is tracked. With shrinkage, each test error curve reaches a lower value, and stays there for many iterations.

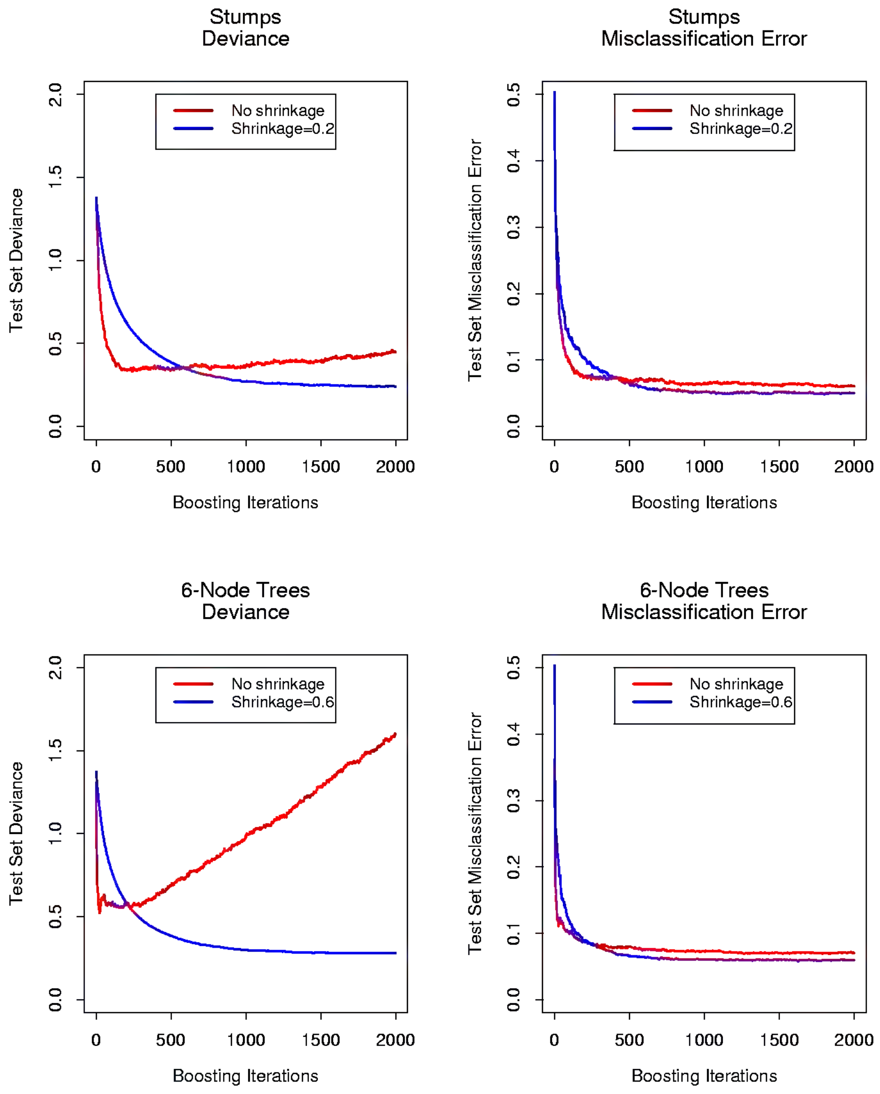

FIGURE 10.11. *Test error curves for simulated example (10.2) of Figure 10.9, using MART. The models were trained using binomial deviance, either stumps or six terminal-node trees, and with or without shrinkage. The left panels report test deviance, while the right panels show misclassification error. The beneficial effect of shrinkage can be seen in all cases, especially for deviance in the left panels.*

10.12.2 Penalized Regression

Intuition for the success of the shrinkage strategy (10.40) can be obtained by drawing analogies with penalized linear regression with a large basis expansion. Consider the set of all possible J-terminal node regression trees $\mathcal{T} = \{T_k\}$ that could be realized on the training data as basis functions in $\mathbb{R}^p$. The linear model is

$$f(x) = \sum_{k=1}^{K} \alpha_k T_k(x), \tag{10.41}$$

where $K = \text{card}(\mathcal{T})$. Suppose the coefficients are to be estimated by least squares. Since the number of such trees is likely to be much larger than even the largest training data sets, penalized least squares is required

$$\hat{\alpha}(\lambda) = \arg\min_{\alpha} \left\{ \sum_{i=1}^{N} \left(y_i - \sum_{k} \alpha_k T_k(x_i) \right)^2 + \lambda \cdot J(\alpha) \right\}, \tag{10.42}$$

where α is the vector of parameters, and $J(\alpha)$ is a function of the coefficients that generally penalizes larger values. Examples are

$$J(\alpha) = \sum_{k=1}^{K} \alpha_k^2 \qquad \text{ridge regression,} \tag{10.43}$$

$$J(\alpha) = \sum_{k=1}^{K} |\alpha_k| \qquad \text{lasso (Section 3.4.3).} \tag{10.44}$$

As discussed in Section 3.4.3, the solution to the lasso problem with moderate to large λ tends to be sparse; many of the $\hat{\alpha}_k(\lambda) = 0$. That is, only a small fraction of all possible trees enter the model (10.41). This seems reasonable since it is likely that only a small fraction of all possible trees will be relevant in approximating any particular target function. However, the relevant subset will be different for different targets. Those coefficients that are not set to zero are shrunk by the lasso in that their absolute values are smaller than their corresponding least squares values: $|\hat{\alpha}_k(\lambda)| < |\hat{\alpha}_k(0)|$. As λ increases, the coefficients all shrink, each one ultimately becoming zero.

Owing to the very large number of basis functions T_k, directly solving (10.42) with the lasso penalty (10.44) is not possible. However, a feasible forward stagewise strategy exists that closely approximates the effect of the lasso, and is very similar to boosting and the forward stagewise Algorithm 10.2. Algorithm 10.4 gives the details. Although phrased in terms of tree basis functions T_k, the algorithm can be used with any set of basis functions. Initially all coefficients are zero in line 1; this corresponds to $\lambda = \infty$ in (10.42). At each successive step, the tree T_{k^*} is selected that

Algorithm 10.4 *Forward stagewise linear regression.*

```
1. Initialize $\hat{\alpha}_k = 0,\ k = 1, \ldots, K$. Set $\varepsilon > 0$ to some small constant,
   and $M$ large.
2. For $m = 1$ to $M$:
   (a) $(\beta^*, k^*) = \arg\min_{\beta,k} \sum_{i=1}^{N} \left( y_i - \sum_{l=1}^{K} \alpha_l T_l(x_i) - \beta T_k(x_i) \right)^2$.
   (b) $\alpha_{k^*} \leftarrow \alpha_{k^*} + \varepsilon \cdot \text{sign}(\beta^*)$.
3. Output $f(x) = \sum_{k=1}^{K} \alpha_k T_k(x)$.
```

best fits the current residuals in line 2(a). Its corresponding coefficient α_{k^*} is then incremented or decremented by an infinitesimal amount in 2(b), while all other coefficients $\alpha_k,\ k \neq k^*$ are left unchanged. In principle, this process could be iterated until either all the residuals are zero, or $\beta^* = 0$. The latter case can occur if $K < N$, and at that point the coefficient values represent a least squares solution. This corresponds to $\lambda = 0$ in (10.42).

After applying Algorithm 10.4 with $M < \infty$ iterations, many of the coefficients will be zero, namely those that have yet to be incremented. The others will tend to have absolute values smaller than their corresponding least squares solution values, $|\,\hat{\alpha}_k(M)\,| < |\,\hat{\alpha}_k(0)\,|$. Therefore this M-iteration solution qualitatively resembles the lasso, with M inversely related to λ.

Figure 10.12 shows an example, using the prostate data studied in Chapter 3. Here, instead of using trees $T_k(X)$ as basis functions, we use the original variables X_k themselves; that is, a multiple linear regression model. The left panel displays the profiles of estimated coefficients from the lasso, for different values of the bound parameter $t = \sum_k |\alpha_k|$. The right panel shows the results of the stagewise Algorithm 10.4, with $M = 250$ and $\varepsilon = 0.01$. The similarity between the two graphs is striking.

In some situations the resemblance is more than qualitative. For example, if all of the basis functions T_k are mutually uncorrelated, then as $\varepsilon \to 0$, Algorithm 10.4 for some $0 < M < \infty$ yields exactly the same set of solutions as the lasso for $\infty \geq \lambda \geq 0$. Of course, tree-based regressors are not uncorrelated. However, the solution sets are also identical if the coefficients $\hat{\alpha}_k(\lambda)$ are all monotone functions of λ. This is often the case. When the $\hat{\alpha}_k(\lambda)$ are not monotone in λ, then the solution sets are not identical, but usually quite close. The solutions sets for Algorithm 10.4 tend to change less rapidly with changing values of the regularization parameter than those of the lasso.

Tree boosting (Algorithm 10.3) with shrinkage (10.40) closely resembles Algorithm 10.4, with the learning rate parameter ν corresponding to ε. For squared error loss, the only difference is that the optimal tree to be selected at each iteration T_{k*} is approximated by the standard top-down

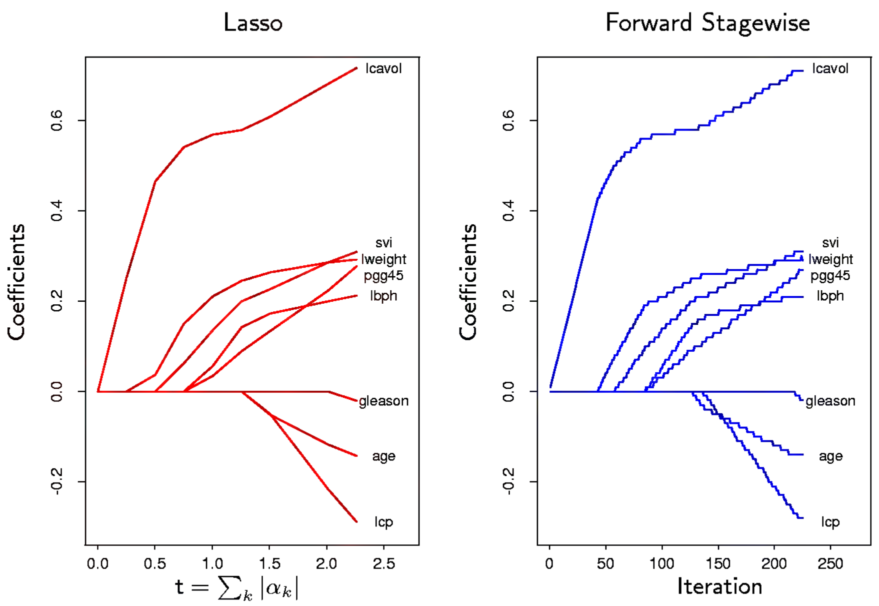

FIGURE 10.12. *Profiles of estimated coefficients from linear regression, for the prostate data studied in Chapter 3. The left panel shows the results from the lasso, for different values of the bound parameter $t = \sum_k |\alpha_k|$. The right panel shows the results of the stagewise linear regression algorithm 10.4, using $M = 250$ consecutive steps of size $\varepsilon = .01$.*

greedy induction algorithm. For other loss criteria, there are no rigorous results comparing shrinkage (10.40) to penalized regression with a particular penalty. However, qualitatively one would expect a correspondence similar to that of least squares. Thus, one can view tree boosting with shrinkage as ill-posed regression on all possible (J-terminal node) trees with the lasso penalty (10.44) as a regularizer.

No shrinkage ($\nu = 1$ in equation (10.40)) is analogous to subset selection which penalizes the number of non zero coefficients $J(\alpha) = \sum_k |\alpha_k|^0$. For prediction, subset selection is well-known to be excessively greedy (Copas, 1983), yielding poor results when compared to less aggressive strategies such as the lasso or ridge regression. The dramatic improvements resulting from shrinkage in the context of boosting are yet another confirmation of this approach.

10.12.3 Virtues of the L_1 Penalty (Lasso) over L_2

As shown in the previous section, boosting's forward stagewise strategy with shrinkage approximately minimizes the same loss function with a lasso-style L_1 penalty. The model is built up slowly, traveling through "model space" and adding shrunken functions of important predictors. In contrast, the L_2 penalty is much easier to deal with, as shown in Section 12.3.6. With the basis functions and L_2 penalty chosen to match a particular positive definite kernel, one can solve the corresponding minimization problem without explicitly searching over individual basis functions.

However, the superior performance of boosting over procedures such as the support vector machine may be largely due to the implicit use of L_1 versus L_2 penalty. The shrinkage resulting from the L_1 penalty is better suited to *sparse* situations, where there are few basis functions with nonzero weights (among all possible choices). Some results supporting this claim, for the specialized setting of wavelet bases, are given by Donoho et al. (1995). Direct minimization of the L_1-penalized problem is much more difficult than that for L_2, but the forward stagewise algorithm of boosting provides an approximate, practical attack on the problem.

10.13 Interpretation

Single decision trees are highly interpretable. The entire model can be completely represented by a simple two-dimensional graphic (binary tree) that is easily visualized. Linear combinations of trees (10.27) lose this important feature, and must therefore be interpreted in a different way.

10.13.1 Relative Importance of Predictor Variables

In data mining applications the input predictor variables are seldom equally relevant. Often only a few of them have substantial influence on the response; the vast majority are irrelevant and could just as well have not been included. It is often useful to learn the relative importance or contribution of each input variable in predicting the response.

For a single decision tree T, Breiman et al. (1984) proposed

$$\mathcal{I}_\ell^2(T) = \sum_{t=1}^{J-1} \hat{\imath}_t^2 \, I(v(t) = \ell) \tag{10.45}$$

as a measure of relevance for each predictor variable X_ℓ. The sum is over the $J-1$ internal nodes of the tree. At each such node t, one of the input variables $X_{v(t)}$ is used to partition the region associated with that node into two subregions; within each a separate constant is fit to the response values. The particular variable chosen is the one that gives maximal estimated improvement $\hat{\imath}_t^2$ in squared error risk over that for a constant fit over the entire region. The squared relative importance of variable X_ℓ is the sum of such squared improvements over all internal nodes for which it was chosen as the splitting variable.

This importance measure is easily generalized to additive tree expansions (10.27); it is simply averaged over the trees

$$\mathcal{I}_\ell^2 = \frac{1}{M}\sum_{m=1}^{M} \mathcal{I}_\ell^2(T_m). \tag{10.46}$$

Due to the stabilizing effect of averaging, this measure turns out to be more reliable than is its counterpart (10.45) for a single tree. Also, because of shrinkage (Section 10.12.1) the masking of important variables by others with which they are highly correlated is much less of a problem. Note that (10.45) and (10.46) refer to *squared* relevance; the actual relevances are their respective square roots. Since these measures are relative, it is customary to assign the largest a value of 100 and then scale the others accordingly. Figure 10.6 shows the relevant importance of the 57 inputs in predicting `spam` versus `email`.

For K-class classification, K separate models $f_k(x), k = 1, 2, \ldots, K$ are induced, each consisting of a sum of trees

$$f_k(x) = \sum_{m=1}^{M} T_{km}(x). \tag{10.47}$$

In this case (10.46) generalizes to

$$\mathcal{I}_{\ell k}^2 = \frac{1}{M}\sum_{m=1}^{M} \mathcal{I}_\ell^2(T_{km}). \tag{10.48}$$

Here $\mathcal{I}_{\ell k}$ is the relevance of X_ℓ in separating the class k observations from the other classes. The overall relevance of x_j is obtained by averaging over all of the classes

$$\mathcal{I}_\ell^2 = \frac{1}{K}\sum_{k=1}^{K} \mathcal{I}_{\ell k}^2. \tag{10.49}$$

Figures 10.19 and 10.20 illustrate the use of these averaged and separate relative importances.

The individual $\mathcal{I}_{\ell k}$ can themselves be quite useful. One can summarize the $p \times K$ matrix of these relevance values in a variety of ways. Individual columns $\mathcal{I}_{\cdot k}$ give the relative variable importances in separating class k. The individual rows $\mathcal{I}_{\ell}$ reveal the influence of X_ℓ in separating the respective classes. One can average the matrix elements (10.48) over chosen subsets of classes to determine variable relevance for that subset. Similarly, one can average over subsets of variables to obtain an idea of which classes the chosen variable subset is most influential in separating.

10.13.2 Partial Dependence Plots

After the most relevant variables have been identified, the next step is to attempt to understand the nature of the dependence of the approximation $f(X)$ on their joint values. Visualization is one of the most powerful such interpretational tools. Graphical renderings of the $f(X)$ as a function of its arguments provides a comprehensive summary of its dependence on the joint values of the input variables.

Unfortunately, such visualization is limited to low-dimensional views. We can easily display functions of one or two arguments, either continuous or discrete (or mixed), in a variety of different ways; this book is filled with such displays. Functions of slightly higher dimensions can be plotted by conditioning on particular sets of values of all but one or two of the arguments, producing a *trellis* of plots (Becker et al., 1996).

For more than two or three variables, viewing functions of the corresponding higher dimensional arguments is more difficult. A useful alternative can sometimes be to view a collection of plots, each one of which shows the partial dependence of the approximation $f(X)$ on a selected small subset of the input variables. Although such a collection can seldom provide a comprehensive depiction of the approximation, it can often produce helpful clues, especially when $f(x)$ is dominated by low-order interactions (10.39).

Consider the subvector $X_{\mathcal{S}}$ of $\ell < p$ of the input predictor variables $X = (X_1, X_2, \ldots, X_p)$, indexed by $\mathcal{S} \subset \{1, 2, \ldots, p\}$. Let $\mathcal{C}$ be the complement set, with $\mathcal{S} \cup \mathcal{C} = \{1, 2, \ldots, p\}$. A general function $f(X)$ will in principle depend on all of the input variables: $f(X) = f(X_{\mathcal{S}}, X_{\mathcal{C}})$. One way to define the average or *partial* dependence of $f(X)$ on $X_{\mathcal{S}}$ is

$$f_{\mathcal{S}}(X_{\mathcal{S}}) = \mathrm{E}_{X_{\mathcal{C}}} f(X_{\mathcal{S}}, X_{\mathcal{C}}). \tag{10.50}$$

This is a marginal average of f, and can serve as a useful description of the effect of the chosen subset on $f(X)$ when, for example, the variables in $X_{\mathcal{S}}$ do not have strong interactions with those in $X_{\mathcal{C}}$.

Partial dependence functions can be used to interpret the results of any "black box" learning method. They can be estimated by

$$\bar{f}_{\mathcal{S}}(X_{\mathcal{S}}) = \frac{1}{N} \sum_{i=1}^{N} f(X_{\mathcal{S}}, x_{i\mathcal{C}}), \tag{10.51}$$

where $\{x_{1\mathcal{C}}, x_{2\mathcal{C}}, \ldots, x_{N\mathcal{C}}\}$ are the values of $X_{\mathcal{C}}$ occurring in the training data. This requires a pass over the data for each set of joint values of $X_{\mathcal{S}}$ for which $\bar{f}_{\mathcal{S}}(X_{\mathcal{S}})$ is to be evaluated. This can be computationally intensive, even for moderately sized data sets. Fortunately with decision trees, $\bar{f}_{\mathcal{S}}(X_{\mathcal{S}})$ (10.51) can be rapidly computed from the tree itself without reference to the data (Friedman, 2001). For additive tree models (10.27), the results are averaged over the constituent trees.

It is important to note that partial dependence functions defined in (10.50) represent the effect of $X_{\mathcal{S}}$ on $f(X)$ after accounting for the (average) effects of the other variables $X_{\mathcal{C}}$ on $f(X)$. They are *not* the effect of $X_{\mathcal{S}}$ on $f(X)$ *ignoring* the effects of $X_{\mathcal{C}}$. The latter is given by the conditional expectation

$$\tilde{f}_{\mathcal{S}}(X_{\mathcal{S}}) = \mathrm{E}(f(X_{\mathcal{S}}, X_{\mathcal{C}})|X_{\mathcal{S}}), \tag{10.52}$$

and is the best least squares approximation to $f(X)$ by a function of $X_{\mathcal{S}}$ alone. The quantities $\tilde{f}_1(X_{\mathcal{S}})$ and $\bar{f}_1(X_{\mathcal{S}})$ will be the same only in the unlikely event of complete independence among all the predictor variables. For example, if the effect of the chosen variable subset happens to be purely additive,

$$f(X) = h_1(X_{\mathcal{S}}) + h_2(X_{\mathcal{C}}). \tag{10.53}$$

Then (10.50) produces the $h_1(X_{\mathcal{S}})$ up to an additive constant. If the effect is purely multiplicative,

$$f(X) = h_1(X_{\mathcal{S}}) \cdot h_2(X_{\mathcal{C}}), \tag{10.54}$$

then (10.50) produces $h_1(X_{\mathcal{S}})$ up to a multiplicative constant factor. On the other hand, (10.52) will not produce $h_1(X_{\mathcal{S}})$ in either case. In fact, (10.52) can produce strong effects on variable subsets for which $f(X)$ has no dependence at all.

Viewing plots of the partial dependence of the boosted-tree approximation (10.27) on selected variables subsets can help to provide a qualitative description of its properties. Illustrations are shown in Sections 10.8 and 10.14. Owing to the limitations of computer graphics, and human perception, the size of the subsets $X_{\mathcal{S}}$ must be small ($l \approx 1, 2, 3$). There are of course a large number of such subsets, but only those chosen from among the usually much smaller set of highly relevant predictors are likely to be informative. Also, those subsets whose effect on $f(X)$ is approximately additive (10.53) or multiplicative (10.54) will be most revealing. Diagnostics for the degree to which this is the case can be obtained by computing the multiple correlation coefficient of $f(X)$ with $\bar{f}_{\mathcal{S}}(X_{\mathcal{S}})$ and $\bar{f}_{\mathcal{C}}(X_{\mathcal{C}})$ for (10.53), and the simple correlation of $f(X)$ with $\bar{f}_{\mathcal{S}}(X_{\mathcal{S}})\cdot\ \bar{f}_{\mathcal{C}}(X_{\mathcal{C}})$ for (10.54).

For K-class classification, there are K separate models (10.47), one for each class. Each one is related to the respective probabilities (10.20) through

$$f_k(X) = \log p_k(X) - \frac{1}{K}\sum_{l=1}^{K} \log p_l(X). \tag{10.55}$$

Thus each $f_k(X)$ is a monotone increasing function of its respective probability on a logarithmic scale. Partial dependence plots of each respective $f_k(X)$ (10.47) on its most relevant predictors (10.48) can help reveal how the log-odds of realizing that class depend on the respective input variables.

10.14 Illustrations

In this section the MART procedure is further illustrated on two larger public domain data sets. In both of the examples the constituent tree size (Section 10.11) was taken to be $J = 6$ terminal nodes, and the learning rate (10.40) was set to $\nu = 0.1$. The Huber loss criterion was used for predicting numeric responses (regression) and multinomial deviance for classification. A random sample of 20% of each data set was set aside as a test set to evaluate performance, and the models were trained on the remaining 80%.

10.14.1 California Housing

This data set (Pace and Barry, 1997) is available from the Carnegie-Mellon STATLIB repository.* It consists of aggregated data from each of 20,460 neighborhoods (1990 census block groups) in California. The response variable Y is the median house value in each neighborhood measured in units of \$100,000. The predictor variables are demographics such as median income `MedInc`, housing density as reflected by the number of houses `House`, and the average occupancy in each house `AveOccup`. Also included as predictors are the location of each neighborhood (`longitude` and `latitude`), and several quantities reflecting the properties of the houses in the neighborhood: average number of rooms `AveRooms` and bedrooms `AveBedrms`. There are thus a total of eight predictors, all numeric.

Figure 10.13 shows the average absolute error

$$AAE = \mathrm{E}\,|y - \hat{f}_M(x)| \tag{10.56}$$

as a function for number of iterations M on both the training data (lower green curve) and test data (upper red curve). The training error has a rough wiggly appearance due to a stochastic aspect of the algorithm described in Friedman (1999). The test error is seen to decrease monotonically with increasing M, more rapidly during the early stages and then leveling off to being nearly constant as iterations increase. Thus, the choice of a particular value of M is not critical, as long as it is not too small. This tends to be the case in nearly all applications. The shrinkage strategy (10.40) tends to eliminate the problem of overfitting, especially for larger data sets.

The value of AAE after 600 iterations is 0.31. This can be compared to that of the optimal constant predictor median$\{y_i\}$ which is 0.89. In terms of more familiar quantities, the squared multiple correlation coefficient of this model is $R^2 = 0.84$. Pace and Barry (1997) use a sophisticated spatial autoregression procedure, where prediction for each neighborhood is based on median house values in nearby neighborhoods, using the other predictors as covariates. Experimenting with transformations they achieved $R^2 = 0.85$,

*http://lib.stat.cmu.edu

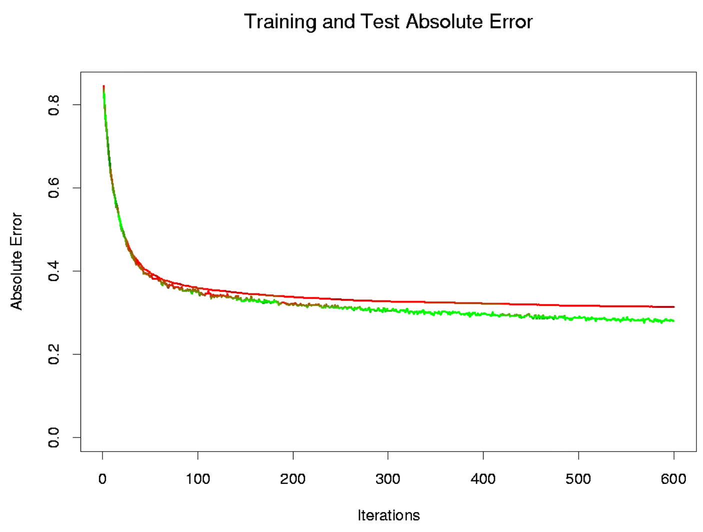

FIGURE 10.13. *Average-absolute error as a function of number of iterations for the California housing data.*

predicting $\log Y$. Using $\log Y$ as the response the corresponding value for MART was $R^2 = 0.86$.

Figure 10.14 displays the relative variable importances for each of the eight predictor variables. Not surprisingly, neighborhood median income was the most relevant predictor. Longitude, latitude, and average occupancy all have roughly half the relevance of income, whereas the others are somewhat less influential.

Figure 10.15 shows single-variable partial dependence plots on the most relevant nonlocation predictors. Note that the plots are not strictly smooth. This is a consequence of using tree-based models. Decision trees produce discontinuous piecewise constant models (10.24). This carries over to sums of trees (10.27), with of course many more pieces. Unlike most of the methods discussed in this book, there is no smoothness constraint imposed on the result. Arbitrarily sharp discontinuities can be modeled. The fact that these curves generally exhibit a smooth trend is because that is what is estimated to best predict the response for this problem. This is often the case.

The hash marks at the base of each plot delineate the deciles of the data distribution of the corresponding variables. Note that here the data density is lower near the edges, especially for larger values. This causes the curves to be somewhat less well determined in those regions. The vertical scales of the plots are the same, and give a visual comparison of the relative importance of the different variables.

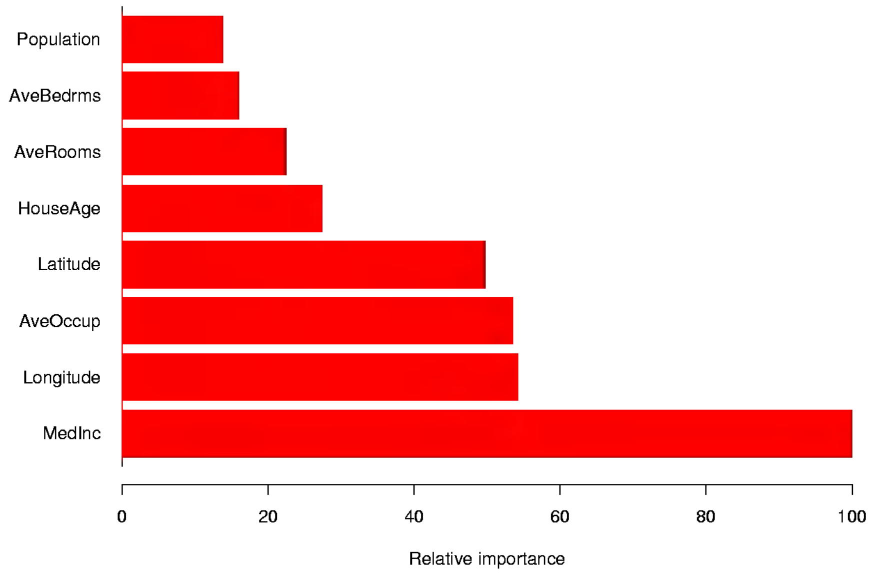

FIGURE 10.14. *Relative importance of the predictors for the California housing data.*

The partial dependence of median house value on median income is monotonic increasing, being nearly linear over the main body of data. House value is generally monotonic decreasing with increasing average occupancy, except perhaps for average occupancy rates less than one. Median house value has a nonmonotonic partial dependence on average number of rooms. It has a minimum at approximately three rooms and is increasing both for smaller and larger values.

Median house value is seen to have a very weak partial dependence on house age that is inconsistent with its importance ranking (Figure 10.14). This suggests that this weak main effect may be masking stronger interaction effects with other variables. Figure 10.16 shows the two-variable partial dependence of housing value on joint values of median age and average occupancy. An interaction between these two variables is apparent. For values of average occupancy greater than two, house value is nearly independent of median age, whereas for values less than two there is a strong dependence on age.

Figure 10.17 shows the two-variable partial dependence contour plot on joint values of longitude and latitude, displayed as a contour. There is clearly a very strong dependence of median house value on the neighborhood location in California. Note that Figure 10.17 is *not* a plot of house value versus location *ignoring* the effects of the other predictors (10.52). Like all partial dependence plots, it represents the effect of location after accounting for the effects of the other neighborhood and house attributes

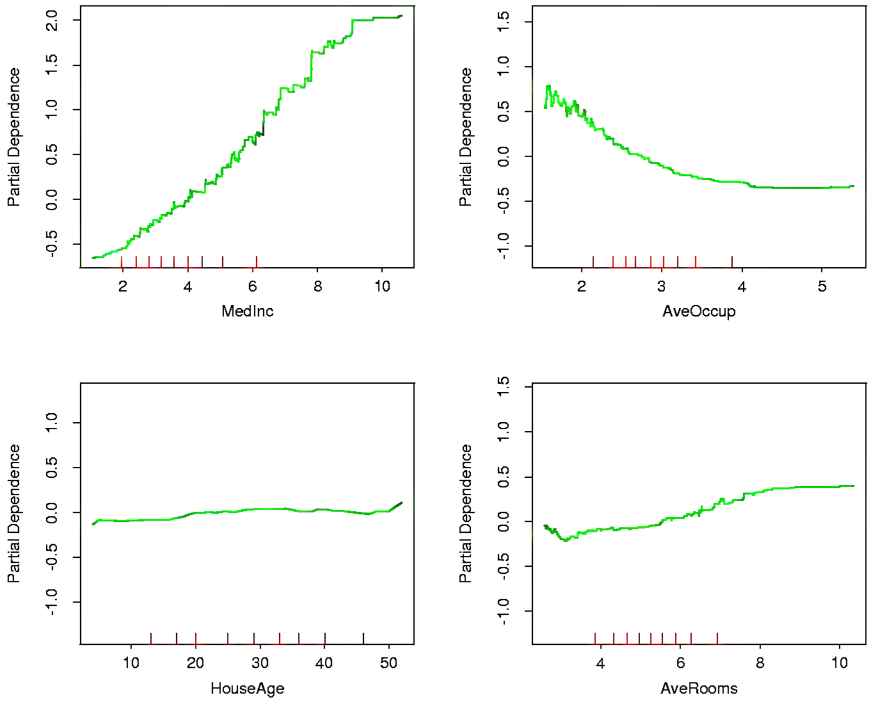

FIGURE 10.15. *Partial dependence of housing value on the nonlocation variables for the California housing data.*

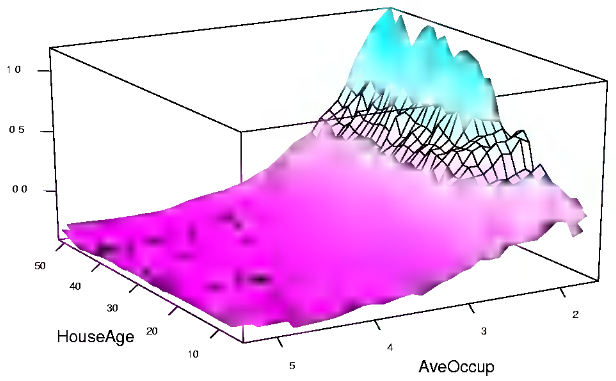

FIGURE 10.16. *Partial dependence of house value on median age and average occupancy. There appears to be a strong interact effect between these two variables.*

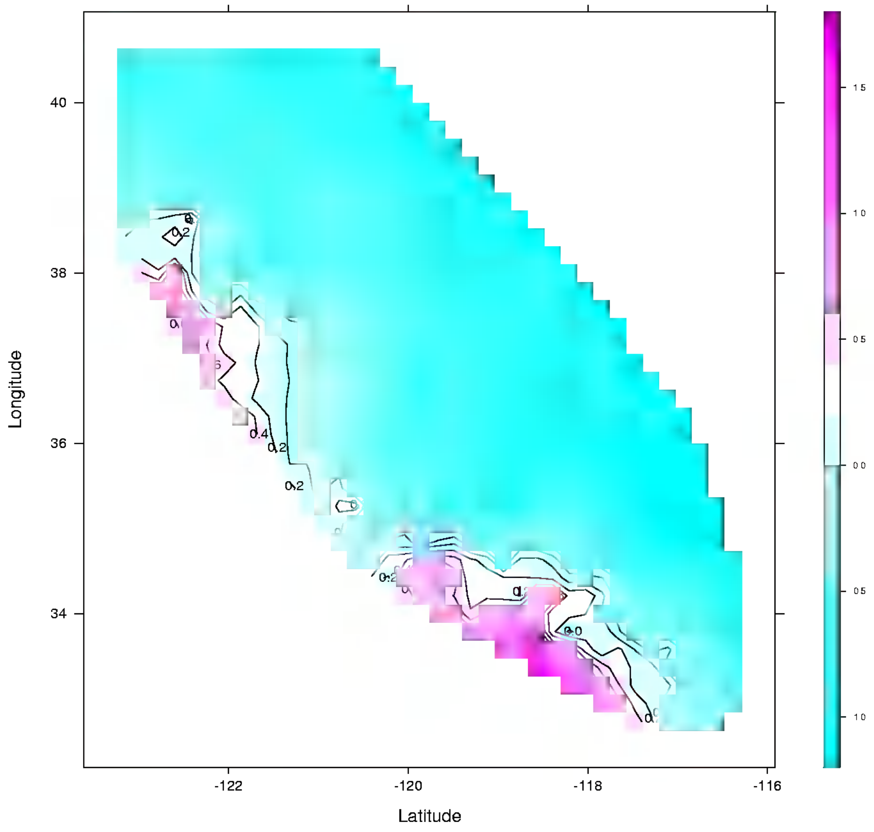

FIGURE 10.17. *Partial dependence of median house value on location in California.*

(10.50). It can be viewed as representing an extra premium one pays for location. This premium is seen to be relatively large near the Pacific coast especially in the Bay Area and Los Angeles–San Diego regions. In the northern, central valley, and southeastern desert regions of California, location costs considerably less.

10.14.2 Demographics Data

In this section MART is illustrated on a multi-class classification problem. The data come from 9243 questionnaires filled out by shopping mall customers in the San Francisco Bay Area (Impact Resources, Inc., Columbus, OH). Among the questions are 14 concerning demographics. For this illustration the goal is to predict occupation using the other 13 variables as predictors, and hence identify demographic variables that discriminate between different occupational categories.

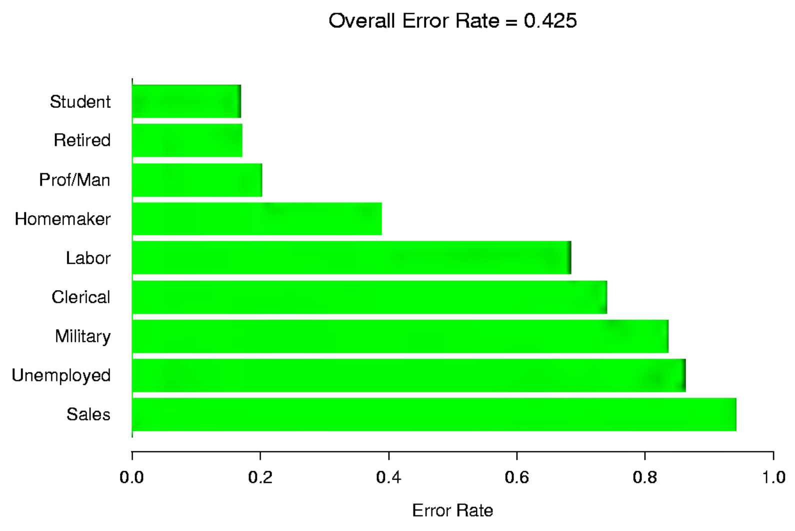

FIGURE 10.18. *Error rate for each occupation in the demographics data.*

Figure 10.18 shows the $K = 9$ occupation class values along with their corresponding error rates. The overall error rate is 42.5%, which can be compared to the null rate of 69% obtained by predicting the most numerous class `Prof/Man` (Professional/Managerial). The four best predicted classes are seen to be `Retired`, `Student`, `Prof/Man`, and `Homemaker`.

Figure 10.19 shows the relative predictor variable importances as averaged over all classes (10.49). Figure 10.20 displays the individual relative importance distributions (10.48) for each of the four best predicted classes. One sees that the most relevant predictors are generally different for each respective class. An exception is `age` which is among the three most relevant for predicting `Retired`, `Student`, and `Prof/Man`.

Figure 10.21 shows the partial dependence of the log-odds (10.55) on `age` for these three classes. The abscissa values are ordered codes for respective equally spaced age intervals. One sees that after accounting for the contributions of the other variables, the odds of being retired are higher for older people, whereas the opposite is the case for being a student. The odds of being professional/managerial are highest for middle-aged people. These results are of course not surprising. They illustrate that inspecting partial dependences separately for each class can lead to sensible results.

Bibliographic Notes

Schapire (1990) developed the first simple boosting procedure in the PAC learning framework (Valiant, 1984; Kearns and Vazirani, 1994). Schapire

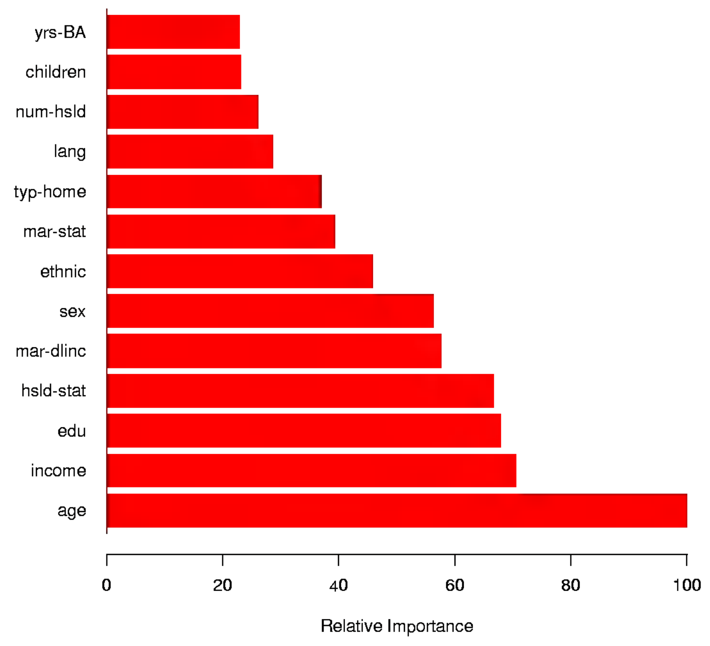

FIGURE 10.19. *Relative importance of the predictors as averaged over all classes for the demographics data.*

showed that a *weak learner* could always improve its performance by training two additional classifiers on filtered versions of the input data stream. A weak learner is an algorithm for producing a two-class classifier with performance guaranteed (with high probability) to be significantly better than a coin-flip. After learning an initial classifier G_1 on the first N training points,

- G_2 is learned on a new sample of N points, half of which are misclassified by G_1;
- G_3 is learned on N points for which G_1 and G_2 disagree;
- the boosted classifier is $G_B = \textit{majority vote}(G_1, G_2, G_3)$.

Schapire's "Strength of Weak Learnability" theorem proves that G_B has improved performance over G_1.

Freund (1995) proposed a "boost by majority" variation which combined many weak learners simultaneously and improved the performance of the simple boosting algorithm of Schapire. The theory supporting both of these algorithms requires the weak learner to produce a classifier with a fixed error rate. This led to the more adaptive and realistic AdaBoost (Freund and Schapire, 1996a) and its offspring, where this assumption was dropped.

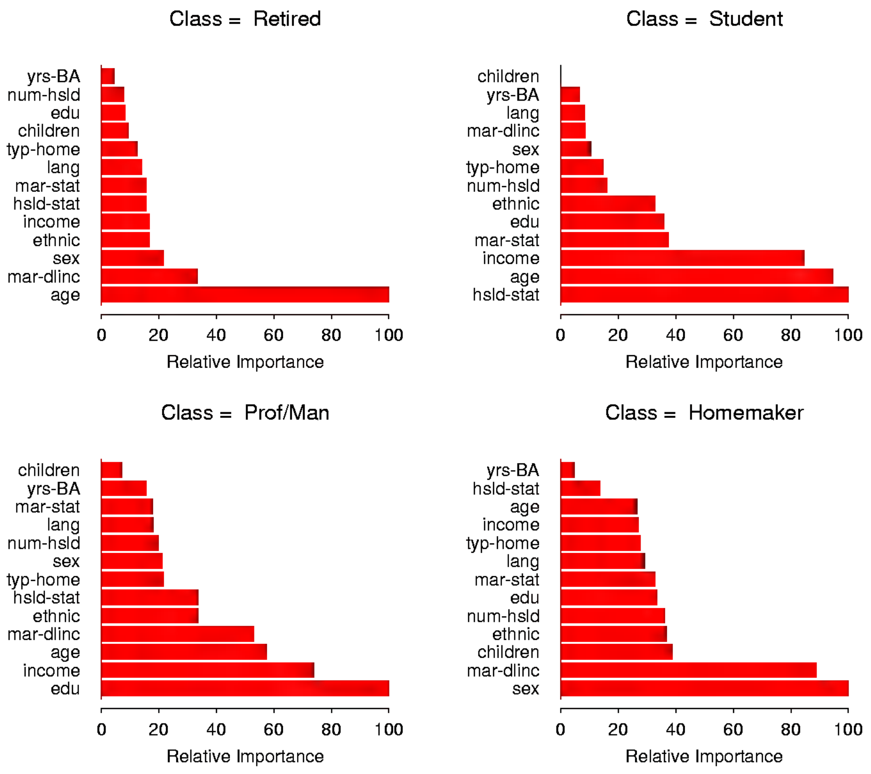

FIGURE 10.20. *Predictor variable importances separately for each of the four classes with lowest error rate for the demographics data.*

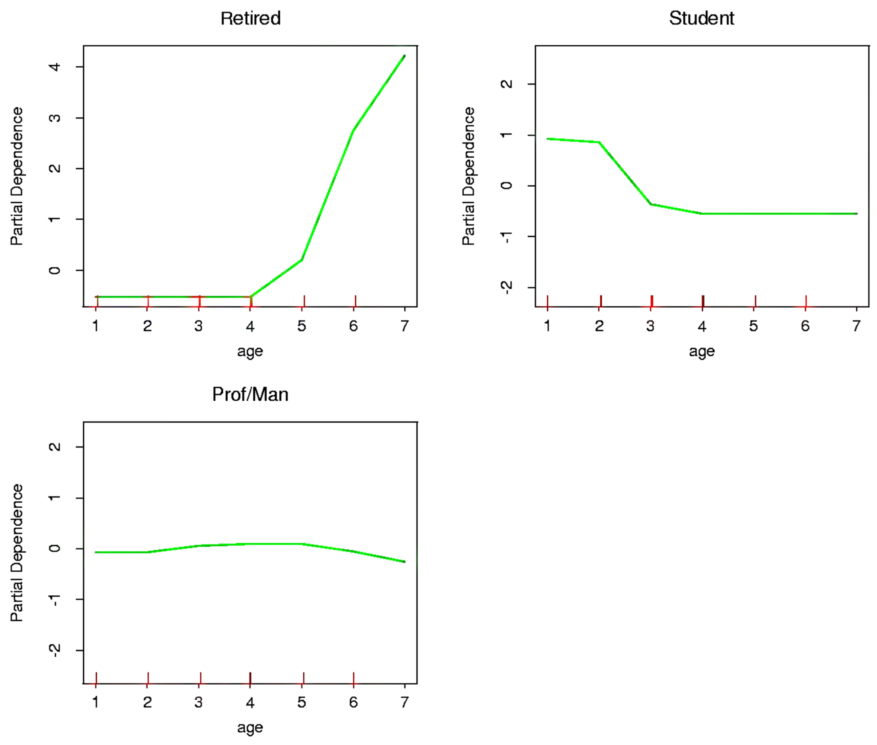

FIGURE 10.21. *Partial dependence of the odds of three different occupations on age, for the demographics data.*

Freund and Schapire (1996a) and Schapire and Singer (1998) provide some theory to support their algorithms, in the form of upper bounds on generalization error. This theory has evolved in the Computational Learning community, initially based on the concepts of PAC learning. Other theories attempting to explain boosting come from game theory (Freund and Schapire, 1996b; Breiman, 1999; Breiman, 1998), and VC theory (Schapire et al., 1998). The bounds and the theory associated with the AdaBoost algorithms are interesting, but tend to be too loose to be of practical importance. In practice, boosting achieves results far more impressive than the bounds would imply. Friedman et al. (2000) and Friedman (2001) form the basis for our exposition in this chapter. Friedman et al. (2000) analyze AdaBoost statistically, derive the exponential criterion, and show that it estimates the log-odds of the class probability. They propose additive tree models, the right-sized trees and ANOVA representation of Section 10.11, and the multi-class logit formulation. Friedman (2001) developed gradient boosting and shrinkage for classification and regression, while Friedman (1999) explored stochastic variants of boosting. As the discussion of Friedman et al. (2000) shows, there is still some controversy about how and why boosting works.

Exercises

Ex. 10.1 Derive expression (10.12) for the update parameter in AdaBoost.

Ex. 10.2 Prove result (10.16), that is, the minimizer of the population version of the AdaBoost criterion, is one-half of the log odds.

Ex. 10.3 Show that the marginal average (10.50) recovers additive and multiplicative functions (10.53) and (10.54), while the conditional expectation (10.52) does not.

Ex. 10.4

(a) Write a program implementing AdaBoost with trees.

(b) Redo the computations for the example of Figure 10.2. Plot the training error as well as test error, and discuss its behavior.

(c) Investigate the number of iterations needed to make the test error finally start to rise.

(d) Change the setup of this example as follows: define two classes, with the features in Class 1 being $X_1, X_2, \dots, X_{10}$, standard independent Gaussian variates. In Class 2, the features $X_1, X_2, \dots, X_{10}$ are also standard independent Gaussian, but conditioned on the event $\sum_j X_j^2 > 12$. Now the classes have significant overlap in feature space. Repeat the AdaBoost experiments as in Figure 10.2 and discuss the results.

Ex. 10.5 Consider a K-class problem where the targets y_{ik} are coded as 1 if observation i is in class k and zero otherwise. Using the symmetric logistic transform (10.55) as the loss function, use the arguments leading to the MART Algorithm 10.3 to derive Algorithm 10.5.

Algorithm 10.5 *MART for K-class classification.*

```
1. Initialize $f_{k0}(x) = 0,\ k = 1, 2, \dots, K$.
2. For $m$=1 to $M$:
    (a) Set
        $$p_k(x) = \frac{e^{f_k(x)}}{\sum_{\ell=1}^{K} e^{f_\ell(x)}},\ k = 1, 2, \dots, K.$$
    (b) For $k = 1$ to $K$:
        i. Compute $r_{ikm} = y_{ik} - p_k(x_i),\ i = 1, 2, \dots, N$.
        ii. Fit a regression tree to the targets $r_{ikm},\ i = 1, 2, \dots, N$,
            giving terminal regions $R_{jkm},\ j = 1, 2, \dots, J_m$.
        iii. Compute
            $$\gamma_{jkm} = \frac{K-1}{K} \frac{\sum_{x_i \in R_{jkm}} r_{ikm}}{\sum_{x_i \in R_{jkm}} |r_{ikm}|(1 - |r_{ikm}|)},\ j = 1, 2, \dots, J_m.$$
        iv. Update $f_{km}(x) = f_{k,m-1}(x) + \sum_{j=1}^{J_m} \gamma_{jkm} I(x \in R_{jkm})$.
3. Output $\hat{f}_k(x) = f_{kM}(x),\ k = 1, 2, \dots, K$.
```

11 Neural Networks

11.1 Introduction

In this chapter we describe a class of learning methods that was developed separately in different fields—statistics and artificial intelligence—based on essentially identical models. The central idea is to extract linear combinations of the inputs as derived features, and then model the target as a nonlinear function of these features. The result is a powerful learning method, with widespread applications in many fields. We first discuss the projection pursuit model, which evolved in the domain of semiparametric statistics and smoothing. The rest of the chapter is devoted to neural network models.

11.2 Projection Pursuit Regression

As in our generic supervised learning problem, assume we have an input vector X with p components, and a target Y. Let ω_m, $m = 1, 2, \dots, M$, be unit p-vectors of unknown parameters. The projection pursuit regression (PPR) model has the form

$$f(X) = \sum_{m=1}^{M} g_m(\omega_m^T X). \tag{11.1}$$

This is an additive model, but in the derived features $V_m = \omega_m^T X$ rather than the inputs themselves. The functions g_m are unspecified and are esti-

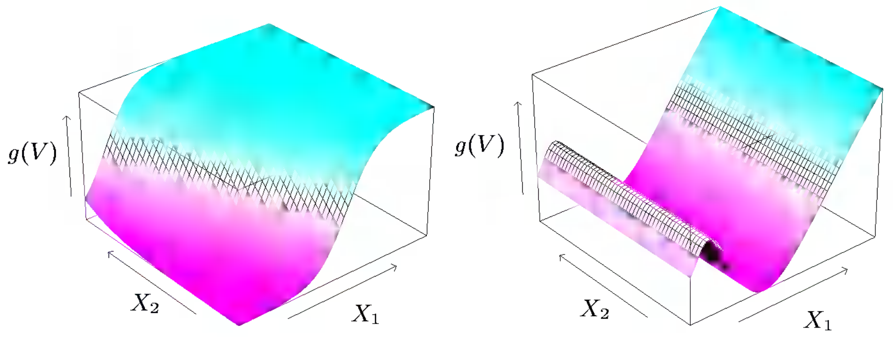

FIGURE 11.1. *Perspective plots of two ridge functions.*
Left: $g(V) = 1/[1 + \exp(-5(V - 0.5))]$, *where* $V = (X_1 + X_2)/\sqrt{2}$.
Right: $g(V) = (V + 0.1)\sin(1/(V/3 + 0.1))$, *where* $V = X_1$.

mated along with the directions ω_m using some flexible smoothing method (see below).

The function $g_m(\omega_m^T X)$ is called a *ridge function* in $\mathbb{R}^p$. It varies only in the direction defined by the vector ω_m. The scalar variable $V_m = \omega_m^T X$ is the projection of X onto the unit vector ω_m, and we seek ω_m so that the model fits well, hence the name "projection pursuit." Figure 11.1 shows some examples of ridge functions. In the example on the left $\omega = (1/\sqrt{2})(1, 1)^T$, so that the function only varies in the direction $X_1 + X_2$. In the example on the right, $\omega = (1, 0)$.

The PPR model (11.1) is very general, since the operation of forming nonlinear functions of linear combinations generates a surprisingly large class of models. For example, the product $X_1 \cdot X_2$ can be written as $[(X_1 + X_2)^2 - (X_1 - X_2)^2]/4$, and higher-order products can be represented similarly.

In fact, if M is taken arbitrarily large, for appropriate choice of g_m the PPR model can approximate any continuous function in $\mathbb{R}^p$ arbitrarily well. Such a class of models is called a *universal approximator*. However this generality comes at a price. Interpretation of the fitted model is usually difficult, because each input enters into the model in a complex and multi-faceted way. As a result, the PPR model is most useful for prediction, and not very useful for producing an understandable model for the data. The $M = 1$ model, known as the *single index model* in econometrics, is an exception. It is slightly more general than the linear regression model, and offers a similar interpretation.

How do we fit a PPR model, given training data (x_i, y_i), $i = 1, 2, \ldots, N$? We seek the approximate minimizers of the error function

$$\sum_{i=1}^{N}\left[y_i - \sum_{m=1}^{M} g_m(\omega_m^T x_i)\right]^2 \tag{11.2}$$

over functions g_m and direction vectors ω_m, $m = 1, 2, \ldots, M$. As in other smoothing problems, we need either explicitly or implicitly to impose complexity constraints on the g_m, to avoid overfit solutions.

Consider just one term ($M = 1$, and drop the subscript). Given the direction vector ω, we form the derived variables $v_i = \omega^T x_i$. Then we have a one-dimensional smoothing problem, and we can apply any scatterplot smoother, such as a smoothing spline, to obtain an estimate of g.

On the other hand, given g, we want to minimize (11.2) over ω. A Gauss–Newton search is convenient for this task. This is a quasi-Newton method, in which the part of the Hessian involving the second derivative of g is discarded. It can be simply derived as follows. Let ω_{old} be the current estimate for ω. We write

$$g(\omega^T x_i) \approx g(\omega_{\text{old}}^T x_i) + g'(\omega_{\text{old}}^T x_i))(\omega - \omega_{\text{old}})^T x_i \tag{11.3}$$

to give

$$\sum_{i=1}^{N} \left[y_i - g(\omega^T x_i)\right]^2 \approx \sum_{i=1}^{N} g'(\omega_{\text{old}}^T x_i)^2 \left[\left(\omega_{\text{old}}^T x_i + \frac{y_i - g(\omega_{\text{old}}^T x_i)}{g'(\omega_{\text{old}}^T x_i)}\right) - \omega^T x_i\right]^2. \tag{11.4}$$

To minimize the right-hand side, we carry out a least squares regression with target $\omega_{\text{old}}^T x_i + (y_i - g(\omega_{\text{old}}^T x_i))/g'(\omega_{\text{old}}^T x_i)$ on the input x_i, with weights $g'(\omega_{\text{old}}^T x_i)^2$ and no intercept (bias) term. This produces the updated coefficient vector ω_{new}.

These two steps, estimation of g and ω, are iterated until convergence. With more than one term in the PPR model, the model is built in a forward stage-wise manner, adding a pair (ω_m, g_m) at each stage.

There are a number of implementation details.

- Although any smoothing method can in principle be used, it is convenient if the method provides derivatives. Local regression and smoothing splines are convenient.

- After each step the g_m's from previous steps can be readjusted using the backfitting procedure described in Chapter 9. While this may lead ultimately to fewer terms, it is not clear whether it improves prediction performance.

- Usually the ω_m are not readjusted (partly to avoid excessive computation), although in principle they could be as well.

- The number of terms M is usually estimated as part of the forward stage-wise strategy. The model building stops when the next term does not appreciably improve the fit of the model. Cross-validation can also be used to determine M.

There are many other applications, such as density estimation (Friedman et al., 1984; Friedman, 1987), where the projection pursuit idea can be used. In particular, see the discussion of ICA in Section 14.6 and its relationship with exploratory projection pursuit. However the projection pursuit regression model has not been widely used in the field of statistics, perhaps because at the time of its introduction (1981), its computational demands exceeded the capabilities of most readily available computers. But it does represent an important intellectual advance, one that has blossomed in its reincarnation in the field of neural networks, the topic of the rest of this chapter.

11.3 Neural Networks

The term *neural network* has evolved to encompass a large class of models and learning methods. Here we describe the most widely used "vanilla" neural net, sometimes called the single hidden layer back-propagation network, or single layer perceptron. There has been a great deal of *hype* surrounding neural networks, making them seem magical and mysterious. As we make clear in this section, they are just nonlinear statistical models, much like the projection pursuit regression model discussed above.

A neural network is a two-stage regression or classification model, typically represented by a *network diagram* as in Figure 11.2. This network applies both to regression or classification. For regression, typically $K = 1$ and there is only one output unit Y_1 at the top. However, these networks can handle multiple quantitative responses in a seamless fashion, so we will deal with the general case.

For K-class classification, there are K units at the top, with the kth unit modeling the probability of class k. There are K target measurements Y_k, $k = 1, \dots, K$, each being coded as a 0-1 variable for the kth class.

Derived features Z_m are created from linear combinations of the inputs, and then the target Y_k is modeled as a function of linear combinations of the Z_m,

$$\begin{aligned} Z_m &= \sigma(\alpha_{0m} + \alpha_m^T X),\ m = 1, \dots, M, \\ T_k &= \beta_{0k} + \beta_k^T Z,\ k = 1, \dots, K, \\ f_k(X) &= g_k(T),\ k = 1, \dots, K, \end{aligned} \tag{11.5}$$

where $Z = (Z_1, Z_2, \dots, Z_M)$, and $T = (T_1, T_2, \dots, T_K)$.

The activation function $\sigma(v)$ is usually chosen to be the *sigmoid* $\sigma(v) = 1/(1+e^{-v})$; see Figure 11.3 for a plot of $1/(1+e^{-v})$. Sometimes Gaussian radial basis functions (Chapter 6) are used for the $\sigma(v)$, producing what is known as a *radial basis function network*.

Neural network diagrams like Figure 11.2 are sometimes drawn with an additional *bias* unit feeding into every unit in the hidden and output layers.

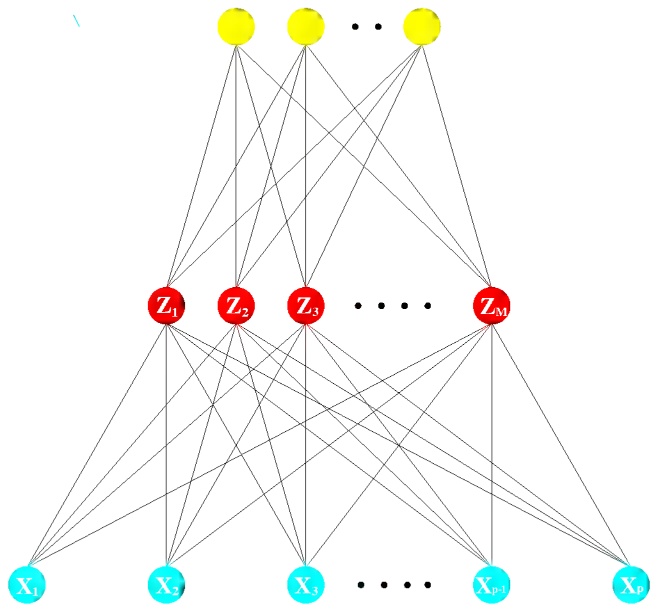

FIGURE 11.2. *Schematic of a single hidden layer, feed-forward neural network.*

Thinking of the constant "1" as an additional input feature, this bias unit captures the intercepts α_{0m} and β_{0k} in model (11.5).

The output function $g_k(T)$ allows a final transformation of the vector of outputs T. For regression we typically choose the identity function $g_k(T) = T_k$. Early work in K-class classification also used the identity function, but this was later abandoned in favor of the *softmax* function

$$g_k(T) = \frac{e^{T_k}}{\sum_{\ell=1}^{K} e^{T_\ell}}. \tag{11.6}$$

This is of course exactly the transformation used in the multilogit model (Section 4.4), and produces positive estimates that sum to one. In Section 4.2 we discuss other problems with linear activation functions, in particular potentially severe masking effects.

The units in the middle of the network, computing the derived features Z_m, are called *hidden units* because the values Z_m are not directly observed. In general there can be more than one hidden layer, as illustrated in the example at the end of this chapter. We can think of the Z_m as a basis expansion of the original inputs X; the neural network is then a standard linear model, or linear multilogit model, using these transformations as inputs. There is, however, an important enhancement over the basis-expansion techniques discussed in Chapter 5; here the parameters of the basis functions are learned from the data.

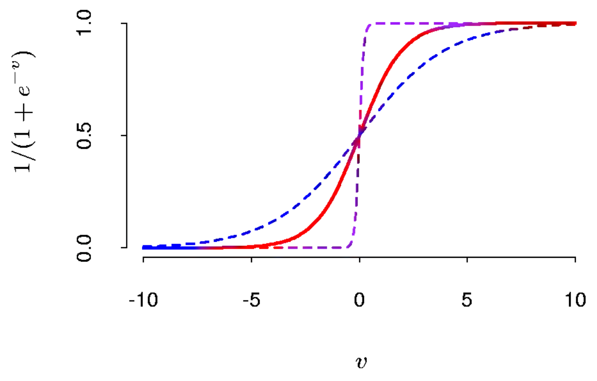

FIGURE 11.3. *Plot of the sigmoid function* $\sigma(v) = 1/(1+\exp(-v))$ *(red curve), commonly used in the hidden layer of a neural network. Included are* $\sigma(sv)$ *for* $s = \frac{1}{2}$ *(blue curve) and* $s = 10$ *(purple curve). The scale parameter* s *controls the activation rate, and we can see that large* s *amounts to a hard activation at* $v = 0$*. Note that* $\sigma(s(v - v_0))$ *shifts the activation threshold from* 0 *to* v_0*.*

Notice that if σ is the identity function, then the entire model collapses to a linear model in the inputs. Hence a neural network can be thought of as a nonlinear generalization of the linear model, both for regression and classification. By introducing the nonlinear transformation σ, it greatly enlarges the class of linear models. In Figure 11.3 we see that the rate of activation of the sigmoid depends on the norm of α_m, and if $\|\alpha_m\|$ is very small, the unit will indeed be operating in the *linear part* of its activation function.

Notice also that the neural network model with one hidden layer has exactly the same form as the projection pursuit model described above. The difference is that the PPR model uses nonparametric functions $g_m(v)$, while the neural network uses a far simpler function based on $\sigma(v)$, with three free parameters in its argument. In detail, viewing the neural network model as a PPR model, we identify

$$\begin{aligned} g_m(\omega_m^T X) &= \beta_m \sigma(\alpha_{0m} + \alpha_m^T X) \\ &= \beta_m \sigma(\alpha_{0m} + \|\alpha_m\|(\omega_m^T X)), \end{aligned} \tag{11.7}$$

where $\omega_m = \alpha_m / \|\alpha_m\|$ is the mth unit-vector. Since $\sigma_{\beta,\alpha_0,s}(v) = \beta\sigma(\alpha_0 + sv)$ has lower complexity than a more general nonparametric $g(v)$, it is not surprising that a neural network might use 20 or 100 such functions, while the PPR model typically uses fewer terms ($M = 5$ or 10, for example).

Finally, we note that the name "neural networks" derives from the fact that they were first developed as models for the human brain. Each unit represents a neuron, and the connections (links in Figure 11.2) represent synapses. In early models, the neurons fired when the total signal passed to that unit exceeded a certain threshold. In the model above, this corresponds to use of a step function for $\sigma(Z)$ and $g_m(T)$. Later the neural network was recognized as a useful tool for nonlinear statistical modeling, and for this purpose the step function is not smooth enough for optimization. Hence the step function was replaced by a smoother threshold function, the sigmoid in Figure 11.3.

11.4 Fitting Neural Networks

The neural network model has unknown parameters, often called *weights*, and we seek values for them that make the model fit the training data well. We denote the complete set of weights by θ, which consists of

$$\begin{aligned} \{\alpha_{0m}, \alpha_m;\ m = 1, 2, \dots, M\} &\quad M(p+1) \text{ weights,} \\ \{\beta_{0k}, \beta_k;\ k = 1, 2, \dots, K\} &\quad K(M+1) \text{ weights.} \end{aligned} \tag{11.8}$$

For regression, we use sum-of-squared errors as our measure of fit (error function)

$$R(\theta) = \sum_{k=1}^{K} \sum_{i=1}^{N} (y_{ik} - f_k(x_i))^2. \tag{11.9}$$

For classification we use either squared error or cross-entropy (deviance):

$$R(\theta) = -\sum_{i=1}^{N} \sum_{k=1}^{K} y_{ik} \log f_k(x_i), \tag{11.10}$$

and the corresponding classifier is $G(x) = \text{argmax}_k f_k(x)$. With the softmax activation function and the cross-entropy error function, the neural network model is exactly a linear logistic regression model in the hidden units, and all the parameters are estimated by maximum likelihood.

Typically we don't want the global minimizer of $R(\theta)$, as this is likely to be an overfit solution. Instead some regularization is needed: this is achieved directly through a penalty term, or indirectly by early stopping. Details are given in the next section.

The generic approach to minimizing $R(\theta)$ is by gradient descent, called *back-propagation* in this setting. Because of the compositional form of the model, the gradient can be easily derived using the chain rule for differentiation. This can be computed by a forward and backward sweep over the network, keeping track only of quantities local to each unit.

Here is back-propagation in detail for squared error loss. Let $z_{mi} = \sigma(\alpha_{0m} + \alpha_m^T x_i)$, from (11.5) and let $z_i = (z_{1i}, z_{2i}, \dots, z_{Mi})$. Then we have

$$\begin{aligned} R(\theta) &\equiv \sum_{i=1}^{N} R_i \\ &= \sum_{i=1}^{N}\sum_{k=1}^{K}(y_{ik} - f_k(x_i))^2, \end{aligned} \tag{11.11}$$

with derivatives

$$\begin{aligned} \frac{\partial R_i}{\partial \beta_{km}} &= -2(y_{ik} - f_k(x_i))g_k'(\beta_k^T z_i)z_{mi}, \\ \frac{\partial R_i}{\partial \alpha_{m\ell}} &= -\sum_{k=1}^{K} 2(y_{ik} - f_k(x_i))g_k'(\beta_k^T z_i)\beta_{km}\sigma'(\alpha_m^T x_i)x_{i\ell}. \end{aligned} \tag{11.12}$$

Given these derivatives, a gradient descent update at the $(r+1)$st iteration has the form

$$\begin{aligned} \beta_{km}^{(r+1)} &= \beta_{km}^{(r)} - \gamma_r \sum_{i=1}^{N} \frac{\partial R_i}{\partial \beta_{km}^{(r)}}, \\ \alpha_{m\ell}^{(r+1)} &= \alpha_{m\ell}^{(r)} - \gamma_r \sum_{i=1}^{N} \frac{\partial R_i}{\partial \alpha_{m\ell}^{(r)}}, \end{aligned} \tag{11.13}$$

where γ_r is the *learning rate*, discussed below.

Now write (11.12) as

$$\begin{aligned} \frac{\partial R_i}{\partial \beta_{km}} &= \delta_{ki} z_{mi}, \\ \frac{\partial R_i}{\partial \alpha_{m\ell}} &= s_{mi} x_{i\ell}. \end{aligned} \tag{11.14}$$

The quantities δ_{ki} and s_{mi} are "errors" from the current model at the output and hidden layer units, respectively. From their definitions, these errors satisfy

$$s_{mi} = \sigma'(\alpha_m^T x_i)\sum_{k=1}^{K}\beta_{km}\delta_{ki}, \tag{11.15}$$

known as the *back-propagation equations*. Using this, the updates in (11.13) can be implemented with a two-pass algorithm. In the *forward pass*, the current weights are fixed and the predicted values $\hat{f}_k(x_i)$ are computed from formula (11.5). In the *backward pass*, the errors δ_{ki} are computed, and then back-propagated via (11.15) to give the errors s_{mi}. Both sets of errors are then used to compute the gradients for the updates in (11.13), via (11.14).

This two-pass procedure is what is known as back-propagation. It has also been called the *delta rule* (Widrow and Hoff, 1960). The computational components for cross-entropy have the same form as those for the sum of squares error function, and are derived in Exercise 11.3.

The advantages of back-propagation are its simple, local nature. In the back propagation algorithm, each hidden unit passes and receives information only to and from units that share a connection. Hence it can be implemented efficiently on a parallel architecture computer.

The updates in (11.13) are a kind of *batch learning*, with the parameter updates being a sum over all of the training cases. Learning can also be carried out online—processing each observation one at a time, updating the gradient after each training case, and cycling through the training cases many times. In this case, the sums in equations (11.13) are replaced by a single summand. A *training epoch* refers to one sweep through the entire training set. Online training allows the network to handle very large training sets, and also to update the weights as new observations come in.

The learning rate γ_r for batch learning is usually taken to be a constant, and can also be optimized by a line search that minimizes the error function at each update. With online learning γ_r should decrease to zero as the iteration $r \to \infty$. This learning is a form of *stochastic approximation* (Robbins and Munro, 1951); results in this field ensure convergence if $\gamma_r \to 0$, $\sum_r \gamma_r = \infty$, and $\sum_r \gamma_r^2 < \infty$ (satisfied, for example, by $\gamma_r = 1/r$).

Back-propagation can be very slow, and for that reason is usually not the method of choice. Second-order techniques such as Newton's method are not attractive here, because the second derivative matrix of R (the Hessian) can be very large. Better approaches to fitting include conjugate gradients and variable metric methods. These avoid explicit computation of the second derivative matrix while still providing faster convergence.

11.5 Some Issues in Training Neural Networks

There is quite an art in training neural networks. The model is generally overparametrized, and the optimization problem is nonconvex and unstable unless certain guidelines are followed. In this section we summarize some of the important issues.

11.5.1 Starting Values

Note that if the weights are near zero, then the operative part of the sigmoid (Figure 11.3) is roughly linear, and hence the neural network collapses into an approximately linear model (Exercise 11.2). Usually starting values for weights are chosen to be random values near zero. Hence the model starts out nearly linear, and becomes nonlinear as the weights increase. Individual units localize to directions and introduce nonlinearities where needed. Use of exact zero weights leads to zero derivatives and perfect symmetry, and the algorithm never moves. Starting instead with large weights often leads to poor solutions.

11.5.2 *Overfitting*

Often neural networks have too many weights and will overfit the data at the global minimum of R. In early developments of neural networks, either by design or by accident, an early stopping rule was used to avoid overfitting. Here we train the model only for a while, and stop well before we approach the global minimum. Since the weights start at a highly regularized (linear) solution, this has the effect of shrinking the final model toward a linear model. A validation dataset is useful for determining when to stop, since we expect the validation error to start increasing.

A more explicit method for regularization is *weight decay*, which is analogous to ridge regression used for linear models (Section 3.4.3). We add a penalty to the error function $R(\theta) + \lambda J(\theta)$, where

$$J(\theta) = \sum_{km} \beta_{km}^2 + \sum_{m\ell} \alpha_{m\ell}^2 \tag{11.16}$$

and $\lambda \geq 0$ is a tuning parameter. Larger values of λ will tend to shrink the weights toward zero: typically cross-validation is used to estimate λ. The effect of the penalty is to simply add terms $2\beta_{km}$ and $2\alpha_{m\ell}$ to the respective gradient expressions (11.13). Other forms for the penalty have been proposed, for example,

$$J(\theta) = \sum_{km} \frac{\beta_{km}^2}{1+\beta_{km}^2} + \sum_{m\ell} \frac{\alpha_{m\ell}^2}{1+\alpha_{m\ell}^2}, \tag{11.17}$$

known as the *weight elimination* penalty. This has the effect of shrinking smaller weights more than (11.16) does.

Figure 11.4 shows the result of training a neural network with ten hidden units, without weight decay (upper panel) and with weight decay (lower panel), to the mixture example of Chapter 2. Weight decay has clearly improved the prediction. Figure 11.5 shows heat maps of the estimated weights from the training (grayscale versions of these are called *Hinton diagrams*.) We see that weight decay has dampened the weights in both layers: the resulting weights are spread fairly evenly over the ten hidden units.

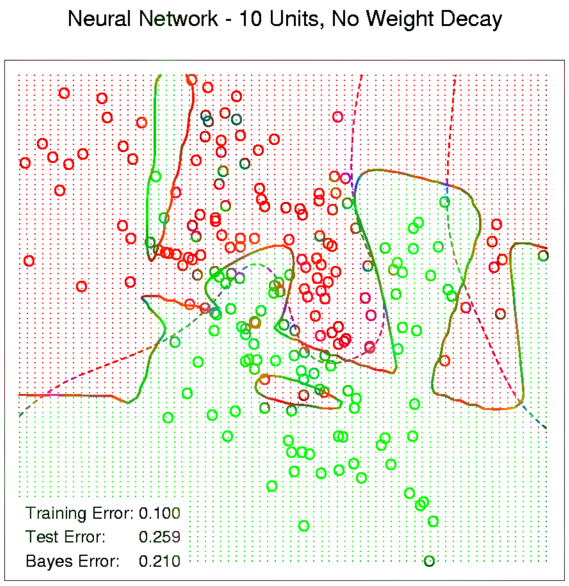

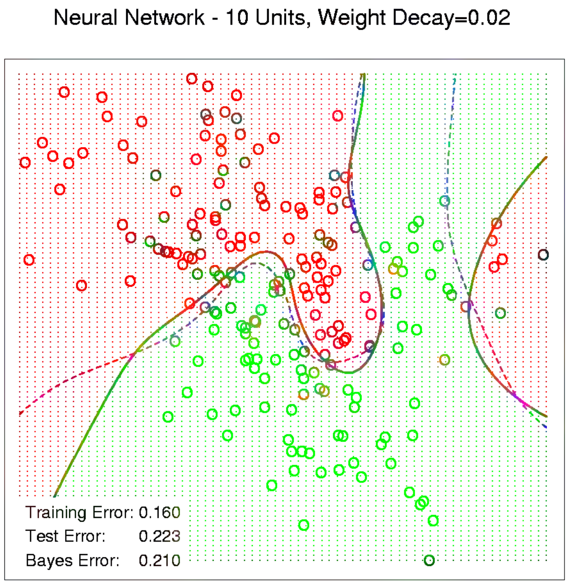

FIGURE 11.4. *A neural network on the mixture example of Chapter 2. The upper panel uses no weight decay, and overfits the training data. The lower panel uses weight decay, and achieves close to the Bayes error rate (broken purple boundary). Both use the softmax activation function and cross-entropy error.*

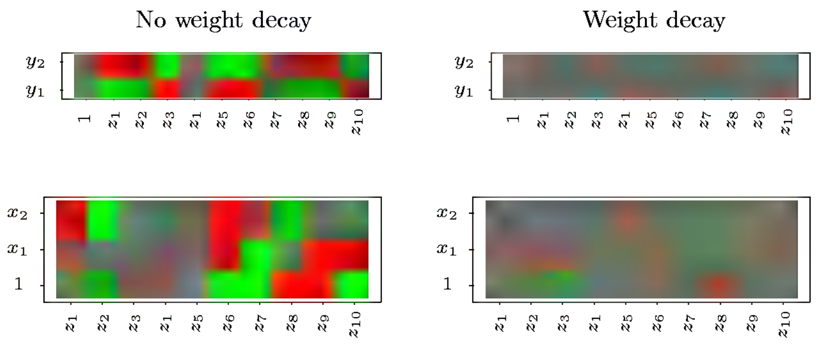

FIGURE 11.5. *Heat maps of the estimated weights from the training of neural networks from Figure 11.4. The display ranges from bright green (negative) to bright red (positive).*

11.5.3 Scaling of the Inputs

Since the scaling of the inputs determines the effective scaling of the weights in the bottom layer, it can have a large effect on the quality of the final solution. At the outset it is best to standardize all inputs to have mean zero and standard deviation one. This ensures all inputs are treated equally in the regularization process, and allows one to choose a meaningful range for the random starting weights. With standardized inputs, it is typical to take random uniform weights over the range $[-0.7, +0.7]$.

11.5.4 Number of Hidden Units and Layers

Generally speaking it is better to have too many hidden units than too few. With too few hidden units, the model might not have enough flexibility to capture the nonlinearities in the data; with too many hidden units, the extra weights can be shrunk toward zero if appropriate regularization is used. Typically the number of hidden units is somewhere in the range of 5 to 100, with the number increasing with the number of inputs and number of training cases. It is most common to put down a reasonably large number of units and train them with regularization. Some researchers use cross-validation to estimate the optimal number, but this seems unnecessary if cross-validation is used to estimate the regularization parameter. Choice of the number of hidden layers is guided by background knowledge and experimentation. Each layer extracts features of the input for regression or classification. Use of multiple hidden layers allows construction of hierarchical features at different levels of resolution. An example of the effective use of multiple layers is given in Section 11.6.

11.5.5 Multiple Minima

The error function $R(\theta)$ is nonconvex, possessing many local minima. As a result, the final solution obtained is quite dependent on the choice of starting weights. One must at least try a number of random starting configurations, and choose the solution giving lowest (penalized) error. Probably a better approach is to use the average predictions over the collection of networks as the final prediction (Ripley, 1996). This is preferable to averaging the weights, since the nonlinearity of the model implies that this averaged solution could be quite poor. Another approach is via *bagging*, which averages the predictions of networks training from randomly perturbed versions of the training data. This is described in Section 8.7.

11.6 Example: Simulated Data

We generated data from two additive error models $Y = f(X) + \varepsilon$:

$$\begin{aligned} \text{Sum of sigmoids: } Y &= \sigma(a_1^T X) + \sigma(a_2^T X) + \varepsilon_1; \\ \text{Radial: } Y &= \prod_{m=1}^{10} \phi(X_m) + \varepsilon_2. \end{aligned}$$

Here $X = (X_1, X_2, \dots, X_p)$, each X_j being a standard Gaussian variate, with $p = 2$ in the first model, and $p = 10$ in the second.

For the sigmoid model, $a_1 = (3, 3)$, $a_2 = (3, -3)$; for the radial model, $\phi(t) = (1/2\pi)^{1/2} \exp(-t^2/2)$. ε_1 and ε_2 are both Gaussian errors, with variance chosen so that the signal-to-noise ratio

$$\frac{\text{Var}(\text{E}(Y|X))}{\text{Var}(Y - \text{E}(Y|X))} = \frac{\text{Var}(f(X))}{\text{Var}(\varepsilon)} \tag{11.18}$$

is 4 in both models. We took a training sample of size 100 and a test sample of size 10000. We fit neural networks with weight decay and various numbers of hidden units, and recorded the average test error $\text{E}_{\text{Test}}(Y - \hat{f}(X))^2$ for each of ten random starting weights. Only one training set was generated, but the results are typical for an "average" training set. The test errors are shown in Figure 11.6. Note that the zero hidden unit model refers to linear least squares regression. The neural network is perfectly suited to the sum of sigmoids model, and the two-unit model does perform the best, achieving an error close to the Bayes rate. (Recall that the Bayes rate for regression with squared error is the error variance; in the figures, we report test error relative to the Bayes error). Notice, however, that with more hidden units, overfitting quickly creeps in, and with some starting weights the model does worse than the linear model (zero hidden unit) model. Even with two hidden units, two of the ten starting weight configurations produced results

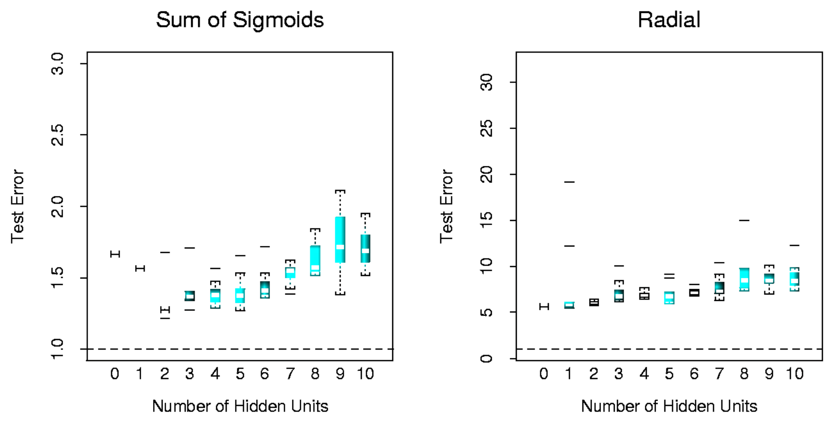

FIGURE 11.6. *Boxplots of test error, for simulated data example, relative to the Bayes error (broken horizontal line). True function is a sum of two sigmoids on the left, and a radial function is on the right. The test error is displayed for ten different starting weights, for a single hidden layer neural network with the number of units as indicated.*

no better than the linear model, confirming the importance of multiple starting values.

A radial function is in a sense the most difficult for the neural net, as it is spherically symmetric and with no preferred directions. We see in the right panel of Figure 11.6 that it does poorly in this case, with the test error staying well above the Bayes error (note the different vertical scale from the left panel). In fact, since a constant fit (such as the sample average) achieves a relative error of 5 (when the SNR is 4), we see that the neural networks perform increasingly worse than the mean.

In this example we used a fixed weight decay parameter of 0.0005, representing a mild amount of regularization. The results in the left panel of Figure 11.6 suggest that more regularization is needed with greater numbers of hidden units.

In Figure 11.7 we repeated the experiment for the sum of sigmoids model, with no weight decay in the left panel, and stronger weight decay ($\lambda = 0.1$) in the right panel. With no weight decay, overfitting becomes even more severe for larger numbers of hidden units. The weight decay value $\lambda = 0.1$ produces good results for all numbers of hidden units, and there does not appear to be overfitting as the number of units increase. Finally, Figure 11.8 shows the test error for a ten hidden unit network, varying the weight decay parameter over a wide range. The value 0.1 is approximately optimal.

In summary, there are two free parameters to select: the weight decay λ and number of hidden units M. As a learning strategy, one could fix either parameter at the value corresponding to the least constrained model, to ensure that the model is rich enough, and use cross-validation to choose

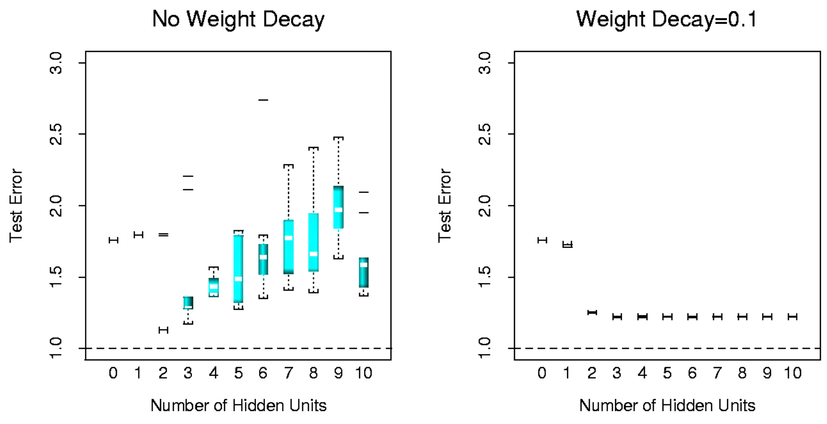

FIGURE 11.7. *Boxplots of test error, for simulated data example, relative to the Bayes error. True function is a sum of two sigmoids. The test error is displayed for ten different starting weights, for a single hidden layer neural network with the number units as indicated. The two panels represent no weight decay (left) and strong weight decay* $\lambda = 0.1$ *(right).*

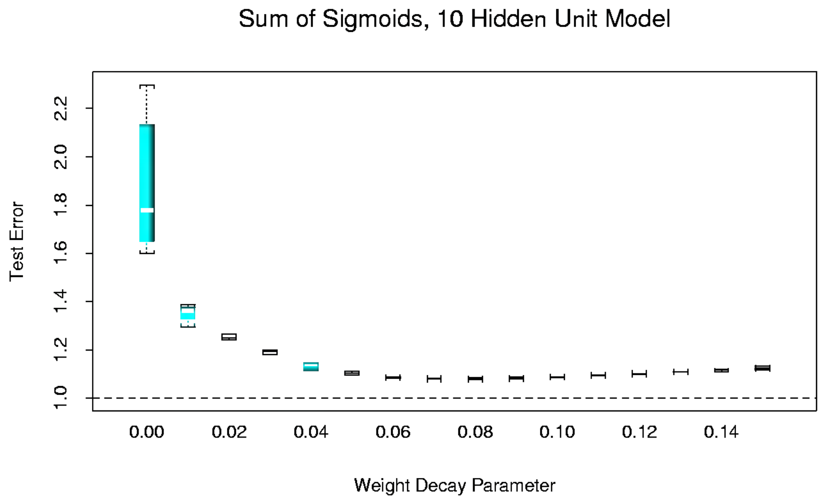

FIGURE 11.8. *Boxplots of test error, for simulated data example. True function is a sum of two sigmoids. The test error is displayed for ten different starting weights, for a single hidden layer neural network with ten hidden units and weight decay parameter value as indicated.*

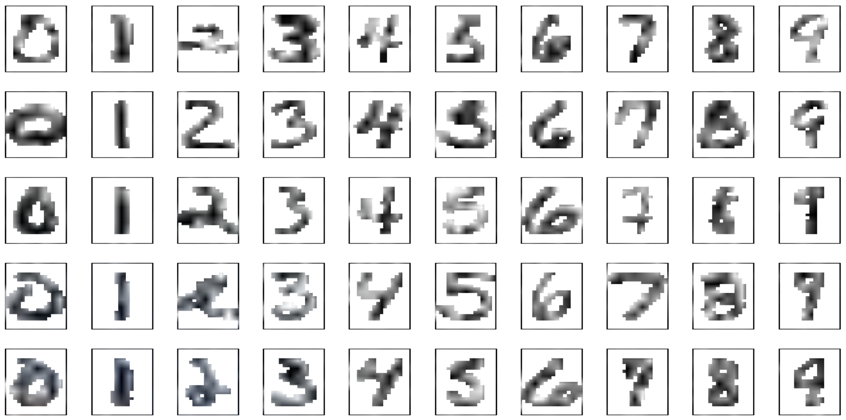

FIGURE 11.9. *Examples of training cases from ZIP code data. Each image is a* 16×16 *8-bit grayscale representation of a handwritten digit.*

the other parameter. Here the least constrained values are zero weight decay and ten hidden units. Comparing the left panel of Figure 11.7 to Figure 11.8, we see that the test error is less sensitive to the value of the weight decay parameter, and hence cross-validation of this parameter would be preferred.

11.7 Example: ZIP Code Data

This example is a character recognition task: classification of handwritten numerals. This problem captured the attention of the machine learning and neural network community for many years, and has remained a benchmark problem in the field. Figure 11.9 shows some examples of normalized handwritten digits, automatically scanned from envelopes by the U.S. Postal Service. The original scanned digits are binary and of different sizes and orientations; the images shown here have been deslanted and size normalized, resulting in 16×16 grayscale images (Le Cun et al., 1990). These 256 pixel values are used as inputs to the neural network classifier.

A *black box* neural network is not ideally suited to this pattern recognition task, partly because the pixel representation of the images lack certain invariances (such as small rotations of the image). Consequently early attempts with neural networks yielded misclassification rates around 4.5% on various examples of the problem. In this section we show some of the pioneering efforts to handcraft the neural network to overcome some these deficiencies (Le Cun, 1989), which ultimately led to the state of the art in neural network performance (Le Cun et al., 1998)*.

Although current digit datasets have tens of thousands of training and test examples, the sample size here is deliberately modest in order to emphasize the effects. The examples were obtained by scanning some actual handdrawn digits, and then generating additional images by random horizontal shifts. Details may be found in Le Cun (1989). There are 320 digits in the training set, and 160 in the test set.

Five different networks were fit to the data:

Net-1: No hidden layer, equivalent to multinomial logistic regression.

Net-2: One hidden layer, 12 hidden units fully connected.

Net-3: Two hidden layers locally connected.

Net-4: Two hidden layers, locally connected with weight sharing.

Net-5: Two hidden layers, locally connected, two levels of weight sharing.

These are depicted in Figure 11.10. Net-1 for example has 256 inputs, one each for the 16×16 input pixels, and ten output units for each of the digits 0–9. The predicted value $\hat{f}_k(x)$ represents the estimated probability that an image x has digit class k, for $k = 0, 2, \ldots, 9$.

The networks all have sigmoidal output units, and were all fit with the sum-of-squares error function. The first network has no hidden layer, and hence is nearly equivalent to a linear multinomial regression model (Exercise 11.4). Net-2 is a single hidden layer network with 12 hidden units, of the kind described above.

The training set error for all of the networks was 0%, since in all cases there are more parameters than training observations. The evolution of the test error during the training epochs is shown in Figure 11.11. The linear network (Net-1) starts to overfit fairly quickly, while test performance of the others level off at successively superior values.

The other three networks have additional features which demonstrate the power and flexibility of the neural network paradigm. They introduce constraints on the network, natural for the problem at hand, which allow for more complex connectivity but fewer parameters.

Net-3 uses local connectivity: this means that each hidden unit is connected to only a small patch of units in the layer below. In the first hidden layer (an 8×8 array), each unit takes inputs from a 3×3 patch of the input layer; for units in the first hidden layer that are one unit apart, their receptive fields overlap by one row or column, and hence are two pixels apart. In the second hidden layer, inputs are from a 5×5 patch, and again units that are one unit apart have receptive fields that are two units apart. The

*The figures and tables in this example were recreated from Le Cun (1989)

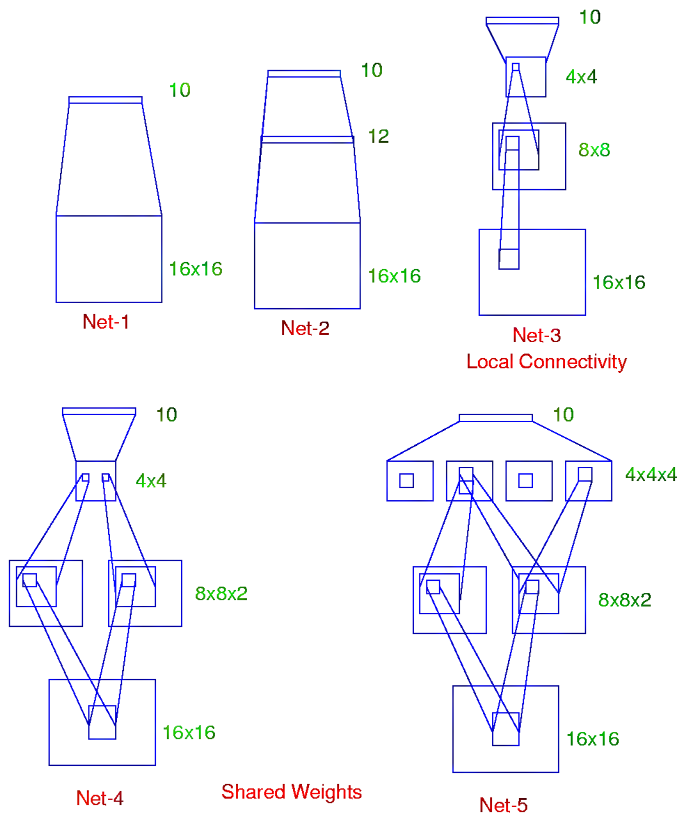

FIGURE 11.10. *Architecture of the five networks used in the ZIP code example.*

weights for all other connections are set to zero. Local connectivity makes each unit responsible for extracting local features from the layer below, and reduces considerably the total number of weights. With many more hidden units than Net-2, Net-3 has fewer links and hence weights (1226 vs. 3214), and achieves similar performance.

Net-4 and Net-5 have local connectivity with shared weights. All units in a local feature map perform the *same* operation on different parts of the image, achieved by sharing the same weights. The first hidden layer of Net-4 has two 8×8 arrays, and each unit takes input from a 3×3 patch just like in Net-3. However, each of the units in a single 8×8 feature map share the same set of nine weights (but have their own bias parameter). This forces the extracted features in different parts of the image to be computed by the same linear functional, and consequently these networks are sometimes known as *convolutional networks.*. The second hidden layer of Net-4 has no weight sharing, and is the same as in Net-3. The gradient of the error function R with respect to a shared weight is the sum of the gradients of R with respect to each connection controlled by the weights in question.

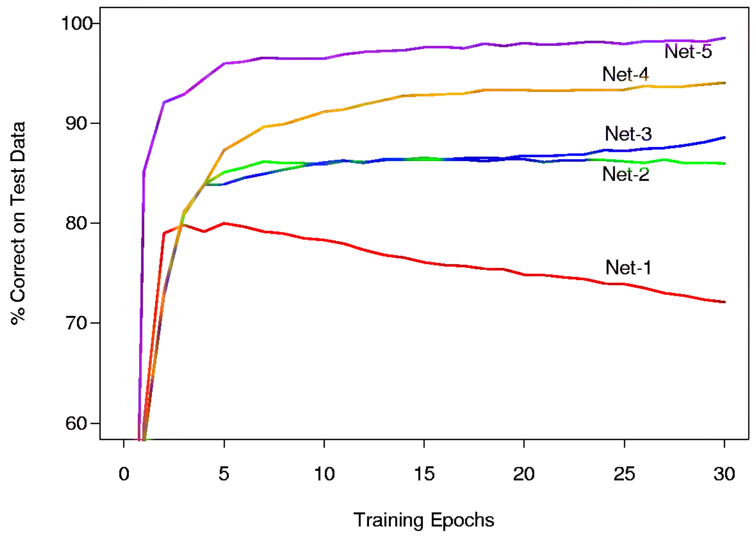

FIGURE 11.11. *Test performance curves, as a function of the number of training epochs, for the five networks of Table 11.1 applied to the ZIP code data (Le Cun, 1989).*

Table 11.1 gives the number of links, the number of weights and the optimal test performance for each of the networks. We see that Net-4 has more links but fewer weights than Net-3, and superior test performance. Net-5 has four 4×4 feature maps in the second hidden layer, each unit connected to a 5×5 local patch in the layer below. Weights are shared in each of these feature maps. We see that Net-5 does the best, having errors of only 1.6%, compared to 13% for the "vanilla" network Net-2. The clever design of network Net-5, motivated by the fact that features of handwriting style should appear in more than one part of a digit, was the result of many person years of experimentation. This and similar networks gave better performance on ZIP code problems than any other learning method at that time (early 1990s). This example also shows that neural

TABLE 11.1. *Test set performance of five different neural networks on a handwritten digit classification example (Le Cun, 1989).*

	Network Architecture	Links	Weights	% Correct
Net-1:	Single layer network	2570	2570	80.0%
Net-2:	Two layer network	3214	3214	87.0%
Net-3:	Locally connected	1226	1226	88.5%
Net-4:	Constrained network 1	2266	1132	94.0%
Net-5:	Constrained network 2	5194	1060	98.4%

networks are not a fully automatic tool, as they are sometimes advertised. As with all statistical models, subject matter knowledge can and should be used to improve their performance.

This network was later outperformed by the tangent distance approach (Simard et al., 1993) described in Section 13.3.3, which explicitly incorporates natural affine invariances. At this point the digit recognition datasets become test beds for every new learning procedure, and researchers worked hard to drive down the error rates. As of this writing, the best error rates on a large database (60000 training, $10,000$ test observations), derived from standard NIST[†] databases, were reported to be the following: (Le Cun et al., 1998):

- 1.1% for tangent distance with a 1-nearest neighbor classifier (Section 13.3.3);
- 0.8% for a degree-9 polynomial SVM (Section 12.3);
- 0.8% for *LeNet-5*, a more complex version of the convolutional network described here;
- 0.7% for boosted *LeNet-4*. Boosting is described in Chapter 8. *LeNet-4* is a predecessor of *LeNet-5*.

Le Cun et al. (1998) report a much larger table of performance results, and it is evident that many groups have been working very hard to bring these test error rates down. They report a standard error of 0.1% on the error estimates, which is based on a binomial average with $N = 10000$ and $p \approx 0.01$. This implies that error rates within 0.1—0.2% of one another are statistically equivalent. Realistically the standard error is even higher, since the test data has been implicitly used in the tuning of the various procedures.

11.8 Discussion

Both projection pursuit regression and neural networks take nonlinear functions of linear combinations ("derived features") of the inputs. This is a powerful and very general approach for regression and classification, and has been shown to compete well with the best learning methods on many problems.

These tools are especially effective in problems with a high signal-to-noise ratio and settings where prediction without interpretation is the goal. They are less effective for problems where the goal is to describe the physical process that generated the data and the roles of individual inputs. Each input

[†]The National Institute of Standards and Technology maintain large databases, including handwritten character databases; `http://www.nist.gov/srd/`

enters into the model in many places, in a nonlinear fashion. Some authors (Hinton, 1989) plot a diagram of the estimated weights into each hidden unit, to try to understand the feature that each unit is extracting. This is limited however by the lack of identifiability of the parameter vectors α_m, $m = 1, \ldots, M$. Often there are solutions with α_m spanning the same linear space as the ones found during training, giving predicted values that are roughly the same. Some authors suggest carrying out a principal component analysis of these weights, to try to find an interpretable solution. In general, the difficulty of interpreting these models has limited their use in fields like medicine, where interpretation of the model is very important.

There has been a great deal of research on the training of neural networks. Unlike methods like CART and MARS, neural networks are smooth functions of real-valued parameters. This facilitates the development of Bayesian inference for these models. Some references are given in the bibliographic notes below.

11.9 Computational Considerations

With N observations, p predictors, M hidden units and L training epochs, a neural network fit typically requires $O(NpML)$ operations. There are many packages available for fitting neural networks, probably many more than exist for mainstream statistical methods. Because the available software varies widely in quality, and the learning problem for neural networks is sensitive to issues such as input scaling, such software should be carefully chosen and tested.

Bibliographic Notes

Projection pursuit was proposed by Friedman and Tukey (1974), and specialized to regression by Friedman and Stuetzle (1981). Huber (1985) gives a scholarly overview, and Roosen and Hastie (1994) present a formulation using smoothing splines. The motivation for neural networks dates back to McCulloch and Pitts (1943), Widrow and Hoff (1960) (reprinted in Anderson and Rosenfeld (1988)) and Rosenblatt (1962). Hebb (1949) heavily influenced the development of learning algorithms. The resurgence of neural networks in the mid 1980s was due to Werbos (1974), Parker (1985) and Rumelhart et al. (1986), who proposed the back-propagation algorithm. Today there are many books written on the topic, for a broad range of audiences. For readers of this book, Hertz et al. (1991), Bishop (1995) and Ripley (1996) may be the most informative. Bayesian learning for neural networks is described in Neal (1996). The ZIP code example was taken from Le Cun (1989); see also Le Cun et al. (1990) and Le Cun et al. (1998).

We do not discuss theoretical topics such as approximation properties of neural networks, such as the work of Barron (1993), Girosi et al. (1995) and Jones (1992). Some of these results are summarized by Ripley (1996).

Exercises

Ex. 11.1 Establish the exact correspondence between the projection pursuit regression model (11.1) and the neural network (11.5). In particular, show that the single-layer regression network is equivalent to a PPR model with $g_m(\omega_m^T x) = \beta_m \sigma(\alpha_{0m} + s_m(\omega_m^T x))$, where ω_m is the mth unit vector. Establish a similar equivalence for a classification network.

Ex. 11.2 Consider a neural network for a quantitative outcome as in (11.5), using squared-error loss and identity output function $g_k(t) = t$. Suppose that the weights α_m from the input to hidden layer are nearly zero. Show that the resulting model is nearly linear in the inputs.

Ex. 11.3 Derive the forward and backward propagation equations for the cross-entropy loss function.

Ex. 11.4 Consider a neural network for a K class outcome that uses cross-entropy loss. If the network has no hidden layer, show that the model is equivalent to the multinomial logistic model described in Chapter 4.

Ex. 11.5

(a) Write a program to fit a single hidden layer neural network (ten hidden units) via back-propagation and weight decay.

(b) Apply it to 100 observations from the model

$$Y = \sigma(a_1^T X) + (a_2^T X)^2 + 0.30 \cdot Z,$$

where σ is the sigmoid function, Z is standard normal, $X = (X_1, X_2)$, each X_j being independent standard normal, and $a_1 = (3, 3), a_2 = (3, -3)$. Generate a test sample of size 1000, and plot the training and test error curves as a function of the number of training epochs, for different values of the weight decay parameter. Discuss the overfitting behavior in each case.

(c) Vary the number of hidden units in the network, from 1 up to 10, and determine the minimum number needed to perform well for this task.

Ex. 11.6 Write a program to carry out projection pursuit regression, using cubic smoothing splines with fixed degrees of freedom. Fit it to the data from the previous exercise, for various values of the smoothing parameter and number of model terms. Find the minimum number of model terms necessary for the model to perform well and compare this to the number of hidden units from the previous exercise.

Ex. 11.7 Fit a neural network to the `spam` data of Section 9.1.2, and compare the results to those for the additive model given in that chapter. Compare both the classification performance and interpretability of the final model.

12
Support Vector Machines and Flexible Discriminants

12.1 Introduction

In this chapter we describe generalizations of linear decision boundaries for classification. Optimal separating hyperplanes are introduced in Chapter 4 for the case when two classes are linearly separable. Here we cover extensions to the nonseparable case, where the classes overlap. These techniques are then generalized to what is known as the *support vector machine*, which produces nonlinear boundaries by constructing a linear boundary in a large, transformed version of the feature space. The second set of methods generalize Fisher's linear discriminant analysis (LDA). The generalizations include *flexible discriminant analysis* which facilitates construction of nonlinear boundaries in a manner very similar to the support vector machines, *penalized discriminant analysis* for problems such as signal and image classification where the large number of features are highly correlated, and *mixture discriminant analysis* for irregularly shaped classes.

12.2 The Support Vector Classifier

In Chapter 4 we discussed a technique for constructing an *optimal* separating hyperplane between two perfectly separated classes. We review this and generalize to the nonseparable case, where the classes may not be separable by a linear boundary.

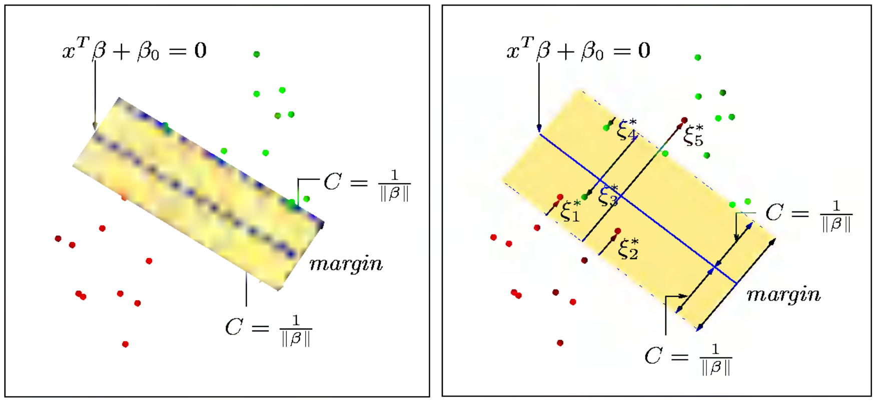

FIGURE 12.1. *Support vector classifiers. The left panel shows the separable case. The decision boundary is the solid line, while broken lines bound the shaded maximal margin of width $2C = 2/\|\beta\|$. The right panel shows the nonseparable (overlap) case. The points labeled ξ_j^* are on the wrong side of their margin by an amount $\xi_j^* = C\xi_j$; points on the correct side have $\xi_j^* = 0$. The margin is maximized subject to a total budget $\sum \xi_i \leq$ constant. Hence $\sum \xi_j^*$ is the total distance of points on the wrong side of their margin.*

Our training data consists of N pairs $(x_1, y_1), (x_2, y_2), \ldots, (x_N, y_N)$, with $x_i \in \mathbb{R}^p$ and $y_i \in \{-1, 1\}$. Define a hyperplane by

$$\{x : f(x) = x^T\beta + \beta_0 = 0\}, \tag{12.1}$$

where β is a unit vector: $\|\beta\| = 1$. A classification rule induced by $f(x)$ is

$$G(x) = \text{sign}[x^T\beta + \beta_0]. \tag{12.2}$$

The geometry of hyperplanes is reviewed in Section 4.5, where we show that $f(x)$ in (12.1) gives the signed distance from a point x to the hyperplane $f(x) = x^T\beta+\beta_0 = 0$. Since the classes are separable, we can find a function $f(x) = x^T\beta + \beta_0$ with $y_i f(x_i) > 0$ $\forall i$. Hence we are able to find the hyperplane that creates the biggest *margin* between the training points for class 1 and -1 (see Figure 12.1). The optimization problem

$$\begin{gathered} \max_{\beta, \beta_0, \|\beta\|=1} C \\ \text{subject to } y_i(x_i^T\beta + \beta_0) \geq C, \; i = 1, \ldots, N, \end{gathered} \tag{12.3}$$

captures this concept. The band in the figure is C units away from the hyperplane on either side, and hence $2C$ units wide. It is called the *margin*.

We showed that this problem can be more conveniently rephrased as

$$\begin{gathered} \min_{\beta, \beta_0} \|\beta\| \\ \text{subject to } y_i(x_i^T\beta + \beta_0) \geq 1, \; i = 1, \ldots, N, \end{gathered} \tag{12.4}$$

where we have dropped the norm constraint on β. Note that $C = 1/\|\beta\|$. Expression (12.4) is the usual way of writing the support vector criterion for separated data. This is a convex optimization problem (quadratic criterion, linear inequality constraints), and the solution is characterized in Section 4.5.2.

Suppose now the classes overlap in feature space. One way to deal with the overlap is to still maximize $\|C\|$, but allow for some points to be on the wrong side of the margin. Define the slack variables $\xi = (\xi_1, \xi_2, \dots, \xi_n)$. There are two natural ways to modify the constraint in (12.3):

$$y_i(x_i^T\beta + \beta_0), \quad \geq \quad C - \xi_i, \tag{12.5}$$

or

$$y_i(x_i^T\beta + \beta_0), \quad \geq \quad C(1 - \xi_i), \tag{12.6}$$

$\forall i,\ \xi_i \geq 0,\ \sum_{i=1}^{N} \xi_i \leq$ constant. The two choices lead to different solutions. While both are equally natural, the second choice leads to the "standard" support vector classifier, and hence we use it.

Here is the idea of the formulation. The value ξ_i in the constraint $y_i(x_i^T\beta + \beta_0) \geq C(1-\xi_i)$ is the proportional amount by which the prediction $f(x_i) = x_i^T\beta + \beta_0$ is on the wrong side of its margin. Hence by bounding the sum $\sum \xi_i$, we bound the total proportional amount by which predictions fall on the wrong side of their margin. Misclassifications occur when $\xi_i > 1$, so bounding $\sum \xi_i$ at a value K say, bounds the total number of training misclassifications at K.

As in (4.44) in Section 4.5.2, we can drop the norm constraint on β, define $C = 1/\|\beta\|$, and write (12.4) in the equivalent form

$$\min \|\beta\| \quad \text{subject to} \quad \begin{cases} y_i(x_i^T\beta + \beta_0) \geq 1 - \xi_i \ \forall i, \\ \xi_i \geq 0,\ \sum \xi_i \leq \text{constant}. \end{cases} \tag{12.7}$$

This is the usual way the support vector classifier is defined for the non-separable case. However we find confusing the presence of the fixed scale "1" in the constraint $y_i(x_i^T\beta + \beta_0) \geq 1 - \xi_i$, and prefer to start with (12.6). The right panel of Figure 12.1 illustrates this overlapping case.

By the nature of the criterion (12.7), we see that points well inside their class boundary do not play a big role in shaping the boundary. This seems like an attractive property, and one that differentiates it from linear discriminant analysis (Section 4.3). In LDA, the decision boundary is determined by the covariance of the class distributions and the positions of the class centroids. We will see in Section 12.3.3 that logistic regression is more similar to the support vector classifier in this regard.

12.2.1 Computing the Support Vector Classifier

The problem (12.7) is quadratic with linear inequality constraints, hence it is a convex optimization problem. We describe a quadratic programming solution using Lagrange multipliers. Computationally it is convenient to re-express (12.7) in the equivalent form

$$\begin{aligned} &\min_{\beta,\beta_0} \frac{1}{2}\|\beta\|^2 + \gamma \sum_{i=1}^{N} \xi_i \\ &\text{subject to } \;\; \xi_i \geq 0, \; y_i(x_i^T\beta x_i + b) \geq 1 - \xi_i \; \forall i, \end{aligned} \tag{12.8}$$

where γ replaces the constant in (12.7); the separable case corresponds to $\gamma = \infty$.

The Lagrange (primal) function is

$$L_P = \frac{1}{2}\|\beta\|^2 + \gamma \sum_{i=1}^{N} \xi_i - \sum_{i=1}^{N} \alpha_i[y_i(x_i^T\beta + \beta_0) - (1 - \xi_i)] - \sum_{i=1}^{N} \mu_i \xi_i, \tag{12.9}$$

which we maximize w.r.t β, β_0 and ξ_i. Setting the respective derivatives to zero, we get

$$\beta = \sum_{i=1}^{N} \alpha_i y_i x_i, \tag{12.10}$$

$$0 = \sum_{i=1}^{N} \alpha_i y_i, \tag{12.11}$$

$$\alpha_i = \gamma - \mu_i, \; \forall i, \tag{12.12}$$

as well as the positivity constraints $\alpha_i, \; \mu_i, \; \xi_i \geq 0 \; \forall i$. By substituting (12.10)–(12.12) into (12.9), we obtain the Lagrangian (Wolfe) dual objective function

$$L_D = \sum_{i=1}^{N} \alpha_i - \frac{1}{2}\sum_{i=1}^{N}\sum_{i'=1}^{N} \alpha_i \alpha_{i'} y_i y_{i'} x_i^T x_{i'}, \tag{12.13}$$

which gives a lower bound on the objective function (12.8) for any feasible point. We maximize L_D subject to $0 \leq \alpha_i \leq \gamma$ and $\sum_{i=1}^{N} \alpha_i y_i = 0$. In addition to (12.10)–(12.12), the Karush–Kuhn–Tucker conditions include the constraints

$$\alpha_i[y_i(x_i^T\beta + \beta_0) - (1 - \xi_i)] = 0, \tag{12.14}$$

$$\mu_i \xi_i = 0, \tag{12.15}$$

$$y_i(x_i^T\beta + \beta_0) - (1 - \xi_i) \geq 0, \tag{12.16}$$

for $i = 1, \ldots, N$. Together these equations (12.10)–(12.16) uniquely characterize the solution to the primal and dual problem.

From (12.10) we see that the solution for β has the form

$$\hat{\beta} = \sum_{i=1}^{N} \hat{\alpha}_i y_i x_i, \tag{12.17}$$

with nonzero coefficients α_i only for those observations i for which the constraints in (12.16) are exactly met (due to (12.14)). These observations are called the *support vectors*, since $\hat{\beta}$ is represented in terms of them alone. Among these support points, some will lie on the edge of the margin ($\xi_i = 0$), and hence from (12.15) and (12.12) will be characterized by $0 < \alpha_i < \gamma$; the remainder ($\xi_i > 0$) have $\alpha_i = \gamma$. From (12.14) we can see that any of these margin points ($0 < \alpha_i$, $\xi_i = 0$) can be used to solve for β_0, and we typically use an average of all the solutions for numerical stability.

Maximizing the dual (12.13) is a simpler convex quadratic programming problem than the primal (12.9), and can be solved with standard techniques (Murray et al., 1981, for example).

Given the solutions $\hat{\beta}_0$ and $\hat{\beta}$, the decision function can be written as

$$\begin{aligned} \hat{G}(x) &= \text{sign}[\hat{f}(x)] \\ &= \text{sign}[x^T\hat{\beta} + \hat{\beta}_0]. \end{aligned} \tag{12.18}$$

The tuning parameter of this procedure is γ.

12.2.2 Mixture Example (Continued)

Figure 12.2 shows the support vector boundary for the mixture example of Figure 2.5 on page 22, with two overlapping classes, for two different values of the tuning parameter γ. The classifiers are rather similar in their performance. Points on the wrong side of the boundary are support vectors. In addition, points on the correct side of the boundary but close to it (in the margin), are also support vectors. The margin is larger for $\gamma = 0.01$ than it is for $\gamma = 10,000$. Hence larger values of γ focus attention more on (correctly classified) points near the decision boundary, while smaller values involve data further away. Either way, misclassified points are given weight, no matter how far away. In this example the procedure is not very sensitive to choices of γ, because of the rigidity of a linear boundary.

The optimal value for γ can be estimated by cross-validation, as discussed in Chapter 7. Interestingly, the leave-one-out cross-validation error can be bounded above by the proportion of support points in the data. The reason is that leaving out an observation that is not a support vector will not change the solution. Hence these observations, being classified correctly by the original boundary, will be classified correctly in the cross-validation process. However this bound tends to be too high, and not generally useful for choosing γ (62% and 85%, respectively, in our examples).

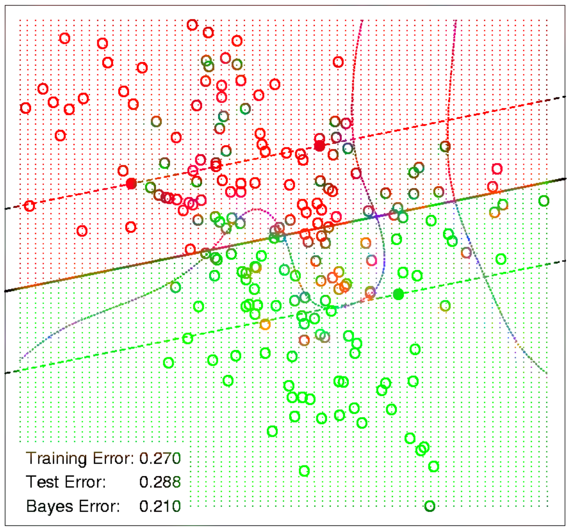

$\gamma = 10000$

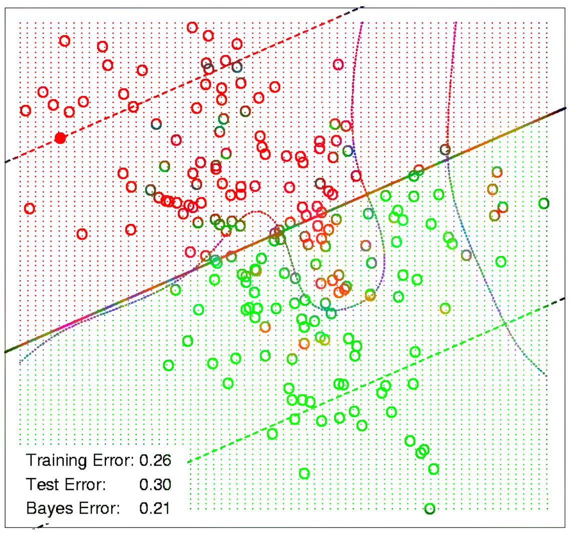

$\gamma = 0.01$

FIGURE 12.2. *The linear support vector boundary for the mixture data example with two overlapping classes, for two different values of γ. The broken lines indicate the margins, where $f(x) = \pm 1$. The support points ($\alpha_i > 0$) are all the points on the wrong side of their margin. The black solid dots are those support points falling exactly on the margin ($\xi_i = 0$, $\alpha_i > 0$). In the upper panel 62% of the observations are support points, while in the lower panel 85% are. The broken purple curve in the background is the Bayes decision boundary.*

12.3 Support Vector Machines

The support vector classifier described so far finds linear boundaries in the input feature space. As with other linear methods, we can make the procedure more flexible by enlarging the feature space using basis expansions such as polynomials or splines (Chapter 5). Generally linear boundaries in the enlarged space achieve better training-class separation, and translate to nonlinear boundaries in the original space. Once the basis functions $h_m(x),\ m = 1, \dots, M$ are selected, the procedure is the same as before. We fit the SV classifier using input features $h(x_i) = (h_1(x_i), h_2(x_i), \dots, h_M(x_i))$, $i = 1, \dots, N$, and produce the (nonlinear) function $\hat{f}(x) = h(x)^T\hat{\beta} + \hat{\beta}_0$. The classifier is $\hat{G}(x) = \text{sign}(\hat{f}(x))$ as before.

The *support vector machine* classifier is an extension of this idea, where the dimension of the enlarged space is allowed to get very large, infinite in some cases. It might seem that the computations would become prohibitive. It would also seem that with sufficient basis functions, the data would be separable, and overfitting would occur. We first show how the SVM technology deals with these issues. We then see that in fact the SVM classifier is solving a function-fitting problem using a particular criterion and form of regularization, and is part of a much bigger class of problems that includes the smoothing splines of Chapter 5. The reader may wish to consult Section 5.8, which provides background material and overlaps somewhat with the next two sections.

12.3.1 Computing the SVM for Classification

We can represent the optimization problem (12.9) and its solution in a special way that only involves the input features via inner products. We do this directly for the transformed feature vectors $h(x_i)$. We then see that for particular choices of h, these inner products can be computed very cheaply.

The Lagrange dual function (12.13) has the form

$$L_D = \sum_{i=1}^{N} \alpha_i - \frac{1}{2}\sum_{i=1}^{N}\sum_{i'=1}^{N} \alpha_i\alpha_{i'}y_iy_{i'}\langle h(x_i), h(x_{i'})\rangle. \tag{12.19}$$

From (12.10) we see that the solution function $f(x)$ can be written

$$\begin{aligned} f(x) &= h(x)^T\beta + \beta_0 \\ &= \sum_{i=1}^{N} \alpha_i y_i \langle h(x), h(x_i)\rangle + \beta_0. \end{aligned} \tag{12.20}$$

As before, given α_i, β_0 can be determined by solving $f(x_i) = 0$ in (12.20) for any (or all) x_i for which $0 < \alpha_i < \gamma$.

So both (12.19) and (12.20) involve $h(x)$ only through inner products. In fact, we need not specify the transformation $h(x)$ at all, but require only knowledge of the kernel function

$$K(x, x') = \langle h(x), h(x') \rangle \tag{12.21}$$

that computes inner products in the transformed space. K should be a symmetric positive (semi-) definite function; see Section 5.8.1.

Three popular choices for K in the SVM literature are

$$\begin{aligned} d\text{th Degree polynomial: } & K(x, x') = (1 + \langle x, x' \rangle)^d, \\ \text{Radial basis: } & K(x, x') = \exp(-\|x - x'\|^2/c), \\ \text{Neural network: } & K(x, x') = \tanh(\kappa_1 \langle x, x' \rangle + \kappa_2). \end{aligned} \tag{12.22}$$

Consider for example a feature space with two inputs X_1 and X_2, and a polynomial kernel of degree 2. Then

$$\begin{aligned} K(X, X') &= (1 + \langle X, X' \rangle)^2 \\ &= (1 + X_1 X_1' + X_2 X_2')^2 \\ &= 1 + 2X_1X_1' + 2X_2X_2' + (X_1X_1')^2 + (X_2X_2')^2 + 2X_1X_1'X_2X_2'. \end{aligned} \tag{12.23}$$

Then $M = 6$, and if we choose $h_1(X) = 1$, $h_2(X) = \sqrt{2}X_1$, $h_3(X) = \sqrt{2}X_2$, $h_4(X) = X_1^2$, $h_5(X) = X_2^2$, and $h_6(X) = \sqrt{2}X_1X_2$, then $K(X, X') = \langle h(X), h(X') \rangle$. From (12.20) we see that the solution can be written

$$\hat{f}(x) = \sum_{i=1}^{N} \hat{\alpha}_i y_i K(x, x_i) + \hat{\beta}_0. \tag{12.24}$$

The role of the parameter γ is clearer in an enlarged feature space, since perfect separation is typically achievable there. A large value of γ will discourage any positive ξ_i, and lead to an overfit wiggly boundary in the original feature space; a small value of γ will encourage a small value of $\|\beta\|$, which in turn causes $f(x)$ and hence the boundary to be smoother. Figure 12.3 show two nonlinear support vector machines applied to the mixture example of Chapter 2. The regularization parameter was chosen in both cases to achieve good test error. The radial basis kernel produces a boundary quite similar to the Bayes optimal boundary for this example; compare Figure 2.5.

In the early literature on support vectors, there were claims that the kernel property of the support vector machine is unique to it and allows one to finesse the curse of dimensionality. Neither of these claims is true, and we go into both of these issues in the next three subsections.

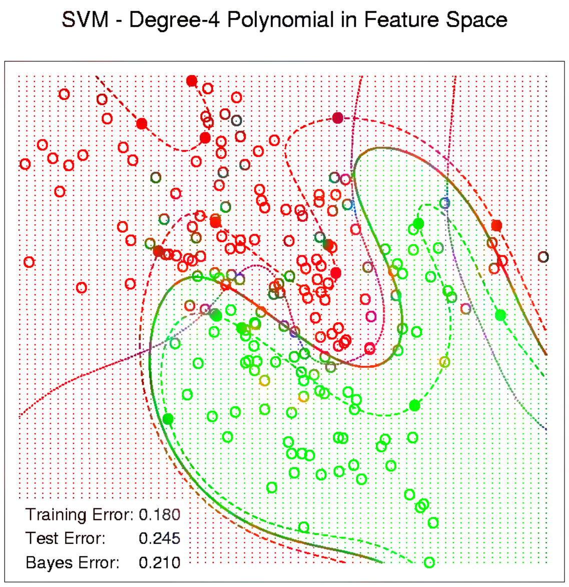

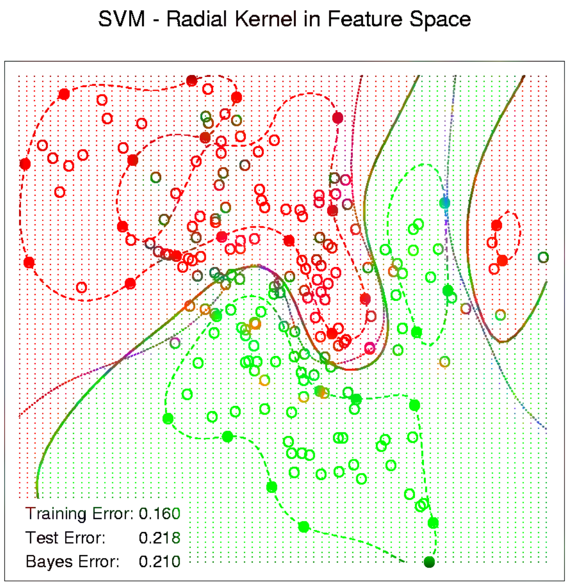

FIGURE 12.3. *Two nonlinear SVMs for the mixture data. The upper plot uses a 4-th degree polynomial kernel, the lower a radial basis kernel. In each case γ was tuned to approximately achieve the best test error performance, and $\gamma = 1$ worked well in both cases. The radial basis kernel performs the best (close to Bayes optimal), as might be expected given the data arise from mixtures of Gaussians. The broken purple curve in the background is the Bayes decision boundary.*

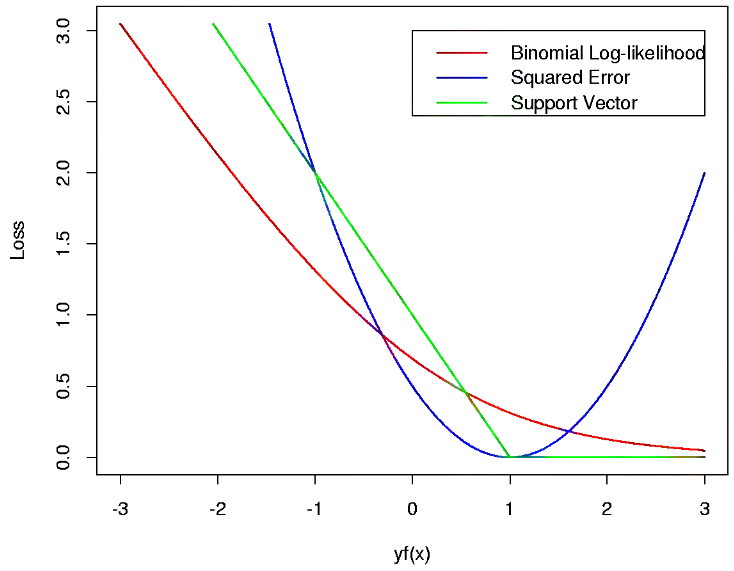

FIGURE 12.4. *The support vector loss function, compared to the (negative) log-likelihood loss for logistic regression, and squared-error loss. All are shown as a function of yf rather than f, because of the symmetry in all three between the $y = +1$ and $y = -1$ case. The log-likelihood has the same asymptotes as the SVM loss, but is rounded in the interior.*

12.3.2 The SVM as a Penalization Method

With $f(x) = h(x)^T\beta + \beta_0$, consider the optimization problem

$$\min_{\beta_0,\,\beta} \sum_{i=1}^{N}[1 - y_i f(x_i)]_+ + \lambda\|\beta\|^2 \tag{12.25}$$

where the subscript "+" indicates positive part. This has the form *loss + penalty*, which is a familiar paradigm in function estimation. It is easy to show (Exercise 12.1) that the solution to (12.25), with $\lambda = 1/(2\gamma)$, is the same as that for (12.8).

Examination of the loss function $L(y, f) = [1 - yf]_+$ shows that it is reasonable for two-class classification, when compared to other more traditional loss functions. Figure 12.4 compares it to the log-likelihood loss for logistic regression, as well as squared-error loss. The (negative) log-likelihood has similar tails as the SVM loss, giving zero penalty to points well inside their margin, and a linear penalty to points on the wrong side and far away. squared-error, on the other hand gives a quadratic penalty, and points well inside their own margin have a strong influence on the model as well.

TABLE 12.1. *The population minimizers for three different loss functions. Logistic regression uses the binomial log-likelihood. Linear discriminant analysis (Exercise (4.51) uses squared-error loss. The SVM loss estimates the mode of the posterior class probabilities.*

Loss function	$L(Y, F(X))$	Minimizing function
$(-)$Binomial Log-likelihood	$\log(1+e^{-Yf(X)})$	$f(X) = \log \dfrac{\Pr(Y=+1\|X)}{\Pr(Y=-1\|X)}$
Squared-error	$(Y - f(X))^2$	$f(X) = \Pr(Y=+1\|X) - \Pr(Y=-1\|X)$
Support vector machine	$[1 - Yf(X)]_+$	$f(X) = \begin{cases} +1, & \text{if } \Pr(Y=+1\|X) \geq \frac{1}{2} \\ -1, & \text{otherwise} \end{cases}$

We can characterize these three loss functions in terms of what they are estimating at the population level. We consider minimizing $\mathrm{E}L(Y, f(X))$. Table 12.1 summarizes the results.

This casts the SVM as a regularized function estimation problem, where the coefficients of the linear expansion $f(x) = \beta_0 + h(x)^T\beta$ are shrunk toward zero (excluding the constant). If $h(x)$ represents a hierarchical basis having some ordered structure (such as ordered in roughness), then the uniform shrinkage makes more sense if the rougher elements h_j in the vector h have smaller norm.

12.3.3 Function Estimation and Reproducing Kernels

Here we describe SVMs in terms of function estimation in reproducing kernel Hilbert spaces, where the kernel property abounds. This material is discussed in some detail in Section 5.8. This provides another view of the support vector classifier, and helps to clarify how it works.

Suppose the basis h arises from the (possibly finite) eigen-expansion of a positive definite kernel K,

$$K(x, x') = \sum_{m=1}^{\infty} \phi_m(x)\phi_m(x')\delta_m \tag{12.26}$$

and $h_m(x) = \sqrt{\delta_m}\phi_m(x)$. Then with $\theta_m = \sqrt{\delta_m}\beta_m$, we can write (12.25) as

$$\min_{\beta_0,\,\theta} \sum_{i=1}^{N} \Big[1 - y_i(\beta_0 + \sum_{m=1}^{\infty} \theta_m \phi_m(x_i))\Big]_+ + \lambda \sum_{m=1}^{\infty} \frac{\theta_m^2}{\delta_m}. \tag{12.27}$$

Now (12.27) is identical in form to (5.49) on page 145 in Section 5.8, and the theory of reproducing kernel Hilbert spaces described there guarantees a finite-dimensional solution of the form

$$f(x) = \beta_0 + \sum_{i=1}^{N} \alpha_i K(x, x_i). \tag{12.28}$$

In particular we see there an equivalent version of the optimization criterion (12.19) (Equation (5.66) in Section 5.8.2; see also Wahba et al. (2000)),

$$\min_{\alpha_0,\alpha} \sum_{i=1}^{N} (1 - y_i f(x_i))_+ + \lambda \alpha^T \mathbf{K} \alpha, \tag{12.29}$$

where $\mathbf{K}$ is the $N \times N$ matrix of kernel evaluations for all pairs of training features (Exercise 12.2).

These models are quite general, and include, for example, the entire family of smoothing splines, additive and interaction spline models discussed in Chapters 5 and 9, and in more detail in Wahba (1990) and Hastie and Tibshirani (1990). They can be expressed more generally as

$$\min_{f \in \mathcal{H}} \sum_{i=1}^{N} [1 - y_i f(x_i)]_+ + \lambda J(f), \tag{12.30}$$

where $\mathcal{H}$ is the structured space of functions, and $J(f)$ an appropriate regularizer on that space. For example, suppose $\mathcal{H}$ is the space of additive functions $f(x) = \sum_{j=1}^{p} f_j(x_j)$, and $J(f) = \sum_j \int f''_j(x_j) dx_j$. Then the solution to (12.30) is an additive cubic spline, and has a kernel representation (12.28) with $K(x, x') = \sum_{j=1}^{p} K_j(x_j, x'_j)$. Each of the K_j is the kernel appropriate for the univariate smoothing spline in x_j (Wahba, 1990).

Conversely this discussion also shows that, for example, *any* of the kernels described in (12.22) above can be used with *any* loss function, and will also lead to a finite-dimensional representation of the form (12.28). Figure 12.5 uses the same kernel functions as in Figure 12.3, except using the binomial log-likelihood as a loss function.* The fitted function is hence an estimate

*Ji Zhu assisted in the preparation of these examples.

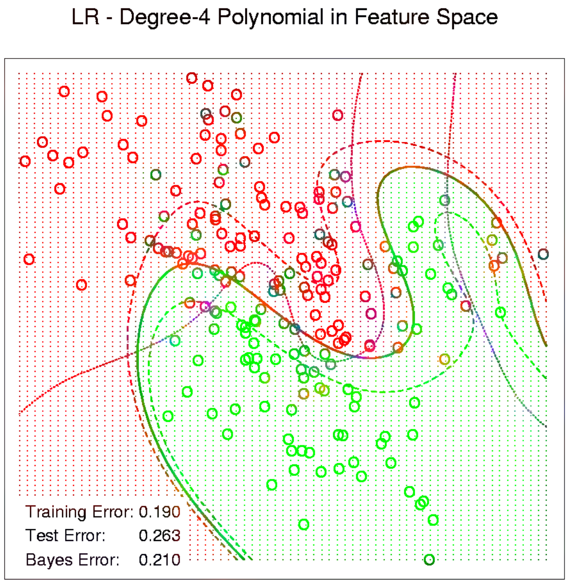

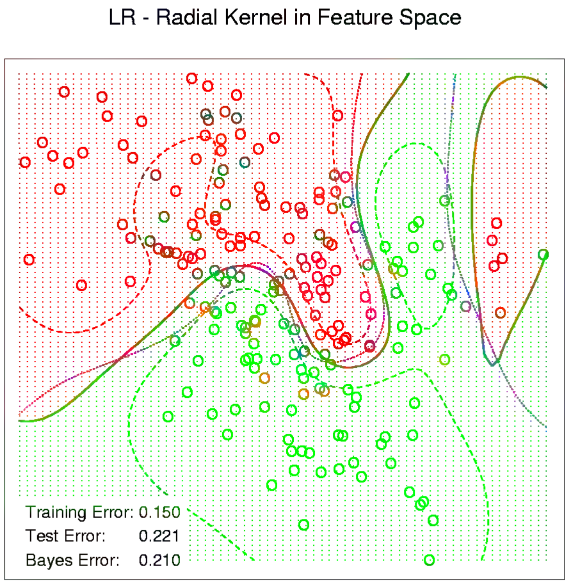

FIGURE 12.5. *The logistic regression versions of the SVM models in Figure 12.3, using the identical kernels and hence penalties, but the log-likelihood loss instead of the SVM loss function. The two broken contours correspond to posterior probabilities of* 0.75 *and* 0.25 *for the +1 class (or vice versa). The broken purple curve in the background is the Bayes decision boundary.*

of the log-odds,

$$\begin{aligned} \hat{f}(x) &= \log \frac{\hat{\Pr}(Y=+1|x)}{\hat{\Pr}(Y=-1|x)} \\ &= \hat{\beta}_0 + \sum_{i=1}^{N} \hat{\alpha}_i K(x, x_i), \end{aligned} \tag{12.31}$$

or conversely we get an estimate of the class probabilities

$$\hat{\Pr}(Y=+1|x) = \frac{1}{1+e^{-\hat{\beta}_0 - \sum_{i=1}^{N} \hat{\alpha}_i K(x,x_i)}}. \tag{12.32}$$

The fitted models are quite similar in shape and performance. Examples and more details are given in Section 5.8.

It does happen that for SVMs, a sizeable fraction of the N values of α_i can be zero (the nonsupport points). In the two examples in Figure 12.3, these fractions are 42% and 45%, respectively. This is a consequence of the L_1 nature of the first part of the criterion (12.25). The lower the class overlap (on the training data), the smaller this fraction will be. Reducing λ will generally reduce the overlap (allowing a more flexible f). A small number of support points means that $\hat{f}(x)$ can be evaluated more quickly, which is important at lookup time. Of course, reducing the overlap too much can lead to poor generalization.

12.3.4 SVMs and the Curse of Dimensionality

In this section, we address the question of whether SVMs have some edge on the curse of dimensionality. Notice that in expression (12.23) we are not allowed a fully general inner product in the space of powers and products. For example, all terms of the form $2X_jX_j'$ are given equal weight, and the kernel cannot adapt itself to concentrate on subspaces. If the number of features p were large, but the class separation occurred only in the linear subspace spanned by say X_1 and X_2, this kernel would not easily find the structure and would suffer from having many dimensions to search over. One would have to build knowledge about the subspace into the kernel; that is, tell it to ignore all but the first two inputs. If such knowledge were available a priori, much of statistical learning would be made much easier. A major goal of adaptive methods is to discover such structure.

We support these statements with an illustrative example. We generated 100 observations in each of two classes. The first class has four standard normal independent features X_1, X_2, X_3, X_4. The second class also has four standard normal independent features, but conditioned on $9 \le \sum X_j^2 \le 16$. This is a relatively easy problem. As a second harder problem, we augmented the features with an additional six standard Gaussian noise features. Hence the second class almost completely surrounds the first,

TABLE 12.2. *Skin of the orange: shown are mean (standard error of the mean) of the test error over five simulations. BRUTO fits an additive spline model adaptively, while MARS fits a low-order interaction model adaptively.*

		Test Error (SE)	
	Method	No Noise Features	Six Noise Features
1	SV Classifier	0.423 (0.006)	0.466 (0.008)
2	SVM/poly 2	0.081 (0.016)	0.172 (0.015)
3	SVM/poly 5	0.212 (0.008)	0.393 (0.004)
4	SVM/poly 10	0.265 (0.011)	0.438 (0.006)
5	BRUTO	0.082 (0.009)	0.080 (0.009)
6	MARS	0.138 (0.016)	0.116 (0.004)
	Bayes	0.061	0.061

like the skin surrounding the orange, in a four-dimensional subspace. The Bayes error rate for this problem is 0.061% (irrespective of dimension). We generated 1000 test observations to compare different procedures. The average test errors over five simulations, with and without noise features, are shown in Table 12.2.

Line 1 uses the support vector classifier in the original feature space. Lines 2–4 refer to the support vector machine with a 2-, 5- and 10-dimensional polynomial kernel. For all support vector procedures, we chose the tuning parameter C to minimize the test error, to be as fair as possible to the method. Line 5 fits an additive spline model to the $(-1, +1)$ response by least squares, using the BRUTO algorithm for additive models, described in Hastie and Tibshirani (1990). Line 6 uses MARS (multivariate adaptive regression splines) allowing interaction of all orders, as described in Chapter 9. Both of these last two have the ability to ignore redundant variables. Test error was not used to choose the smoothing parameters in either of lines 5 or 6.

In the original feature space, a hyperplane cannot separate the classes and the support vector classifier (line 1) does poorly. The polynomial support vector machine makes a substantial improvement in test error rate, but is adversely affected by the six noise features It is also very sensitive to the choice of kernel: the second degree polynomial kernel (line 2) does best since the true decision boundary is a second degree polynomial. However, higher-degree polynomial kernels (lines 3 and 4) do much worse. The additive model and MARS adapt well and achieve test error rates close to the Bayes rate.

12.3.5 Support Vector Machines for Regression

In this section we show how SVMs can be adapted for regression with a quantitative response, in ways that inherit some of the properties of the

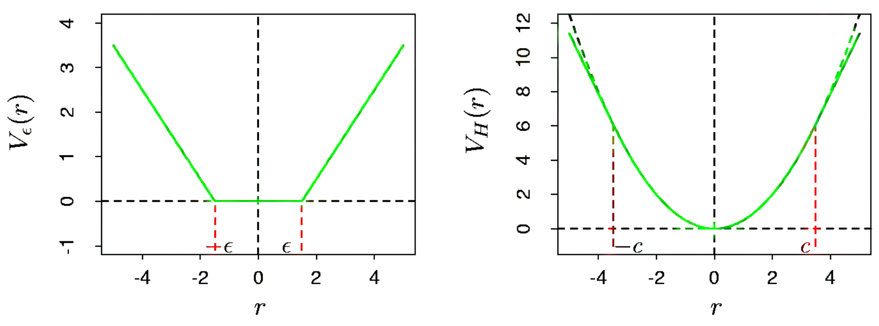

FIGURE 12.6. *The left panel shows the ϵ-insensitive error function used by the support vector regression machine. The right panel shows the error function used in Huber's robust regression (green curve). Beyond $|c|$, the function changes from quadratic to linear.*

SVM classifier. We first discuss the linear regression model

$$f(x) = x^T\beta + \beta_0, \tag{12.33}$$

and then handle nonlinear generalizations. To estimate β, we consider minimization of

$$H(\beta, \beta_0) = \sum_{i=1}^{N} V(y_i - f(x_i)) + \frac{\lambda}{2}\|\beta\|^2, \tag{12.34}$$

where

$$V_\epsilon(t) = \begin{cases} 0 & \text{if } |t| < \epsilon, \\ |t| - \epsilon, & \text{otherwise.} \end{cases} \tag{12.35}$$

This is an "ϵ-insensitive" error measure, ignoring errors of size less than ϵ (left panel of Figure 12.6). There is a rough analogy with the support vector classification setup, where points on the correct side of the decision boundary and far away from it, are ignored in the optimization. In regression, these "low error" points are the ones with small residuals.

It is interesting to contrast this with error measures used in robust regression in statistics. The most popular, due to Huber (1964), has the form

$$V_H(r) = \begin{cases} r^2/2 & \text{if } |r| \le c, \\ c|r| - c^2/2, & |r| > c, \end{cases} \tag{12.36}$$

shown in the right panel of Figure 12.6. This function reduces from quadratic to linear the contributions of observations with absolute residual greater than a prechosen constant c. This makes the fitting less sensitive to outliers. The support vector error measure (12.35) also has linear tails (beyond

ϵ), but in addition it flattens the contributions of those cases with small residuals.

If $\hat{\beta}$, $\hat{\beta}_0$ are the minimizers of H, the solution function can be shown to have the form

$$\begin{aligned}\hat{\beta} &= \sum_{i=1}^{N}(\hat{\alpha}_i^* - \hat{\alpha}_i)x_i, \quad (12.37)\\ \hat{f}(x) &= \sum_{i=1}^{N}(\hat{\alpha}_i^* - \hat{\alpha}_i)\langle x, x_i\rangle + \beta_0, \quad (12.38)\end{aligned}$$

where α_i, α_i^* are positive and solve the quadratic programming problem

$$\min_{\alpha_i,\alpha_i^*} \epsilon\sum_{i=1}^{N}(\alpha_i^* + \alpha_i) - \sum_{i=1}^{N} y_i(\alpha_i^* - \alpha_i) + \frac{1}{2}\sum_{i,i'=1}^{N}(\alpha_i^* - \alpha_i)(\alpha_{i'}^* - \alpha_{i'})\langle x_i, x_{i'}\rangle$$

subject to the constraints

$$\begin{aligned} 0 \le \alpha_i,\ \alpha_i^* &\le 1/\lambda,\\ \sum_{i=1}^{N}(\alpha_i^* - \alpha_i) &= 0, \quad (12.39)\\ \alpha_i\alpha_i^* &= 0.\end{aligned}$$

Due to the nature of these constraints, typically only a subset of the solution values $(\alpha_i^* - \alpha_i)$ are nonzero, and the associated data values are called the support vectors. As was the case in the classification setting, the solution depends on the input values only through the inner products $\langle x_i, x_{i'}\rangle$. Thus we can generalize the methods to richer spaces by defining an appropriate inner product, for example, one of those defined in (12.22).

Note that there are parameters, ϵ and λ, associated with the criterion (12.34). These seem to play different roles. ϵ is a parameter of the loss function V_ϵ, just like c is for V_H. Note that both V_ϵ and V_H depend on the scale of y and hence r. If we scale our response (and hence use $V_H(r/\sigma)$ and $V_\epsilon(r/\sigma)$ instead), then we might consider using preset values for c and ϵ (the value $c = 1.345$ achieves 95% efficiency for the Gaussian). The quantity λ is a more traditional regularization parameter, and can be estimated for example by cross-validation.

12.3.6 Regression and Kernels

As discussed in Section 12.3.3, this kernel property is not unique to support vector machines. Suppose we consider approximation of the regression function in terms of a set of basis functions $\{h_m(x)\}, m = 1, 2, \dots, M$:

$$f(x) = \sum_{m=1}^{M} \beta_m h_m(x) + \beta_0. \tag{12.40}$$

To estimate β and β_0 we minimize

$$H(\beta, \beta_0) = \sum_{i=1}^{N} V(y_i - f(x_i)) + \frac{\lambda}{2} \sum \beta_m^2 \tag{12.41}$$

for some general error measure $V(r)$. For any choice of $V(r)$, the solution $\hat{f}(x) = \sum \hat{\beta}_m h_m(x) + \hat{\beta}_0$ has the form

$$\hat{f}(x) = \sum_{i=1}^{N} \hat{a}_i K(x, x_i) \tag{12.42}$$

with $K(x, y) = \sum_{m=1}^{M} h_m(x) h_m(y)$. Notice that this has same form as both the radial basis function expansion and a regularization estimate, discussed in Chapters 5 and 6.

For concreteness, let's work out the case $V(r) = r^2$. Let $\mathbf{H}$ be the $N \times M$ basis matrix with imth element $h_m(x_i)$, and suppose that $M > N$ is large. For simplicity we assume that $\beta_0 = 0$, or that the constant is absorbed in h; see Exercise 12.3 for an alternative.

We estimate β by minimizing the penalized least squares criterion

$$H(\beta) = (\mathbf{y} - \mathbf{H}\beta)^T (\mathbf{y} - \mathbf{H}\beta) + \lambda \|\beta\|^2. \tag{12.43}$$

The solution is

$$\hat{\mathbf{y}} = \mathbf{H}\hat{\beta} \tag{12.44}$$

with $\hat{\beta}$ determined by

$$-\mathbf{H}^T(\mathbf{y} - \mathbf{H}\hat{\beta}) + \lambda\hat{\beta} = 0. \tag{12.45}$$

From this it appears that we need to evaluate the $M \times M$ matrix of inner products in the transformed space. However, we can premultiply by $\mathbf{H}$ to give

$$\mathbf{H}\hat{\beta} = (\mathbf{H}\mathbf{H}^T + \lambda I)^{-1} \mathbf{H}\mathbf{H}^T \mathbf{y}. \tag{12.46}$$

The $N \times N$ matrix $\mathbf{H}\mathbf{H}^T$ consists of inner products between pairs of observations i, i'; that is, the evaluation of an inner product kernel $\{\mathbf{H}\mathbf{H}^T\}_{i,i'} = K(x_i, x_{i'})$. It is easy to show (12.42) directly in this case, that the predicted values at an arbitrary x satisfy

$$\begin{aligned} \hat{f}(x) &= h(x)^T \hat{\beta} \\ &= \sum_{i=1}^{N} \hat{\alpha}_i K(x, x_i), \end{aligned} \tag{12.47}$$

where $\hat{\alpha} = (\mathbf{H}\mathbf{H}^T + \mathbf{I})^{-1}\mathbf{y}$. As in the support vector machine, we need not specify or evaluate the large set of functions $h_1(x), h_2(x), \ldots, h_M(x)$. Only the inner product kernel $K(x_i, x_{i'})$ need be evaluated, at the N training points for each i, i' and at points x for predictions there. Careful choice of h_m (such as the eigenfunctions of particular, easy-to-evaluate kernels K) means, for example, that $\mathbf{H}\mathbf{H}^T$ can be computed at a cost of $N^2/2$ evaluations of K, rather than the direct cost N^2M.

Note, however, that this property depends on the choice of squared norm $\|\beta\|^2$ in the penalty. It does not hold, for example, for the L_1 norm $|\beta|$, which may lead to a superior model.

12.3.7 Discussion

The support vector machine can be extended to multiclass problems, essentially by solving many two-class problems. A classifier is built for each pair of classes, and the final classifier is the one that dominates the most (Kressel, 1999; Friedman, 1996; Hastie and Tibshirani, 1998). Alternatively, one could use the multinomial loss function along with a suitable kernel, as in Section 12.3.3. SVMs have applications in many other supervised and unsupervised learning problems. At the time of this writing, empirical evidence suggests that it performs well in many real learning problems.

Finally, we mention the connection of the support vector machine and structural risk minimization (7.9). Suppose the training points (or their basis expansion) are contained in a sphere of radius R, and let $G(x) = \text{sign}[f(x)] = \text{sign}[\beta^T x + \beta_0]$ as in (12.2). Then one can show that the class of functions $\{G(x), \|\beta\| \leq A\}$ has VC-dimension h satisfying

$$h \leq R^2A^2. \tag{12.48}$$

If $f(x)$ separates the training data, optimally for $\|\beta\| \leq A$, then with probability at least $1 - \eta$ over training sets (Vapnik, 1996, page 139):

$$\text{Error}_{\text{Test}} \leq 4\frac{h(\log(2N/h) + 1) - \log(\eta/4)}{N}. \tag{12.49}$$

The support vector classifier was one of the first practical learning procedures for which useful bounds on the VC dimension could be obtained, and hence the SRM program could be carried out. However in the derivation, balls are put around the data points—a process that depends on the observed values of the features. Hence in a strict sense, the VC complexity of the class is not fixed a priori, before seeing the features.

The regularization parameter γ controls an upper bound on the VC dimension of the classifier. Following the SRM paradigm, we could choose γ by minimizing the upper bound on the test error, given in (12.49). However, it is not clear that this has any advantage over the use of cross-validation for choice of γ.

12.4 Generalizing Linear Discriminant Analysis

In Section 4.3 we discussed linear discriminant analysis (LDA), a fundamental tool for classification. For the remainder of this chapter we discuss a class of techniques that produce better classifiers than LDA by directly generalizing LDA.

Some of the virtues of LDA are as follows:

- It is a simple prototype classifier. A new observation is classified to the class with closest centroid. A slight twist is that distance is measured in the Mahalanobis metric, using a pooled covariance estimate.

- LDA is the estimated Bayes classifier if the observations are multivariate Gaussian in each class, with a common covariance matrix. Since this assumption is unlikely to be true, this might not seem to be much of a virtue.

- The decision boundaries created by LDA are linear, leading to decision rules that are simple to describe and implement.

- LDA provides natural low-dimensional views of the data. For example, Figure 12.10 is an informative two-dimensional view of data in 256 dimensions with ten classes.

- Often LDA produces the best classification results, because of its simplicity and low variance. LDA was among the top three classifiers for 11 of the 22 datasets studied in the STATLOG project (Michie et al., 1994).[†]

Unfortunately the simplicity of LDA causes it to fail in a number of situations as well:

- Often linear decision boundaries do not adequately separate the classes. When N is large, it is possible to estimate more complex decision boundaries. Quadratic discriminant analysis (QDA) is often useful here, and allows for quadratic decision boundaries. More generally we would like to be able to model irregular decision boundaries.

- The aforementioned shortcoming of LDA can often be paraphrased by saying that a single prototype per class is insufficient. LDA uses a single prototype (class centroid) plus a common covariance matrix to describe the spread of the data in each class. In many situations, several prototypes are more appropriate.

- At the other end of the spectrum, we may have way too many (correlated) predictors, for example, in the case of digitized analogue signals

[†]This study predated the emergence of SVMs.

and images. In this case LDA uses too many parameters, which are estimated with high variance, and its performance suffers. In cases such as this we need to restrict or regularize LDA even further.

In the remainder of this chapter we describe a class of techniques that attend to all these issues by generalizing the LDA model. This is achieved largely by three different ideas.

The first idea is to recast the LDA problem as a linear regression problem. Many techniques exist for generalizing linear regression to more flexible, nonparametric forms of regression. This in turn leads to more flexible forms of discriminant analysis, which we call FDA. In most cases of interest, the regression procedures can be seen to identify an enlarged set of predictors via basis expansions. FDA amounts to LDA in this enlarged space, the same paradigm used in SVMs.

In the case of too many predictors, such as the pixels of a digitized image, we do not want to expand the set: it is already too large. The second idea is to fit an LDA model, but penalize its coefficients to be smooth or otherwise coherent in the spatial domain, that is, as an image. We call this procedure *penalized discriminant analysis* or PDA. With FDA itself, the expanded basis set is often so large that regularization is also required (again as in SVMs). Both of these can be achieved via a suitably regularized regression in the context of the FDA model.

The third idea is to model each class by a mixture of two or more Gaussians with different centroids, but with every component Gaussian, both within and between classes, sharing the same covariance matrix. This allows for more complex decision boundaries, and allows for subspace reduction as in LDA. We call this extension *mixture discriminant analysis* or MDA.

All three of these generalizations use a common framework by exploiting their connection with LDA.

12.5 Flexible Discriminant Analysis

In this section we describe a method for performing LDA using linear regression on derived responses. This in turn leads to nonparametric and flexible alternatives to LDA. As in Chapter 4, we assume we have observations with a quantitative response G falling into one of K classes $\mathcal{G} = \{1, \dots, K\}$, each having measured features X. Suppose $\theta : \mathcal{G} \mapsto \mathbb{R}^1$ is a function that assigns scores to the classes, such that the transformed class labels are optimally predicted by linear regression on X: If our training sample has the form $(g_i, x_i),\ i = 1, 2, \dots, N$, then we solve

$$\min_{\beta,\theta} \sum_{i=1}^{N} \left(\theta(g_i) - x_i^T\beta\right)^2, \tag{12.50}$$

with a restrictions on θ to avoid a trivial solution (mean zero and unit variance over the training data). This produces a one-dimensional separation between the classes.

More generally, we can find up to $L \leq K-1$ sets of independent scorings for the class labels, $\theta_1, \theta_2, \ldots, \theta_L$, and L corresponding linear maps $\eta_\ell(X) = X^T\beta_\ell$, $\ell = 1, \ldots, L$, chosen to be optimal for multiple regression in $\mathbb{R}^p$. The scores $\theta_\ell(g)$ and the maps β_ℓ are chosen to minimize the average squared residual,

$$ASR = \frac{1}{N}\sum_{\ell=1}^{L}\left[\sum_{i=1}^{N}\left(\theta_\ell(g_i) - x_i^T\beta_\ell\right)^2\right]. \tag{12.51}$$

The set of scores are assumed to be mutually orthogonal and normalized with respect to an appropriate inner product to prevent trivial zero solutions.

Why are we going down this road? It can be shown that the sequence of discriminant (canonical) vectors ν_ℓ derived in 4.3.3 are identical to the sequence β_ℓ up to a constant (Mardia et al., 1979; Hastie et al., 1995). Moreover, the Mahalanobis distance of a test point x to the kth class centroid $\hat{\mu}_k$ is given by

$$\delta_J(x, \hat{\mu}_k) = \sum_{\ell=1}^{K-1} w_\ell(\hat{\eta}_\ell(x) - \bar{\eta}_\ell^k)^2 + D(x), \tag{12.52}$$

where $\bar{\eta}_\ell^k$ is the mean of the $\hat{\eta}_\ell(x_i)$ in the kth class, and $D(x)$ does not depend on k. Here w_ℓ are coordinate weights that are defined in terms of the mean squared residual r_ℓ^2 of the ℓth optimally scored fit

$$w_\ell = \frac{1}{r_\ell^2(1-r_\ell^2)}. \tag{12.53}$$

In Section 4.3.2 we saw that these canonical distances are all that is needed for classification in the Gaussian setup, with equal covariances in each class. To summarize:

> LDA can be performed by a sequence of linear regressions, followed by classification to the closest class centroid in the space of fits. The analogy applies both to the reduced rank version, or the full rank case when $L = K-1$.

The real power of this result is in the generalizations that it invites. We can replace the linear regression fits $\eta_\ell(x) = x^T\beta_\ell$ by far more flexible, nonparametric fits, and by analogy achieve a more flexible classifier than LDA. We have in mind generalized additive fits, spline functions, MARS models and the like. In this more general form the regression problems are

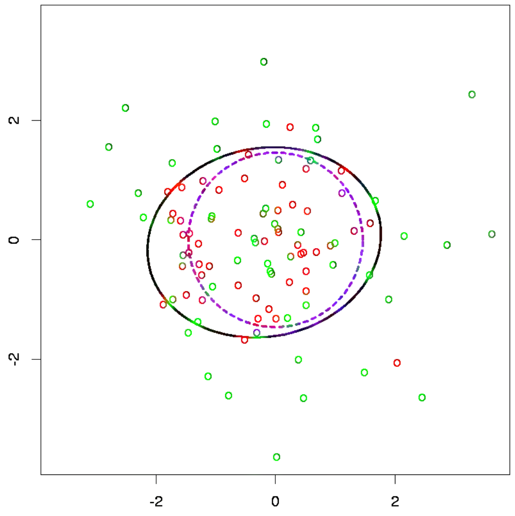

FIGURE 12.7. *The data consist of* 50 *points generated from each of* $N(0, I)$ *and* $N(0, \frac{9}{4}I)$. *The solid black ellipse is the decision boundary found by FDA using degree-two polynomial regression. The dashed purple circle is the Bayes decision boundary.*

defined via the criterion

$$ASR(\{\theta_\ell, \eta_\ell\}_{\ell=1}^L) = \frac{1}{N}\sum_{\ell=1}^{L}\left[\sum_{i=1}^{N}(\theta_\ell(g_i) - \eta_\ell(x_i))^2 + \lambda J(\eta_\ell)\right], \qquad (12.54)$$

where J is a regularizer appropriate for some forms of nonparametric regression, such as smoothing splines, additive splines and lower-order ANOVA spline models. Also included are the classes of functions and associated penalties generated by kernels, as in Section 12.3.3.

Before we describe the computations involved in this generalization, let us consider a very simple example. Suppose we use degree-two polynomial regression for each η_ℓ. The decision boundaries implied by the (12.52) will be quadratic surfaces, since each of the fitted functions is quadratic, and as in LDA their squares cancel out when comparing distances. We could have achieved *identical* quadratic boundaries in a more conventional way, by augmenting our original predictors with their squares and cross-products. In the enlarged space one performs an LDA, and the linear boundaries in the enlarged space map down to quadratic boundaries in the original space. A classic example is a pair of multivariate Gaussians centered at the origin, one having covariance matrix I, and the other cI for $c > 1$; Figure 12.7 illustrates. The Bayes decision boundary is the sphere $\|x\| = \frac{pc\log c}{2(c-1)}$, which is a linear boundary in the enlarged space.

Many nonparametric regression procedures operate by generating a basis expansion of derived variables, and then performing a linear regression in the enlarged space. The MARS procedure (Chapter 9) is exactly of this form. Smoothing splines and additive spline models generate an extremely large basis set ($N \times p$ basis functions for additive splines), but then perform a penalized regression fit in the enlarged space. SVMs do as well; see also the kernel-based regression example in Section 12.3.6. FDA in this case can be shown to perform a *penalized linear discriminant analysis* in the enlarged space. We elaborate in Section 12.6. Linear boundaries in the enlarged space map down to nonlinear boundaries in the reduced space. This is exactly the same paradigm that is used with support vector machines (Section 12.3).

We illustrate FDA on the speech recognition example used in Chapter 4.), with $K = 11$ classes and $p = 10$ predictors. The classes correspond to 11 vowel sounds, each contained in 11 different words. Here are the words, preceded by the symbols that represent them:

vowel	word	vowel	word	vowel	word	vowel	word
i:	heed	O	hod	I	hid	C:	hoard
E	head	U	hood	A	had	u:	who'd
a:	hard	3:	heard	Y	hud		

Each of eight speakers spoke each word six times in the training set, and likewise seven speakers in the test set. The ten predictors are derived from the digitized speech in a rather complicated way, but standard in the speech recognition world. There are thus 528 training observations, and 462 test observations. Figure 12.8 shows two-dimensional projections produced by LDA and FDA. The FDA model used adaptive additive-spline regression functions to model the $\eta_\ell(x)$, and the points plotted in the right plot have coordinates $\hat{\eta}_1(x_i)$ and $\hat{\eta}_2(x_i)$. The routine used in S-PLUS is called `bruto`, hence the heading on the plot and in Table 12.3. We see that flexible modeling has helped to separate the classes in this case. Table 12.3 shows training and test error rates for a number of classification techniques. FDA/MARS refers to Friedman's multivariate adaptive regression splines; degree = 2 means pairwise products are permitted. Notice that for FDA/MARS, the best classification results are obtained in a reduced-rank subspace.

12.5.1 Computing the FDA Estimates

The computations for the FDA coordinates can be simplified in many important cases, in particular when the nonparametric regression procedure can be represented as a linear operator. We will denote this operator by $\mathbf{S}_\lambda$; that is, $\hat{\mathbf{y}} = \mathbf{S}_\lambda \mathbf{y}$, where $\mathbf{y}$ is the vector of responses and $\hat{\mathbf{y}}$ the vector of fits. Additive splines have this property, if the smoothing parameters are fixed, as does MARS once the basis functions are selected. The subscript λ denotes the entire set of smoothing parameters. In this case optimal scoring is equivalent to a canonical correlation problem, and the solution can be

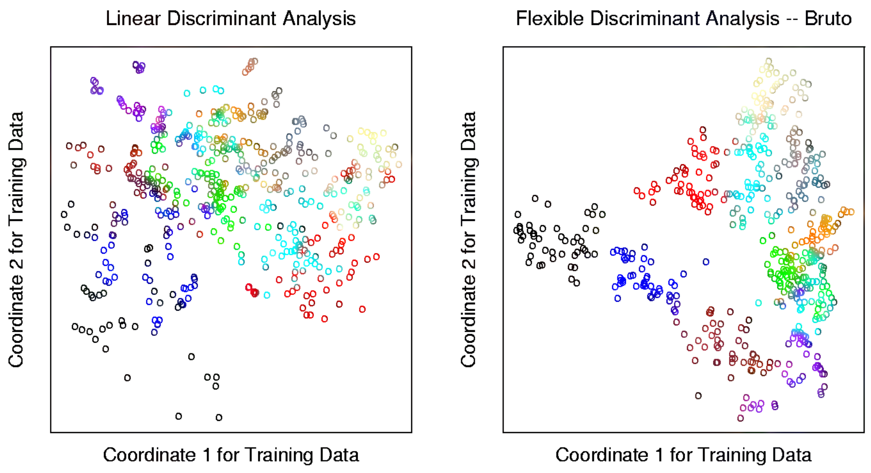

FIGURE 12.8. *The left plot shows the first two LDA canonical variates for the vowel training data. The right plot shows the corresponding projection when FDA/BRUTO is used to fit the model; plotted are the fitted regression functions $\hat{\eta}_1(x_i)$ and $\hat{\eta}_2(x_i)$. Notice the improved separation. The letters label the vowel sounds.*

computed by a single eigen-decomposition. This is pursued in Exercise 12.6, and the resulting algorithm is presented here.

We create an $N \times K$ *indicator response matrix* $\mathbf{Y}$ from the responses g_i, such that $y_{ik} = 1$ if $g_i = k$, otherwise $y_{ik} = 0$. For a five-class problem $\mathbf{Y}$ might look like the following:

$$\begin{array}{c} \\ g_1 = 2 \\ g_2 = 1 \\ g_3 = 1 \\ g_4 = 5 \\ g_5 = 4 \\ \vdots \\ g_N = 3 \end{array} \begin{array}{c} \begin{array}{ccccc} C_1 & C_2 & C_3 & C_4 & C_5 \end{array} \\ \begin{pmatrix} 0 & 1 & 0 & 0 & 0 \\ 1 & 0 & 0 & 0 & 0 \\ 1 & 0 & 0 & 0 & 0 \\ 0 & 0 & 0 & 0 & 1 \\ 0 & 0 & 0 & 1 & 0 \\ & & \vdots & & \\ 0 & 0 & 1 & 0 & 0 \end{pmatrix} \end{array}$$

Here are the computational steps:

1. *Multivariate nonparametric regression.* Fit a multiresponse, adaptive nonparametric regression of $\mathbf{Y}$ on $\mathbf{X}$, giving fitted values $\hat{\mathbf{Y}}$. Let $\mathbf{S}_\lambda$ be the linear operator that fits the final chosen model, and $\eta^*(x)$ be the vector of fitted regression functions.

2. *Optimal scores.* Compute the eigen-decomposition of $\mathbf{Y}^T\hat{\mathbf{Y}} = \mathbf{Y}^T\mathbf{S}_\lambda\mathbf{Y}$, where the eigenvectors Θ are normalized: $\Theta^T\mathbf{D}_\pi\Theta = \mathbf{I}$. Here $\mathbf{D}_\pi =$

TABLE 12.3. *Vowel recognition data performance results. The results for neural networks are the best among a much larger set, taken from a neural network archive. The notation FDA/BRUTO refers to the regression method used with FDA.*

	Technique	Error Rates	
		Training	Test
(1)	LDA	0.32	0.56
	Softmax	0.48	0.67
(2)	QDA	0.01	0.53
(3)	CART	0.05	0.56
(4)	CART (linear combination splits)	0.05	0.54
(5)	Single-layer perceptron		0.67
(6)	Multi-layer perceptron (88 hidden units)		0.49
(7)	Gaussian node network (528 hidden units)		0.45
(8)	Nearest neighbor		0.44
(9)	FDA/BRUTO	0.06	0.44
	Softmax	0.11	0.50
(10)	FDA/MARS (degree = 1)	0.09	0.45
	Best reduced dimension (=2)	0.18	0.42
	Softmax	0.14	0.48
(11)	FDA/MARS (degree = 2)	0.02	0.42
	Best reduced dimension (=6)	0.13	0.39
	Softmax	0.10	0.50

$\mathbf{Y}^T\mathbf{Y}/N$ is a diagonal matrix of the estimated class prior probabilities.

3. *Update* the model from step 1 using the optimal scores: $\eta(x) = \Theta^T\eta^*(x)$.

The first of the K functions in $\eta(x)$ is the constant function— a trivial solution; the remaining $K-1$ functions are the discriminant functions. The constant function, along with the normalization, causes all the remaining functions to be centered.

Again $\mathbf{S}_\lambda$ can correspond to any regression method. When $\mathbf{S}_\lambda = \mathbf{H}_X$, the linear regression projection operator, then FDA is linear discriminant analysis. The software that we reference in the bibliographic notes makes good use of this modularity; the `fda` function has a `method=` argument that allows one to supply *any* regression function, as long as it follows some natural conventions. The regression functions we provide allow for polynomial regression, adaptive additive models and MARS. They all efficiently handle multiple responses, so step (1) is a single call to a regression routine. The eigen-decomposition in step (2) simultaneously computes all the optimal scoring functions.

In Section 4.2 we discussed the pitfalls of using linear regression on an indicator response matrix as a method for classification. In particular, severe masking can occur with three or more classes. FDA uses the fits from such a regression in step (1), but then transforms them further to produce useful discriminant functions that are devoid of these pitfalls. Exercise 12.9 takes another view of this phenomenon.

12.6 Penalized Discriminant Analysis

Although FDA is motivated by generalizing optimal scoring, it can also be viewed directly as a form of regularized discriminant analysis. Suppose the regression procedure used in FDA amounts to a linear regression onto a basis expansion $h(X)$, with a quadratic penalty on the coefficients:

$$ASR(\{\theta_\ell, \beta_\ell\}_{\ell=1}^L) = \frac{1}{N}\sum_{\ell=1}^L \left[\sum_{i=1}^N (\theta_\ell(g_i) - h^T(x_i)\beta_\ell)^2 + \lambda \beta_\ell^T \Omega \beta_\ell\right]. \quad (12.55)$$

The choice of Ω depends on the problem. If $\eta_\ell(x) = h(x)\beta_\ell$ is an expansion on spline basis functions, Ω might constrain η_ℓ to be smooth over $\mathbb{R}^p$. In the case of additive splines, there are N spline basis functions for each coordinate, resulting in a total of Np basis functions in $h(x)$; Ω in this case is $Np \times Np$ and block diagonal.

The steps in FDA can then be viewed as a generalized form of LDA, which we call *penalized discriminant analysis*, or PDA:

- Enlarge the set of predictors X via a basis expansion $h(X)$.
- Use (penalized) LDA in the enlarged space, where the penalized Mahalanobis distance is given by

$$D(x, \mu) = (h(x) - h(\mu))^T (\Sigma_W + \Omega)^{-1} (h(x) - h(\mu)), \quad (12.56)$$

  where Σ_W is the within-class covariance matrix of the derived variables $h(x_i)$.
- Decompose the classification subspace using a penalized metric:

$$\max u^T \Sigma_{\text{Bet}} u \text{ subject to } u^T(\Sigma_W + \Omega)u = 1.$$

Loosely speaking, the penalized Mahalanobis distance tends to give less weight to "rough" coordinates, and more weight to "smooth" ones; since the penalty is not diagonal, the same applies to linear combinations that are rough or smooth.

For some classes of problems, the first step, involving the basis expansion, is not needed; we already have far too many (correlated) predictors. A leading example is when the objects to be classified are digitized analog signals:

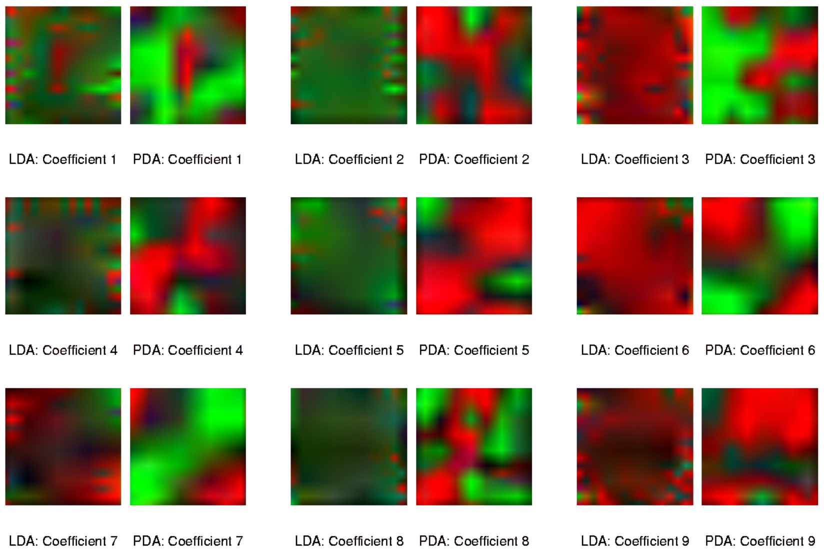

FIGURE 12.9. *The images appear in pairs, and represent the nine discriminant coefficient functions for the digit recognition problem. The left member of each pair is the LDA coefficient, while the right member is the PDA coefficient, regularized to enforce spatial smoothness.*

- the log-periodogram of a fragment of spoken speech, sampled at a set of 256 frequencies; see Figure 5.5 on page 125.
- the grayscale pixel values in a digitized image of a handwritten digit.

It is also intuitively clear in these cases why regularization is needed. Take the digitized image as an example. Neighboring pixel values will tend to be correlated, being often almost the same. This implies that the pair of corresponding LDA coefficients for these pixels can be wildly different and opposite in sign, and thus cancel when applied to similar pixel values. Positively correlated predictors lead to noisy, negatively correlated coefficient estimates, and this noise results in unwanted sampling variance. A reasonable strategy is to regularize the *coefficients* to be smooth over the spatial domain, as with images. This is what PDA does. The computations proceed just as for FDA, except that an appropriate penalized regression method is used. Here $h^T(X)\beta_\ell = X\beta_\ell$, and Ω is chosen so that $\beta_\ell^T\Omega\beta_\ell$ penalizes roughness in β_ℓ when viewed as an image. Figure 1.2 on page 4 shows some examples of handwritten digits. Figure 12.9 shows the discriminant variates using LDA and PDA. Those produced by LDA appear as *salt-and-pepper* images, while those produced by PDA are smooth images. The first smooth image can be seen as the coefficients of a linear contrast functional for separating images with a dark central vertical strip (ones,

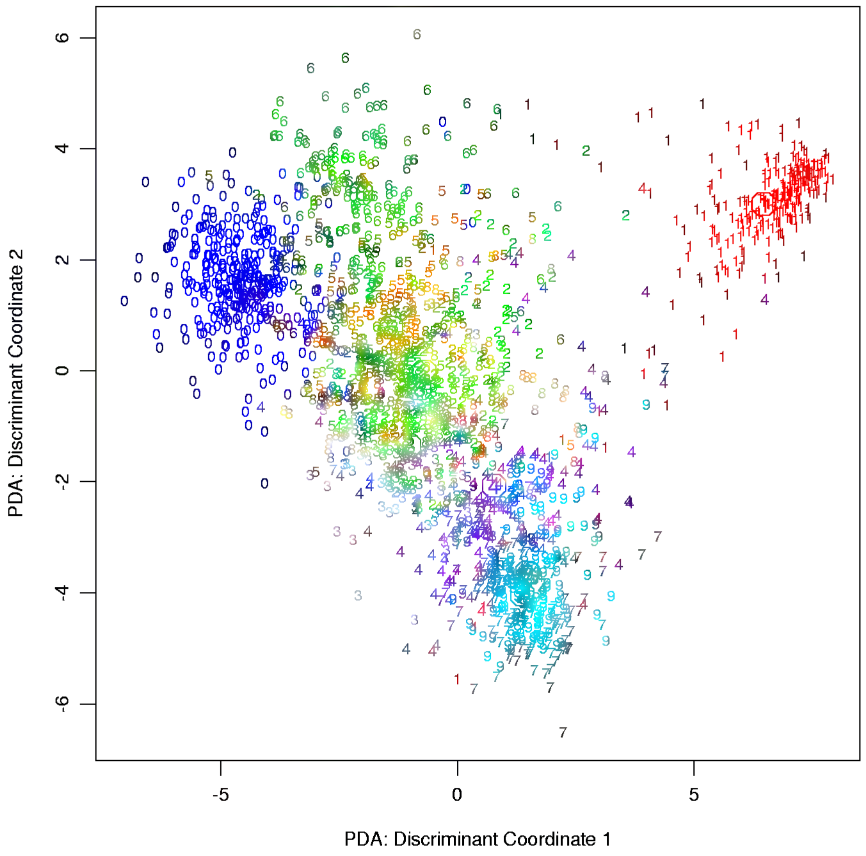

FIGURE 12.10. *The first two penalized canonical variates, evaluated for the test data. The circles indicate the class centroids. The first coordinate contrasts mainly* 0*'s and* 1*'s, while the second contrasts* 6*'s and* 7/9*'s.*

possibly sevens) from images that are hollow in the middle (zeros, some fours). Figure 12.10 supports this interpretation, and with more difficulty allows an interpretation of the second coordinate. This and other examples are discussed in more detail in Hastie et al. (1995), who also show that the regularization improves the classification performance of LDA on independent test data by a factor of around 25% in the cases they tried.

12.7 Mixture Discriminant Analysis

Linear discriminant analysis can be viewed as a *prototype* classifier. Each class is represented by its centroid, and we classify to the closest using an appropriate metric. In many situations a single prototype is not sufficient to represent inhomogeneous classes, and mixture models are more appropriate. In this section we review Gaussian mixture models and show how they can be generalized via the FDA and PDA methods discussed earlier. A Gaussian mixture model for the kth class has density

$$P(X|G=k)=\sum_{r=1}^{R_k}\pi_{kr}\phi(X;\mu_{kr},\Sigma), \tag{12.57}$$

where the *mixing proportions* π_{kr} sum to one. This has R_k prototypes for the kth class, and in our specification, the same covariance matrix Σ is used as the metric throughout. Given such a model for each class, the class posterior probabilities are given by

$$P(G=k|X=x)=\frac{\sum_{r=1}^{R_k}\pi_{kr}\phi(X;\mu_{kr},\Sigma)\Pi_k}{\sum_{\ell=1}^{K}\sum_{r=1}^{R_\ell}\pi_{\ell r}\phi(X;\mu_{\ell r},\Sigma)\Pi_\ell}, \tag{12.58}$$

where Π_k represent the class prior probabilities.

We saw these calculations for the special case of two components in Chapter 8. As in LDA, we estimate the parameters by maximum likelihood, using the joint log-likelihood based on $P(G,X)$:

$$\sum_{k=1}^{K}\sum_{g_i=k}\log\left[\sum_{r=1}^{R_k}\pi_{kr}\phi(x_i;\mu_{kr},\Sigma)\Pi_k\right]. \tag{12.59}$$

The sum within the log makes this a rather messy optimization problem if tackled directly. The classical and natural method for computing the maximum-likelihood estimates (MLEs) for mixture distributions is the EM algorithm (Dempster et al., 1977), which is known to possess good convergence properties. EM alternates between the two steps:

E-step: Given the current parameters, compute the *responsibility* of subclass c_{kr} within class k for each of the class-k observations ($g_i=k$):

$$W(c_{kr}|x_i,g_i)=\frac{\pi_{kr}\phi(x_i;\mu_{kr},\Sigma)}{\sum_{\ell=1}^{R_k}\pi_{k\ell}\phi(x_i;\mu_{k\ell},\Sigma)}. \tag{12.60}$$

M-step: Compute the weighted MLEs for the parameters of each of the component Gaussians within each of the classes, using the weights from the E-step.

In the E-step, the algorithm apportions the unit weight of an observation in class k to the various subclasses assigned to that class. If it is close to the centroid of a particular subclass, and far from the others, it will receive a mass close to one for that subclass. On the other hand, observations halfway between two subclasses will get approximately equal weight for both.

In the M-step, an observation in class k is used R_k times, to estimate the parameters in each of the R_k component densities, with a different weight for each.

The EM algorithm is studied in detail in Chapter 8. The algorithm requires initialization, which can have an impact, since mixture likelihoods are generally multimodal. Our software (referenced in the bibliographic notes) allows several strategies; here we describe the default. The user supplies the number R_k of subclasses per class. Within class k, a k-means clustering model, with multiple random starts, is fitted to the data. This partitions the observations into R_k disjoint groups, from which an initial weight matrix, consisting of zeros and ones, is created.

Our assumption of an equal component covariance matrix Σ throughout buys an additional simplicity; we can incorporate rank restrictions in the mixture formulation just like in LDA. To understand this, we review a little-known fact about LDA. The rank-L LDA fit (Section 4.3.3) is equivalent to the maximum-likelihood fit of a Gaussian model,where the different mean vectors in each class are confined to a rank-L subspace of $\mathbb{R}^p$ (Exercise 4.8). We can inherit this property for the mixture model, and maximize the log-likelihood (12.59) subject to rank constraints on *all* the $\sum_k R_k$ centroids: $\text{rank}\{\mu_{k\ell}\} = L$.

Again the EM algorithm is available, and the M-step turns out to be a weighted version of LDA, with $R = \sum_{k=1}^{K} R_k$ "classes." Furthermore, we can use optimal scoring as before to solve the weighted LDA problem, which allows us to use a weighted version of FDA or PDA at this stage. One would expect, in addition to an increase in the number of "classes," a similar increase in the number of "observations" in the kth class by a factor of R_k. It turns out that this is not the case if linear operators are used for the optimal scoring regression. The enlarged indicator $\mathbf{Y}$ matrix collapses in this case to a *blurred* response matrix $\mathbf{Z}$, which is intuitively pleasing. For example, suppose there are $K = 3$ classes, and $R_k = 3$ subclasses per class. Then $\mathbf{Z}$ might be

$$\begin{array}{c} \\ g_1 = 2 \\ g_2 = 1 \\ g_3 = 1 \\ g_4 = 3 \\ g_5 = 2 \\ \vdots \\ g_n = 3 \end{array} \begin{array}{c} \begin{array}{ccccccccc} c_{11} & c_{12} & c_{13} & c_{21} & c_{22} & c_{23} & c_{31} & c_{32} & c_{33} \end{array} \\ \begin{pmatrix} 0 & 0 & 0 & 0.3 & 0.5 & 0.2 & 0 & 0 & 0 \\ 0.9 & 0.1 & 0.0 & 0 & 0 & 0 & 0 & 0 & 0 \\ 0.1 & 0.8 & 0.1 & 0 & 0 & 0 & 0 & 0 & 0 \\ 0 & 0 & 0 & 0 & 0 & 0 & 0.5 & 0.4 & 0.1 \\ 0 & 0 & 0 & 0.7 & 0.1 & 0.2 & 0 & 0 & 0 \\ & & & \vdots & & & & & \\ 0 & 0 & 0 & 0 & 0 & 0 & 0.1 & 0.1 & 0.8 \end{pmatrix} \end{array}, \quad (12.61)$$

where the entries in a class-k row correspond to $W(c_{kr}|x, g_i)$.

The remaining steps are the same:

$$\left.\begin{array}{l}\hat{\mathbf{Z}} = \mathbf{S}\mathbf{Z}\\ \mathbf{Z}^T\hat{\mathbf{Z}} = \Theta\mathbf{D}\Theta^T\\ \text{Update } \pi\text{s and } \Pi\text{s}\end{array}\right\} \text{M-step of MDA.}$$

These simple modifications add considerable flexibility to the mixture model:

- The dimension reduction step in LDA, FDA or PDA is limited by the number of classes; in particular, for $K = 2$ classes no reduction is possible. MDA substitutes subclasses for classes, and then allows us to look at low-dimensional views of the subspace spanned by these subclass centroids. This subspace will often be an important one for discrimination.

- By using FDA or PDA in the M-step, we can adapt even more to particular situations. For example, we can fit MDA models to digitized analog signals and images, with smoothness constraints built in.

Figure 12.11 compares FDA and MDA on the mixture example.

12.7.1 Example: Waveform Data

We now illustrate some of these ideas on a popular simulated example, taken from Breiman et al. (1984, pp. 49–55), and used in Hastie and Tibshirani (1996b) and elsewhere. It is a three-class problem with 21 variables, and is considered to be a difficult pattern recognition problem. The predictors are defined by

$$\begin{array}{rcll} X_j &=& Uh_1(j) + (1-U)h_2(j) + \epsilon_j & \text{Class 1,}\\ X_j &=& Uh_1(j) + (1-U)h_3(j) + \epsilon_j & \text{Class 2,}\\ X_j &=& Uh_2(j) + (1-U)h_3(j) + \epsilon_j & \text{Class 3,}\end{array} \tag{12.62}$$

where $j = 1, 2, \ldots, 21$, U is uniform on $(0, 1)$, ϵ_j are standard normal variates, and the h_ℓ are the shifted triangular waveforms: $h_1(j) = \max(6 - |j - 11|, 0)$, $h_2(j) = h_1(j - 4)$ and $h_3(j) = h_1(j + 4)$. Figure 12.12 shows some example waveforms from each class.

Table 12.4 shows the results of MDA applied to the waveform data, as well as several other methods from this and other chapters. Each training sample has 300 observations, and equal priors were used, so there are roughly 100 observations in each class. We used test samples of size 500. The two MDA models are described in the caption.

Figure 12.13 shows the leading canonical variates for the penalized MDA model, evaluated at the test data. As we might have guessed, the classes appear to lie on the edges of a triangle. This is because the $h_j(i)$ are represented by three points in 21-space, thereby forming vertices of a triangle,

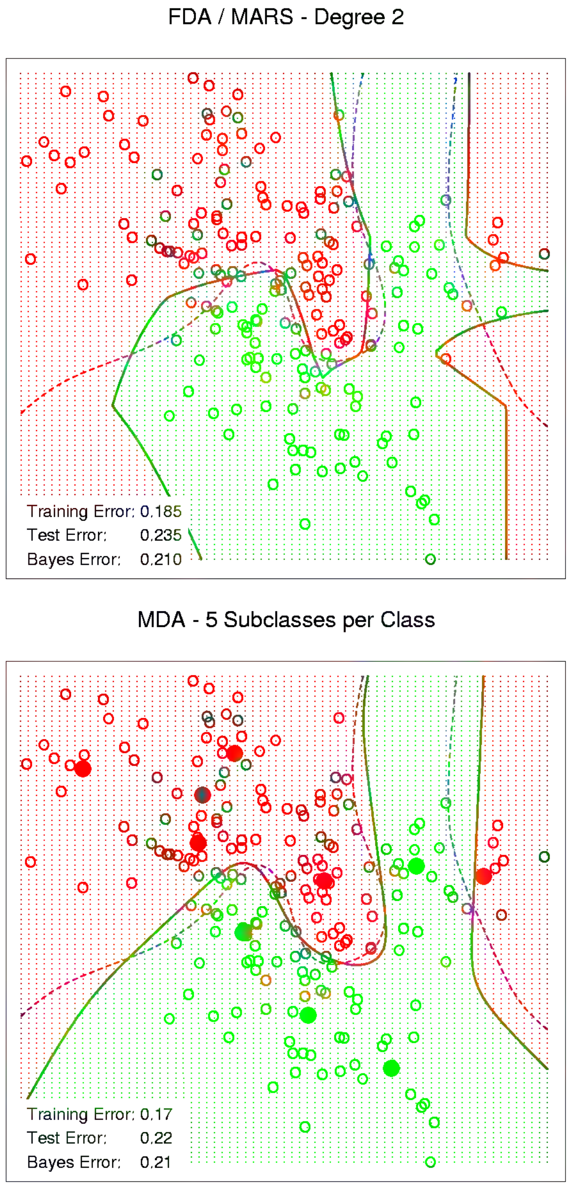

FIGURE 12.11. *FDA and MDA on the mixture data. The upper plot uses FDA with MARS as the regression procedure. The lower plot uses MDA with five mixture centers per class (indicated). The MDA solution is close to Bayes optimal, as might be expected given the data arise from mixtures of Gaussians. The broken purple curve in the background is the Bayes decision boundary.*

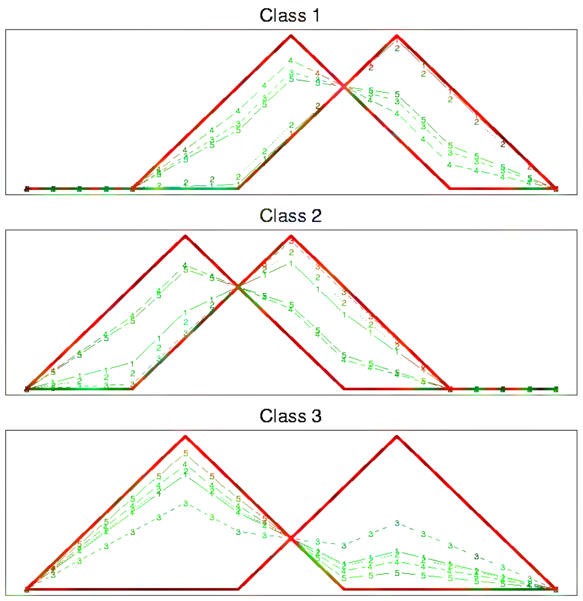

FIGURE 12.12. *Some examples of the waveforms generated from model (12.62) before the Gaussian noise is added.*

TABLE 12.4. *Results for waveform data. The values are averages over ten simulations, with the standard error of the average in parentheses. The five entries above the line are taken from Hastie et al. (1994). The first model below the line is MDA with three subclasses per class. The next line is the same, except that the discriminant coefficients are penalized via a roughness penalty to effectively* 4df. *The third is the corresponding penalized LDA or PDA model.*

Technique	Error Rates	
	Training	Test
LDA	0.121(0.006)	0.191(0.006)
QDA	0.039(0.004)	0.205(0.006)
CART	0.072(0.003)	0.289(0.004)
FDA/MARS (degree = 1)	0.100(0.006)	0.191(0.006)
FDA/MARS (degree = 2)	0.068(0.004)	0.215(0.002)
MDA (3 subclasses)	0.087(0.005)	0.169(0.006)
MDA (3 subclasses, penalized 4 df)	0.137(0.006)	0.157(0.005)
PDA (penalized 4 df)	0.150(0.005)	0.171(0.005)
Bayes		0.140

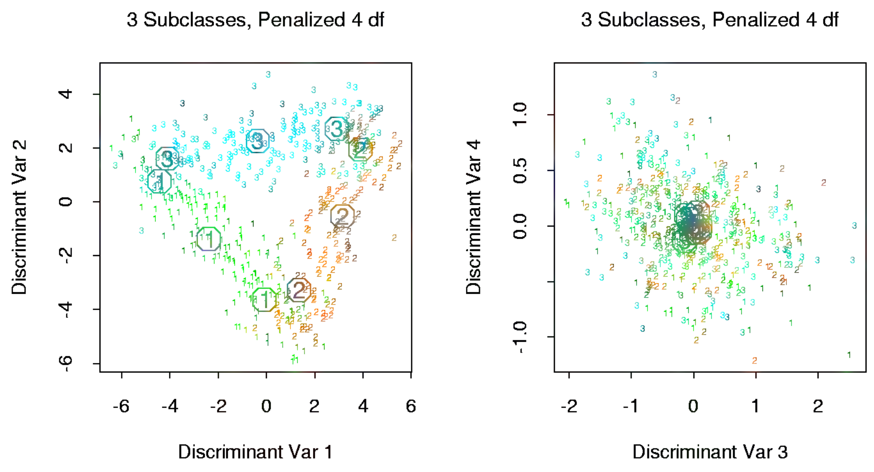

FIGURE 12.13. *Some two-dimensional views of the MDA model fitted to a sample of the waveform model. The points are independent test data, projected on to the leading two canonical coordinates (left panel), and the third and fourth (right panel). The subclass centers are indicated.*

and each class is represented as a convex combination of a pair of vertices, and hence lie on an edge. Also it is clear visually that all the information lies in the first two dimensions; the percentage of variance explained by the first two coordinates is 99.8%, and we would lose nothing by truncating the solution there. The Bayes risk for this problem has been estimated to be about 0.14 (Breiman et al., 1984). MDA comes close to the optimal rate, which is not surprising since the structure of the MDA model is similar to the generating model.

Computational Considerations

With N training cases, p predictors, and m support vectors, the support vector machine requires $m^3 + mN + mpN$ operations, assuming $m \approx N$. They do not scale well with N, although computational shortcuts are available (Platt, 1999). Since these are evolving rapidly, the reader is urged to search the web for the latest technology.

LDA requires $Np^2 + p^3$ operations, as does PDA. The complexity of FDA depends on the regression method used. Many techniques are linear in N, such as additive models and MARS. General splines and kernel-based regression methods will typically require N^3 operations.

Software in S-PLUS for fitting FDA, PDA and MDA models is available in the public archive at `http://lib/stat.cmu/edu/S/mda`.

Bibliographic Notes

The theory behind support vector machines is due to Vapnik and is described in Vapnik (1996). There is a burgeoning literature on SVMs; an online bibliography, created and maintained by Alex Smola and Bernhard Schölkopf, can be found at:

`http://www.kernel-machines.org/publications.html.`

Our treatment is based on Wahba et al. (2000) and Evgeniou et al. (2001), and the tutorial by Burges (Burges, 1998).

Linear discriminant analysis is due to Fisher (1936) and Rao (1973). The connection with optimal scoring dates back at least to Breiman and Ihaka (1984), and in a simple form to Fisher (1936). There are strong connections with correspondence analysis (Greenacre, 1984). The description of flexible, penalized and mixture discriminant analysis is taken from Hastie et al. (1994), Hastie et al. (1995) and Hastie and Tibshirani (1996b), and all three are summarized in Hastie et al. (1998); see also Ripley (1996).

Exercises

Ex. 12.1 Show that the criteria (12.25) and (12.8) are equivalent.

Ex. 12.2 Show that the the solution to (12.29) is the same as the solution to (12.25) or (12.25).

Ex. 12.3 Consider a modification to (12.41) where you do not penalize the constant. Formulate the problem, and characterize its solution.

Ex. 12.4 Suppose you perform a reduced-subspace linear discriminant analysis for a K-group problem. You compute the canonical variables of dimension $L \leq K-1$ given by $z = \mathbf{U}^T x$, where U is the $p \times L$ matrix of discriminant coefficients, and $p > K$ is the dimension of x.

(a) If $L = K - 1$ show that

$$\|z - \bar{z}_k\|^2 - \|z - \bar{z}_{k'}\|^2 = \|x - \bar{x}_k\|_W^2 - \|x - \bar{x}_{k'}\|_W^2 ,$$

where $\|\cdot\|_W$ denotes *Mahalanobis* distance with respect to the covariance $\mathbf{W}$.

(b) If $L < K - 1$, show that the same expression on the left measures the difference in Mahalanobis squared distances for the distributions projected onto the subspace spanned by $\mathbf{U}$.

Ex. 12.5 The data in `phoneme.subset`, available from this book's website

`http://www-stat.stanford.edu/ElemStatLearn` consists of digitized log-periodograms for phonemes uttered by 60 speakers, each speaker having produced phonemes from each of five classes. It is appropriate to plot each vector of 256 "features" against the frequencies 0–255.

(a) Produce a separate plot of all the phoneme curves against frequency for each class.

(b) You plan to use a nearest prototype classification scheme to classify the curves into phoneme classes. In particular, you will use a K-means clustering algorithm in each class (`kmeans()` in S-PLUS), and then classify observations to the class of the closest cluster center. The curves are high-dimensional and you have a rather small sample-size-to-variables ratio. You decide to restrict all the prototypes to be smooth functions of frequency. In particular, you decide to represent each prototype m as $m = B\theta$ where B is a $256 \times J$ matrix of natural spline basis functions with J knots uniformly chosen in $(0, 255)$ and boundary knots at 0 and 255. Describe how to proceed analytically, and in particular, how to avoid costly high-dimensional fitting procedures. (*Hint:* It may help to restrict B to be orthogonal.)

(c) Implement your procedure on the phoneme data, and try it out. Divide the data into a training set and a test set (50-50), making sure that speakers are not split across sets (why?). Use $K = 1, 3, 5, 7$ centers per class, and for each use $J = 5, 10, 15$ knots (taking care to start the K-means procedure at the same starting values for each value of J), and compare the results.

Ex. 12.6 Suppose that the regression procedure used in FDA (Section 12.5.1) is a linear expansion of basis functions $h_m(x)$, $m = 1, \dots, M$. Let $\mathbf{D}_\pi = \mathbf{Y}^T\mathbf{Y}/N$ be the diagonal matrix of class proportions.

(a) Show that the optimal scoring problem (12.50) can be written in vector notation as

$$\min_{\theta,\beta} \|\mathbf{Y}\theta - \mathbf{H}\beta\|^2, \tag{12.63}$$

where θ is a vector of K real numbers, and $\mathbf{H}$ is the $N \times M$ matrix of evaluations $h_j(x_i)$.

(b) Suppose that the normalization on θ is $\theta^T\mathbf{D}_\pi 1 = 0$ and $\theta^T\mathbf{D}_\pi\theta = 1$. Interpret these normalizations in terms of the original scored $\theta(g_i)$.

(c) Show that, with this normalization, (12.63) can be partially optimized w.r.t. β, and leads to

$$\max_{\theta} \theta^T\mathbf{S}\theta, \tag{12.64}$$

subject to the normalization constraints, where $\mathbf{S}$ is the projection operator corresponding to the basis matrix H.

(d) Suppose that the h_j include the constant function. Show that the largest eigenvalue of $\mathbf{S}$ is 1.

(e) Let Θ be a $K \times K$ matrix of scores (in columns), and suppose the normalization is $\Theta^T \mathbf{D}_\pi \Theta = \mathbf{I}$. Show that the solution to (12.51) is given by the complete set of eigenvectors of $\mathbf{S}$; the first eigenvector is trivial, and takes care of the centering of the scores. The remainder characterize the optimal scoring solution.

Ex. 12.7 Derive the solution to the penalized optimal scoring problem (12.55).

Ex. 12.8 Show that coefficients β_ℓ found by optimal scoring are proportional to the discriminant directions ν_ℓ found by linear discriminant analysis.

Ex. 12.9 Let $\hat{\mathbf{Y}} = \mathbf{X}\hat{\mathbf{B}}$ be the fitted $N \times K$ indicator response matrix after linear regression on the $N \times p$ matrix $\mathbf{X}$, where $p > K$. Consider the reduced features $x_i^* = \hat{\mathbf{B}}^T x_i$. Show that LDA using x_i^* is equivalent to LDA in the original space.

Ex. 12.10 *Kernels and linear discriminant analysis.* Suppose you wish to carry out a linear discriminant analysis (two classes) using a vector of transformations of the input variables $h(x)$. Since $h(x)$ is high-dimensional, you will use a regularized within-class covariance matrix $\mathbf{W}_h + \gamma\mathbf{I}$. Show that the model can be estimated using only the inner products $K(x_i, x_{i'}) = \langle h(x_i), h(x_{i'})\rangle$. Hence the kernel property of support vector machines is also shared by regularized linear discriminant analysis.

Ex. 12.11 The MDA procedure models each class as a mixture of Gaussians. Hence each mixture center belongs to one and only one class. A more general model allows each mixture center to be shared by all classes. We take the joint density of labels and features to be

$$P(G, X) = \sum_{r=1}^{R} \pi_r P_r(G, X), \qquad (12.65)$$

a mixture of joint densities. Furthermore we assume

$$P_r(G, X) = P_r(G)\phi(X; \mu_r, \Sigma). \qquad (12.66)$$

This model consists of regions centered at μ_r, and for each there is a class profile $P_r(G)$. The posterior class distribution is given by

$$P(G = k|X = x) = \frac{\sum_{r=1}^{R} \pi_r P_r(G = k)\phi(x; \mu_r, \Sigma)}{\sum_{r=1}^{R} \pi_r \phi(x; \mu_r, \Sigma)}, \qquad (12.67)$$

where the denominator is the marginal distribution $P(X)$.

(a) Show that this model (called MDA2) can be viewed as a generalization of MDA since

$$P(X|G=k) = \frac{\sum_{r=1}^{R} \pi_r P_r(G=k)\phi(x;\mu_r,\Sigma)}{\sum_{r=1}^{R} \pi_r P_r(G=k)}, \tag{12.68}$$

where $\pi_{rk} = \pi_r P_r(G = k)/\sum_{r=1}^{R} \pi_r P_r(G = k)$ corresponds to the mixing proportions for the kth class.

(b) Derive the EM algorithm for MDA2.

(c) Show that if the initial weight matrix is constructed as in MDA, involving separate k-means clustering in each class, then the algorithm for MDA2 is identical to the original MDA procedure.

13
Prototype Methods and Nearest-Neighbors

13.1 Introduction

In this chapter we discuss some simple and essentially model-free methods for classification and pattern recognition. Because they are highly unstructured, they typically aren't useful for understanding the nature of the relationship between the features and class outcome. However, as *black box* prediction engines, they can be very effective, and are often among the best performers in real data problems. The nearest-neighbor technique can also be used in regression; this was touched on in Chapter 2 and works reasonably well for low-dimensional problems. However, with high-dimensional features, the bias–variance tradeoff does not work as favorably for nearest-neighbor regression as it does for classification.

13.2 Prototype Methods

Throughout this chapter, our training data consists of the N pairs (x_1, g_1), $\dots$, (x_n, g_N) where g_i is a class label taking values in $\{1, 2, \dots , K\}$. Prototype methods represent the training data by a set of points in feature space. These prototypes are typically not examples from the training sample, except in the case of 1-nearest-neighbor classification discussed later.

Each prototype has an associated class label, and classification of a query point x is made to the class of the closest prototype. "Closest" is usually defined by Euclidean distance in the feature space, after each feature has been standardized to have overall mean 0 and variance 1 in the training sample. Euclidean distance is appropriate for quantitative features. We discuss distance measures between qualitative and other kinds of feature values in Chapter 14.

These methods can be very effective if the prototypes are well positioned to capture the distribution of each class. Irregular class boundaries can be represented, with enough prototypes in the right places in feature space. The main challenge is to figure out how many prototypes to use and where to put them. Methods differ according to the number and way in which prototypes are selected.

13.2.1 *K-means Clustering*

K-means clustering is a method for finding clusters and cluster centers in a set of unlabeled data. One chooses the desired number of cluster centers, say R, and the K-means procedure iteratively moves the centers to minimize the total within cluster variance.* Given an initial set of centers, the K-means algorithm alternates the two steps:

- for each center we identify the subset of training points (its cluster) that is closer to it than any other center;
- the means of each feature for the data points in each cluster are computed, and this mean vector becomes the new center for that cluster.

These two steps are iterated until convergence. Typically the initial centers are R randomly chosen observations from the training data. Details of the K-means procedure, as well as generalizations allowing for different variable types and more general distance measures, are given in Chapter 14.

To use K-means clustering for classification of labeled data, the steps are:

- apply K-means clustering to the training data in each class separately, using R prototypes per class;
- assign a class label to each of the $K \times R$ prototypes;
- classify a new feature x to the class of the closest prototype.

Figure 13.1 (upper panel) shows a simulated example with three classes and two features. We used $R = 5$ prototypes per class, and show the classification regions and the decision boundary. Notice that a number of the

*The "K" in K-means refers to the number of cluster centers. Since we have already reserved K to denote the number of classes, we denote the number of clusters by R.

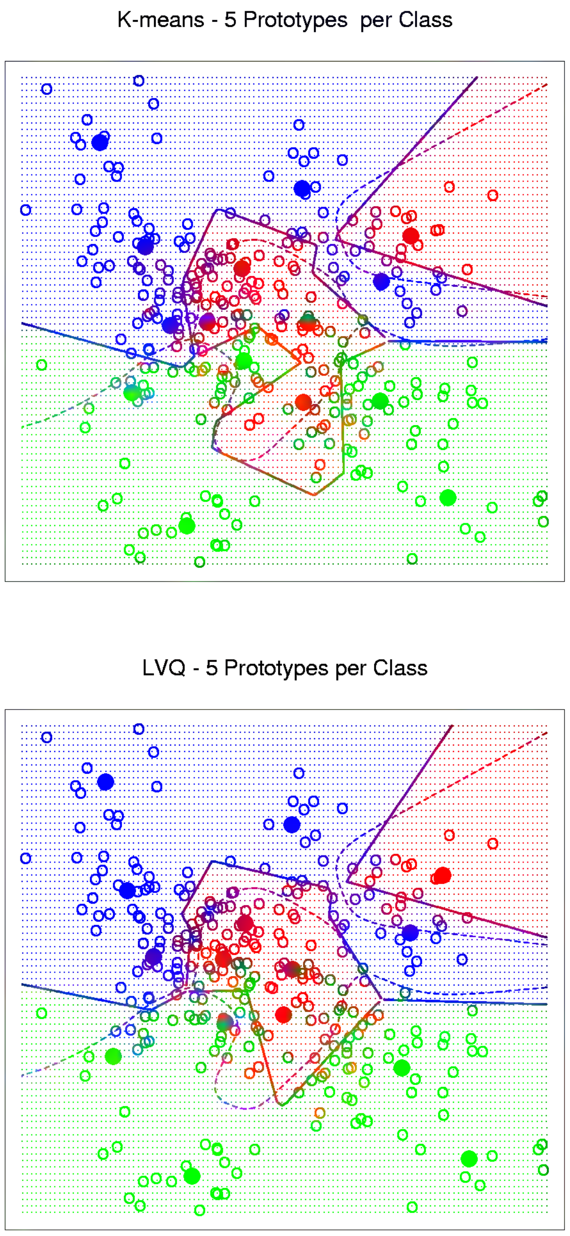

FIGURE 13.1. *Simulated example with three classes and five prototypes per class. The data in each class are generated from a mixture of Gaussians. In the upper panel, the prototypes were found by applying the K-means clustering algorithm separately in each class. In the lower panel, the LVQ algorithm (starting from the K-means solution) moves the prototypes away from the decision boundary. The broken purple curve in the background is the Bayes decision boundary.*

Algorithm 13.1 Learning Vector Quantization—LVQ.

1. Choose R initial prototypes for each class: $m_1(k), m_2(k), \ldots, m_R(k)$, $k = 1, 2, \ldots, K$, for example by sampling R training points at random from each class.

2. Sample a training point x_i randomly (with replacement), and let (j, k) index the closest prototype $m_j(k)$ to x_i.

   (a) If $g_i = k$ (i.e., they are in the same class), move the prototype towards the training point:

   $$m_j(k) \leftarrow m_j(k) + \epsilon(x_i - m_j(k)),$$

   where ϵ is the *learning rate*.

   (b) If $g_i \neq m_j(k)$ (i.e., they are in different classes), move the prototype away from the training point:

   $$m_j(k) \leftarrow m_j(k) - \epsilon(x_i - m_j(k)).$$

3. Repeat step 2, decreasing the learning rate ϵ with each iteration to zero.

---

prototypes are near the class boundaries, leading to potential misclassification errors for points near these boundaries. This results from an obvious shortcoming with this method: for each class, the other classes do not have a say in the positioning of the prototypes for that class. A better approach, discussed next, uses all of the data to position all prototypes.

13.2.2 Learning Vector Quantization

In this technique due to Kohonen (1989), prototypes are placed strategically with respect to the decision boundaries in an ad-hoc way. LVQ is an *online* algorithm—observations are processed one at a time.

The idea is that the training points attract prototypes of the correct class, and repel other prototypes. When the iterations settle down, prototypes should be close to the training points in their class. The learning rate ϵ is decreased to zero with each iteration, following the guidelines for stochastic approximation learning rates (Section 11.4.)

Figure 13.1 (lower panel) shows the result of LVQ, using the K-means solution as starting values. The prototypes have tended to move away from the decision boundaries, and away from prototypes of competing classes.

The procedure just described is actually called LVQ1. Modifications (LVQ2, LVQ3, etc.) have been proposed, that can sometimes improve performance. A drawback of learning vector quantization methods is the fact that they are defined by algorithms, rather than optimization of some fixed criteria; this makes it difficult to understand their properties.

13.2.3 Gaussian Mixtures

The Gaussian mixture model can also be thought of as a prototype method, similar in spirit to K-means and LVQ. We discuss Gaussian mixtures in some detail in Sections 6.8, 8.5 and 12.7. Each cluster is described in terms of a Gaussian density, which has a centroid (as in K-means), and a covariance matrix. The comparison becomes crisper if we restrict the component Gaussians to have a scalar covariance matrix (Exercise 13.1). The two steps of the alternating EM algorithm are very similar to the two steps in K-means:

- In the E-step, each observation is assigned a *responsibility* or weight for each cluster, based on the likelihood of each of the corresponding Gaussians. Observations close to the center of a cluster will most likely get weight 1 for that cluster, and weight 0 for every other cluster. Observations half-way between two clusters divide their weight accordingly.

- In the M-step, each observation contributes to the weighted means (and covariances) for *every* cluster.

As a consequence, the Gaussian mixture model is often referred to as a *soft* clustering method, while K-means is *hard*.

Similarly, when Gaussian mixture models are used to represent the feature density in each class, it produces smooth posterior probabilities $\hat{p}(x) = \{\hat{p}_1(x), \dots, \hat{p}_K(x)\}$ for classifying x (see (12.58) on page 400.) Often this is interpreted as a soft classification, while in fact the classification rule is $\hat{G}(x) = \arg\max_k \hat{p}_k(x)$. Figure 13.2 compares the results of K-means and Gaussian mixtures on the simulated mixture problem of Chapter 2. We see that although the decision boundaries are roughly similar, those for the mixture model are smoother (although the prototypes are in approximately the same positions.) We also see that while both procedures devote a green prototype (incorrectly) to a region in the northwest, the Gaussian mixture classifier can ultimately ignore this region, while K-means cannot. LVQ gave very similar results to K-means on this example, and is not shown.

13.3 k-Nearest-Neighbor Classifiers

These classifiers are *memory-based*, and require no model to be fit. Given a query point x_0, we find the k training points $x_{(r)}, r = 1, \dots, k$ closest in distance to x_0, and then classify using majority vote among the k neighbors.

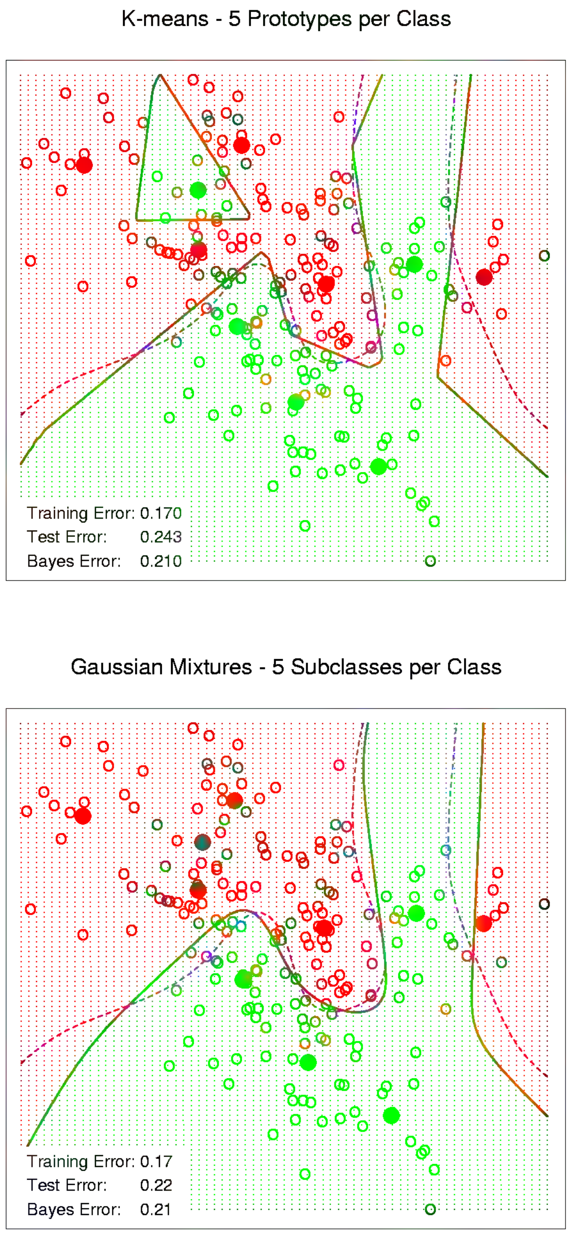

FIGURE 13.2. *The upper panel shows the K-means classifier applied to the mixture data example. The decision boundary is piecewise linear. The lower panel shows a Gaussian mixture model with a common covariance for all component Gaussians. The EM algorithm for the mixture model was started at the K-means solution. The broken purple curve in the background is the Bayes decision boundary.*

Ties are broken at random. For simplicity we will assume that the features are real-valued, and we use Euclidean distance in feature space:

$$d_{(i)} = ||x_{(i)} - x_0||. \tag{13.1}$$

Typically we first standardize each of the features to have mean zero and variance 1, since it is possible that they are measured in different units. In Chapter 14 we discuss distance measures appropriate for qualitative and ordinal features, and how to combine them for mixed data. Adaptively chosen distance metrics are discussed later in this chapter.

Despite its simplicity, k-nearest-neighbors has been successful in a large number of classification problems, including handwritten digits, satellite image scenes and EKG patterns. It is often successful where each class has many possible prototypes, and the decision boundary is very irregular. Figure 13.3 (upper panel) shows the decision boundary of a 15-nearest-neighbor classifier applied to the three-class simulated data. The decision boundary is fairly smooth compared to the lower panel, where a 1-nearest-neighbor classifier was used. There is a close relationship between nearest-neighbor and prototype methods: in 1-nearest-neighbor classification, each training point is a prototype.

Figure 13.4 shows the training, test and tenfold cross-validation errors as a function of the neighborhood size, for the two-class mixture problem. Since the tenfold CV errors are averages of ten numbers, we can estimate a standard error.

Because it uses only the training point closest to the query point, the bias of the 1-nearest-neighbor estimate is often low, but the variance is high. A famous result of Cover and Hart (1967) shows that asymptotically the error rate of the 1-nearest-neighbor classifier is never more than twice the Bayes rate. The rough idea of the proof is as follows (using squared-error loss). We assume that the query point coincides with one of the training points, so that the bias is zero. This is true asymptotically if the dimension of the feature space is fixed and the training data fills up the space in a dense fashion. Then the error of the Bayes rule is just the variance of a Bernoulli random variate (the target at the query point), while the error of 1-nearest-neighbor rule is *twice* the variance of a Bernoulli random variate, one contribution each for the training and query targets.

We now give more detail for misclassification loss. At x let k^* be the dominant class, and $p_k(x)$ the true conditional probability for class k. Then

$$\begin{aligned}\text{Bayes error} &= 1 - p_{k^*}(x), & (13.2)\\ \text{1-Nearest-Neighbor error} &= \sum_{k=1}^{K} p_k(x)(1 - p_k(x)), & (13.3)\\ &\geq 1 - p_{k^*}(x). & (13.4)\end{aligned}$$

The asymptotic 1-nearest-neighbor error rate is that of a random rule; we pick both the classification and the test point at random with probabil-

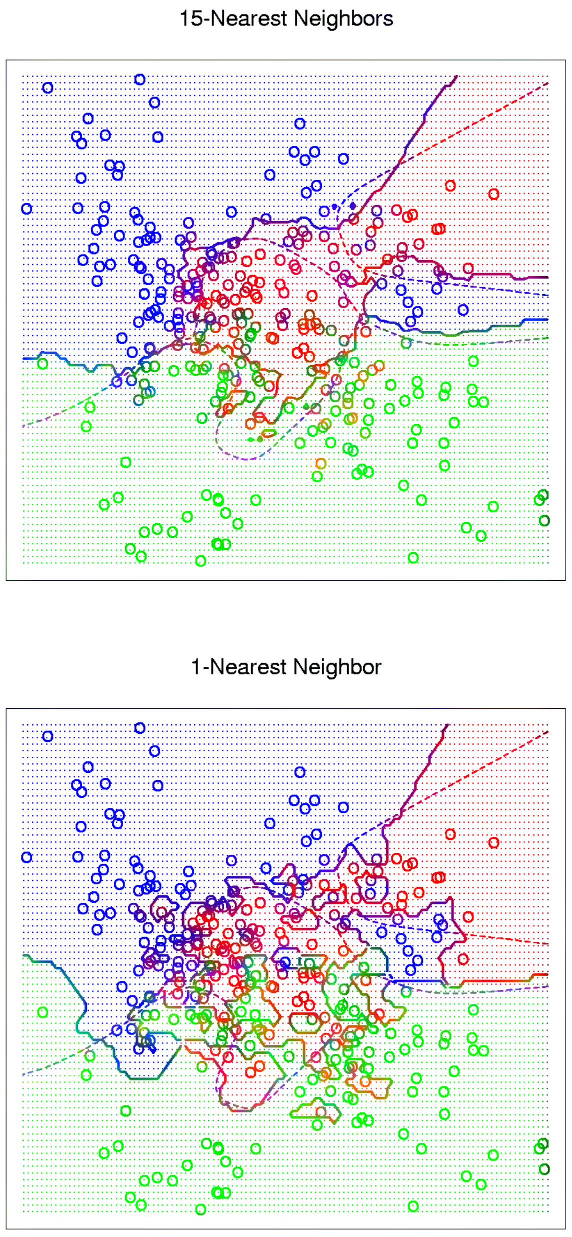

FIGURE 13.3. *k-nearest-neighbor classifiers applied to the simulation data of Figure 13.1. The broken purple curve in the background is the Bayes decision boundary.*

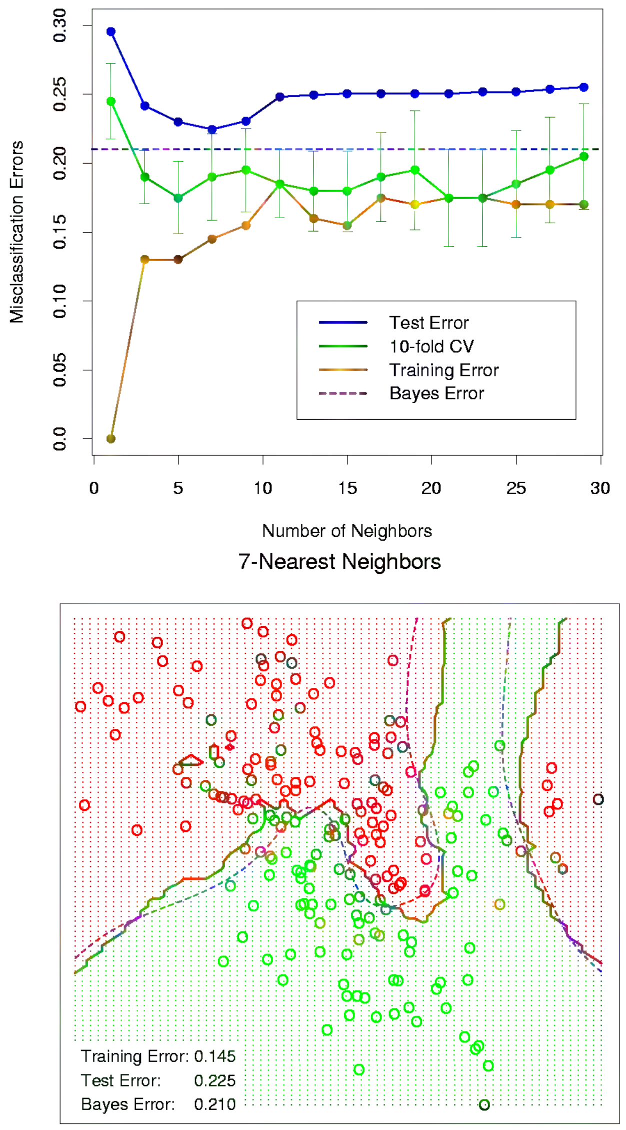

FIGURE 13.4. *k-nearest-neighbors on the two-class mixture data. The upper panel shows the misclassification errors as a function of neighborhood size. Standard error bars are included for 10-fold cross validation. The lower panel shows the decision boundary for 7-nearest-neighbors, which appears to be optimal for minimizing test error. The broken purple curve in the background is the Bayes decision boundary.*

ities $p_k(x)$, $k = 1, \dots, K$. For $K = 2$ the 1-nearest-neighbor error rate is $2p_{k^*}(x)(1 - p_{k^*}(x)) \leq 2(1 - p_{k^*}(x))$ (twice the Bayes error rate). More generally, one can show (Exercise 13.3)

$$\sum_{k=1}^{K} p_k(x)(1 - p_k(x)) \leq 2(1 - p_{k^*}(x)) - \frac{K}{K-1}(1 - p_{k^*}(x))^2. \tag{13.5}$$

Many additional results of this kind have been derived; Ripley (1996) summarizes a number of them.

This result can provide a rough idea about the best performance that is possible in a given problem. For example, if the 1-nearest-neighbor rule has a 10% error rate, then asymptotically the Bayes error rate is at least 5%. The kicker here is the asymptotic part, which assumes the bias of the nearest-neighbor rule is zero. In real problems the bias can be substantial. The adaptive nearest-neighbor rules, described later in this chapter, are an attempt to alleviate this bias. For simple nearest-neighbors, the bias and variance characteristics can dictate the optimal number of near neighbors for a given problem. This is illustrated in the next example.

13.3.1 Example: A Comparative Study

We tested the nearest-neighbors, K-means and LVQ classifiers on two simulated problems. There are 10 independent features X_j, each uniformly distributed on $[0, 1]$. The two-class 0-1 target variable is defined as follows:

$$\begin{aligned} Y &= I\left(X_1 > \frac{1}{2}\right); \quad \text{problem 1: “easy”,} \\ Y &= I\left(\text{sign}\left\{\prod_{j=1}^{3}\left(X_j - \frac{1}{2}\right)\right\} > 0\right); \quad \text{problem 2: “difficult.”} \end{aligned} \tag{13.6}$$

Hence in the first problem the two classes are separated by the hyperplane $X_1 = 1/2$; in the second problem, the two classes form a checkerboard pattern in the hypercube defined by the first three features. The Bayes error rate is zero in both problems. There were 100 training and 1000 test observations.

Figure 13.5 shows the mean and standard error of the misclassification error for nearest-neighbors, K-means and LVQ over ten realizations, as the tuning parameters are varied. We see that K-means and LVQ give nearly identical results. For the best choices of their tuning parameters, K-means and LVQ outperform nearest-neighbors for the first problem, and they perform similarly for the second problem. Notice that the best value of each tuning parameter is clearly situation dependent. For example 25-nearest-neighbors outperforms 1-nearest-neighbor by a factor of 70% in the

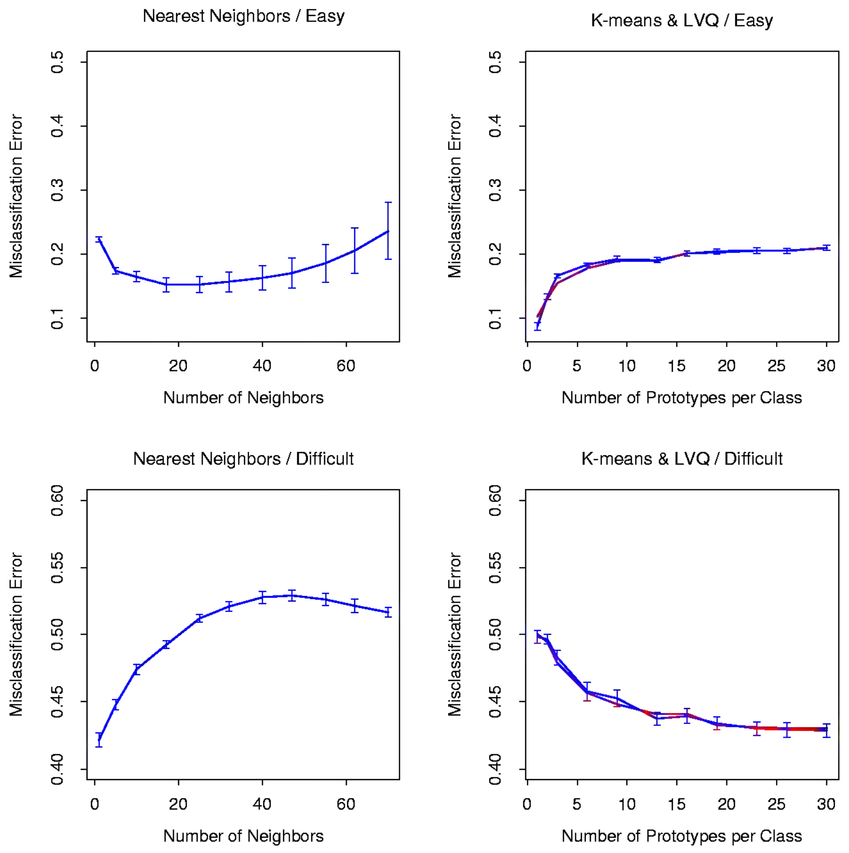

FIGURE 13.5. *Mean $\pm$ one standard error of misclassification error for nearest-neighbors, K-means (blue) and LVQ (red) over ten realizations for two simulated problems: "easy" and "difficult," described in the text.*

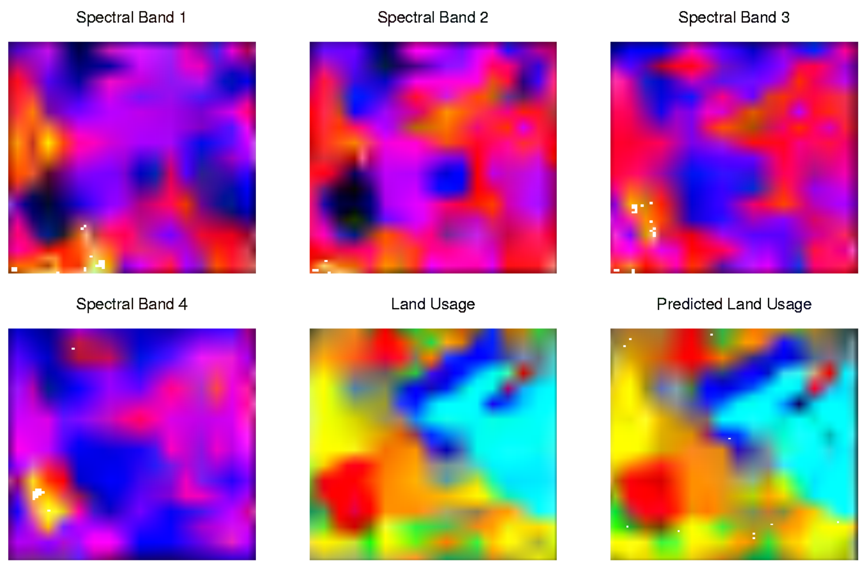

FIGURE 13.6. *The first four panels are LANDSAT images for an agricultural area in four spectral bands, depicted by heatmap shading. The remaining two panels give the actual land usage (color coded) and the predicted land usage using a five-nearest-neighbor rule described in the text.*

first problem, while 1-nearest-neighbor is best in the second problem by a factor of 18%. These results underline the importance of using an objective, data-based method like cross-validation to estimate the best value of a tuning parameter (see Figure 13.4 and Chapter 7).

13.3.2 Example: k-Nearest-Neighbors and Image Scene Classification

The STATLOG project (Michie et al., 1994) used part of a LANDSAT image as a benchmark for classification (82×100 pixels). Figure 13.6 shows four heat-map images, two in the visible spectrum and two in the infrared, for an area of agricultural land in Australia. Each pixel has a class label from the 7-element set $\mathcal{G} = \{$*red soil, cotton, vegetation stubble, mixture, gray soil, damp gray soil, very damp gray soil*$\}$, determined manually by research assistants surveying the area. The lower middle panel shows the actual land usage, shaded by different colors to indicate the classes. The objective is to classify the land usage at a pixel, based on the information in the four spectral bands.

Five-nearest-neighbors produced the predicted map shown in the bottom right panel, and was computed as follows. For each pixel we extracted an 8-neighbor feature map—the pixel itself and its eight immediate neighbors

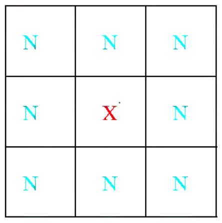

FIGURE 13.7. *A pixel and its eight-neighbor feature map.*

(see Figure 13.7). This is done separately in the four spectral bands, giving $(1+8)\times 4 = 36$ input features per pixel. Then five-nearest-neighbors classification was carried out in this 36-dimensional feature space. The resulting test error rate was about 9.5% (see Figure 13.8). Of all the methods used in the STATLOG project, including LVQ, CART, neural networks, linear discriminant analysis and many others, k-nearest-neighbors performed best on this task. Hence it is likely that the decision boundaries in $\mathbb{R}^{36}$ are quite irregular.

13.3.3 Invariant Metrics and Tangent Distance

In some problems, the training features are invariant under certain natural transformations. The nearest-neighbor classifier can exploit such invariances by incorporating them into the metric used to measure the distances between objects. Here we give an example where this idea was used with great success, and the resulting classifier outperformed all others at the time of its development (Simard et al., 1993).

The problem is handwritten digit recognition, as discussed is Chapter 1 and Section 11.7. The inputs are grayscale images with $16 \times 16 = 256$ pixels; some examples are shown in Figure 13.9. At the top of Figure 13.10, a "3" is shown, in its actual orientation (middle) and rotated 7.5° and 15° in either direction. Such rotations can often occur in real handwriting, and it is obvious to our eye that this "3" is still a "3" after small rotations. Hence we want our nearest-neighbor classifier to consider these two "3"s to be close together (similar). However the 256 grayscale pixel values for a rotated "3" will look quite different from those in the original image, and hence the two objects can be far apart in Euclidean distance in $\mathbb{R}^{256}$.

We wish to remove the effect of rotation in measuring distances between two digits of the same class. Consider the set of pixel values consisting of the original "3" and its rotated versions. This is a one-dimensional curve in $\mathbb{R}^{256}$, depicted by the green curve passing through the "3" in Figure 13.10. Figure 13.11 shows a stylized version of $\mathbb{R}^{256}$, with two images indicated by x_i and $x_{i'}$. These might be two different "3"s, for example. Through each image we have drawn the curve of rotated versions of that image,

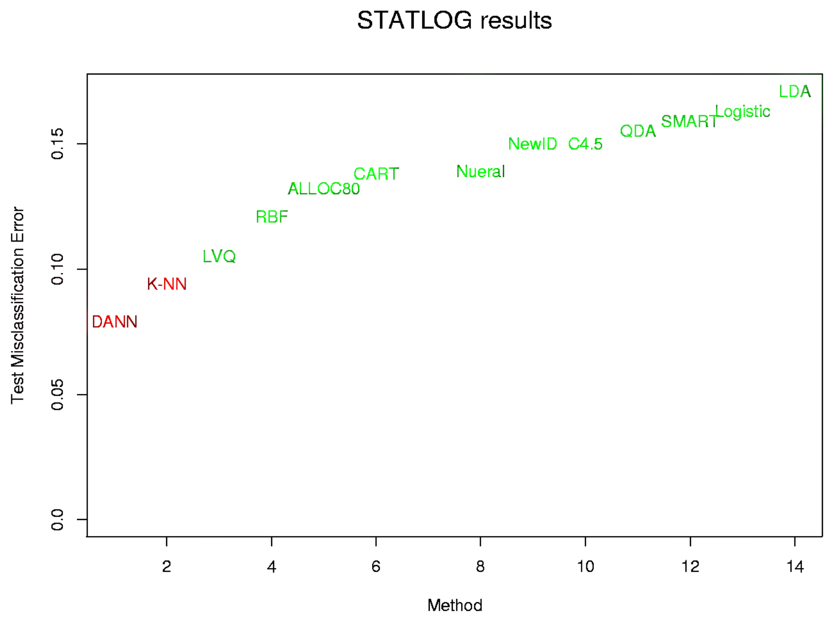

FIGURE 13.8. *Test-error performance for a number of classifiers, as reported by the STATLOG project. The entry DANN is a variant of k-nearest neighbors, using an adaptive metric (Section 13.4.2).*

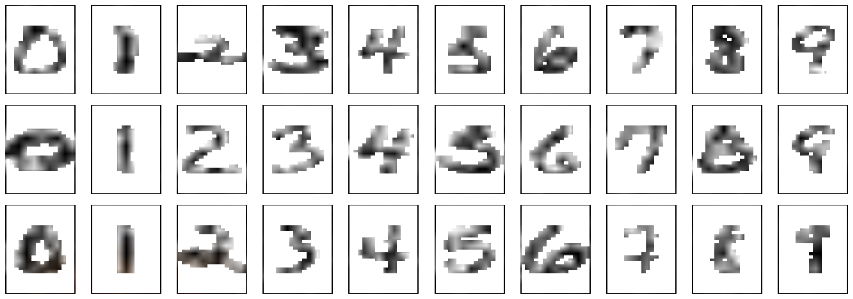

FIGURE 13.9. *Examples of grayscale images of handwritten digits.*

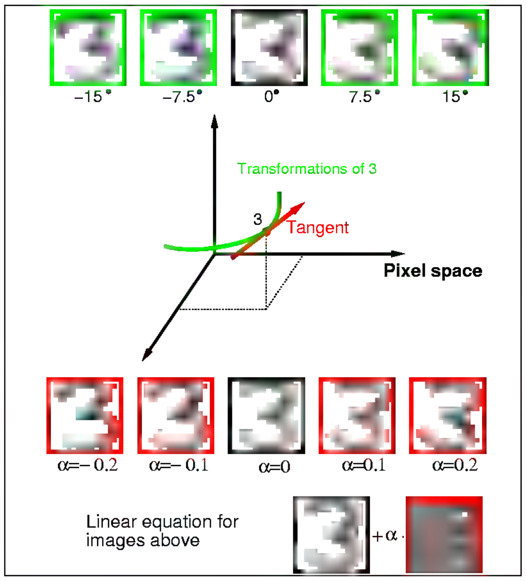

FIGURE 13.10. *The top row shows a "3" in its original orientation (middle) and rotated versions of it. The green curve in the middle of the figure depicts this set of rotated "3" in 256-dimensional space. The red line is the tangent line to the curve at the original image, with some "3"s on this tangent line, and its equation shown at the bottom of the figure.*

called *invariance manifolds* in this context. Now rather than using the usual Euclidean distance between the two images, we use the shortest distance between the two curves. In other words, the distance between the two images is taken to be the shortest Euclidean distance between any rotated version of first image, and any rotated version of the second image. This distance is called an *invariant metric.*

In principle one could carry out 1-nearest-neighbor classification using this invariant metric. However there are two problems with it. First, it is very difficult to calculate for real images. Second, it allows large transformations that can lead to poor performance. For example a "6" would be considered close to a "9" after a rotation of 180^o. We need to restrict attention to small rotations.

The use of *tangent distance* solves both of these problems. As shown in Figure 13.10, we can approximate the invariance manifold of the image "3" by its tangent at the original image. This tangent can be computed by estimating the direction vector from small rotations of the image, or by more sophisticated spatial smoothing methods (Exercise 13.4.) For large rotations, the tangent image no longer looks like a "3", so the problem with large transformations is alleviated.

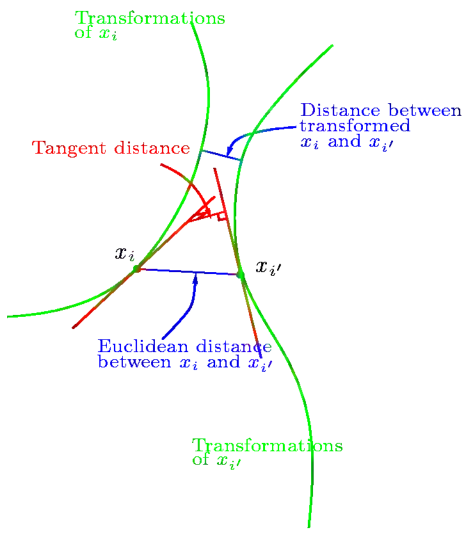
Transformations of x_i
Distance between transformed x_i and $x_{i'}$
Tangent distance
x_i
$x_{i'}$
Euclidean distance between x_i and $x_{i'}$
Transformations of $x_{i'}$

FIGURE 13.11. *Tangent distance computation for two images x_i and $x_{i'}$. Rather than using the Euclidean distance between x_i and $x_{i'}$, or the shortest distance between the two curves, we use the shortest distance between the two tangent lines.*

The idea then is to compute the invariant tangent line for each training image. For a query image to be classified, we compute its invariant tangent line, and find the closest line to it among the lines in the training set. The class (digit) corresponding to this closest line is our predicted class for the query image. In Figure 13.11 the two tangent lines intersect, but this is only because we have been forced to draw a two-dimensional representation of the actual 256-dimensional situation. In $\mathbb{R}^{256}$ the probability of two such lines intersecting is effectively zero.

Now a simpler way to achieve this invariance would be to add into the training set a number of rotated versions of each training image, and then just use a standard nearest-neighbor classifier. This idea is called “hints” in Abu-Mostafa (1995), and works well when the space of invariances is small. So far we have presented a simplified version of the problem. In addition to rotation, there are six other types of transformations under which we would like our classifier to be invariant. There are translation (two directions), scaling (two directions), sheer, and character thickness. Hence the curves and tangent lines in Figures 13.10 and 13.11 are actually 7-dimensional manifolds and hyperplanes. It is infeasible to add transformed versions of each training image to capture all of these possibilities. The tangent manifolds provide an elegant way of capturing the invariances.

Table 13.1 shows the test misclassification error for a problem with 7291 training images and 2007 test digits (the U.S. Postal Services database), for a carefully constructed neural network, and simple 1-nearest-neighbor and

TABLE 13.1. *Test error rates for the handwritten ZIP code problem.*

Method	Error rate
Neural-net	0.049
1-nearest-neighbor/Euclidean distance	0.055
1-nearest-neighbor/tangent distance	0.026

tangent distance 1-nearest-neighbor rules. The tangent distance nearest-neighbor classifier works remarkably well, with test error rates near those for the human eye (this is a notoriously difficult test set). In practice, it turned out that nearest-neighbors are too slow for online classification in this application (see Section 13.5), and neural network classifiers were subsequently developed to mimic it.

13.4 Adaptive Nearest-Neighbor Methods

When nearest-neighbor classification is carried out in a high-dimensional feature space, the nearest neighbors of a point can be very far away, causing bias and degrading the performance of the rule.

To quantify this, consider N data points uniformly distributed in the unit cube $[-\frac{1}{2}, \frac{1}{2}]^p$. Let R be the radius of a 1-nearest-neighborhood centered at the origin. Then

$$\text{median}(R) = v_p^{-1/p}\Big(1 - \frac{1}{2}^{1/N}\Big)^{1/p}, \tag{13.7}$$

where $v_d r^p$ is the volume of the sphere of radius r in p dimensions. Figure 13.12 shows the median radius for various training sample sizes and dimensions. We see that median radius quickly approaches 0.5, the distance to the edge of the cube.

What can be done about this problem? Consider the two-class situation in Figure 13.13. There are two features, and a nearest-neighborhood at a query point is depicted by the circular region. Implicit in near-neighbor classification is the assumption that the class probabilities are roughly constant in the neighborhood, and hence simple averages give good estimates. However, in this example the class probabilities vary only in the horizontal direction. If we knew this, we would stretch the neighborhood in the vertical direction, as shown by the tall rectangular region. This will reduce the bias of our estimate and leave the variance the same.

In general, this calls for adapting the metric used in nearest-neighbor classification, so that the resulting neighborhoods stretch out in directions for which the class probabilities don't change much. In high-dimensional feature space, the class probabilities might change only a low-dimensional subspace and hence there can be considerable advantage to adapting the metric.

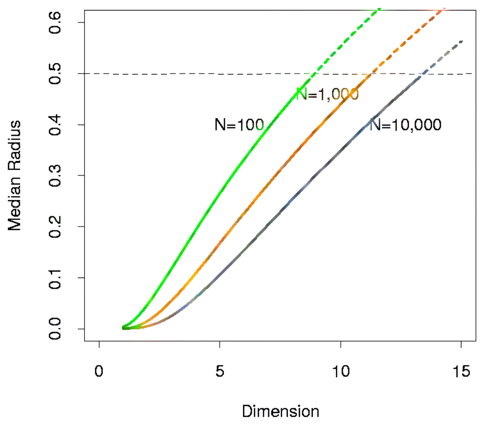

FIGURE 13.12. *Median radius of a 1-nearest-neighborhood, for uniform data with N observations in p dimensions.*

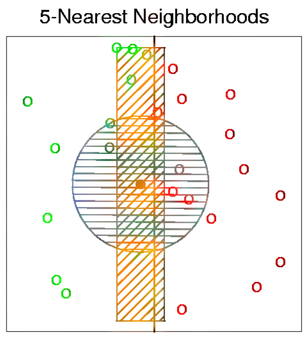

FIGURE 13.13. *The points are uniform in the cube, with the vertical line separating class red and green. The vertical strip denotes the* 5*-nearest-neighbor region using only the horizontal coordinate to find the nearest-neighbors for the target point (solid dot). The sphere shows the* 5*-nearest-neighbor region using both coordinates, and we see in this case it has extended into the class-red region (and is dominated by the wrong class in this instance).*

Friedman (1994a) proposed a method in which rectangular neighborhoods are found adaptively by successively carving away edges of a box containing the training data. Here we describe the *discriminant adaptive nearest-neighbor* (DANN) rule of Hastie and Tibshirani (1996a). Earlier, related proposals appear in Short and Fukunaga (1981) and Myles and Hand (1990).

At each query point a neighborhood of say 50 points is formed, and the class distribution among the points is used to decide how to deform the neighborhood—that is, to adapt the metric. The adapted metric is then used in a nearest-neighbor rule at the query point. Thus at each query point a potentially different metric is used.

In Figure 13.13 it is clear that the neighborhood should be stretched in the direction orthogonal to line joining the class centroids. This direction also coincides with the linear discriminant boundary, and is the direction in which the class probabilities change the least. In general this direction of maximum change will not be orthogonal to the line joining the class centroids (see Figure 4.9 on page 94.) Assuming a local discriminant model, the information contained in the local within- and between-class covariance matrices is all that is needed to determine the optimal shape of the neighborhood.

The *discriminant adaptive nearest-neighbor* (DANN) metric at a query point x_0 is defined by

$$D(x, x_0) = (x - x_0)^T \mathbf{\Sigma}(x - x_0), \tag{13.8}$$

where

$$\begin{aligned} \mathbf{\Sigma} &= \mathbf{W}^{-1/2}[\mathbf{W}^{-1/2}\mathbf{B}\mathbf{W}^{-1/2} + \epsilon\mathbf{I}]\mathbf{W}^{-1/2} \\ &= \mathbf{W}^{-1/2}[\mathbf{B}^* + \epsilon\mathbf{I}]\mathbf{W}^{-1/2}. \end{aligned} \tag{13.9}$$

Here $\mathbf{W}$ is the pooled within-class covariance matrix $\sum_{k=1}^K \pi_k \mathbf{W}_k$ and $\mathbf{B}$ is the between class covariance matrix $\sum_{k=1}^K \pi_k(\bar{x}_k - \bar{x})(\bar{x}_k - \bar{x})^T$, with $\mathbf{W}$ and $\mathbf{B}$ computed using only the 50 nearest neighbors around x_0. After computation of the metric, it is used in a nearest-neighbor rule at x_0.

This complicated formula is actually quite simple in its operation. It first spheres the data with respect to $\mathbf{W}$, and then stretches the neighborhood in the zero-eigenvalue directions of $\mathbf{B}^*$ (the between-matrix for the sphered data). This makes sense, since locally the observed class means do not differ in these directions. The ϵ parameter rounds the neighborhood, from an infinite strip to an ellipsoid, to avoid using points far away from the query point. The value of $\epsilon = 1$ seems to work well in general. Figure 13.14 shows the resulting neighborhoods for a problem where the classes form two concentric circles. Notice how the neighborhoods stretch out orthogonally to the decision boundaries when both classes are present in the neighborhood. In the pure regions with only one class, the neighborhoods remain circular;

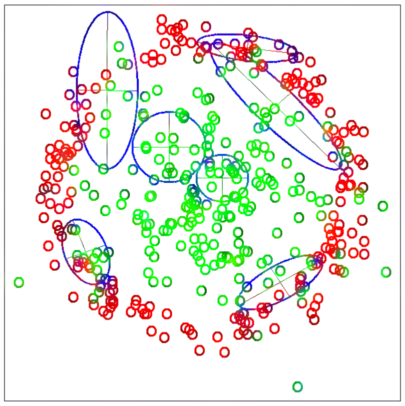

FIGURE 13.14. *Neighborhoods found by the DANN procedure, at various query points (centers of the crosses). There are two classes in the data, with one class surrounding the other.* 50 *nearest-neighbors were used to estimate the local metrics. Shown are the resulting metrics used to form* 15*-nearest-neighborhoods.*

in these cases the between matrix $\mathbf{B} = 0$, and the $\mathbf{\Sigma}$ in (13.8) is the identity matrix.

13.4.1 Example

Here we generate two-class data in ten dimensions, analogous to the two-dimensional example of Figure 13.14. All ten predictors in class 1 are independent standard normal, conditioned on the radius being greater than 22.4 and less than 40, while the predictors in class 2 are independent standard normal without the restriction. There are 250 observations in each class. Hence the first class almost completely surrounds the second class in the full ten-dimensional space.

In this example there are no pure noise variables, the kind that a nearest-neighbor subset selection rule might be able to weed out. At any given point in the feature space, the class discrimination occurs along only one direction. However, this direction changes as we move across the feature space and all variables are important somewhere in the space.

Figure 13.15 shows boxplots of the test error rates over ten realizations, for standard 5-nearest-neighbors, LVQ, and discriminant adaptive 5-nearest-neighbors. We used 50 prototypes per class for LVQ, to make it comparable to 5 nearest-neighbors (since $250/5 = 50$). The adaptive metric significantly reduces the error rate, compared to LVQ or standard nearest-neighbors.

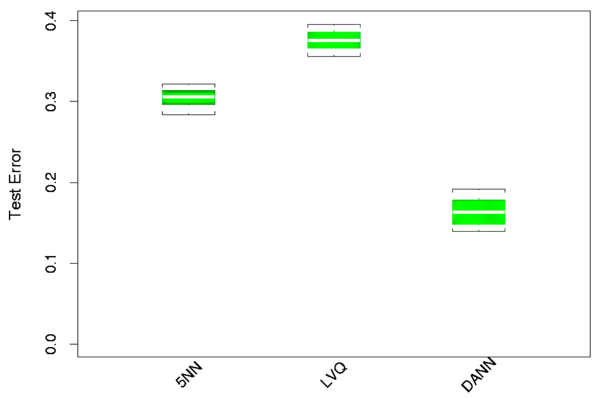

FIGURE 13.15. *Ten-dimensional simulated example: boxplots of the test error rates over ten realizations, for standard* 5*-nearest-neighbors, LVQ with* 50 *centers, and discriminant-adaptive* 5*-nearest-neighbors*

13.4.2 Global Dimension Reduction for Nearest-Neighbors

The discriminant-adaptive nearest-neighbor method carries out local dimension reduction—that is, dimension reduction separately at each query point. In many problems we can also benefit from global dimension reduction, that is, apply a nearest-neighbor rule in some optimally chosen subspace of the original feature space. For example, suppose that the two classes form two nested spheres in four dimensions of feature space, and there are an additional six noise features whose distribution is independent of class. Then we would like to discover the important four-dimensional subspace, and carry out nearest-neighbor classification in that reduced subspace. Hastie and Tibshirani (1996a) discuss a variation of the discriminant-adaptive nearest-neighbor method for this purpose. At each training point x_i, the between-centroids sum of squares matrix $\mathbf{B}_i$ is computed, and then these matrices are averaged over all training points:

$$\bar{\mathbf{B}} = \frac{1}{N}\sum_{i=1}^{N}\mathbf{B}_i. \tag{13.10}$$

Let $e_1, e_2, \dots, e_p$ be the eigenvectors of the matrix $\bar{\mathbf{B}}$, ordered from largest to smallest eigenvalue θ_k. Then these eigenvectors span the optimal subspaces for global subspace reduction. The derivation is based on the fact that the best rank-L approximation to $\bar{\mathbf{B}}$, $\bar{\mathbf{B}}_{[L]} = \sum_{\ell=1}^{L}\theta_\ell e_\ell e_\ell^T$, solves the least squares problem

$$\min_{\text{rank}(\mathbf{M})=L}\sum_{i=1}^{N}\text{trace}[(\mathbf{B}_i - \mathbf{M})^2]. \tag{13.11}$$

Since each $\mathbf{B}_i$ contains information on (a) the local discriminant subspace, and (b) the strength of discrimination in that subspace, (13.11) can be seen as a way of finding the best approximating subspace of dimension L to a series of N subspaces by weighted least squares (Exercise 13.5.)

In the four-dimensional sphere example mentioned above and examined in Hastie and Tibshirani (1996a), four of the eigenvalues θ_ℓ turn out to be large (having eigenvectors nearly spanning the interesting subspace), and the remaining six are near zero. Operationally, we project the data into the leading four-dimensional subspace, and then carry out nearest neighbor classification. In the satellite image classification example in Section 13.3.2, the technique labeled `DANN` in Figure 13.8 used 5-nearest-neighbors in a globally reduced subspace. There are also connections of this technique with the *sliced inverse regression* proposal of Duan and Li (1991). These authors use similar ideas in the regression setting, but do global rather than local computations. They assume and exploit spherical symmetry of the feature distribution to estimate interesting subspaces.

13.5 Computational Considerations

One drawback of nearest-neighbor rules in general is the computational load, both in finding the neighbors and storing the entire training set. With N observations and p predictors, nearest-neighbor classification requires Np operations to find the neighbors per query point. There are fast algorithms for finding nearest-neighbors (Friedman et al., 1975; Friedman et al., 1977) which can reduce this load somewhat. Hastie and Simard (1998) reduce the computations for tangent distance by developing analogs of K-means clustering in the context of this invariant metric.

Reducing the storage requirements is more difficult, and various *editing* and *condensing* procedures have been proposed. The idea is to isolate a subset of the training set that suffices for nearest-neighbor predictions, and throw away the remaining training data. Intuitively, it seems important to keep the training points that are near the decision boundaries and on the correct side of those boundaries, while some points far from the boundaries could be discarded.

The *multi-edit* algorithm of Devijver and Kittler (1982) divides the data cyclically into training and test sets, computing a nearest neighbor rule on the training set and deleting test points that are misclassified. The idea is to keep homogeneous clusters of training observations.

The *condensing* procedure of Hart (1968) goes further, trying to keep only important exterior points of these clusters. Starting with a single randomly chosen observation as the training set, each additional data item is processed one at a time, adding it to the training set only if it is misclassified by a nearest-neighbor rule computed on the current training set.

These procedures are surveyed in Dasarathy (1991) and Ripley (1996). They can also be applied to other learning procedures besides nearest-neighbors. While such methods are sometimes useful, we have not had much practical experience with them, nor have we found any systematic comparison of their performance in the literature.

Bibliographic Notes

The nearest-neighbor method goes back at least to Fix and Hodges (1951). The extensive literature on the topic is reviewed by Dasarathy (1991); Chapter 6 of Ripley (1996) contains a good summary. K-means clustering is due to Lloyd (1957) and MacQueen (1967). Kohonen (1989) introduced learning vector quantization. The tangent distance method is due to Simard et al. (1993). Hastie and Tibshirani (1996a) proposed the discriminant adaptive nearest-neighbor technique.

Exercises

Ex. 13.1 Consider a Gaussian mixture model where the covariance matrices are assumed to be scalar: $\mathbf{\Sigma}_r = \sigma\mathbf{I}\ \forall r = 1, \dots, R$, and σ is a fixed parameter. Discuss the analogy between the K-means clustering algorithm and the EM algorithm for fitting this mixture model in detail. Show that in the limit $\sigma \to 0$ the two methods coincide.

Ex. 13.2 Derive formula (13.7) for the median radius of the 1-nearest-neighborhood.

Ex. 13.3 Let E^* be the error rate of the Bayes rule in a K-class problem, where the true class probabilities are given by $p_k(x),\ k = 1, \dots, K$. Assuming the test point and training point have identical features x, prove (13.5)

$$\sum_{k=1}^{K} p_k(x)(1 - p_k(x)) \le 2(1 - p_{k^*}(x)) - \frac{K}{K-1}(1 - p_{k^*}(x))^2.$$

where $k^* = \arg\max_k p_k(x)$. Hence argue that the error rate of the 1-nearest-neighbor rule converges in L_1, as the size of the training set increases, to a value E_1, bounded above by

$$E^*\Big(2 - E^*\frac{K}{K-1}\Big). \tag{13.12}$$

[This statement of the theorem of Cover and Hart (1967) is taken from Chapter 6 of Ripley (1996), where a short proof is also given].

Ex. 13.4 Consider an image to be a function $F(x): \mathbb{R}^2 \mapsto \mathbb{R}^1$ over the two-dimensional spatial domain (paper coordinates). Then $F(c+x_0+\mathbf{A}(x-x_0))$ represents an affine transformation of the image F, where $\mathbf{A}$ is a 2×2 matrix.

1. Decompose $\mathbf{A}$ (via Q-R) in such a way that parameters identifying the four affine transformations (two scale, shear and rotation) are clearly identified.
2. Using the chain rule, show that the derivative of $F(c+x_0+\mathbf{A}(x-x_0))$ w.r.t. each of these parameters can be represented in terms of the two spatial derivatives of F.
3. Using a two-dimensional kernel smoother (Chapter 6), describe how to implement this procedure when the images are quantized to 16×16 pixels.

Ex. 13.5 Let $\mathbf{B}_i, i = 1, 2, \ldots, N$ be square $p \times p$ positive semi-definite matrices and let $\bar{\mathbf{B}} = (1/N)\sum \mathbf{B}_i$. Write the eigen-decomposition of $\bar{\mathbf{B}}$ as $\sum_{\ell=1}^{p} \theta_\ell e_\ell e_\ell^T$ with $\theta_\ell \geq \theta_{\ell-1} \geq \cdots \geq \theta_1$. Show that the best rank-L approximation for the $\mathbf{B}_i$,

$$\min_{\text{rank}(\mathbf{M})=L} \sum_{i=1}^{N} \text{trace}[(\mathbf{B}_i - \mathbf{M})^2],$$

is given by $\bar{\mathbf{B}}_{[L]} = \sum_{\ell=1}^{L} \theta_\ell e_\ell e_\ell^T$. (*Hint:* Write $\sum_{i=1}^{N} \text{trace}[(\mathbf{B}_i - \mathbf{M})^2]$ as

$$\sum_{i=1}^{N} \text{trace}[(\mathbf{B}_i - \bar{\mathbf{B}})^2] + \sum_{i=1}^{N} \text{trace}[(\mathbf{M} - \bar{\mathbf{B}})^2]).$$

Ex. 13.6 Here we consider the problem of *shape averaging*. In particular, $\mathbf{L}_i$, $i = 1, \ldots, M$ are each $N \times 2$ matrices of points in $\mathbb{R}^2$, each sampled from corresponding positions of handwritten (cursive) letters. We seek an *affine invariant average* $\mathbf{V}$, also $N \times 2$, $\mathbf{V}^T\mathbf{V} = I$, of the M letters $\mathbf{L}_i$ with the following property: $\mathbf{V}$ minimizes

$$\sum_{j=1}^{M} \min_{\mathbf{A}_j} \|\mathbf{L}_j - \mathbf{V}\mathbf{A}_j\|^2 .$$

Characterize the solution.

This solution can suffer if some of the letters are *big* and dominate the average. An alternative approach is to minimize instead:

$$\sum_{j=1}^{M} \min_{\mathbf{A}_j} \left\|\mathbf{L}_j\mathbf{A}_j^* - \mathbf{V}\right\|^2 .$$

Derive the solution to this problem. How do the criteria differ? Use the SVD of the $\mathbf{L}_j$ to simplify the comparison of the two approaches.

Ex. 13.7 Consider the application of nearest-neighbors to the “easy” and “hard” problems in the left panel of Figure 13.5.

1. Replicate the results in the left panel of Figure 13.5.
2. Estimate the misclassification errors using fivefold cross-validation, and compare the error rate curves to those in 1.
3. Consider an “AIC-like” penalization of the training set misclassification error. Specifically, add $2t/N$ to the training set misclassification error, where t is the approximate number of parameters N/r, r being the number of nearest-neighbors. Compare plots of the resulting penalized misclassification error to those in 1 and 2. Which method gives a better estimate of the optimal number of nearest-neighbors: cross-validation or AIC?

Ex. 13.8 Generate data in two classes, with two features. These features are all independent Gaussian variates with standard deviation 1. Their mean vectors are $(-1,-1)$ in class 1 and $(1,1)$ in class 2. To each feature vector apply a random rotation of angle θ, θ chosen uniformly from 0 to 2π. Generate 50 observations from each class to form the training set, and 500 in each class as the test set. Apply four different classifiers:

1. Nearest-neighbors.
2. Nearest-neighbors with hints: ten randomly rotated versions of each data point are added to the training set before applying nearest-neighbors.
3. Invariant metric nearest-neighbors, using Euclidean distance invariant to rotations about the origin.
4. Tangent distance nearest-neighbors.

In each case choose the number of neighbors by tenfold cross-validation. Compare the results.

14
Unsupervised Learning

14.1 Introduction

The previous chapters have been concerned with predicting the values of one or more outputs or response variables $Y = (Y_1, \dots, Y_m)$ for a given set of input or predictor variables $X = (X_1, \dots, X_p)$. Denote by $x_i = (x_{i1}, \dots, x_{ip})$ the inputs for the ith training case, and let y_i be a response measurement. The predictions are based on the training sample $(x_1, y_1), \dots, (x_N, y_N)$ of previously solved cases, where the joint values of all of the variables are known. This is called *supervised learning* or "learning with a teacher." Under this metaphor the "student" presents an answer $\hat{y}_i$ for each x_i in the training sample, and the supervisor or "teacher" provides either the correct answer and/or an error associated with the student's answer. This is usually characterized by some loss function $L(y, \hat{y})$, for example, $L(y, \hat{y}) = (y - \hat{y})^2$.

If one supposes that (X, Y) are random variables represented by some joint probability density $\Pr(X, Y)$, then supervised learning can be formally characterized as a density estimation problem where one is concerned with determining properties of the conditional density $\Pr(Y|X)$. Usually the properties of interest are the "location" parameters μ that minimize the expected error at each x,

$$\mu(x) = \operatorname*{argmin}_{\theta} E_{Y|X} L(Y, \theta). \tag{14.1}$$

From Bayes theorem one has

$$\Pr(X, Y) = \Pr(Y|X) \cdot \Pr(X),$$

where $\Pr(X)$ is the joint marginal density of the X values alone. In supervised learning $\Pr(X)$ is typically of no direct concern. One is interested mainly in the properties of the conditional density $\Pr(Y|X)$. Since Y is often of low dimension (usually one), and only its location $\mu(x)$ is of interest, the problem is greatly simplified. As discussed in the previous chapters, there are many approaches for successfully addressing supervised learning in a variety of contexts.

In this chapter we address *unsupervised learning* or "learning without a teacher." In this case one has a set of N observations $(x_1, x_2, \ldots, x_N)$ of a random p-vector X having joint density $\Pr(X)$. The goal is to directly infer the properties of this probability density without the help of a supervisor or teacher providing correct answers or degree-of-error for each observation. The dimension of X is sometimes much higher than in supervised learning, and the properties of interest are often more complicated than simple location estimates. These factors are somewhat mitigated by the fact that X represents all of the variables under consideration; one is not required to infer how the properties of $\Pr(X)$ change, conditioned on the changing values of another set of variables.

In low-dimensional problems (say $p \leq 3$), there are a variety of effective nonparametric methods for directly estimating the density $\Pr(X)$ itself at all X-values, and representing it graphically (Silverman, 1986, e.g.). Owing to the curse of dimensionality, these methods fail in high dimensions. One must settle for estimating rather crude global models, such as Gaussian mixtures or various simple descriptive statistics that characterize $\Pr(X)$.

Generally, these descriptive statistics attempt to characterize X-values, or collections of such values, where $\Pr(X)$ is relatively large. Principal components, multidimensional scaling, self-organizing maps, and principal curves, for example, attempt to identify low-dimensional manifolds within the X-space that represent high data density. This provides information about the associations among the variables and whether or not they can be considered as functions of a smaller set of "latent" variables. Cluster analysis attempts to find multiple convex regions of the X-space that contain modes of $\Pr(X)$. This can tell whether or not $\Pr(X)$ can be represented by a mixture of simpler densities representing distinct types or classes of observations. Mixture modeling has a similar goal. Association rules attempt to construct simple descriptions (conjunctive rules) that describe regions of high density in the special case of very high dimensional binary-valued data.

With supervised learning there is a clear measure of success, or lack thereof, that can be used to judge adequacy in particular situations and to compare the effectiveness of different methods over various situations.

Lack of success is directly measured by expected loss over the joint distribution $\Pr(X, Y)$. This can be estimated in a variety of ways including cross-validation. In the context of unsupervised learning, there is no such direct measure of success. It is difficult to ascertain the validity of inferences drawn from the output of most unsupervised learning algorithms. One must resort to heuristic arguments not only for motivating the algorithms, as is often the case in supervised learning as well, but also for judgments as to the quality of the results. This uncomfortable situation has led to heavy proliferation of proposed methods, since effectiveness is a matter of opinion and cannot be verified directly.

In this chapter we present those unsupervised learning techniques that are among the most commonly used in practice, and additionally, a few others that are favored by the authors.

14.2 Association Rules

Association rule analysis has emerged as a popular tool for mining commercial data bases. The goal is to find joint values of the variables $X = (X_1, X_2, \ldots, X_p)$ that appear most frequently in the data base. It is most often applied to binary-valued data $X_j \in \{0, 1\}$, where it is referred to as "market basket" analysis. In this context the observations are sales transactions, such as those occurring at the checkout counter of a store. The variables represent all of the items sold in the store. For observation i, each variable X_j is assigned one of two values; $x_{ij} = 1$ if the jth item is purchased as part of the transaction, whereas $x_{ij} = 0$ if it was not purchased. Those variables that frequently have joint values of one represent items that are frequently purchased together. This information can be quite useful for stocking shelves, cross-marketing in sales promotions, catalog design, and consumer segmentation based on buying patterns.

More generally, the basic goal of association rule analysis is to find a collection of prototype X-values $v_l, \ldots, v_L$ for the feature vector X, such that the probability density $\Pr(v_l)$ evaluated at each of those values is relatively large. In this general framework, the problem can be viewed as "mode finding" or "bump hunting." As formulated, this problem is impossibly difficult. A natural estimator for each $\Pr(v_l)$ is the fraction of observations for which $X = v_l$. For problems that involve more than a small number of variables, each of which can assume more than a small number of values, the number of observations for which $X = v_l$ will nearly always be too small for reliable estimation. In order to have a tractable problem, both the goals of the analysis and the generality of the data to which it is applied must be greatly simplified.

The first simplification modifies the goal. Instead of seeking *values* x where $\Pr(x)$ is large, one seeks *regions* of the X-space with high probability content relative to their size or support. Let $\mathcal{S}_j$ represent the set of all possible values of the jth variable (its *support*), and let $s_j \subseteq \mathcal{S}_j$ be a subset of these values. The modified goal can be stated as attempting to find subsets of variable values $s_1, \ldots, s_p$ such that the probability of each of the variables simultaneously assuming a value within its respective subset

$$\Pr\left[\bigcap_{j=1}^{p}(X_j \in s_j)\right] \tag{14.2}$$

is relatively large. The intersection of subsets $\cap_{j=1}^{p}(X_j \in s_j)$ is called a *conjunctive rule*. For quantitative variables the subsets s_j are contiguous intervals; for categorical variables the subsets are delineated explicitly. Note that if the subset s_j is in fact the entire set of values $s_j = \mathcal{S}_j$, as is often the case, the variable X_j is said *not* to appear in the rule (14.2).

14.2.1 Market Basket Analysis

General approaches to solving (14.2) are discussed in Section 14.2.5. These can be quite useful in many applications. However, they are not feasible for the very large ($p \approx 10^4$, $N \approx 10^8$) commercial data bases to which market basket analysis is often applied. Several further simplifications of (14.2) are required. First, only two types of subsets are considered; either s_j consists of a *single* value of X_j, $s_j = v_{0j}$, or it consists of the entire set of values that X_j can assume, $s_j = \mathcal{S}_j$. This simplifies the problem (14.2) to finding subsets of the integers $\mathcal{J} \subset \{1, \ldots, p\}$, and corresponding values v_{0j}, $j \in \mathcal{J}$, such that

$$\Pr\left[\bigcap_{j\in\mathcal{J}}(X_j = v_{0j})\right] \tag{14.3}$$

is large. Figure 14.1 illustrates this assumption.

One can apply the technique of *dummy variables* to turn (14.3) into a problem involving only binary-valued variables. Here we assume that the support $\mathcal{S}_j$ is finite for each variable X_j. Specifically, a new set of variables $Z_1, \ldots, Z_K$ is created, one such variable for each of the values v_{lj} attainable by each of the original variables $X_1, \ldots, X_p$. The number of dummy variables K is

$$K = \sum_{j=1}^{p} |\mathcal{S}_j|,$$

where $|\mathcal{S}_j|$ is the number of distinct values attainable by X_j. Each dummy variable is assigned the value $Z_k = 1$ if the variable with which it is associated takes on the corresponding value to which Z_k is assigned, and

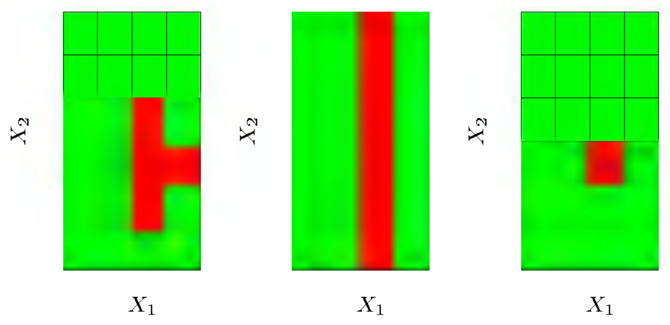

FIGURE 14.1. *Simplifications for association rules. Here there are two inputs X_1 and X_2, taking four and six distinct values, respectively. The red squares indicate areas of high density. To simplify the computations, we assume that the derived subset corresponds to either a single value of an input or all values. With this assumption we could find either the middle or right pattern, but not the left one.*

$Z_k = 0$ otherwise. This transforms (14.3) to finding a subset of the integers $\mathcal{K} \subset \{1, \ldots, K\}$ such that

$$\Pr\left[\bigcap_{k\in\mathcal{K}} (Z_k = 1)\right] = \Pr\left[\prod_{k\in\mathcal{K}} Z_k = 1\right] \tag{14.4}$$

is large. This is the standard formulation of the market basket problem. The set $\mathcal{K}$ is called an "item set." The number of variables Z_k in the item set is called its "size" (note that the size is no bigger than p). The estimated value of (14.4) is taken to be the fraction of observations in the data base for which the conjunction in (14.4) is true:

$$\widehat{\Pr}\left[\prod_{k\in\mathcal{K}} (Z_k = 1)\right] = \frac{1}{N}\sum_{i=1}^{N}\prod_{k\in\mathcal{K}} z_{ik}. \tag{14.5}$$

Here z_{ik} is the value of Z_k for this ith case. This is called the "support" or "prevalence" $T(\mathcal{K})$ of the item set $\mathcal{K}$. An observation i for which $\prod_{k\in\mathcal{K}} z_{ik} = 1$ is said to "contain" the item set $\mathcal{K}$.

In association rule mining a lower support bound t is specified, and one seeks *all* item sets $\mathcal{K}_l$ that can be formed from the variables $Z_1, \ldots, Z_K$ with support in the data base greater this lower bound t

$$\{\mathcal{K}_l | T(\mathcal{K}_l) > t\}. \tag{14.6}$$

14.2.2 The Apriori Algorithm

The solution to this problem (14.6) can be obtained with feasible computation for very large data bases provided the threshold t is adjusted so that

(14.6) consists of only a small fraction of all 2^K possible item sets. The "Apriori" algorithm (Agrawal et al., 1995) exploits several aspects of the curse of dimensionality to solve (14.6) with a small number of passes over the data. Specifically, for a given support threshold t:

- The cardinality $|\{\mathcal{K}|\, T(\mathcal{K}) > t\}|$ is relatively small.
- Any item set $\mathcal{L}$ consisting of a subset of the items in $\mathcal{K}$ must have support greater than or equal to that of $\mathcal{K}$, $\mathcal{L} \subseteq \mathcal{K} \Rightarrow T(\mathcal{L}) \geq T(\mathcal{K})$.

The first pass over the data computes the support of all single-item sets. Those whose support is less than the threshold are discarded. The second pass computes the support of all item sets of size two that can be formed from pairs of the single items surviving the first pass. In other words, to generate all frequent itemsets with $|\mathcal{K}| = m$, we need to consider only candidates such that *all* of their m ancestral item sets of size $m-1$ are frequent. Those size-two item sets with support less than the threshold are discarded. Each successive pass over the data considers only those item sets that can be formed by combining those that survived the previous pass with those retained from the first pass. Passes over the data continue until all candidate rules from the previous pass have support less than the specified threshold. The Apriori algorithm requires only one pass over the data for each value of $|\mathcal{K}|$, which is crucial since we assume the data cannot be fitted into a computer's main memory. If the data are sufficiently sparse (or if the threshold t is high enough), then the process will terminate in reasonable time even for huge data sets.

There are many additional tricks that can be used as part of this strategy to increase speed and convergence (Agrawal et al., 1995). The Apriori algorithm represents one of the major advances in data mining technology.

Each high support item set $\mathcal{K}$ (14.6) returned by the Apriori algorithm is cast into a set of "association rules." The items Z_k, $k \in \mathcal{K}$, are partitioned into two disjoint subsets, $A \cup B = \mathcal{K}$, and written

$$A \Rightarrow B. \tag{14.7}$$

The first item subset A is called the "antecedent" and the second B the "consequent." Association rules are defined to have several properties based on the prevalence of the antecedent and consequent item sets in the data base. The "support" of the rule $T(A \Rightarrow B)$ is the fraction of observations in the union of the antecedent and consequent, which is just the support of the item set $\mathcal{K}$ from which they were derived. It can be viewed as an estimate (14.5) of the probability of simultaneously observing both item sets $\Pr(A \text{ and } B)$ in a randomly selected market basket. The "confidence" or "predictability" $C(A \Rightarrow B)$ of the rule is its support divided by the support of the antecedent

$$C(A \Rightarrow B) = \frac{T(A \Rightarrow B)}{T(A)}, \tag{14.8}$$

which can be viewed as an estimate of $\Pr(B \mid A)$. The notation $\Pr(A)$, the probability of an item set A occurring in a basket, is an abbreviation for $\Pr(\prod_{k\in A} Z_k = 1)$. The "expected confidence" is defined as the support of the consequent $T(B)$, which is an estimate of the unconditional probability $\Pr(B)$. Finally, the "lift" of the rule is defined as the confidence divided by the expected confidence

$$L(A \Rightarrow B) = \frac{C(A \Rightarrow B)}{T(B)}.$$

This is an estimate of the association measure $\Pr(A \text{ and } B)/\Pr(A)\Pr(B)$.

As an example, suppose the item set $\mathcal{K} = \{$`peanut butter, jelly, bread`$\}$ and consider the rule $\{$`peanut butter, jelly`$\} \Rightarrow \{$`bread`$\}$. A support value of 0.03 for this rule means that `peanut butter`, `jelly`, and `bread` appeared together in 3% of the market baskets. A confidence of 0.82 for this rule implies that when `peanut butter` and `jelly` were purchased, 82% of the time `bread` was also purchased. If bread appeared in 43% of all market baskets then the rule $\{$`peanut butter, jelly`$\} \Rightarrow \{$`bread`$\}$ would have a lift of 1.95.

The goal of this analysis is to produce association rules (14.7) with both high values of support and confidence (14.8). The Apriori algorithm returns all item sets with high support as defined by the support threshold t (14.6). A confidence threshold c is set, and all rules that can be formed from those item sets (14.6) with confidence greater than this value

$$\{A \Rightarrow B \mid C(A \Rightarrow B) > c\} \tag{14.9}$$

are reported. For each item set $\mathcal{K}$ of size $|\mathcal{K}|$ there are $2^{|\mathcal{K}|-1} - 1$ rules of the form $A \Rightarrow (\mathcal{K} - A)$, $A \subset \mathcal{K}$. Agrawal et al. (1995) present a variant of the Apriori algorithm that can rapidly determine which rules survive the confidence threshold (14.9) from all possible rules that can be formed from the solution item sets (14.6).

The output of the entire analysis is a collection of association rules (14.7) that satisfy the constraints

$$T(A \Rightarrow B) > t \quad \text{and} \quad C(A \Rightarrow B) > c.$$

These are generally stored in a data base that can be queried by the user. Typical requests might be to display the rules in sorted order of confidence, lift or support. More specifically, one might request such a list conditioned on particular items in the antecedent or especially the consequent. For example, a request might be the following:

Display all transactions in which ice skates are the consequent that have confidence over 80% *and support of more than* 2%.

This could provide information on those items (antecedent) that predicate sales of ice skates. Focusing on a particular consequent casts the problem into the framework of supervised learning.

Association rules have become a popular tool for analyzing very large commercial data bases in settings where market basket is relevant. That is when the data can be cast in the form of a multidimensional contingency table. The output is in the form of conjunctive rules (14.4) that are easily understood and interpreted. The Apriori algorithm allows this analysis to be applied to huge data bases, much larger that are amenable to other types of analyses. Association rules are among data mining's biggest successes.

Besides the restrictive form of the data to which they can be applied, association rules have other limitations. Critical to computational feasibility is the support threshold (14.6). The number of solution item sets, their size, and the number of passes required over the data can grow exponentially with decreasing size of this lower bound. Thus, rules with high confidence or lift, but low support, will not be discovered. For example, a high confidence rule such as `vodka` $\Rightarrow$ `caviar` will not be uncovered owing to the low sales volume of the consequent `caviar`.

14.2.3 Example: Market Basket Analysis

We illustrate the use of Apriori on a moderately sized demographics data base. This data set consists of $N = 9409$ questionnaires filled out by shopping mall customers in the San Francisco Bay Area (Impact Resources, Inc., Columbus OH, 1987). Here we use answers to the first 14 questions, relating to demographics, for illustration. These questions are listed in Table 14.1. The data are seen to consist of a mixture of ordinal and (unordered) categorical variables, many of the latter having more than a few values. There are many missing values.

We used a freeware implementation of the Apriori algorithm due to Christian Borgelt. [*] After removing observations with missing values, each ordinal predictor was cut at its median and coded by two dummy variables; each categorical predictor with k categories was coded by k dummy variables. This resulted in a 6876×50 matrix of 6876 observations on 50 dummy variables.

The algorithm found a total of 6288 association rules, involving ≤ 5 predictors, with support of at least 10%. Understanding this large set of rules is itself a challenging data analysis task. We will not attempt this here, but only illustrate in Figure 14.2 the relative frequency of each dummy variable in the data (top) and the association rules (bottom). Prevalent categories tend to appear more often in the rules, for example, the first category in language (English). However, others such as occupation are under-represented, with the exception of the fourth occupation (clerical/service worker).

Here are three examples of association rules found by the Apriori algorithm:

[*] See `http://fuzzy.cs.uni-magdeburg.de/~borgelt`

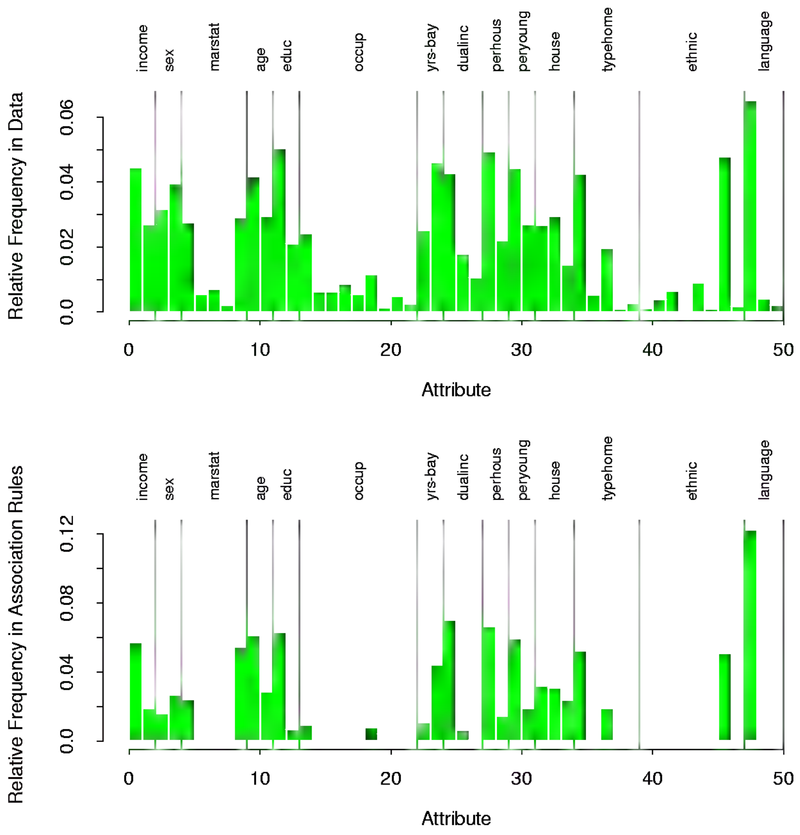

FIGURE 14.2. *Market basket analysis: relative frequency of each dummy variable (coding an input category) in the data (top), and the association rules found by the Apriori algorithm (bottom).*

TABLE 14.1. *Inputs for the demographic data.*

Feature	Demographic	# values	Type
1	sex	2	categorical
2	marital status	5	categorical
3	age	7	ordinal
4	education	6	ordinal
5	occupation	9	categorical
6	income	9	ordinal
7	years in Bay Area	5	ordinal
8	dual incomes	3	categorical
9	number in household	9	ordinal
10	number of children	9	ordinal
11	householder status	3	categorical
12	type of home	5	categorical
13	ethnic classification	8	categorical
14	language in home	3	categorical

Association rule 1: Support 25%, confidence 99.7% and lift 1.03.

$$\begin{bmatrix} \text{number in household} & = & \textit{1} \\ \text{number of children} & = & \textit{0} \end{bmatrix}$$
$$\Downarrow$$
$$\text{language in home} = \textit{English}$$

Association rule 2: Support 13.4%, confidence 80.8%, and lift 2.13.

$$\begin{bmatrix} \text{language in home} & = & \textit{English} \\ \text{householder status} & = & \textit{own} \\ \text{occupation} & = & \{\textit{professional/managerial}\} \end{bmatrix}$$
$$\Downarrow$$
$$\text{income} \geq \textit{\$40,000}$$

Association rule 3: Support 26.5%, confidence 82.8% and lift 2.15.

$$\begin{bmatrix} \text{language in home} & = & \textit{English} \\ \text{income} & < & \textit{\$40,000} \\ \text{marital status} & = & \textit{not married} \\ \text{number of children} & = & \textit{0} \end{bmatrix}$$
$$\Downarrow$$
$$\text{education} \notin \{\textit{college graduate, graduate study}\}$$

We chose the first and third rules based on their high support. The second rule is an association rule with a high-income consequent, and could be used to try to target high-income individuals.

As stated above, we created dummy variables for each category of the input predictors, for example, $Z_1 = I(\text{income} < \$40,000)$ and $Z_2 = I(\text{income} \geq \$40,000)$ for below and above the median income. If we were interested only in finding associations with the high-income category, we would include Z_2 but not Z_1. This is often the case in actual market basket problems, where we are interested in finding associations with the presence of a relatively rare item, but not associations with its absence.

14.2.4 Unsupervised as Supervised Learning

Here we discuss a technique for transforming the density estimation problem into one of supervised function approximation. This forms the basis for the generalized association rules described in the next section.

Let $g(x)$ be the unknown data probability density to be estimated, and $g_0(x)$ be a specified probability density function used for reference. For example, $g_0(x)$ might be the uniform density over the range of the variables. Other possibilities are discussed below. The data set $x_1, x_2, \ldots, x_N$ is presumed to be an *i.i.d.* random sample drawn from $g(x)$. A sample of size N_0 can be drawn from $g_0(x)$ using Monte Carlo methods. Pooling these two data sets, and assigning mass $w = N_0/(N + N_0)$ to those drawn from $g(x)$, and $w_0 = N/(N + N_0)$ to those drawn from $g_0(x)$, results in a random sample drawn from the mixture density $(g(x) + g_0(x))/2$. If one assigns the value $Y = 1$ to each sample point drawn from $g(x)$ and $Y = 0$ those drawn from $g_0(x)$, then

$$\begin{aligned} \mu(x) = E(Y \,|\, x) &= \frac{g(x)}{g(x) + g_0(x)} \\ &= \frac{g(x)/g_0(x)}{1 + g(x)/g_0(x)} \end{aligned} \tag{14.10}$$

can be estimated by supervised learning using the combined sample

$$(y_1, x_1), (y_2, x_2), \ldots, (y_{N+N_0}, x_{N+N_0}) \tag{14.11}$$

as training data. The resulting estimate $\hat{\mu}(x)$ can be inverted to provide an estimate for $g(x)$

$$\hat{g}(x) = g_0(x) \frac{\hat{\mu}(x)}{1 - \hat{\mu}(x)}. \tag{14.12}$$

Generalized versions of logistic regression (Section 4.4) are especially well suited for this application since the log-odds,

$$f(x) = \log \frac{g(x)}{g_0(x)}, \tag{14.13}$$

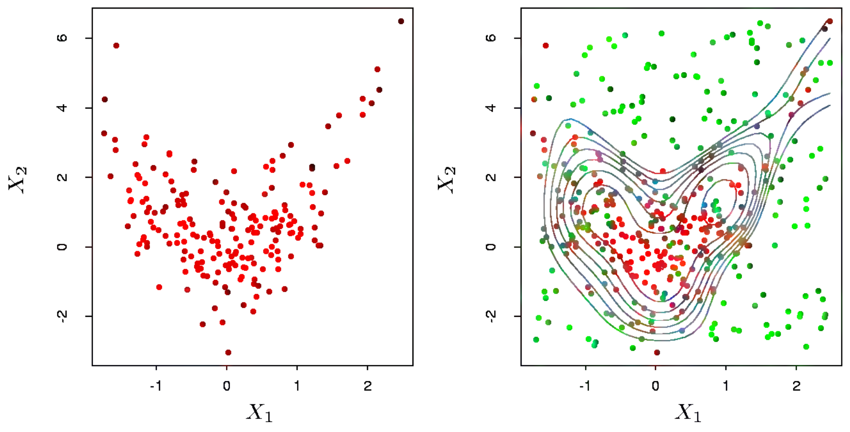

FIGURE 14.3. *Density estimation via classification. Left panel: Training set of* 200 *data points. Right panel: Training set plus* 200 *reference data points, generated uniformly over the rectangle containing the training data. The training sample was labeled as class* 1*, and the reference sample class* 0*, and a semiparametric logistic regression model was fit to the data. Some contours for* $\hat{g}(x)$ *are shown.*

are estimated directly. In this case one has

$$\hat{g}(x) = g_0(x)\, e^{\hat{f}(x)}. \tag{14.14}$$

An example is shown in Figure 14.3. We generated a training set of size 200 shown in the left panel. The right panel shows the reference data (green) generated uniformly over the rectangle containing the training data. The training sample was labeled as class 1, and the reference sample class 0, and a logistic regression model, using a tensor product of natural splines (Section 5.2.1), was fit to the data. Some probability contours of $\hat{\mu}(x)$ are shown in the right panel; these are also the contours of the density estimate $\hat{g}(x)$, since $\hat{g}(x) = \hat{\mu}(x)/(1 - \hat{\mu}(x))$, is a monotone function. The contours roughly capture the data density.

In principle any reference density can be used for $g_0(x)$ in (14.14). In practice the accuracy of the estimate $\hat{g}(x)$ can depend greatly on particular choices. Good choices will depend on the data density $g(x)$ and the procedure used to estimate (14.10) or (14.13). If accuracy is the goal, $g_0(x)$ should be chosen so that the resulting functions $\mu(x)$ or $f(x)$ are approximated easily by the method being used. However, accuracy is not always the primary goal. Both $\mu(x)$ and $f(x)$ are monotonic functions of the density ratio $g(x)/g_0(x)$. They can thus be viewed as "contrast" statistics that provide information concerning departures of the data density $g(x)$ from the chosen reference density $g_0(x)$. Therefore, in data analytic settings, a choice for $g_0(x)$ is dictated by types of departures that are deemed most interesting in the context of the specific problem at hand. For example, if departures from uniformity are of interest, $g_0(x)$ might be the a uniform density over the range of the variables. If departures from joint normality are of interest, a good choice for $g_0(x)$ would be a Gaussian distribution with the same mean vector and covariance matrix as the data; we pursue this further in Section 14.6.4 in the context of *Independent Components Analysis*. Departures from independence could be investigated by using

$$g_0(x) = \prod_{j=1}^{p} g_j(x_j), \tag{14.15}$$

where $g_j(x_j)$ is the marginal data density of X_j, the jth coordinate of X. A sample from this independent density (14.15) is easily generated from the data itself by applying a different random permutation to the data values of each of the variables.

As discussed above, unsupervised learning is concerned with revealing properties of the data density $g(x)$. Each technique focuses on a particular property or set of properties. Although this approach of transforming the problem to one of supervised learning (14.10)–(14.14) seems to have been part of the statistics folklore for some time, it does not appear to have had much impact despite its potential to bring well-developed supervised learning methodology to bear on unsupervised learning problems. One reason may be that the problem must be enlarged with a simulated data set generated by Monte Carlo techniques. Since the size of this data set should be at least as large as the data sample $N_0 \geq N$, the computation and memory requirements of the estimation procedure are at least doubled. Also, substantial computation may be required to generate the Monte Carlo sample itself. Although perhaps a deterrent in the past, these increased computational requirements are becoming much less of a burden as increased resources become routinely available. We illustrate the use of supervising learning methods for unsupervised learning in the next section.

14.2.5 Generalized Association Rules

The more general problem (14.2) of finding high-density regions in the data space can be addressed using the supervised learning approach described above. Although not applicable to the huge data bases for which market basket analysis is feasible, useful information can be obtained from moderately sized data sets. The problem (14.2) can be formulated as finding subsets of the integers $\mathcal{J} \subset \{1, 2, \ldots, p\}$ and corresponding value subsets $s_j,\ j \in \mathcal{J}$ for the corresponding variables X_j, such that

$$\widehat{\Pr}\left(\bigcap_{j\in\mathcal{J}} (X_j \in s_j)\right) = \frac{1}{N}\sum_{i=1}^{N} I\left(\bigcap_{j\in\mathcal{J}} (x_{ij} \in s_j)\right) \tag{14.16}$$

is large. Following the nomenclature of association rule analysis, $\{(X_j \in s_j\}_{j\in\mathcal{J}}$ will be called a "generalized" item set. The subsets s_j corresponding to quantitative variables are taken to be contiguous intervals within their range of values, and subsets for categorical variables can involve more than a single value. The ambitious nature of this formulation precludes a thorough search for all generalized item sets with support (14.16) greater than a specified minimum threshold, as was possible in the more restrictive setting of market basket analysis. Heuristic search methods must be employed, and the most one can hope for is to find a useful collection of such generalized item sets.

Both market basket analysis (14.5) and the generalized formulation (14.16) implicitly reference the uniform probability distribution. One seeks item sets that are more frequent than would be expected if all joint data values $(x_1, x_2, \dots, x_N)$ were uniformly distributed. This favors the discovery of item sets whose marginal constituents $(X_j \in s_j)$ are *individually* frequent, that is, the quantity

$$\frac{1}{N}\sum_{i=1}^{N} I(x_{ij} \in s_j) \tag{14.17}$$

is large. Conjunctions of frequent subsets (14.17) will tend to appear more often among item sets of high support (14.16) than conjunctions of marginally less frequent subsets. This is why the rule `vodka` $\Rightarrow$ `caviar` is not likely to be discovered in spite of a high association (lift); neither item has high marginal support, so that their joint support is especially small. Reference to the uniform distribution can cause highly frequent item sets with low associations among their constituents to dominate the collection of highest support item sets.

Highly frequent subsets s_j are formed as disjunctions of the most frequent X_j-values. Using the product of the variable marginal data densities (14.15) as a reference distribution removes the preference for highly frequent values of the individual variables in the discovered item sets. This is because the density ratio $g(x)/g_0(x)$ is uniform if there are no associations among the variables (complete independence), regardless of the frequency distribution of the individual variable values. Rules like `vodka` $\Rightarrow$ `caviar` would have a chance to emerge. It is not clear however, how to incorporate reference distributions other than the uniform into the Apriori algorithm. As explained in Section 14.2.4, it is straightforward to generate a sample from the product density (14.15), given the original data set.

After choosing a reference distribution, and drawing a sample from it as in (14.11), one has a supervised learning problem with a binary-valued output variable $Y \in \{0, 1\}$. The goal is to use this training data to find regions

$$R = \bigcap_{j \in \mathcal{J}} (X_j \in s_j) \tag{14.18}$$

for which the target function $\mu(x) = E(Y \mid x)$ is relatively large. In addition, one might wish to require that the *data* support of these regions

$$T(R) = \int_{x \in R} g(x)\, dx \tag{14.19}$$

not be too small.

14.2.6 Choice of Supervised Learning Method

The regions (14.18) are defined by conjunctive rules. Hence supervised methods that learn such rules would be most appropriate in this context. The terminal nodes of a CART decision tree are defined by rules precisely of the form (14.18). Applying CART to the pooled data (14.11) will produce a decision tree that attempts to model the target (14.10) over the entire data space by a disjoint set of regions (terminal nodes). Each region is defined by a rule of the form (14.18). Those terminal nodes t with high average y-values

$$\bar{y}_t = \text{ave}(y_i \mid x_i \in t)$$

are candidates for high-support generalized item sets (14.16). The actual (data) support is given by

$$T(R) = \bar{y}_t \cdot \frac{N_t}{N + N_0},$$

where N_t is the number of (pooled) observations within the region represented by the terminal node. By examining the resulting decision tree, one might discover interesting generalized item sets of relatively high-support. These can then be partitioned into antecedents and consequents in a search for generalized association rules of high confidence and/or lift.

Another natural learning method for this purpose is the patient rule induction method PRIM described in Section 9.3. PRIM also produces rules precisely of the form (14.18), but it is especially designed for finding high-support regions that maximize the average target (14.10) value within them, rather than trying to model the target function over the entire data space. It also provides more control over the support/average-target-value tradeoff.

14.2.7 Example: Market Basket Analysis (Continued)

We illustrate the use of PRIM on the demographics data of Table 14.1.

Three of the high-support generalized item sets emerging from the PRIM analysis were the following:

Item set 1: Support= 24%.

$$\begin{bmatrix} \text{marital status} & = & \textit{married} \\ \text{householder status} & = & \textit{own} \\ \text{type of home} & \neq & \textit{apartment} \end{bmatrix}$$

Item set 2: Support= 24%.

$$\begin{bmatrix} \text{age} & \leq & 24 \\ \text{marital status} & \in & \{\textit{living together-not married, single}\} \\ \text{occupation} & \notin & \{\textit{professional, homemaker, retired}\} \\ \text{household status} & \in & \{\textit{rent, live with family}\} \end{bmatrix}$$

Item set 3: Support= 15%.

$$\begin{bmatrix} \text{householder status} & = & \textit{rent} \\ \text{type of home} & \neq & \textit{house} \\ \text{number in household} & \leq & 2 \\ \text{number of children} & = & 0 \\ \text{occupation} & \notin & \{\textit{homemaker, student, unemployed}\} \\ \text{income} & \in & [\$20{,}000, \$150{,}000] \end{bmatrix}$$

Generalized association rules derived from these item sets with confidence (14.8) greater than 95% are the following:

Association rule 1: Support 25%, confidence 99.7% and lift 1.35.

$$\begin{bmatrix} \text{marital status} & = & \textit{married} \\ \text{householder status} & = & \textit{own} \end{bmatrix}$$
$$\Downarrow$$
$$\text{type of home} \neq \textit{apartment}$$

Association rule 2: Support 25%, confidence 98.7% and lift 1.97.

$$\begin{bmatrix} \text{age} & \leq & 24 \\ \text{occupation} & \notin & \{\textit{professional, homemaker, retired}\} \\ \text{household status} & \in & \{\textit{rent, live with family}\} \end{bmatrix}$$
$$\Downarrow$$
$$\text{marital status} \in \{\textit{single, living together-not married}\}$$

Association rule 3: Support 25%, confidence 95.9% and lift 2.61.

$$\begin{bmatrix} \text{householder status} & = & \textit{own} \\ \text{type of home} & \neq & \textit{apartment} \end{bmatrix}$$
$$\Downarrow$$
$$\text{marital status} = \textit{married}$$

Association rule 4: Support 15%, confidence 95.4% and lift 1.50.

$$\left[\begin{array}{rcl} \text{householder status} & = & \textit{rent} \\ \text{type of home} & \neq & \textit{house} \\ \text{number in household} & \leq & 2 \\ \text{occupation} & \notin & \{\textit{homemaker, student,unemployed}\} \\ \text{income} & \in & [\$20{,}000, \$150{,}000] \end{array}\right]$$
$$\Downarrow$$
$$\text{number of children} = 0$$

There are no great surprises among these particular rules. For the most part they verify intuition. In other contexts where there is less prior information available, unexpected results have a greater chance to emerge. These results do illustrate the type of information generalized association rules can provide, and that the supervised learning approach, coupled with a ruled induction method such as CART or PRIM, can uncover item sets exhibiting high associations among their constituents.

How do these generalized association rules compare to those found earlier by the Apriori algorithm? Since the Apriori procedure gives thousands of rules, it is difficult to compare them. However some general points can be made. The Apriori algorithm is exhaustive—it finds *all* rules with support greater than a specified amount. In contrast, PRIM is a greedy algorithm and is not guaranteed to give an "optimal" set of rules. On the other hand, the Apriori algorithm can deal only with dummy variables and hence could not find some of the above rules. For example, since *apartment* is a categorical input, with a dummy variable for each level, Apriori could not find a rule involving the set

$$\text{type of home} \neq \textit{apartment}.$$

To find this set, we would have to code a dummy variable for *apartment* versus the other categories of type of home. It will not generally be feasible to precode all such potentially interesting comparisons.

14.3 Cluster Analysis

Cluster analysis, also called data segmentation, has a variety of goals. All relate to grouping or segmenting a collection of objects into subsets or "clusters," such that those within each cluster are more closely related to one another than objects assigned to different clusters. An object can be described by a set of measurements, or by its relation to other objects. In addition, the goal is sometimes to arrange the clusters into a natural hierarchy. This involves successively grouping the clusters themselves so

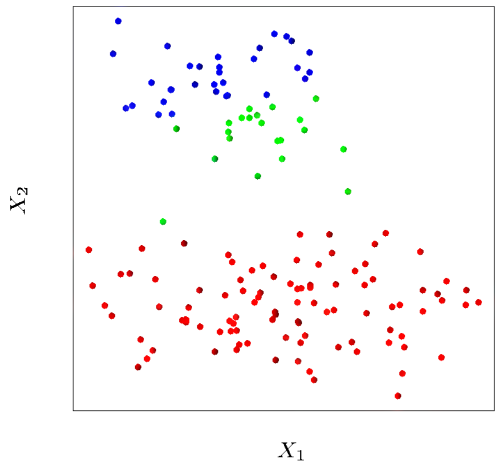

FIGURE 14.4. *Simulated data in the plane, clustered into three classes (represented by red, blue and green) by the K-means clustering algorithm*

that at each level of the hierarchy, clusters within the same group are more similar to each other than those in different groups.

Cluster analysis is also used to form descriptive statistics to ascertain whether or not the data consists of a set distinct subgroups, each group representing objects with substantially different properties. This latter goal requires an assessment of the degree of difference between the objects assigned to the respective clusters.

Central to all of the goals of cluster analysis is the notion of the degree of similarity (or dissimilarity) between the individual objects being clustered. A clustering method attempts to group the objects based on the definition of similarity supplied to it. This can only come from subject matter considerations. The situation is somewhat similar to the specification of a loss or cost function in prediction problems (supervised learning). There the cost associated with an inaccurate prediction depends on considerations outside the data.

Figure 14.4 shows some simulated data clustered into three groups via the popular K-means algorithm. In this case two of the clusters are not well separated, so that "segmentation" more accurately describes the part of this process than "clustering." K-means clustering starts with guesses for the three cluster centers. Then it alternates the following steps until convergence:

- for each data point, the closest cluster center (in Euclidean distance) is identified;

- each cluster center is replaced by the coordinatewise average of all data points that are closest to it.

We describe K-means clustering in more detail later, including the problem of how to choose the number of clusters (three in this example). K-means clustering is a *top-down* procedure, while other cluster approaches that we discuss are *bottom-up*. Fundamental to all clustering techniques is the choice of distance or dissimilarity measure between two objects. We first discuss distance measures before describing a variety of algorithms for clustering.

14.3.1 Proximity Matrices

Sometimes the data is represented directly in terms of the proximity (alikeness or affinity) between pairs of objects. These can be either *similarities* or *dissimilarities* (difference or lack of affinity). For example, in social science experiments, participants are asked to judge by how much certain objects differ from one another. Dissimilarities can then be computed by averaging over the collection of such judgments. This type of data can be represented by an $N \times N$ matrix $\mathbf{D}$, where N is the number of objects, and each element $d_{ii'}$ records the proximity between the ith and i'th objects. This matrix is then provided as input to the clustering algorithm.

Most algorithms presume a matrix of dissimilarities with nonnegative entries and zero diagonal elements: $d_{ii} = 0,\ i = 1, 2, \dots, N$. If the original data were collected as similarities, a suitable monotone-decreasing function can be used to convert them to dissimilarities. Also, most algorithms assume symmetric dissimilarity matrices, so if the original matrix $\mathbf{D}$ is not symmetric it must be replaced by $(\mathbf{D} + \mathbf{D}^T)/2$. Subjectively judged dissimilarities are seldom *distances* in the strict sense, since the triangle inequality $d_{ii'} \leq d_{ik} + d_{i'k}$, for all $k \in \{1, \dots, N\}$ does not hold. Thus, some algorithms that assume distances cannot be used with such data.

14.3.2 Dissimilarities Based on Attributes

Most often we have measurements x_{ij} for $i = 1, 2, \dots, N$, on variables $j = 1, 2, \dots, p$ (also called *attributes*). Since most of the popular clustering algorithms take a dissimilarity matrix as their input, we must first construct pairwise dissimilarities between the observations. In the most common case, we define a dissimilarity $d_j(x_{ij}, x_{i'j})$ between values of the jth attribute, and then define

$$D(x_i, x_{i'}) = \sum_{j=1}^{p} d_j(x_{ij}, x_{i'j}) \qquad (14.20)$$

as the dissimilarity between objects i and i'. By far the most common choice is squared distance

$$d_j(x_{ij}, x_{i'j}) = (x_{ij} - x_{i'j})^2. \tag{14.21}$$

However, other choices are possible, and can lead to potentially different results. For nonquantitative attributes (e.g., categorical data), squared distance may not be appropriate. In addition, it is sometimes desirable to weigh attributes differently rather than giving them equal weight as in (14.20).

We first discuss alternatives in terms of the attribute type:

- *Quantitative variables.* Measurements of this type of variable or attribute are represented by continuous real-valued numbers. It is natural to define the "error" between them as a monotone-increasing function of their absolute difference

  $$d(x_i, x_{i'}) = l(|x_i - x_{i'}|).$$

  Besides squared-error loss $(x_i - x_{i'})^2$, a common choice is the identity (absolute error). The former places more emphasis on larger differences than smaller ones. Alternatively, clustering can be based on the correlation

  $$\rho(x_i, x_{i'}) = \frac{\sum_j (x_{ij} - \bar{x}_i)(x_{i'j} - \bar{x}_{i'})}{\sqrt{\sum_j (x_{ij} - \bar{x}_i)^2 \sum_j (x_{i'j} - \bar{x}_{i'})^2}}, \tag{14.22}$$

  with $\bar{x}_i = \sum_j x_{ij}/p$. Note that this is averaged over *variables*, not observations. If the inputs are first standardized, then $\sum_j (x_{ij} - x_{i'j})^2 = 2(1 - \rho(x_i, x_{i'}))$. Hence clustering based on correlation (similarity) is equivalent to that based on squared distance (dissimilarity).

- *Ordinal variables.* The values of this type of variable are often represented as contiguous integers, and the realizable values are considered to be an ordered set. Examples are academic grades (A, B, C, D, F), degree of preference (can't stand, dislike, OK, like, terrific). Rank data are a special kind of ordinal data. Error measures for ordinal variables are generally defined by replacing their M original values with

  $$\frac{i - 1/2}{M}, \; i = 1, \ldots, M \tag{14.23}$$

  in the prescribed order of their original values. They are then treated as quantitative variables on this scale.

- *Categorical variables.* With unordered categorical (also called nominal) variables, the degree-of-difference between pairs of values must be delineated explicitly. If the variable assumes M distinct values, these can be arranged in a symmetric $M \times M$ matrix with elements $L_{rr'} = L_{r'r}, L_{rr} = 0, L_{rr'} \geq 0$. The most common choice is $L_{rr'} = 1$ for all $r \neq r$, while unequal losses can be used to emphasize some errors more than others.

14.3.3 Object Dissimilarity

Next we define a procedure for combining the p-individual attribute dissimilarities $d_j(x_{ij}, x_{i'j}),\ j = 1, 2, \ldots, p$ into a single overall measure of dissimilarity $D(x_i, x_{i'})$ between two objects or observations $(x_i, x_{i'})$ possessing the respective attribute values. This is nearly always done by means of a weighted average (convex combination)

$$D(x_i, x_{i'}) = \sum_{j=1}^{p} w_j \cdot d_j(x_{ij}, x_{i'j}); \quad \sum_{j=1}^{p} w_j = 1. \tag{14.24}$$

Here w_j is a weight assigned to the jth attribute regulating the relative influence of that variable in determining the overall dissimilarity between objects. This choice should be based on subject matter considerations.

It is important to realize that setting the weight w_j to the same value for each variable (say, $w_j = 1 \ \forall \ j$) does *not* necessarily give all attributes equal influence. The influence of the jth attribute X_j on object dissimilarity $D(x_i, x_{i'})$ (14.24) depends upon its relative contribution to the average object dissimilarity measure over all pairs of observations in the data set

$$\bar{D} = \frac{1}{N^2} \sum_{i=1}^{N} \sum_{i'=1}^{N} D(x_i, x_{i'}) = \sum_{j=1}^{p} w_j \cdot \bar{d}_j,$$

with

$$\bar{d}_j = \frac{1}{N^2} \sum_{i=1}^{N} \sum_{i'=1}^{N} d_j(x_{ij}, x_{i'j}) \tag{14.25}$$

being the average dissimilarity on the jth attribute. Thus, the relative influence of the jth variable is $w_j \cdot \bar{d}_j$, and setting $w_j \backsim 1/\bar{d}_j$ would give all attributes equal influence in characterizing overall dissimilarity between objects. For example, with p quantitative variables and squared-error distance used for each coordinate, then (14.24) becomes the (weighted) squared Euclidean distance

$$D_I(x_i, x_{i'}) = \sum_{j=1}^{p} w_j \cdot (x_{ij} - x_{i'j})^2 \tag{14.26}$$

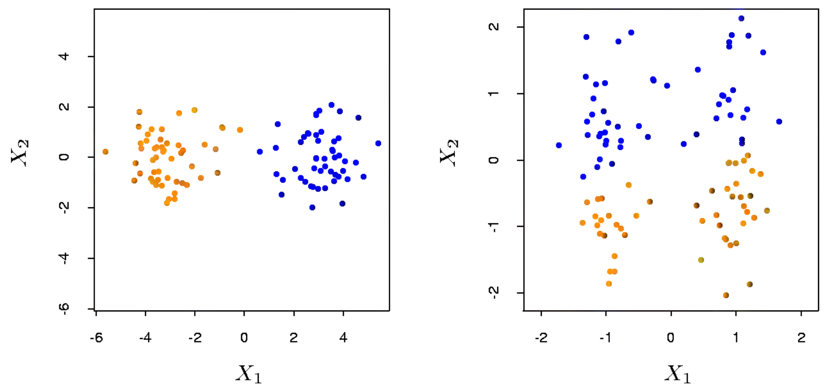

FIGURE 14.5. *Simulated data: on the left, K-means clustering (with $K=2$) has been applied to the raw data. The two colors indicate the cluster memberships. One the right, the features were first standardized before clustering. This is equivalent to using feature weights $1/[2 \cdot \text{var}(X_j)]$. The standardization has obscured the two well-separated groups. Note that each plot uses the same units in the horizontal and vertical axes.*

between pairs of points in an $\mathbb{R}^p$, with the quantitative variables as axes. In this case (14.25) becomes

$$\bar{d}_j = \frac{1}{N^2}\sum_{i=1}^{N}\sum_{i'=1}^{N}(x_{ij} - x_{i'j})^2 = 2 \cdot \text{var}_j, \tag{14.27}$$

where var_j is the sample estimate of $\text{Var}(X_j)$. Thus, the relative importance of each such variable is proportional to its variance over the data set. In general, setting $w_j = 1/\bar{d}_j$ for all attributes, irrespective of type, will cause each one of them to equally influence the overall dissimilarity between pairs of objects $(x_i, x_{i'})$. Although this may seem reasonable, and is often recommended, it can be highly counterproductive. If the goal is to segment the data into groups of similar objects, all attributes may not contribute equally to the (problem-dependent) notion of dissimilarity between objects. Some attribute value differences may reflect greater actual object dissimilarity in the context of the problem domain.

If the goal is to discover natural groupings in the data, some attributes may exhibit more of a grouping tendency than others. Variables that are more relevant in separating the groups should be assigned a higher influence in defining object dissimilarity. Giving all attributes equal influence in this case will tend to obscure the groups to the point where a clustering algorithm cannot uncover them. Figure 14.5 shows an example.

Although simple generic prescriptions for choosing the individual attribute dissimilarities $d_j(x_{ij}, x_{i'j})$ and their weights w_j can be comforting, there is no substitute for careful thought in the context of each individual problem. Specifying an appropriate dissimilarity measure is far more important in obtaining success with clustering than choice of clustering algorithm. This aspect of the problem is emphasized less in the clustering literature than the algorithms themselves, since it depends on domain knowledge specifics and is less amenable to general research.

Finally, often observations have *missing values* in one or more of the attributes. The most common method of incorporating missing values in dissimilarity calculations (14.24) is to omit each observation pair $x_{ij}, x_{i'j}$ having at least one value missing, when computing the dissimilarity between observations x_i and x_i'. This method can fail in the circumstance when both observations have no measured values in common. In this case both observations could be deleted from the analysis. Alternatively, the missing values could be imputed using the mean or median of each attribute over the nonmissing data. For categorical variables, one could consider the value "missing" as just another categorical value, if it were reasonable to consider two objects as being similar if they both have missing values on the same variables.

14.3.4 Clustering Algorithms

The goal of cluster analysis is to partition the observations into groups ("clusters") so that the pairwise dissimilarities between those assigned to the same cluster tend to be smaller than those in different clusters. Clustering algorithms fall into three distinct types: combinatorial algorithms, mixture modeling, and mode seeking.

Combinatorial algorithms work directly on the observed data with no direct reference to an underlying probability model. *Mixture modeling* supposes that the data is an *i.i.d* sample from some population described by a probability density function. This density function is characterized by a parameterized model taken to be a mixture of component density functions; each component density describes one of the clusters. This model is then fit to the data by maximum likelihood or corresponding Bayesian approaches. *Mode seekers* ("bump hunters") take a nonparametric perspective, attempting to directly estimate distinct modes of the probability density function. Observations "closest" to each respective mode then define the individual clusters.

Mixture modeling is described in Section 6.8. The PRIM algorithm, discussed in Sections 9.3 and 14.2.5, is an example of mode seeking or "bump hunting." We discuss combinatorial algorithms next.

14.3.5 Combinatorial Algorithms

The most popular clustering algorithms directly assign each observation to a group or cluster without regard to a probability model describing the data. Each observation is uniquely labeled by an integer $i \in \{1, \cdots, N\}$. A prespecified number of clusters $K < N$ is postulated, and each one is labeled by an integer $k \in \{1, \ldots, K\}$. Each observation is assigned to one and only one cluster. These assignments can be characterized by a many-to-one mapping, or *encoder* $k = C(i)$, that assigns the ith observation to the kth cluster. One seeks the particular encoder $C^*(i)$ that achieves the required goal (details below), based on the dissimilarities $d(x_i, x_{i'})$ between every pair of observations. These are specified by the user as described above. Generally, the encoder $C(i)$ is explicitly delineated by giving its value (cluster assignment) for each observation i. Thus, the "parameters" of the procedure are the individual cluster assignments for each of the N observations. These are adjusted so as to *minimize* a "loss" function that characterizes the degree to which the clustering goal is *not* met.

One approach is to directly specify a mathematical loss function and attempt to minimize it through some combinatorial optimization algorithm. Since the goal is to assign close points to the same cluster, a natural loss (or "energy") function would be

$$W(C) = \frac{1}{2}\sum_{k=1}^{K}\sum_{C(i)=k}\sum_{C(i')=k} d(x_i, x_{i'}). \tag{14.28}$$

This criterion characterizes the extent to which observations assigned to the same cluster tend to be close to one another. It is sometimes referred to as the "within cluster" point scatter since

$$T = \frac{1}{2}\sum_{i=1}^{N}\sum_{i'=1}^{N} d_{ii'} = \frac{1}{2}\sum_{k=1}^{K}\sum_{C(i)=k}\left(\sum_{C(i')=k} d_{ii'} + \sum_{C(i')\neq k} d_{ii'}\right),$$

or

$$T = W(C) + B(C),$$

where $d_{ii'} = d(x_i, x_{i'})$. Here T is the *total* point scatter, which is a constant given the data, independent of cluster assignment. The quantity

$$B(C) = \frac{1}{2}\sum_{k=1}^{K}\sum_{C(i)=k}\sum_{C(i')\neq k} d_{ii'} \tag{14.29}$$

is the *between-cluster* point scatter. This will tend to be large when observations assigned to different clusters are far apart. Thus one has

$$W(C) = T - B(C)$$

and minimizing $W(C)$ is equivalent to *maximizing* $B(C)$.

Cluster analysis by combinatorial optimization is straightforward in principle. One simply minimizes W or equivalently maximizes B over all possible assignments of the N data points to K clusters. Unfortunately, such optimization by complete enumeration is feasible only for very small data sets. The number of distinct assignments is (Jain and Dubes, 1988)

$$S(N,K) = \frac{1}{K!}\sum_{k=1}^{K}(-1)^{K-k}\binom{K}{k}k^N. \tag{14.30}$$

For example, $S(10,4) = 34,105$ which is quite feasible. But, $S(N,K)$ grows very rapidly with increasing values of its arguments. Already $S(19,4) \simeq 10^{10}$, and most clustering problems involve much larger data sets than $N = 19$. For this reason, practical clustering algorithms are able to examine only a very small fraction of all possible encoders $k = C(i)$. The goal is to identify a small subset that is likely to contain the optimal one, or at least a good suboptimal partition.

Such feasible strategies are based on iterative greedy descent. An initial partition is specified. At each iterative step, the cluster assignments are changed in such a way that the value of the criterion is improved from its previous value. Clustering algorithms of this type differ in their prescriptions for modifying the cluster assignments at each iteration. When the prescription is unable to provide an improvement, the algorithm terminates with the current assignments as its solution. Since the assignment of observations to clusters at any iteration is a perturbation of that for the previous iteration, only a very small fraction of all possible assignments (14.30) are examined. However, these algorithms converge to *local* optima which may be highly suboptimal when compared to the global optimum.

14.3.6 K-means

The K-means algorithm is one of the most popular iterative descent clustering methods. It is intended for situations in which all variables are of the quantitative type, and squared Euclidean distance

$$d(x_i, x_{i'}) = \sum_{j=1}^{p}(x_{ij} - x_{i'j})^2 = ||x_i - x_{i'}||^2$$

is chosen as the dissimilarity measure. Note that weighted Euclidean distance can be used by redefining the x_{ij} values (Exercise 14.1).

The within-point scatter (14.28) can be written as

$$W(C) \quad = \quad \frac{1}{2}\sum_{k=1}^{K}\sum_{C(i)=k}\sum_{C(i')=k}||x_i - x_{i'}||^2$$

Algorithm 14.1 *K-means clustering.*

1. For a given cluster assignment C, the total cluster variance (14.33) is minimized with respect to $\{m_1, \ldots, m_K\}$ yielding the means of the currently assigned clusters (14.32).

2. Given a current set of means $\{m_1, \ldots, m_K\}$, (14.33) is minimized by assigning each observation to the closest (current) cluster mean. That is,

$$C(i) = \underset{1 \leq k \leq K}{\operatorname{argmin}} ||x_i - m_k||^2. \tag{14.34}$$

3. Steps 1 and 2 are iterated until the assignments do not change.

$$= \sum_{k=1}^{K} \sum_{C(i)=k} ||x_i - \bar{x}_k||^2, \tag{14.31}$$

where $\bar{x}_k = (\bar{x}_{1k}, \ldots, \bar{x}_{pk})$ is the mean vector associated with the kth cluster. Thus, the criterion is minimized by assigning the N observations to the K clusters in such a way that within each cluster the average dissimilarity of the observations from the cluster mean, as defined by the points in that cluster, is minimized.

An iterative descent algorithm for solving

$$C^* = \min_C \sum_{k=1}^{K} \sum_{C(i)=k} ||x_i - \bar{x}_k||^2$$

can be obtained by noting that for any set of observations S

$$\bar{x}_S = \underset{m}{\operatorname{argmin}} \sum_{i \in S} ||x_i - m||^2. \tag{14.32}$$

Hence we can obtain C^* by solving the enlarged optimization problem

$$\min_{C, \{m_k\}_1^K} \sum_{k=1}^{K} \sum_{C(i)=k} ||x_i - m_k||^2. \tag{14.33}$$

This can be minimized by an alternating optimization procedure given in Algorithm 14.1.

Each of steps 1 and 2 reduces the value of the criterion (14.33), so that convergence is assured. However, the result may represent a suboptimal local minimum. The algorithm of Hartigan and Wong (1979) goes further, and ensures that there is no single switch of an observation from one group to another group that will decrease the objective. In addition, one should start the algorithm with many different random choices for the starting means, and choose the solution having smallest value of the objective function.

Figure 14.6 shows some of the K-means iterations for the simulated data of Figure 14.4. The centroids are depicted by "O"s. The straight lines show the partitioning of points, each sector being the set of points closest to each centroid. This partitioning is called the *Voronoi tessellation*. After 20 iterations the procedure has converged.

14.3.7 Gaussian Mixtures as Soft K-means Clustering

The K-means clustering procedure is closely related to the EM algorithm for estimating a certain Gaussian mixture model. (Sections 6.8 and 8.5.1). The M-step of the EM algorithm assigns "responsibilities" for each data point based in its relative density under each mixture component, while the E-step recomputes the component density parameters based on the current responsibilities. Suppose we specify K mixture components, each with a Gaussian density having scalar covariance matrix $\sigma^2\mathbf{I}$. Then the relative density under each mixture component is a monotone function of the Euclidean distance between the data point and the mixture center. Hence in this setup EM is a "soft" version of K-means clustering, making probabilistic (rather than deterministic) assignments of points to cluster centers. As the variance $\sigma^2 \to 0$, these probabilities become 0 and 1, and the two methods coincide. Details are given in Exercise 14.2. Figure 14.7 illustrates this result for two clusters on the real line.

14.3.8 Example: Human Tumor Microarray Data

We apply K-means clustering to the human tumor microarray data described in Chapter 1. This is an example of high-dimensional clustering. The data are a 6830×64 matrix of real numbers, each representing an expression measurement for a gene (row) and sample (column). Here we cluster the samples, each of which is a vector of length 6830, corresponding to expression values for the 6830 genes. Each sample has a label such as `breast` (for breast cancer), `melanoma`, and so on; we don't use these labels in the clustering, but will examine posthoc which labels fall into which clusters.

We applied K-means clustering with K running from 1 to 10, and computed the total within-sum of squares for each clustering, shown in Figure 14.8. Typically one looks for a kink in the sum of squares curve (or its logarithm) to locate the optimal number of clusters (see Section 14.3.11). Here there is no clear indication: for illustration we chose $K = 3$ giving the three clusters shown in Table 14.2.

We see that the procedure is successful at grouping together samples of the same cancer. In fact, the two breast cancers in the second cluster were

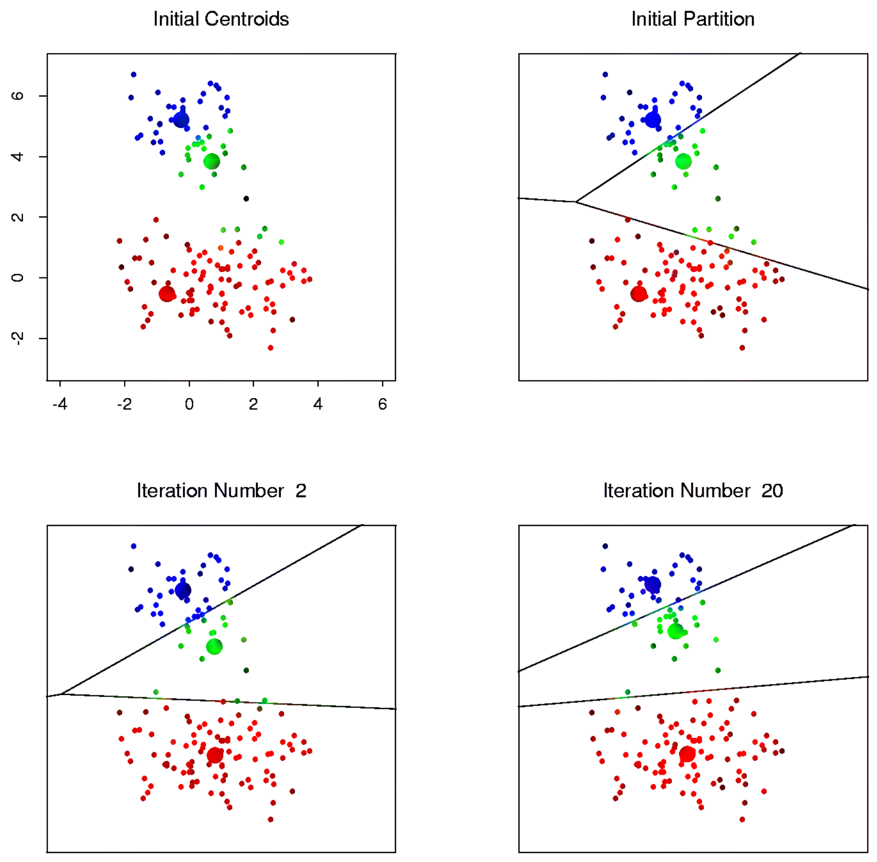

FIGURE 14.6. *Successive iterations of the K-means clustering algorithm for the simulated data of Figure 14.4.*

TABLE 14.2. *Human tumor data: number of cancer cases of each type, in each of the three clusters from K-means clustering.*

Cluster	`Breast`	`CNS`	`Colon`	`K562`	`Leukemia`	`MCF7`
1	3	5	0	0	0	0
2	2	0	0	2	6	2
3	2	0	7	0	0	0
Cluster	`Melanoma`	`NSCLC`	`Ovarian`	`Prostate`	`Renal`	`Unknown`
1	1	7	6	2	9	1
2	7	2	0	0	0	0
3	0	0	0	0	0	0

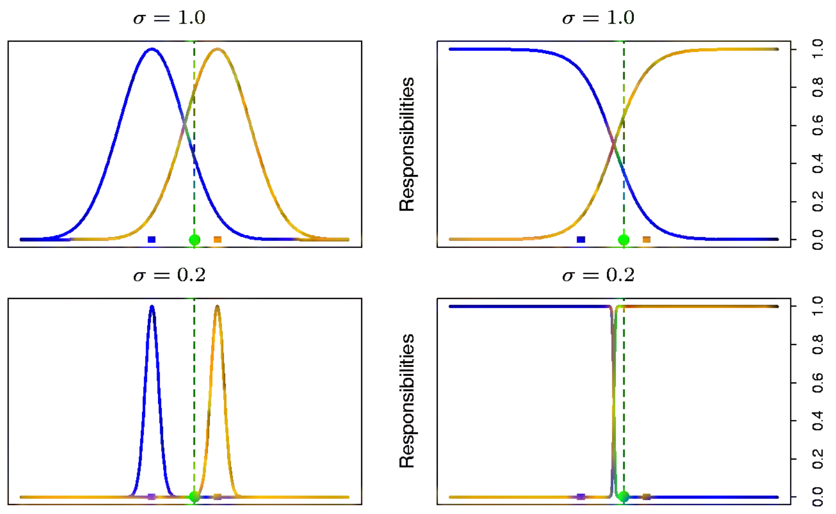

FIGURE 14.7. *Left panels: two Gaussian densities* $g_0(x)$ *and* $g_1(x)$ *(blue and orange) on the real line, and a single data point (green dot) at* $x = 0.5$*. The colored squares are plotted at* $x = -1.0$ *and* $x = 1.0$*, the means of each density. Right panels: the relative densities* $g_0(x)/(g_0(x)+g_1(x))$ *and* $g_1(x)/(g_0(x)+g_1(x))$*, called the "responsibilities" of each cluster, for this data point. In the top panels, the Gaussian standard deviation* $\sigma = 1.0$*; in the bottom panels* $\sigma = 0.2$*. The EM algorithm uses these responsibilities to make a "soft" assignment of each data point to each of the two clusters. When* σ *is fairly large, the responsibilities can be near 0.5 (they are 0.36 and 0.64 in the top right panel). As* $\sigma \to 0$*, the responsibilities* $\to 1$*, for the cluster center closest to the target point, and* 0 *for all other clusters. This "hard" assignment is seen in the bottom right panel.*

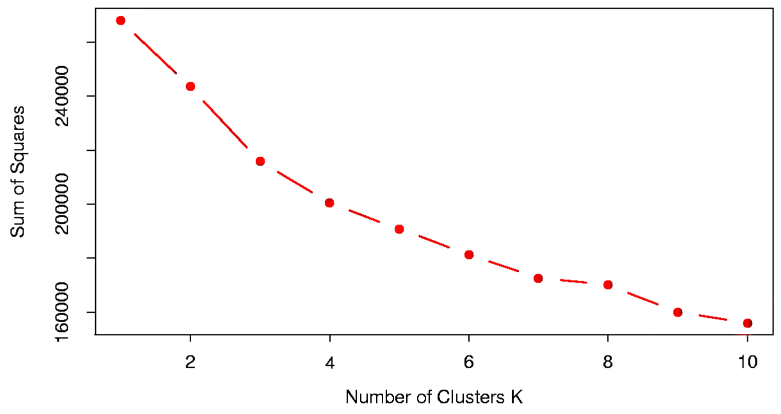

FIGURE 14.8. *Total within-cluster sum of squares for K-means clustering applied to the human tumor microarray data.*

later found to be misdiagnosed and were melanomas that had metastesized. However, K-means clustering has shortcomings in this application. For one, it does not give a linear ordering of objects within a cluster: we have simply listed them in alphabetic order above. Secondly, as the number of clusters K is changed, the cluster memberships can change in arbitrary ways. That is, with say four clusters, the clusters need not be nested within the three clusters above. For these reasons, hierarchical clustering (described later), is probably preferable for this application.

14.3.9 Vector Quantization

The K-means clustering algorithm represents a key tool in the apparently unrelated area of image and signal compression, particularly in *vector quantization* or VQ (Gersho and Gray, 1992). The left image in Figure 14.9[†] is a digitized photograph of a famous statistician, Sir Ronald Fisher. It consists of 1024×1024 pixels, where each pixel is a grayscale value ranging from 0 to 255, and hence requires 8 bits of storage per pixel. The entire image occupies 1 megabyte of storage. The center image is a VQ-compressed version of the left panel, and requires 0.239 of the storage (at some loss in quality). The right image is compressed even more, and requires only 0.0625 of the storage (at a considerable loss in quality).

The version of VQ implemented here first breaks the image into small blocks, in this case 2×2 blocks of pixels. Each of the 512×512 blocks of four

[†]This example was prepared by Maya Gupta.

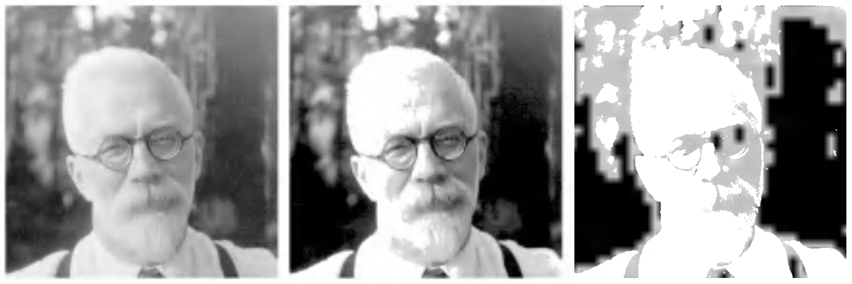

FIGURE 14.9. *Sir Ronald A. Fisher (1890-1962) was one of the founders of modern day statistics, to whom we owe maximum-likelihood, sufficiency, and many other fundamental concepts. The image on the left is a* 1024×1024 *grayscale image at* 8 *bits per pixel. The center image is the result of* 2×2 *block VQ, using* 200 *code vectors, with a compression rate of* 1.9 *bits/pixel. The right image uses only four code vectors, with a compression rate of* 0.50 *bits/pixel*

numbers is regarded as a vector in $\mathbb{R}^4$. A K-means clustering algorithm (also known as Lloyd's algorithm in this context) is run in this space. The center image uses $K = 200$, while the right image $K = 4$. Each of the 512×512 pixel blocks (or points) is approximated by its closest cluster centroid, known as a codeword. The clustering process is called the *encoding* step, and the collection of centroids is called the *codebook*.

To represent the approximated image, we need to supply for each block the identity of the codebook entry that approximates it. This will require $\log_2(K)$ bits per block. We also need to supply the codebook itself, which is $K \times 4$ real numbers (typically negligible). Overall, the storage for the compressed image amounts to $\log_2(K)/(4 \cdot 8)$ of the original (0.239 for $K = 200$, 0.063 for $K = 4$). This is typically expressed as a *rate* in bits per pixel: $\log_2(K)/4$, which are 1.91 and 0.50, respectively. The process of constructing the approximate image from the centroids is called the *decoding* step.

Why do we expect VQ to work at all? The reason is that for typical everyday images like photographs, many of the blocks look the same. In this case there are many almost pure white blocks, and similarly pure gray blocks of various shades. These require only one block each to represent them, and then multiple pointers to that block.

What we have described is known as *lossy* compression, since our images are degraded versions of the original. The degradation or *distortion* is usually measured in terms of mean squared error. In this case $D = 0.89$ for $K = 200$ and $D = 16.95$ for $K = 4$. More generally a rate/distortion curve would be used to assess the tradeoff. One can also perform *lossless* compression using block clustering, and still capitalize on the repeated patterns. If you took the original image and losslessly compressed it, the best you would do is 4.48 bits per pixel.

We claimed above that $\log_2(K)$ bits were needed to identify each of the K codewords in the codebook. This uses a fixed-length code, and is inefficient if some codewords occur many more times than others in the image. Using Shannon coding theory, we know that in general a variable length code will do better, and the rate then becomes $-\sum_{\ell=1}^{K} p_\ell \log_2(p_\ell)/4$. The term in the numerator is the entropy of the distribution p_ℓ of the codewords in the image. Using variable length coding our rates come down to 1.42 and 0.39, respectively. Finally, there are many generalization of VQ that have been developed: for example, tree-structured VQ finds the centroids with a top-down, 2-means style algorithm, as alluded to in Section 14.3.12. This allows successive refinement of the of the compression. Further details may be found in Gersho and Gray (1992).

14.3.10 K-medoids

As discussed above, the K-means algorithm is appropriate when the dissimilarity measure is taken to be squared Euclidean distance $D(x_i, x_{i'})$ (14.74). This requires all of the variables to be of the quantitative type. In addition, using *squared* Euclidean distance places the highest influence on the largest distances. This causes the procedure to lack robustness against outliers that produce very large distances. These restrictions can be removed at the expense of computation.

The only part of the K-means algorithm that assumes squared Euclidean distance is the minimization step (14.32); the cluster representatives $\{m_1, \ldots, m_K\}$ in (14.33) are taken to be the means of the currently assigned clusters. The algorithm can be generalized for use with arbitrarily defined dissimilarities $D(x_i, x_{i'})$ by replacing this step by an explicit optimization with respect to $\{m_1, \ldots, m_K\}$ in (14.33). In the most common form, centers for each cluster are restricted to be one of the observations assigned to the cluster, as summarized in Algorithm 14.2. This algorithm assumes attribute data, but the approach can also be applied to data described *only* by proximity matrices (Section 14.3.1). There is no need to explicitly compute cluster centers; rather we just keep track of the indices i_k^*.

Solving (14.32) for each provisional cluster k requires an amount of computation proportional to the number of observations assigned to it, whereas for solving (14.35) the computation increases to $O(N_k^2)$. Given a set of cluster "centers," $\{i_1, \ldots, i_K\}$, obtaining the new assignments

$$C(i) = \underset{1 \le k \le K}{\operatorname{argmin}}\, d_{ii_k^*} \tag{14.37}$$

requires computation proportional to $K \cdot N$ as before. Thus, K-medoids is far more computationally intensive than K-means.

Algorithm 14.2 *K-medoids clustering.*

1. For a given cluster assignment C find the observation in the cluster minimizing total distance to other points in that cluster:
$$i_k^* = \operatorname*{argmin}_{\{i:C(i)=k\}} \sum_{C(i')=k} D(x_i, x_{i'}). \tag{14.35}$$
Then $m_k = x_{i_k^*}$, $k = 1, 2, \ldots, K$ are the current estimates of the cluster centers.

2. Given a current set of cluster centers $\{m_1, \ldots, m_K\}$, minimize the total error by assigning each observation to the closest (current) cluster center:
$$C(i) = \operatorname*{argmin}_{1\le k\le K} D(x_i, m_k). \tag{14.36}$$

3. Iterate steps 1 and 2 until the assignments do not change.

Alternating between (14.35) and (14.37) represents a particular heuristic search strategy for trying to solve
$$\min_{C,\ \{i_k\}_1^K} \sum_{k=1}^{K} \sum_{C(i)=k} d_{ii_k}. \tag{14.38}$$
Kaufman and Rousseeuw (1990) propose an alternative strategy for directly solving (14.38) that provisionally exchanges each center i_k with an observation that is not currently a center, selecting the exchange that produces the greatest reduction in the value of the criterion (14.38). This is repeated until no advantageous exchanges can be found. Massart et al. (1983) derive a branch-and-bound combinatorial method that finds the global minimum of (14.38) that is practical only for very small data sets.

Example: Country Dissimilarities

This example, taken from Kaufman and Rousseeuw (1990), comes from a study in which political science students were asked to provide pairwise dissimilarity measures for 12 countries: Belgium, Brazil, Chile, Cuba, Egypt, France, India, Israel, United States, Union of Soviet Socialist Republics, Yugoslavia and Zaire. The average dissimilarity scores are given in Table 14.3. We applied 3-medoid clustering to these dissimilarities. Note that K-means clustering could not be applied because we have only distances rather than raw observations. The left panel of Figure 14.10 shows the dissimilarities reordered and blocked according to the 3-medoid clustering. The right panel is a two-dimensional multidimensional scaling plot, with

TABLE 14.3. *Data from a political science survey: values are average pairwise dissimilarities of countries from a questionnaire given to political science students.*

	BEL	BRA	CHI	CUB	EGY	FRA	IND	ISR	USA	USS	YUG
BRA	5.58										
CHI	7.00	6.50									
CUB	7.08	7.00	3.83								
EGY	4.83	5.08	8.17	5.83							
FRA	2.17	5.75	6.67	6.92	4.92						
IND	6.42	5.00	5.58	6.00	4.67	6.42					
ISR	3.42	5.50	6.42	6.42	5.00	3.92	6.17				
USA	2.50	4.92	6.25	7.33	4.50	2.25	6.33	2.75			
USS	6.08	6.67	4.25	2.67	6.00	6.17	6.17	6.92	6.17		
YUG	5.25	6.83	4.50	3.75	5.75	5.42	6.08	5.83	6.67	3.67	
ZAI	4.75	3.00	6.08	6.67	5.00	5.58	4.83	6.17	5.67	6.50	6.92

the 3-medoid clusters assignments indicated by colors (multidimensional scaling is discussed in Section 14.7.) Both plots show three well-separated clusters, but the MDS display indicates that "Egypt" falls about halfway between two clusters.

14.3.11 Practical Issues

In order to apply K-means or K-medoids one must select the number of clusters K^* and an initialization. The latter can be defined by specifying an initial set of centers $\{m_1, \dots, m_K\}$ or $\{i_1, \dots, i_K\}$ or an initial encoder $C(i)$. Usually specifying the centers is more convenient. Suggestions range from simple random selection to a deliberate strategy based on forward stepwise assignment. At each step a new center i_k is chosen to minimize the criterion (14.33) or (14.38), given the centers $i_1, \dots, i_{k-1}$ chosen at the previous steps. This continues for K steps, thereby producing K initial centers with which to begin the optimization algorithm.

A choice for the number of clusters K depends on the goal. For data segmentation K is usually defined as part of the problem. For example, a company may employ K sales people, and the goal is to partition a customer data base into K segments, one for each sales person, such that the customers assigned to each one are as similar as possible. Often, however, cluster analysis is used to provide a descriptive statistic for ascertaining the extent to which the observations comprising the data base fall into natural distinct groupings. Here the number of such groups K^* is unknown and one requires that it, as well as the groupings themselves, be estimated from the data.

Data-based methods for estimating K^* typically examine the within-cluster dissimilarity W_K as a function of the number of clusters K. Separate

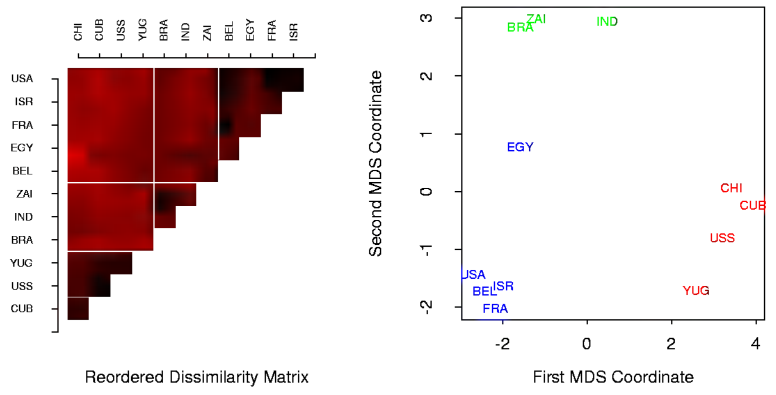

FIGURE 14.10. *Survey of country dissimilarities. Left panel: dissimilarities reordered and blocked according to* 3*-medoid clustering. Heat map is coded from most similar (dark red) to least similar (bright red). Right panel: two-dimensional multidimensional scaling plot, with* 3*-medoid clusters indicated by different colors.*

solutions are obtained for $K \in \{1, 2, \ldots, K_{\max}\}$. The corresponding values $\{W_1, W_2, \ldots, W_{K_{\max}}\}$ generally decrease with increasing K. This will be the case even when the criterion is evaluated on an independent test set, since a large number of cluster centers will tend to fill the feature space densely and thus will be close to all data points. Thus cross-validation techniques, so useful for model selection in supervised learning, cannot be utilized in this context.

The intuition underlying the approach is that if there are actually K^* distinct groupings of the observations (as defined by the dissimilarity measure), then for $K < K^*$ the clusters returned by the algorithm will each contain a subset of the true underlying groups. That is, the solution will not assign observations in the same naturally occurring group to different estimated clusters. To the extent that this is the case, the solution criterion value will tend to decrease substantially with each successive increase in the number of specified clusters, $W_{K+1} \ll W_K$, as the natural groups are successively assigned to separate clusters. For $K > K^*$, one of the estimated clusters must partition at least one of the natural groups into two subgroups. This will tend to provide a smaller decrease in the criterion as K is further increased. Splitting a natural group, within which the observations are all quite close to each other, reduces the criterion less than partitioning the union of two well-separated groups into their proper constituents.

To the extent this scenario is realized, there will be a sharp decrease in successive differences in criterion value, $W_K - W_{K+1}$, at $K = K^*$. That is, $\{W_K - W_{K+1} \,|\, K < K^*\} \ll \{W_K - W_{K+1} \,|\, K \geq K^*\}$. An estimate

$\hat{K}^*$ for K^* is then obtained by identifying a "kink" in the plot of W_K as a function of K. As with other aspects of clustering procedures, this approach is somewhat heuristic.

The recently proposed *Gap statistic* (Tibshirani et al., 2001) compares the curve $\log W_K$ to the curve obtained from data uniformly distributed over a rectangle containing the data. It estimates the optimal number of clusters to be the place where the gap between the two curves in largest. Essentially this is an automatic way of locating the aforementioned "kink." It also works reasonably well when the data fall into a single cluster, and in that case will tend to estimate the optimal number of clusters to be one. This is the scenario where most other competing methods fail.

Figure 14.11 shows the result of the Gap statistic applied to simulated data of Figure 14.4. The left panel shows $\log W_K$ for $k = 1, 2, \ldots, 8$ clusters (solid curve) and the expected value of $\log W_K$ over 20 simulations from uniform data (broken curve). The right panel shows the gap curve, which is the expected curve minus the observed curve. Shown also are error bars of half-width $s'_K = s_K\sqrt{1 + 1/20}$, where s_K is the standard deviation of $\log W_K$ over the 20 simulations. The Gap curve is maximized at $K = 2$ clusters. If $G(K)$ is the Gap curve at K clusters, the formal rule for estimating K^* is

$$K^* = \underset{K}{\operatorname{argmin}}\{K | G(K) \geq G(K+1) - s'_{K+1}\}. \tag{14.39}$$

This gives $K^* = 2$, which looks reasonable from Figure 14.4.

14.3.12 Hierarchical Clustering

The results of applying K-means or K-medoids clustering algorithms depend on the choice for the number of clusters to be searched and a starting configuration assignment. In contrast, hierarchical clustering methods do not require such specifications. Instead, they require the user to specify a measure of dissimilarity between (disjoint) *groups* of observations, based on the pairwise dissimilarities among the observations in the two groups. As the name suggests, they produce hierarchical representations in which the clusters at each level of the hierarchy are created by merging clusters at the next lower level. At the lowest level, each cluster contains a single observation. At the highest level there is only one cluster containing all of the data.

Strategies for hierarchical clustering divide into two basic paradigms: *agglomerative* (bottom-up) and *divisive* (top-down). Agglomerative strategies start at the bottom and at each level recursively merge a selected pair of clusters into a single cluster. This produces a grouping at the next higher level with one less cluster. The pair chosen for merging consist of the two groups with the smallest intergroup dissimilarity. Divisive methods start at the top and at each level recursively split one of the existing clusters at

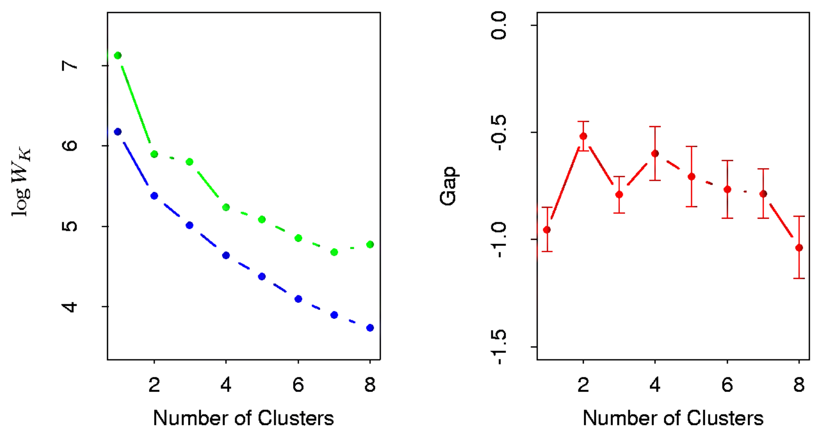

FIGURE 14.11. *Left panel: observed (green) and expected (blue) values of* $\log W_K$ *for the simulated data of Figure 14.4. Right panel: Gap curve, equal to the difference between the observed and expected values of* $\log W_K$*. The Gap estimate* K^* *is the smallest* K *producing a gap within one standard deviation of the maximum; here* $K^* = 2$.

that level into two new clusters. The split is chosen to produce two new groups with the largest between-group dissimilarity. With both paradigms there are $N - 1$ levels in the hierarchy.

Each level of the hierarchy represents a particular grouping of the data into disjoint clusters of observations. The entire hierarchy represents an ordered sequence of such groupings. It is up to the user to decide which level (if any) actually represents a "natural" clustering in the sense that observations within each of its groups are sufficiently more similar to each other than to observations assigned to different groups at that level. The Gap statistic described earlier can be used for this purpose.

Recursive binary splitting/agglomeration can be represented by a rooted binary tree. The nodes of the trees represent groups. The root node represents the entire data set. The N terminal nodes each represent one of the individual observations (singleton clusters). Each nonterminal node ("parent") has two daughter nodes. For divisive clustering the two daughters represent the two groups resulting from the split of the parent; for agglomerative clustering the daughters represent the two groups that were merged to form the parent.

All agglomerative and some divisive methods (when viewed bottom-up) possess a monotonicity property. That is, the dissimilarity between merged clusters is monotone increasing with the level of the merger. Thus the binary tree can be plotted so that the height of each node is proportional to the value of the intergroup dissimilarity between its two daughters. The

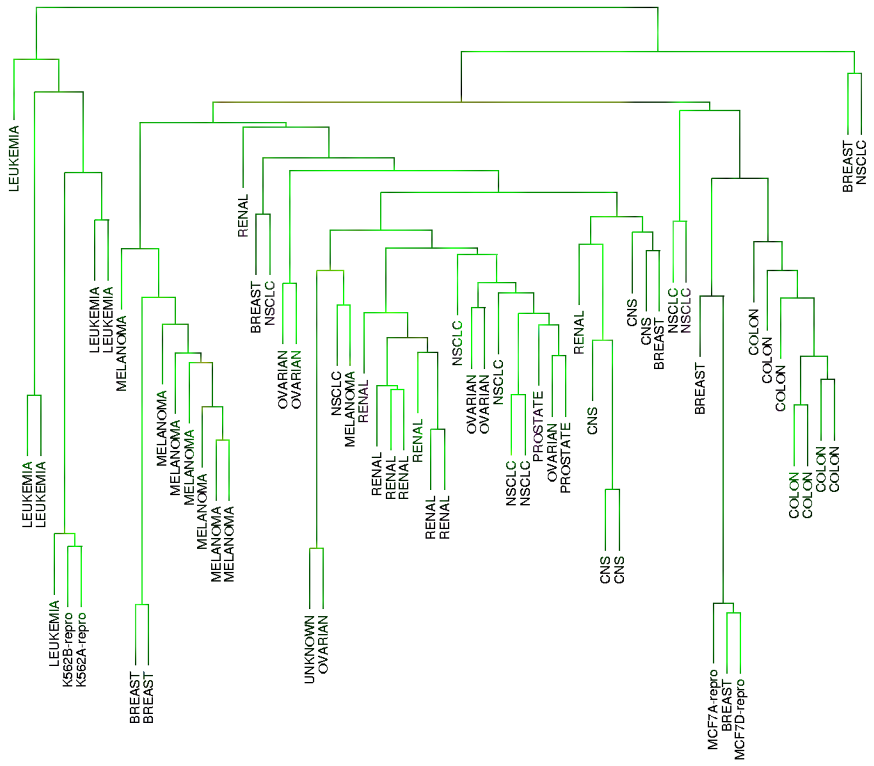

FIGURE 14.12. *Dendrogram from agglomerative hierarchical clustering with average linkage to the human tumor microarray data.*

terminal nodes representing individual observations are all plotted at zero height. This type of graphical display is called a *dendrogram*.

A dendrogram provides a highly interpretable complete description of the hierarchical clustering in a graphical format. This is one of the main reasons for the popularity of hierarchical clustering methods.

For the microarray data, Figure 14.12 shows the dendrogram resulting from agglomerative clustering with average linkage; agglomerative clustering and this example are discussed in more detail later in this chapter. Cutting the dendrogram horizontally at a particular height partitions the data into disjoint clusters represented by the vertical lines that intersect it. These are the clusters that would be produced by terminating the procedure when the optimal intergroup dissimilarity exceeds that threshold cut value. Groups that merge at high values, relative to the merger values of the subgroups contained within them lower in the tree, are candidates for natural clusters. Note that this may occur at several different levels, indicating a clustering hierarchy: that is, clusters nested within clusters.

Such a dendrogram is often viewed as a graphical summary of the data itself, rather than a description of the results of the algorithm. However, such interpretations should be treated with caution. First, different hierarchical methods (see below), as well as small changes in the data, can lead to quite different dendrograms. Also, such a summary will be valid only to the extent that the pairwise *observation* dissimilarities possess the hierarchical structure produced by the algorithm. Hierarchical methods impose hierarchical structure whether or not such structure actually exists in the data.

The extent to which the hierarchical structure produced by a dendrogram actually represents the data itself can be judged by the *cophenetic correlation coefficient*. This is the correlation between the $N(N-1)/2$ pairwise observation dissimilarities $d_{ii'}$ input to the algorithm and their corresponding *cophenetic* dissimilarities $d_{ii'}$ derived from the dendrogram. The cophenetic dissimilarity $C_{ii'}$ between two observations (i, i') is the intergroup dissimilarity at which observations i and i' are first joined together in the same cluster.

The cophenetic dissimilarity is a very restrictive dissimilarity measure. First, the $C_{ii'}$ over the observations must contain many ties, since only $N-1$ of the total $N(N-1)/2$ values can be distinct. Also these dissimilarities obey the *ultrametric inequality*

$$C_{ii'} \leq \max\{C_{ik}, C_{i'k}\} \tag{14.40}$$

for any three observations (i, i', k). As a geometric example, suppose the data were represented as points in a Euclidean coordinate system. In order for the set of interpoint distances over the data to conform to (14.40), the triangles formed by all triples of points must be isosceles triangles with the unequal length no longer than the length of the two equal sides (Jain and Dubes, 1988). Therefore it is unrealistic to expect general dissimilarities over arbitrary data sets to closely resemble their corresponding cophenetic dissimilarities as calculated from a dendrogram, especially if there are not many tied values. Thus the dendrogram should be viewed mainly as a description of the *clustering* structure of the data as imposed by the particular algorithm employed.

Agglomerative Clustering

Agglomerative clustering algorithms begin with every observation representing a singleton cluster. At each of the $N-1$ steps the closest two (least dissimilar) clusters are merged into a single cluster, producing one less cluster at the next higher level. Therefore, a measure of dissimilarity between two clusters (groups of observations) must be defined.

Let G and H represent two such groups. The dissimilarity $d(G, H)$ between G and H is computed from the set of pairwise observation dissimilarities $d_{ii'}$ where one member of the pair i is in G and the other i' is

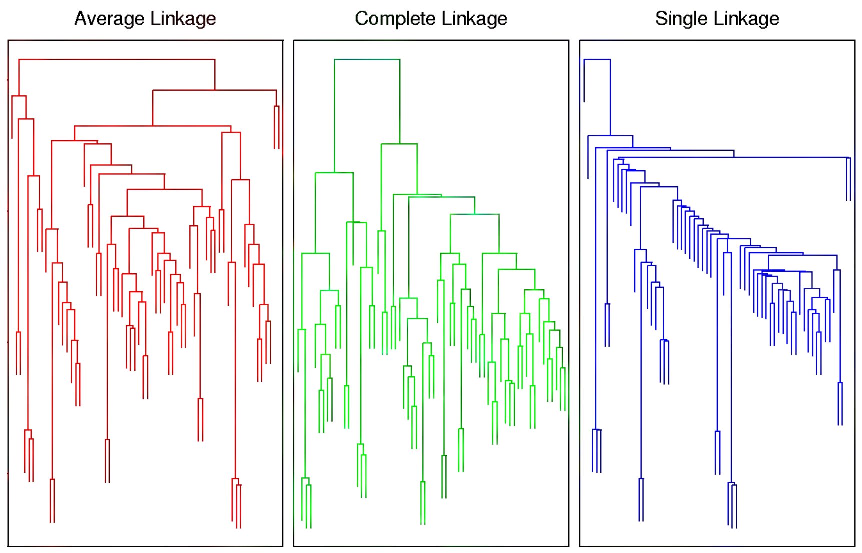

FIGURE 14.13. *Dendrograms from agglomerative hierarchical clustering of human tumor microarray data.*

in H. *Single linkage* (SL) agglomerative clustering takes the intergroup dissimilarity to be that of the closest (least dissimilar) pair

$$d_{SL}(G,H) = \min_{\substack{i\in G\\ i'\in H}} d_{ii'}. \tag{14.41}$$

This is also often called the *nearest-neighbor* technique. *Complete linkage* (CL) agglomerative clustering (*furthest-neighbor* technique) takes the intergroup dissimilarity to be that of the furthest (most dissimilar) pair

$$d_{CL}(G,H) = \max_{\substack{i\in G\\ i'\in H}} d_{ii'}. \tag{14.42}$$

Group average (GA) clustering uses the average dissimilarity between the groups

$$d_{GA}(G,H) = \frac{1}{N_G N_H}\sum_{i\in G}\sum_{i'\in H} d_{ii'} \tag{14.43}$$

where N_G and N_H are the respective number of observations in each group. Although there have been many other proposals for defining intergroup dissimilarity in the context of agglomerative clustering, the above three are the ones most commonly used. Figure 14.13 shows examples of all three.

If the data dissimilarities $\{d_{ii'}\}$ exhibit a strong clustering tendency, with each of the clusters being compact and well separated from others, then all three methods produce similar results. Clusters are compact if the all of the observations within them are relatively close together (small dissimilarities) as compared with observations in different clusters. To the extent this is not the case, results will differ.

Single linkage (14.41) only requires that a single dissimilarity $d_{ii'}$, $i \in G$ and $i' \in H$, be small for two groups G and H to be considered close together, irrespective of the other observation dissimilarities between the groups. It will therefore have a tendency to combine, at relatively low thresholds, observations linked by a series of close intermediate observations. This phenomenon, referred to as *chaining*, is often considered a defect of the method. The clusters produced by single linkage can violate the "compactness" property that all observations within each cluster tend to be similar to one another, based on the supplied observation dissimilarities $\{d_{ii'}\}$. If we define the *diameter* D_G of a group of observations as the largest dissimilarity among its members

$$D_G = \max_{\substack{i \in G \\ i' \in G}} d_{ii'}, \tag{14.44}$$

then single linkage can produce clusters with very large diameters.

Complete linkage (14.42) represents the opposite extreme. Two groups G and H are considered close only if all of the observations in their union are relatively similar. It will tend to produce compact clusters with small diameters (14.44). However, it can produce clusters that violate the "closeness" property. That is, observations assigned to a cluster can be much closer to members of other clusters than they are to some members of their own cluster.

Group average clustering (14.43) represents a compromise between the two extremes of single and complete linkage. It attempts to produce *relatively* compact clusters that are *relatively* far apart. However, its results depend on the numerical scale on which the observation dissimilarities $d_{ii'}$ are measured. Applying a monotone strictly increasing transformation $h(\cdot)$ to the $d_{ii'}$, $h_{ii'} = h(d_{ii'})$, can change the result produced by (14.43). In contrast, (14.41) and (14.42) depend only on the ordering of the $d_{ii'}$ and are thus invariant to such monotone transformations. This invariance is often used as an argument in favor of single or complete linkage over group average methods.

Kelly and Rice (1990) argue that group average clustering has a statistical consistency property violated by single and complete linkage. Assume we have attribute-value data $X = (X_1, \dots, X_p)$ and that each cluster k is a random sample from some population joint density $g_k(x)$. The complete data set is a random sample from a mixture of K such densities. The group average dissimilarity $d_{GA}(G, H)$ (14.43) is an estimate of

$$\int\int d(x, x')\, p_G(x)\, p_H(x')\, dx\, dx', \tag{14.45}$$

where $d(x, x')$ is the dissimilarity between points x and x' in the space of attribute values. As the sample size N approaches infinity $d_{GA}(G, H)$ (14.43) approaches (14.45), which is a characteristic of the relationship between the two densities $p_G(x)$ and $p_H(x)$. For single linkage, $d_{SL}(G, H)$ (14.41) approaches zero as $N \to \infty$ independent of $p_G(x)$ and $p_H(x)$. For complete linkage, $d_{CL}(G, H)$ (14.42) becomes infinite as $N \to \infty$, again independent of the two densities. Thus, it is not clear what aspects of the population distribution are being estimated by $d_{SL}(G, H)$ and $d_{CL}(G, H)$.

Example: Human Cancer Microarray Data (Continued)

The left panel of Figure 14.13 shows the dendrogram resulting from average linkage agglomerative clustering of the samples (columns) of the microarray data. The middle and right panels show the result using complete and single linkage. Average and complete linkage gave similar results, while single linkage produced unbalanced groups with long thin clusters. We focus on the average linkage clustering.

Like K-means clustering, hierarchical clustering is successful at clustering simple cancers together. However it has other nice features. By cutting off the dendrogram at various heights, different numbers of clusters emerge, and the sets of clusters are nested within one another. Secondly, it gives some partial ordering information about the samples. In Figure 14.14, we have arranged the genes (rows) and samples (columns) of the expression matrix in orderings derived from hierarchical clustering.

Note that if we flip the orientation of the branches of a dendrogram at any merge, the resulting dendrogram is still consistent with the series of hierarchical clustering operations. Hence to determine an ordering of the leaves, we must add a constraint. To produce the row ordering of Figure 14.14, we have used the default rule in S-PLUS: at each merge, the subtree with the tighter cluster is placed to the left (toward the bottom in the rotated dendrogram in the figure.) Individual genes are the tightest clusters possible, and merges involving two individual genes place them in order by their observation number. The same rule was used for the columns. Many other rules are possible—for example, ordering by a multidimensional scaling of the genes; see Section 14.7.

The two-way rearrangement of Figure14.14 produces an informative picture of the genes and samples. This picture is more informative than the randomly ordered rows and columns of Figure 1.3 of Chapter 1. Furthermore, the dendrograms themselves are useful, as biologists can, for example, interpret the gene clusters in terms of biological processes.

Divisive Clustering

Divisive clustering algorithms begin with the entire data set as a single cluster, and recursively divide one of the existing clusters into two daughter clusters at each iteration in a top-down fashion. This approach has not

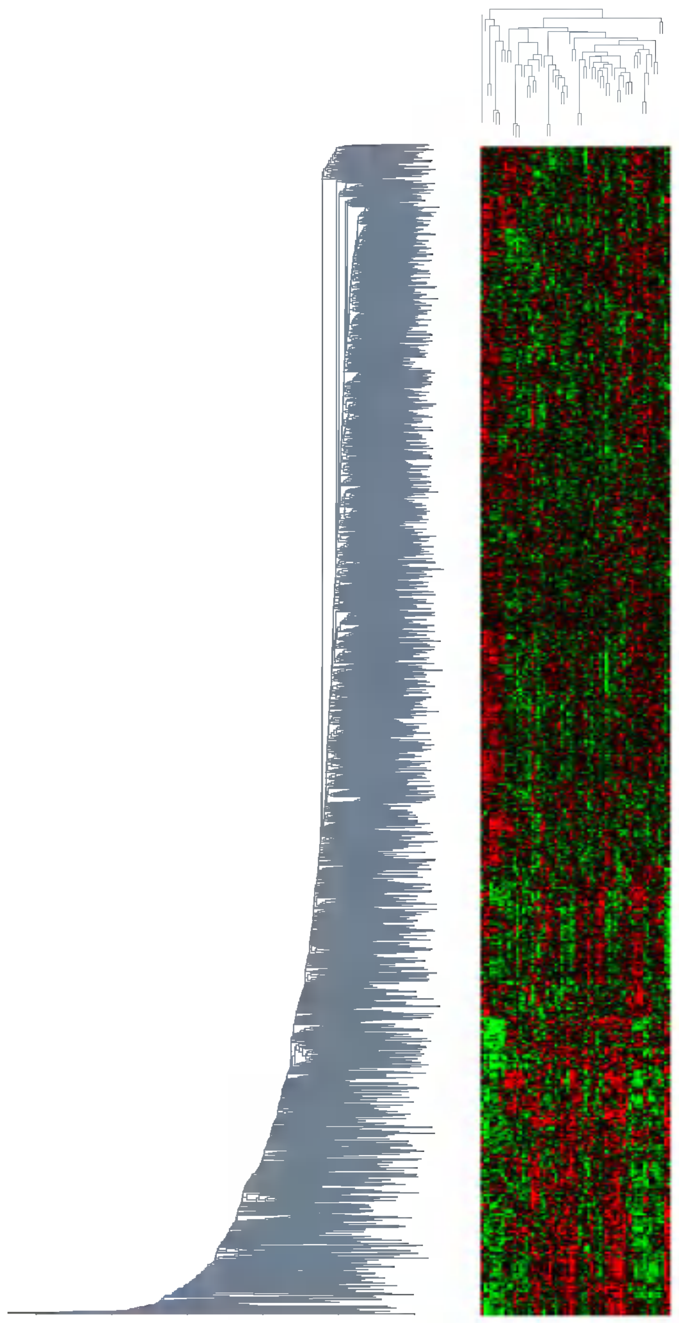

FIGURE 14.14. *DNA microarray data: average linkage hierarchical clustering has been applied independently to the rows (genes) and columns (samples), determining the ordering of the rows and columms (see text). The colors range from bright green (negative, underexpressed) to bright red (positive, overexpressed).*

been studied nearly as extensively as agglomerative methods in the clustering literature. It has been explored somewhat in the engineering literature (Gersho and Gray, 1992) in the context of compression. In the clustering setting, a potential advantage of divisive over agglomerative methods can occur when interest is focused on partitioning the data into a relatively *small* number of clusters.

The divisive paradigm can be employed by recursively applying any of the combinatorial methods such as K-means (Section 14.3.6) or K-medoids (Section 14.3.10), with $K = 2$, to perform the splits at each iteration. However, such an approach would depend on the starting configuration specified at each step. In addition, it would not necessarily produce a splitting sequence that possesses the monotonicity property required for dendrogram representation.

A divisive algorithm that avoids these problems was proposed by Macnaughton Smith et al. (1965). It begins by placing all observations in a single cluster G. It then chooses that observation whose average dissimilarity from all the other observations is largest. This observation forms the first member of a second cluster H. At each successive step that observation in G whose average distance from those in H, minus that for the remaining observations in G is largest, is transferred to H. This continues until the corresponding difference in averages becomes negative. That is, there are no longer any observations in G that are, on average, closer to those in H. The result is a split of the original cluster into two daughter clusters, the observations transferred to H, and those remaining in G. These two clusters represent the second level of the hierarchy. Each successive level is produced by applying this splitting procedure to one of the clusters at the previous level. Kaufman and Rousseeuw (1990) suggest choosing the cluster at each level with the largest diameter (14.44) for splitting. An alternative would be to choose the one with the largest average dissimilarity among its members

$$\bar{d}_G = \frac{1}{N_G} \sum_{i \in G} \sum_{i' \in G} d_{ii'}.$$

The recursive splitting continues until all clusters either become singletons or all members of each one have zero dissimilarity from one another.

14.4 Self-Organizing Maps

This method can be viewed as a constrained version of K-means clustering, in which the prototypes are encouraged to lie in a one- or two-dimensional manifold in the feature space. The resulting manifold is also referred to as a *constrained topological map*, since the original high-dimensional observations can be mapped down onto the two-dimensional coordinate system.

The original SOM algorithm was online—observations are processed one at a time—and later a batch version was proposed. The technique also bears a close relationship to *principal curves and surfaces*, which are discussed in the next section.

We consider a SOM with a two-dimensional rectangular grid of K prototypes $m_j \in \mathbb{R}^p$ (other choices, such as hexagonal grids, can also be used). Each of the K prototypes are parametrized with respect to an integer coordinate pair $\ell_j \in \mathcal{Q}_1 \times \mathcal{Q}_2$. Here $\mathcal{Q}_1 = \{1, 2, \dots, q_1\}$, similarly $\mathcal{Q}_2$, and $K = q_1 \cdot q_2$. The m_j are initialized, for example, to lie in the two-dimensional principal component plane of the data (next section). We can think of the prototypes as "buttons," "sewn" on the principal component plane in a regular pattern. The SOM procedure tries to bend the plane so that the buttons approximate the data points as well as possible. Once the model is fit, the observations can be mapped down onto the two-dimensional grid.

The observations x_i are processed one at a time. We find the closest prototype m_j to x_i in Euclidean distance in $\mathbb{R}^p$, and then for all neighbors m_k of m_j, move m_k toward x_i via the update

$$m_k \leftarrow m_k + \alpha(x_i - m_k). \tag{14.46}$$

The "neighbors" of m_j are defined to be all m_k such that the distance between ℓ_j and ℓ_k is small. The simplest approach uses Euclidean distance, and "small" is determined by a threshold r. This neighborhood always includes the closest prototype m_j itself.

Notice that distance is defined in the space $\mathcal{Q}_1 \times \mathcal{Q}_2$ of integer topological coordinates of the prototypes, rather than in the feature space $\mathbb{R}^p$. The effect of the update (14.46) is to move the prototypes closer to the data, but also to maintain a smooth two-dimensional spatial relationship between the prototypes.

The performance of the SOM algorithm depends on the learning rate α and the distance threshold r. Typically α is decreased from say 1.0 to 0.0 over a few thousand iterations (one per observation). Similarly r is decreased linearly from from starting value R to 1 over a few thousand iterations. We illustrate a method for choosing R in the example below.

We have described the simplest version of the SOM. More sophisticated versions modify the update step according to distance:

$$m_k \leftarrow m_k + \alpha h(\|\ell_j - \ell_k\|)(x_i - m_k), \tag{14.47}$$

where the *neighborhood function h* gives more weight to prototypes m_k with indices ℓ_k closer to ℓ_j than to those further away.

If we take the distance r small enough so that each neighborhood contains only one point, then the spatial connection between prototypes is lost. In that case one can show that the SOM algorithm is an online version of K-means clustering, and eventually stabilizes at one of the local minima found by K-means. Since the SOM is a constrained version of K-means

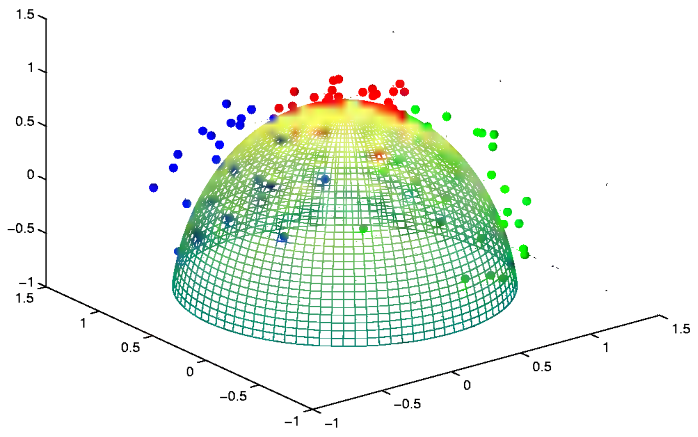

FIGURE 14.15. *Simulated data in three classes, near the surface of a half-sphere.*

clustering, it is important to check whether the constraint is reasonable in any given problem. One can do this by computing the reconstruction error $\|x - m_j\|^2$, summed over observations, for both methods. This will necessarily be smaller for K-means, but should not be much smaller if the SOM is a reasonable approximation.

As an illustrative example, we generated 90 data points in three dimensions, near the surface of a half sphere of radius 1. The points were in each of three clusters—red, green, and blue—located near $(0, 0, 1)$, $(1, 0, 0)$ and $(0, 0, 1)$. The data are shown in Figure 14.15

By design, the red cluster was much tighter than the green or blue ones. (Full details of the data generation are given in Exercise 14.5.) A 5×5 grid of prototypes was used, with initial grid size $R = 2$; this meant that about a third of the prototypes were initially in each neighborhood. We did a total of 40 passes through the dataset of 90 observations, and let r and α decrease linearly over the 3600 iterations.

In Figure 14.16 the prototypes are indicated by circles, and the points that project to each prototype are plotted randomly within the corresponding circle. The left panel shows the initial configuration, while the right panel shows the final one. The algorithm has succeeded in separating the clusters; however, the separation of the red cluster indicates that the the manifold has folded back on itself (see Figure 14.17). Since the distances in the two-dimensional display are not used, there is little indication in the SOM projection that the red cluster is tighter than the others.

Figure 14.18 shows the reconstruction error, equal to the total sum of squares of each data point around its prototype. For comparison we carried

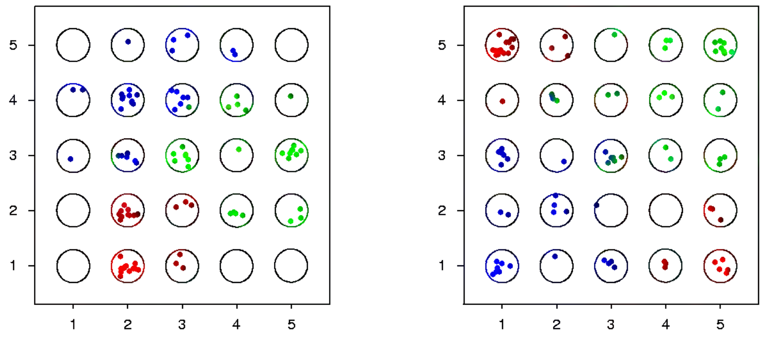

FIGURE 14.16. *Self-organizing map applied to half-sphere data example. Left panel is the initial configuration, right panel the final one. The* 5×5 *grid of prototypes are indicated by circles, and the points that project to each prototype are plotted randomly within the corresponding circle.*

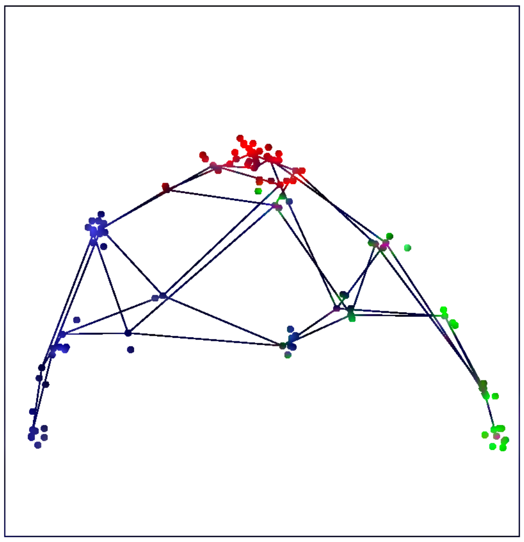

FIGURE 14.17. *Wiremesh representation of the fitted SOM model in* $\mathbb{R}^3$. *The lines represent the horizontal and vertical edges of the topological lattice. The double lines indicate that the surface was folded diagonally back on itself in order to model the red points. The cluster members have been jittered to indicate their color, and the purple points are the node centers.*

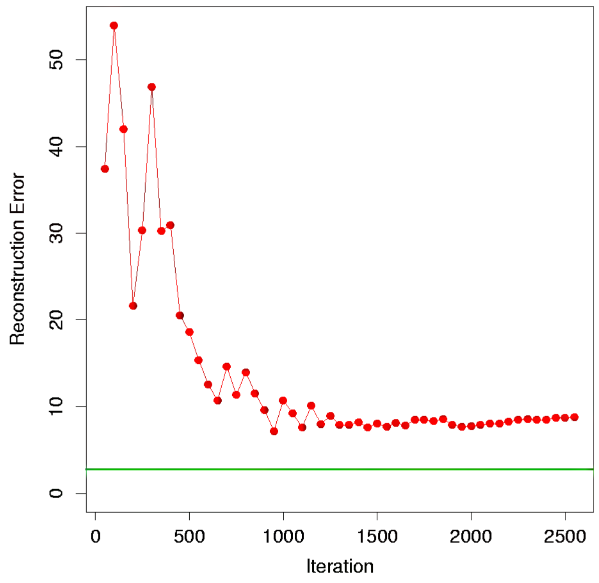

FIGURE 14.18. *Half-sphere data: reconstruction error for the SOM as a function of iteration. Error for k-means clustering is indicated by the horizontal line.*

out a K-means clustering with 25 centroids, and indicate its reconstruction error by the horizontal line on the graph. We see that the SOM significantly decreases the error, nearly to the level of the K-means solution. This provides evidence that the two-dimensional constraint used by the SOM is reasonable for this particular dataset.

In the batch version of the SOM, we update each m_j via

$$m_j = \frac{\sum w_k x_k}{\sum w_k}. \tag{14.48}$$

The sum is over points x_k that mapped (i.e., were closest to) neighbors m_k of m_j. The weight function may be rectangular, that is, equal to 1 for the neighbors of m_k, or may decrease smoothly with distance $\|\ell_k - \ell_j\|$ as before. If the neighborhood size is chosen small enough so that it consists only of m_k, with rectangular weights, this reduces to the K-means clustering procedure described earlier. It can also be thought of as a discrete version of principal curves and surfaces, described in Section 14.5.

Example: Document Organization and Retrieval

Document retrieval has gained importance with the rapid development of the Internet and the Web, and SOMs have proved to be useful for organizing and indexing large corpii. This example is taken from the WEBSOM homepage `http://websom.hut.fi/websom/` (Kohonen et al., 2000). Figure 14.19 represents a SOM fit to 12,088 newsgroup `comp.ai.neural-nets` articles. The labels are generated automatically by the WEBSOM software and provide a guide as to the typical content of a node.

In applications such as this, the documents have to be reprocessed in order to create a feature vector. A *term-document* matrix is created, where each row represents a single document. The entries in each row are the relative frequency of each of a predefined set of terms. These terms could be a large set of dictionary entries (50,000 words), or an even larger set of bigrams (word pairs), or subsets of these. These matrices are typically very sparse, and so often some preprocessing is done to reduce the number of features (columns). Sometimes the SVD (next section) is used to reduce the matrix; Kohonen et al. (2000) use a randomized variant thereof. These reduced vectors are then the input to the SOM.

In this application the authors have developed a "zoom" feature, which allows one to interact with the map in order to get more detail. The final level of zooming retrieves the actual news articles, which can then be read.

14.5 Principal Components, Curves and Surfaces

14.5.1 Principal Components

The principal components of a set of data in $\mathbb{R}^p$ provide a sequence of best linear approximations to that data, of all ranks $q \leq p$.

Denote the observations by $x_1, x_2, \ldots, x_N$, and consider the rank-q linear model for representing them

$$f(\lambda) = \mu + \mathbf{V}_q \lambda, \tag{14.49}$$

where μ is a location vector in $\mathbb{R}^p$, $\mathbf{V}_q$ is a $p \times q$ matrix with q orthogonal unit vectors as columns, and λ is a q vector of parameters. This is the parametric representation of an affine hyperplane of rank q. Figures 14.20 and 14.21 illustrate for $q = 1$ and $q = 2$, respectively. Fitting such a model to the data by least squares amounts to minimizing the *reconstruction error*

$$\min_{\mu, \{\lambda_i\}, \mathbf{V}_q} \sum_{i=1}^{N} \|x_i - \mu - \mathbf{V}_q \lambda_i\|^2. \tag{14.50}$$

We can partially optimize for μ and the λ_i (Exercise 14.7) to obtain

$$\hat{\mu} = \bar{x}, \tag{14.51}$$

$$\hat{\lambda}_i = \mathbf{V}_q^T (x_i - \bar{x}). \tag{14.52}$$

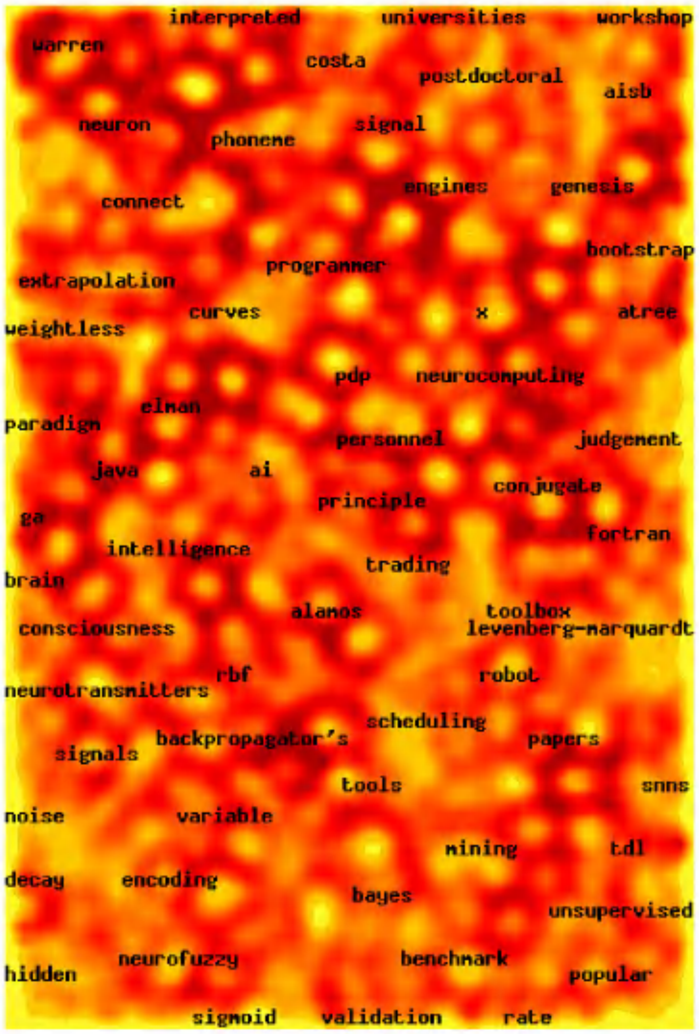

FIGURE 14.19. *Heatmap representation of the SOM model fit to a corpus of* 12,088 *newsgroup* `comp.ai.neural-nets` *contributions (courtesy WEBSOM homepage). The lighter areas indicate higher density areas. Populated nodes are automatically labelled according to typical content.*

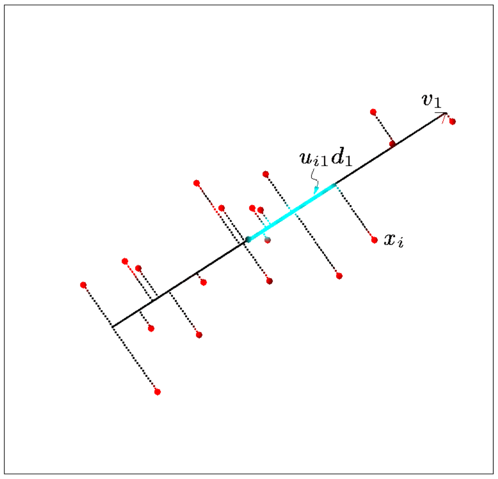

FIGURE 14.20. *The first linear principal component of a set of data. The line minimizes the total squared distance from each point to its orthogonal projection onto the line.*

This leaves us to find the orthogonal matrix $\mathbf{V}_q$:

$$\min_{\mathbf{V}_q} \sum_{i=1}^{N} ||(x_i - \bar{x}) - \mathbf{V}_q \mathbf{V}_q^T (x_i - \bar{x})||^2. \tag{14.53}$$

For convenience we assume that $\bar{x} = 0$ (otherwise we simply replace the observations by their centered versions $\tilde{x}_i = x_i - \bar{x}$). The $p \times p$ matrix $\mathbf{H}_q = \mathbf{V}_q \mathbf{V}_q^T$ is a *projection matrix*, and maps each point x_i onto its rank-q reconstruction $\mathbf{H}_q x_i$, the orthogonal projection of x_i onto the subspace spanned by the columns of $\mathbf{V}_q$. The solution can be expressed as follows. Stack the (centered) observations into the rows of an $N \times p$ matrix $\mathbf{X}$. We construct the *singular value decomposition* of $\mathbf{X}$:

$$\mathbf{X} = \mathbf{U}\mathbf{D}\mathbf{V}^T. \tag{14.54}$$

This is a standard decomposition in numerical analysis, and many algorithms exist for its computation (Golub and Van Loan, 1983, for example). Here $\mathbf{U}$ is an $N \times p$ orthogonal matrix ($\mathbf{U}^T\mathbf{U} = \mathbf{I}_p$) whose columns $\mathbf{u}_j$ are called the *left singular vectors*; $\mathbf{V}$ is a $p \times p$ orthogonal matrix ($\mathbf{V}^T\mathbf{V} = \mathbf{I}_p$) with columns v_j called the *right singular vectors*, and $\mathbf{D}$ is a $p \times p$ diagonal matrix, with diagonal elements $d_1 \geq d_2 \cdots \geq d_p \geq 0$ known as the *singular values*. For each rank q, the solution $\mathbf{V}_q$ to (14.53) consists of the first q columns of $\mathbf{V}$. The columns of $\mathbf{UD}$ are called the principal components of

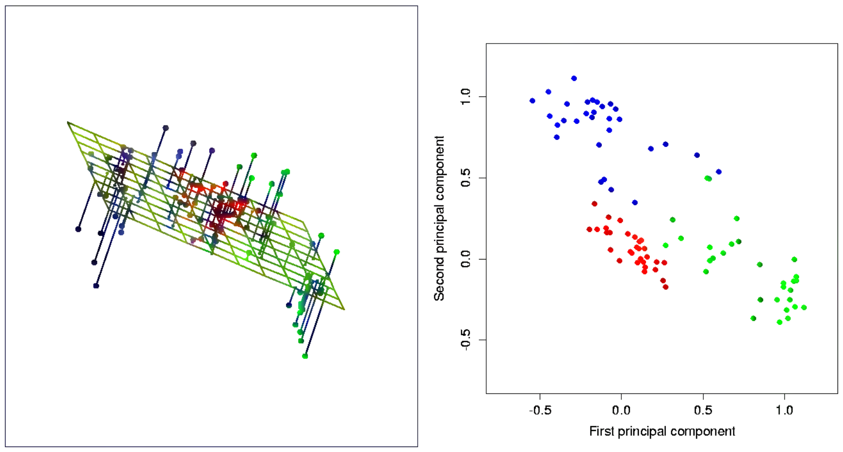

FIGURE 14.21. *The best rank-two linear approximation to the half-sphere data. The right panel shows the projected points with coordinates given by* $\mathbf{U}_2\mathbf{D}_2$, *the first two principal components of the data.*

$\mathbf{X}$ (see Section 3.4.4). The N optimal $\hat{\lambda}_i$ in (14.52) are given by the first q principal components (the N rows of the $N \times q$ matrix $\mathbf{U}_q\mathbf{D}_q$).

The one-dimensional principal component line in $\mathbb{R}^2$ is illustrated in Figure 14.20. For each data point x_i, there is a closest point on the line, given by $u_{i1}d_1v_1$. Here v_1 is the direction of the line and $\hat{\lambda}_i = u_{i1}d_1$ measures distance along the line from the origin. Similarly Figure 14.21 shows the two-dimensional principal component surface fit to the half-sphere data (left panel). The right panel shows the projection of the data onto the first two principal components. This projection was the basis for the initial configuration for the SOM method shown earlier. The procedure is quite successful at separating the clusters. Since the half-sphere is nonlinear, a nonlinear projection will do a better job, and this is the topic of the next section.

Principal components have many other nice properties, for example, the linear combination $\mathbf{X}v_1$ has the highest variance among all linear combinations of the features; $\mathbf{X}v_2$ has the highest variance among all linear combinations satisfying v_2 orthogonal to v_1, and so on.

Example: Handwritten Digits

Principal components are a useful tool for dimension reduction and compression. We illustrate this feature on the handwritten digits data described in Chapter 1. Figure 14.22 shows a sample of 130 handwritten threes, each a digitized 16×16 grayscale image, from a total of 658 such threes. We see considerable variation in writing styles, character thickness and orien-

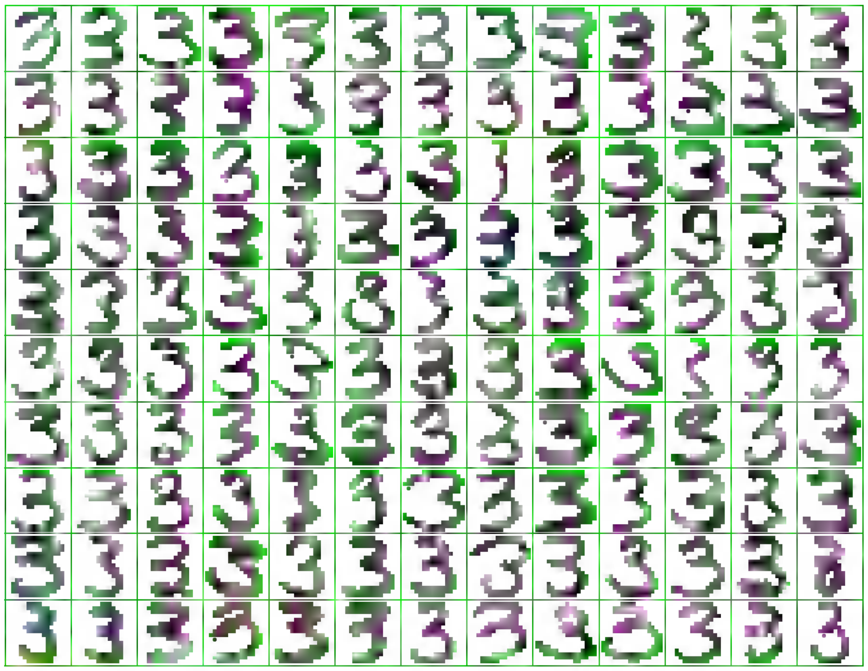

FIGURE 14.22. *A sample of* 130 *handwritten threes shows a variety of writing styles.*

tation. We consider these images as points x_i in $\mathbb{R}^{256}$, and compute their principal components via the SVD (14.54).

Figure 14.23 shows the first two principal components of these data. For each of these first two principal components u_{i1} and u_{i2}, we computed the 5%, 25%, 50%, 75% and 95% quantile points, and used them to define the rectangular grid superimposed on the plot. The circled points indicate those images close to the vertices of the grid, where the distance measure focuses mainly on these projected coordinates, but gives some weight to the components in the orthogonal subspace. The right plot shows the images corresponding to these circled points. This allows us to visualize the nature of the first two principal components. We see that the v_1 (horizontal movement) mainly accounts for the lengthening of the lower tail of the three, while v_2 (vertical movement) accounts for character thickness. In terms of the parametrized model (14.49), this two-component model has the form

$$\hat{f}(\lambda) = \bar{x} + \lambda_1 v_1 + \lambda_2 v_2$$

$=$ 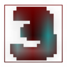 $+ \lambda_1 \cdot$ 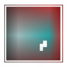 $+ \lambda_2 \cdot$ 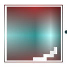 .

Here we have displayed the first two principal component directions, v_1 and v_2, as images. Although there are a possible 256 principal components,

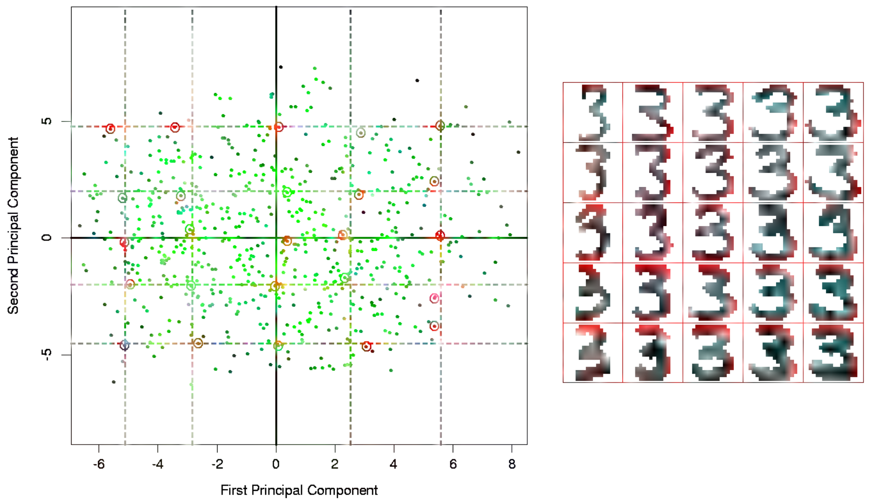

FIGURE 14.23. *Left plot: the first two principal components of the handwritten threes. The circled points are the closest projected images to the vertices of a grid, defined by the marginal quantiles of the principal components. Right plot: the images corresponding to the red-circled points. These show the nature of the first two principal components.*

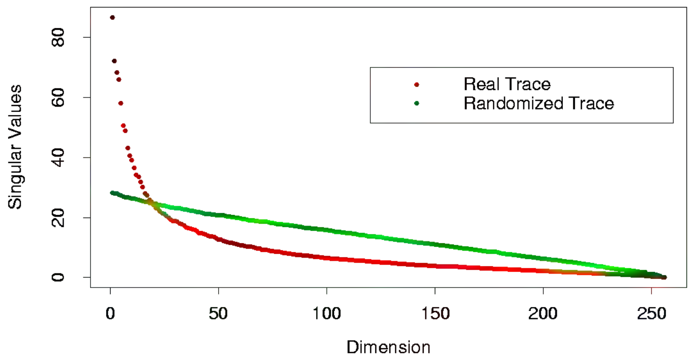

FIGURE 14.24. *The* 256 *singular values for the digitized threes, compared to those for a randomized version of the data (each column of* **X** *was scrambled).*

approximately 50 account for 90% of the variation in the threes, 12 account for 63%. Figure 14.24 compares the singular values to those obtained for equivalent uncorrelated data, obtained by randomly scrambling each column of $\mathbf{X}$. The pixels in a digitized image are inherently correlated, and since these are all the same digit the correlations are even stronger. A relatively small subset of the principal components serve as excellent lower-dimensional features for representing the high-dimensional data.

14.5.2 Principal Curves and Surfaces

Principal curves generalize the principal component line, providing a smooth one-dimensional curved approximation to a set of data points in $\mathbb{R}^p$. A principal surface is more general, providing a curved manifold approximation of dimension 2 or more.

We will first define principal curves for random variables $X \in \mathbb{R}^p$, and then move to the finite data case. Let $f(\lambda)$ be a parameterized smooth curve in $\mathbb{R}^p$. Hence $f(\lambda)$ is a vector function with p coordinates, each a smooth function of the single parameter λ. The parameter λ can be chosen, for example, to be arc-length along the curve from some fixed origin. For each data value x, let $\lambda_f(x)$ define the closest point on the curve to x. Then $f(\lambda)$ is called a principal curve for the distribution of the random vector X if

$$f(\lambda) = \mathrm{E}(X|\lambda_f(X) = \lambda). \tag{14.55}$$

This says $f(\lambda)$ is the average of all data points that project to it, that is, the points for which it is "responsible." This is also known as a *self-consistency* property. Although in practice, continuous multivariate distributes have infinitely many principal curves (Duchamp and Stuetzle, 1996), we are interested mainly in the smooth ones. A principal curve is illustrated in Figure 14.25.

Principal points are an interesting related concept. Consider a set of k prototypes and for each point x in the support of a distribution, identify the closest prototype, that is, the prototype that is responsible for it. This induces a partition of the feature space into so-called Voronoi regions. The set of k points that minimize the expected distance from X to its prototype are called the principal points of the distribution. Each principal point is self-consistent, in that it equals the mean of X in its Voronoi region. For example, with $k = 1$, the principal point of a circular normal distribution is the mean vector; with $k = 2$ they are a pair of points symmetrically placed on a ray through the mean vector. Principal points are the distributional analogs of centroids found by K-means clustering. Principal curves can be viewed as $k = \infty$ principal points, but constrained to lie on a smooth curve, in a similar way that a SOM constrains K-means cluster centers to fall on a smooth manifold.

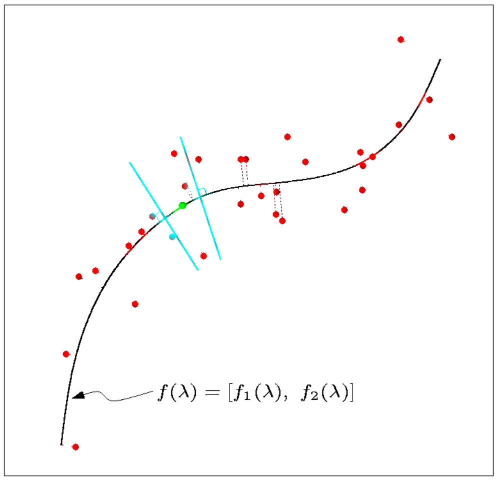

FIGURE 14.25. *The principal curve of a set of data. Each point on the curve is the average of all data points that project there.*

To find a principal curve $f(\lambda)$ of a distribution, we consider its coordinate functions $f(\lambda) = [f_1(\lambda), f_2(\lambda), \dots, f_p(\lambda)]$ and let $X = (X_1, X_2, \dots, X_p)$. Consider the following alternating steps:

$$\begin{array}{lrcl} \text{(a)} & \hat{f}_j(\lambda) & \leftarrow & \mathrm{E}(X_j|\lambda(X) = \lambda);\ j = 1, 2, \dots, p, \\ \text{(b)} & \hat{\lambda}_f(x) & \leftarrow & \mathrm{argmin}_{\lambda'} \,||x - \hat{f}(\lambda')||^2. \end{array} \tag{14.56}$$

The first equation fixes λ and enforces the self-consistency requirement (14.55). The second equation fixes the curve and finds the closest point on the curve to each data point. With finite data, the principal curve algorithm starts with the linear principal component, and iterates the two steps in (14.56) until convergence. A scatterplot smoother is used to estimate the conditional expectations in step (a) by smoothing each X_j as a function of the arc-length $\hat{\lambda}(X)$, and the projection in (b) is done for each of the observed data points. Proving convergence in general is difficult, but one can show that if a linear least squares fit is used for the scatterplot smoothing, then the procedure converges to the first linear principal component, and is equivalent to the *power method* for finding the largest eigenvector of a matrix.

Principal surfaces have exactly the same form as principal curves, but are of higher dimension. The mostly commonly used is the two-dimensional principal surface, with coordinate functions

$$f(\lambda_1, \lambda_2) = [f_1(\lambda_1, \lambda_2), \dots, f_p(\lambda_1, \lambda_2)].$$

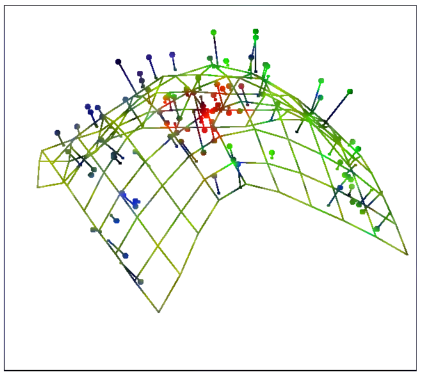

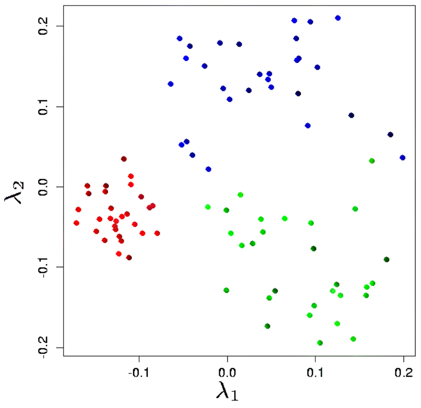

FIGURE 14.26. *Principal surface fit to half-sphere data. Left panel: fitted two-dimensional surface. Right panel: projections of data points onto the surface, resulting in coordinates* $\hat{\lambda}_1, \hat{\lambda}_2$.

The estimates in step (a) above are obtained from two-dimensional surface smoothers. Principal surfaces of dimension greater than two are rarely used, since the visualization aspect is less attractive, as is smoothing in high dimensions.

Figure 14.26 shows the result of a principal surface fit to the half-sphere data. Plotted are the data points as a function of the estimated nonlinear coordinates $\hat{\lambda}_1(x_i), \hat{\lambda}_2(x_i)$. The class separation is evident.

Principal surfaces are very similar to self-organizing maps. If we use a kernel surface smoother to estimate each coordinate function $f_j(\lambda_1, \lambda_2)$, this has the same form as the batch version of SOMs (14.48). The SOM weights w_k are just the weights in the kernel. There is a difference, however: the principal surface estimates a separate prototype $f(\lambda_1(x_i), \lambda_2(x_i))$ for each data point x_i, while the SOM shares a smaller number of prototypes for all data points. As a result, the SOM and principal surface will agree only as the number of SOM prototypes grows very large.

There also is a conceptual difference between the two. Principal surfaces provide a smooth parameterization of the entire manifold in terms of its coordinate functions, while SOMs are discrete and produce only the estimated prototypes for approximating the data. The smooth parameterization in principal surfaces preserves distance locally: in Figure 14.26 it reveals that the red cluster is tighter than the green or blue clusters. In simple examples the estimates coordinate functions themselves can be informative: see Exercise 14.9.

14.6 Independent Component Analysis and Exploratory Projection Pursuit

Multivariate data are often viewed as multiple indirect measurements arising from an underlying source, which typically cannot be directly measured. Examples include the following:

- Educational and psychological tests use the answers to questionnaires to measure the underlying intelligence and other mental abilities of subjects.
- EEG brain scans measure the neuronal activity in various parts of the brain indirectly via electromagnetic signals recorded at sensors placed at various positions on the head.
- The trading prices of stocks change constantly over time, and reflect various unmeasured factors such as market confidence, external influences, and other driving forces that may be hard to identify or measure.

Factor analysis is a classical technique developed in the statistical literature that aims to identify these latent sources. Factor analysis models are typically wed to Gaussian distributions, which has to some extent hindered their usefulness. More recently, independent component analysis has emerged as a strong competitor to factor analysis, and as we will see, relies on the non-Gaussian nature of the underlying sources for its success.

14.6.1 Latent Variables and Factor Analysis

The singular-value decomposition $\mathbf{X} = \mathbf{UDV}^T$ (14.54) has a latent variable representation. Writing $\mathbf{S} = \sqrt{N}\mathbf{U}$ and $\mathbf{A}^T = \mathbf{DV}^T/\sqrt{N}$, we have $\mathbf{X} = \mathbf{SA}^T$, and hence each of the columns of $\mathbf{X}$ is a linear combination of the columns of $\mathbf{S}$. Now since $\mathbf{U}$ is orthogonal, and assuming as before that the columns of $\mathbf{X}$ (and hence $\mathbf{U}$) each have mean zero, this implies that the columns of $\mathbf{S}$ have zero mean, are uncorrelated and have unit variance. In terms of random variables, we can interpret the SVD, or the corresponding principal component analysis (PCA) as an estimate of a latent variable model

$$\begin{aligned} X_1 &= a_{11}S_1 + a_{12}S_2 + \cdots + a_{1p}S_p \\ X_2 &= a_{21}S_1 + s_{22}S_2 + \cdots + a_{2p}S_p \\ \vdots \quad & \qquad \vdots \\ X_p &= a_{p1}S_1 + s_{p2}S_2 + \cdots + a_{pp}S_p, \end{aligned} \tag{14.57}$$

or simply $X = \mathbf{A}S$. The correlated X_j are each represented as a linear expansion in the uncorrelated, unit variance variables S_ℓ. This is not too satisfactory, though, because given any orthogonal $p \times p$ matrix $\mathbf{R}$, we can write

$$\begin{aligned} X &= \mathbf{A}S \\ &= \mathbf{A}\mathbf{R}^T\mathbf{R}S \\ &= \mathbf{A}^*S^*, \end{aligned} \tag{14.58}$$

and $\text{Cov}(S^*) = \mathbf{R}\,\text{Cov}(S)\,\mathbf{R}^T = \mathbf{I}$. Hence there are many such decompositions, and it is therefore impossible to identify any particular latent variables as unique underlying sources. The SVD decomposition does have the property that any rank $q < p$ truncated decomposition approximates $\mathbf{X}$ in an optimal way.

The classical *factor analysis* model, developed primarily by researchers in psychometrics, alleviates these problems to some extent; see, for example, Mardia et al. (1979). With $q < p$, a factor analysis model has the form

$$\begin{aligned} X_1 &= a_{11}S_1 + \cdots + a_{1p}S_q + \varepsilon_1 \\ X_2 &= a_{21}S_1 + \cdots + a_{2p}S_q + \varepsilon_2 \\ &\vdots \\ X_p &= a_{p1}S_1 + \cdots + a_{pp}S_q + \varepsilon_p, \end{aligned} \tag{14.59}$$

or $X = \mathbf{A}S + \varepsilon$. Here S is a vector of $q < p$ underlying latent variables or factors, $\mathbf{A}$ is a $p \times q$ matrix of factor *loadings*, and the ε_j are uncorrelated zero-mean disturbances. The idea is that the latent variables S_ℓ are common sources of variation amongst the X_j, and account for their correlation structure, while the uncorrelated ε_j are unique to each X_j and pick up the remaining unaccounted variation. Typically the S_j and the ε_j are modelled as Gaussian random variables, and the model is fit by maximum likelihood. The parameters all reside in the covariance matrix

$$\mathbf{\Sigma} = \mathbf{A}\mathbf{A}^T + \mathbf{D}_\varepsilon, \tag{14.60}$$

where $\mathbf{D}_\varepsilon = \text{diag}[\text{Var}(\varepsilon_1), \ldots, \text{Var}(\varepsilon_p)]$. The S_j being Gaussian and uncorrelated makes them statistically independent random variables. Thus a battery of educational test scores would be thought to be driven by the independent underlying factors such as *intelligence*, *drive* and so on. The columns of $\mathbf{A}$ are referred to as the *factor loadings*, and are used to name and interpret the factors.

Unfortunately the identifiability issue (14.58) remains, since $\mathbf{A}$ and $\mathbf{A}\mathbf{R}^T$ are equivalent in (14.60) for any $q \times q$ orthogonal $\mathbf{R}$. This leaves a certain subjectivity in the use of factor analysis, since the user can search for rotated versions of the factors that are more easily interpretable. This aspect has left many analysts skeptical of factor analysis, and may account for its lack of popularity in contemporary statistics. Although we will not go into details here, the SVD plays a key role in the estimation of (14.60). For example, if the $\text{Var}(\varepsilon_j)$ are all assumed to be equal, the leading q components of the SVD identify the subspace determined by $\mathbf{A}$.

Because of the separate disturbances ε_j for each X_j, factor analysis can be seen to be modelling the correlation structure of the X_j rather than the covariance structure. This can be easily seen by standardizing the covariance structure in (14.60) (Exercise 14.10). This is an important distinction between factor analysis and PCA, although not central to the discussion here. Exercise 14.11 discusses a simple example where the solutions from factor analysis and PCA differ dramatically because of this distinction.

14.6.2 Independent Component Analysis

The independent component analysis (ICA) model has exactly the same form as (14.57), except the S_i are assumed to be *statistically independent* rather than uncorrelated. Intuitively, lack of correlation determines the second-degree cross-moments (covariances) of a multivariate distribution, while in general statistical independence determines all of the cross-moments. These extra moment conditions allow us to identify the elements of $\mathbf{A}$ uniquely. Since the multivariate Gaussian distribution is determined by its second moments alone, it is the exception, and any Gaussian independent components can be determined only up to a rotation, as before. Hence identifiability problems in (14.57) and (14.59) can be avoided if we assume that the S_i are independent and *non-Gaussian*.

Here we will discuss the full p-component model as in (14.57), where the S_ℓ are independent with unit variance; ICA versions of the factor analysis model (14.59) exist as well. Our treatment is based on the survey article by Hyvärinen and Oja (2000).

We wish to recover the mixing matrix $\mathbf{A}$ in $X = \mathbf{A}S$. Without loss of generality, we can assume that X has already been *whitened* to have $\text{Cov}(X) = \mathbf{I}$; this is typically achieved via the SVD described above. This in turn implies that $\mathbf{A}$ is orthogonal, since S also has covariance $\mathbf{I}$. So solving the ICA problem amounts to finding an orthogonal $\mathbf{A}$ such that the components of the vector random variable $S = \mathbf{A}^T X$ are independent (and non-Gaussian).

Figure 14.27 shows the power of ICA in separating two mixed signals. This is an example of the classical *cocktail party problem*, where different microphones X_j pick up mixtures of different independent sources S_ℓ (music, speech from different speakers, etc.). ICA is able to perform *blind source separation*, by exploiting the independence and non-Gaussianity of the original sources.

Many of the popular approaches to ICA are based on entropy. The differential entropy H of a random variable Y with density $g(y)$ is given by

$$H(Y) = -\int g(y) \log g(y) dy. \tag{14.61}$$

A well-known result in information theory says that among all random variables with with equal variance, Gaussian variables have maximum en-

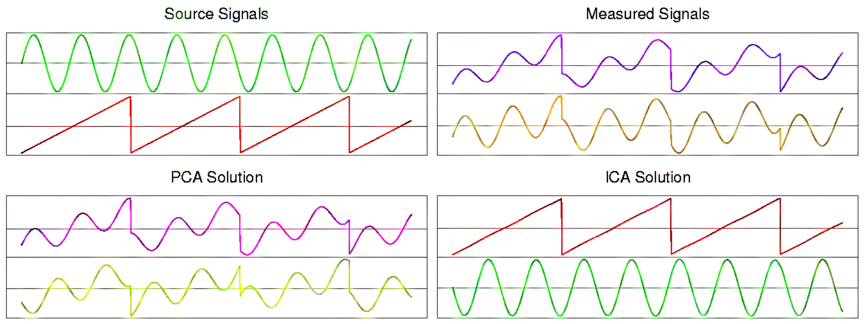

FIGURE 14.27. *Illustration of ICA vs. PCA on artificial time-series data. The upper left panel shows the two source signals, measured at* 1000 *uniformly spaced time points. The upper right panel shows the observed mixed signals. The lower two panels show the principal components and independent component solutions.*

tropy. Finally, the *mutual information* $I(Y)$ between the components of the random vector Y is a natural measure of dependence:

$$I(Y) = \sum_{j=1}^{p} H(Y_j) - H(Y). \tag{14.62}$$

The quantity $I(Y)$ is called the *Kullback–Leibler distance* between the density $g(y)$ of Y and its independence version $\prod_{j=1}^{p} g_j(y_j)$, where $g_j(y_j)$ is the marginal density of Y_j. Now if X has covariance $\mathbf{I}$, and $Y = \mathbf{A}^T X$ with $\mathbf{A}$ orthogonal, then it is easy to show that

$$\begin{aligned} I(Y) &= \sum_{j=1}^{p} H(Y_j) - H(X) - \log|\det \mathbf{A}| & (14.63)\\ &= \sum_{j=1}^{p} H(Y_j) - H(X). & (14.64) \end{aligned}$$

Finding an $\mathbf{A}$ to minimize $I(Y) = I(\mathbf{A}^T X)$ looks for the orthogonal transformation that leads to the most independence between its components. In light of (14.63) this is equivalent to minimizing the sum of the entropies of the separate components of Y, which in turn amounts to maximizing their departures from Gaussianity.

For convenience, rather than using the entropy $H(Y_j)$, Hyvärinen and Oja (2000) use the *negentropy* measure $J(Y_j)$ defined by

$$J(Y_j) = H(Z_j) - H(Y_j), \tag{14.65}$$

where Z_j is a Gaussian random variable with the same variance as Y_j. Negentropy is nonnegative, and measures the departure of Y_j from Gaussianity. They propose simple approximations to negentropy which can be

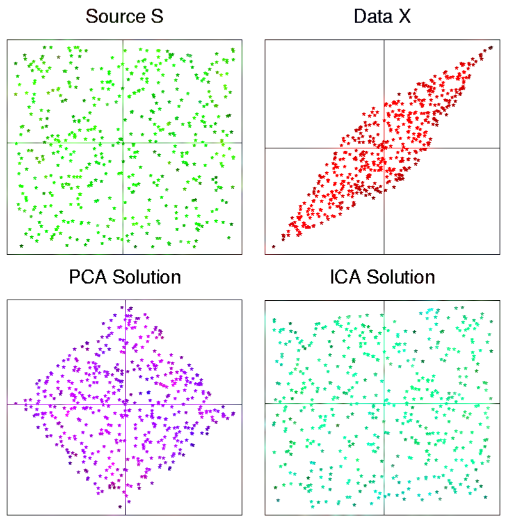

FIGURE 14.28. *Mixtures of independent uniform random variables. The upper left panel shows* 500 *realizations from the two independent uniform sources, the upper right panel their mixed versions. The lower two panels show the PCA and ICA solutions, respectively.*

computed and optimized on data. The ICA solutions shown in Figures 14.27 and 14.28 use the approximation

$$J(Y_j) \approx [\mathrm{E}G(Y_j) - \mathrm{E}G(Z_j)]^2, \tag{14.66}$$

where $G(u) = \frac{1}{a}\log\cosh(au)$ for $1 \leq a \leq 2$. When applied to a sample of x_i, the expectations are replaced by data averages. More classical (and less robust) measures are based on fourth moments, and hence look for departures from the Gaussian via kurtosis. See Hyvärinen and Oja (2000) for more details, and for a simple Newton algorithm for finding the optimal directions.

In summary then, ICA applied to multivariate data looks for a sequence of orthogonal projections such that the projected data look as far from Gaussian as possible. With pre-whitened data, this amounts to looking for components that are as independent as possible.

ICA starts from essentially a factor analysis solution, and looks for rotations that lead to independent components. From this point of view, ICA is just another factor rotation method, along with the traditional "varimax" and "quartimax" methods used in psychometrics.

Example: Handwritten Digits

We revisit the handwritten threes analyzed by PCA in Section 14.5.1. Figure 14.29 compares the first five (standardized) principal components with

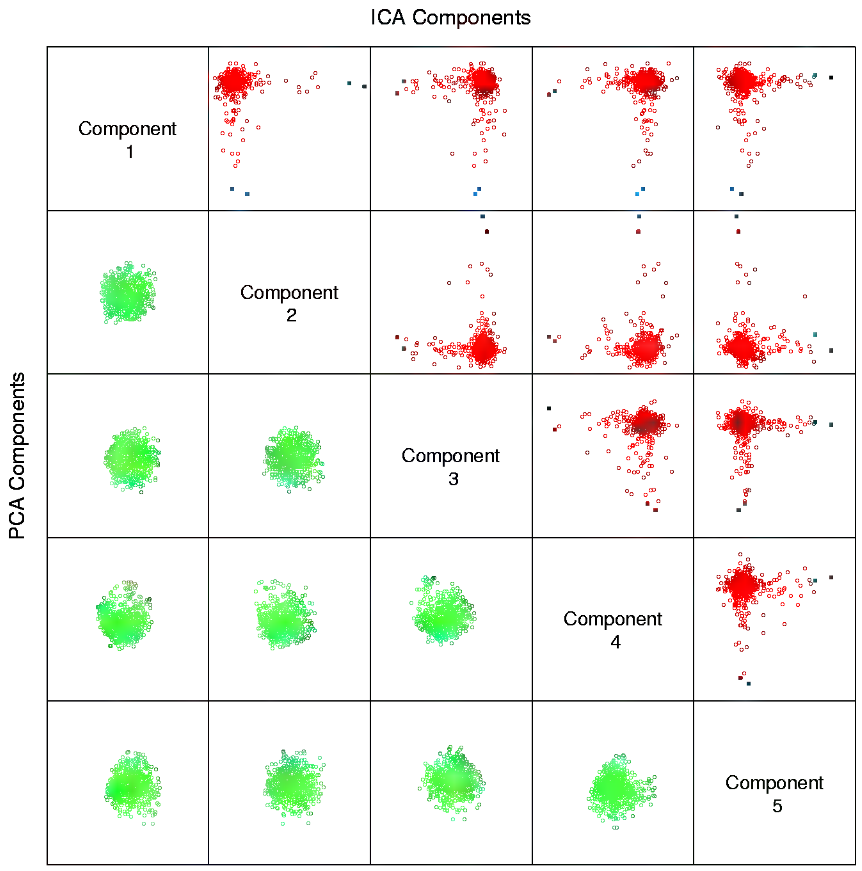

FIGURE 14.29. *A comparison of the first five ICA components (above diagonal) with the first five PCA components(below diagonal). Each component is standardized to have unit variance.*

the first five ICA components, all shown in the same standardized units. Note that each plot is a two-dimensional projection from a 256-dimensional space. While the PCA components all appear to have joint Gaussian distributions, the ICA components have long-tailed distributions. This is not too surprising, since PCA focusses on variance, while ICA specifically looks for non-Gaussian distributions. All the components have been standardized, so we do not see the decreasing variances of the principal components.

For each ICA component we have highlighted two of the extreme digits, as well as a pair of central digits and displayed them in Figure 14.30. This illustrates the nature of each of the components. For example, ICA component five picks up the long sweeping tailed threes.

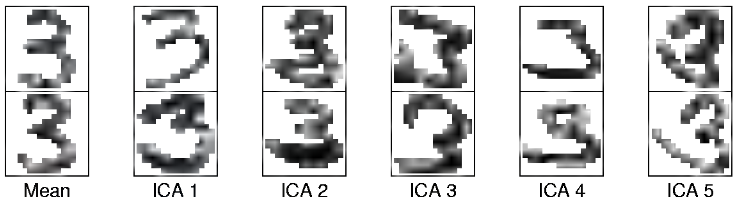

FIGURE 14.30. *The highlighted digits from Figure 14.29. By comparing with the mean digits, we see the nature of the ICA component.*

14.6.3 Exploratory Projection Pursuit

Friedman and Tukey (1974) proposed *exploratory projection pursuit,* a graphical exploration technique for visualizing high-dimensional data. Their view was that most low (one- or two-dimensional) projections of high-dimensional data look Gaussian. Interesting structure, such as clusters or long tails, would be revealed by non-Gaussian projections. They proposed a number of *projection indices* for optimization, each focussing on a different departure from Gaussianity. Since their initial proposal, a variety of improvements have been suggested (Huber, 1985; Friedman, 1987), and a variety of indices, including entropy, are implemented in the interactive graphics package Xgobi (Swayne et al., 1991). These projection indices are exactly of the same form as $J(Y_j)$ above, where $Y_j = a_j^T X$, and normalized linear combination of the components of X. In fact, some of the approximations and substitutions for cross-entropy coincide with indices proposed for projection pursuit. Typically with projection pursuit, the directions a_j are not constrained to be orthogonal. Friedman (1987) transforms the data to look Gaussian in the chosen projection, and then searches for subsequent directions. Despite their different origins, ICA and exploratory projection pursuit are quite similar, at least in the representation described here.

14.6.4 A Different Approach to ICA

Independent components have by definition a joint product density, and so to find them we can estimate their product density. Using the trick of Section 14.2.4, we can simplify things by casting the density estimation task as a two-class classification problem. The observed data points are assigned to class $G = 1$ and a background sample is generated from a density $g_0(x)$, and assigned to class $G = 0$. For illustration consider a bivariate problem $X = (X_1, X_2)$ and a two-term model of the form

$$\log \frac{\Pr(G=1)}{1-\Pr(G=1)} = f_1(a_1^T X) + f_2(a_2^T X). \tag{14.67}$$

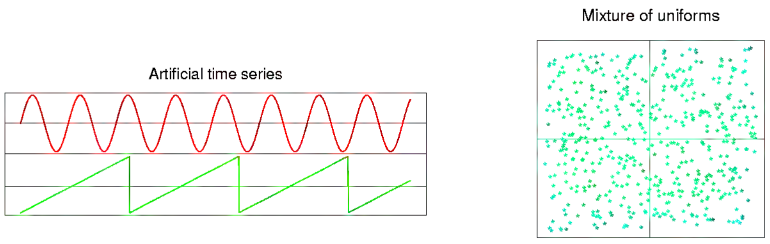

FIGURE 14.31. *Projection-pursuit solutions to the artificial time series problem of Figure 14.27 (left panel), and the mixture of uniforms problem of Figure 14.28 (right panel). These solutions were obtained using the generalized logistic regression model (14.67).*

By the arguments in Section (14.2.4), this additive model for the logit gives a data density of the form

$$\begin{aligned} g(X) &= g_0(X)\cdot\exp\{f_1(a_1^TX)+f_2(a_2^TX)\} \\ &= g_0(X)\cdot\exp\{f_1(a_1^TX)\}\cdot\exp\{f_2(a_2^TX)\}. \end{aligned} \tag{14.68}$$

We seek components a_1^TX and a_2^TX that are independent, and hence have a joint density that factors:

$$h(a_1^TX, a_2^TX) = h_1(a_1^TX)\cdot h_2(a_2^TX). \tag{14.69}$$

A change of variables is needed to get from expression (14.68) to expression (14.69), and it is easy to see that $g_0(a_1^TX, a_2^TX)$ must factor into a product. This occurs only if g_0 is the density of a multivariate Gaussian distribution and a_1 is orthogonal to a_2 in the metric of the inverse of the covariance matrix $\mathbf{\Sigma}$ of X. As before we first transform the data so as to have identity covariance, which then allows us to use for g_0 a spherical Gaussian distribution.

Hence to apply this procedure, we sphere the observed data, generate the background data from a spherical Gaussian distribution, and then fit model (14.67) with the constraint that a_1 be orthogonal to a_2.

Model (14.67) is a generalization of logistic regression, and hence we can use the local scoring algorithm (9.2) to fit it. The right hand side of the model has the form of projection pursuit regression, and so we use the PPR algorithm (11.2) in step 2(c) of local scoring. We tried this on the artificial time series data of Figure 14.27, and the mixture of uniforms data of Figure 14.28. The resulting components $\hat{a}_1^TX$ and $\hat{a}_2^TX$ for each case are shown in Figure 14.31 and reproduce the original source signals.

Like ICA, the above procedure finds independent components by finding orthogonal, non-Gaussian projections of the data. It has the apparent advantage of not requiring the choice of a non-normality index, but instead uses background Gaussian data to judge non-normality of projections. However, the index is implicit in the binomial deviance loss function used to measure separation between the original and background data in a given projection (Exercise 14.12). While this procedure appears to work well on the examples presented here, at the time of writing it is largely untested.

14.7 Multidimensional Scaling

Both self-organizing maps and principal curves and surfaces map data points in $\mathbb{R}^p$ to a lower-dimensional manifold. Multidimensional scaling (MDS) has a similar goal, but approaches the problem in a somewhat different way.

We start with observations $x_1, x_2, \ldots, x_N \in \mathbb{R}^p$, and let d_{ij} be the distance between observations i and j. Often we choose Euclidean distance $d_{ij} = ||x_i - x_j||$, but other distances may be used. Further, in some applications we may not even have available the data points x_i, but only have some *dissimilarity* measure d_{ij} (see Section 14.3.10). For example, in a wine tasting experiment, d_{ij} might be a measure of how different a subject judged wines i and j, and the subject provides such a measure for all pairs of wines i, j. MDS requires only the dissimilarities d_{ij}, in contrast to the SOM and principal curves and surfaces which need the data points x_i.

Multidimensional scaling seeks values $z_1, z_2, \ldots, z_N \in \mathbb{R}^k$ to minimize the so-called *stress function*

$$S_D(z_1, z_2, \ldots, z_N) = \left[\sum_{i \neq i'} (d_{ii'} - ||z_i - z_i'||)^2 \right]^{1/2}. \qquad (14.70)$$

This is known as *least squares* or *Kruskal–Shephard* scaling. The idea is to find a lower-dimensional approximation of the data so as to preserve the pairwise distances as well as possible. Notice that the approximation is in terms of the distances rather that squared distances: the square root on the outside is just a convention. A gradient descent algorithm is used to minimize S_D.

A variation on least squares scaling is the so-called *Sammon mapping* which minimizes

$$\sum_{i \neq i'} \frac{(d_{ii'} - ||z_i - z_i'||)^2}{d_{ii'}}. \qquad (14.71)$$

Here more emphasis is put on preserving smaller pairwise distances.

In *classical scaling*, we instead start with similarities $s_{ii'}$: often we use the centered inner product $s_{ii'} = \langle x_i - \bar{x}, x_i' - \bar{x} \rangle$. The problem then is to minimize

$$\sum_{i \neq i'} (s_{ii'} - \langle z_i - \bar{z}_i, z_i' - \bar{z}_i' \rangle)^2 \tag{14.72}$$

over $z_1, z_2, \ldots, z_N \in \mathbb{R}^k$. This is attractive because there is an explicit solution in terms of eigenvectors: see Exercise 14.8. Classical scaling is not equivalent to least squares scaling, since inner products rely on a choice of origin while pairwise distances do not. A set of inner products determines a set of pairwise distances but not vice versa.

Least squares and classical scaling are referred to as *metric* scaling methods, in the sense that the actual dissimilarities or similarities are approximated. *Shephard–Kruskal nonmetric scaling* effectively uses only ranks. Nonmetric scaling seeks to minimize the stress function

$$\frac{\sum_{i,i'} [\theta(||z_i - z_i'||) - d_{ii'}]^2}{\sum_{i,i'} d_{ii'}^2} \tag{14.73}$$

over the $d_{ii'}$ and an arbitrary increasing function $\theta(\cdot)$. With $\theta(\cdot)$ fixed,we minimize over $d_{ii'}$ by gradient descent. With the $d_{ii'}$ fixed, the method of isotonic regression is used to find the best monotonic approximation $\theta(\cdot)$. These steps are iterated until the solutions stabilize.

Like the self-organizing map, multidimensional scaling projects the data onto a lower-dimensional manifold, but does not give a parameterization of the manifold, as with principal surfaces. In a principal surface and SOM, points close together in the original feature space should map close together on the manifold, but points far apart in feature space might also map close together. This is less likely in multidimensional scaling since it explicitly tries to preserve all pairwise distances.

Figure 14.32 shows the first two MDS coordinates from classical scaling for the half-sphere example. There is clear separation of the clusters, and the tighter nature of the red cluster is apparent.

Bibliographic Notes

There are many books on clustering, including Hartigan (1975), Gordon (1999) and Kaufman and Rousseeuw (1990). K-means clustering goes back at least to Lloyd (1957), Forgy (1965), Jancey (1966) and MacQueen (1967). Applications in engineering, especially in image compression via vector quantization, can be found in Gersho and Gray (1992). The k-medoid procedure is described in Kaufman and Rousseeuw (1990). Association rules are outlined in Agrawal et al. (1995). The self-organizing map was proposed by Kohonen (1989) and Kohonen (1990); Kohonen et al. (2000) give a more recent account. Principal components analysis and multidimensional scaling are described in standard books on multivariate analysis, for example,

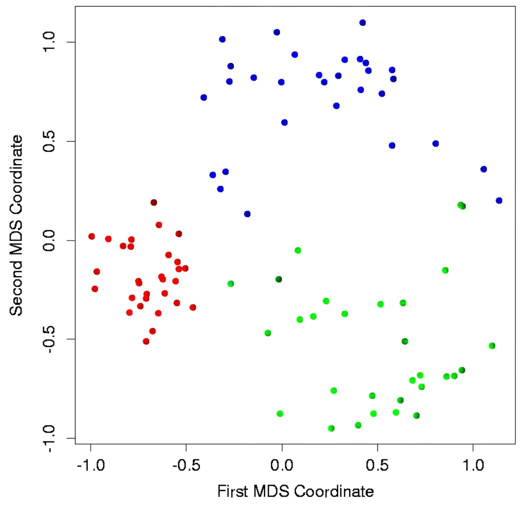

FIGURE 14.32. *First two coordinates for half-sphere data, from classical multidimensional scaling.*

Mardia et al. (1979). Buja et al. (1999) have implemented a powerful environment called XGvis for multidimensional scaling, and the user manual contains a lucid overview of the subject. Figures 14.17, 14.21 (left panel) and 14.26 (left panel) where produced in XGobi, a multidimensional data visualization package by the same authors. Principal curves and surfaces were proposed in Hastie (1984) and Hastie and Stuetzle (1989). The idea of principal points was formulated in Flury (1990), Tarpey and Flury (1996) give an exposition of the general concept of self-consistency. Independent component analysis was proposed by Comon (1994), with subsequent developments by Bell and Sejnowski (1995); our treatment in Section 14.6 is based on (Hyvärinen and Oja, 2000). Projection pursuit was proposed by (Friedman and Tukey, 1974), and is discussed in detail in (Huber, 1985). A dynamic projection pursuit algorithm is implemented in XGobi.

Exercises

Ex. 14.1 *Weights for clustering.* Show that weighted Euclidean distance

$$d_e^{(w)}(x_i, x_{i'}) = \frac{\sum_{l=1}^{p} w_l (x_{il} - x_{i'l})^2}{\sum_{l=1}^{p} w_l}$$

satisfies

$$d_e^{(w)}(x_i, x_{i'}) = d_e(z_i, z_{i'}) = \sum_{l=1}^{p}(z_{il} - z_{i'l})^2, \tag{14.74}$$

where

$$z_{il} = x_{il} \cdot \left(\frac{w_l}{\sum_{l=1}^{p} w_l}\right)^{1/2}. \tag{14.75}$$

Thus weighted Euclidean distance based on x is equivalent to unweighted Euclidean distance based on z.

Ex. 14.2 Consider a mixture model density in p-dimensional feature space,

$$g(x) = \sum_{k=1}^{K} \pi_k g_k(x), \tag{14.76}$$

where $g_k = N(\mu_k, \mathbf{I} \cdot \sigma^2)$ and $\pi_k \geq 0 \; \forall k$ with $\sum_k \pi_k = 1$. Here $\{\mu_k, \pi_k\}, k = 1, \ldots, K$ and σ^2 are unknown parameters.

Suppose we have data $x_1, x_2, \ldots, x_N \sim g(x)$ and we wish to fit the mixture model.

1. Write down the log-likelihood of the data
2. Derive an EM algorithm for computing the maximum likelihood estimates (see Section 8.1).
3. Show that if σ has a known value in the mixture model and we take $\sigma \to 0$, then in a sense this EM algorithm coincides with K-means clustering.

Ex. 14.3 Show how the K-means procedure can be viewed as a special case of the EM algorithm (Chapter 8) applied to an appropriate mixture of Gaussian densities model.

Ex. 14.4 Cluster the the demographic data of Table 14.1 using a classification tree. Specifically, generate a reference sample of the same size of the training set, by randomly permuting the values within each feature. Build a classification tree to the training sample (class 1) and the reference sample (class 0) and describe the terminal nodes having highest estimated class 1 probability. Compare the results to the PRIM results near Table 14.1 and also to the results of K-means clustering applied to the same data.

Ex. 14.5 Generate data with three features, with 30 data points in each of three classes as follows:

$$\theta_1 = U(-\pi/8, \pi/8)$$

$$\begin{aligned}
\phi_1 &= U(0, 2\pi) \\
x_1 &= \sin(\theta_1)\cos(\phi_1) + W_{11} \\
y_1 &= \sin(\theta_1)\sin(\phi_1) + W_{12} \\
z_1 &= \cos(\theta_1) + W_{13} \\
\\
\theta_2 &= U(\pi/2 - \pi/4, \pi/2 + \pi/4) \\
\phi_2 &= U(-\pi/4, \pi/4) \\
x_2 &= \sin(\theta_2)\cos(\phi_2) + W_{21} \\
y_2 &= \sin(\theta_2)\sin(\phi_2) + W_{22} \\
z_2 &= \cos(\theta_2) + W_{23} \\
\\
\theta_3 &= U(\pi/2 - \pi/4, \pi/2 + \pi/4) \\
\phi_3 &= U(\pi/2 - \pi/4, \pi/2 + \pi/4) \\
x_3 &= \sin(\theta_3)\cos(\phi_3) + W_{31} \\
y_3 &= \sin(\theta_3)\sin(\phi_3) + W_{32} \\
z_3 &= \cos(\theta_3) + W_{33}
\end{aligned}$$

Here $U(a, b)$ indicates a uniform variate on the range $[a, b]$ and W_{jk} are independent normal variates with standard deviation 0.6. Hence the data lie near the surface of a sphere in three clusters centered at $(1, 0, 0)$, $(0, 1, 0)$ and $(0, 0, 1)$.

Write a program to fit a SOM to these data, using the learning rates given in the text. Carry out a K-means clustering of the same data, and compare the results to those in the text.

Ex. 14.6 Write programs to implement K-means clustering and a self-organizing map (SOM), with the prototype lying on a two-dimensional grid. Apply them to the columns of the human tumor microarray data, using $K = 2, 5, 10, 20$ centroids for both. Demonstrate that as the size of the SOM neighborhood is taken to be smaller and smaller, the SOM solution becomes more similar to the K-means solution.

Ex. 14.7 Derive (14.51) and (14.52) in Section 14.5.1. Show that $\hat{\mu}$ is not unique, and characterize the family of equivalent solutions.

Ex. 14.8 *Classical multidimensional scaling.* Let $\mathbf{S}$ be the centered inner product matrix with elements $\langle x_i - \bar{x}, x_j - \bar{x}\rangle$. Let $\lambda_1 > \lambda_2 \cdots > \lambda_k$ be the k largest eigenvalues of $\mathbf{S}$, with associated eigenvectors $\mathbf{E}_k = (\mathbf{e}_1, \mathbf{e}_2, \ldots, \mathbf{e}_k)$. Let $\mathbf{D}_k$ be a diagonal matrix with diagonal entries $\sqrt{\lambda_1}, \sqrt{\lambda_2}, \ldots, \sqrt{\lambda_k}$.

Show that the solutions z_i to the classical scaling problem (14.72) are the *rows* of $\mathbf{E}_k\mathbf{D}_k$.

Ex. 14.9 Generate 200 data points with three features, lying close to a *helix*. In detail, define $X_1 = \cos(s) + 0.1 \cdot Z_1$, $X_2 = \sin(s) + 0.1 \cdot Z_2$, $X_3 = s + 0.1 \cdot Z_3$ where s takes on 200 equally spaced values between 0 and 2π, and Z_1, Z_2, Z_3 are independent and have standard Gaussian distributions.

(a) Fit a principal curve to the data and plot the estimated coordinate functions. Compare them to the underlying functions $\cos(s), \sin(s)$ and s.

(b) Fit a self-organizing map to the same data, and see if you can discover the helical shape of the original point cloud.

Ex. 14.10 Pre and post-multiply equation (14.60) by a diagonal matrix containing the inverse variances of the X_j. Hence obtain an equivalent decomposition for the correlation matrix, in the sense that a simple scaling is applied to the matrix **A**.

Ex. 14.11 Generate 200 observations of three variates X_1, X_2, X_3 according to

$$\begin{aligned} X_1 &\sim Z_1 \\ X_2 &= X_1 + .001 \cdot Z_2 \\ X_3 &= 10 \cdot Z_3 \end{aligned} \tag{14.77}$$

where Z_1, Z_2, Z_3 are independent standard normal variates. Compute the leading principal component and factor analysis directions. Hence show that the leading principal component aligns itself in the maximal variance direction X_3, while the leading factor essentially ignores the uncorrelated component X_3, and picks up the correlated component $X_2 + X_1$. [Geoffrey Hinton, personal communication]

Ex. 14.12 *ICA and projection pursuit (Section 14.6.4).*

(a) Suppose that the true density at a point x is $f(x)$, and denote the Gaussian density by $g(x)$. Show that the probability that a point selected at random comes from f is

$$p(x) = \Pr(y = 1|x) = \frac{f(x)}{f(x) + g(x)},$$

and its logit is

$$\text{logit}(p(x)) = \log(f(x)) - \log(g(x)).$$

(b) Show that the expected binomial log-likelihood for a model $\tilde{p}(x)$ is

$$E_X\left[p(x)\log(\tilde{p}(x)) + (1 - p(x))\log(1 - \tilde{p}(x))\right]$$

(c) Assuming that $\tilde{p}$ is modelled nonparametrically and is close to the true p, we can replace it by p.

Hence we have an index of non-normality

$$\kappa(p) = E_x p(x)\log(p(x)) + (1 - p)\log(1 - p(x)),$$

and we seek projection directions a to maximize $\kappa(p_a)$, where $p_a(x) = p(a^T x)$.

Now $\kappa(p_a)$ is maximized when p_a is zero or one - extremes - and hence $\text{logit}(p_a(x) = \log(f_a(x)) - \log(g_a(x))$ is large in absolute value. So by maximizing the likelihood with respect to a, we are looking for the direction for which the projected data is as far from the Gaussian density as possible, in this binomial entropy metric.

Expand κ in a Taylor series about $p_a = .5$, to show that

$$\kappa(p_a) \approx E_X \frac{f_a(x) g_a(x)}{f_a(x) + g_a(x)} \left[\log(f_a(x)) - \log(g_a(x))\right]^2 .$$

Compare the measure of non-normality on the righthand side to those discussed in Section 14.6.2.

References

Abu-Mostafa, Y. (1995). Hints, *Neural Computation* **7**: 639–671.

Agrawal, R., Mannila, H., Srikant, R., Toivonen, H. and Verkamo, A. I. (1995). Fast discovery of association rules, *Advances in Knowledge Discovery and Data Mining*, AAAI/MIT Press, Cambridge, MA.

Akaike, H. (1973). Information theory and an extension of the maximum likelihood principle, *Second International Symposium on Information Theory*, pp. 267–281.

Allen, D. (1977). The relationship between variable selection and data augmentation and a method of prediction, *Technometrics* **16**: 125–7.

Anderson, J. and Rosenfeld, E. (eds) (1988). *Neurocomputing: Foundations of Research*, MIT Press, Cambridge, MA.

Barron, A. (1993). Universal approximation bounds for superpositions of a sigmoid function, *IEEE transactions on Information Theory* **39**: 930–945.

Becker, R., Cleveland, W. and Shyu, M. (1996). The visual design and control of trellis display, *Journal of Computational and Graphical Statistics* **5**: 123–155.

Bell, A. and Sejnowski, T. (1995). An information-maximization approach to blind separation and blind deconvolution, *Neural Computation* **7**: 1129–1159.

Bellman, R. E. (1961). *Adaptive Control Processes*, Princeton University Press.

Bishop, C. (1995). *Neural Networks for Pattern Recognition*, Clarendon Press, Oxford.

Breiman, L. (1992). The little bootstrap and other methods for dimensionality selection in regression: X-fixed prediction error, *J. Amer. Statist. Assoc* **87**: 738–754.

Breiman, L. (1996a). Bagging predictors, *Machine Learning* **26**: 123–140.

Breiman, L. (1996b). Stacked regressions, *Machine Learning* **24**: 51–64.

Breiman, L. (1998). Arcing classifiers (with discussion), *Annals of Statistics* **26**: 801–849.

Breiman, L. (1999). Prediction games and arcing algorithms, *Neural Computation* pp. 1493–1517.

Breiman, L. and Friedman, J. (1997). Predicting multivariate responses in multiple linear regression (with discussion), *J. Roy. Statist. Soc. B.* **59**: 3–37.

Breiman, L., Friedman, J., Olshen, R. and Stone, C. (1984). *Classification and Regression Trees*, Wadsworth.

Breiman, L. and Ihaka, R. (1984). Nonlinear discriminant analysis via scaling and ACE, *Technical report*, Univ. of California, Berkeley.

Breiman, L. and Spector, P. (1992). Submodel selection and evaluation in regression: the X-random case, *Intern. Statist. Rev* **60**: 291–319.

Bruce, A. and Gao, H. (1996). *Applied Wavelet Analysis with S-PLUS*, Springer.

Buja, A., Hastie, T. and Tibshirani, R. (1989). Linear smoothers and additive models (with discussion), *Annals of Statistics* **17**: 453–555.

Buja, A., Swayne, D., Littman, M. and Dean, N. (1999). Xgvis: A system for multidimensional scaling and graph layout in any dimension, *Technical report*, AT&T Laboratories.

Burges, C. J. C. (1998). A Tutorial on Support Vector Machines for Pattern Recognition, *Knowledge Discovery and Data Mining* **2**(2): 121–167.

Chambers, J. and Hastie, T. (1991). *Statistical Models in S*, Wadsworth/Brooks Cole, Pacific Grove, CA.

Cherkassky, V. and Mulier, F. (1998). *Learning from Data*, Wiley, New York.

Chui, C. (1992). *An Introduction to Wavelets*, Academic Press, London.

Comon, P. (1994). Independent component analysis — a new concept?, *Signal Processing* **36**: 287–314.

Copas, J. B. (1983). Regression, prediction and shrinkage (with discussion), *Journal of the Royal Statistical Society, Series B, Methodological* **45**: 311–354.

Cover, T. and Hart, P. (1967). Nearest neighbor pattern classification, *Proc. IEEE Trans. Inform. Theory* **IT-11**: 21–27.

Cover, T. and Thomas, J. (1991). *Elements of Information Theory*, Wiley, New York.

Cox, D. and Hinkley, D. (1974). *Theoretical Statistics*, Chapman and Hall, London.

Cressie, N. A. C. (1993). *Statistics for Spatial Data (Revised Edition)*, Wiley-Interscience, New York.

Csiszar, I. and Tusnády, G. (1984). Information geometry and alternating minimization procedures, *Statistics & Decisions Supplement Issue* **1**: 205–237.

Dasarathy, B. (1991). *Nearest Neighbor Pattern Classification Techniques*, IEEE Computer Society Press.

Daubechies, I. (1992). *Ten Lectures in Wavelets*, Society for Industrial and Applied Mathematics, Philadelphia, PA.

de Boor, C. (1978). *A Practical Guide to Splines*, Springer-Verlag, New York.

Dempster, A., Laird, N. and Rubin, D. (1977). Maximum likelihood from incomplete data via the EM algorithm (with discussion), *J. R. Statist. Soc. B.* **39**: 1–38.

Devijver, P. and Kittler, J. (1982). *Pattern Recognition: a Statistical Approach*, Prentice-Hall, Englewood Cliffs, N.J.

Donoho, D. and Johnstone, I. (1994). Ideal spatial adaptation by wavelet shrinkage, *Biometrika* **81**: 425–455.

Donoho, D., Johnstone, I., Kerkyachairan, G. and Picard, D. (1995). Wavelet shrinkage; asymptopia? (with discussion), *J. Royal. Statist. Soc.* **57**: 201–337.

Duan, N. and Li, K.-C. (1991). Slicing regression: a link-free regression method, *Annals of Statistics* **19**: 505–530.

Duchamp, T. and Stuetzle, W. (1996). Extremal properties of principal curves in the plane, *The Annals of Statistics* **24**: 1511–1520.

Duda, R., Hart, P. and Stork, D. (2000). *Pattern Classification (Second Edition)*, Wiley, New York.

Efron, B. (1975). The efficiency of logistic regression compared to normal discriminant analysis, *J. Amer. Statist. Assoc.* **70**: 892–898.

Efron, B. (1979). Bootstrap methods: another look at the jackknife, *Annals of Statistics* **7**: 1–26.

Efron, B. (1983). Estimating the error rate of a prediction rule: some improvements on cross-validation, *J. Amer. Statist. Assoc.* **78**: 316–331.

Efron, B. (1986). How biased is the apparent error rate of a prediction rule?, *J. Amer. Statist. Assoc.* **81**: 461–70.

Efron, B. and Tibshirani, R. (1991). Statistical analysis in the computer age, *Science* **253**: 390–395.

Efron, B. and Tibshirani, R. (1993). *An Introduction to the Bootstrap*, Chapman and Hall, London.

Efron, B. and Tibshirani, R. (1997). Improvements on cross-validation: the 632+ bootstrap: method, *J. Amer. Statist. Assoc.* **92**: 548–560.

Evgeniou, T., Pontil, M. and Poggio, T. (2001). Regularization networks and support vector machines, *Advances in Computational Mathematics (to appear)* .

Fan, J. and Gijbels, I. (1996). *Local Polynomial Modelling and Its Applications*, Chapman and Hall, London.

Fisher, R. A. (1936). The use of multiple measurements in taxonomic problems, *Eugen.* **7**: 179–188.

Fix, E. and Hodges, J. (1951). Discriminatory analysis- nonparametric discrimination: Consistency properties, *Technical Report 21-49-004,4*, US Air Force, School of Aviation Medicine, Randolph Field, TX.

Flury, B. (1990). Principal points, *Biometrika* **77**: 33–41.

Forgy, E. (1965). Cluster analysis of multivariate data: Efficiency vs. interpretability of classifications (abstract), *Biometrics* **21**: 768–769.

Frank, I. and Friedman, J. (1993). A statistical view of some chemometrics regression tools (with discussion), *Technometrics* **35**(2): 109–148.

Freund, Y. (1995). Boosting a weak learning algorithm by majority, *Information and Computation* **121**(2): 256–285.

Freund, Y. and Schapire, R. (1996a). Experiments with a new boosting algorithm, *Machine Learning: Proceedings of the Thirteenth International Conference*, Morgan Kauffman, San Francisco, pp. 148–156.

Freund, Y. and Schapire, R. (1996b). Game theory, on-line prediction and boosting, *Proceedings of the Ninth Annual Conference on Computational Learning Theory*, pp. 325–332.

Freund, Y. and Schapire, R. (1997). A decision-theoretic generalization of online learning and an application to boosting, *Journal of Computer and System Sciences* **55**: 119–139.

Friedman, J. (1987). Exploratory projection pursuit, *Journal of the American Statistical Association* **82**: 249–266.

Friedman, J. (1989). Regularized discriminant analysis, *Journal of the American Statistical Association* **84**: 165–175.

Friedman, J. (1991). Multivariate adaptive regression splines (with discussion), *Annals of Statistics* **19**(1): 1–141.

Friedman, J. (1994a). Flexible metric nearest-sneighbour classification, *Technical report*, Stanford University.

Friedman, J. (1994b). An overview of predictive learning and function approximation, *in* V. Cherkassky, J. Friedman and H. Wechsler (eds), *From Statistics to Neural Networks*, Vol. 136 of *NATO ISI Series F*, Springer Verlag, New York.

Friedman, J. (1996). Another approach to polychotomous classification, *Technical report*, Stanford University.

Friedman, J. (1997). On bias, variance, 0-1 loss and the curse of dimensionality, *J. Data Mining and Knowledge Discovery* **1**: 55–77.

Friedman, J. (1999). Stochastic gradient boosting, *Technical report*, Stanford University.

Friedman, J. (2001). Greedy function approximation: the gradient boosting machine, *Annals of Statistics* . to appear.

Friedman, J., Baskett, F. and Shustek, L. (1975). An algorithm for finding nearest neighbors, *IEEE transactions on computers* **24**: 1000–1006.

Friedman, J., Bentley, J. and Finkel, R. (1977). An algorthm for finding best matches in logarithmic expected time, *ACM Transactions on Mathematical Software* **3**: 209–226.

Friedman, J. and Fisher, N. (1999). Bump hunting in high dimensional data, *Statistics and Computing* **9**: 123–143.

Friedman, J., Hastie, T. and Tibshirani, R. (2000). Additive logistic regression: a statistical view of boosting (with discussion), *Annals of Statistics* **28**: 337–307.

Friedman, J. and Silverman, B. (1989). Flexible parsimonious smoothing and additive modelling (with discussion), *Technometrics* **31**: 3–39.

Friedman, J. and Stuetzle, W. (1981). Projection pursuit regression, *Journal of the American Statistical Association* **76**: 817–823.

Friedman, J., Stuetzle, W. and Schroeder, A. (1984). Projection pursuit density estimation, *Journal of the American Statistical Association* **79**: 599–608.

Friedman, J. and Tukey, J. (1974). A projection pursuit algorithm for exploratory data analysis, *IEEE trans. on computers, Ser. C* **23**: 881–889.

Furnival, G. and Wilson, R. (1974). Regression by leaps and bounds, *Technometrics* **16**: 499–511.

Gelfand, A. and Smith, A. (1990). Sampling based approaches to calculating marginal densities, *J. Amer. Statist. Assoc.* **85**: 398–409.

Gelman, A., Carlin, J., Stern, H. and Rubin, D. (1995). *Bayesian Data Analysis*, CRC Press, Boca Raton, FL.

Geman, S. and Geman, D. (1984). Stochastic relaxation, Gibbs distributions and the Bayesian restoration of images, *IEEE Transactions on Pattern Analysis and Machine Intelligence* **6**: 721–741.

Gersho, A. and Gray, R. (1992). *Vector Quantization and Signal Compression*, Kluwer Academic Publishers, Boston, MA.

Girosi, F., Jones, M. and Poggio, T. (1995). Regularization theory and neural network architectures, *Neural Computation* **7**: 219–269.

Golub, G., Heath, M. and Wahba, G. (1979). Generalized cross-validation as a method for choosing a good ridge parameter, *Technometrics* **21**: 215–224.

Golub, G. and Van Loan, C. (1983). *Matrix Computations*, Johns Hopkins University Press, Baltimore.

Gordon, A. (1999). *Classification (2nd edition)*, Chapman and Hall/CRC press, London.

Green, P. and Silverman, B. (1994). *Nonparametric Regression and Generalized Linear Models: A Roughness Penalty Approach*, Chapman and Hall, London.

Greenacre, M. (1984). *Theory and Applications of Correspondence Analysis*, Academic Press, New York.

Hall, P. (1992). *The Bootstrap and Edgeworth Expansion*, Springer-Verlag, New York.

Hand, D. (1981). *Discrimination and Classification*, Wiley, Chichester.

Hart, P. (1968). The condensed nearest-neighbor rule, *IEEE Trans. Inform. Theory* **14**: 515–516.

Hartigan, J. A. (1975). *Clustering Algorithms*, Wiley, New York.

Hartigan, J. A. and Wong, M. A. (1979). [(Algorithm AS 136] A k-means clustering algorithm (AS R39: 81v30 p355-356), *Applied Statistics* **28**: 100–108.

Hastie, T. (1984). Principal curves and surfaces, *Technical report*, Stanford University.

Hastie, T., Botha, J. and Schnitzler, C. (1989). Regression with an ordered categorical response, *Statistics in Medicine* **43**: 884–889.

Hastie, T., Buja, A. and Tibshirani, R. (1995). Penalized discriminant analysis, *Annals of Statistics* **23**: 73–102.

Hastie, T. and Herman, A. (1990). An analysis of gestational age, neonatal size and neonatal death using nonparametric logistic regression, *Journal of Clinical Epidemiology* **43**: 1179–90.

Hastie, T. and Simard, P. (1998). Models and metrics for handwritten digit recognition, *Statistical Science* **13**: 54–65.

Hastie, T. and Stuetzle, W. (1989). Principal curves, *Journal of the American Statistical Association* **84**(406): 502–516.

Hastie, T. and Tibshirani, R. (1987). Nonparametric logistic and proportional odds regression, *Applied Statistics* **36**: 260–276.

Hastie, T. and Tibshirani, R. (1990). *Generalized Additive Models*, Chapman and Hall, London.

Hastie, T. and Tibshirani, R. (1996a). Discriminant adaptive nearest-neighbor classification, *IEEE Pattern Recognition and Machine Intelligence* **18**: 607–616.

Hastie, T. and Tibshirani, R. (1996b). Discriminant analysis by Gaussian mixtures, *J. Royal. Statist. Soc. B.* **58**: 155–176.

Hastie, T. and Tibshirani, R. (1998). Classification by pairwise coupling, *Annals of Statistics* **26**(2).

Hastie, T., Tibshirani, R. and Buja, A. (1994). Flexible discriminant analysis by optimal scoring, *J. Amer. Statist. Assoc.* **89**: 1255–1270.

Hastie, T., Tibshirani, R. and Buja, A. (1998). Flexible discriminant and mixture models, *in* J. Kay and M. Titterington (eds), *Statistics and Artificial Neural Networks*, Oxford University Press.

Hathaway, R. J. (1986). Another interpretation of the EM algorithm for mixture distributions, *Statistics & Probability Letters* **4**: 53–56.

Hebb, D. (1949). *The Organization of Behavior*, Wiley, New York.

Hertz, J., Krogh, A. and Palmer, R. (1991). *Introduction to the Theory of Neural Computation*, Addison Wesley, Redwood City, CA.

Hinton, G. (1989). Connectionist learning procedures, *Artificial Intelligence* **40**: 185–234.

Hoerl, A. E. and Kennard, R. (1970). Ridge regression: Biased estimation for nonorthogonal problems, *Technometrics* **12**: 55–67.

Huber, P. (1964). Robust estimation of a location parameter, *Annals of Math. Stat.* **53**: 73–101.

Huber, P. (1985). Projection pursuit, *Annals of Statistics* **13**: 435–475.

Hyvärinen, A. and Oja, E. (2000). Independent component analysis: Algorithms and applications, *Neural Networks* **13**: 411–430.

Izenman, A. (1975). Reduced-rank regression for the multivariate linear model, *Journal of Multivariate Analysis* **5**: 248–264.

Jacobs, R., Jordan, M., Nowlan, S. and Hinton, G. (1991). Adaptive mixtures of local experts, *Neural computation* **3**: 79–87.

Jain, A. and Dubes, R. (1988). *Algorithms for Clustering Data*, Prentice-Hall.

Jancey, R. (1966). Multidimensional group analysis, *Austral. J. Botany* **14**: 127–130.

Jones, L. (1992). A simple lemma on greedy approximation in Hilbert space and convergence rates for projection pursuit regression and neural network training, *Ann. Stat.* **20**: 608–613.

Jordan, M. and Jacobs, R. (1994). Hierachical mixtures of experts and the EM algorithm, *Neural Computation* **6**: 181–214.

Kaufman, L. and Rousseeuw, P. (1990). *Finding Groups in Data: An Introduction to Cluster Analysis*, Wiley, New York.

Kearns, M. and Vazirani, U. (1994). *An Introduction to Computational Learning Theory*, MIT Press.

Kelly, C. and Rice, J. (1990). Monotone smoothing with application to dose-response curves and the assessment of synergism, *Biometrics* **46**: 1071–1085.

Kohonen, T. (1989). *Self-Organization and Associative Memory (3rd edition)*, Springer-Verlag, Berlin.

Kohonen, T. (1990). The self-organizing map, *Proc. of IEEE* **78**: 1464–1479.

Kohonen, T., Kaski, S., Lagus, K., Salojärvi, J., Paatero, A. and Saarela, A. (2000). Self organization of a massive document collection, *IEEE Transactions on Neural Networks* **11**(3): 574–585. Special Issue on Neural Networks for Data Mining and Knowledge Discovery.

Kressel, U. (1999). Pairwise classification and support vector machines, *in* B. Sch olkopf, C. Burges and A. Smola (eds), *Advances in Kernel Methods - Support Vector Learning*, MIT Press, Cambridge, MA., pp. 255–268.

Lawson, C. and Hansen, R. (1974). *Solving Least Squares Problems*, Prentice-Hall, Englewood Cliffs, NJ.

Le Cun, Y. (1989). Generalization and network design strategies, *Technical Report CRG-TR-89-4*, Dept. of Comp. Sci,. Univ. of Toronto.

Le Cun, Y., Boser, B., Denker, J., Henderson, D., Howard, R., Hubbard, W. and Jackel, L. (1990). Handwritten digit recognition with a back-propogation network, *in* D. Touretzky (ed.), *Advances in Neural Information Processing Systems*, Vol. 2, Morgan Kaufman, Denver, CO.

Le Cun, Y., Bottou, L., Bengio, Y. and Haffner, P. (1998). Gradient-based learning applied to document recognition, *Proceedings of the IEEE* **86**(11): 2278–2324.

Leblanc, M. and Tibshirani, R. (1996). Combining estimates in regression and classification, *J. Amer. Statist. Assoc.* **91**: 1641–1650.

Lin, H., McCulloch, C., Turnbull, B., Slate, E. and Clark, L. (2000). A latent class mixed model for analyzing biomarker trajectories in longitudinal data with irregularly scheduled observations., *Statistics in Medicine* **19**: 1303–1318.

Little, R. and Rubin, D. (1987). *Statistical Analysis with Missing Data*, Wiley, New York.

Lloyd, S. (1957). Least squares quantization in PCM., *Technical report*, Bell Laboratories. Published in 1982 in IEEE Trans. Inf. Theory **28** 128-137.

Loader, C. (1999). *Local Regression and Likelihood*, Springer–Verlag.

Macnaughton Smith, P., Williams, W., Dale, M. and Mockett, L. (1965). Dissimilarity analysis: a new technique of hierarchical subdivision, *Nature* **202**: 1034–1035.

MacQueen, J. (1967). Some methods for classification and analysis of multivariate observations, *Proceedings of the Fifth Berkeley Symposium on Mathematical Statistics and Probability, eds. L.M. LeCam and J. Neyman*, Univ. of California Press, pp. 281–297.

Madigan, D. and Raftery, A. (1994). Model selection and accounting for model uncertainty using occam's window., *J. Amer. Statist. Assoc.* **89**: 1535–46.

Mardia, K., Kent, J. and Bibby, J. (1979). *Multivariate Analysis*, Academic Press.

Massart, D., Plastria, F. and Kaufman, L. (1983). Non-hierarchical clustering with MASLOC, *The Journal of the Pattern Recognition Society* **16**: 507–516.

McCulloch, W. and Pitts, W. (1943). A logical calculus of the ideas immenent in nervous activity, *Bull. Math. Biophys.* **5**: 115–133. pp 96-104; Reprinted in Andersen and Rosenfeld (1988).

McLachlan, G. J. (1992). *Discriminant Analysis and Statistical Pattern Recognition*, Wiley, New York.

Michie, D., Spiegelhalter, D. and Taylor, C. (eds) (1994). *Machine Learning, Neural and Statistical Classification*, Ellis Horwood Series in Artificial Intelligence, Ellis Horwood.

Morgan, J. N. and Sonquist, J. A. (1963). Problems in the analysis of survey data, and a proposal, *Journal of the American Statistical Association* pp. 415–434.

Murray, W., Gill, P., and Wright, M. (1981). *Practical Optimization*, Academic Press.

Myles, J. and Hand, D. (1990). The multiclass metric problem in nearest neighbor clasification, *Pattern Recognition* **23**: 1291–1297.

Neal, R. (1996). *Bayesian Learning for Neural Networks*, Springer-Verlag, New York.

Neal, R. and Hinton, G. (1998). *A view of the EM algorithm that justifies incremental, sparse, and other variants; in Learning in Graphical Models, M. Jordan (ed.),*, Dordrecht: Kluwer Academic Publishers, Boston, MA., pp. 355–368.

Pace, R. K. and Barry, R. (1997). Sparse spatial autoregressions, *Statistics & Probability Letters* **33**: 291–297.

Parker, D. (1985). Learning logic, *Technical Report TR-87*, Cambridge MA: MIT Center for Reserach in Computational Economics and Management Science.

Platt, J. (1999). Fast training of support vector machines using sequential minimal optimization, *in* B. Schölkopf, C. J. C. Burges and A. J. Smola (eds), *Advances in Kernel Methods — Support Vector Learning*, MIT Press, Cambridge, MA., pp. 185–208.

Quinlan, R. (1993). *C4.5: Programs for Machine Learning*, Morgan Kaufmann, San Mateo.

Ramsay, J. and Silverman, B. (1997). *Functional Data Analysis*, Springer Verlag.

Rao, C. R. (1973). *Linear Statistical Inference and Its Applications*, Wiley, New York.

Ripley, B. D. (1996). *Pattern Recognition and Neural Networks*, Cambridge University Press.

Rissanen, J. (1983). A universal prior for integers and estimation by minimum description length, *Annals of Statistics* **11**: 416–431.

Robbins, H. and Munro, S. (1951). A stochastic approximation method, *Ann. Math. Stat.* **22**: 400–407.

Roosen, C. and Hastie, T. (1994). Automatic smoothing spline projection pursuit, *Journal of Computational and Graphical Statistics* **3**: 235–248.

Rosenblatt, F. (1958). The perceptron: a probabilistic model for information storage and organization in the brain, *Psychological Review* **65**: 386–408.

Rosenblatt, F. (1962). *Principles of Neurodynamics: Perceptrons and the Theory of Brain Mechanisms*, Spartan, Washington, D.C.

Rousseauw, J., du Plessis, J., Benade, A., Jordaan, P., Kotze, J., Jooste, P. and Ferreira, J. (1983). Coronary risk factor screening in three rural communities, *South African Medical Journal* **64**: 430–436.

Rumelhart, D., Hinton, G. and Williams, R. (1986). *Learning internal representations by error propagation in Parallel Distributed Processing: Explorations in the Microstructure of Cognition (Rumelhart, D.E. and McClelland, J. L eds.)*, The MIT Press, Cambridge, MA., pp. 318–362.

Schapire, R. (1990). The strength of weak learnability, *Machine Learning* **5**(2): 197–227.

Schapire, R., Freund, Y., Bartlett, P. and Lee, W. (1998). Boosting the margin: a new explanation for the effectiveness of voting methods, *Annals of Statistics* **26**(5): 1651–1686.

Schapire, R. and Singer, Y. (1998). Improved boosting algorithms using confidence-rated predictions, *Proceedings of the Eleventh Annual Conference on Computational Learning Theory.*

Schwartz, G. (1979). Estimating the dimension of a model, *Annals of Statistics* **6**: 461–464.

Scott, D. (1992). *Multivariate Density Estimation: Theory, Practice, and Visualization*, Wiley, New York.

Seber, G. (1984). *Multivariate Observations*, Wiley, New York.

Shao, J. (1996). Bootstrap model selection, *J. Amer. Statist. Assoc.* **91**: 655–665.

Short, R. and Fukunaga, K. (1981). The optimal distance measure for nearest neighbor classification, *IEEE Transactions on Information Theory* **27**: 622–627.

Silverman, B. (1986). *Density Estimation for Statistics and Data Analysis*, Chapman and Hall, London.

Silvey, S. (1975). *Statistical Inference*, Halsted.

Simard, P., Le Cun, Y. and Denker, J. (1993). Efficient pattern recognition using a new transformation distance, *Advances in Neural Information Processing Systems*, Morgan Kaufman, San Mateo, CA, pp. 50–58.

Spiegelhalter, D., Best, N., Gilks, W. and Inskip, H. (1996). Hepatitis B: a case study in MCMC methods, *in* W. Gilks, S. Richardson and D. Spegelhalter (eds), *Markov Chain Monte Carlo in Practice*, Interdisciplinary Statistics, Chapman and Hall, London.

Stamey, T., Kabalin, J., McNeal, J., Johnstone, I., Freiha, F., Redwine, E. and Yang, N. (1989). Prostate specific antigen in the diagnosis and treatment of adenocarcinoma of the prostate II. radical prostatectomy treated patients, *Journal of Urology* **16**: 1076–1083.

Stone, C., Hansen, M., Kooperberg, C. and Truong, Y. (1997). Polynomial splines and their tensor products (with discussion), *Annals of Statistics* **25**(4): 1371–1470.

Stone, M. (1974). Cross-validatory choice and assessment of statistical predictions, *J. Roy. Statist. Soc.* **36**: 111–147.

Stone, M. (1977). An asymptotic equivalence of choice of model by cross-validation and Akaike's criterion, *J. Roy. Statist. Soc.* **39**: 44–7.

Stone, M. and Brooks, R. J. (1990). Continuum regression: Cross-validated sequentially constructed prediction embracing ordinary least squares, partial least squares and principal components regression (Corr: V54 p906-907), *Journal of the Royal Statistical Society, Series B, Methodological* **52**: 237–269.

Swayne, D., Cook, D. and Buja, A. (1991). Xgobi: Interactive dynamic graphics in the X window system with a link to S, *ASA Proceedings of Section on Statistical Graphics*, pp. 1–8.

Tanner, M. and Wong, W. (1987). The calculation of posterior distributions by data augmentation (with discussion), *J. Amer. Statist. Assoc.* **82**: 528–550.

Tarpey, T. and Flury, B. (1996). Self-consistency: A fundamental concept in statistics, *Statistical Science* **11**: 229–243.

Tibshirani, R. (1996). Regression shrinkage and selection via the lasso, *J. Royal. Statist. Soc. B.* **58**: 267–288.

Tibshirani, R. and Knight, K. (1999). Model search and inference by bootstrap "bumping, *J. Comp. and Graph. Stat.* **8**: 671–686.

Tibshirani, R., Walther, G. and Hastie, T. (2001). Estimating the number of clusters in a dataset via the gap statistic, *J. Royal. Statist. Soc. B. (to appear)* .

Valiant, L. G. (1984). A theory of the learnable, *Communications of the ACM* **27**: 1134–1142.

van der Merwe, A. and Zidek, J. (1980). Multivariate regression analysis and canonical variates, *The Canadian Journal of Statistics* **8**: 27–39.

Vapnik, V. (1996). *The Nature of Statistical Learning Theory*, Springer-Verlag, New York.

Vidakovic, B. (1999). *Statistical Modeling by Wavelets*, Wiley, New York.

Wahba, G. (1980). Spline bases, regularization, and generalized cross-validation for solving approximation problems with large quantities of noisy data, *Proceedings of the International Conference on Approximation theory in Honour of George Lorenz*, Academic Press, Austin, Texas.

Wahba, G. (1990). *Spline Models for Observational Data*, SIAM, Philadelphia.

Wahba, G., Lin, Y. and Zhang, H. (2000). GACV for support vector machines, *in* A. Smola, P. Bartlett, B. Schölkopf and D. Schuurmans (eds), *Advances in Large Margin Classifiers*, MIT Press, Cambridge, MA., pp. 297–311.

Weisberg, S. (1980). *Applied Linear Regression*, Wiley, New York.

Werbos, P. (1974). *Beyond regression*, PhD thesis, Harvard University.

Wickerhauser, M. (1994). *Adapted Wavelet Analysis from Theory to Software*, A.K. Peters Ltd, Natick, MA.

Widrow, B. and Hoff, M. (1960). Adaptive switching curcuits, Vol. 4, IRE WESCON Convention record. pp 96-104; Reprinted in Andersen and Rosenfeld (1988).

Wold, H. (1975). Soft modelling by latent variables: The nonlinear iterative partial least squares (NIPALS) approach, *Perspectives in Probability and Statistics, In Honor of M. S. Bartlett*, pp. 117– 144.

Wolpert, D. (1992). Stacked generalization, *Neural Networks* **5**: 241–259.

Yee, T. and Wild, C. (1996). Vector generalized additive models, *Journal of the Royal Statistical Society, Series B.* **58**: 481–493.

Zhang, P. (1993). Model selection via multifold cross-validation, *Ann. Statist.* **21**: 299–311.

Author Index

Index